UNIVERSITY OF NATAL

SCHOOL OF GEOLOGICAL AND COMPUTER SCIENCES

THE PHYSICAL VOLCANOLOGY AND GEOCHEMISTRY OF THE NSUZE GROUP, PONGOLA SUPERGROUP, OF NORTHERN KWAZULU-NATAL AND SOUTHEASTERN MPUMALANGA

By

Claire Elizabeth Grant

B.Sc. (Honours)

Submitted in fulfilment of the academic
requirements for the degree of
Master of Science in the
School of Geological and
Computer Sciences,
University of Natal
Durban

November 2003

ABSTRACT

The Nsuze Group forms the lower, predominantly volcanic succession of the Pongola Supergroup. The 2.9Ga Nsuze Group outcrops in southeastern Mpumalanga, northern KwaZulu-Natal and Swaziland. The volcanic rocks of the Nsuze Group are basalts, basaltic andesites, andesites, dacites and rhyolites preserved as both lava and pyroclastic deposits. The oldest volcanic sequence of the Nsuze Group is the basaltic Wagondrift Formation. The younger Bivane Subgroup represents the main volcanic component of the Nsuze Group. The White River Section represents a complex volcanic history of magma storage, fractionation, and eruption, supplied by a multi-level system of magma chambers. The basaltic and basaltic andesite rocks of the White Mfolozi Inlier represent the steady and non-violent eruption of lavas from related volcanic centres. The Nsuze Group rocks have been metamorphosed by high heat flow burial metamorphism to lower greenschist facies. Geochemically, elements display well-defined fractionation trends, with evident sub-trends within each phase group of samples. These sub-trends are related to the fractionation of key minerals, in particular plagioclase. The REE patterns show that evolution of magma was largely controlled by the fractionation of plagioclase. All REE patterns show LREE enrichment relative to the HREE. The Wagondrift Formation was derived from a more depleted source than the younger Bivane Subgroup volcanic rocks and exhibits a within-plate tectonic signature. The volcanic rocks of the Bivane Subgroup in the White River Section and the White Mfolozi Inlier are geochemically similar. The volcanic rocks of the Bivane Subgroup of both the White River Section and the White Mfolozi Inlier have a subduction zone tectonic signature, in particular a Ta-Nb negative anomaly. Tectonic discrimination diagrams suggest an enriched source related to a continental-arc setting. The geochemistry suggests an eclogitic source for the Nsuze Group volcanic rocks. The formation of eclogite in the mantle requires subduction of basaltic material. Archaean models for subduction-like processes include decoupling of oceanic crust and subsequent underplating of the continental lithosphere, and low-angle subduction which minimises the effect of the mantle wedge. It is possible that a combination of these processes resulted in an enriched eclogitic source for the magmas of the Nsuze Group.

This study was undertaken in the School of Geological and Computer Sciences, University of Natal, Durban, from April 2001 to September 2003, under the supervision of Professor Allan H. Wilson.

This dissertation represents original work by the author and has not otherwise been submitted in any form for any degree or diploma to any tertiary institution. Where use has been made of the work of others, it is duly acknowledged in the text.

Claire Elizabeth Grant

CONTENTS

CHAPTER 1
INTRODUCTION

1.1 GENERAL

The Pongola Supergroup is a meso-Archaean volcano-sedimentary succession that outcrops in southeastern Mpumalanga, northern KwaZulu-Natal and Swaziland (Figure 1.1). It is divided into two distinct sequences – the lower Nsuze Group and the upper Mozaan Group. The Nsuze Group is mainly composed of volcanic rocks while sedimentary rocks dominate the Mozaan Group. The Pongola Supergroup has been regionally metamorphosed to lower greenschist facies, although amphibolite facies is observed in some exposures in southeastern Swaziland (SACS, 1980).

The Pongola Supergroup is unique in terms of global geological history as it represents the first known stable cratonic cover sequence. While volcano-sedimentary successions of an equivalent age (2.98-2.97Ga, Griffin, 2002), are preserved as greenstone belts on the Zimbabwe and Australian Cratons, the Pongola Supergroup on the southeastern margin of the Kaapvaal Craton, is relatively undeformed and well preserved (Armstrong, 1980).

The eastern and southern limits of the Pongola Supergroup also characterise the eastern and southeastern margins of the Kaapvaal Craton, and interpretation of the depositional environment would provide an understanding of the evolution of the margins of the craton (Matthews, 1990). The Pongola Supergroup is preserved as a number of inliers, exposed where uplift and erosion have removed younger Natal Group and Karoo Supergroup cover sequences.

The Nsuze Group and Mozaan Group have been lithologically correlated with the Dominion Group and Witwatersrand Supergroup respectively (Beukes and Cairncross, 1991). While dating indicates that the deposition of these volcano-sedimentary successions was consanguineous, it is debatable as to the extent of the specific relationship between their tectonic and depositional environments.

1.2 PURPOSE AND AIMS

The Pongola Supergroup has been the focus of numerous studies in the 1980's and early 1990's. These investigations were however concerned with the regional geology of individual inliers of the Pongola Supergroup and did not look at the supergroup as a whole.

The project aims:

- to investigate the physical nature of the volcanism that produced the Nsuze Group. This includes environment of eruption; characteristics of different flow units and their relationship to one another; characteristics of pyroclastic material.
- to study the petrology of the Nsuze volcanic rocks to gain a better understanding of the mineralogical variations of the different rock types and the effect of low-grade regional metamorphism on the mineral assemblages.
- to interpret all geochemical data to determine the nature of the Nsuze Group volcanism.
- to explain the tectonic setting responsible for eruption of the Nsuze Group using immobile trace elements as determined by ICP-MS and XRF. Certain trace elements were not determined in previous studies due to their exceptionally low concentrations.

The achievement of these aims is based on both field and laboratory work. The study incorporates previous mapping by various authors and fieldwork, which involved detailed mapping of unique and well-preserved outcrops that exhibited relationships between differing volcanic units. Sampling of individual volcanic units for the purpose of geochemistry and petrological studies was carried out in different geographic areas in order to obtain a comprehensive and consistent data set over the entire stratigraphic succession. It is not the purpose of this study to provide a stratigraphic framework but rather to describe the physical and geochemical changes in volcanic activity over the time of Nsuze Group formation.

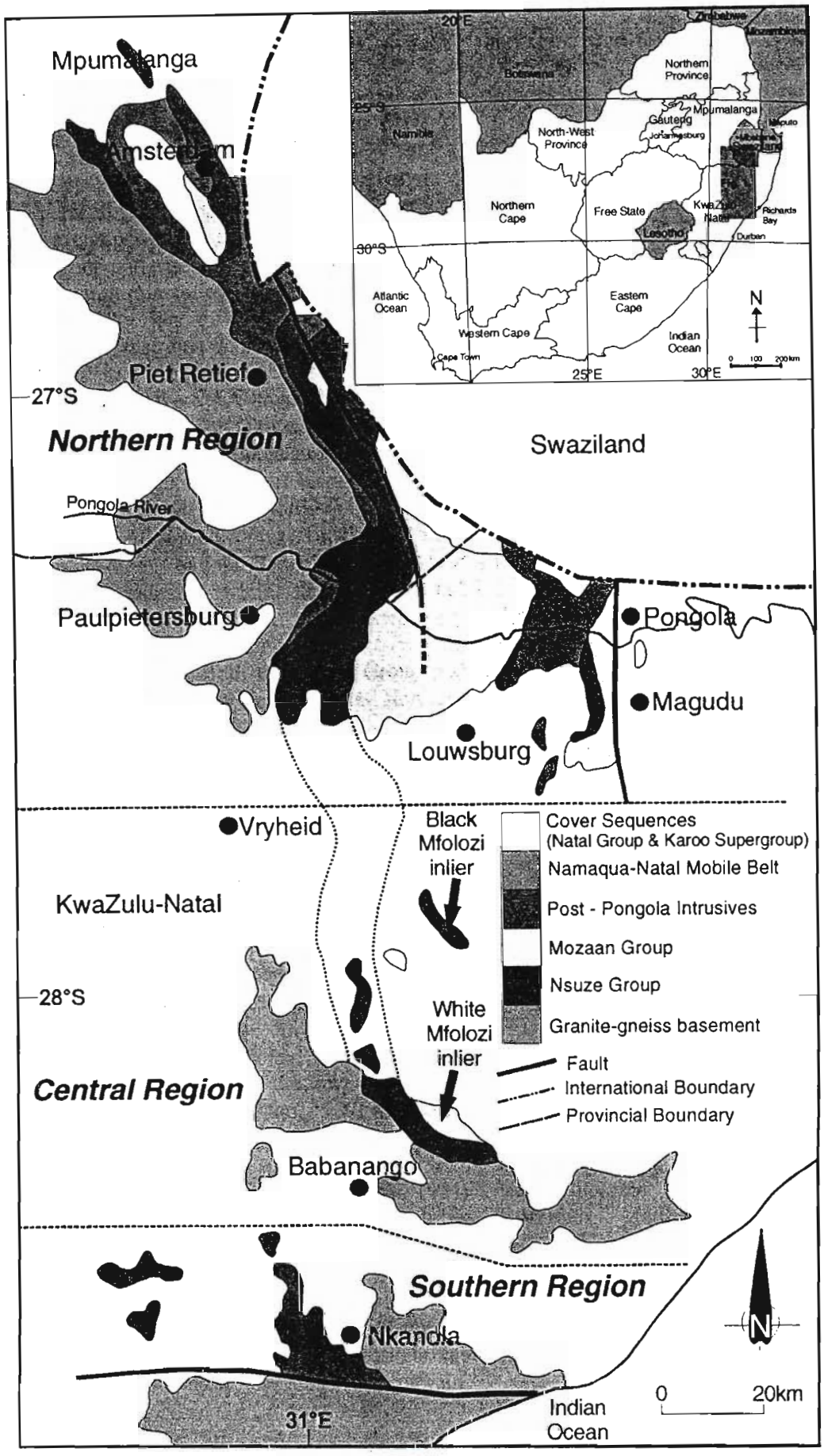

Figure 1.1 Locality map of the Pongola Supergroup, showing the outcrop of the Nsuze and Mozaan Groups in the Northern, Central and Southern Regions. (Modified after Gold, 1993)

1.3 LOCATION AND PHYSIOGRAPHY OF STUDY AREA

The Pongola Supergroup is exposed as a series of inliers that can be broadly divided into a Northern Region, a Central Region and a Southern Region (Figure 1.1). The Northern Region comprises the type area of the Pongola Supergroup and extends approximately 125km in a north-south orientation, from east of Piet Retief to south of the Bivane River, covering an area of 1100km^2 (Armstrong, 1980; Hatfield, 1990). In this area the Pongola Supergroup is at it's stratigraphic thickest. A small-elongated inlier (~200km^2) also exists around the town of Amsterdam in eastern Mpumalanga and outcrops are found throughout southern Swaziland. The western margin of the Northern Region is relatively undisturbed, preserving the basal contact of the Pongola Supergroup on older granitoid basement, while the eastern and northeastern margins have been extensively deformed by the intrusion of post-Pongola granitoid plutons. Both the Nsuze Group and Mozaan Group are present in the Northern Region (Matthews, 1990).

The Central Region is made up of the Black Mfolozi (40km^2; Preston, 1987) and White Mfolozi Inliers (Figure 1.1). Northwest trending outcrops of pre-Pongola granitoid basement, unconformably overlain by northeast dipping Pongola lithologies characterize the area. This outcrop pattern was formed by extensive block faulting in the region resulting in repetition of the stratigraphy (Matthews, 1990). While the Black Mfolozi Inlier contains only Nsuze Group lithologies, the White Mfolozi Inlier comprises both the Nsuze Group and the lower lithologies of the Mozaan Group (Preston, 1987; Matthews, 1967).

The Nkandla Inlier (280km^2; Groenewald, 1984) constitutes the Southern Region, which is dominated by east-west trending folds and thrust faults (Matthews, 1990) (Figure 1.1). No Mozaan Group strata are found in the Nkandla Inlier, and the Nsuze Group lithologies present are not directly correlatable with those in the Northern and Central Regions (Groenewald, 1984).

Vegetation throughout northern KwaZulu-Natal and southeastern Mpumalanga is typically Acacia thorn scrub and grassland, although vast areas are used for forestry. The topography is generally rugged, with rivers and streams flowing through steep valleys, providing the best exposures. Access is via old main roadways, farm roads and recently constructed 4x4 recreation tracks.

1.4 PREVIOUS WORK

The Pongola Series was first attributed to a succession of lavas and sediments found along the Pongola River in southeastern Mpumalanga by Humphrey (1912). Humphrey described a Lower Unit comprising quartzites, phyllites and dominated by lavas. Quartzites and shales dominate the Upper Unit. Although Humphrey initially correlated the Upper Unit to the Witwatersrand System, in 1914, he assigned both the Upper and Lower Units of the Pongola Series to the Swaziland System.

Krige re-classified the Pongola Series to the Pongola System in 1931. The Lower Unit was therefore known as the Lower Pongola Series and the Upper Unit as the Upper Pongola Series. Krige correlated the Pongola System with the Swaziland System (Krige, 1931).

Hatch (1910) described a succession of quartzites, conglomerates and schists, found outcropping west of Nkandla, KwaZulu-Natal. He named this succession the Insuzi Series (original spelling). Du Toit (1931), correlated the succession, based on the unconformable basal contact with granitoid basement, to the Lower Pongola Series, described by Krige (1931) and Humphrey (1912).

The Insuzi Series was correlated to the Dominion Reef System by Matthews (1959), who also recognised clear intrusive relationships between the Insuzi Series and certain granite intrusions, which became known as the post-Pongola granitoids. Matthews (1979a) also determined the importance of the low grade of metamorphism of the Pongola System, in comparison to older high-grade metamorphic basement, representing a major unconformity at the base of the succession.

The Upper Pongola Series was renamed the Mozaan Series and correlated with the lower division of the Witwatersrand System (Truter, 1950). SACS (1980) assigned the Pongola System, supergroup status, containing the Nsuze

sedimentary succession's extensive geographic and stratigraphic nature.

Matthews (1979b) mapped the Piet Retief Area and the Pongola and Bivane Valleys in the Northern Region of the Pongola Supergroup. The Nsuze Group in the Pongola and Bivane Valleys, in the Northern Region, were the focus of a field and geochemical study by Armstrong (1980). Hatfield (1990) studied the outcrop area to the east of Piet Retief. Watchorn (1978) researched the Mozaan sediments of the Northern Region. Van Vuuren (1965) mapped the area in the region of Amsterdam, while Hammerbeck (1977) studied the most northerly exposures of the Northern Region. The Swaziland Area of the Northern Region has been the focus of work by Hunter (1961), Mabuza (1993) and Nhleko (1998).

The Central Region of the Pongola Supergroup, incorporating the Black Mfolozi and White Mfolozi Inliers, were reported on by Preston (1987) and Matthews (1967) respectively. Von Brunn and Mason (1977) studied the stromatilites of the Nsuze Group in the White Mfolozi Inlier.

The Southern Region of the Pongola Supergroup, comprising the Nkandla Inlier, was mapped and interpreted by Matthews (1967) and Groenewald (1984).

The Pongola Supergroup, and its unique significance in terms of Archaean geological history, has been discussed in many publications (Hunter, 1974; Burke *et al.*, 1985 and Matthews, 1990).

CHAPTER 2
GEOLOGICAL OVERVIEW OF THE PONGOLA SUPERGROUP AND LITHOLOGICAL ASSOCIATIONS

2.1 INTRODUCTION

The volcano-sedimentary succession of the Pongola Supergroup formed during two distinct depositional phases. The older Nsuze Group is predominantly volcanic, while sediments and minor volcanic rocks form the younger Mozaan Group. The Pongola Supergroup is exposed where the Phanerozoic cover sequences have been eroded to reveal a number of inliers found throughout southeastern Mpumalanga, southern Swaziland and northern KwaZulu-Natal (Figure 1.1). A general time interval of between 3100Ma and 2840Ma has been postulated for the deposition of the Pongola Supergroup (Hegner *et al.*, 1984).

This chapter will discuss in detail the lithostratigraphy of the Pongola Supergroup and pre- and post-Pongola depositional and intrusive events and associated environments of formation. It is based on work by a number of authors who have studied specific areas or aspects of the geology of the Pongola Supergroup. The aim of the chapter is to provide the reader with an overview of the complete stratigraphic succession present in southeastern Mpumalanga and northern KwaZulu-Natal.

2.2 PRE-PONGOLA BASEMENT

2.2.1 Northern Region

In the Northern Region, in the area west of Amsterdam (Figure 1.1), the Mpuluzi (previously known as Lochiel) granitoid sheet forms the basement to the Pongola Supergroup. The leucocratic granodiorite is dated at 3028±14Ma (Rb-Sr whole rock; Barton *et al.*, 1983) and 3107±4Ma (U-Pb single zircon; Kamo *et al.*, 1990) and has an unconformable relationship with the overlying Nsuze Group (Visser *et al.*, 1947; Grandstaff *et al.*, 1986). The most recent ages (U-Pb on zircons) for Pre-Pongola lithologies are 3147±13Ma for gneissic granite near Piet Retief, 3267±21Ma for the Hoopwel granitoid and 3427±24Ma for the Tsawela Gneiss component of the Ancient Gneiss Complex (Griffin, 2002).

The basal contact of the Nsuze Group has been obscured by the post-Pongola Usushwana Complex, intruded between the Pre-Pongola basement and Nsuze Group lithologies in the area east of Piet Retief (Hatfield, 1990) (Figure 1.1 and Figure 2.1). The Archaean basement rocks in this area are gneissic granitoids and probably formed the original depositional platform for the Nsuze Group sequence (Hunter and Wilson, 1988).

Further south, along the Pongola River, the Nsuze Group lies unconformably on Archaean basement rocks. Banded gneisses, potassic granites and granodiorites, containing xenoliths of amphibolite constitute the basement lithologies (Armstrong, 1980). The gneisses are composed of alternating bands of leuco-tonalite and amphibolite, which are complexly folded and intruded by aplites and pegmatitic phases. Thin layers of metasediments (orthoquartzite) and metavolcanics rocks are found within the gneisses. The strike orientation of the foliation of the gneisses is consistent with those recorded for the Ancient Gneiss Complex in Swaziland (Armstrong, 1980). The gneissic component of the pre-Pongola basement is restricted to the northwestern portion of the area of interest of this study. Dating of the Ancient Gneiss Complex in Swaziland (correlated to the gneisses of the Pre-Pongola basement by Armstrong, 1980) reveals an age of quartz monzonite gneiss of 3450±40Ma (Sm-Nd; Carlson *et al.*, 1983). Armstrong considered the gneisses as the oldest part of the Pre-Pongola basement. The granites of the basement rocks have yielded ages of 3223±3Ma by Pb-Pb single zircon evaporation (Meyer *et al.*, 1993) and 3292±20 by Pb-Pb whole rock (Matthews *et al.*, 1989).

The basement rocks south of the Pongola River in the Northern Region are dominated by a coarse-grained, leucocratic, potassic granite. The granite is generally unfoliated, although small areas of gneissic granite are also found. Amphibolite xenoliths, aplites and pegmatites are also located within the granite (Armstrong, 1980). Granodiorites comprise a small percentage of the Pre-Pongola basement. They are found in the south of the Northern Region

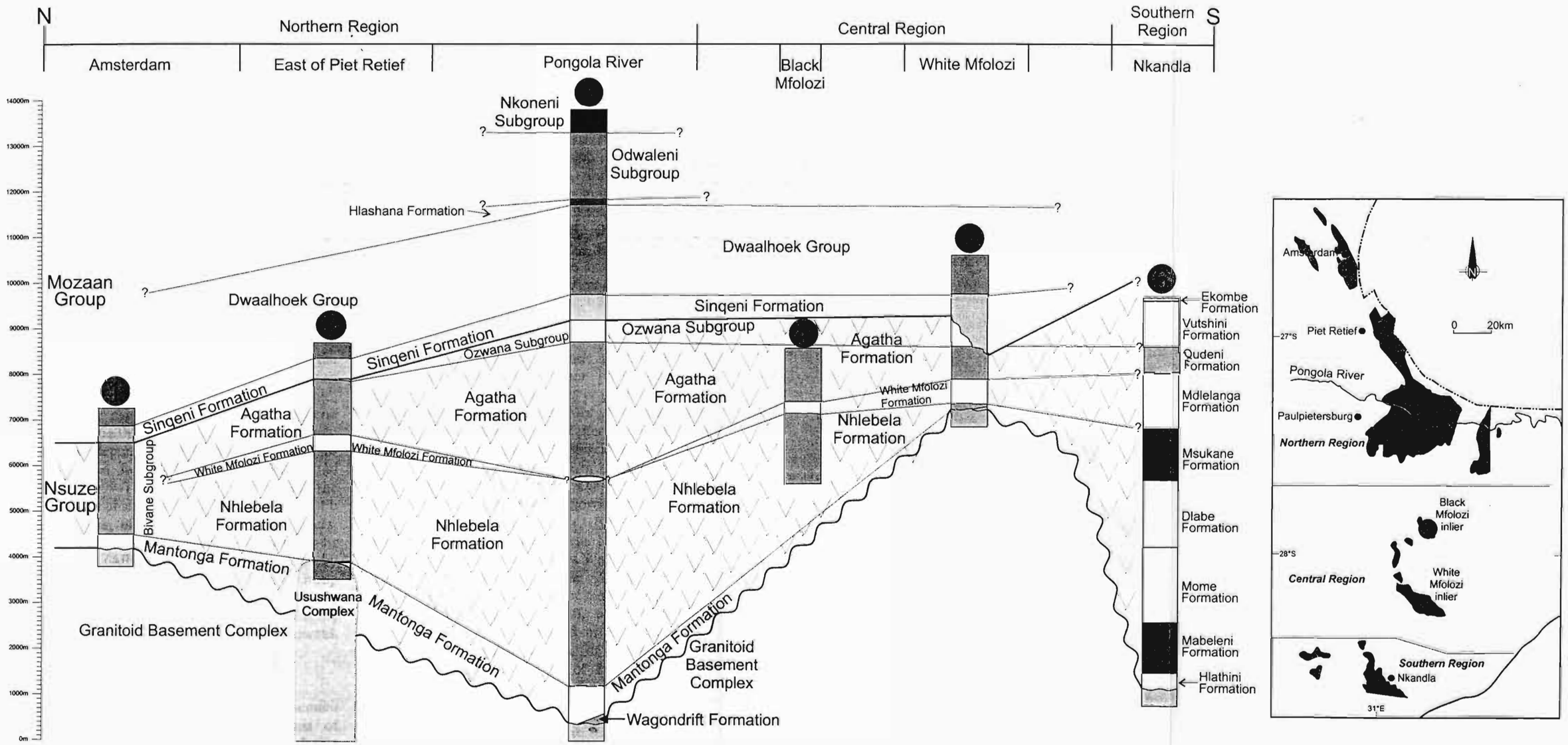

Figure 2.1 Stratigraphic columns representative of each prominent area of Pongola Supergroup outcrop.
(after SACS, 1980; Beukes and Cairncross, 1991; Armstrong *et al.*, 1982; Groenewald, 1984; Hatfield, 1990; Preston, 1987; Gold, 1993; Linstrom, 1987; Matthews, 1967)

and are generally medium grained and massive (Armstrong, 1980).

2.2.2 Central Region

The basal contact of the Pongola Supergroup is not exposed in the Black Mfolozi Inlier (Preston, 1987). In the White Mfolozi Inlier, however, a nonconformable contact between granite-gneiss basement and Nsuze Group sedimentary sequence is exposed in the White Mfolozi River (Matthews, 1967). The validity of this contact has been contested by Cole (1994) who states that the basal contact of the Nsuze Group and the granitoid basement has, for the large part, been obscured by granitoid intrusives, in the outcrop area of the White Mfolozi River.

2.2.3 Southern Region

In the southern Nkandla area, the Nsuze Group and its relationship to older units has been obscured by structural events. The older lithologies of the basement include the Nondweni Greenstone Belt, which has been intruded by tonalitic granitoids (Groenewald, 1984). The age of the Nondweni Greenstone Belt is 3406±3Ma (whole rock zircon, Annual Technical Report of the Geological Survey of South Africa for 1988 cited in Wilson and Versfeld, 1994) and therefore predates the tonalitic basement, which has yielded U-Pb zircon dates of 3138±38Ma (Burger, pers. comm., cited by Groenewald, 1984) and Rb-Sr 3160±80Ma (Allsopp, unpublished data cited by Burger and Coertze, 1973). The Nsuze Group rests unconformably on this granite-greenstone terrane. A basement high is found between the White Mfolozi and Nkandla inliers (Groenewald, 1984).

2.2.4 Palaeosaprolite

The contact between the Pre-Pongola basement and the Nsuze Group, in the area east of Paulpietersburg, is marked by a well-developed quartz – sericite palaeosaprolite (Matthews and Scharrer, 1968). A saprolite is decomposed residue of a rock, in this case granite, formed in situ by subaerial chemical weathering (Matthews and Scharrer, 1968). The palaeosaprolite, as described by Armstrong (1980), varies from 2 to 10m in thickness, and grades into the underlying granite. A distinct lack of feldspars and an abundance of micaceous minerals distinguish it from the underlying granite. The contact between the palaeosaprolite and the basal Nsuze sediments was observed by Armstrong (1980) to be sharp, the saprolite providing material for the quartz wackes. The limited thickness, but considerable lateral extent of the saprolite is evidence for extremely low topographical relief prior to the deposition of the Pongola Supergroup lithologies (Matthews and Scharrer, 1968).

Grandstaff *et al.* (1986) investigated the pre-Pongola palaeosaprolite to the west of Amsterdam in the Northern Region (Figure 1.1). The minimum thickness of the saprolite is 6.2m. Major losses of CaO, MgO, Na_2O and MnO are in agreement with weathering under humid conditions. The oxygen content of the Archaean atmosphere was greater than 0.02% - 0.05% PAL P_{O2} i.e. low oxygen pressures. P_{CO2} would have been equal to 5-30 PAL in order to maintain rates of chemical weathering (Grandstaff *et al.*, 1986).

2.3 NSUZE GROUP

The Nsuze Group comprises basic through to acid volcanic rocks, with minor intercalated lenses of clastic sediments. The proportion of sediments within the group increases towards the south. The Nsuze Group, named after the Nsuze River, trends north-south and is present as far as Nkandla in the Southern Region, a distance of nearly 200km (SACS, 1980). Dating of the Nsuze lavas has yielded the following results: Pb-Pb bulk zircon 3090±90Ma (Burger and Coertze, 1973); Pb-Pb single zircon evaporation 2978±2Ma (unpubl. data, cited by Walraven and Pape, 1994); U-Pb bulk zircon 2940±14Ma (Hegner *et al.*, 1984) and the same sample redated in Hegner *et al.* (1994), using U-Pb single zircon chemistry, resulted in an age of 2985±1Ma. The oldest lava unit of the Nsuze Group has a U-Pb zircon age of 2980±10Ma (Griffin, 2002). A rhyolitic unit found near the top of the Nsuze Group has a U-Pb zircon age of 2968±6Ma (Griffin, 2002).

The Nsuze Group can be divided into three broad lithological units and researchers have assigned different subgroup and formation names for the different areas mapped. Large-scale lateral variations are evident, but subgroups and formations are correlated broadly on the dominance of volcanic versus sedimentary rocks. The correlation for the Nsuze Group used in this thesis, is based on that proposed by Gold (unpublished data). The Nsuze Group is divided into three subunits. The basal Mantonga Formation is predominantly clastic sediments

with minor pyroclastic and lava lenses, the middle Bivane Subgroup is a succession of lavas and pyroclastic rocks and the upper Ozwana Subgroup is a pyroclastic, both primary and reworked, and sedimentary sequence (Figure 2.1). The Southern Region i.e. the area around Nkandla (Figure 1.1) is the only area, which is inconsistent with the broad correlation of the Nsuze lithostratigraphic units.

The Nsuze Group in the Northern Region, in the area east of Piet Retief, is approximately 4000m thick (Hatfield, 1990), and increases to a maximum thickness of approximately 9000m along the Pongola River (Armstrong *et al.*, 1982) (Figure 2.1). The White Mfolozi and Black Mfolozi Inliers dominate the Nsuze Group in the Central Region. The proportion of sediments to lavas is far greater in the Central Region compared with the Northern Region. The overall thickness of the group is approximately 1070m (Cole, 1994) in the White Mfolozi Inlier and a minimum thickness of 2500m in the Black Mfolozi Inlier (Preston, 1987) (Figure 2.1). Although lithostratigraphic units are similar, the thickness of the Nsuze Group in the Southern Region is markedly different to the northerly exposures. The true thickness of the group is also debatable due to difficulty in correlating within the region itself (Figure 2.1). This is as a result of a large number of tectonic contacts due to extensive faulting and folding in the area. The thickness of the Nsuze Group in the Southern Region as determined by Matthews (1967) is 2440m.

2.3.1 Mantonga Formation

The Mantonga Formation is considered to encompass the predominantly sedimentary succession developed at the base of the Nsuze Group (Figure 2.1). It is named after the Mantonga Tributary of the Pongola River, in which the succession is best preserved and is stratigraphically thickest (SACS, 1980). The formation can be identified in all outcrop exposures of the Pongola Supergroup from north to south. It has, however, not been exposed in the Black Mfolozi Inlier as the basal contact of the Nsuze Group lies beneath Karoo Supergroup cover rocks.

2.3.1.1 Northern Region

The Mantonga Formation, in the Northern Region, is composed of sandstones with intercalated lenses of intermediate and acid lavas, and volcaniclastics[1]. It is approximately 800m thick east of Paulpietersburg along the Pongola River (Armstrong, 1980) and has been correlated to the basal sedimentary unit to the north, east of Piet Retief (Hatfield, 1990) (Figure 2.1). The true thickness of the Mantonga Formation in this area has been obscured by the intrusion of the Usushwana Complex but a minimum thickness can be estimated at 150m (Hatfield, 1990) (Figure 2.1). Hammerbeck (1977) described a predominantly sedimentary unit at the base of the Nsuze Group in the area around Amsterdam as approximately 250m thick (Figure 2.1). The Mantonga Formation, around Amsterdam, in southeastern Mpumalanga (Figure 1.1), is predominantly quartzite. A layer of basaltic lava, approximately 30m thick, is exposed in the middle of the quartzites and a thin ferruginous zone is found sporadically near the base of the formation (Hammerbeck, 1977).

The area east of Piet Retief has exposures of the Mantonga Formation, although they are highly discontinuous, as the basal contact of the Nsuze Group has been eliminated by intrusions of the Usushwana Complex (Hatfield, 1990) (Figure 2.1). The lithologies exposed in this area are fine- to course-grained quartz arenites and quartz wackes. Minor sedimentary phases include argillaceous units and reworked pyroclastics. Sedimentary structures preserved include planar bedding and poorly defined cross bedding (Hatfield, 1990).

While Armstrong *et al.* (1982) recognised the Mantonga Formation in the area north and south of the Pongola River, they also identified a volcanic wedge, which is terminated by the Usushwana Complex in the White River. Evidence for this wedge, named the Wagondrift Formation is found in the White River Valley, where the Mantonga Formation is seen to overly it. The Wagondrift Formation is predominantly basaltic lava with minor quartz wacke lenses. Armstrong *et al.* (1982) described the lavas as chemically and petrologically similar to the basaltic lavas of the Bivane Subgroup.

[1] The term volcaniclastic includes all clastic volcanic materials formed by any process and deposited by any form of transportation in any environment. These rocks may then be divided into pyroclastics (primary fragments formed by volcanic eruption processes) and epiclastics (the weathered fragments from original volcanic outcrops re-deposited to form sedimentary rocks) (Fisher and Schmincke, 1984).

The Mantonga Formation in the Pongola River area consists of a succession of immature medium to very coarse-grained quartz wackes with minor intercalated lenses of quartz and arkosic arenites and conglomerates. The succession generally represents a series of fining-upward cycles, with basal conglomerates overlying irregular erosion surfaces (Armstrong *et al.*, 1982). Sedimentary structures are poorly preserved but Watchorn and Armstrong (1980) have interpreted the depositional environment as a braided river system with flow direction generally towards the southeast, although a subordinate direction of northeast has also been recorded (Watchorn and Armstrong, 1980).

Lava flows within the Mantonga Formation are a minor component and are generally found to the south of the Bivane River. The lavas range in composition from basalt through to rhyolite. Flows are laterally limited and are generally less than 10m thick. Pyroclastic rocks are mainly air-fall tuffs, with minor agglomerates and welded ash-flow units. Bombs and lapilli are found in the clastic rock units. The nature of the volcanic rocks indicates explosivity, contemporaneously deposited with the sediments (Armstrong *et al.*, 1982).

2.3.1.2 Central Region

The Mantonga Formation is not exposed in the Black Mfolozi Inlier, however quartzite boulders are found in the vicinity of the basal sequence of the Bivane Subgroup, and therefore suggest the presence of a sedimentary unit (Preston, 1987). This is in keeping with the proposed stratigraphy of the Nsuze Group (Matthews, 1967; Watchorn and Armstrong, 1980).

In the White Mfolozi Inlier, the Mantonga Formation forms a unit of variable thickness (0–60m) but of considerable lateral extent, overlying the basement granites (Matthews, 1967) (Figure 2.1). The Mantonga Formation is composed of quartz arenites with impersistent arkosic layers found near the base. A thin conglomerate, containing well-rounded quartz pebbles, marks the basal contact of the formation (Matthews, 1967).

2.3.2 Bivane Subgroup

The Bivane Subgroup is predominantly volcanic containing both lavas and pyroclastic rocks. It is named after the Bivane River, a tributary of the Pongola River, in northern KwaZulu-Natal, which cuts through the entire section of volcanic rocks from west to east. The proportion of sedimentary rocks to volcanic rocks increases progressively from north to south. The subgroup is divided into the volcanic Nhlebela Formation at the base, the sedimentary White Mfolozi Formation, followed by the volcanic Agatha Formation at the top of the subgroup. The White Mfolozi Formation is laterally impersistent in the Northern Region, but increases in thickness towards the south, reaching its maximum thickness in the White Mfolozi Inlier of the Central Region (Hammerbeck, 1977; Hatfield, 1990; Armstrong *et al.*, 1982; Matthews, 1967).

The Bivane Subgroup has been estimated at 7500m thick in the central and southern areas of the Northern Region, thinning to approximately 3800m in the north of the Northern Region. In the Central Region, the Bivane Subgroup attains a minimum thickness (due to its limited exposure) of 2420m in the Black Mfolozi Inlier (Preston, 1987). The entire succession of the Bivane Subgroup is exposed along the White Mfolozi River and is approximately 900m thick (Cole, 1994) (Figure 2.1).

Hammerbeck (1977) did not identify any sedimentary phases within the Bivane Subgroup around Amsterdam, in the north of the Northern Region. As a result, the Bivane Subgroup in this area is not divided into the usual three formations (Figure 2.1).

2.3.3 Nhlebela Formation

The Nhlebela Formation is considered to represent the lowermost, predominantly volcanic, unit of the Bivane Subgroup. It is separated from the Agatha Formation higher up in the succession, by a hiatus in volcanic activity that resulted in the deposition of sedimentary units, namely the White Mfolozi Formation. The Nhlebela River is found in the White Mfolozi River Valley and lends its name to the formation through which it flows (SACS, 1980).

2.3.3.1 Northern Region

The Bivane Subgroup lavas exposed in the Amsterdam area do not contain any known sedimentary units. As a result, the entire volcanic succession will be discussed under the Nhlebela Formation. The dominant lava compositions are basalts and andesites. The lavas are generally amygdaloidal, although porphyritic varieties with feldspar phenocrysts

are found within the sequence (van Vuuren, 1965; Hammerbeck, 1977).

Hatfield (1990) described the lower volcanic unit of the Bivane Subgroup, in the north of the Northern Region, as felsic, comprising rhyolites and dacites. Minor air-fall and reworked tuffs, as well as associated quartz wackes are found within the formation. Rhyolites are considered to be pyroclastic in origin. Dacites are often porphyritic, containing plagioclase phenocrysts (Hatfield, 1990).

Armstrong (1980) described the volcanic rocks in the area adjacent to the Pongola River as predominantly basaltic andesite to andesite in composition, although basaltic units are also present. Thin rhyolitic and dacitic flows are found in the upper portion of the Nhlebela Formation. Porphyritic and non-porphyritic varieties of rhyolite are found within the formation as well as porphyritic dacites. The andesites and basaltic andesites are often porphyritic with plagioclase phenocrysts and most commonly amygdaloidal. They are often flow banded, and plagioclase phenocrysts may show a preferred orientation. Basalts are generally amygdaloidal, aphanitic and lack phenocrysts (Armstrong, 1980). The contacts between flows of differing and similar compositions are either sharp or show evidence of mixing and interfingering. This is evidence for contemporaneous extrusion of lavas of differing compositions (Armstrong, 1980).

2.3.3.2 Central Region

The Nhlebela Formation in the White Mfolozi Inlier conformably overlies the Mantonga Formation with a sharp contact. The formation comprises basalts, basaltic andesites and andesites. It is estimated to be 130m thick, although the intrusion of dolerite sills has resulted in a greater apparent thickness of the formation. The lavas are aphanitic and amygdaloidal with pillow-structures near the base of the formation (Matthews, 1967).

Preston (1987) identified a northern and southern facies of the Nhlebela Formation in the Black Mfolozi Inlier. The general stratigraphy of the Nhlebela Formation comprises a mafic sequence overlain by a felsic sequence, the different facies representing distal and proximal variations of the same depositional events (Preston, 1987). Polygonal fracturing of the lavas is prominent in the lower portions of the mafic sequence of the northern facies (Preston, 1987). Pillow-like or ovoid structures are found within the fractured lavas, suggested to have formed by hydrothermal activity. The upper parts of the mafic sequence are generally amygdaloidal and vesicular, with isolated patches of intense alteration (Preston, 1987). In the south, the lower units of the Nhlebela Formation do not exhibit evidence of hydrothermal alteration (i.e. fracturing and ovoid structures) although the lavas contain varying degrees of development of vesicles and amygdales. The mafic lavas of the northern and southern facies are texturally and petrographically similar and represent the same phase of mafic volcanism (Preston, 1987).

The felsic sequence of the northern and southern facies is predominately pyroclastic, representing numerous ash-flow deposits (Preston, 1987). A block and ash deposit, that overlies these ash-flow deposits, represents the terminal phase of volcanicity (Preston, 1987). Preston (1987) identified the source of the volcanic material as lying to the north of the Black Mfolozi Inlier, although evidence of eruptive centres is not visible, due to the lateral variation in the ash-flow deposits. The main body of the flows is located in the north, while the well-stratified heads of the ignimbrite flows are found in the southern area (Preston, 1987).

2.3.4 White Mfolozi Formation

The White Mfolozi Formation represents a pause in volcanic activity, allowing sedimentary processes to resume. It is best developed in the Central Region, in the White Mfolozi River valley, where is reaches a maximum thickness of 480m and derives its name (Cole, 1994) (Figure 2.1).

2.3.4.1 Northern Region

The White Mfolozi Formation is not recognised in the Nsuze Group lithogies around Amsterdam (Hammerbeck, 1977). Hatfield (1990) identified and described, in the area east of Piet Retief, a pyroclastic – volcanosedimentary unit that correlates with the White Mfolozi Formation. The basal lithology of the formation is horizontally laminated argillites of variable thickness (0 – 100m) (Hatfield, 1990). This is conformably overlain by fine-grained volcanic tuffs, with limited lenses of lapilli and agglomerate (Hatfield, 1990). The succession is dominated by air-fall tuffs, containing

interbedded mudstones and siltstones, including 1m thick ferruginous shale. Subordinate lava flows occur throughout the formation. They range in composition from basaltic to rhyolitic and are generally laterally impersistent. A prominent agglomerate layer occurs near the top of the formation. The top of the unit is marked by a medium- to fine-grained quartz arenite, 25m thick (Hatfield, 1990).

While Armstrong (1980) mapped quartzite units with minor argillaceous lenses as well as pyroclastic lenses in the middle of the Bivane Subgroup in the area adjacent to the Pongola River, he did not ascribe them to a separate unit. These sedimentary units are not laterally extensive and are generally poorly exposed, as are the pyroclastic units (Armstrong, 1980). Whether the White Mfolozi Formation does in fact exist in this area is debatable, but the sedimentary and pyroclastic lenses are found at a similar stratigraphic level to exposures in the north and south (Figure 2.1).

2.3.4.2 Central Region

The outcrop along the White Mfolozi River provides the type section for the White Mfolozi Formation. The basal unit of the formation is a quartzite, although a dolerite sill has intruded along its base. A 14m thick diamictite overlies the poorly exposed quartzite. The diamictite contains angular to subrounded clasts in a muddy matrix. Clast lithologies include quartzite, chert, shale, lava and granite. A 65m thick sequence of shale conformably overlies the diamictite. The finely laminated shale coarsens upwards into a quartzite. Sedimentary structures include trough and planar cross bedding, as well as occasional herringbone cross bedding. The quartzite grades into a series of fining upwards sequences comprising alternating quartzite-siltstone-shale, with calcareous arenites at the top of each cycle. This alternating sequence is overlain by 40m-thick sequence of well-bedded quartzite. The beds alternate between medium- to fine-grained quartzite and very coarse-grained quartzite. Layers of grit are found throughout the unit, as well as shale rip-up clasts. The quartzite is overlain by a massive diamictite containing angular to sub-rounded quartz, feldspar and volcanolithic fragments, set in a chloritic matrix (Matthews, 1967; Beukes and Lowe, 1989).

The Chobeni Member overlies the diamictite. It is a 20m thick carbonate-rich succession, consisting of quartzitic dolomite, dolomitic quartzite and calcareous siltstone and partly silicified dolomite. Stromatilites form the top 4.5m of the Chobeni Member (Beukes and Lowe, 1989). The Chobeni Member is overlain by a 75m thick coarse-grained quartzite. The unit is bedded, with well-developed trough cross-beds. Shale rip-up clasts as well as gritstone lags are found throughout the quartzite. A massive diamictite overlies the quartzite. The matrix is composed of sand to mud sized fractions of chlorite, quartz and carbonate, containing quartz, potassic feldspar and lithic clasts. The diamictite is overlain by a 27m thick coarse-grained quartzite, containing trough cross-beds and grit lags. This unit is in turn overlain by a carbonate-cemented coarse-grained arenite that grades into a fine dolomite unit. This unit is non-stromatolitic. The dolomite grades upwards into a medium- to coarse-grained calcareous quartzite. The uppermost unit of the White Mfolozi Formation is a quartzite. It is coarse-grained and poorly sorted at the base, but fines upwards into a fine-grained well sorted quartzite at the top of the succession. Trough and planar cross-beds are well developed (Matthews, 1967; Beukes and Lowe, 1989).

The Black Mfolozi Inlier also exhibits a sedimentary unit between the two volcanic sequences. The sedimentary sequence has maximum thickness of 260m. The formation can be divided into three lithofacies (Preston, 1987). The 100m thick basal facies is predominantly quartz arenites, with superimposed herringbone cross bedding. Other sedimentary structures include ripples, rip-up clasts and trough cross bedding (Preston, 1987). The middle facies is rhymically layered with alternating arenites, siltstones and mudstones. It is approximately 75m thick. The arenites contain ripples and herringbone cross bedding. The argillaceous beds are generally structureless, but fine horizontal laminae are observed at certain exposures. Soft-sediment deformation is present at the top of the sequence, where volcanic bombs have fallen onto wet sediment during deposition (Preston, 1987). The upper arenite unit is estimated at 85m thick. The quartz grains, in contrast to the basal unit, show extensive recrystallization. Herringbone cross-beds are present as well as planar cross bedding (Preston, 1987).

2.3.5 Agatha Formation

The Agatha Formation unconformably overlies the White Mfolozi Formation. It is predominantly volcanic, although the proportion of pyroclastics in the formation is greater than in the Nhlebela Formation. The Agatha Formation is named after the Agatha Tributary that flows into the White River, a tributary of the Pongola River.

2.3.5.1 Northern Region

As stated previously, the lack of sediments within the Bivane Subgroup, means that the lavas in the Amsterdam area cannot be subdivided into the Nhlebela and Agatha Formations. The Agatha Formation found in the area east of Piet Retief is predominantly composed of andesitic lava types, with minor phases of basaltic andesite and basalt. Flows are generally amygdaloidal, and are not obviously porphyritic (Hatfield, 1990).

Armstrong (1980) did not differentiate between the Nhlebela and the Agatha Formations. The characteristics of the Agatha Formation are however based on the upper volcanic units described along the Pongola River. The Agatha Formation is lithologically very similar to the lower Nhlebela lava units. It comprises andesites, basaltic andesites and basalts. An acid phase of volcanism can be identified at the base of the formation, resulting in the formation of rhyolitic and dacitic flow units. The rhyolites are characterised by devitrification and recrystallization and where flow banding is evident, are characteristically highly distorted. Acid volcanic units are often porphyritic. South of the Pongola River, the proportion of pyroclastic units increases. These pyroclastic units include ash and lapilli tuffs and agglomerates (Armstrong, 1980).

2.3.5.2 Central Region

The Agatha Formation, in the Black Mfolozi Inlier, is dominated by mafic lavas overlain by felsic volcaniclastics (Preston, 1987). The formation unconformably overlies the White Mfolozi Formation, and has a minimum thickness of 1160m. The unit is stratigraphically similar to the Nhlebela Formation of the inlier, i.e. a mafic lava sequence overlain by a felsic volcaniclastic sequence. The lower mafic lava unit overlies the White Mfolozi Formation in the west and the Nhlebela Formation in the east. The unconformable contact between the Agatha Formation and the White Mfolozi Formation shows evidence for tectonic movement along the contact (Preston, 1987).

The lower mafic unit reaches a minimum stratigraphic thickness of 480m. The contact zone displays pèpèrite structures, where fragments of angular mafic rock are set in an arenaceous matrix, formed as a result of the fluidization of underlying sediments during eruption of the mafic lavas (Preston, 1987). The mafic unit is generally aphanitic and randomly amygdaloidal. Polygonal fracturing is common towards the top of the mafic sequence. Field evidence i.e. amygdales, siliceous veining, ovoid structures and fracturing, suggests extensive post-eruption hydrothermal activity (Preston, 1987).

The mafic unit is unconformably overlain by a felsic sequence of volcaniclastics. The upper contact of the unit is not exposed and a minimum thickness of 680m has been calculated. The sequence comprises a series of ash-flow units overlain by a 90m thick block and ash deposit at the top (Preston, 1987).

The Agatha Formation truncates the upper most quartzite bed of the White Mfolozi Formation in the White Mfolozi Inlier. The lavas of the Agatha Formation are generally amygdaloidal, and exhibit pillow structures in certain flow units. The composition of the lavas is predominantly andesitic (Matthews, 1967).

2.3.6 Ozwana Subgroup

The upper Ozwana Subgroup is a highly variable volcaniclastic – sedimentary succession. It is named for the Ozwana River, a tributary of the Pongola River (SACS, 1980). The Ozwana Subgroup is varies from 6-500m thick in the area adjacent to the Pongola River (Armstrong *et al.*, 1982). This unit is highly variable (0 - 50m thick) to the east of Piet Retief, and Hatfield (1990) did not ascribe it to a separate unit from the Bivane Subgroup. The subgroup is not exposed in the area around Amsterdam. This may be due to non-deposition or pre-Mozaan erosion (Hammerbeck, 1977). The Ozwana Subgroup has not been recognised in the Central Region by Cole (1994). Sediments do however overlie the Agatha Formation lavas and underlie the Mozaan Group in the northern area of the White Mfolozi Inlier (SACS, 1980). The poor exposure of these sedimentary units may be due

to the overstepping nature of the Mozaan Group contact in the area (Matthews, 1967). The Ozwana Subgroup is divided into the lower Langfontein Formation and the upper Mkuzane Formation (Gold, 1993).

2.3.6.1 Langfontein Formation

The Langfontein Formation generally comprises sandstones, clast-supported conglomerates, interpreted as lahars, and minor siltstones (Gold, 1993). It is best exposed in a faulted block of Pongola Supergroup lithologies in the east of the Northern Region, south of the town of Pongola (Figure 1.1).

Hatfield (1990) described the upper portion of the Nsuze Group, in the area east of Piet Retief, as being mainly volcaniclastic units, i.e. reworked tuffs, quartz wackes and pyroclastic breccias. Armstrong (1980) described the uppermost lithologies of the Nsuze Group, as being dominated by fine-grained rocks, in particular, argillites (volcanogenic sediments) and air-fall tuffs, with minor arenites and acid lava units. Epiclastic volcanic breccia and accretionary lapilli lenses are also found within the volcanogenic sediments (Armstrong, 1980).

In the Black Mfolozi Inlier in the Central Region, the Ozwana Subgroup is not known, as the top of the Nsuze as well as the Mozaan Group, is not exposed (Preston, 1987). The Nsuze Group exposures of the Black Mfolozi Inlier are unconformably overlain by Phanerozoic cover sequences. The Langfontein Formation in the White Mfolozi Inlier is only exposed in the north of the area due to the unconformable overstepping Mozaan Group contact. It is a sequence of ferruginous shales and minor quartzites estimated as approximately 530m thick (SACS, 1980).

2.3.6.2 Mkuzane Formation

The Mkuzane Formation comprises laterally extensive banded siltstone. Alternating light and dark layering form the 1-5cm thick laminations (Gold, 1993). The formation is not preserved in the Central Region.

The presence of the Mkuzane Formation in the area adjacent to the Pongola River is 40m thick (Gold, 1993). Gold (1993) described the upper unit of the Nsuze Group as banded siltstone. Armstrong (1980) identified the first unit of the Mozaan Group as being argillaceous. This could possibly be the Mkuzane Formation, and not the basal unit of the Mozaan Group as proposed by Armstrong (1980). This is supported by the fact that the Mozaan – Nsuze contact is described as unconformable to the north and south of the Pongola River area, yet is described by Armstrong (1980) as being gradational (Beukes and Cairncross, 1991).

2.3.7 Southern Region

The Nkandla Inlier is made up entirely of units correlated with the Nsuze Group and is divided into eight official formations (SACS, 1980).

a. The basal unit, the *Hlathini Formation*, is a 450m thick sequence of alternating quartzites and shales, unconformably overlying granite-greenstone terrane (Linström and Matthews, 1990a).
b. The Hlathini Formation is conformably overlain by the 1100m thick *Mabaleni Formation*. This formation comprises mature sandstones, overlain by shales, containing a banded iron unit (Linström and Matthews, 1990b).
c. The *Mome Formation*, which conformably overlies the Mabaleni Formation, represents a thick orthoquartzite, overlain by shale and banded iron-formation. The shales are associated with subordinate amygdaloidal basalts to andesites (Linström and Matthews, 1990c).
d. The *Dlabe Formation* consists almost entirely of quartzites, although it does contain amygdaloidal basalt near its upper contact. It conformably overlies the underlying Mome Formation (Linström and Matthews, 1990c).
e. The *Msukane Formation* is 1130m of phyllites with intercalated sheared amygdaloidal lavas. It overlies the Dlabe Formation (SACS, 1980).

A thrust fault separates the lower five formations in the south from the upper four formations to the north. While a lower unit than the Mdlelanga exists to the north of the thrust front, it cannot be separated into the five formations. It is marked on the 1:250 000 geological sheet of the area (Dundee 2830) as undifferentiated Nsuze Group (Linström, 1987).

f. The *Mdlelanga Formation* is predominantly quartz wackes and quartz

arenites and is approximately 1200m thick. Volcaniclastic and epiclastic sediments form wedges within the Mdlelanga Formation (Groenewald, 1984).

g. The *Qudeni Formation* is the only formation dominated by volcanics, and is 580m thick. The lavas range from basaltic andesites to dacites (Groenewald, 1984).

h. The *Vutshini Formation* has been correlated with the Langefontein Formation of the Northern and Central Regions. It is a 1000m combination of sandstones and shales (Groenewald, 1984).

i. The *Mankane Formation* represents the uppermost unit of Nsuze Group deposition. It is a thin unit approximately 60m, comprising andesitic lavas (Groenewald, 1984).

2.3.8 Depositional Environment of the Nsuze Group

The Mantonga Formation in the Northern Region is interpreted as a distal braided stream environment. Rapid lateral migration of channels resulted in the deposition of tabular sandstones, with limited mudstone layers (Watchorn and Armstrong, 1980; Hatfield, 1990). According to Matthews (1967) the Mantonga Formation exposed in the Central Region, represents a near-littoral environment, with deposition occurring in a transgressive sea. The shoreline must therefore have been situated between the two regions.

The lack of feldspathic material in the quartz wackes indicates that the detritus was derived from the weathering of the palaeosaprolite. The source rocks for the subordinate arkosic arenites was unweathered granitic basement (Watchorn and Armstrong, 1980; Matthews, 1967). The palaeocurrent directions vary from the northeast to the southeast (Watchorn and Armstrong, 1980). The higher proportion of conglomerates at the base of the Mantonga Formation represents a gradual degradation of the source area with time (Armstrong *et al.*, 1982). The extrusion of lavas and pyroclastics was contemporaneous with sedimentation in a continental subaerial environment. The source of the volcanism was to the north of the region. Down warping of the granitic crust with simultaneous uplift of adjacent areas, resulted in the initiation of Nsuze sedimentation. Degradation of the provenance area resulted in the termination of sedimentary processes, coupled with the increasing volcanic activity (Armstrong, 1980).

The Bivane Subgroup was formed by a massive eruptive phase. The lavas in the Northern Region were erupted subaerially, as there is little evidence to suggest a submarine environment i.e. pillow lavas (Armstrong, 1980). The Nhlebela Formation in the Central Region does not offer evidence for submarine eruption, although the high level of hydrothermal alteration supports the presence of secondary aqueous interaction (Preston, 1987; Matthews, 1967). In contrast, the White Mfolozi Formation in the Central Region has been interpreted by von Brunn (1974), von Brunn and Mason (1977), Preston (1987) and Beukes and Lowe (1989) to represent a prograding tidal environment. The lack of development of the White Mfolozi Formation in the Northern Region indicates that the shoreline transgressed between the two regions. This is supported by the development of the White Mfolozi Formation east of Piet Retief considered by Hatfield (1990), to have formed as a result of fluvial processes. The nature of the thin fluvial sedimentary units along the Pongola River, suggest contemporaneous eruption and sedimentation. The lavas associated with the sediments are acid in composition suggesting they are proximal to the volcanic source as due to their high viscosity, acid lavas tend to build up close to the source of eruption (Armstrong, 1980; Hall, 1987). This would explain the lack of lavas and presence of pyroclastic units in other areas of the depository. The shoreline regressed southwards in order for eruption of the Agatha Formation to be dominantly subaerial in the Northern and Central Regions (Hatfield, 1990; Preston, 1987; Armstrong, 1980; Matthews, 1967).

The Ozwana Subgroup marks the onset of sedimentation. The lithologies of the Central Region were deposited in a predominantly shallow-water marine shelf environment (Preston, 1987). The Northern Region marks the shoreline as both fluvial and marine deposits are evident in the Ozwana lithologies (Armstrong, 1980).

In the Southern Region, the lithologies are representative of tidal to distal shelf deposition, indicated by the sedimentary rock types.

Palaeocurrent indicators show south – southeast dipping palaeoslopes, indicating a northeast – southwest trending coastline. Sediments are more mature and possibly represent a distal phase of deposition. This may also be true due to a reduction in the proportion of volcanic products (Groenewald, 1984).

2.4 NSUZE – MOZAAN CONTACT

The contact between the Nsuze and Mozaan Groups is gradational in the Northern Region and was regarded by Armstrong *et al.* (1982) and Hatfield (1990) as representing the stratigraphic level above which volcanic rocks (lavas, pyroclastics or volcanogenic sediments) are absent. Beukes and Cairncross (1991) suggested that the Sinqeni Formation of the Mozaan Group does not conformably overlie the argillaceous units of the Mkuzane Formation. Instead, the contact is unconformable, with the Mozaan Group overstepping the Nsuze Group in both a northerly and southerly direction (Beukes and Cairncross, 1991).

In the Central Region, the Nsuze – Mozaan contact, is an angular unconformity. The basal Sinqeni Formation of the Mozaan Group oversteps the upper units of the Nsuze Group. This overstepping has eliminated approximately 1200m of Nsuze Group stratigraphy of the Ozwana Subgroup (Matthews, 1967). This is evident in the White Mfolozi Inlier, where the sandstones of the Mozaan Group, unconformably overlie the lavas of the Agatha Formation. Further north in the White Mfolozi Inlier, in the Nsileni River, the unconformity overlies ferruginous shales of the Nsuze Group, possibly belonging to the Langfontein Formation (SACS, 1980). This would then provide evidence for the Ozwana Subgroup in the Central Region, being overstepped by the Mozaan Group sediments.

2.5 MOZAAN GROUP

The Mozaan Group is preserved in the Northern and Central Regions, but is completely absent from the Southern Region i.e. the Nkandla Inlier. It is named after the Mozana River, a tributary of the Pongola River in the Northern Region (SACS, 1980). Walraven and Pape (1994) dated the ferruginous shale of the Sinqeni Formation in the Amsterdam area. The resultant age, using Pb-Pb whole rock analysis, was 2860±26Ma. Recent research by Griffin (2002) reported a U-Pb zircon age of 2954±9Ma for an andesite lava flow found within the Tobolsk Member.

The Mozaan Group is dominantly sedimentary, with minor volcaniclastic lenses near the base of the succession and in the uppermost lithogies. In the Northern Region, where the section is best developed, Beukes and Cairncross (1991) have identified nine formations. The stratigraphy of the Mozaan Group is summarised in Table 2.1.

The Sinqeni Formation is the basal formation of the Mozaan Group. It is approximately 650m thick along the Pongola River, in the Northern Region (Gold, 1993). The Sinqeni Formation is named after the Sinqeni Mountain where it is best exposed (SACS, 1980). The formation is divided into two quartzite units, the Dipka and Kwaaiman Members, separated by a shale unit, the Vlakhoek Member (Beukes and Cairncross, 1991) (Table 2.1).

In the Central Region the Sinqeni Formation outcrops in the White Mfolozi Inlier only. Due to the overstepping nature of the Mozaan –Nsuze contact, the basal units form a wedge structure, increasing in thickness towards the southeast. The basal units of the formation therefore pinch out against the unconformity. The gold-bearing Denny Dalton conglomerates are found in the White Mfolozi Inlier and are equivalent of the Dipka Member (Matthews, 1967) (Table 2.1).

The Dwaalhoek Subgroup conformably overlies the Sinqeni Formation with a sharp contact. It is named after the Dwaalhoek Farm situated approximately 15km south of the Pongola River. It reaches a maximum thickness of 2020m in the Northern Region, along the Pongola River, but thins to the north near Amsterdam and to the south, along the White Mfolozi River. The subgroup is divided into the lower argillaceous Ntombe Formation and the upper quartzitic Thalu Formation (Beukes and Cairncross, 1991) (Table 2.1). The Ntombe Formation represents the uppermost unit of the Pongola Supergroup exposed in the Central Region (Beukes and Cairncross, 1991). It is unknown as to the true extent of the Mozaan Group sedimentary succession that lies beneath the Phanerozoic cover rocks in the Central Region.

The Hlashana Formation is 125m thick in the area south of the Pongola River (Table 2.1). The

Table 2.1 Lithological Subdivision of the Mozaan Group, Pongola Supergroup (Matthews, 1967; Beukes and Cairncross, 1991; Gold, 1993)

Maximum Thickness	Subgroup	Formation	Northern Region	Central Region
540m	Nkoneni	Ntanyana	140m thick Shale at base overlain by med- to coarse-grained quartzites Uppermost layer is quartzite Youngest layer exposed of Mozaan Group	Not exposed
		Gabela	150m thick Volcaniclastic succession Base marked by agglomerate grading into massive tuffaceous unit Minor amygdaloidal lava flows in tuffs Andesitic to dacitic compositions Minor layers of shale and quartzite	Not exposed
		Bongaspoort	250m thick Coarse-grained, moderately sorted quartzites Argillaceous units at base but lessen towards top of unit	Not exposed
1530m	Odwaleni	Khiphunyawa	500m thick Ferruginous shale and quartzite layers Tobolsk Member - 40-50m thick volcanic unit Amygdaloidal lavas with tuffs beds at top and bottom of member Bombs and pillows preserved in lower part of upper tuff layer	Not exposed
		Delfkom	1030m thick Lower lithologies – two upward coarsening shale-quartzite sequences Upper lithologies – quartzites Klipwal and Mpatheni Members – diamictites formed by glaciers (Young *et al.*, 1998)	Not exposed
125m		Hlashana	Fine- to medium-grained quartzites, with pebble lags & minor siltstone lenses	Not exposed
2020m	Dwaalhoek	Thalu	720m thick Upward coarsening successions of shale – shale/siltstone and siltstone capped by quartzite Quartzite marked by pebble lag at basal contact with underlying siltstone Vary from 10m to 100m thick Banded iron formations mark base of two successions Scots Hill Member - lower iron formation	Not exposed
		Ntombe	1300m thick Argillaceous unit with increasing quartzite layers towards the top Coarsening upward cycles of shale and siltstone Cycles capped by orthoquartzite 3m iron formation in upper part of formation	320m thick Shales with thin quartzite lenses Uppermost layer of Mozaan Group exposed in Central Region
650m		Sinqeni	Kwaaiman Member - 170m thick Medium-grained orthoquartzite with minor gritty layers Small pebble conglomerate at top of unit	Fine-to medium-grained quartzite Minor gritty layers Thin argillaceous layers
			Vlakhoek Member - 80m thick Carbonaceous laminated shale 5m banded iron formation Small lenses of banded iron throughout unit	Ferruginous shales 5m magnetite-jasper banded iron formation
			Dipka Member - 400m thick Lower quartzites med to coarse-grained, grading into gritty quartzites Small pebble layers at base of fining up cycles Capped by grit layer	Mature, well-bedded quartzites Gold-bearing Denny Dalton conglomerates

hill Kwa-Hlashana is composed of quartzite, and hence the name (SACS, 1980).

The Odwaleni Subgroup is approximately 1530m thick. It is only exposed in the Northern Region in the areas to the north and south of the Pongola River. It rests with a sharp contact on the underlying Hlashana Formation. It is divided into the Delfkom Formation, a shale-quartzite succession, and Khiphunyawa Formation, a volcano-sedimentary sequence (Beukes and Cairncross, 1991) (Table 2.1).

The 540m-thick Nkoneni Subgroup overlies the Khiphunyawa Formation with a very sharp contact. The subgroup is named after Nkoneni Ridge that overlooks the farm Mozaan. The Subgroup represents a sequence of quartzites (Bongaspoort Formation), volcanic rocks (Gabela Formation) and feldspathic quartzites (Ntanyana Formation) (Beukes and Cairncross, 1991) (Table 2.1). The Ntanyana Formation represents the top-most outcrop of the Pongola Supergroup preserved on the Kaapvaal Craton (Beukes and Cairncross, 1991).

2.5.1 Depositional Environment of the Mozaan Group

The depositional evolution of the Mozaan sedimentary sequence has been investigated by Beukes and Cairncross (1991), Watchorn (1980) and Gold (1993). The 4800m thick Mozaan Group is estimated to have accumulated over a period of 70Ma, at a sedimentation rate of 0.07m/1000years (Beukes and Cairncross, 1991).

Armstrong (1980) considered the Mozaan basin to have formed in response to the mass outpourings of the Nsuze lavas, which resulted in subsidence of the Kaapvaal crust. This subsidence resulted in the formation of a shallow epeiric sea (Gold, 1993). Beukes and Cairncross (1991) identified the mature and sheetlike character of the lithogies of the Mozaan Group as been indicative of a passive margin or continental seaway depositional setting.

Alternating sequences of arenaceous and argillaceous sediments represent several cycles of marine transgression and regression. Watchorn (1980) identified three interacting sedimentary environments – braided alluvial plain, offshore shelf and tidalites. Beukes and Cairncross (1991) only identified two dominant environments i.e. shallow marine shelf and fluvial braidplain. Shoreline deposits only account for a minor component of the Mozaan Group sediments. According to Beukes and Cairncross (1991), a tide-dominated environment can only be interpreted for one lithofacies with any certainty. This lithofacies is the lowermost zone of the Kwaaiman Member of the Sinqeni Formation. This lithofacies relates to intertidal sequence described in the Sinqeni Formation of the White Mfolozi Inlier, by von Brunn and Mason (1977).

The braided fluvial systems show complex palaeocurrent directions. Generally, the direction of palaeoslope was towards the south in the Sinqeni and Bongaspoort Formations and towards the southeast in the Hlashana Formation and the lower half of the Delfkom Formation. The upper half of the Delkom Formation suggests a flow direction towards the northeast (Beukes and Cairncross, 1991).

The lack of true shoreline deposits, i.e. interaction between fluvial and marine environments, is best explained by the nature of the fluvial system that would have developed in the Archaean. The lack of vegetation would have resulted in a shallow widespread braided river system, that would have had rapid and continuous shifting river mouths, which would not allow the development of deltaic wedges (Beukes and Cairncross, 1991).

The provenance for the Mozaan Group is considered by Beukes and Cairncross (1991) to be first-cycle sediments from the granite basement terrain. A unique combination of tropical climate, extremely low relief and slow sedimentation rates is required in order for this to occur. The Mozaan Group does not, however, fulfil the last two criteria, as grain sorting is poor and grain size generally coarse. The environment of erosion and subsequent deposition must have been warm and humid, with acidic surface water related to the CO_2- rich Archaean atmosphere. This condition would have resulted in extremely effective chemical weathering of the granitoid basement complex (Beukes and Cairncross, 1991).

The palaeomagnetic pole determined for the Klipwal Member, Delfkom Formation, Odwaleni Subgroup, is distinct from other poles determined

for the meso-Archaean. This finding supports the concept that cratonic movement was active during the Archaean (Nhleko *et al.*, 2002). The palaeolatitude of the southeastern portion of the Kaapvaal Craton, during deposition of the Mozaan Group is approximately 48°, indicating that normal glaciation conditions were probable (Nhleko *et al.*, 2002).

2.6 TECTONIC SETTING OF THE PONGOLA SUPERGROUP

While it is widely considered that volcanism occurred in a dominantly continental environment, the true nature of the tectonic setting is still under debate. Nsuze volcanism is thought by Hegner *et al.* (1984), Burke *et al.* (1985), Crow *et al.* (1989) and Matthews (1990) to be due to continental extension, resulting in the formation of a rift basin. Alternatively, Armstrong (1980) and Armstrong *et al.* (1986) considered the Nsuze Group a result of non-orogenic continental magmatism due to plumes beneath the Kaapvaal Craton. Tankard *et al.* (1982) suggested a possible volcanic arc setting due to the occurrence of andesites and calc-alkaline REE patterns in the Nsuze volcanic rocks. Griffin (2002) recently proposed a tectonic setting of a convergent continental margin.

Armstrong *et al.* (1986) considered that the low proportion of pyroclastic material to lavas (<5%) is indicative of divergent plate boundaries and within plate tectonic settings. The dominance of intermediate to acid volcanic rocks excludes continental flood basaltic volcanism as a possible tectonic setting. While a certain degree of extension must have taken place to enable parental magma rise, the lack of alkaline magmatism also precludes continental rifting from the list of tectonic settings. This evidence put forward by Armstrong *et al.* (1986) suggested that the Nsuze Group does not have an exact modern day analogy.

Hegner *et al.* (1984) on the basis of structural, lithological and chemical evidence suggested rifting as the origin of the Pongola Supergroup intracratonic depositional basin. These authors also suggested the development of extraordinarily high crust formation of the Archaean Kaapvaal Craton was due to extensive underplating of primary magmas, rather than through marginal horizontal accretion due to subduction (Hegner *et al.*, 1984).

Burke *et al.* (1985) suggested a continental rift setting based on rapid lateral variations in thickness, the character of the sediments, the volcanic composition range, coarse basement-derived conglomerates and thick sequences of shallow water sedimentary facies. Crow *et al.* (1989) considered that the structural and sedimentological data do not support any single tectonic environment for the Nsuze group, but tended to favour a continental rift setting. The enrichment in LILE and relative depletion of Nb-Ta supports a subduction zone component. Crow *et al.* (1989) therefore considered the Nsuze Group to have been erupted in subduction-related rift. Similar subduction zone signatures have also been recorded in lavas erupted in intracratonic rift settings. This is generally due to continental contamination or derivation of the melt from an enriched LILE parental source (Crow *et al.*, 1989).

Matthews (1990) considered a continental rift setting based on a north south trending asymmetric outcrop pattern. The overlapping of the Mozaan Group onto the Nsuze Group and the isopach data interpreted by Matthews (1990) suggested that the Nsuze volcanic rocks were erupted into a major half-graben syndepositional rift basin, while the Mozaan sedimentary rocks represent the post-rift thermal subsidence event. These two features together represent an aulacogen structure and is the setting proposed for the Northern and Central Regions (Matthews, 1990). Matthews (1990) discussed the Southern Region as having been formed in a slowly subsiding epicratonic basin. The dominantly sedimentary succession was deposited along an extensive continental margin. Subsequent uplift and erosion followed as well as listric faulting which down faulted the Nsuze Group into northward dipping half-graben structures. These were truncated by erosion prior to the regional subsidence that resulted in the deposition of the Mozaan Group sedimentary sequence. This accounts for the unconformity at the Nsuze – Mozaan boundary (Matthews, 1990).

Griffin (2002) suggested that the tectonic setting of the Pongola Supergroup was a convergent margin represented as a continental arc. This conclusion is based on the full spectrum of volcanic rocks present in the Pongola

Supergroup and the arc-like geochemical characteristics of the suite of volcanic rocks.

2.7 METAMORPHISM

Regional low-grade metamorphism has affected the Nsuze and Mozaan Group lithologies. Metamorphism is lower greenschist facies except in contact metamorphic aureoles of mafic - ultramafic and granitic intrusives (Hammerbeck, 1977). The greenschist facies assemblage (tremolite-actinolite, albite, chlorite, zoisite-clinozoisite) for mafic to intermediate volcanics are consistent with the low temperature facies of low-grade metamorphism (Armstrong, 1980). Contact metamorphism in proximity to the post-Pongola granitoids has resulted in the local transition from actinolite to hornblende, as well as the presence of andalusite (Hatfield, 1990).

Hydrothermal and deuteric alteration formed contemporaneously with eruption and deposition of the volcanic sequences (Preston, 1987). This alteration of the volcanic pile has resulted in varying stages of chloritization, epidotization, silicification and calcitization (Armstrong, 1980).

Dynamic metamorphism is related to shear zones, resulting in the milling of the matrix around porphyroclasts, resulting in a preferred orientation of all minerals (Armstrong, 1980).

Due to various alteration and metamorphic processes that have affected the Pongola Supergroup lithologies, certain elements may have been enriched or depleted over the past 3Ga. The recrystallization of plagioclase to form albite released Ca (Armstrong, 1980). This resulted in the formation of Ca-rich minerals like epidote and calcite. Mafic minerals have been altered to chlorite and saussuritised aggregates. Quartz overgrowths show evidence for silicification. While element exchange has definitely taken place, it is questionable whether concentrations of some elements have been introduced and others released from the bulk rock geochemistry. Condie *et al.* (1977), based on work on Barberton tholeiites, identified that Sr, Fe^{3+} and Ca are enriched and H_2O, Na, Mg, Fe^{2+}, K, Rb, Ba, Si, Ti, P, Ni, Zn, Cu and Zr are depleted during epidotization. CO_2, H_2O, Fe^{2+}, Ti, Zn, Y, Nb and light REE elements are enriched and Na, Sr, Cr, Ba, Fe^{3+}, Ca, and Mn are depleted during calcitization –chloritization. Condie *et al.* (1977) also identified that Cr and REE are least affected by epidotization and Ni, Zr and the heavy REE are least affected by calcitization – chloritization. It was further stated that up to 10% calcitization and 60% epidotization of tholeiitic rocks does not affect the interpretation of trace element models for magma generation. Using the work of Condie *et al.* (1977), Armstrong (1980) deemed the geochemistry of the Nsuze Group volcanic rocks adequate for the establishment of petrogenetic models. He identified Na and Sr as the elements most susceptible to loss or gain in the bulk rock geochemistry. Armstrong (1980) did, however, also state that metasomatism did not play a major role in the redistribution of alkalis, due to the relative immobility of K.

2.8 DEFORMATION

The Northern Region has been affected by numerous deformation events generally oriented north and northwest. Two major perisynclinal folds, Piensrand and Tobolsk, separated by the Bethu anticlinal saddle define the current outcrop pattern (Gold and von Veh, 1995).

Three Late Archaean deformational events have been identified. The D1 event involves compression resulting in north-northwest directed thrusting. Evidence of this event is the Izermijn and the Klipwal shear zones. Open east northeast trending folding developed contemporaneously with thrusting (Gold and von Veh, 1995).

Southeastern-directed extension is indicative of the D2 event. This extension is related to the extrusion of the upper Mozaan volcanics of the Nkoneni Subgroup and the emplacement of the Usushwana Complex. The northwest striking Mahamba shear zone possibly defined the eastern boundary of the half-graben during the eruption of the Nsuze lavas as discussed by Matthews (1990) and (Gold and von Veh, 1995). The Mahamba shear zone reactivated during the D2 extensional event, resulting in thicker quartzites to the east of the shear zone (Gold and von Veh, 1995).

The D3 event involved compression from the northeast leading to the refolding of D1 folds into a dome-and-basin interference pattern. The development of strikeslip shear zones resulted in the displacement of the limbs of the Betha anticline. The D3 event appears to be the only

event to have deformed the post-Pongola granitoids (Gold and von Veh, 1995).

The focus area of the White River Section is exposed as easterly to east southeasterly dipping strata which has for the large part been unaffected by extensive faulting. Broad stratigraphic relationships can therefore be determined without extensive structural interpretation.

The Central Region is characterised by repetitive blocks of northeast dipping Pongola Supergroup strata overlying Archaean granitoid basement. Matthews (1990) identified extensive block-faulting as the cause for the repetitive nature of the Central Regions inliers. The overstepping nature of the Mozaan – Nsuze contact is inferred by Matthews (1990) to be due to the uplift, tilting and erosion of the Nsuze Group prior to the southward expansion of the Mozaan basin. The Nhlebela and Agatha Formation have for the large part been preserved as complete blocks, while the middle White Mfolozi Formation is known to have duplication of units due to faulting. The uppermost lava flows of the Agatha Formation that outcrop within the White Mfolozi River are not preserved due to the overstepping nature of the Nsuze – Mozaan contact.

The Nsuze Group in the Southern Region has been deformed into tight to isoclinal folding in an east – west orientation (Groenewald, 1984). The cause of this deformation is unknown although it is unrelated to the 1000Ma Natal Thrust Front. The unconformity between the Ntingwe Group and the Nsuze Group shows that the Nsuze strata were deformed prior to Ntingwe conglomerate deposition. The Ntingwe Group was subsequently overridden from the south by the 1000Ma Natal Thrust Front as slices of Ntingwe strata are found, undeformed, at the forefront of the thrust zone (Matthews, 1959; Matthews, 1990).

2.9 POST – PONGOLA INTRUSIVES

2.9.1 Usushwana Complex

The Usushwana Complex is essentially made up of two dyke-like intrusions that strike northwest, one cutting through Amsterdam and the other lies 45km east of Amsterdam in southwestern Swaziland. They are linked by a sheet of gabbro and granophyre, which intruded along the base of the Nsuze Group (Armstrong, 1980) (Figure 1.1).

Dating on the Usushwana has generally been done on samples taken from the oldest group of pyroxenites in the suite, so as to better constrain the Pongola Supergroup. Hegner *et al.* (1984) used Sm-Nd whole rock analyses to provide a series of ages of the pyroxenites of the Thole Suite. These dates are 2873±31Ma, 2826±98Ma and 3086±95Ma (Hegner *et al.*, 1984). Hegner *et al.* (1984) considered this dating possibly problematic because whole rock mineral determinations reflect partial disturbance of the mineral isotopic systems, as well as the influence of mixing on the isotopic systematics of the pyroxenites. Walraven and Pape (1994) dated a magnetitite of the Piet Retief Suite, which provided an age of 2671±18Ma (Pb-Pb whole rock).

There were three phases of intrusion as identified by Hammerbeck (1982). The first phase resulted in the emplacement of ultramafic to mafic sills at various levels of the Pongola stratigraphy, but predominantly in the Mozaan Group. They are called the Thole ultramafics by SACS (1980). The second phase was an extrusive event known as the Amsterdam Formation, containing a lower dacitic formation and an upper rhyolitic formation (Hammerbeck, 1982; SACS, 1980). The Piet Retief Suite and the Hleho Suite conclude the Usushwana Complex. The Piet Retief suite comprises gabbros and quartz gabbros, while the younger acid phase, the Hleho Suite, is composed of granophyric granite, microgranite and granodiorite.

2.9.2 Sicunusa Granite Pluton

Minor porphyritic dykes have intruded the far northern area of the Northern Region. A plagioclase, quartz and microcline matrix surrounds the large microcline phenocrysts. Hatfield (1990) associated these dykes with the Sicunusa Granite, which extends into southwestern Swaziland. The Sicunusa Granite intrudes the Usushwana Complex (Hammerbeck, 1977). Griffin (2002) reported an age of 2717±11Ma (U-Pb Zircon) for the Sicunusa pluton.

2.9.3 Post-Pongola Granitoids

Post-Pongola granitoids outcrop in southern Swaziland, southeastern Mpumalanga and the far northern reaches of KwaZulu-Natal. These

intrusions are generally potassic granites. They take the form of gneissic domes, tabular bodies and discordant plutons. The Nhlangano gneiss forms northwest trending elongated domes, separated by steeply dipping Mozaan Group sediments. The Nhlangano Gneiss has an age of 2961±14Ma (U-Pb zircon; Griffin, 2002) and is older than the other post-Pongola granitoids. The Hluti Gneiss is found in southeastern Swaziland. It trends in a northeasterly direction is well foliated and contains a large proportion of meta-volcanic xenoliths (Hunter and Wilson, 1988).

The Hlatikulu granite intrudes into the Nhlangano gneiss domes. The Hlatikulu granite has an age of 2742±22Ma (U-Pb zircon; Griffin, 2002). The Mozaan Group forms the roof of the intrusion. The discordant granite plutons are the Kwetta granodiorite (2720±10Ma U-Pb zircon; Griffin, 2002), the Mhlosheni pluton (2837±6Ma U-Pb zircon; Griffin, 2002) and the Mooihoek granite (Hunter, 1974; Hunter and Wilson, 1988). The Mooihoek granite intruded into the Kwetta granite (Hunter, 1974).

2.9.4 Other Pre-Karoo Intrusives

A number of mafic and ultramafic sills and dykes are found throughout the north of the Northern Region. The ultramafic intrusives range in composition from harzburgite to pyroxenite (Hatfield, 1990). The age relationships of these intrusions have not been determined (Hatfield, 1990).

2.10 PHANEROZOIC LITHOLOGIES

2.10.1 Natal Group

The Natal Group sediments are exposed in the Southern Region. They were deposited on a highly variable palaeotopographical surface formed by the extensive erosion of the Nsuze Group. The Natal Group consists of conglomerates, feldspathic arenites and siltstones and shales. The Natal Group is thought to have developed in an extensive braided river system (Linström, 1987).

2.10.2 Karoo Supergroup

The most recent cover sequence of the Pongola Supergroup is the Karoo Supergroup. The various Karoo lithologies form most of the high lying areas of southeastern Mpumalanga and northern KwaZulu-Natal.

2.10.2.1 Dwyka Formation

The Dwyka Group is composed of sediments derived from glacial activity on Gondwana 270Ma ago (evidence provided by numerous glacial pavements in the Northern and Central Regions). The formation is found covering the Pongola Supergroup throughout the Northern, Central and Southern Regions. The Dwyka sediments were deposited on a rugged palaeotopography scoured out by moving glaciers. The formation consists predominantly of characteristic tillite, as well as diamictite (of undetermined origin), siltstones and sandstones (Armstrong, 1980; Groenewald, 1984).

2.10.2.2 Ecca Group

The Ecca Group sediments are exposed only in the topographically highest areas of the Northern, and Southern Region, and unconformably overly the Dwyka Formation. The shales exposed represent the Pietermaritzburg Formation, the lowest unit of the Ecca Group. The shales are considered to have formed from suspension deposits in a large relatively shallow body of water (Groenewald, 1984).

2.10.2.3 Karoo Dolerites

The Karoo Dolerites, associated with the Drakensberg Group lavas, are found throughout the Northern, Central and Southern Regions. They intrude all lithologies and range in size from less than 1m wide to 50m wide, and can be up to several kilometres in length (Armstrong, 1980; Linström, 1987).

2.11 CONCLUSION

Due to the extensive and varied localities of the Nsuze Group outcrop, the author has selected two main focus areas where almost complete and continuous volcanic sequences have been preserved. These two areas are the outcrops north of the Pongola River, along the White River, in the Northern Region and in the White Mfolozi River, in the Central Region. Extensive use has therefore been made of existing literature discussed in this chapter to gain overall impressions of the Nsuze Group's geological evolution.

CHAPTER 3
PHYSICAL VOLCANOLOGY

3.1 INTRODUCTION

This chapter focuses on the interpretation of field observations using a volcanological facies approach. This allows for an understanding of the processes associated with depositional setting, eruption mechanisms, transport mechanisms, and the resultant deposits of the volcanic stages of the Nsuze Group, in particular the Bivane Subgroup. The aim was not to investigate every outcrop area of the Nsuze Group, but rather to record detailed observations to provide a framework for the geochemical sampling. The bias was towards pristine outcrops and well exposed areas. Correlation of flow units across the rugged topography is difficult but a general idea of the changes in volcanicity can be interpreted from the compositions and characteristics of the outcrops.

The study of the physical volcanology of both ancient and modern volcano-sedimentary provinces includes factors controlling eruption mechanisms, and processes governing subaerial and subaqueous transportation and deposition of lavas, pyroclastics and volcaniclastics (Mueller *et al.*, 2000). While active volcanic environments are well documented, ancient sequences require more insight and investigation. As a result, ancient volcanic sequences are more often studied from tectonic and geodynamic perspectives, rather than from the aspect of volcanological facies (Cas and Wright, 1987). The majority of subaerially deposited volcanic and volcaniclastic rocks of the Archaean and Proterozoic are poorly preserved due to their susceptibility to erosive processes and deformation events. The Kaapvaal Craton is considered to be unique in this regard, as the volcano-sedimentary successions of the Pongola Supergroup, Witwatersrand Supergroup, Ventersdorp Supergroup and the Transvaal Supergroup are extensively developed and well preserved (Mueller *et al.*, 2000).

This study focuses on two geographical areas of Nsuze Group outcrop. The most extensive outcrop is found in the Northern Region, and is well preserved along the White River, a tributary of the Pongola River (Appendix 1) and is termed the White River Section. This study serves to build on the previous work in this area of Armstrong (1980) by applying a facies approach combined with more intensive geochemical sampling. The second geographical focus area is found in the Central Region, in the White Mfolozi Inlier (Figure 1.1). The volcanic rocks of the Nsuze Group are well preserved along the White Mfolozi River and have not previously been described in detail. References in this chapter, to the compositional type of volcanic rock identified in the various outcrops, are based on petrographic and geochemical criteria and are discussed in Chapter 4 Petrology and Chapter 5 Geochemistry respectively.

3.2 WAGONDRIFT FORMATION - WHITE RIVER SECTION

The basal unit of the Nsuze Group is largely sedimentary, with minor volcanic and volcaniclastic phases. Armstrong *et al.* (1982) estimated the Mantonga Formation to be 800m thick. North of the White River, in the northwest of the White River Section, a lava wedge of approximately 300m thick lies unconformably on the granite-gneiss basement (Armstrong, 1980) (Appendix 1). The exact relationship between the lava wedge, termed the Wagondrift Formation by Armstrong *et al.* (1982), and the Mantonga Formation is unclear, although Armstrong (1980) suggested based on field evidence that it preceded the Mantonga sedimentary succession. Compositionally these lavas are basalts to andesites. The lavas are massive with vesicular flow tops, typical of basaltic lava flows (Cas and Wright, 1987) (Figure 3.1). The outcrop section has been affected by diorite / granodiorite intrusions. The relationships between the lava flows have been obscured by the granodiorite intrusions, identified by Watchorn and Armstrong (1980), as belonging to the Acid Suite of the Usushwana Complex. These intrusions appear to be have been emplaced by stoping, as they contain a large number of variable sizes of basaltic lava xenoliths. Stoping is an intrusion mechanism, whereby magma forces its way along existing joints and other structural weaknesses (i.e. flow surfaces) in the country rock. This causes blocks of country rock to become detached and sink into the magma (Hall, 1987). The outcrops of lavas

sampled in the White River may therefore represent large xenoliths in the intrusion, and not the original outcrop (Appendix 1). This is supported by mapping carried out by Armstrong (1980), as he did not identify the Wagondrift Formation outcrop in the White River, but rather recognised the presence of outcrops of approximately 0.06km^2 to 0.16km^2 (Armstrong, 1980) within the diorite. The stratigraphic association of these blocks to the main Wagondrift Formation outcrop to the northwest, however, suggests that they have not been displaced far from their original position (Appendix 1).

3.3 MANTONGA FORMATION / BIVANE SUBGROUP CONTACT – WHITE RIVER SECTION

Two acid volcanic units, interbedded with quartzite layers, are exposed in the White River on the northwestern boundary of the Mkhunyane Eco-reserve, represented by CG01/122 on Appendix 1 (Figure 3.2). These volcanic units are generally massive with scattered patches of vesicles[2]. The massive areas are commonly columnar jointed (Figure 3.3). The lower volcanic unit forms a lens within the quartzite. The upper unit overlies the quartzite, but its upper contact is obscured by alluvium and vegetation. There is little evidence available to suggest whether these units represent lava flows or pyroclastic flow deposits. Younger volcanic units to the east of the locality are basic in composition.

Armstrong (1980) described lava and pyroclastic layers within the predominantly sedimentary Mantonga Formation. It is, however, debatable whether these volcanic units observed, lie in the uppermost layers of the Mantonga Formation. They may possibly form the base of the Bivane Subgroup (the units are acid as opposed to the basic composition of the lower Bivane Subgroup) or represent a transitional phase from predominantly sedimentary to volcanic processes.

3.4 BIVANE SUBGROUP – WHITE RIVER SECTION

Discussion of the volcanology of the Bivane Subgroup will highlight the characteristic and interpretative features. It is difficult to identify continuous sequences of individual lava flows and pyroclastic layers due to the incomplete nature of the outcrop along the White River, but interpretation of the style of volcanism can be made based on general changes in the character of the volcanic lithologies. A possible feeder dyke system to the lavas of the Bivane Subgroup is discussed in Section 3.4.6. The Bivane Subgroup in the White River Section has been divided into five phases of volcanism based on stratigraphic, geographic and structural observations (Appendix 1). Stratigraphic divisions are based on orientation of the lava units (striking N-S to NNE-SSW, dipping E to ESE) and their field relationships to one another. The effect of the rugged topography on the stratigraphic succession has been taken into account (Appendix 1). Geographic position has been used to create subphases if the outcrop areas are possibly stratigraphically equal but a sufficient distance apart or divided by a topographical feature (Appendix 1). Any structural observations were taken into account so as to recognise any duplication of volcanic units. These divisions will be used in this chapter as well as Chapter 5 Geochemistry. Figure 3.4 is a stratigraphic column relating the different phases and their characteristics.

3.4.1 Phase 1

The oldest lava flows of the Bivane Subgroup are basaltic (Figure 3.4). These outcrops are susceptible to spheroidal weathering, which has obscured primary structures. There is evidence for epidote alteration and extensive quartz veining. The epidote alteration is present as green spherical patches. A possible origin of this alteration was by the inundation of small pools of water with lava. The steam rose through the fractures in the lava causing localised areas of hydrothermal alteration. Certain areas of the outcrop are pyroclastic in origin; while others are highly vesicular possibly representing volatile-rich lava flows. The pyroclastic units are tuffaceous with thin laminae preserved.

[2] The term vesicle is applied to all gas cavities preserved within the lava flows. The majority of these preserved gas bubbles are infilled by various minerals e.g. quartz, epidote, calcite, zeolite, forming amygdales. Amygdales, however, formed as a result of a secondary process, and the original structure name of vesicle is therefore used in this chapter where the focus is on the primary volcanological processes.

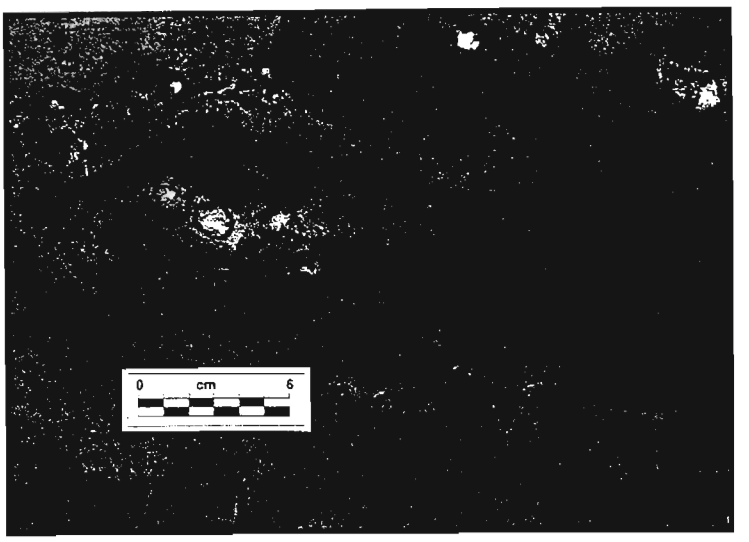

Figure 3.1 Amygdaloidal flow top of a basalt, Wagondrift Formation, White River. (sample CG01/19; 27.2445 S, 31.0562 E)

Figure 3.2 Lava flow between two quartzite units, Mantonga Formation, White River. (Facing west, dip direction towards the east) (sample CG01/122; 27.2635 S, 31.0785 E)

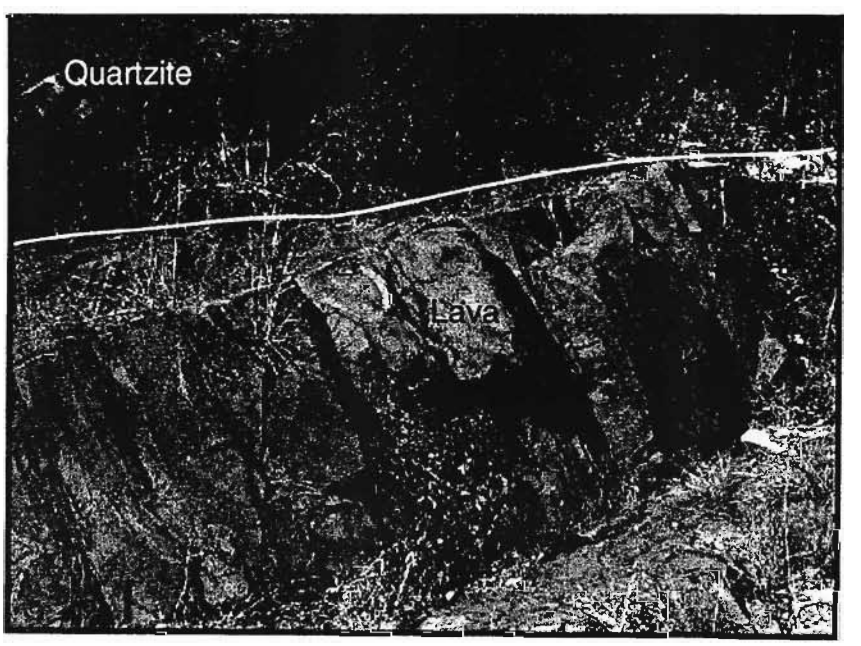

Figure 3.3 Columnar jointing in lava flow, Mantonga Formation, White River. (Facing south, dip direction towards the east)(sample CG01/122; 27.2635 S, 31.0785 E)

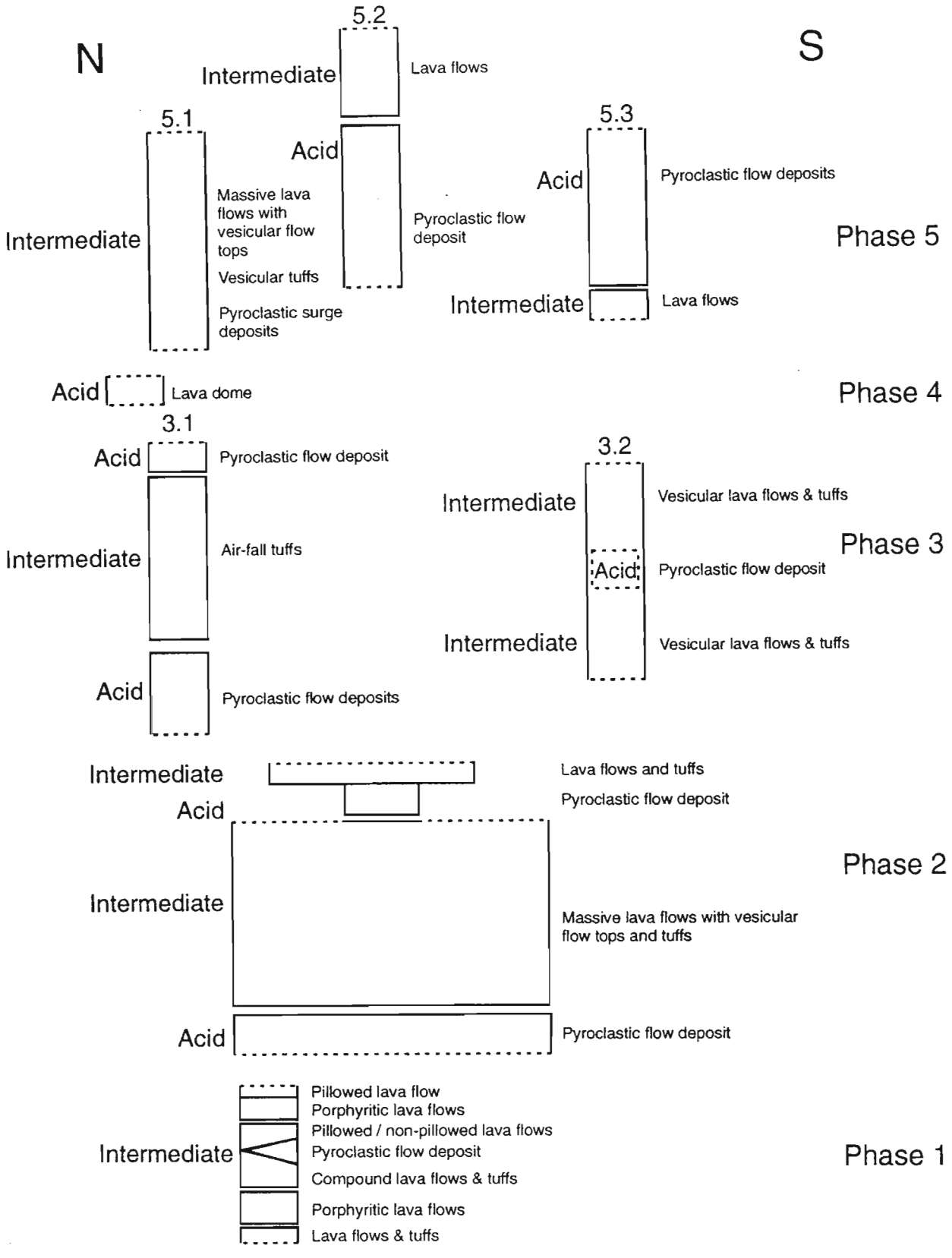

Figure 3.4 Schematic stratigraphic column of the eruption phases of Bivane Subgroup, White River Section, showing relative geographic relationships, dominant compositions, and nature of the volcanic rocks.

The highly altered sequence described above is overlain by a distinct series of andesitic units containing plagioclase phenocrysts of varying sizes (Figure 3.4). The porphyritic andesite phase is approximately 200m thick and porphyritic units are interbedded with non-porphyritic units (Figure 3.5). Phenocrysts are generally randomly orientated but show a localised preferred orientation (Figure 3.6; Figure 3.7). The phenocrysts range in size from <0.5cm to 2.5cm in long axis. The top of the porphyritic andesite sequence contains localised pillow structures of 20cm to 1m in diameter (Figure 3.8a-c). This may be due to the viscous nature of the porphyritic melt and its tendency not to form pillow structures. The higher the yield strength of lava (due to a high viscosity), the less susceptible the lava is to deform within a skin that results in structures like pillows or toes (Cas and Wright, 1987). The depth of the water body may also not have been sufficient to allow for the continued formation of pillow structures.

Overlying the porphyritic andesite unit is a sequence of lavas, well preserved in a cliff section sub-parallel to strike (Figure 3.9; Figure 3.10). The cliff section was investigated in detail providing an understanding of volcanism in the early stages of the Bivane Subgroup. The volcanic lithologies exposed on the cliff can be broadly grouped into four eruption phases (Figure 3.4; Figure 3.9). The oldest phase formed as a series of compound andesitic lava flows, interbedded with ash-fall layers. The second event is a fine-grained andesite layer pinching out towards the north. This is overlain by a pillowed / non-pillowed andesitic lava which is in turn overlain by a porphyritic lava of andesitic composition.

Andesitic lavas and ash layers form a compound flow field found at the base of the cliff section (Figure 3.4; Figure 3.9; Figure 3.10). The complex relationship of the lava flows suggests they are part of the same eruptive episode and represent lobes and toes that interfinger and overlap each other (Figure 3.11a-b). The flow units vary from <0.5m to 4m thick. Pillow lava structures (and lava toe structures) are found at the base at the northern end of the cliff (Figure 3.12). These pillow lava structures are generally less than 10cm in diameter and are confined to the flow surface of one flow unit (Figure 3.13a-b). The limited distribution of the pillow lavas is reminiscent of the pillow lavas found in older porphyritic andesites, suggesting isolated areas of water, possibly in a fluvial system. The lava surfaces are not regular but display undulations and domes. These domes represent tumuli, or gas blisters that rose to the surface of the lava flow unit, which caused the crust of the lava to rise (Figure 3.14). Tumuli are common features on the flow surfaces of pahoehoe lava flow fields (Walker, 1991). The pahoehoe nature of the lava flow field is supported by the presence of rough pahoehoe texture preserved on a flow surface (Figure 3.15). Ash layers are found at the top of the certain lava flow units (Figure 3.16). The presence of thin layers of ash (5-15cm) as well as andesitic lava flows suggests that these units formed through cyclical eruption of pyroclastic material followed by lava outpourings from a single vent. Vesicles are small (<1 – 3mm) and spherical. They are concentrated at the base and top of the lava flow units. There are few large irregular shaped vesicles and pipe vesicles are only found in the flow units thicker than 3m. This is due to the limited thickness of the lava flow units, which did not allow time for bubble coalescence and bubble migration prior to solidification (Wilmoth and Walker, 1993).

The fine-grained andesite pinches out towards the north and thickens to the south of the cliff section (Figure 3.4; Figure 3.9). The interior of the andesite is structurally massive and exhibits columnar jointing (Figure 3.17). There are also clasts or brecciated fragments preserved in the unit as well as isolated patches of vesicles found within the andesite (Figure 3.18). The upper and lower contacts of the andesite show differing textures. The lower contact varies from a sharp to a non-mixed contact. A lava skin marks the sharp lower contact between lower compound lavas and the fine-grained andesite (Figure 3.19). A non-mixed contact is thought to have formed because the underlying magma was not yet solid when the fine-grained andesite was emplaced over it (Figure 3.20). This resulted in two slightly differing compositions interacting with one another but due to their rheological differences could not have easily mixed. This resulted in the globules of the fine-grained andesite forming within the lower lava, which then solidified. The sharp contact has formed with an older flow unit than the flow unit responsible for the non-mixed contact (see locality of Figure 3.19 with respect to Figure 3.20 on Figure 3.10). The upper contact of the fine-grained andesite is flow banded on a scale of

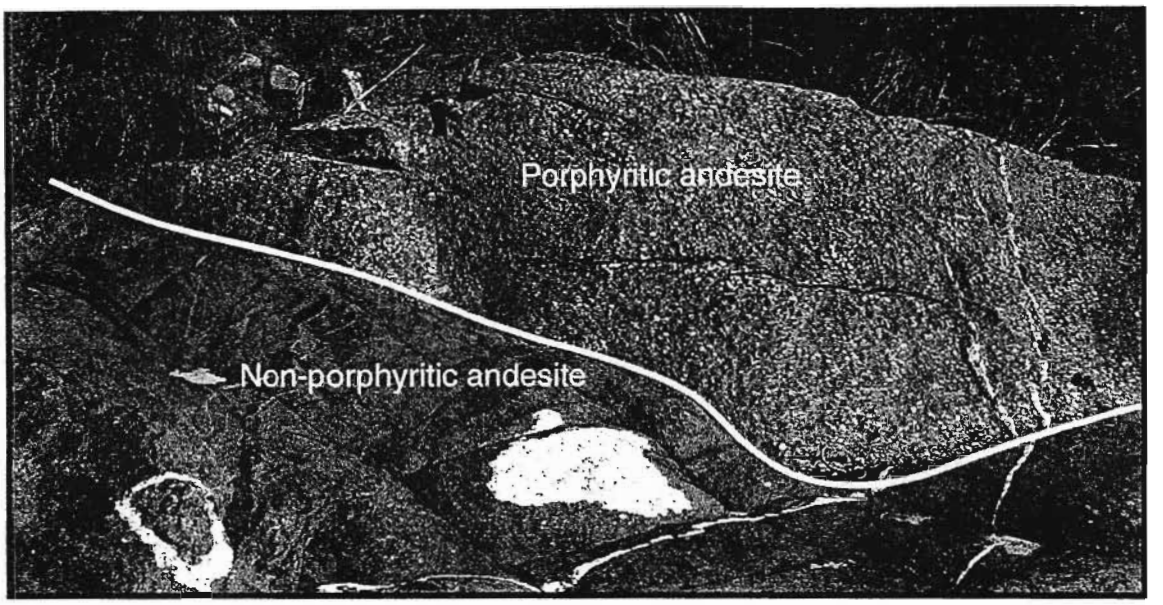

Figure 3.5 Contact between porphyritic and non-porphyritic andesite lava flows, Bivane Subgroup, White River. (Facing west, dip direction towards the east) (27.2722 S, 31.0838 E)

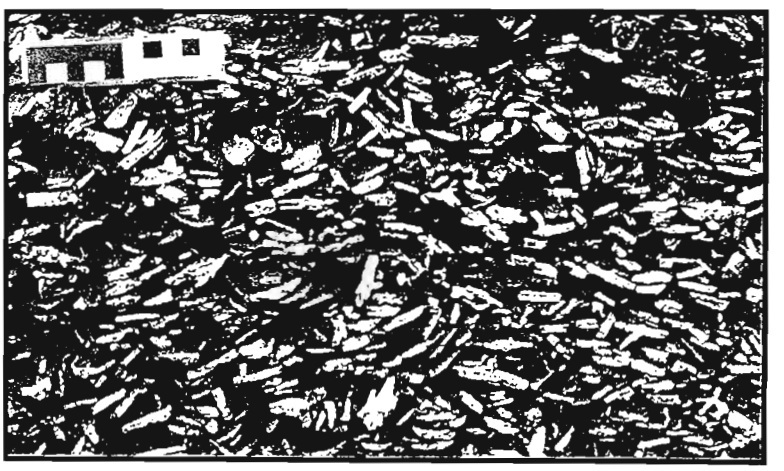

Figure 3.6 Random orientation of plagioclase phenocrysts in andesite, Bivane Subgroup, White River. (Facing east) (27.2722 S, 31.0838 E)

Figure 3.7 Localised preferred orientation of plagioclase phenocrysts in andesite, Bivane Subgroup, White River. (Facing south) (27.2738 S, 31.0845 E)

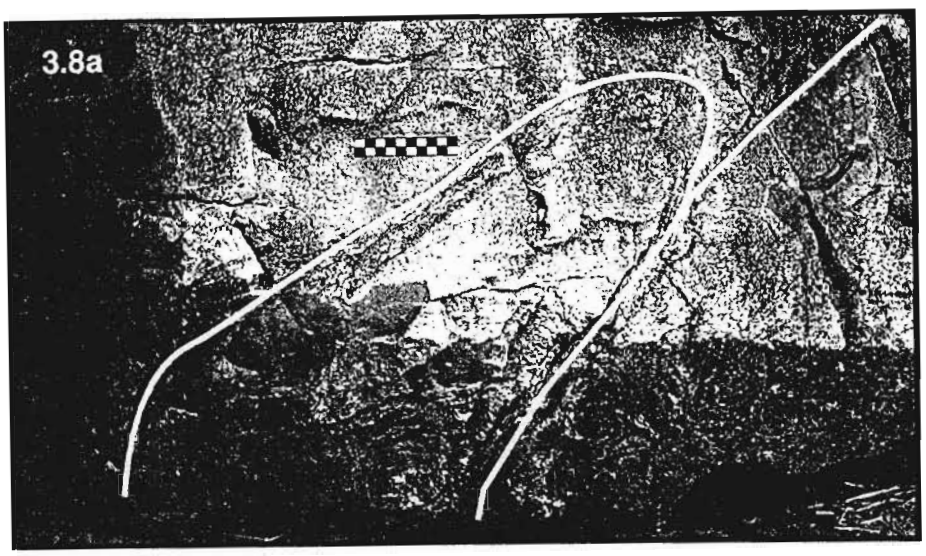

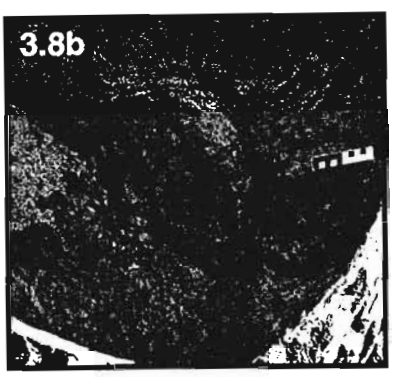

Figure 3.8a-c Localised pillow lava structures in porphyritic andesite, suggesting a limited body of water, Bivane Subgroup, White River. (Facing south) (27.2738 S, 31.0845 E)

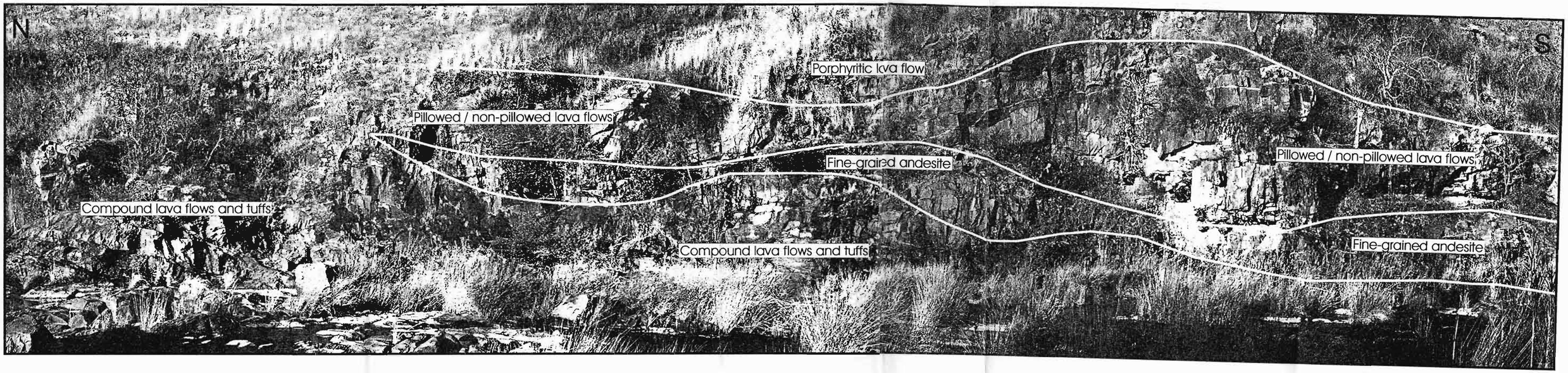

Figure 3.9 Cliff section along White River, showing the four andesitic eruption events - compound lava flows and tuffs; fine-grained andesite; pillowed / non-pillowed lava flows; porphyritic lava flow. See Figure 3.10 for detailed interpretation and samples of cliff section. (Facing east) (27.2729 S, 31.0897 E)

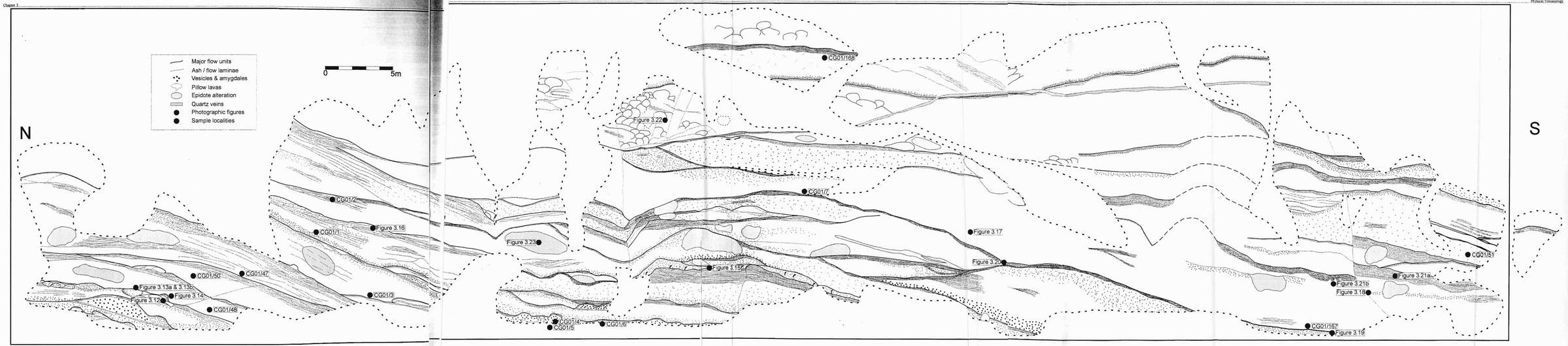

Figure 3.10 Detailed drawing of cliff section, Bivane Subgroup, White River. (See Figure 3.9 for photographic image- red outline represents extent of photograph) (27.2729 S, 31.0897 E

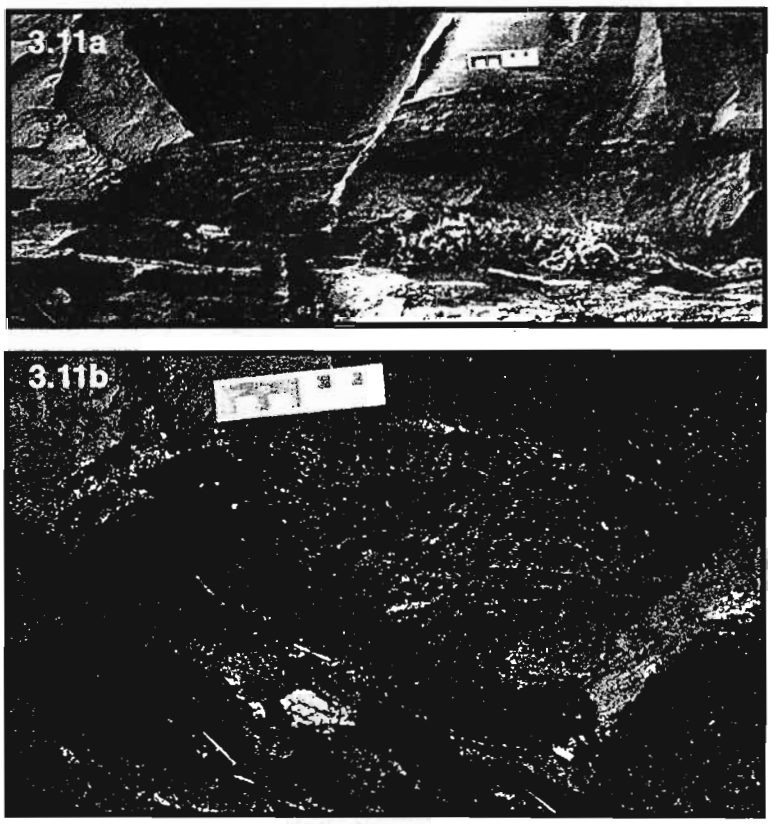

Figure 3.11a-b Lava toes in a compound lava flow on cliff section, Bivane Subgroup, White River. See Figure 3.10 for location of photographs. (Facing east)

Figure 3.12 Pillow structures in compound lava flow on cliff section, Bivane Subgroup, White River. See Figure 3.10 for location of photograph. (Facing east)

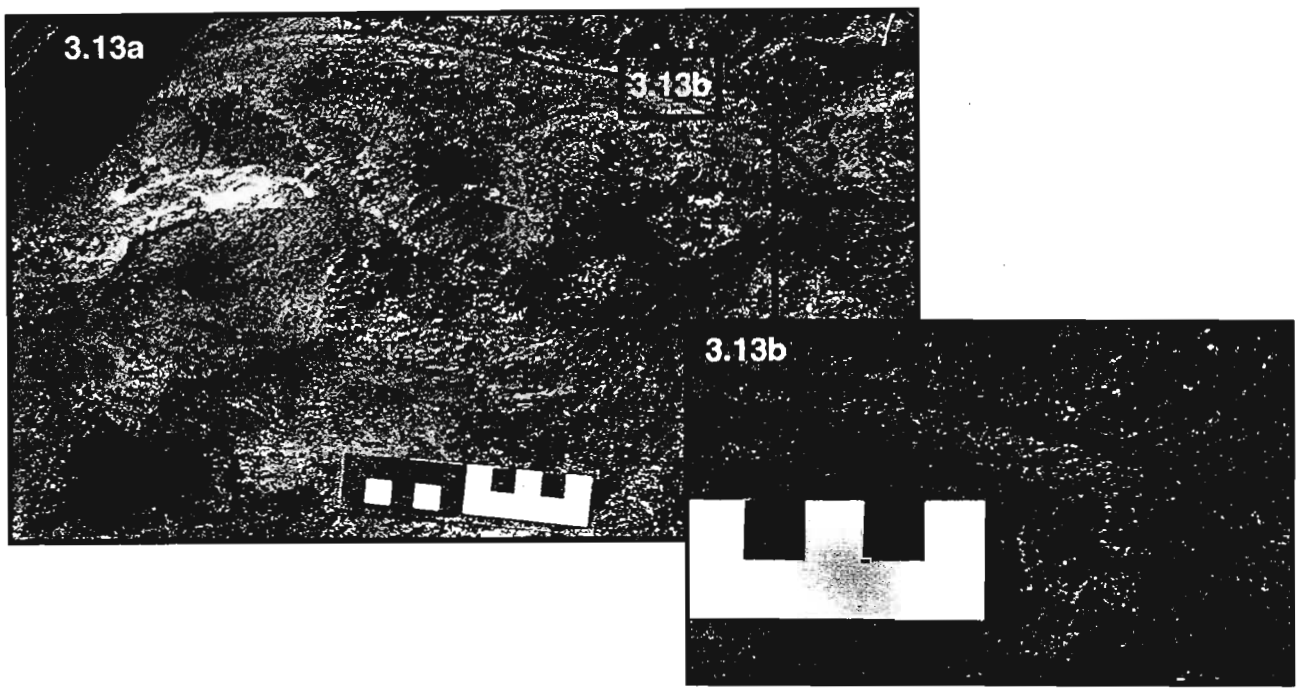

Figure 3.13a-b Pillow lava structure in compound lava flow on cliff section, Bivane Subgroup, White River. Figure 3.13b shows a close up of the vesicular pillow rim. See Figure 3.10 for location of photographs. (Facing east)

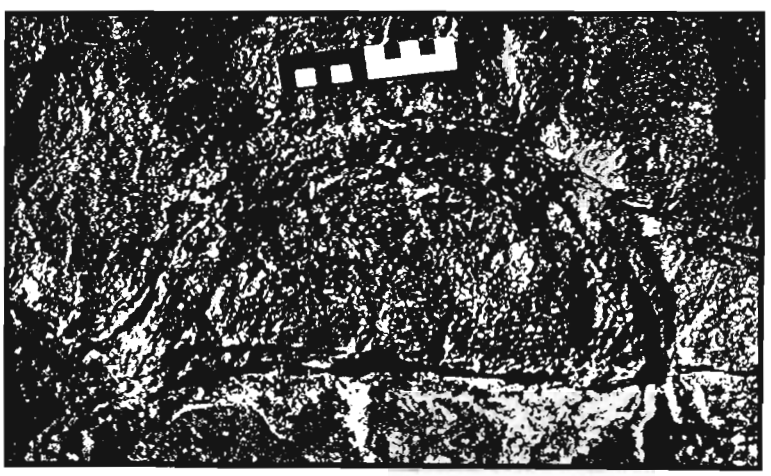

Figure 3.14 Dome on the surface of a compound lava flow on cliff section, Bivane Subgroup, White River. See Figure 3.10 for location of photograph. (Facing east)

Figure 3.15 Pahoehoe texture on a compound lava flow surface on cliff section, Bivane Subgroup, White River.
See Figure 3.10 for location of photograph. (Facing east)

Figure 3.16 Ash layers on compound lava flow surface on cliff section, Bivane Subgroup, White River.
See Figure 3.10 for location of photograph. (Facing east)

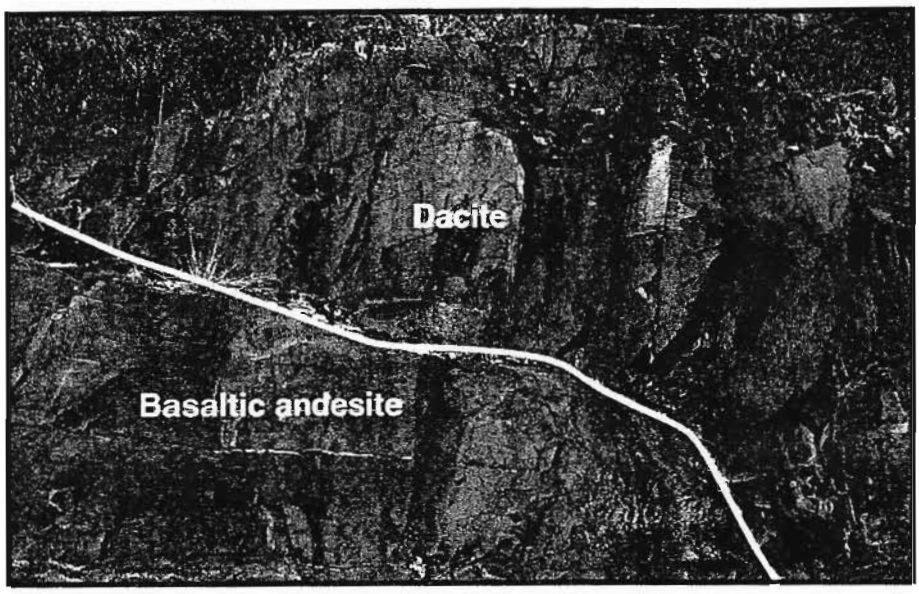

Figure 3.17 Columnar jointing in fine-grained andesite on cliff section, Bivane Subgroup, White River. See Figure 3.10 for location of photograph. (Facing east)

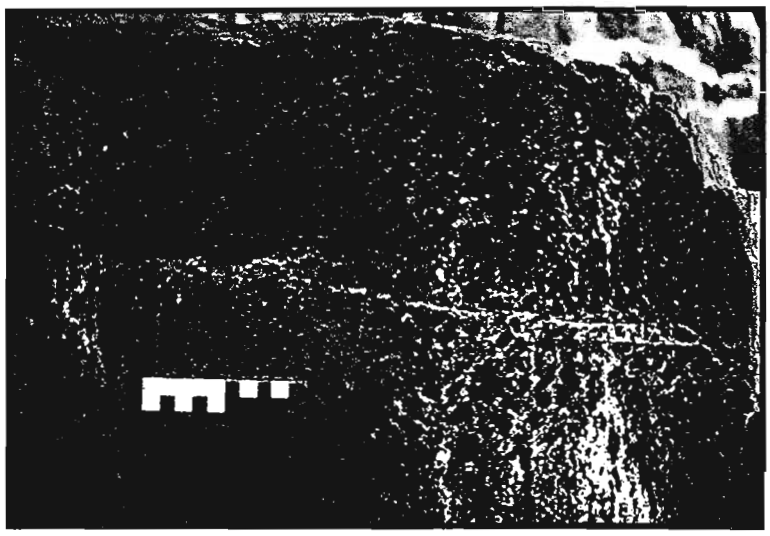

Figure 3.18 Vesicles in fine-grained andesite on cliff section, Bivane Subgroup, White River. See Figure 3.10 for location of photograph. (Facing south)

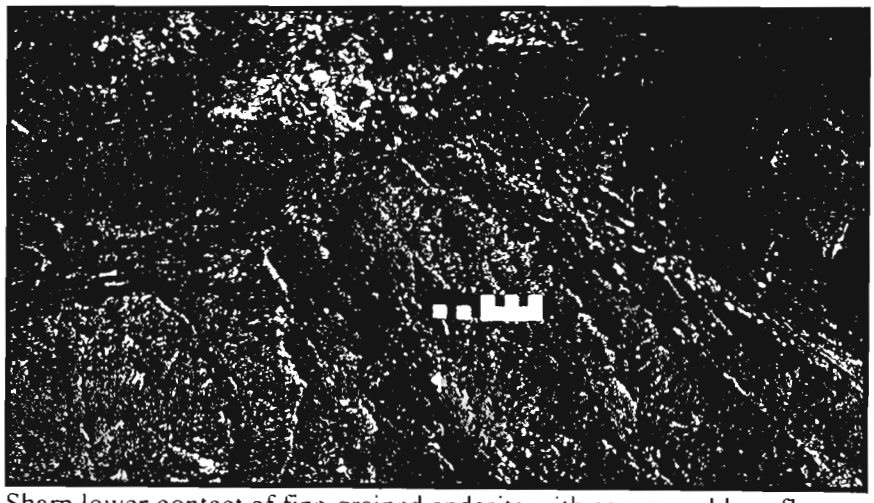

Figure 3.19 Sharp lower contact of fine-grained andesite with compound lava flow on cliff section, Bivane Subgroup, White River.
See Figure 3.10 for location of photograph. (Facing east)

1cm to 15cm. Pre-solidification movement has formed minor folds within the pyroclastic material (Figure 3.21a-b). The fine-grained andesite unit possibly represents the edge of a pyroclastic flow event. Andesitic lava flows are usually porphyritic with phenocrysts preserved as euhedral crystals (Cas and Wright, 1987). In this case the andesite is very fine grained with no phenocrysts suggesting its bulk is made up of fragmented glass shards (Cas and Wright, 1987). Facies associated with pyroclastic flows are easily eroded if they are unwelded (Fisher and Schmincke, 1984). Welded pyroclastic flow deposits are often characterised by columnar jointing (Freundt *et al.*, 2000). If a period of quiescence followed the emplacement of the fine-grained andesite (as would be expected after a pyroclastic event), the ash and breccia facies component of the pyroclastic flows could have been eroded away. This would have also allowed for the re-establishment of a fluvial system (possibly the mechanism of erosion) that would influence the morphology and flow characteristics of lavas of the subsequent eruption.

The subsequent eruption produced andesitic lava flows similar in composition to the compound flow field located at the base of the cliff section (Figure 3.4; Figure 3.10). This lava flow unit has pillow structures in the central area of the cliff (Figure 3.22). The pillow structures are not laterally extensive throughout the lava flow unit suggesting that the lava flowed into a shallow, localised body of water as might be found in a fluvial system (Figure 3.10). The pillows, generally flattened, vary in size from <10cm rounded to 1m. These shapes are consistent with structures formed by lava flowing passively into a body of water. The lava would have had a relatively low viscosity, low volatile content and would have flowed very slowly (Gregg and Fink, 1995). The rest of the pillowed andesitic flow is relatively structureless. This flow unit is overlain by a porphyritic andesite, which is in turn overlain by another pillowed unit close to sample site CG01/168 on Figure 3.10 (Figure 3.4). The phenocrysts are <1cm long axis and vesicles are present at the top and bottom of the flow. The overlying pillowed unit is obscured by vegetation so its true lateral and vertical extent is unknown (Figure 3.10).

Epidote alteration is present throughout the outcrop area, but appears to be confined to the lava and ash units and as noted previously formed as a result of lava flowing over puddles of water (Figure 3.23). This type of alteration is also commonly associated with silicification. The presence of water is prevalent in Phase 1. While in the volcanic units, the effects of water are at different stratigraphic levels, it suggests that this area was dominated by a variable fluvial system over a period of time with the rapid re-establishment of river channels during periods of volcanic inactivity.

3.1.1 Phase 2

Phase 2 represents a younger stage of eruption than Phase 1, and is characterised by the presence of acid volcanic rocks, as well as intermediate compositions. The oldest unit of Phase 2 is acid and is identified by two outcrops along the White River represented on Appendix 1 by samples CG01/28 and CG01/93 (Figure 3.4). Dacites are columnar jointed (Figure 3.24) and outcrops in the south of Phase 2 contain ash layering (Figure 3.25). The acid unit is estimated at <60m thick. It represents the fine-grained welded component of a pyroclastic flow deposit resulting from the collapse of an eruption column (Freundt *et al.*, 2000). The complete lateral extent of the flow has not been determined.

Stratigraphically overlying the acid unit is a sequence of andesitic volcanic rocks, dominated by massive lavas with vesicular to highly vesicular flow tops (Figure 3.4; Figure 3.26). Many of the vesicles have been infilled to form amygdales. Pahoehoe surface texture is observed at one locality (Figure 3.27). Evidence for andesite ash tuffs are found throughout the sequence, in particular towards the north of Phase 2 (Appendix 1). There is little evidence to differentiate which tuffs are fall deposits and which are flow deposits. The tuffs are pitted possibly representing unconsolidated ash that was subjected to weathering prior to diagenesis.

Spheroidal textures are preserved in an outcrop in the White River (Figure 3.28a-b). These spherical globules are found at the top of a flow unit. They are preserved as individual ellipse shapes or as cuspate trains of ellipses. In thin section, these spheroidal structures are plagioclase, quartz and minor epidote intergrowths surrounded by a rim of biotite with minor chlorite. This texture is interpreted to be a non-mixing zone between two slightly different

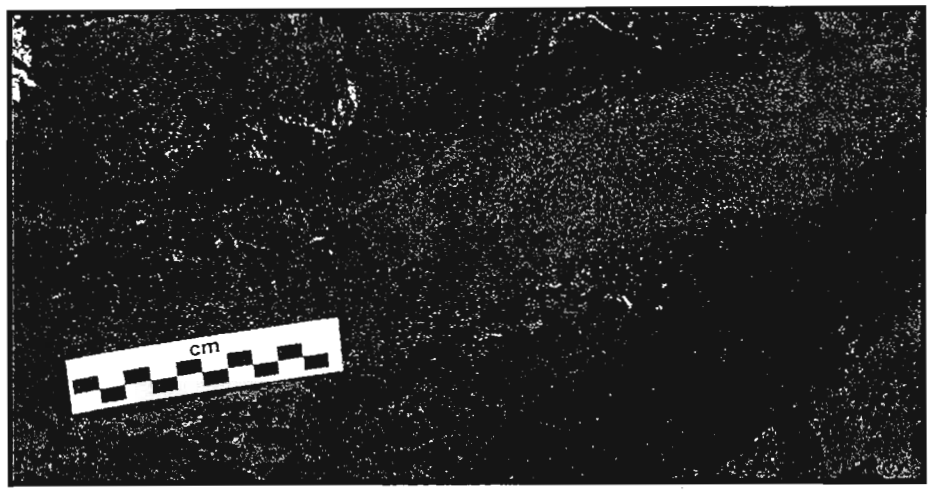

Figure 3.20 Lower non-mixing contact of fine-grained andesite with compound lava flow on cliff section, Bivane Subgroup, White River.
See Figure 3.10 for location of photograph. (Facing east)

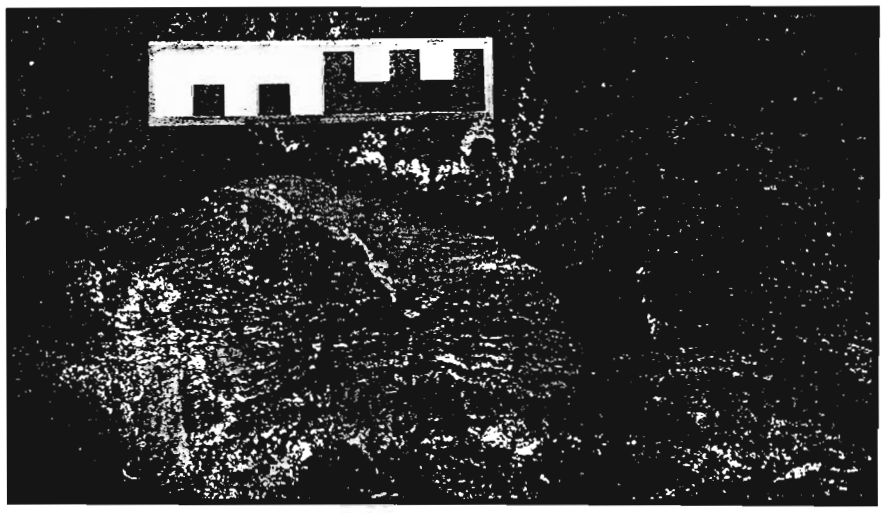

Figure 3.21a Upper flow banded contact of fine-grained andesite with pillowed / non-pillowed lava flow on cliff section, Bivane Subgroup, White River.
See Figure 3.10 for location of photograph. (Facing east)

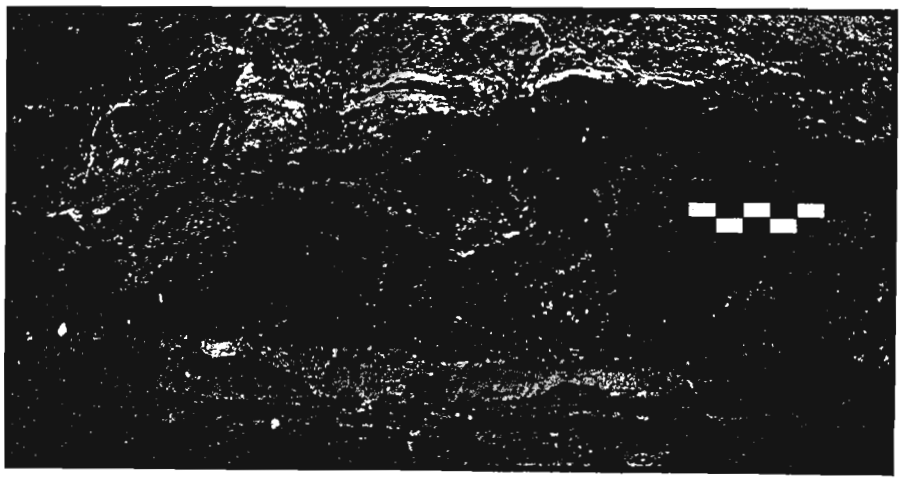

Figure 3.21b Folded flow banding in upper contact of fine-grained andesite with pillowed / non-pillowed lava flow on cliff section, Bivane Subgroup, White River.
See Figure 3.10 for location of photograph. (Facing east)

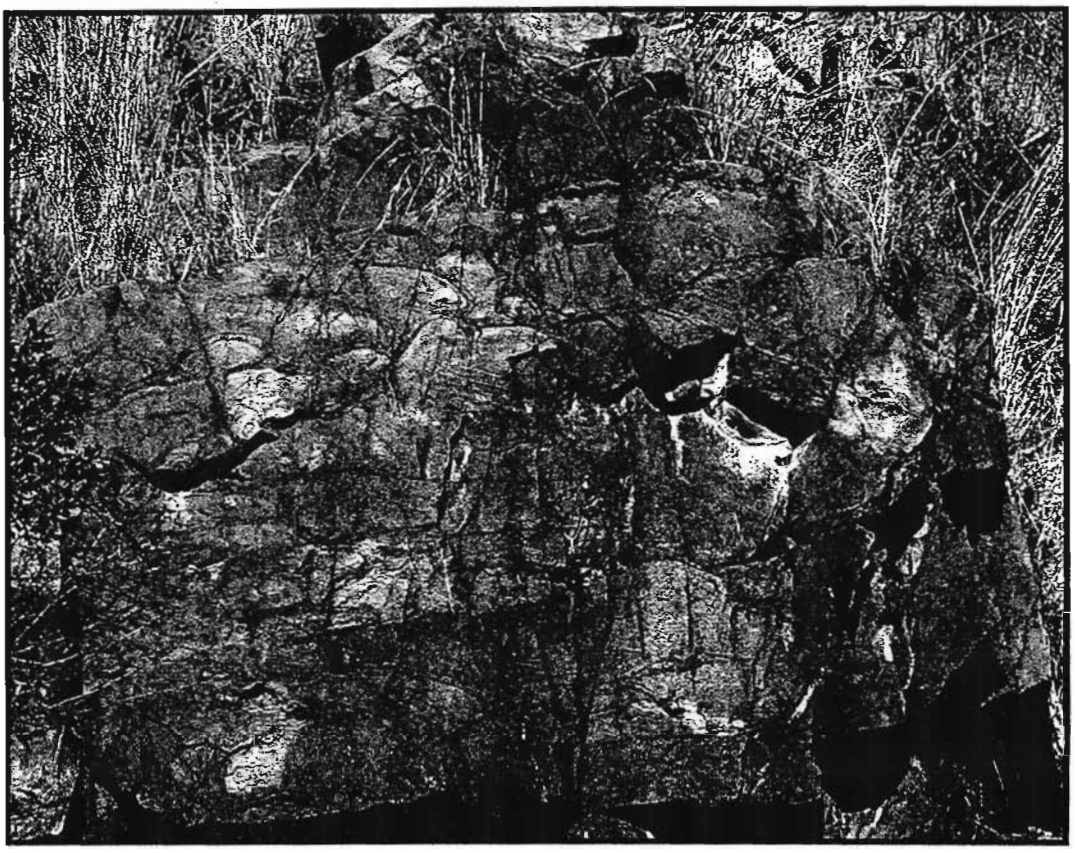

Figure 3.22 Pillow structures in pillowed / non-pillowed lava flow on cliff section, Bivane Subgroup, White River.
See Figure 3.10 for location of photograph. (FOV = 7m; Facing east)

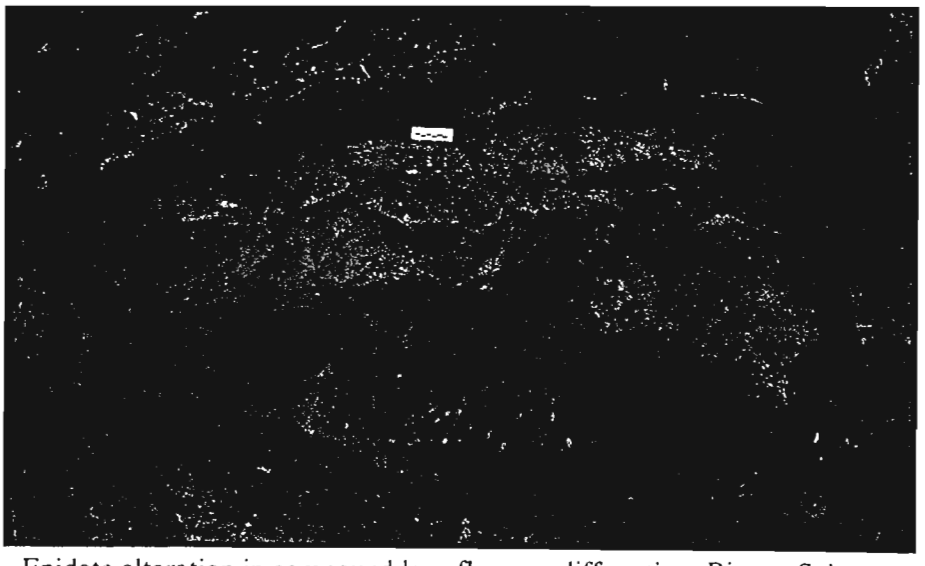

Figure 3.23 Epidote alteration in compound lava flow on cliff section, Bivane Subgroup, White River.
See Figure 3.10 for location of photograph. (Facing east)

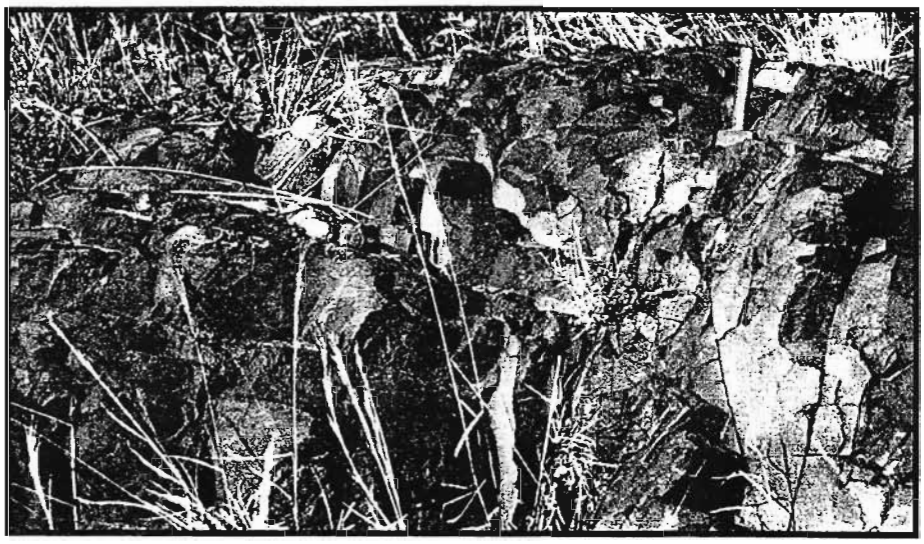

Figure 3.24 Columnar jointing in dacite, Bivane Subgroup, White River. (sample CG01/93; 27.2835 S, 31.0900 E)

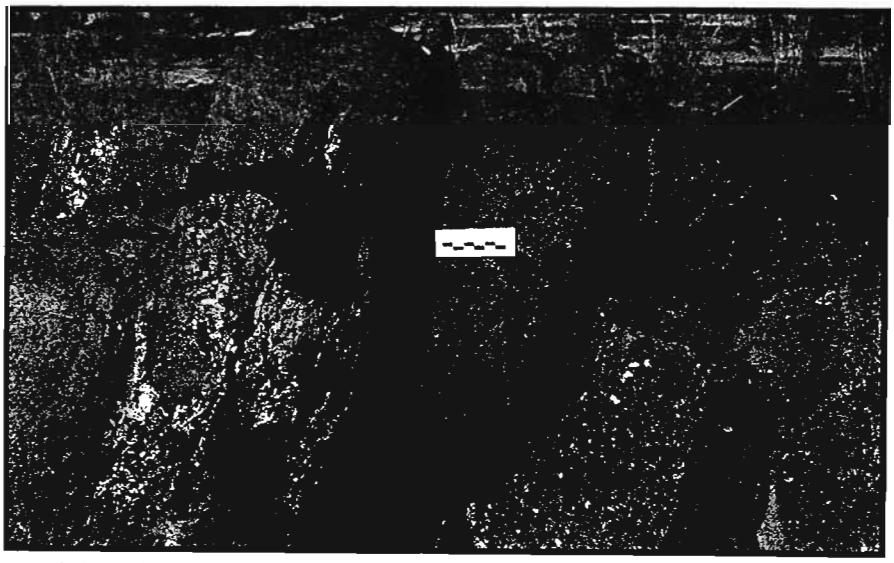

Figure 3.25 Ash layering in dacite, Bivane Subgroup, White River. (sample CG01/28; 27.977 S, 31.0865 E)

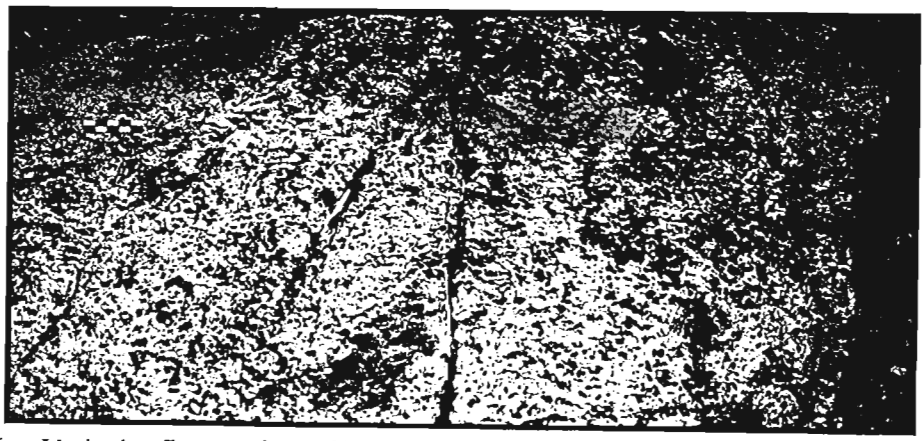

Figure 3.26 Vesicular flow surface of basaltic andesite, Bivane Subgroup, White River. (sample CG01/151; 27.2910 S, 31.0888 E)

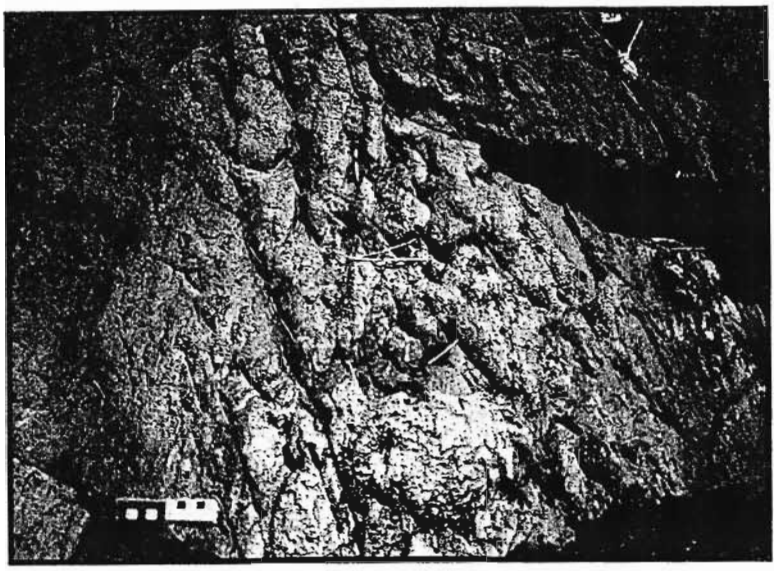

Figure 3.27 Pahoehoe flow surface in basaltic andesite, Bivane Subgroup, White River. (sample CG01/151; 27.2910 S, 31.0888 E)

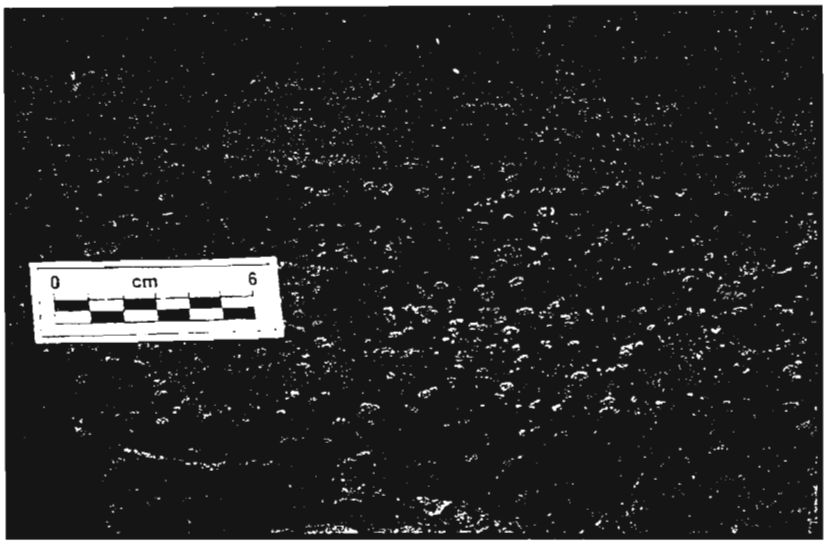

Figure 3.28a Non-mixing of felsic and mafic components in andesite, Bivane Subgroup, White River. (sample CG01/24; 27.2887 S, 31.0913 E)

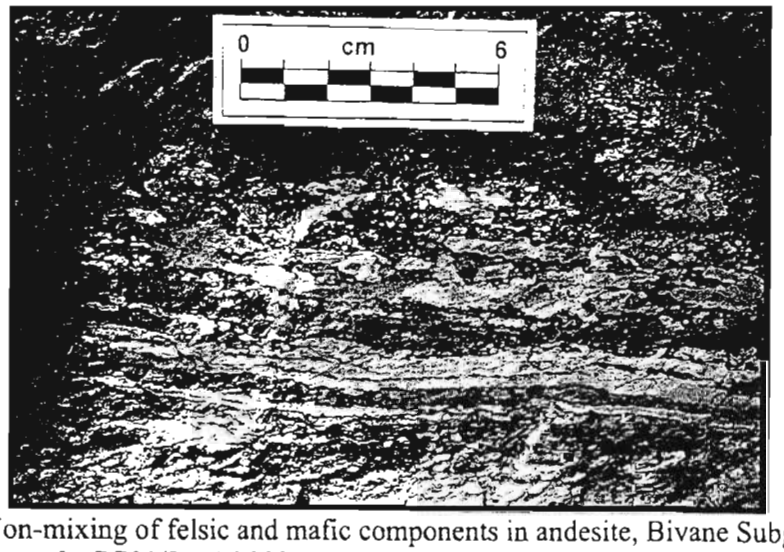

Figure 3.28b Non-mixing of felsic and mafic components in andesite, Bivane Subgroup, White River. (sample CG01/24; 27.2887 S, 31.0913 E)

magma types, where the more mafic components could not fully blend with the felsic components.

An acid volcanic unit is represented by samples CG01/82 to CG01/84 at the confluence of the White River and the Beki-Beki Tributary in Phase 2 and by sample CG01/25 towards the south. Columnar jointing is the only feature of the acid unit in the south of Phase 2 (Figure 3.29). Figure 3.30 depicts three flows within the unit. The oldest massive unit (CG01/84) is overlain by an ash deposit (CG01/83), which in turn is overlain by a lapilli unit (CG01/85). The lower unit may represent a welded ash-fall, while the overlying ash is unwelded (Figure 3.31). The lapilli are small (1-3mm) and some particles may be classified as coarse ash (Fisher and Schmincke, 1984). The massive structure of the acid unit in the south suggest that it forms part of a pyroclastic flow deposit, while the lithologies in the north of the unit have characteristics more typical of fall deposits.

Overlying this acid flow unit is a sequence of highly vesicular andesitic lava flows (CG01/85 on Figure 3.30). A massive andesite unit associated with the vesicular andesitic lava flows may constitute a cryptodome (CG01/86 on Figure 3.30). Cryptodomes form by the near-surface intrusion of magma into existing volcanic layers resulting in dome-like uplift of the surface rocks (Cas and Wright, 1987). The andesite that lies adjacent to the acid unit and which underlies the vesicular andesite, is glassy and massive and has a domed surface. The andesite lava flows present in the remaining area of Phase 2 are highly vesicular (preserved as amygdaloidal) and the tuffs are finely laminated.

3.1.2 Phase 3

Phase 3 is found in the north and south of the White River Section (Appendix 1). Phase 3 in the north is termed Phase 3.1, while in the south it is called Phase 3.2. A north – south trending ridge (identified as the western half of Phase 5.2 on Appendix 1) separates the two geographic areas of Phase 3. Due to the elevation of the ridge and the easterly dipping nature of the strata, the ridge area cannot be included in the low lying Phase 3 stage of eruption.

Phase 3.1 is exposed in the Beki Beki Tributary (Appendix 1). This phase is made up predominantly of andesites and dacites with the lower volcanic units comprising mainly dacites. These units represent a complex history of pyroclastic activity. The alternating units of massive, finely laminated, and brecciated dacite represent a series of pyroclastic flow deposits. Freundt *et al.* (2000) described three layers that can be found within a pyroclastic flow deposit. Layer 1, at the base, is deposited at the flow front and is dominated by lithic fragments; layer 2 is made up of the main body and tail of the flow and comprises a basal ash layer overlain by lithic and pumice breccias; and layer 3 is formed by the ash-fall from the suspended cloud over the flow. Textures associated with these different layers are present in the dacite outcrops where massive zones represent lower layer 2, brecciated dacite forms part of layer 1 or upper layer 2 and finely laminated tuffs represent layer 3. The dacite pyroclastic rocks are followed by finely layered andesitic air-fall tuffs, which are heavily quartz veined. The uppermost units of Phase 3.1 comprise dacite. The sequence observed in Phase 3.1 represents a series of violent eruptions from a proximal source resulting in pyroclastic flow deposits. The andesitic ash is possibly derived from a more distal source as ash can be transported great distances from its point of origin (Fisher and Schmincke, 1984).

Phase 3.2 in the south of the Mkhunyane Eco-reserve represents a sequence of highly vesicular basaltic andesites, with a minor acid phase (Appendix 1). The basaltic andesite lavas have a less vesicular base, which grades into a dense vesicular flow top. No flow surface structures are observed although there is a localised development of a matrix-supported breccia comprising angular clasts in a highly vesicular matrix (Figure 3.32a-b). The fragments are predominantly pumice with minor lithic clasts that vary in size from <0.5cm to 10cm. The fragments are poorly sorted and show no preferred orientation. Flattened pumice clasts and glass fragments form alternating layers resulting in flow banding preserved in the rock (Figure 3.33). This flow banding and the nature of the large fragments are indicative of welding in a pyroclastic flow deposit (Fisher and Schmincke, 1984; Cas and Wright, 1987). Some fragments have been deformed due to high temperature ductile deformation characteristics. The vesicular nature of the matrix as well as the severe angularity of the fragments, suggests a highly volatile source. There is however no evidence for gas escape structures, generally associated with pyroclastic flow deposits (Cas

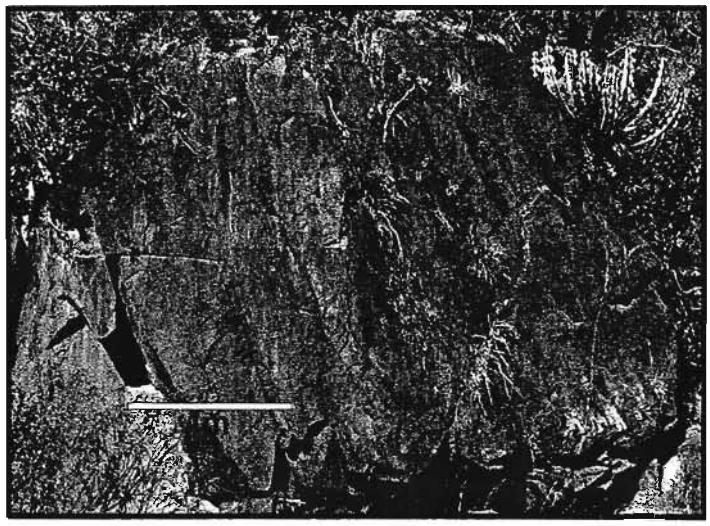

Figure 3.29 Columnar jointing in rhyolite, Bivane Subgroup, White River. (sample CG01/25; 27.2890 S, 31.0928 E)

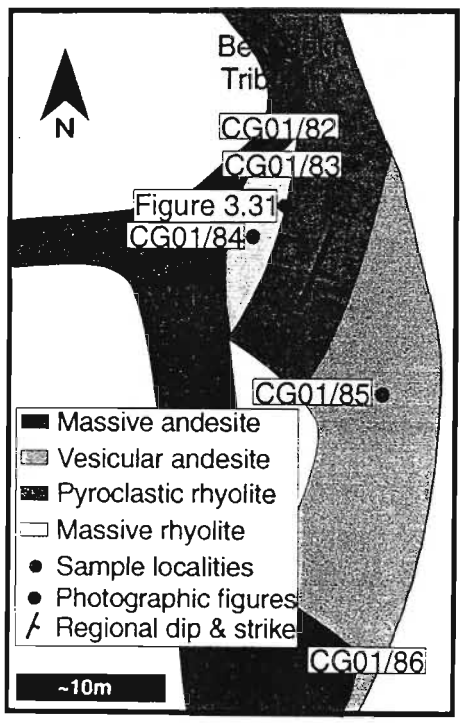

Figure 3.30 Schematic map of outcrop where Beki-Beki Tributary flows into the White River. (27.2782 S, 31.0958 E)

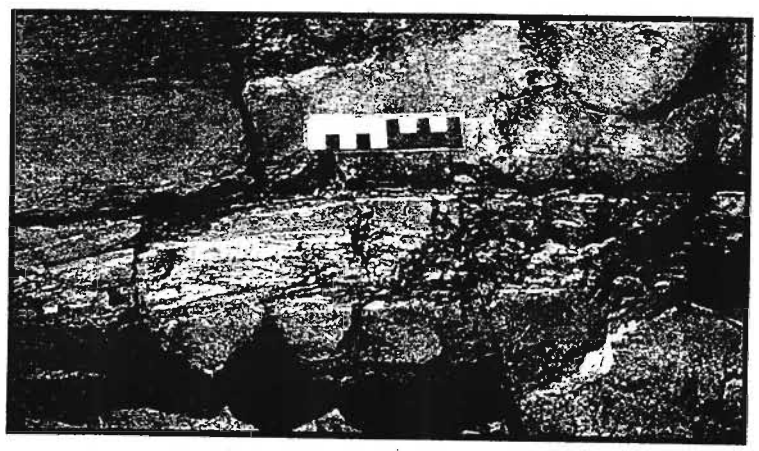

Figure 3.31 Contact of massive rhyolite (below) with pyroclastic rhyolite (above). See Figure 3.30 for location of photograph

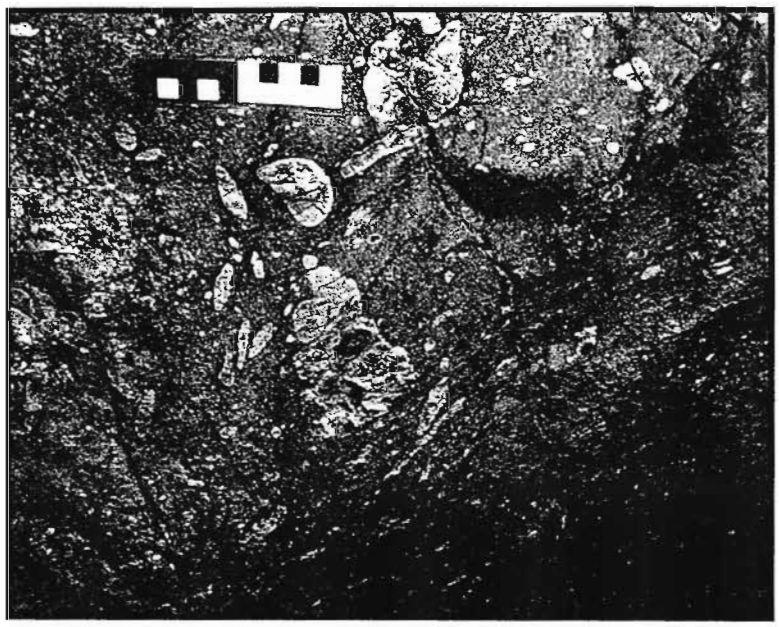

Figure 3.32a Angular clasts in pyroclastic breccia, Bivane Subgroup, White River. (27.3144 S, 31.0977 E)

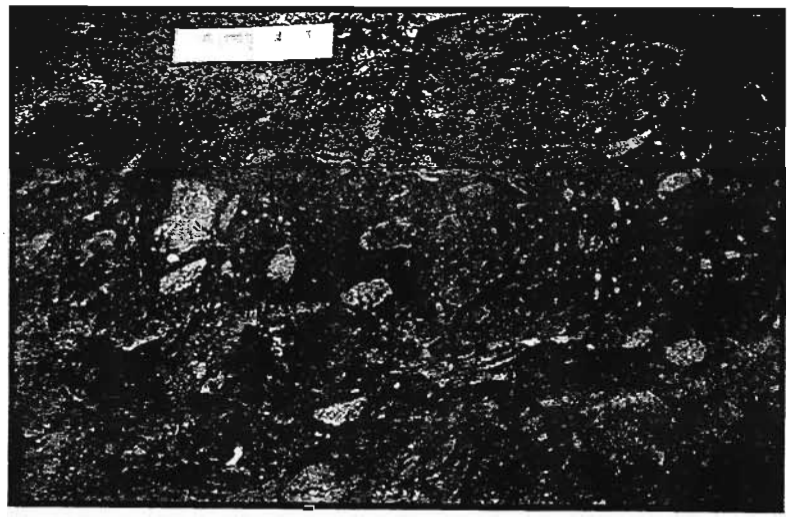

Figure 3.32b Angular clasts in acid pyroclastic breccia, Bivane Subgroup, White River. (27.3144 S, 31.0977 E)

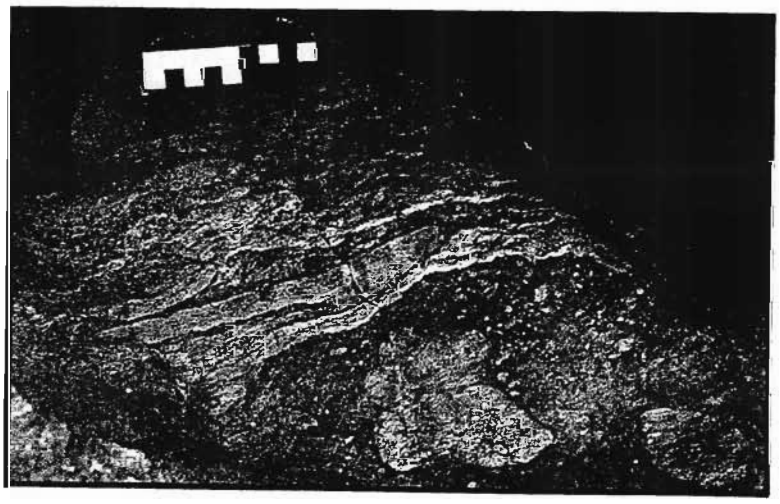

Figure 3.33 Flow banding in acid pyroclastic breccia, Bivane Subgroup, White River. (27.3144 S, 31.0977 E)

and Wright, 1987). The maximum size of the fragments (10cm) suggests that the outcrop best represents an ignimbrite that developed more than 3km from the volcanic source (Cas and Wright, 1987). The massive acid unit in Phase 3.2 may be related to this pyroclastic breccia, and represents a fine-grained welded ash facies of the ignimbrite (Cas and Wright, 1987). The stratigraphic relationship between these units would indicate that the acid unit overlies the breccia and that the breccia and acid lithologies are representative of layer 2 and layer 3 of ignimbrite flow units respectively (Freundt *et al.*, 2000).

3.1.1 Phase 4

A porphyritic rhyolite lava flow representing Phase 4 is found in the northern area of the White River Section (Appendix 1). The rhyolite caps the top of a hill and as a result outcrop is poor and obscured beneath grassland. The actual shape of the rhyolite flow is unknown but the estimated size is $<4km^2$ and thickness >80m. This size is consistent with a low lava dome or coulée (Francis, 1993). In order for the rhyolite to form a coulée, a certain degree of flow must have occurred to cause an asymmetric shape however this cannot be determined due to the disrupted western margin by a granodiorite intrusion. It is possible the dome formed in the hiatus of volcanic activity that resulted in the White Mfolozi Formation elsewhere in the Nsuze Group stratigraphy. It represents the effusive lava stage that often follows a pyroclastic flow stage (possibly represented by the units of Phase 3.1) associated with intermediate to acid volcanicity (Cas and Wright, 1987). This would support the concept of a proximal acid volcanic centre.

3.1.2 Phase 5

Phase 5 is represented in three areas in and around the Mkhunyane Eco-reserve. Phase 5.1 is found along the Beki Beki Tributary; Phase 5.2 forms the ridge to the east of the White River; Phase 5.3 is found just outside the southeastern boundary of the reserve, along the Agatha tributary (Appendix 1).

Phase 5.1 represents an andesitic phase of volcanism outcropping in the Beki Beki Tributary (Appendix 1). The andesite lava flows have both massive and vesicular surfaces, supporting the multiphase nature of the sequence. The massive zones of the andesite are columnar jointed. Vesicles are small (<5mm), spherical and in places have been infilled by secondary material to form amygdales (Figure 3.34). A tuff unit appears to be cross-bedded yet has an amygdaloidal surface; characteristics related to vesicular tuff units (Figure 3.35). Vesicular tuffs are associated with water and are rarely found more than 2-3km from their source. While vesicular tuffs are most often associated with phreatomagmatic eruptions, evidence has been found to suggest that the water may be introduced by rainfall (Fisher and Schmincke, 1984). Rain is a common occurrence during volcanic eruptions and is a likely scenario as there is a lack of evidence for a subaqueous environment. Pyroclastic surge deposits would be the cause of low-angled cross-bedded ash deposits (Fisher and Schmincke, 1984).

The subsequent eruptive activity is preserved in a possible lapilli-tuff (pyroclastic rock containing 25-75% ash with the balance made up of lapilli) (Schmid, 1981). The lapilli are ellipsoid and rounded (Figure 3.36a-b) and are relatively uniform in size from 10-15mm. These lapilli may be accretionary lapilli i.e. they were formed by ash nucleating around nuclei, often rain (Fisher and Schmincke, 1984). This would therefore indicate that the accretionary lapilli are related to the eruption that formed the vesicular tuff. Fisher and Schmincke (1984) state that lapilli are commonly associated with vesicular tuffs due to the water factor. The ellipsoid shape of the lapilli is also suggestive of accretionary lapilli as they are flattened on impact with the ground (Fisher and Schmincke, 1984). The size of lapilli means that they are rarely transported further than 10km from the source, unless the eruption is particularly violent. The distance of the source was probably ~3km from the outcrop. This would be in keeping with the weak eruption status commonly associated with andesite eruptions (Fisher and Schmincke, 1984).

The acid volcanics of Phase 5.2 form a large hill to the east of the White River and incorporate the lower western side of the Pypklipberg Mountain (Appendix 1). The rhyolites are perlitic and flow banded and the flow bands are composed of alternating layers of pumice and glass formed by welding (Figure 3.37). Perlite is formed by the hydration of obsidian and is characterised by fracturing caused by the expansion of the volcanic glass. This is a common feature observed in ancient obsidians (Fisher and

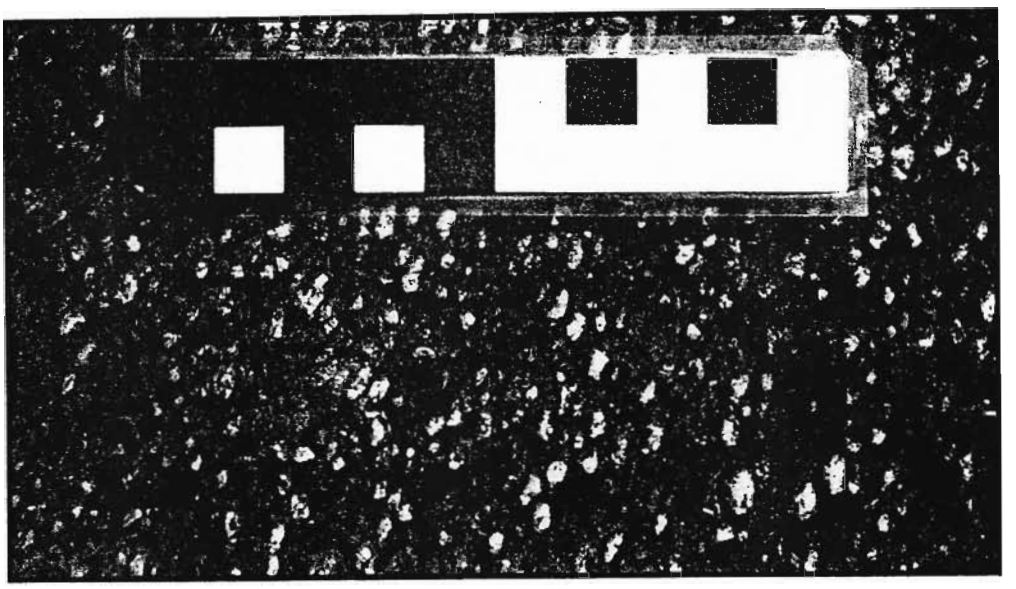

Figure 3.34 Amygdaloidal basaltic andesite, Bivane Subgroup, Beki-Beki Tributary. (sample CG01/107; 27.2555, 31.1240 E)

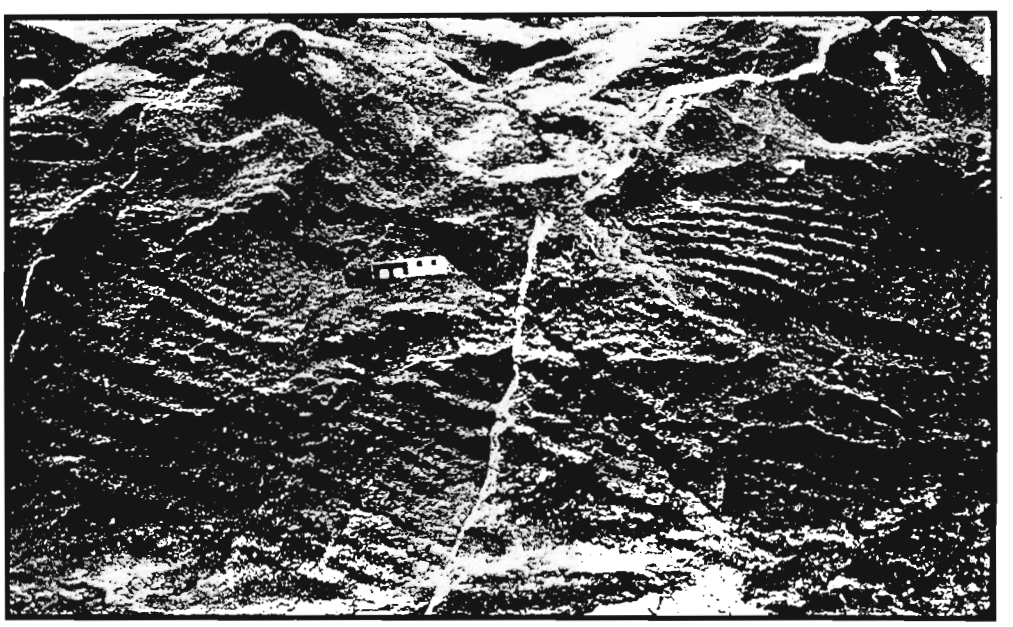

Figure 3.35 Cross-bedded andesitic tuff, Bivane Subgroup, Beki-Beki Tributary. (27.2536 S, 31.1156 E)

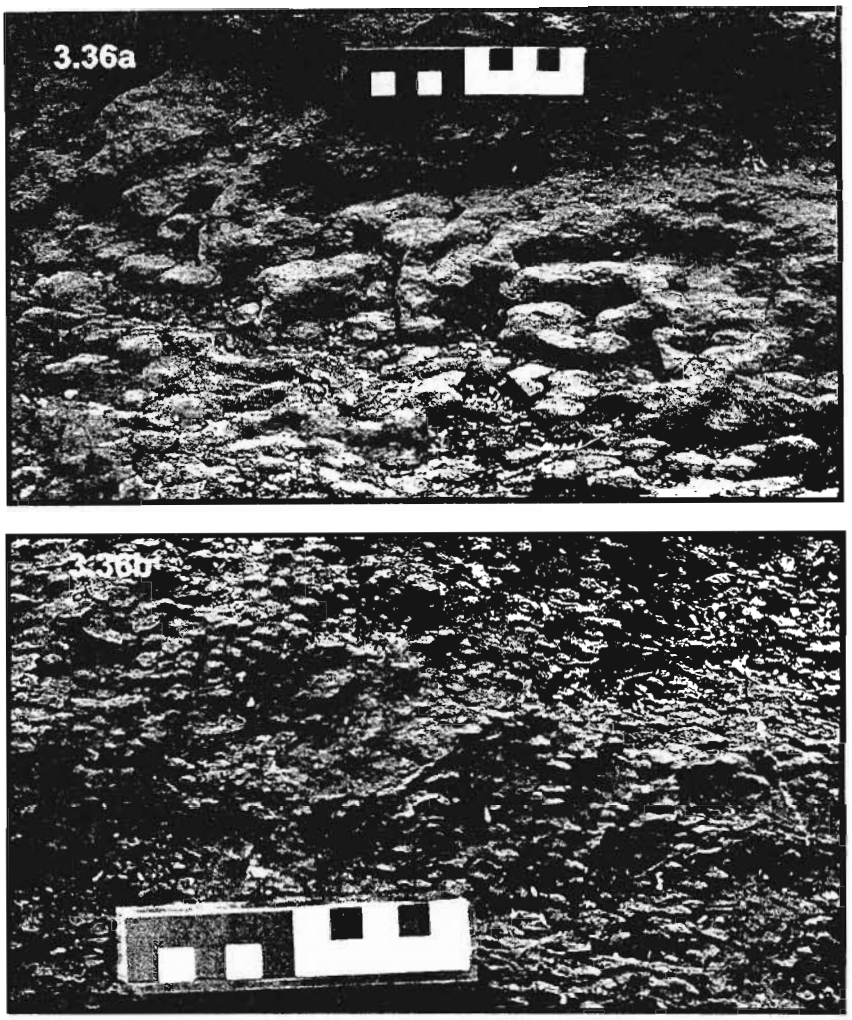

Figure 3.36a-b Accretionary lapilli in andesite, Bivane Subgroup, Beki-Beki Tributary. (sample CG01/106, CG01/108; 27.2524 S, 31.1169 E)

Figure 3.37 Flow banded rhyolite, Bivane Subgroup, Pypklipberg Mountain. (sample CG01/43; 27.2711 S, 31.1192 E)

Schmincke, 1984). Extreme welding can transform an ignimbrite into homogenous solid glass very similar to obsidian (Fisher and Schmincke, 1984). It can therefore be assumed that the perlite actually originated from highly welded glass shards. The rhyolitic volcanic unit is interpreted as a welded ignimbrite. Float of volcanic spindle bombs are found at the base of the mountain, carried down by a recent landslide (Figure 3.38). While the original outcrop has not been found, it signifies that that pyroclastic activity was prevalent towards the end of the Bivane Subgroup. It is also significant as it means that the volcanic source was proximal to the locality of the Pypklipberg Mountain.

The initial activity of Phase 5.3 is represented by andesite (Appendix 1). The andesite outcrops are severely weathered and in some places appear to be affected by shearing. Field observations reveal that small (<5mm) phenocrysts have been preferentially weathered from the andesite indicating that the primary rock type may be a porphyritic andesite.

Phase 5.3 is dominated by acid volcanicity. The rhyolite can be divided into two main types: porphyritic and banded. The porphyritic rhyolite is found at the base of a waterfall in the Agatha Tributary. The K-feldspar phenocrysts are <1mm and are set in a fine-grained, foliated, glassy matrix (Griffin, 2002). The preservation of phenocrysts suggests a low degree of welding (Cas and Wright, 1987).

The banded rhyolite has alternating layers of glass and collapsed pumice fragments. The rhyolite therefore forms part of a pyroclastic unit (Fisher and Schmincke, 1984; Cas and Wright, 1987). This flow banding forms a series of folds on a centimetre scale (Figure 3.39; Figure 3.40). This is indicative of rheomorphism or secondary mass flowage of the tuff indicating that once welding had taken place due to compaction, intergranular friction in the tuff was eliminated and the tuff was then free to flow as a coherent viscous liquid (Cas and Wright, 1987; Freundt *et al.*, 2000). Rheomorphism is commonly associated with ignimbrites and results in the stretching and boudinaging of flattened pumice fragments, the formation of fold structures on all scales and the production of features similar to those that may be produced by lava of similar composition (Freundt *et al.*, 2000). The entire rhyolite represents a pyroclastic flow deposit with varying degrees of welding. Phase 5.2 and 5.3 may form part of the same acid eruption event.

The rhyolite is overlain by andesites located at the top of the Pypklipberg Mountain (represented by CG01/45 and CG01/46 in Appendix 1). The outcrop is disrupted by vegetation and little detail is known about them. They appear to be massive.

3.1.3 Detailed investigation of feeder dyke system

A possible feeder dyke system, trending north – south, is exposed in Phase 2 in the south of the White River Section (Appendix 1). The dyke system intruded a highly vesicular (now amygdaloidal) basaltic andesite (Figure 3.41). The dyke system is composed of a central acid dyke (6m wide) that has a basic dyke (0.3-0.5m) on either side of it termed the east and west dykes (Figure 3.42).

The basic dykes have chill margins on the east side of the east dyke (Figure 3.43) and the west side of the west dyke (Figure 3.44). The lack of a chill zone on the inner margins of the eastern and western dykes suggests that they intruded first as a single entity. The central dyke has chill margins on its western and eastern margins, supporting its late stage emplacement by splitting the basic dyke into an eastern and western component (represented as dashed line on Figure 3.42). The central dyke contains phenocrysts that have a preferred orientation of north – south, and are concentrated along the east and west margins of the dyke (Figure 3.45). Flow banding is found throughout the central dyke (Figure 3.46a-b). The flow banding is generally orientated north – south, but has been distorted into folds in places. These folds have wrap-around structures that determine that the flow direction was towards the south.

3.1.4 Discussion of volcanology of the White River Section

The investigated section along the White River in the Northern Region provides a continuous example of volcanism throughout the depositional history of the Nsuze Group. The Wagondrift Formation, considered by Armstrong *et al.* (1982) to represent the earliest phase of volcanism of the Nsuze Group, is a sequence of basic to intermediate volatile-poor lava flows. As the outcrop of the Wagondrift Formation is

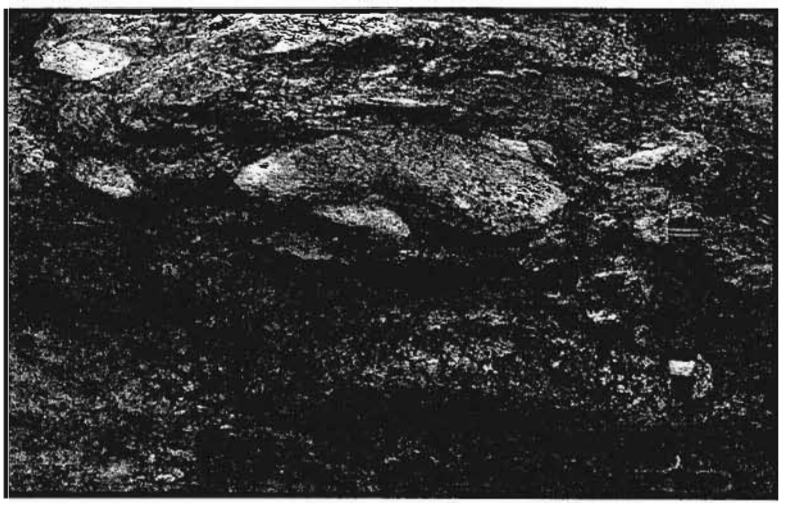

Figure 3.38 Bomb tuff, Bivane Subgroup, Pypklipberg Camp.
(27.2689 S; 31.1152 E)

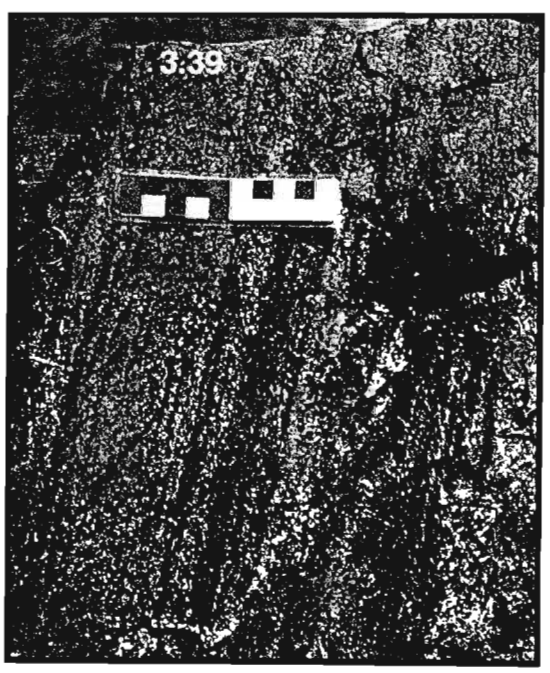

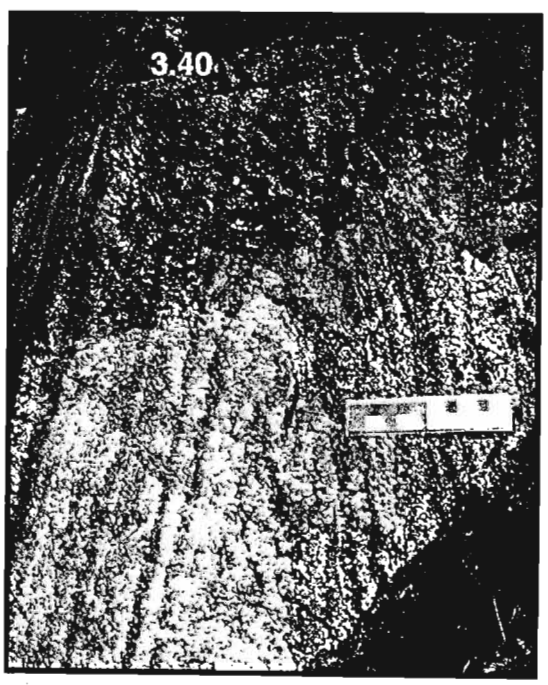

Figure 3.39 & 3.40 Folded flow banding in rhyolite, Bivane Subgroup, Agatha Tributary.
(sample CG01/100; 27.3110 S, 31.1230 E)

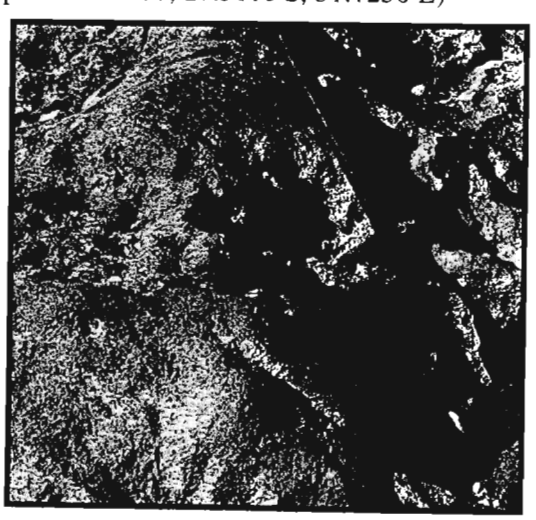

Figure 3.41 Vesicular basaltic andesite, Bivane Subgroup, White River.
(sample CG01/30; 27.2978 S, 31.0867 E)

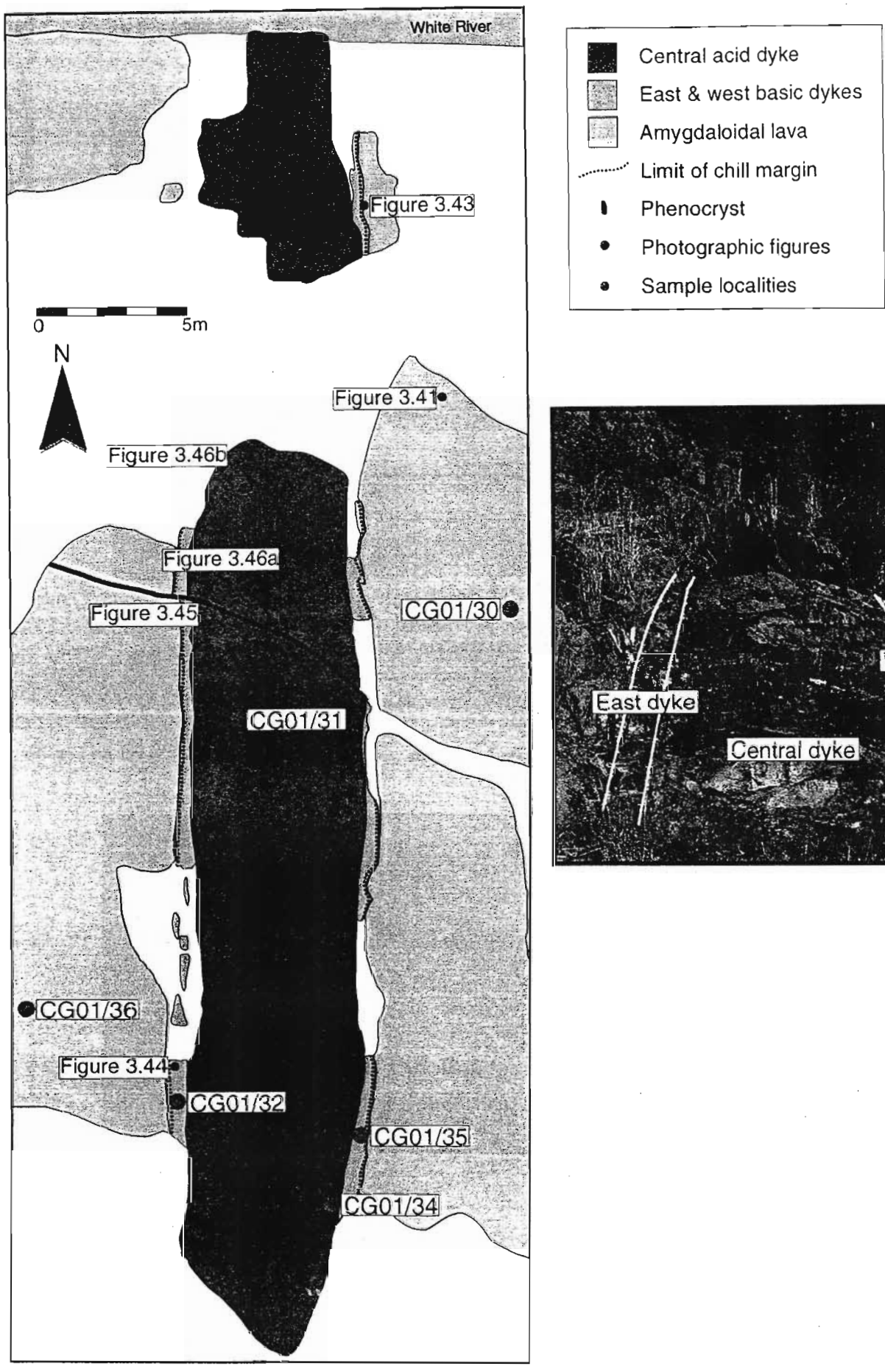

Figure 3.42 Plan of feeder dyke system, White River, showing sample and photographic figure localities. (27.2987 S, 31.0861 E)

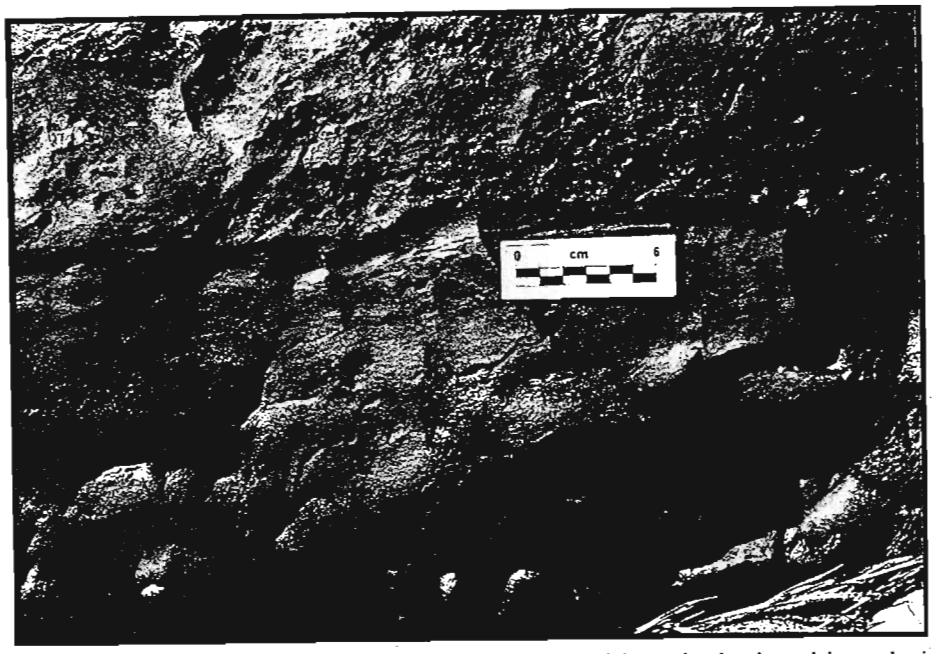

Figure 3.43 Chill margin on eastern margin of east dyke with vesicular basaltic andesite. Feeder dyke system , White River.
See Figure 3.42 for location of photograph. (Facing east)

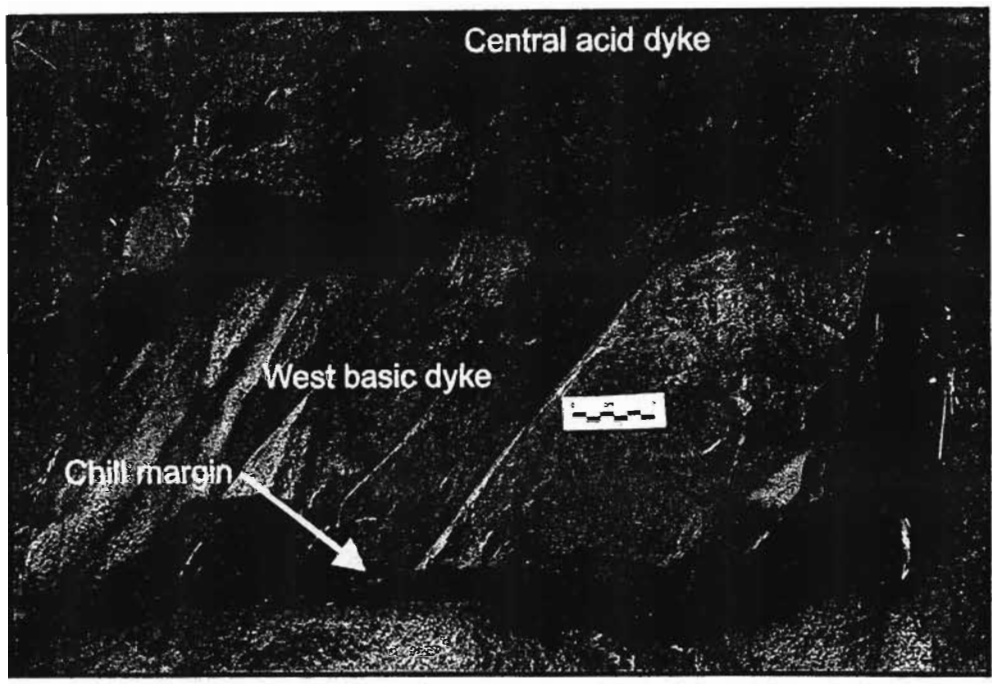

Figure 3.44 West dyke showing chill margin on western side with basaltic andesite and no apparent chill margin on eastern side with central dyke, Feeder dyke system, White River.
See Figure 3.42 for location of photograph. (Facing east)

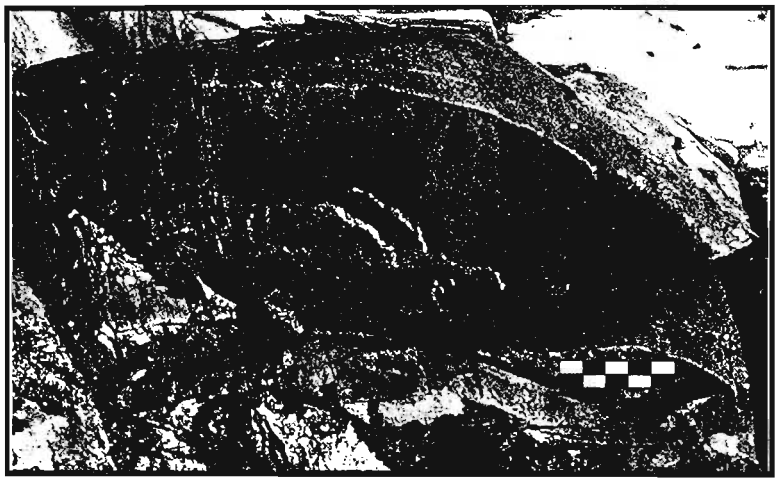

Figure 3.45 Phenocrysts orientated N-S in central dyke, Feeder dyke system , White River. See Figure 3.42 for location of photograph. (Facing south)

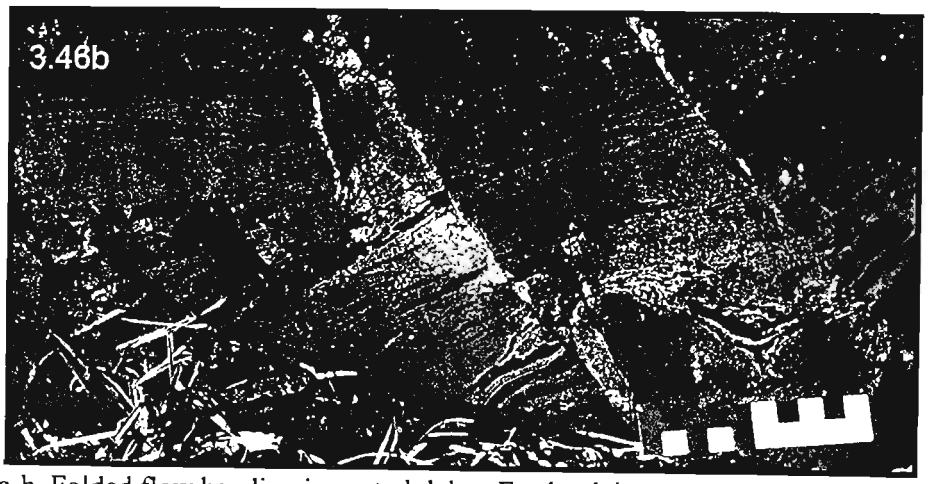

Figure 3.46a-b Folded flow banding in central dyke, Feeder dyke system, White River. See Figure 3.42 for location of photograph. (Facing east)

not laterally extensive, it can be interpreted that the succession represents a limited volcanic event, where effusion rates were low and lavas did not travel great distances from the vent. Contemporaneously clastic sediments derived from the granite-gneiss basement were being deposited by a complex fluvial system to form the Mantonga Formation (Watchorn and Armstrong, 1980). The Mantonga Formation, while predominantly sedimentary, contains lava and pyroclastic units. The proportion of volcanic units to sedimentary lithologies is greatest in the north of the White River Section and decreases southwards (Armstrong *et al.*, 1982). The volume of extrusive material was not sufficient to halt sedimentary processes. The volcanic source is therefore considered to lie to the north of the White River Section.

A marked increase in effusion rate terminated sedimentary processes and allowed for the development of a landscape completely dominated by volcanic lithologies. The Bivane Subgroup in the White River Section is 100% volcanic, although Armstrong (1980) identified sedimentary lenses to the south of the Pongola River. The initial stage of volcanism, represented by Phase 1, lacks acid compositions and pyroclastic deposits are limited to relatively thin air-fall tuffs and one laterally impersistent pyroclastic flow deposit. The eruptive source is estimated to have been greater than 1km but probably less than 5km away from the location of the White River. This is based on the lack of coarse-grained pyroclastic material but the presence of high viscosity porphyritic lavas that could not have travelled long distances from their source. A hiatus in eruption or volcanic material was being deposited elsewhere, would have resulted in the re-establishment of fluvial channels. Pillow structures formed when the localised water bodies were inundated with lava flows.

Phase 2 indicates the first occurrence of acid compositions. The acid units represent pyroclastic flows, possibly as a result of high-level fractionation of the magma under existing, possibly blocked volcanic centres. Eventually the pressure within the centre would exceed that of the plug and a violent explosion would result, depositing material over a large area through the collapse of the eruption column and the ash fall out. The occurrence of intermediate tuffs and lavas suggests new vents and fissures were constantly forming allowing the passage of less evolved compositions that had not been trapped beneath blocked craters.

Phase 3 is a complex sequence of acid pyroclastic flow deposits and intermediate lavas and air-fall tuffs. This would again suggest that fractionation beneath well established craters would allow for the development of acid compositions which would periodically erupt in violent explosions, while the intermediate lavas and tuffs would erupt out of newly developed eruptive centres. The acid pyroclastic flow deposits in Phase 3.1 are more proximal than those in Phase 3.2. If these events are related, it suggests that the volcanic source lies just north of the area marked as Phase 3.1 (Appendix 1). This is supported by the presence of Phase 4, which is situated to the west and northwest of Phase 3.1 and is stratigraphically younger. Phase 4 is an acid lava flow and must therefore be proximal to its source. It may therefore form the lava flow that followed a pyroclastic eruption and may have sealed that specific crater.

If the dominant crater in the northern area of the White River Section was plugged by the rhyolitic lava flow of Phase 4, a subsidiary vent may have formed to allow the intermediate eruption of Phase 5.1. The presence of pyroclastic surge deposits, vesicular tuffs and lapilli suggest that the vent was <3km from the Beki-Beki Tributary locality of Phase 5.1 (Appendix 1). Acid pyroclastic flow deposits dominate Phase 5.2 and Phase 5.3. The presence of a bomb tuff in Phase 5.2, indicates a very proximal source of <1km.

Overall the White River Section represents a maturing volcanic crater field, where intermediate lavas erupted with minor explosions resulting in ash deposits. Fractionation beneath older, possibly plugged, craters resulted in the development of acid magmas, which exploded violently resulting in huge eruption columns of ash, pumice and glass. The collapse of these eruption columns resulted in pyroclastic flow deposits covering the White River Section area. New craters and fissures developed that allowed for the continued passage and eruption of intermediate composition lava and ash. A complex multi-level magma chamber system would allow for the differing levels of fractionation observed within the Bivane Subgroup volcanic rocks.

3.1 WHITE MFOLOZI INLIER

The White Mfolozi Inlier is present in the Central Region of the Pongola Supergroup, where the lithologies are best exposed along the White Mfolozi River (Figure 1.1). The sedimentary Mantonga Formation, the volcano-sedimentary Bivane Subgroup and the overstepping sedimentary Ozwana Subgroup constitute the Nsuze Group stratigraphic units present in the White Mfolozi Inlier. The Bivane Subgroup is divided into the lower volcanic Nhlebela Formation, the middle sedimentary White Mfolozi Formation and the upper volcanic Agatha Formation. For the purposes of this study, the focus lies with the volcanic sequences of the Nhlebela and Agatha Formations.

3.1.1 Nhlebela Formation

The Nhlebela Formation of the White Mfolozi Inlier conformably overlies the older sedimentary Mantonga Formation (Figure 3.47). The Nhlebela Formation can be divided into a lower 70m thick hydroclastic lava type and an upper 60m thick amygdaloidal lava type.

Brecciated fragments and pillow structures dominate the oldest hydroclastic lava flow units (Figure 3.48). The pillow structures have highly altered reaction rims. Angular fragments are found between the pillows. Hydrothermal alteration is extensive. The water involved in the early stages of eruption is likely to have been the same fluvial system that deposited the sediment of the Mantonga Formation in the area.

The transition from a slightly subaqueous to a completely subaerial environment is gradational. The intermittent phase exhibits highly vesicular pillow structures but there are no hydrothermal altered fragments found between them. Instead dense chilled lava is present between the pseudo-pillow structures. The pillows themselves do not have reaction rims (Figure 3.49). This would suggest that these structures might in fact be lobate flows or toes of a subaerial eruption.

A thin mafic fine-grained intrusion is found in the upper flow units of these fragmented lavas. The intrusion is approximately 1.5m wide and a broken bridge is present (Figure 3.50). The dyke is orientated northeast – southwest. It is fine-grained and has a chilled appearance.

A breccia is present at the top of the hydroclastic lava flows (Figure 3.51). It has a limited lateral extent of approximately 150m^2. The breccia is no more than 5m thick, although the vertical extent of the outcrop appears to be variable. The heterolithic clasts are angular to subrounded glass, basaltic lava and highly altered clasts. The matrix supported clasts range in size from 5cm to 20cm in diameter and are set in a fine-grained matrix. There is no obvious sorting or grading visible in the breccia. The breccia has a gradational contact with the surrounding volcanic rock (Figure 3.52). It is likely that this breccia represents a lahar or volcanic debris flow. Cas and Wright (1987) classified a matrix supported breccia with angular to subrounded clasts as being representative of cohesive debris flows and lahars. The lack of gas escape pipes and other hot state emplacement structures and the basaltic composition of the deposit exclude it from having been formed by a pyroclastic flow (Cas and Wright, 1987). Lahars follow pre-existing valleys, which may explain the limited outcrop pattern (Fisher and Schmincke, 1984). In order for a lahar to form, water must be added to loose debris, which is then disturbed. The involvement of water in the lavas underlying the lahar is evident, and it can therefore be assumed that water was present to form the debris flow. The disturbance that caused the debris to flow may have been directly related to volcanic activity i.e. eruption during heavy rains or indirectly related to an eruption i.e. earthquakes or expansion of volcanic centre causing an avalanche (Fisher and Schmincke, 1984).

The amygdaloidal lava flow units form the upper 60m of the Nhlebela Formation. These lava flows have densely vesicular flow tops and massive interiors (Figure 3.53). The vesicles have been infilled by secondary fluids to form amygdales after solidification of the lava. The vesicles are of two populations, small and spherical and large and irregular. Flow surfaces are not preserved which makes conclusions about the nature of the volcanism difficult. The middle zones of the lava flows are massive, rarely exhibiting even columnar jointing. Vesicles are observed where the bases of lava flow units are exposed. Shearing has deformed the youngest lava flows of the Nhlebela Formation and primary volcanological structures have been destroyed.

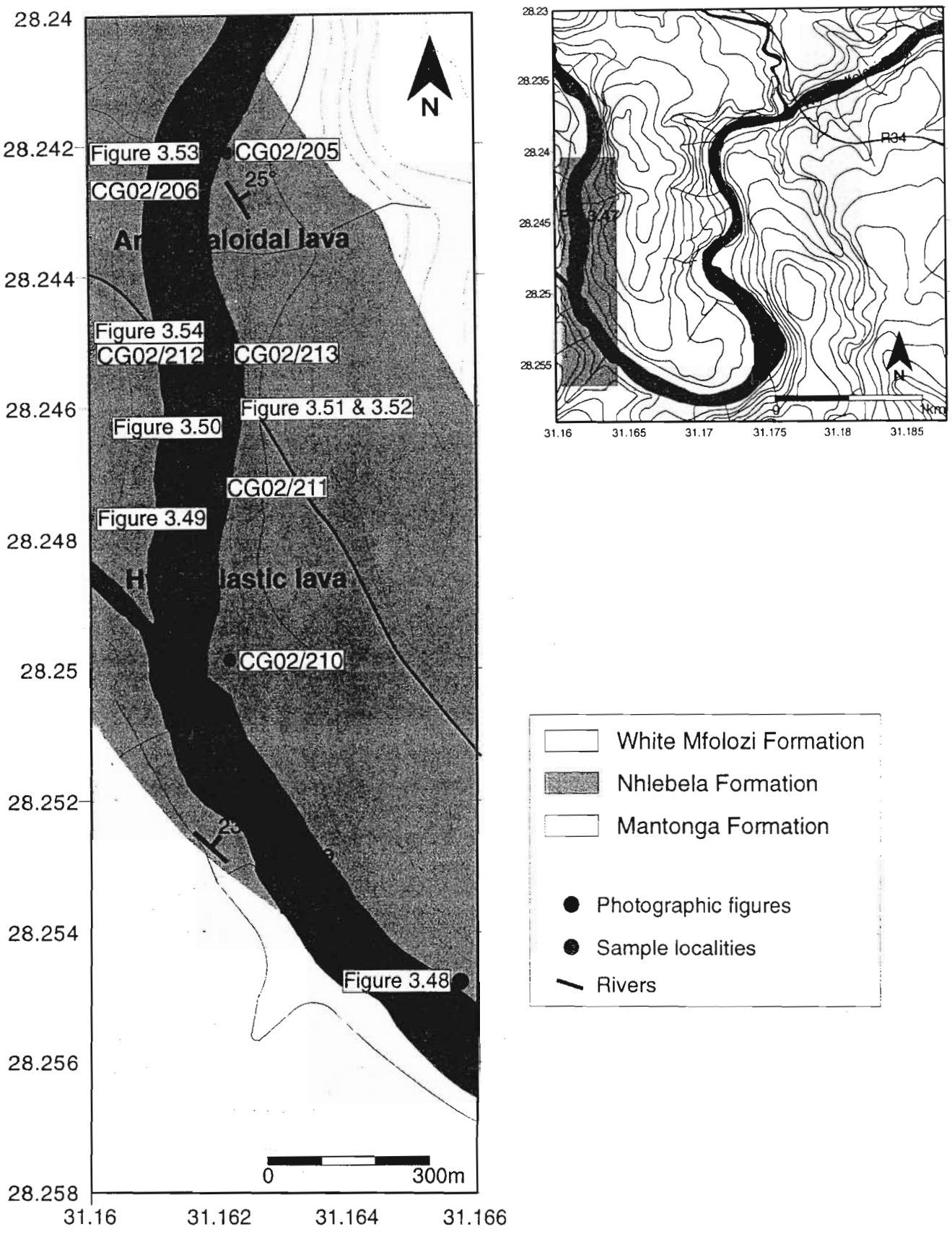

Figure 3.47 Map of Nhlebela Formation, along the White Mfolozi River in the White Mfolozi Inlier, showing sample and photographic figure localities.

Figure 3.48 Hydroclastic breccia between two pillow structures, Nhlebela Formation, White Mfolozi River. See Figure 3.47 for location of photograph.

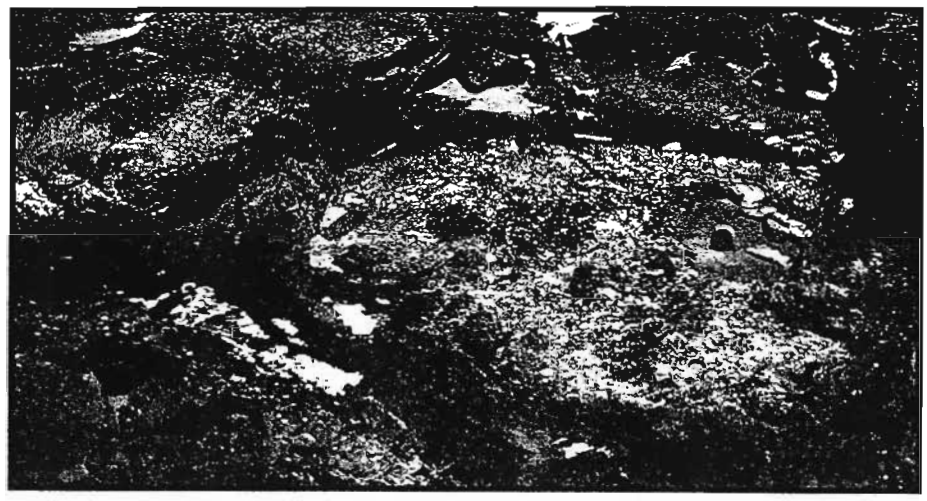

Figure 3.49 Vesicular pillow structures with dense chilled margins, Nhlebela Formation, White Mfolozi River. See Figure 3.47 for location of photograph.

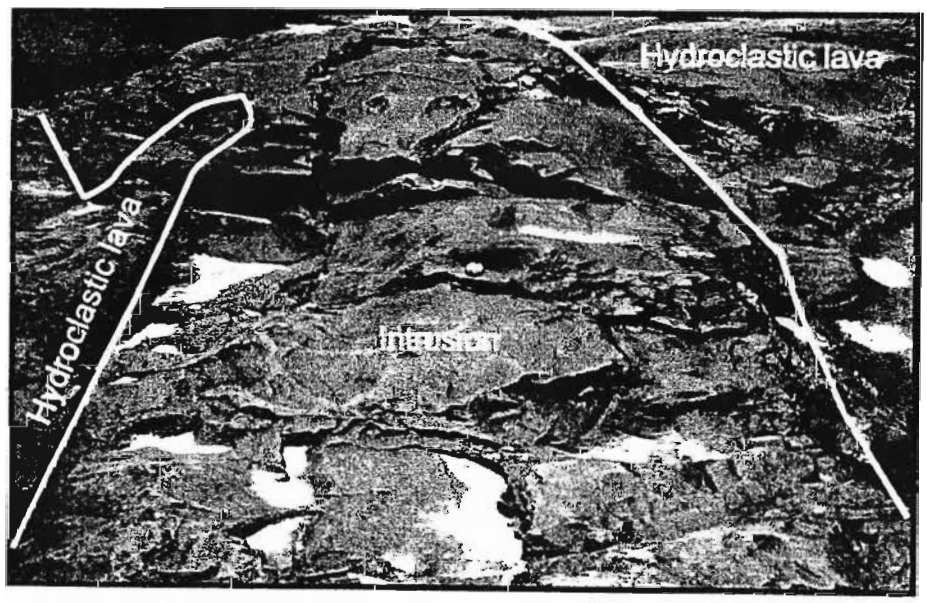

Figure 3.50 Intrusion into hydroclastic lava, Nhlebela Formation, White Mfolozi River. See Figure 3.47 for location of photograph.

Figure 3.51 Breccia formed by pyroclastic debris flow, Nhlebela Formation, White Mfolozi River.
See Figure 3.47 for location of photograph.

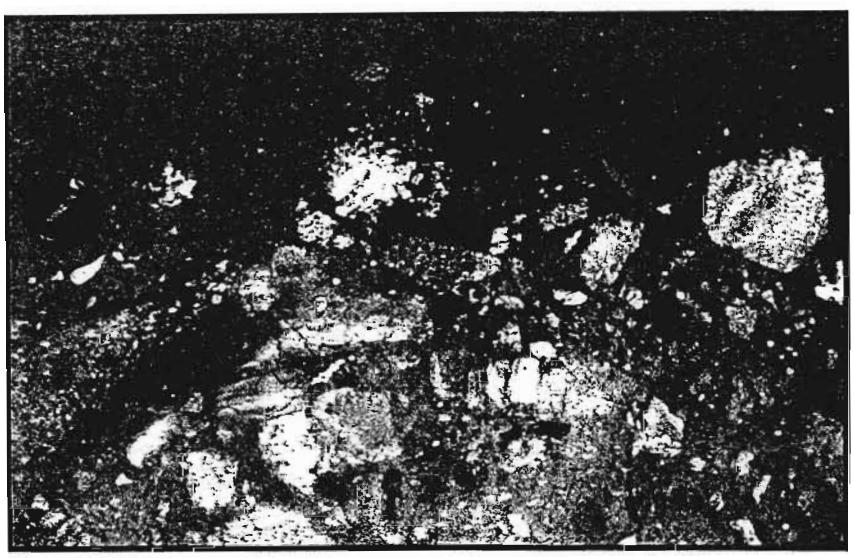

Figure 3.52 Gradational contact of breccia with surrounding volcanic unit, Nhlebela Formation, White Mfolozi River.
See Figure 3.47 for location of photograph.

A zone of banding, sub-horizontal to the flow top, is observed near the top of a lava flow unit near the base of the amygdaloidal lavas. These lines may represent strand lines (Figure 3.54). Williams and McBirney (1979) described strand lines as lines marked onto the sidewalls of an active lava tube by the fluctuating level of flowing lava within it.

The average thickness of the lava flows of the Nhlebela Formation is approximately 5-7m thick. This is too thick for traditional compound pahoehoe lavas. It is therefore possible that these lavas were either tube pahoehoe lava flows, where the flowing lava thermally eroded into underlying units, or inflated lava flows, where a new influx of lava causes the crust to rise (Wilmoth and Walker, 1993).

3.1.2 Agatha Formation

A section of the Agatha Formation exposed along the White Mfolozi River, in the White Mfolozi Inlier, has been studied in detail. The volcanological structures preserved in this riverside outcrop provide an excellent insight into the nature of the Nsuze Group volcanism in this area (Figure 3.55; Figure 3.56). The lavas under investigation exhibit textures and structures characteristic of basaltic to basaltic andesite compositions and are consistent with the geochemical classification (see Chapter 5 Geochemistry). Two detailed traverses were undertaken. The first traverse was along the northern bank of the White Mfolozi River, and covered a horizontal distance of 285m in an east-northeast direction, approximately parallel to the average dip direction (Figure 3.55; Figure 3.56). The second traverse follows the southern bank of the White Mfolozi River and covers a horizontal distance of 375m in a northeast direction, 15° off the average dip direction of the strata (Figure 3.55; Figure 3.56). Therefore approximately a horizontal distance of 300m between Traverse 1 and 2, and 150m horizontal distance upsection of Traverse 2 are not included in the detailed description. The exclusion of these areas is due to the poor condition of outcrop or lack of good exposure. General observations have however been made and will be included in the overall observations of the Agatha Formation.

It is difficult to determine the lateral extent of the lava flows as well as their relationship to one another i.e. whether the units are part of the same flow field or subsequent eruption events. The exposed area along the White Mfolozi River is not extensive enough to determine the true lateral nature of the volcanism, but provides a stratigraphic representation of the volcanicity. The tilting of the lava flow units from their original position and subsequent erosion has resulted in numerous well exposed outcrops that represent the entire section of a flow from base to surface. This provides a unique opportunity to investigate the nature of the volcanism of the Nsuze Group in the White Mfolozi Inlier.

3.1.2.1 Structures and textures preserved in lava units of Traverse 1

Four different types of lava flows can be identified in the 300m section of the Agatha Formation studied in detail along the White Mfolozi River (Figure 3.56). These types are hydroclastic breccia / aa lava combination, aa lava, pahoehoe lava and massive lava.

The basal contact of the Agatha Formation with the underlying sedimentary White Mfolozi Formation shows structures that may represent pèpèrites (Figure 3.57). Pèpèrites result when lava or magma and poorly consolidated, often wet sediment come into contact. This results in the melting and mixing of the two components (Batiza and White, 2000). This would therefore suggest that the Agatha Formation volcanism terminated the White Mfolozi Formation sedimentation and the relationship between the two processes is for the large part conformable. It is also significant that there are no intercalated sedimentary units at the base of the Agatha Formation.

The oldest flow units (units 1-4) of the Agatha Formation are highly fragmented and brecciated (Figure 3.58) as well as exhibiting pseudo-pillow structures. These lower flow units are 4-7m thick. Pseudo-pillow structures are fragments of broken lava that show rim alteration and preserved core features similar to those of true sub-aqueous volcanism pillows. Where lava squeezed between the breccia blocks, lava ribbons have been preserved (Figure 3.59). Large irregular vesicles and amygdales (generally filled with quartz) represent the preservation of gas blisters within the lava flows. The blocky and fragmented nature of the surface of the lava units suggest that while brecciation may have been partly due to interaction of hot lava and cold water, the nature of the lava itself may also have been responsible for the aa lava

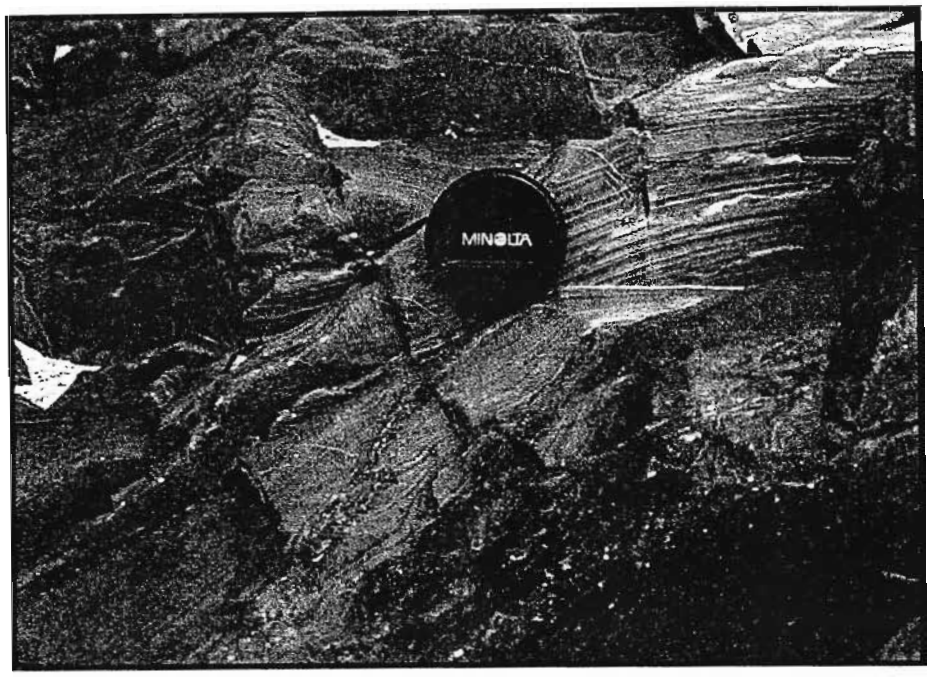

Figure 3.53 Strand lines in amygdaloidal lavas, Nhlebela Formation, White Mfolozi River. See Figure 3.47 for location of photograph.

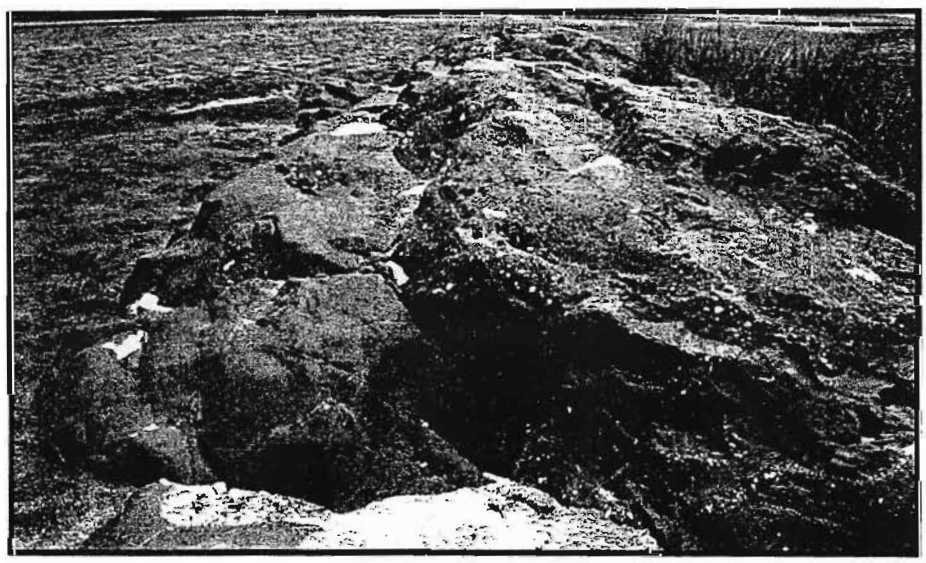

Figure 3.54 Massive interior and vesicular flow top of an amygdaloidal lava, Nhlebela Formation, White Mfolozi River. See Figure 3.47 for location of photograph.

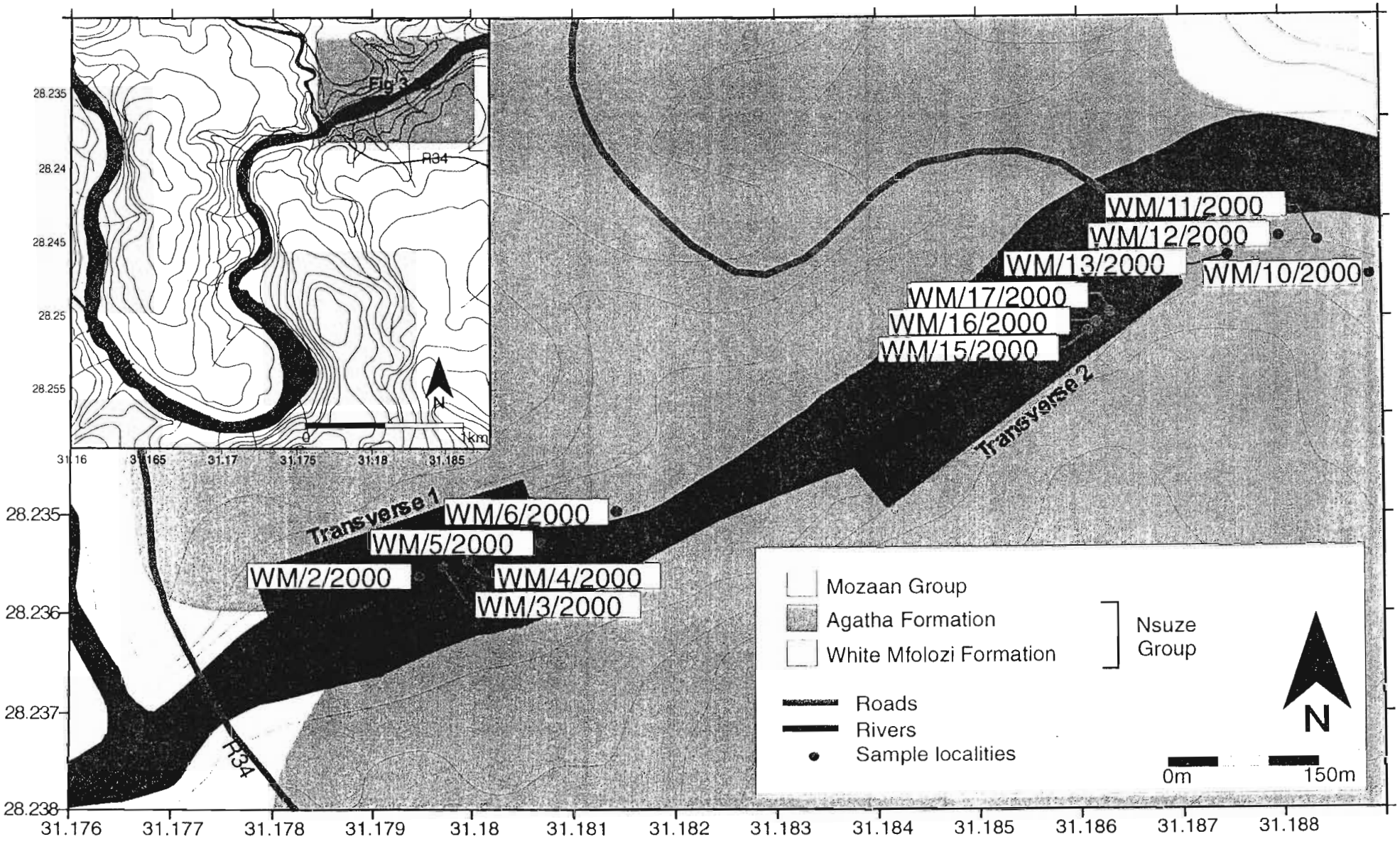

Figure 3.55 Map of the Agatha Formation, along the White Mfolozi River in the White Mfolozi Inlier, showing sample localities and location of Traverse 1 & Traverse 2.

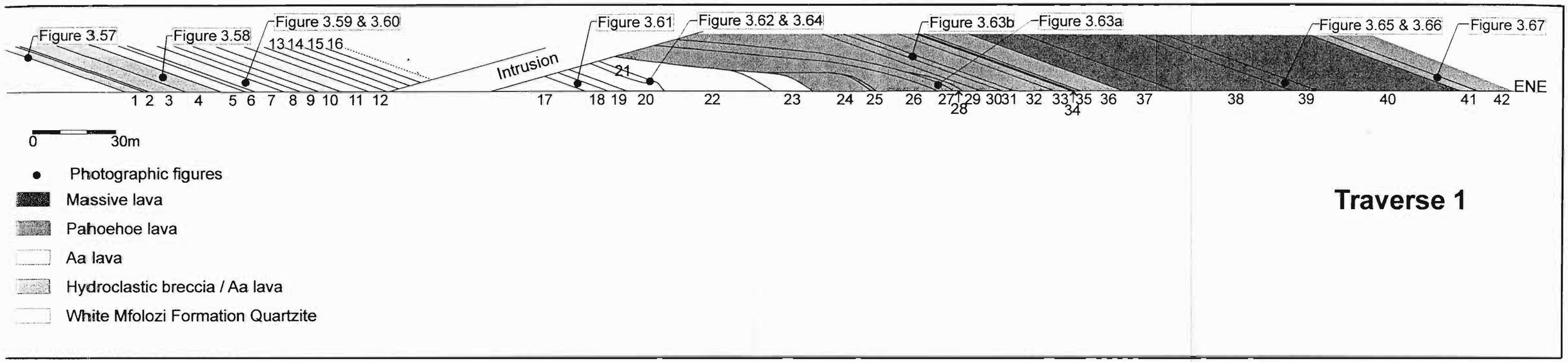

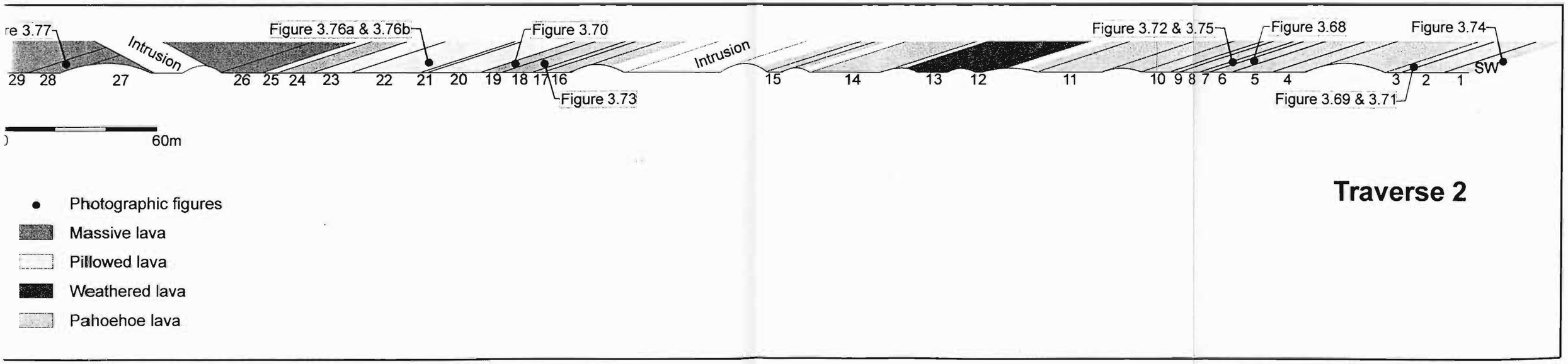

3.56 Schematic sections along traverse 1 and traverse 2, showing different lava types and photographic figure localities.

Figure 3.57 Peperite on contact between White Mfolozi Formation and Agatha Formation, White Mfolozi River. See Figure 3.56 for location of photograph.

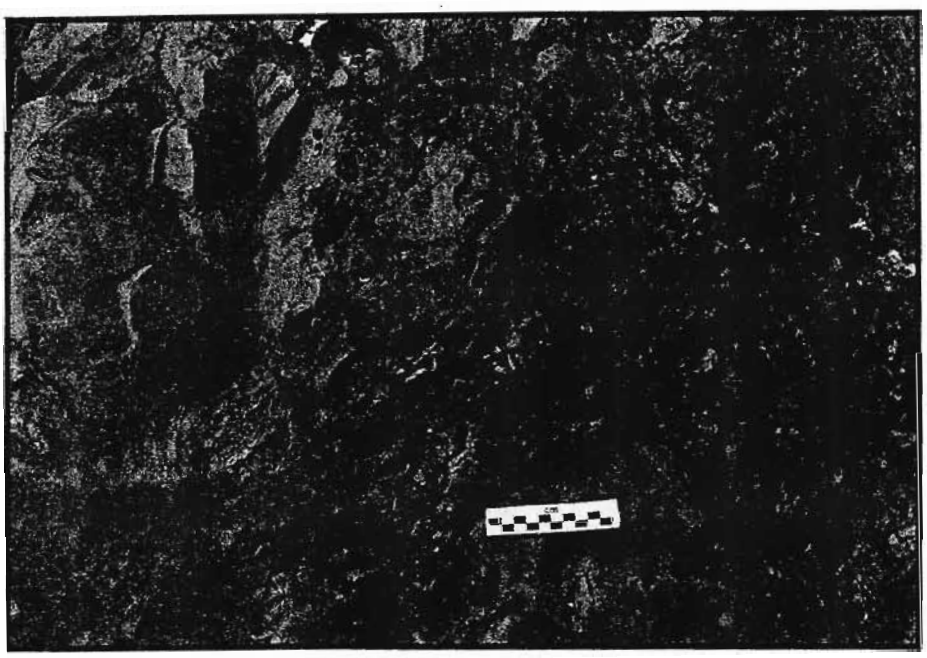

Figure 3.58 Highly fragmented flow surface, Agatha Formation, White Mfolozi River. See Figure 3.56 for location of photograph.

surface of the lower lava flow units (Figure 3.60). A thin clinkered flow surface of relatively small fragments is indicative of proximal aa lava (Rowland and Walker, 1987). A true cross section through aa lava depicts a massive interior with blocky joints (Cas and Wright, 1987). These lower lava units are therefore possibly a combination of hydroclastic and aa lava resulting in breccia with the presence of hydrothermal alteration suggesting an aqueous influence. The thickness of the flow units (4-7m) and the presence of elongated gas blisters also support the aa nature of the erupting lava (Cas and Wright, 1987). The altered nature of the lava fragments and absence of true pillow lavas suggests that the lava flows were erupted into a wet yet sub-aerial environment, possibly the lagoon and shoreline environment proposed for the White Mfolozi Formation (Matthews, 1967).

The transition from hydroclastic breccia / aa combination to aa lava is not clearly defined and hydroclastic fragments occur in flow units throughout the aa lava zone. The lava flows from unit 5 to unit 23 exhibit a more typical aa lava structure i.e. a massive interior with rough fragmented flow top (Cas and Wright, 1987) (Figure 3.61). Flow units range from 3m to more than 10m thick (although thicker units are recorded, the poor exposure may mean that these thick units are actually composed of thinner flows) (Figure 3.56). Features of the aa lavas include columnar jointing in the massive interiors of the flow units and gas blisters preserved as large irregular vesicles and amygdales. Clinkered flow surfaces are not well preserved but field observations indicate that the flow tops were relatively thin suggesting the locality to be proximal to the original volcanic source (Rowland and Walker, 1987). The flow units of the lower Agatha Formation appear to be simple rather than compound although this can only be said with certainty on a local scale.

The nature of the volcanism would have been the same as the hydroclastic breccia / aa lava combination except the environment of eruption would not have been influenced by a subaqueous component. This may be a local observation, as the previous flows would have lifted the topography away from any local water level. This is not to say that the interaction of these aa flows with aqueous bodies did not take place in other unexposed areas of the flow units.

The lava must have been relatively viscous at this point to form aa lava. If the viscosity was high enough to allow aa formation, this would suggest that effusion rates from the volcanic centre were high (Cas and Wright, 1987). This would be in line with the initial phase of eruption from a dormant volcanic centre. The apparent simple nature of the aa lava flow units would suggest viscosity of between 10^5 – 10^7 poise (water = 1poise) and an effusion rate greater than $10^1 m^3 s^{-1}$ (Walker, 1971). Flows of this character generally cover long distances (Cas and Wright, 1987).

The first occurrence of a pahoehoe lava surface is at the top of unit 20 (Figure 3.62). This is however not taken as the top of the aa lava zone as several flows units overlie it that are typical aa lava units. Flow unit 20 and its exposed interaction with unit 21 show the brief formation of compound pahoehoe lavas (Figure 3.56). This may be due to a drop in effusion rate of the erupting volcanic centre. The evidence for pahoehoe and aa features on the same lava surface suggests that this may represent the critical transition from pahoehoe to aa lava formation where sufficient cooling and crystallization had occurred to raise the viscosity (Cas and Wright, 1987). The irregular appearance of the flow surface of unit 20 suggests that the lava flowing over the steeper areas would have experienced higher rates of shear therefore allowing the development of aa lavas before those areas of the lava flowing over shallower gradients (Cas and Wright, 1987).

The transition from aa to pahoehoe surfaces of the flow units is not definite although attempts to form pahoehoe lava are evident on the surface of unit 24 and are present in some form or another in all younger flows until unit 36 (Figure 3.63a-b). It is important to bear in mind that the surface of a lava flow cannot change from aa into pahoehoe (Cas and Wright, 1987) and that the main transition discussed here is preserved in separate and subsequent flow units.

The lava flows develop a compound flow pattern from unit 22. The complexity of the relationships between the lava flows seems to increase from this point to unit 30 suggesting a compound nature to the flows. This would indicate a decrease in effusion rate, a decrease in viscosity or most probably a combination of both factors. This observation is however limited due

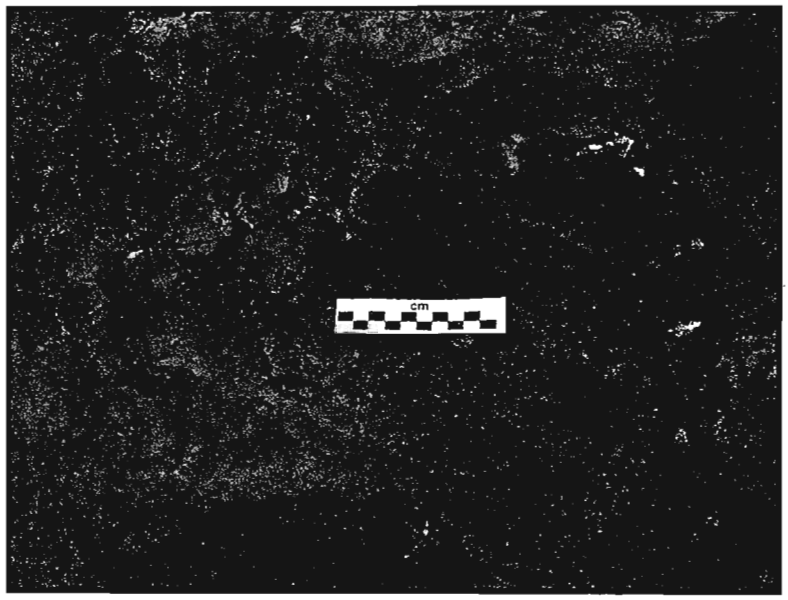

Figure 3.59 Lava ribbons in fragmented lava, Agatha Formation, White Mfolozi River. See Figure 3.56 for location of photograph.

Figure 3.60 Fragmented aa flow top, Agatha Formation, White Mfolozi River. See Figure 3.56 for location of photograph.

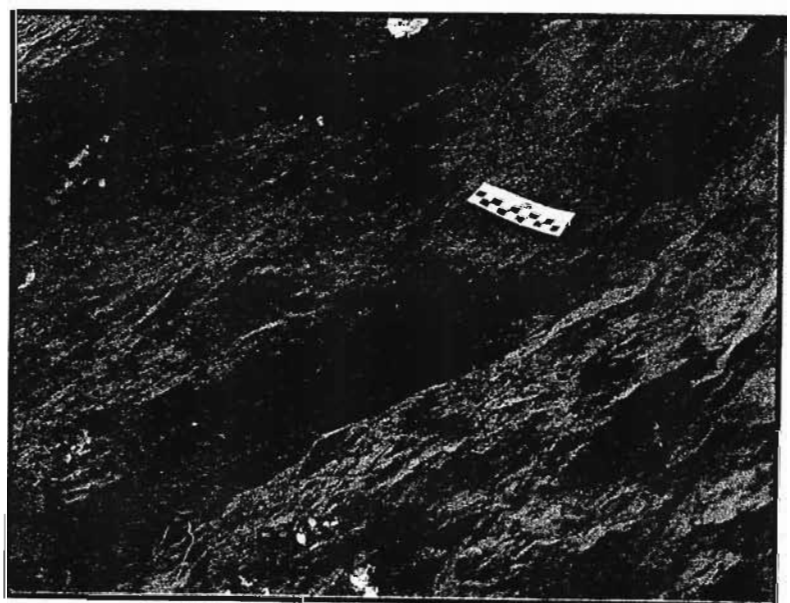

Figure 3.61 Irregular fragmented flow surface, Agatha Formation, White Mfolozi River. See Figure 3.56 for location of photograph.

Figure 3.62 Pahoehoe flow surface, Agatha Formation, White Mfolozi River. See Figure 3.56 for location of photograph.

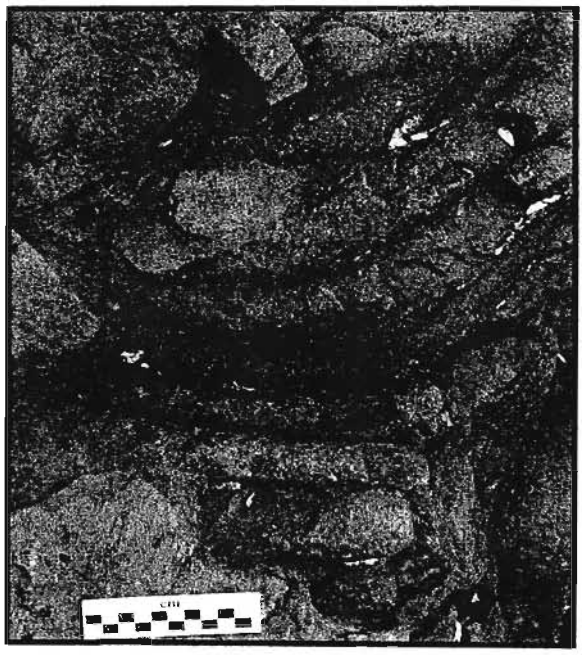

Figure 3.63a Pahoehoe flow surface, Agatha Formation, White Mfolozi River. See Figure 3.56 for location of photograph.

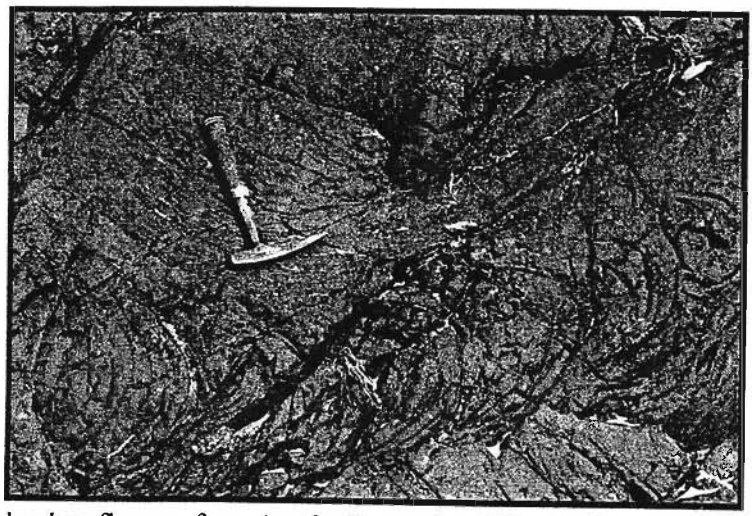

Figure 3.63b Pahoehoe flow surface, Agatha Formation, White Mfolozi River. See Figure 3.56 for location of photograph.

to the lack of well-preserved outcrop in the area. The pahoehoe lava surfaces are remarkably well preserved which suggests that while the effusion rate from the vent did decrease, it did not reduce sufficiently to expose flow surfaces for long periods of time to allow weathering to take effect (Cas and Wright, 1987). Structures present in the crust of a flow surface are evident at the top of unit 20 (Figure 3.64). The pahoehoe surface is underlain by a 2-3cm zone of small columnar joints, which in turn is underlain by a vesicle zone. The boundary of the vesicle and jointed zones shows evidence of shearing indicating movement of the crust relative to the underlying lava. This is consistent with the behaviour of pahoehoe lava flows (Cas and Wright, 1987). The internal structure of the pahoehoe flows is generally massive, although pseudo-pillows and brecciated areas are not uncommon. This is likely to be as a result of the presence of water, possibly collected in depressions in the palaeotopography, during a brief hiatus in eruption activity. The presence of froth zones within the lower pahoehoe lava flows (units 24 and 25) and the dominance of small, regular, spheroidal vesicles is typical of pahoehoe lava flows, which may contain between 20 – 50% vesicles (Cas and Wright, 1987).

The thickness of the pahoehoe flow units varies from <1m to 4m. Two flow units i.e. units 26 and 32, are approximately 8-10m thick. This is unusual for pahoehoe lava flows (which are generally <2m thick, Cas and Wright, 1987) and it is possible that the thicker units may in fact represent a series of thinner flows but individual flow surfaces may not be exposed.

The pahoehoe lava type present in Traverse 1 appears to be ropy pahoehoe. While flow directions can be determined by using the convex trains of the ropes, the extent of the exposed surfaces is not sufficient for palaeoflow evaluation as some pahoehoe ropes may have formed due to localised eddies on the flow surface (Cas and Wright, 1987).

Massive lava flows (units 37-40) range from 8m thick to >20m thick. These flows may have been formed as a result of aa flows, where the surface of the lava has not been preserved, but the massive columnar jointed interior is the result. The thick flow units may represent thinner units, where the flow surfaces are not exposed or are difficult to determine due to the limited outcrop and the presence of large-scale debris adjacent to the White Mfolozi River. Unit 37 is characterised by exfoliation weathering resulting in the poor quality of preservation of primary flow structures. Gas blisters and vesicles are spread throughout the massive lava units. A smooth glassy lava toe overlying another smooth glassy flow is preserved in unit 39 (Figure 3.65). No pahoehoe is present although limited areas of breccia occur. Large vesicles and amygdales can be found near the surface of the flow. Breakout features, where lava broke through the surface of the crust, are also preserved in unit 39m (Figure 3.66).

Unit 41 is a thin flow of approximately 3m thick and has a pahoehoe flow surface (Figure 3.67). It is possible that the overlying flows returned to a thin pahoehoe lava stage as the effusion rate of the volcanic centre decreased.

3.1.1.1 Structures and textures preserved in lava units of Traverse 2

Traverse 2, on the southern bank of the White Mfolozi River, represents a section through the upper lava flow units of the Agatha Formation in the White Mfolozi Inlier (Figure 3.55; Figure 3.56). The lava flows of Traverse 2 can be divided into three general types, pahoehoe, pillowed and massive. By far the most abundant lava flow type is pahoehoe lava. Weathered lava is found within the pahoehoe lavas, and is differentiated because no primary structures are preserved. The pillowed lava flow units are found near the top of the pahoehoe unit. The uppermost lava flows are of the massive type and generally contain few textures or structures.

The pahoehoe flow type is evident in flow units 1 to 19 of Traverse 2 along the White Mfolozi River (Figure 3.56). The pahoehoe flow type units do not show well-developed ropey pahoehoe texture as seen in Traverse 1. If the flow surfaces are preserved, they show a gentle undulatory surface with a rough and rugged texture. It is therefore assumed that either the ropey lava surfaces were eroded prior to subsequent burying eruptions or that the flow texture itself has changed, indicating differing conditions. The latter scenario is supported by observations of lava flows on Mount Etna by Kilburn (1990) and Hawaii by Rowland and Walker (1988). The flow surfaces from Traverse 2 resemble what Kilburn (1990) described as ripply pahoehoe, and Rowland and Walker

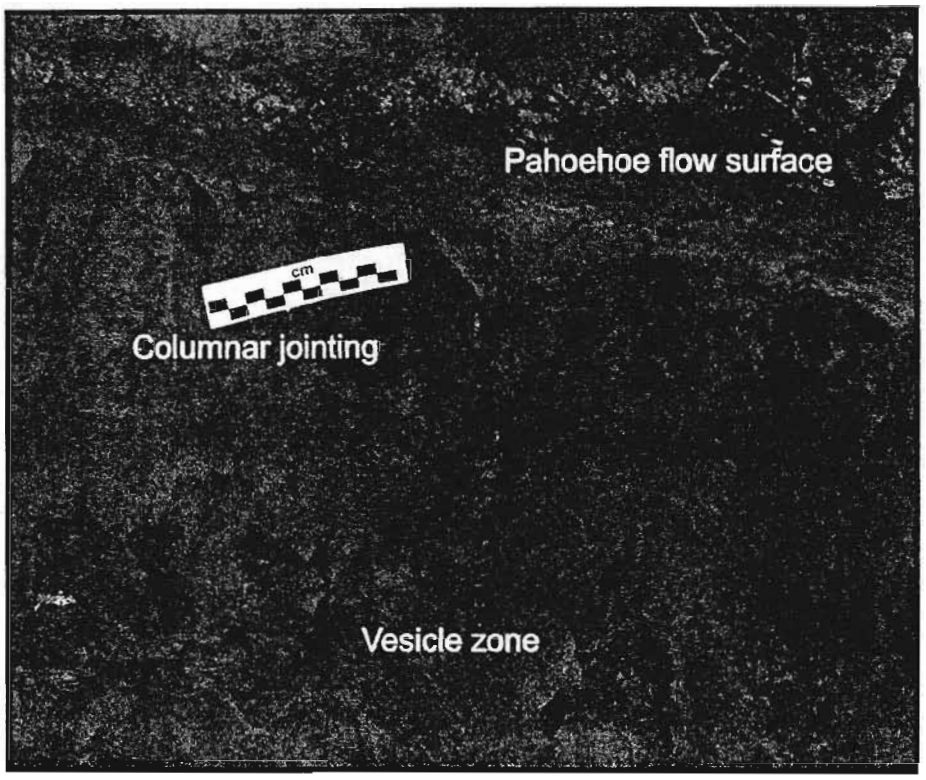

Figure 3.64 Lava flow crust showing pahoehoe surface, columnar jointing and vesicle zones. Agatha Formation, White Mfolozi River.
See Figure 3.56 for location of photograph.

Figure 3.65 Smooth glassy lava toe over another smooth lava flow, Agatha Formation, White Mfolozi River. See Figure 3.56 for location of photograph.

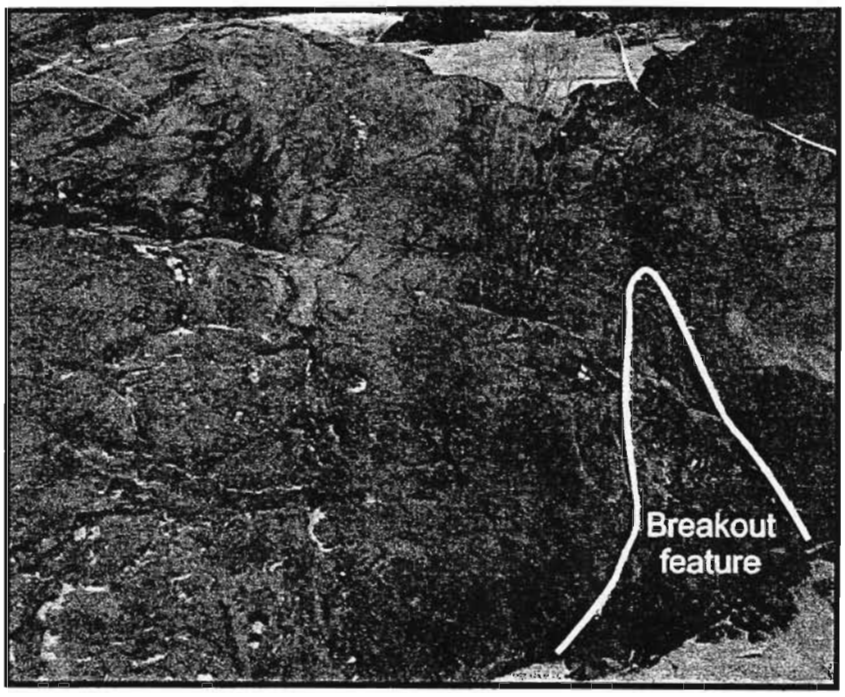

Figure 3.66 Breakout feature on flow surface, Agatha Formation, White Mfolozi River. See Figure 3.56 for location of photograph.

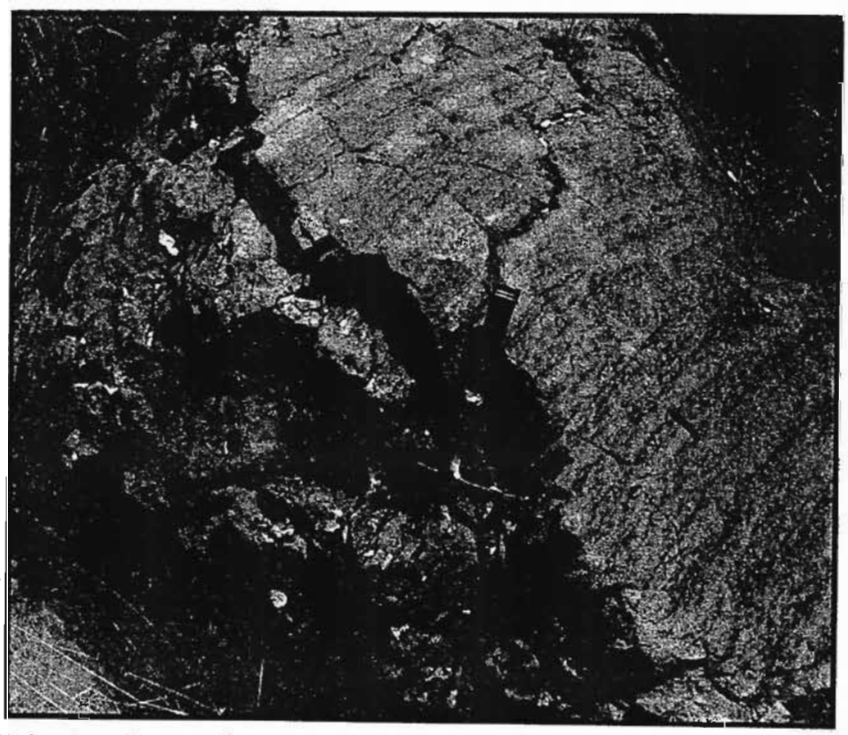

Figure 3.67 Pahoehoe flow surface, Agatha Formation, White Mfolozi River. See Figure 3.56 for location of photograph.

(1988) termed rough and toothpaste pahoehoe (Figure 3.68). The texture resembles asymmetrical ripples found in sedimentary rocks and is thought to have formed by irregular tearing of the exposed crust of the lava flow (Kilburn, 1990). This results in a rugged appearance on the surface of the emerging lava flow (Kilburn, 1990). This type of lava flow surface is considered by Rowland and Walker (1988) to represent a transitional phase between pahoehoe and aa lava. This type of lava flow surface forms from a late breakout in a pahoehoe flow field. The rough pahoehoe surface therefore forms on flow surfaces where the lava is slightly more viscous than the lava that formed ropey pahoehoe lava (Rowland and Walker, 1988). Toothpaste lava forms from more viscous lava than that which results in rough pahoehoe lava surfaces. The surface of toothpaste lava is covered with spines and longitudinal grooves and ridges (Rowland and Walker, 1987). The spinose features have long since been eroded away but the rough, slightly undulatory surface of the lava flow units remains. While a relatively high viscosity is required to form toothpaste lava, the characteristic that distinguishes it from otherwise forming aa lava is the slow flow rate of the lava. The torque is therefore not sufficient to tear the skin apart to form clinker and rubble (Rowland and Walker, 1987). In order for a low flow rate to result from an eruption either effusion rates must be low or the gradient over which the lava is flowing must be gentle (Rowland and Walker, 1987). Flow units associated with rough pahoehoe and toothpaste lava are generally thicker than traditional pahoehoe lava flows and the formation of lava tubes is rare. This is thought to be due to the shallowly inclined surface on which this type of lava flow forms (Rowland and Walker, 1987).

Apparent ropey pahoehoe is found as isolated patches within the rough / ripply pahoehoe and toothpaste lava (Figure 3.69). This can be seen on the surfaces of approximately 10% of the pahoehoe type lava flow units. This may be construed as squeeze ups that have pushed through the surface of the tearing rough / ripply pahoehoe and toothpaste lava flow tops. This has resulted in glassy pahoehoe toes protruding through the rough flow surface. These features are typically associated with small regular shaped vesicles (1-3mm diameter) in the thin crust, which can be seen in the flow surface examples of Traverse 2. The vesicles have since undergone secondary infilling to form predominantly epidote and quartz amygdales. Glassy, smooth roll over structures are also found on certain flow surfaces (Figure 3.70).

The flow tops of the pahoehoe type lava flow units are generally marked by a sudden increase in the amount of vesicles present (Figure 3.71). The flow top of the lava flow units is considered to start at the first indication of dense vesicle accumulation up to and including the lava flow surface. The flow tops are generally highly vesicular containing two distinct size populations of vesicles. Small spherical vesicles are less than 3mm in diameter and are densely packed. The large irregular vesicles are generally between 5cm and 20cm in long axis. It has been observed that the large vesicles are concentrated at the base of the flow top, exhibiting a decrease in vesicle size upwards towards the flow surface. The flow surface is dominated by small spherical vesicles (Figure 3.72). Densities of small vesicles are so great on certain flow surfaces that they were most likely frothy prior to solidification. On the basis of mathematical modelling, Sahagain (1985) determined that the volume of vesicles preserved at the flow surface is representative of the minimum initial vesicularity of the lava flow. Wilmoth and Walker (1993) recorded a similar observation that the upper crust of a lava flow represents the volume of gas bubbles present in the lava when it emerged from the vent or tube system. Flow 18 exhibits large vesicles that are not present in any of the other flows. The vesicles are large 15-20cm wide and 10-15cm high (Figure 3.73). The tops of the vesicles are convex while the bottom surface is concave. Migration trails are evidence at the two points where the convex and concave surfaces meet. These migration trails are generally fractures and thin elongated cavities that have formed perpendicular to the surface of the lava flow as the large gas bubble rose through the liquid lava. McMillan *et al.* (1987) have described similar structures, termed domed vesicles, in the Cohasset Flow of the Grande Ronde Basalt in south-central Washington, U.S.A. The domed vesicles identified in the Agatha Formation along the White Mfolozi River fall within the size and shape range documented by McMillan *et al.* (1987). These domed vesicles are formed by relatively few nuclei that experience exceptional growth by accumulation of smaller gas bubbles. The domed shape of the vesicles is formed by

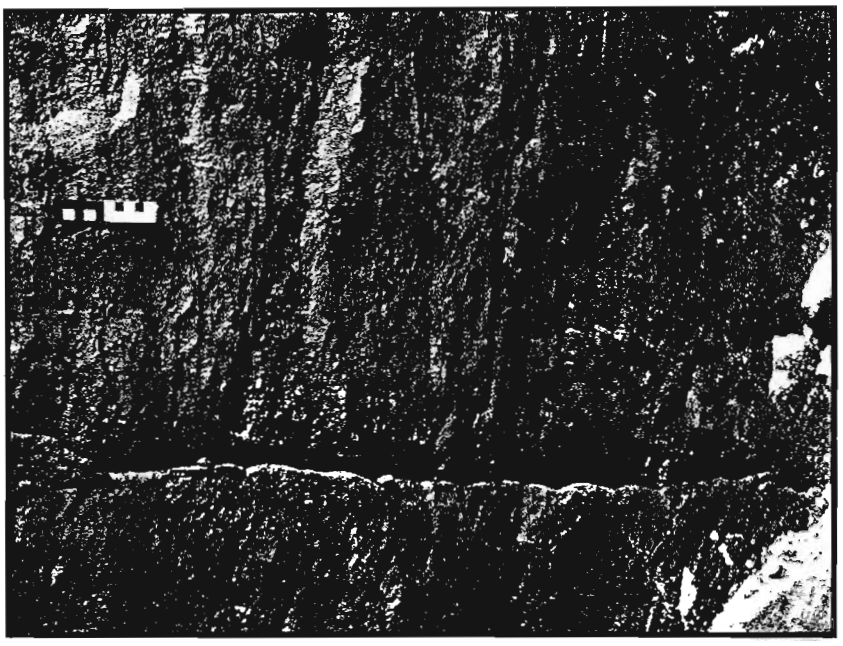

Figure 3.68 Rough pahoehoe flow surface texture, Agatha Formation, White Mfolozi River. See Figure 3.56 for location of photograph.

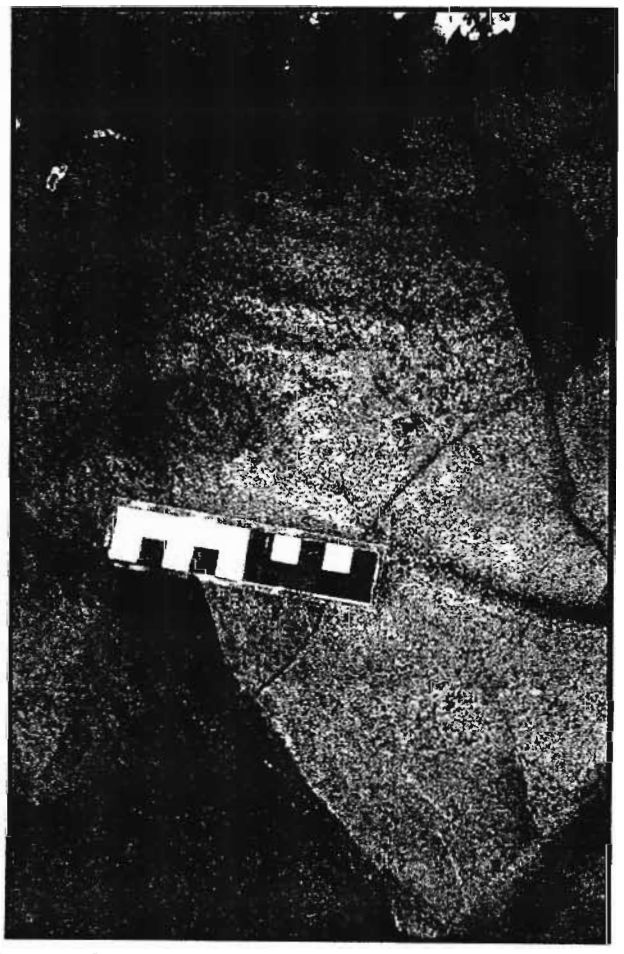

Figure 3.69 Pahoehoe flow surface, Agatha Formation, White Mfolozi River. See Figure 3.56 for location of photograph.

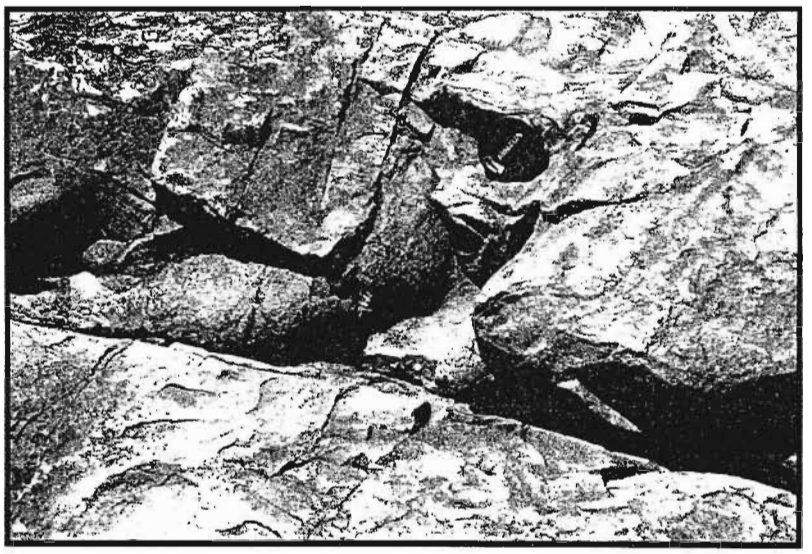

Figure 3.70 Smooth glassy lava toe, Agatha Formation, White Mfolozi River. See Figure 3.56 for location of photograph.

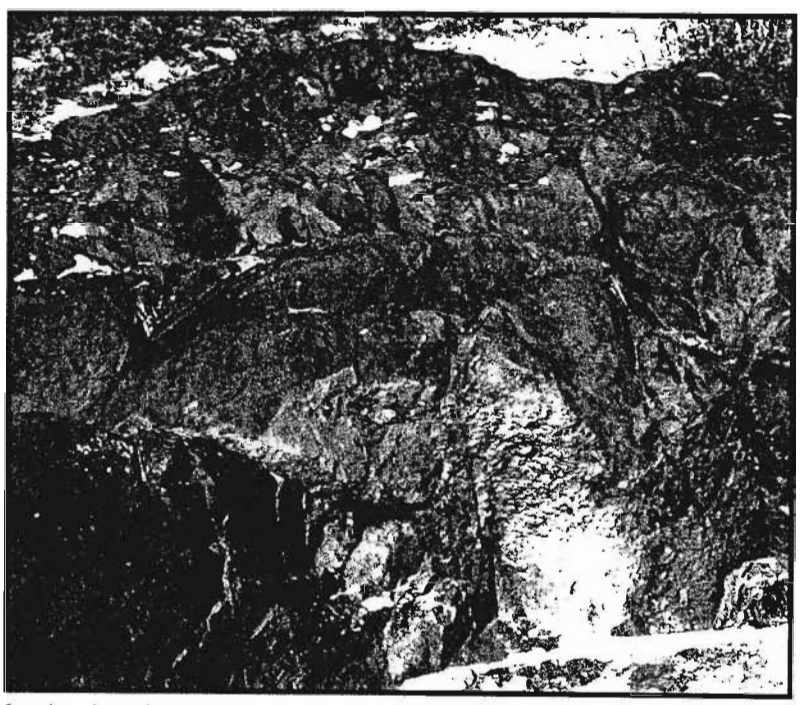

Figure 3.71 Massive interior and vesicular flow top, Agatha Formation, White Mfolozi River. See Figure 3.56 for location of photograph.

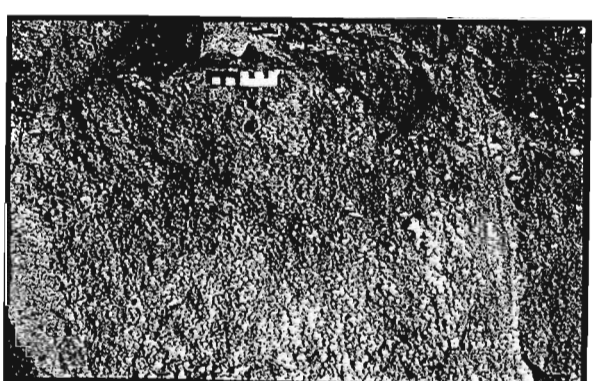

Figure 3.72 Vesicular flow surface, Agatha Formation, White Mfolozi River. See Figure 3.56 for location of photograph.

hydrodynamic forces acting on the large vesicle as it moves upward in a viscous lava (McMillan *et al.*, 1987).

A chill margin / crust is preserved on the flow surfaces of certain flow units. This chill zone is vesicle-poor and is often glassy (Figure 3.74). The middle of the flows is commonly massive. It has however been observed that the thinner the flow, the more vesicles to be found within the middle zone as a result of the more rapid solidification. Small spherical vesicles are found within the middle zone in minor proportions, most often towards the top of the zone. The thicker lava flow units have a crude columnar jointing.

Where the base of the flow has been exposed, the lower portion is vesicular. These vesicles are small and spherical (<2mm diameter) and / or elongated approximately 2mm wide and 2-6cm long (Figure 3.75). This lower vesicular zone varies between 5cm and 15cm, although poorly exposed for many of the flow units and an exact thickness range can therefore not be determined.

Wilmoth and Walker (1993) identified two main types of Hawaiian pahoehoe lava, S-type and P-type. S-type or spongy lava exhibits a high density of small spherical vesicles throughout the lava flow unit. This type of pahoehoe lava is not evident in Traverse 2. Wilmoth and Walker (1993) described P-type or pahoehoe lava as containing large vesicle sizes and pipe vesicles at the base of the flow unit. P-type or pahoehoe lava is much less vesicular than S-type pahoehoe lava. Three zones can be identified in lava flows: a basal vesicle zone, a middle vesicle deficient or massive zone and an upper vesicle rich zone (Aubele *et al.*, 1988; Cashman and Kauahikaua, 1997). A vesicle poor crust or chill margin often marks the extremities of the lava flow units. These features are all exhibited in the lava flow units of Traverse 2 to a certain degree and the lavas present along the White Mfolozi River are therefore similar in character to the P-type pahoehoe lava flow units described by Wilmoth and Walker (1993). The lavas flowed over an area of shallow gradient (<4°). This type of pahoehoe lava is associated with tumuli and lava rises. While these features have not been identified, the presence of squeeze ups and lava ribbons suggests that fresh lava was being injected beneath the pahoehoe crust. Cashman and Kauahikaua (1997) determined vesicle patterns almost identical to those identified in Traverse 2. The observed pattern of three zones, the upper and lower being vesicular and the decreasing of vesicle density downwards from the top, together with an increase in vesicle size through the upper zone, is indicative of inflated pahoehoe lava flows. It is also observed that P-type pahoehoe lava flow units as described by Wilmoth and Walker (1993) are always associated with regions of inflation, but not all inflated flows have pipe vesicles at the base (Cashman and Kauahikaua, 1997). Inflated flows are observed in Hawaii on near horizontal slopes and completely absent where slopes are steeper than 2° (Cashman and Kauahikaua, 1997). The formation of a lava flow by inflation requires the upper and lower flow surfaces to cool conductively to form rigid upper and lower flow crusts. The steady flow of lava between these flow crusts results in the lifting of the upper crust causing lava ridges and tumuli to form (Cashman and Kauahikaua, 1997).

Highly weathered lava is found within the pahoehoe type lava flows, in what has been identified as flow unit 12 and 13 (although they may in fact form part of a single larger flow unit). Spheroidal weathering has obliterated any structures that may have represented any internal features. The only preserved physical characteristic of these lavas is patchy areas of small spherical vesicles, approximately 1-3mm in diameter. The reason that these lava flow units have been so severely affected by weathering is not fully understood. A similar occurrence was found in Traverse 1 where a series of flows exhibit intense spheroidal weathering. This localised spheroidal weathering may be attributed to a combination of lithological and environmental factors. Basaltic lava with a high density of cooling joints would be more susceptible to the development of a spheroidal weathering pattern. Mineralogically basalts are also more prone to breakdown than intermediate or acid volcanic rocks. If the lava surface were exposed to the atmosphere for an extended period of time, forming a soil horizon, the basaltic lava flows would have been already in an advanced state of weathering before they were covered by subsequent eruptions.

At the top of the pahoehoe lava flow type lies a complex mixture of pillowed lava, minor pahoehoe units and massive lava flows. The true nature of the pillow lavas is difficult to determine. While the structures appear to be true pillows, they may easily be lava toes (Figure 3.76a-b).

Figure 3.73 Domed vesicles with migration trails, Agatha Formation, White Mfolozi River. See Figure 3.56 for location of photograph.

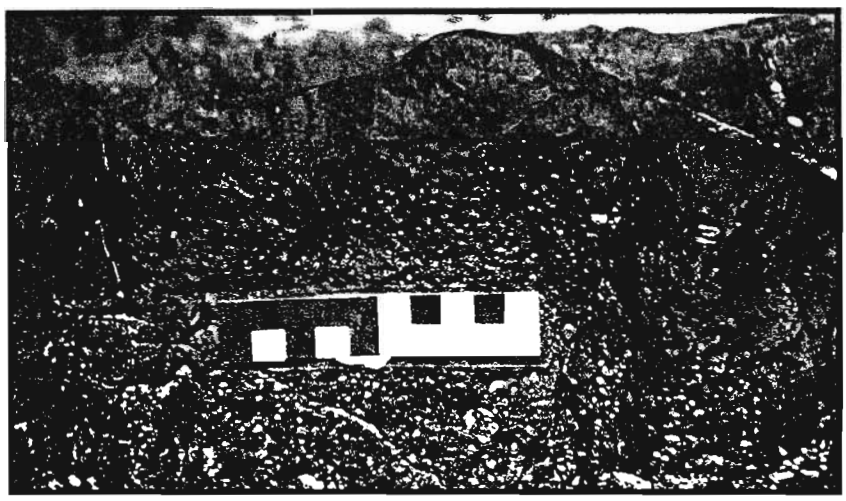

Figure 3.74 Vesicle-poor chill zone on flow surface , Agatha Formation, White Mfolozi River. See Figure 3.56 for location of photograph.

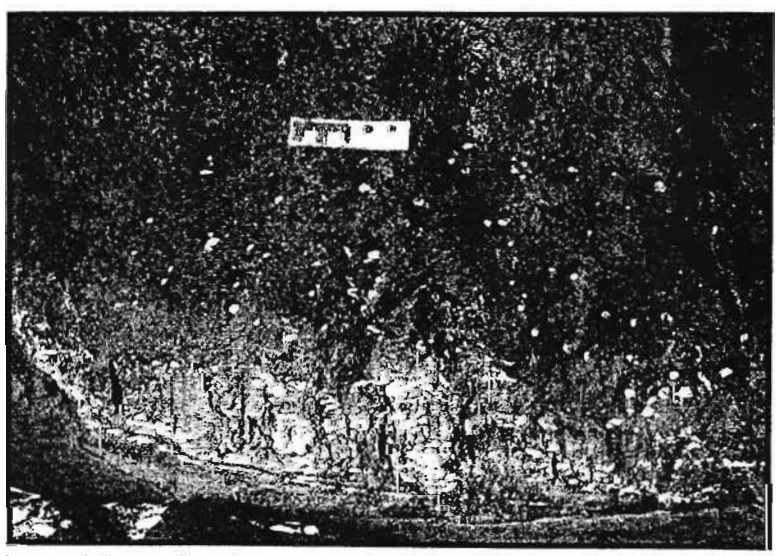

Figure 3.75 Pipe vesicles at flow base, Agatha Formation, White Mfolozi River. See Figure 3.56 for location of photograph.

These "pillow" lava structures appear to form the basal portion of flow units 21, 22 and 25. The distinct lack of hydroclastic breccias implies the absence of explosive fragmentation in these lava flows suggesting that emplacement was quiet. Passive emplacement of lavas into water bodies requires moderate to low effusion rates, a shallow gradient and minimum disruption in the water itself i.e. waves (Carr and Jones, 2001). The features that form in the water are lobes, sheets and pillows. The formation of pillows represents the lowest effusion rate of lava (Gregg and Fink, 1995). Increasing slope and effusion rates result in the pillows becoming larger and flatter, eventually forming lobate flows. The difference with lobate flows is that the crust swells to accommodate the new influx of lava but does not crack. This is because the effusion rate is almost equal to the crustal growth rate. The lobate flows therefore lack the striated surfaces of the pillow lavas (Gregg and Fink, 1995). Unfortunately the pillow lavas exposed along the White Mfolozi River are only a two-dimensional representation and no flow surfaces are exposed. The shapes of the pillows are in places somewhat large and flat and may suggest that they are in fact toes to lobate flows. The nature of the eruption at this time had a low effusion rate with lava flow units moving over a very shallow gradient of less than 3°.

The middle and upper zones of the pillowed lava flows resemble the upper portions of the pahoehoe lava flow type. Above the pillows, the sequence is generally massive, and capped by a flow top containing both large and small vesicles. Flow units 23 and 24 appear to be massive with little internal features apart from the vesicular flow tops. This sequence of lava flows appears to be relatively compound in nature and may therefore represent a complex flow field. The surfaces of these lava flow units are not adequately preserved for interpretation.

Massive lava flows mark the last and stratigraphically highest phase of volcanism of the Agatha Formation in the White Mfolozi Inlier. Within Traverse 2 the massive units are the uppermost flow units 26 to 28 (Figure 3.77). The flow units above Traverse 2 to the unconformable Mozaan contact are however also of the massive type. These lavas are generally devoid of features and textures. Few vesicles are present and the determination of flow tops is difficult. Columnar jointing is prominent in these flows and they have weathered to form a blocky outcrop. These lava flow units may represent thick aa lava flows, where a significant period elapsed between subsequent flows allowing for the removable of the rubbly surface, and preserving the massive interior often associated with aa lava flows (Cas and Wright, 1987). The flow tops of proximal aa lava flows generally have surface rubble of scoriaceous fragments with highly spinose textures. These flow tops are generally relatively thin and there is often a lack of internal shear structure within the lava flows (Rowland and Walker, 1987). It would therefore take little geological time to remove the thin clinkered surface to expose the massive interior of the aa lava flow. There is no evidence for internal shearing preserved within the massive lava flows.

3.1.2 Discussion of volcanology of White Mfolozi Inlier

The nature of lava erupted in the White Mfolozi Inlier suggests that volcanism was not explosive, i.e. the exsolved volatile content was considerably low. The Nhelbela Formation represents the steady and non-violent eruption of lava from one or multiple eruptive centres, where effusion rates were high and viscosities of the lavas low. The initial stages of eruption resulted in the interaction of the lava with an aqueous phase. This aqueous phase was a result of the fluvial system that existed prior to the development of the responsible eruptive source. Pillow structures and hydroclastic breccia define the lower lava flow units of the Nhelbela Formation. The upper amygdaloidal lava flows of the Nhlebela Formation show no interaction with water. Volcanism was terminated for a substantial period of time resulting in the development of the sedimentary White Mfolozi Formation in a littoral depositional environment.

The renewed outpourings of lava to form the Agatha Formation terminated the sedimentary processes of the White Mfolozi Formation. The presence of well-preserved lava flow-top structures indicates an absence of widespread explosive activity in the area, resulting in lava flows rather than extensive pyroclastic deposits. The locations of the original volcanic sources are however unknown, and it is therefore possible that local vent accumulation of pyroclastics associated with more basic compositions occurred e.g. scoria cones.

Although the well preserved outcrop is limited to the banks of the White Mfolozi River, a localised

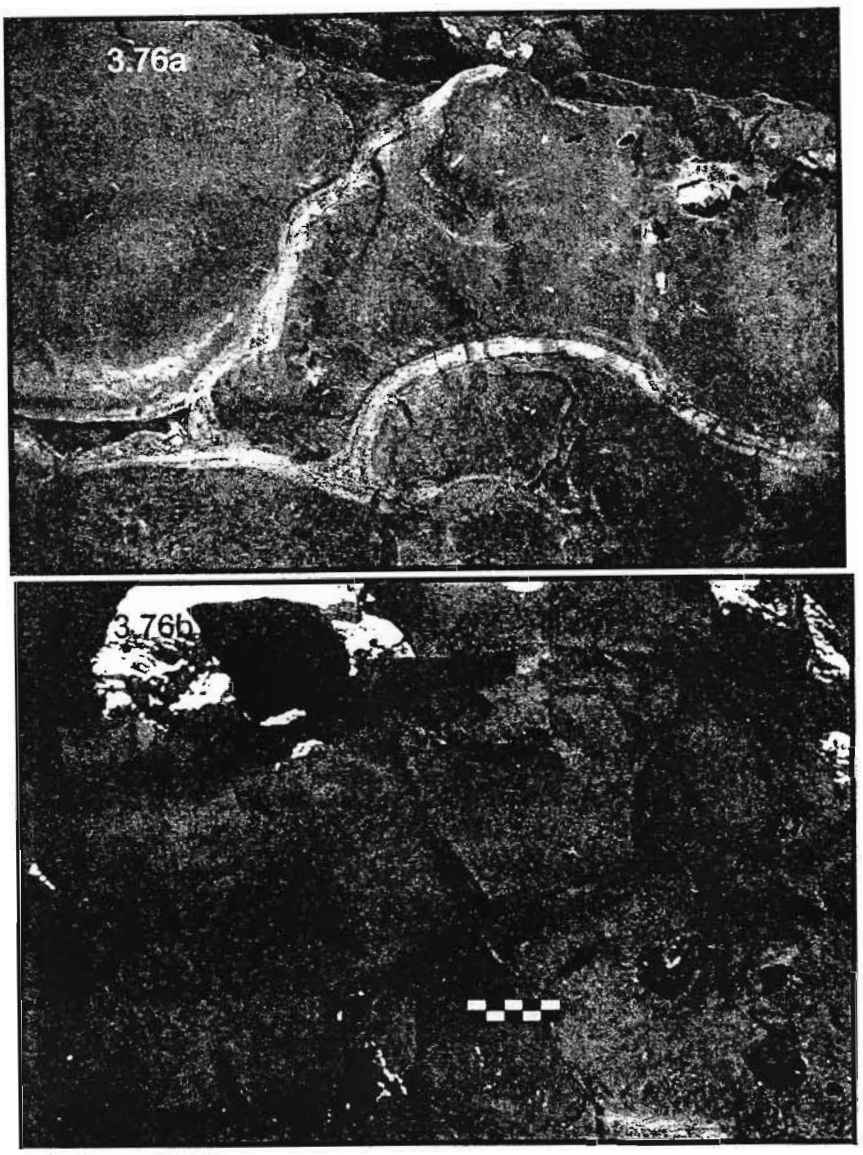

Figure 3.76a-b Pillow lava structures, Agatha Formation, White Mfolozi River. See Figure 3.56 for location of photograph.

Figure 3.77 Massive lavas, showing jointing, Agatha Formation, White Mfolozi River. See Figure 3.56 for location of photograph.

istory of the basic volcanicity can be determined. Initially effusion rates were relatively high as demonstrated by the presence of aa lava flows closer to the source. The presence of an aqueous phase resulted in hydroclastic brecciation of the lava flows as well as associated hydrothermal alteration. The build up of the volcanic pile or the disappearance of the water, resulted in true subaerial lava flows. A combination of a drop in effusion rate from the volcanic centre as well as a decrease in viscosity due to the loss of volatiles, resulted in the pahoehoe surface of the lava flows extending to further from the vent. A temporary increase in effusion rate may have been the cause of thicker, more massive flows that then gave way to a quieter period of eruption again. Low effusion rates over sub-horizontal topography resulted in the formation of lava flows that are transitional between pahoehoe and aa lava. The flow surfaces of these lava flows suggest that the viscosities of the lava had increased forming a rough surface. The internal structure of the lava flows signifies inflation once the crust of the lavas had been formed. The possible localised introduction of an aqueous body resulted in the formation of pillow lavas. The eruptions at this time were still slow over a very gentle gradient. This passive phase of volcanism gave way to an increase in effusion of lava, but with periods of quiescence between lava flows or when lava was flowing in a different direction. There is a suggestion that the volcanism of the Agatha Formation occurred relatively proximal to the volcanic source.

3.2 COMPARISON OF VOLCANOLOGY OF THE WHITE RIVER SECTION AND THE WHITE MFOLOZI INLIER

The fundamental differences between the White River Section volcanic lithologies and those of the White Mfolozi Inlier are the lack of pyroclastics and acid compositions in the rocks of the Central Region of the Nsuze Group. The White River Section also does not have the break in volcanism within the Bivane Subgroup that the White Mfolozi Formation in the White Mfolozi Inlier represents. The volume of the volcanic material in the White River Section far exceeds that in the White Mfolozi Inlier. It can therefore be assumed that these two areas had different volcanic centres and possibly different magma sources. While the volcanic rocks of the White River Section were allowed to evolve in multiple levels of magma chambers, the White Mfolozi Inlier has a less complex plumbing system and less fractionation therefore took place prior to eruption. This may be due to contrasting tectonic stresses that impacted on each area. The less evolved the magma, the less likely explosive volcanic conditions are to form. The reservoirs of magma maintained beneath the craters of the White River Section would have allowed for the continued eruption of volcanic material (suggested by the slow growth of the acid lava dome of Phase 4) during the hiatus of eruptive activity that resulted in the sedimentary sequence of the White Mfolozi Formation in the Central Region. While the eruption of volcanic material from the White River Section and the White Mfolozi Inlier was contemporaneous, and the area most probably form different parts of the same tectonic event, it is unlikely they shared any volcanic centres.

CHAPTER 4
PETROLOGY

4.1 INTRODUCTION

A range of basalts, basaltic andesites, andesites, dacites and rhyolites were petrographically investigated under transmitted light. The criterion for classification is based on geochemistry and is discussed in Chapter 5. The aphanitic nature and the metamorphic state of the volcanic rocks prevent detailed work of the fine-grained components. Observations have, however, been made about the dominant minerals and textures present in thin sections.

4.2 BASALTS

4.2.1 White River Section

True basalts are rare in the northern region, and are generally restricted to the Wagondrift Formation and form several smaller units within the Bivane Subgroup. Secondary minerals have replaced all primary minerals in the basalts. In certain examples primary textures have however been preserved. Minerals present in significant quantities are chlorite, plagioclase, actinolite and devitrified basaltic glass. Calcite, quartz, epidote and opaque minerals are present in less significant quantities (Figure 4.1a-b). By far the most dominant mineral is chlorite, pleochroic green under plane polarised light and often exhibiting anomalous blue interference colours under cross polars. The relatively strong pleochroism of the green chlorite suggests high iron content. This is supported by the anomalous blue interference colours, which are also indicative of Fe-rich chlorites (Deer *et al.*, 1992). The presence of chlorite in large quantities can represent either greenschist facies metamorphism or hydrothermal alteration of pyroxenes and amphiboles. The composition of the plagioclase cannot be determined using optical properties due to the small nature of the crystals. Actinolite is present as a major phase in the basalts. This mineral is characteristic of low-temperature regionally metamorphosed ultrabasic to basic igneous rocks and results from the breakdown of Mg-rich ferromagnesian minerals. Devitrified basaltic glass forms spherulitic oval structures that overprint existing minerals and associated textures (Figure 4.1b). Although amygdales were observed in the field, none were examined in thin section.

4.2.2 White Mfolozi Inlier

Two basalt suites have been investigated from the Nsuze Group volcanic rocks in the White Mfolozi Inlier. Basalts dominate the older Nhlebela Formation and the younger Agatha Formation, although andesitic compositions are found at the top of both units. Alteration and metamorphic minerals have replaced primary minerals. The most prominent minerals present in the basalts are chlorite, albite, actinolite and basaltic glass. Minor quantities of calcite, quartz, epidote and opaque minerals are also present. As with the Northern Region basalts, the chlorite is Fe-rich (green pleochroism and anomalous blue interference colours). Plagioclase has an An content of 0-10 mol%, and can therefore be classified as albite. Albite is not commonly associated with basic volcanic rocks and it can therefore be assumed that the albite is a secondary low temperature mineral that replaced the original Ca-rich plagioclase of basaltic igneous rocks. Devitrified basaltic glass is a collective term applied to murky brown patches found throughout the basalt thin sections.

Groundmass in the Nhlebela Formation is coarser than that of the Agatha Formation. Plagioclase crystals (less than 0.1mm) are prevalent in the Nhlebela Formation forming glomeroporphyritic texture in places (Figure 4.2). Chlorite pseudomorphs mafic phenocrysts, where the original mineral may have been orthopyroxene as the green pleochroism of the chlorite suggests high iron content (Figure 4.3). Remnant larger plagioclase phenocrysts (0.5-1mm) are present in the basalts of the Agatha Formation, although the groundmass is finely crystalline (Figure 4.4). A suggestion for this difference in crystal sizes of the groundmass is relative thickness of lava flows. The lava flows of the Nhlebela Formation are generally thicker than those of the Agatha Formation, and would therefore have allowed for larger crystal growth during slower cooling times.

Amygdales are present in the basalts of the Nhlebela Formation. These amygdales are highly irregular in shape and form a complex zoned texture of calcite, quartz and chlorite (Figure 4.5a-b). Calcite forms part of the outer

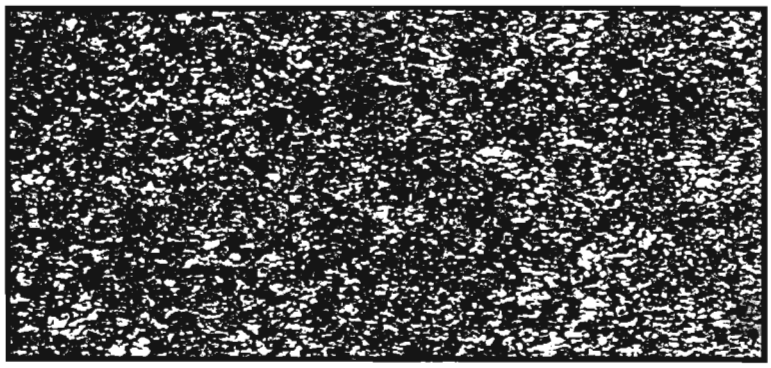

Figure 4.1a Chlorite, actinolite, plagioclase, epidote, devitrified basaltic glass, quartz and calcite make up the basalts of the Wagondrift Formation. (CG01/13; ppl; width of view = 10mm)

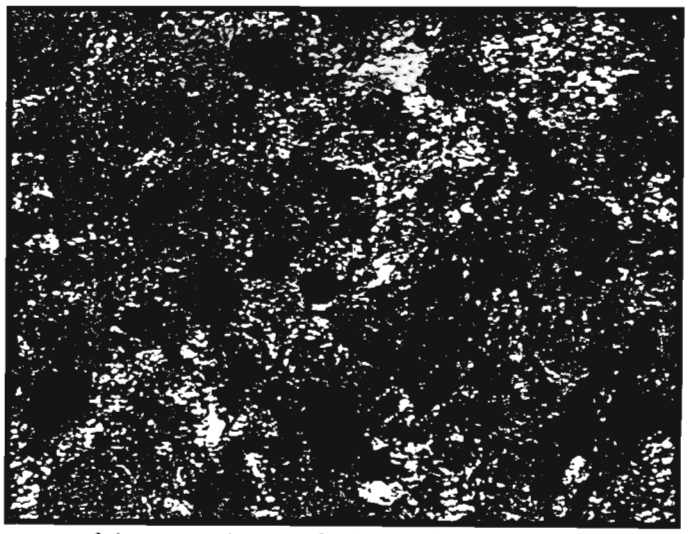

Figure 4.1b Close up of the groundmass of a basalt from the Wagondrift Formation showing chlorite, epidote, actinolite, devitrified basaltic glass and plagioclase. (CG01/13; ppl; width of view = 1.5mm)

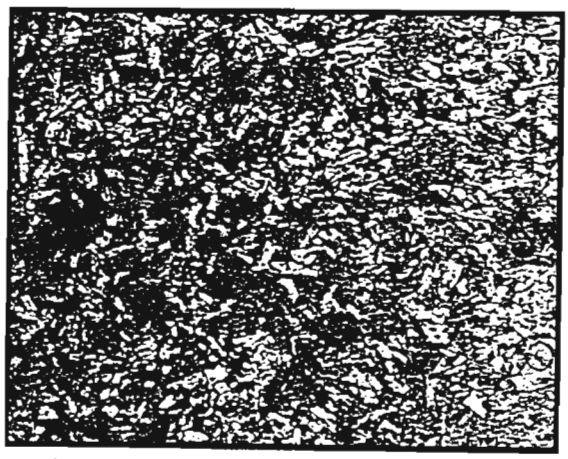

Figure 4.2 Plagioclase phenocrysts in a chlorite, actinolite and devitrified basaltic glass groundmass, Nhlebela Formation, White Mfolozi Inlier. (CG01/211; ppl; width of view = 8mm)

Figure 4.3 Chlorite phenocrysts in a chlorite, actinolite, plagioclase and devitrified basaltic glass groundmass, Nhlebela Formation, White Mfolozi Inlier. Chlorite has probably replaced orthopyroxene phenocrysts. (CG02/213; ppl; width of view = 8mm)

Figure 4.4 Fine groundmass of a basalt from the Agatha Formation, White Mfolozi Inlier showing chlorite, epidote, actinolite, devitrified basaltic glass, quartz and plagioclase. (WM3/2000; ppl; width of view = 9mm)

rim of only the largest vesicles otherwise the rim is composed of quartz surrounding a chlorite core. Certain amygdales have alternating layers of quartz and chlorite, with a quartz interior. Amygdales of the Agatha Formation are more spherical. They are often exhibit concentric layers of quartz aggregate, calcite and epidote (Figure 4.6).

4.3 BASALTIC ANDESITES

Basaltic andesites have a similar groundmass to basalts and the more mafic andesites, containing chlorite, actinolite, epidote, albite and quartz. The samples selected for petrographic study exhibit crystal sizes bordering on cryptocrystalline, have few phenocrysts (less than 0.2mm) and no amygdales (Figure 4.7). They have been differentiated from basalts and andesites on the basis of geochemistry (Chapter 5).

4.4 ANDESITES

Andesites vary from mafic through to more acid varieties and therefore exhibit similar mineral assemblages that differs in modal proportions. Andesites are the dominant composition of the Bivane Subgroup in the Northern Region. The original mineral assemblages are no longer present but have been replaced by various secondary minerals. Groundmass of andesites is dominated by chlorite and actinolite with varying amounts of epidote and biotite, as well as quartz and feldspar. Minor amounts of calcite and sphene (altered to leucoxene) are also present. The groundmass crystal size ranges from microcrystalline to cryptocrystalline (Figure 4.8a-b). The groundmass appears as aggregates of irregular crystals or small acicular crystals that form an interlocking weave pattern. Evidence for devitrification structures of intermediate glass include the spherulitic texture of amphibole (Figure 4.9).

Both phenocrysts and amygdales occur in abundance and often together. Where preserved the phenocrysts have undergone saussuritisation and are pseudomorphed by aggregates of albite, epidote, calcite and sericite (Figure 4.10). The phenocrysts vary in size from 0.2mm to 10mm (in thin section samples) and form glomeroporphyritic texture in certain samples.

Amygdales are generally spherical and contain quartz, calcite, zeolite and occasionally epidote. In certain samples, it can be seen that a calcite phase of amygdale growth developed prior to the development of a quartz phase (Figure 4.11). Certain amygdales appear to be surrounded by a chill margin, comprising cryptocrystalline groundmass (Figure 4.12). Veining is common and is predominantly composed of quartz, calcite, epidote and chlorite (Figure 4.13a-b).

Foliation is evident in certain samples. It is important to be able to distinguish between primary layering and flow bandings and secondary structural foliation. CG01/107 exhibits foliation produced by shearing (a shear zone is situated to the northeast of the sample locality) (Figure 4.14a-d). This has been identified by the presence of shear textures within the amygdales of the sample. Had the foliation been caused by primary flow movement, the vesicles would have been more flattened and subsequent infilling to form amygdales would not show signs of shear deformation. A needle like texture, not unlike the quenching texture associated with komatiites, is preserved in CG01/166 (Figure 4.15). It is unknown whether this is an alteration texture or was formed due to rapid cooling of lava.

4.5 DACITES AND RHYOLITES

The dacite and rhyolite samples will be discussed in the same section. Acid volcanic rocks are not found in the White Mfolozi Inlier. The acid volcanic rocks of the White River Section formed as a result of pyroclastic and lava eruption. It is often difficult to distinguish between the two mechanisms of formation.

The rhyolitic and dacitic volcanic rocks comprise mainly quartz and feldspar, with minor phases of calcite, biotite, actinolite and chlorite. Accessory minerals include epidote, sphene and zircon. The biotite and chlorite appear to form outlines that depict original crystal structures of phenocrysts (Figure 4.16a-b). Devitrification of silicic glass is present at varying stages of development, from stage 3 to advanced stage 4 (Lofgren, 1971). Stage 3 devitrification involves the formation of spherulitic structures often oval in shape. These may join together to form cuspate trains (Figure 4.17). The spherulites are made up of cryptocrystalline quartz and K-feldspar. The more circular the spherulites, the

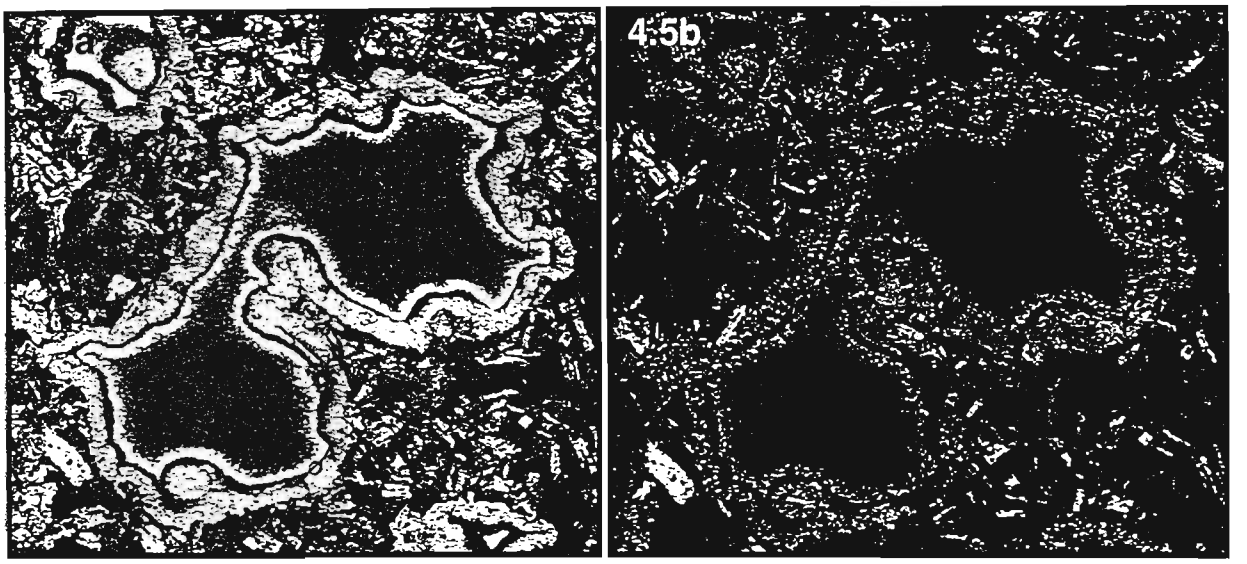

Figure 4.5a-b Irregular shaped amygdales in basalts of the Nhlebela Formation, White Mfolozi Inlier. A calcite rim is present on the right side of the large amygdale, while the rest of the rim is quartz aggregate. Internally, the amygdale has concentric layers of chlorite, quartz and chlorite again. (CG02/206; a-ppl; b-xpl; width of view = 4.5mm)

Figure 4.6 Amygdale in a basalt from the Agatha Formation, White Mfolozi Inlier. The amygdale has a rim of quartz and calcite aggregate and a core of calcite overprinted by epidote. (WM3/2000; xpl; width of view = 3mm)

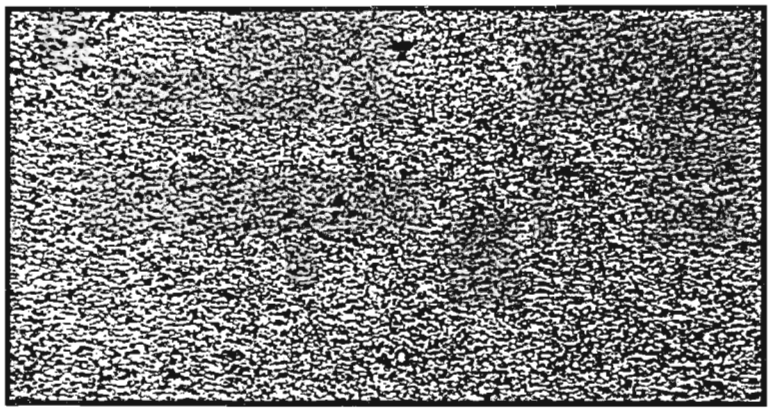

Figure 4.7 Very fine groundmass of a basaltic andesite, Bivane Subgroup, Northern Region. The groundmass is made up of chlorite, actinolite, epidote, plagioclase and quartz.
(CG01/30; ppl; width of view = 10mm)

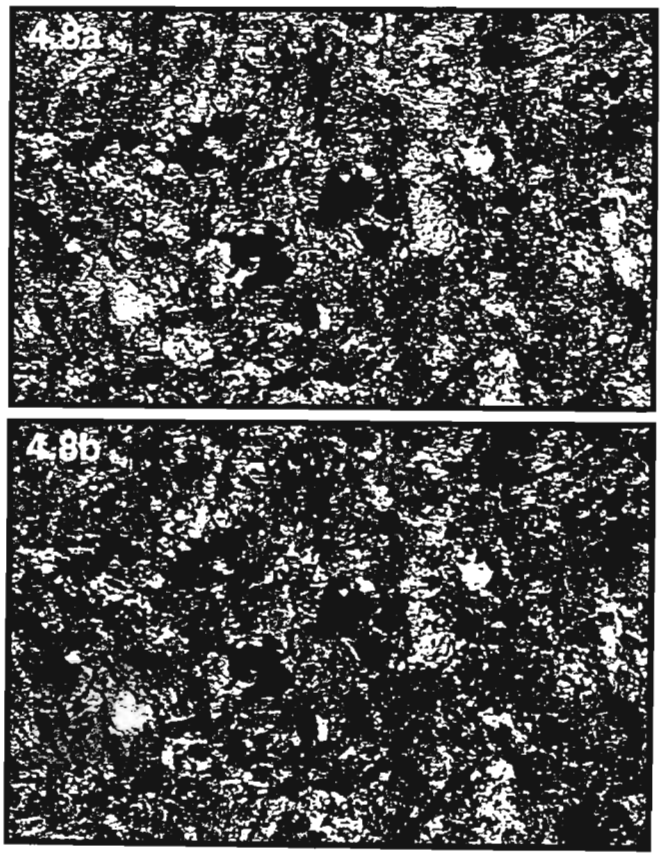

Figure 4.8a-b Close up of groundmass of an andesite from the Bivane Subgroup Northern Region. The groundmass is made up of epidote, chlorite actinolite, plagioclase, quartz and devitrified glass.
(CG01/49; a-ppl; b-xpl; width of view = 1.5mm)

Figure 4.9 Sphericle devitrification textures in an andesite, Bivane Subgroup, Northern Region.
(CG01/24; ppl; width of view = 9mm)

Figure 4.10a Plagioclase phenocryst remnant in an andesite, Bivane Subgroup, Northern Region. (CG01/130; ppl; width of view = 10mm)

Figure 4.10b Plagioclase phenocryst remnants in an andesite, Bivane Subgroup, Northern Region. (CG01/168; ppl; width of view = 11mm)

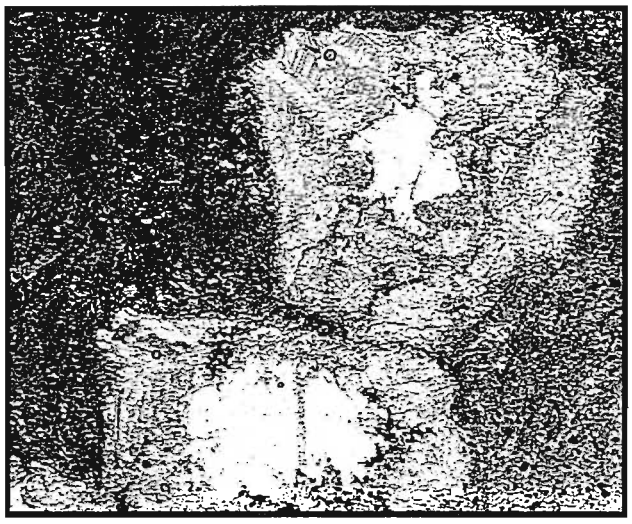

Figure 4.11a Amygdale in an andesite, Bivane Subgroup, Northern Region. Amygdale is formed by quartz aggregate, calcite and minor chlorite. (CG01/76; ppl; width of view = 8mm)

Figure 4.11b Amygdale in an andesite, Bivane Subgroup, Northern Region. Amygdale is made up of calcite, zeolite, quartz and chlorite. (CG01/70; ppl; width of view = 2mm)

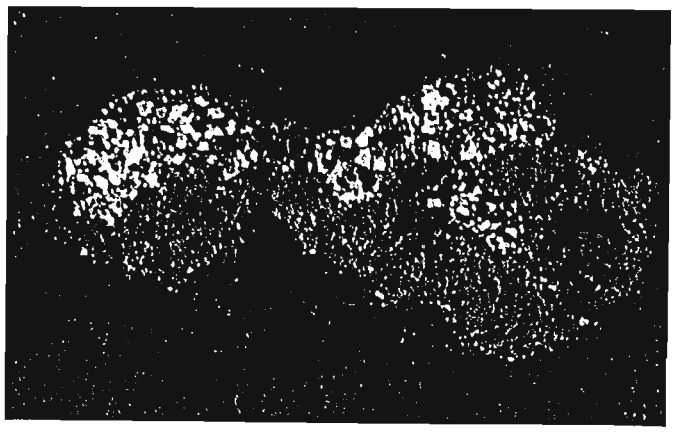

Figure 4.11c Quartz aggregate and calcite amygdale in an andesite, Bivane Subgroup, Northern Region. (CG01/176; xpl; width of view = 11mm)

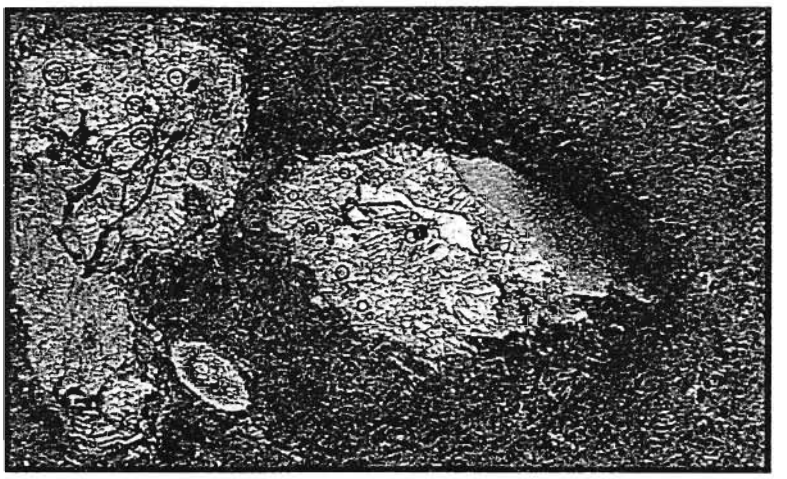

Figure 4.12 Chilled zone around an amygdale in an andesite, Bivane Subgroup, Northern Region. Chilled zone is marked by finer groundmass around the amygdale. Amygdale is filled with quartz aggregate, calcite, zeolite and minor chlorite.
(CG01/76; ppl; width of view = 11mm)

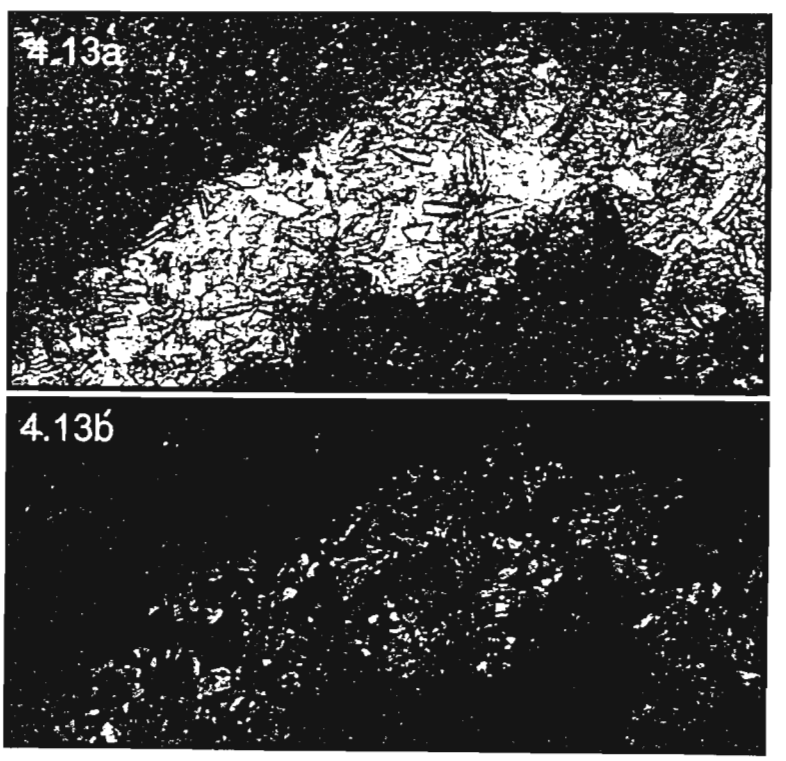

Figure 4.13a-b An epidote and quartz vein in an andesite, Bivane Subgroup, Northern Region. (CG01/125; a-ppl; b-xpl; width of view = 1.75mm)

Figure 4.14a Shearing foliation in an amygdaloidal andesite, Bivane Subgroup, Northern Region. Note the pressure shadows around the quartz amygdales. (CG01/107; ppl; width of view = 7mm)

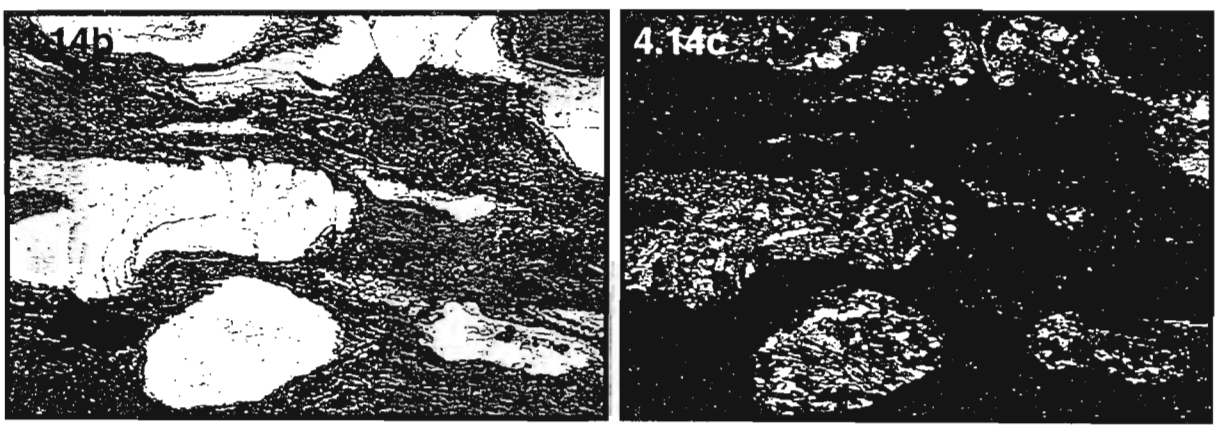

Figure 4.14b-c Shearing foliation in an amygdaloidal andesite, Bivane Subgroup, Northern Region. The quartz and zeolite have been deformed within the amygdales in the same orientation as the groundmass. (CG01/107; a-ppl; b-xpl; width of view = 10mm)

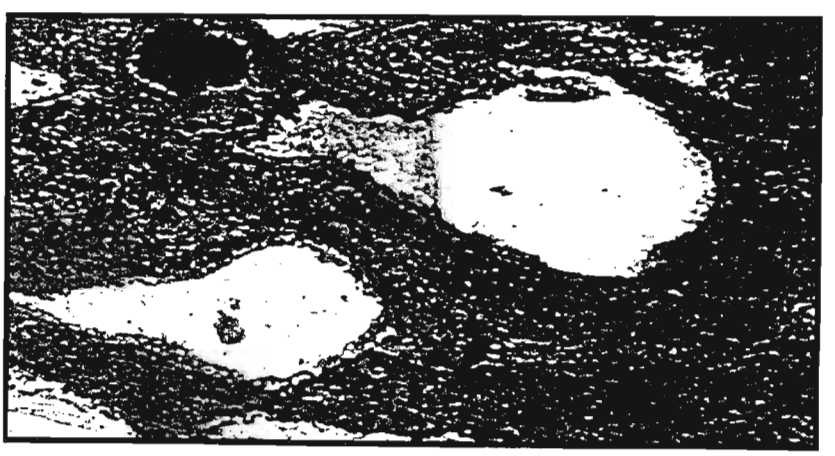

Figure 4.14d Pressure tails formed behind quartz amygdales in an andesite, Bivane Subgroup, Northern Region. (CG01/107; ppl; width of view = 8mm)

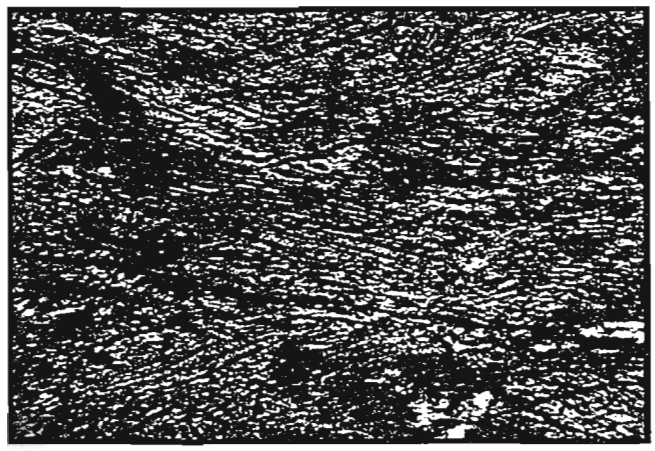

Figure 4.15 Needle like growths in an andesite, Bivane Subgroup, Northern Region. (CG01/166; ppl; width of view = 3mm)

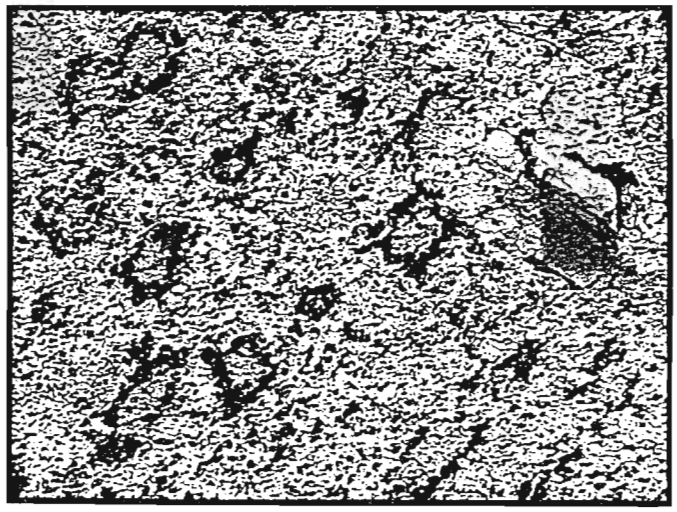

Figure 4.16a Biotite outlining possible remnant phenocrysts in a rhyolite, Bivane Subgroup, Northern Region.
(CG01/98; ppl; width of view = 6mm)

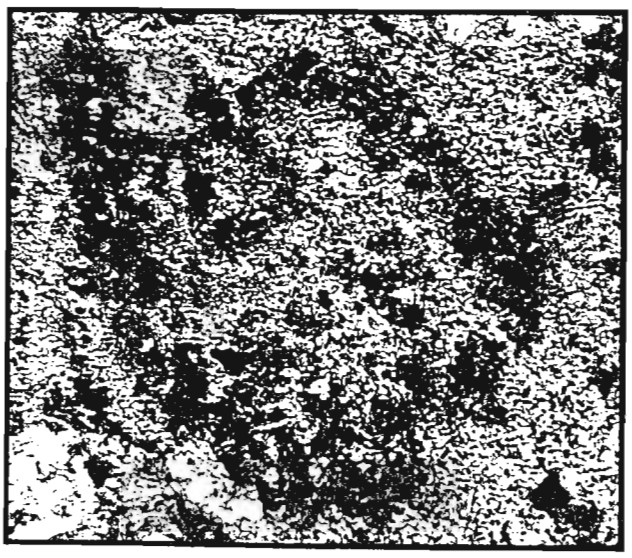

Figure 4.16b Biotite and chlorite have pseudomorphed this phenocryst in a dacite, Bivane Subgroup, Northern Region.
(CG01/85; ppl; width of view = 1.5mm)

lower the temperatures that the rocks experienced since formation. An oval shape indicates that the temperature did not or rarely exceeded 400°C (Lofgren, 1971). Stage 4 devitrification results in a granophyric texture and represents the complete recrystallization of the volcanic rocks (Figure 4.18a-b). Quartz and K-feldspar intergrowths radiate from K-feldspar or plagioclase phenocrysts. The texture is not unlike that found in acid plutonic igneous rocks.

Remnants of feldspathic phenocrysts are evident in dacitic samples, and certain rhyolitic samples (Figure 4.19). Phenocrysts are predominantly albite and K-feldspar in composition, but the albite composition may not represent primary mineral composition. Phenocrysts have been saussuritised and exist as a combination of sericite, albite and epidote. Large quartz crystals may represent phenocrysts or subsequent silica growth.

Foliation is common in acid volcanic rocks of the Northern Region. The foliation for all samples investigated under transmitted light has been interpreted as primary layering or flow banding. This deduction has been based on field observations associated with the relevant samples or through a lack of shearing textures in secondary quartz structures. Two types of layering are evident – flow banding and tuffaceous layering. Flow banding forms irregular layers of clay and mica minerals (originally pumice) and devitrified acid glass (Figure 4.20a-b). Tuffaceous layering is formed by the alignment of minerals predominantly biotite (not the original mineral) when ash settled through a flow or fall mechanism (Figure 4.21). Subsequent movement of the unconsolidated ash may have resulted in certain flow textures developing.

4.6 METAMORPHISM

The metabasic volcanic rocks clearly show evidence for low-grade metamorphism. The acid volcanic rocks, on the other hand, do not contain the necessary mafic minerals to reflect the metamorphism. The mineral assemblages found in the acid volcanic rocks are most likely due to deuteric alteration processes, although a similar assemblage results. The dominant minerals identified from the metabasic volcanic rocks are chlorite, epidote, actinolite, quartz, albite (sericite) as well as minor amounts of calcite, biotite, K-feldspar and sphene (leucoxene). These minerals are indicative of the chlorite and biotite zones of the greenschist facies of the Barrovian Zones (Yardley, 1989). A reaction that is relevant to this mineral assemblage is: chlorite + calcite $\rightarrow$ epidote + actinolite + CO_2 – H_2O fluid. The lack of hornblende determines that the transition to amphibolite facies has not occurred (Yardley, 1989). Temperatures required for the formation of greenschist facies metamorphic mineral assemblages are between 300° - 400°C. This is in keeping with the determination that the temperature applied to the acid volcanics did not exceed 400°C. Pressures did not exceed 3kbar (Yardley, 1989). These P-T conditions suggest regional metamorphic conditions as a result of either burial metamorphism or subduction zone metamorphism (Yardley, 1989).

It is interesting to note that the Pongola Supergroup overlies older Archaean greenstone belt remnants i.e. Commondale and Nondweni Greenstone Belts. These greenstone belts contain primary mineral assemblages, namely pyroxene and olivine, while the Nsuze Group volcanic rocks have no primary minerals preserved (Wilson, per. comm., Hunter and Wilson, 1988). Both the Pongola Supergroup and the greenstone belts have undergone the same burial and regional metamorphism. While the answer is speculative, it is possibly the Nsuze Group's association with hydrous phases has caused the primary minerals to metamorphose to a greenschist facies assemblage.

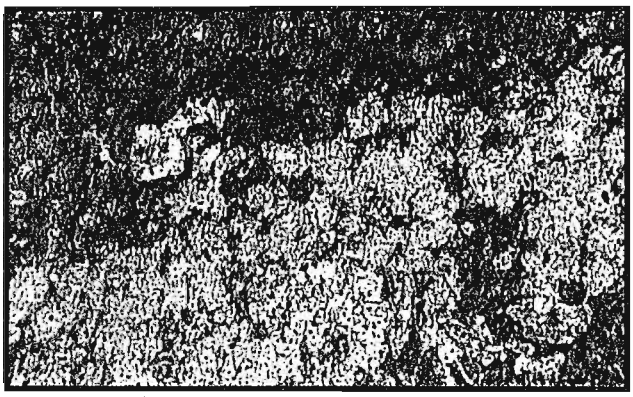

Figure 4.17 Third stage acidic glass devitrification spherulitic textures in a rhyolite, Bivane Subgroup, Northern Region. (CG01/142; ppl; width of view = 11mm)

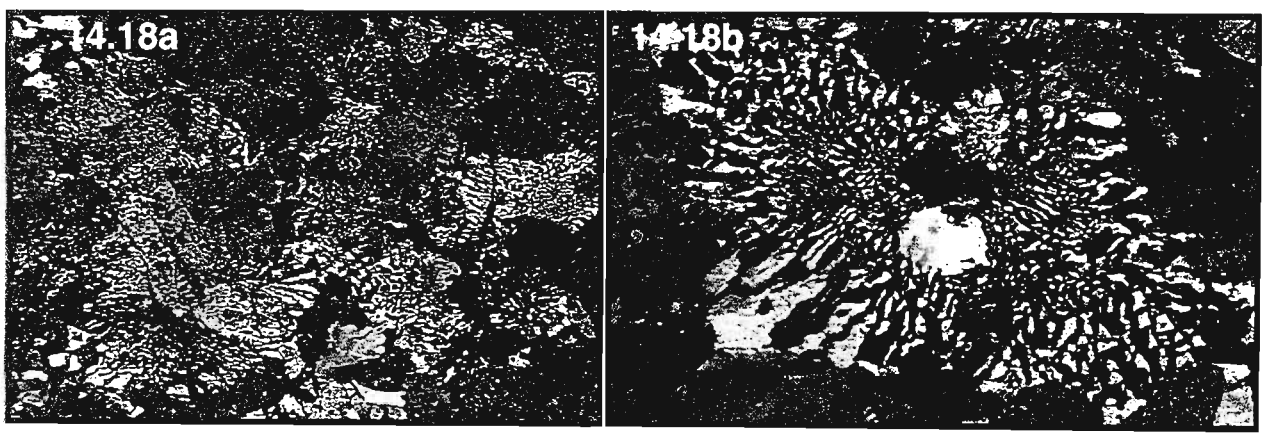

Figure 4.18a-b Fourth stage devitrification of acidic glass forming granophyric texture in a rhyolite of the Bivane Subgroup, Northern Region. (CG01/109; xpl; width of view = a-1.75mm, b-10mm)

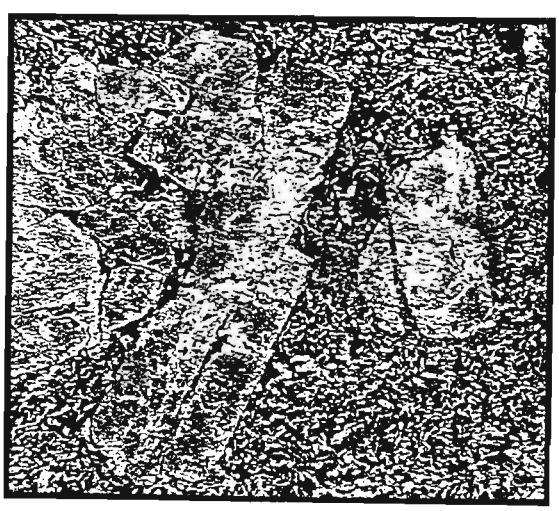

Figure 4.19 K-feldspar phenocrysts in a rhyolite, Bivane Subgroup, Northern Region. (CG01/157; ppl; width of view = 10mm)

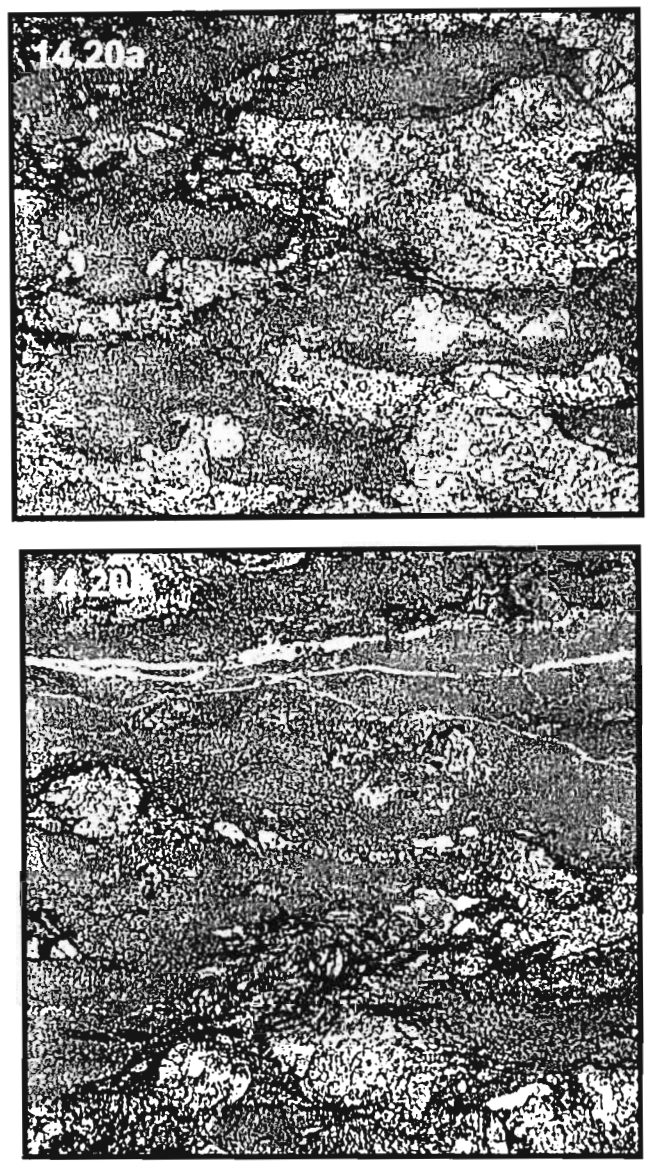

Figure 4.20a-b Flow banding of broken down pumice and volcanic glass in a rhyolite of the Bivane Subgroup, Northern Region. (CG01/100; ppl; width of view = 11mm)

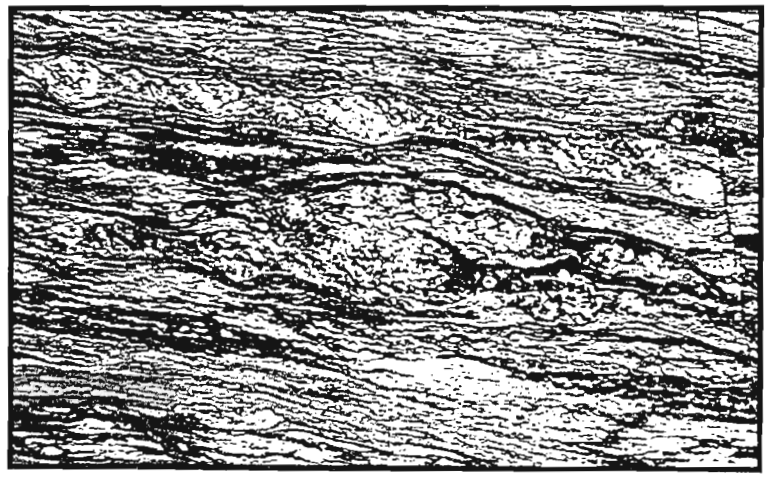

Figure 4.21 Tuffaceous layering in a rhyolite, Bivane Subgroup, Northern Region. (CG01/84; ppl; width of view = 7mm)

CHAPTER 5
GEOCHEMISTRY

5.1 INTRODUCTION

Localities (including GPS co-ordinates) and brief descriptions of all samples collected during the project are recorded in Appendix 2. Appendix 2 also differentiates between samples processed for geochemical analyses, samples collected for thin section description and samples collected for hand specimen records. Samples were collected across the entire Pongola Supergroup, including Pre-Pongola Supergroup and Post-Pongola Supergroup lithologies, in Swaziland, Mpumalanga and northern KwaZulu-Natal (see Figure 1.1). For the purpose of this study, the volcanic samples from two specific areas of the Nsuze Group have been investigated, the White River Section in the Northern Region (Appendix 1) and the White Mfolozi Inlier in the Central Region (Figure 3.47 and Figure 3.55) of the Pongola Supergroup. Samples, collected in the field for geochemical analyses, were considered to be unweathered and as unaltered as possible. Some field samples had to be cut using a diamond saw to obtain a fresh, unweathered sample. Subsequent petrographic analysis has shown however that all samples show alteration to a greater or lesser degree (see Chapter 4). All geochemical samples were analysed for major and minor elements using X-ray Fluorescence (XRF) (description of XRF process and procedures in Appendix 3). Suitable samples, selected from the XRF data, were analysed for trace elements, including rare earth elements (REE), using Inductively Coupled Plasma Emission Mass Spectrometry (ICP-MS) (description of ICP-MS process and procedures in Appendix 3). All major, minor and trace element data for samples used in this study are recorded in Appendix 4.

Geochemical data for the White River Section have been interpreted using five eruption phases deduced for Chapter 3 Physical Volcanology. These eruption phases are interpreted on the basis of stratigraphic relationships using topography, outcrop patterns and regional dip and strike of strata. Phases 3 and 5 have been further divided into sub-phases based on geographic locality. These eruption phases are represented in Appendix 1. The White Mfolozi occurrence has been divided into two volcanic stratigraphic groups, the older Nhlebela Formation and the younger Agatha Formation (see Chapter 2 and Chapter 3 for stratigraphic and volcanological descriptions).

5.2 IMMOBILITY OF ELEMENTS

The determination of the immobility of elements is crucial to understanding the geochemistry of an Archaean suite of volcanic rocks. Due to various forms of alteration: silicification, epidotization, chloritization, sericitization and metamorphic processes, certain elements may have been enriched or depleted over geological time. The whole rock geochemistry of the rock therefore may not entirely represent the primary element concentrations at the time of the rock's formation. The Nsuze Group volcanic rocks have been metamorphosed to greenschist facies (Chapter 4 Petrology). Elements that are not accommodated in the greenschist facies stable mineral assemblage may be lost from the rock (Gunn, 1976). Brewer and Atkin (1989) warned against element mobility due to low-grade metamorphic events. In a study carried out on a Proterozoic volcano-sedimentary succession in Norway, Brewer and Atkin (1989) identified that the sequence had been subjected to three metamorphic events: burial-type, regional greenschist and thermal metamorphism; all metamorphism types that the Nsuze Group volcanic rocks have been subjected to a lesser or greater degree. Both burial and regional greenschist metamorphism have affected the entire Pongola Supergroup, whereas thermal metamorphism has occurred in the Northern Region due to the intrusion of Post-Pongola granitoids and the Usushwana Complex (Hatfield, 1990; Armstrong, 1980). Brewer and Atkin (1989) discussed the use of major element whole rock analyses where the volcanic rock has been subjected to combinations of these types of metamorphism as invalid. The mobility of a trace element relies on its solubility in alteration and metamorphic fluids and it's ability to be accommodated in the new mineral assemblage of the low-grade metamorphic rock (Brewer and Atkin, 1989). Conclusions drawn by Brewer and Atkin (1989) are that burial metamorphism can cause the enrichment of Ca, Sr and Si, the depletion of Al, Ti, and the relative immobility

of Nb (Y and Zr proved immobile in the least altered zones). Regional greenschist metamorphism resulted in the enrichment of K, Rb and Ba, the depletion of Si, with Zr, Nb and Y being considered immobile (Brewer and Atkin, 1989). Thermal metamorphism resulted in all elements been depleted or enriched to a larger or lesser degree, including the rare earth elements (REE) (Brewer and Atkin, 1989).

The alkali elements Na and K are regarded as being highly mobile under changes in pressure, temperature or the introduction of fluids (Rollinson, 1993). A plot of SiO_2 vs Na_2O shows wide scatter with no trends evident (Figure 5.1a). A plot of SiO_2 vs K_2O shows a general positive trend (Figure 5.1b). It is therefore evident that Na is far more mobile than K. This observation can be used as an indicator of the degree of alteration in the Nsuze Group rocks. The degree of mobilisation of K, a commonly mobile element, is therefore limited in the Nsuze Group rocks. It is therefore suggested that other less mobile elements may still be representative of their primary concentrations. In support of the relative immobility of K, silica is plotted against Rb (Figure 5.1c). Rb often substitutes for K in alkali minerals. The graph almost mimics that of SiO_2 vs K_2O, suggesting that the concentrations of K and Rb in the Nsuze Group rocks have not been seriously affected since formation.

A method of testing mobility of elements involves binary plots. Linear arrays with high correlation coefficients represent the least mobile elements (MacLean and Kranidiotis, 1987). It is useful to start with elements widely considered to be immobile through most low-grade alteration and metamorphic processes e.g. Zr, Nb, Y and the Rare Earth Elements (REE) (Cann, 1970; Floyd and Winchester, 1978). Problems arise if there is more than one fractionation pattern or if there are sub-trends within the overall fractionation, which may be interpreted as scatter. Resulting binary plots are shown in Appendix 5. Only elements to be used in the geochemical interpretation of the Nsuze Group have been tested for mobility. The REE (La, Ce, Pr, Nd, Sm, Eu, Gd, Tb, Dy, Ho, Er, Tm, Yb, Lu) are immobile. Eu shows a degree of scatter in the more acid compositions but this is possibly differentiation between porphyritic and non-porphyritic varieties. Other immobile trace elements include Hf, Nb, Y, Ta and Zr. The elements Cr, Ni, Cu, Pb, Th, U, Rb, Ba and W show a degree of scatter but an overall linear trend. The scatter may be due to sub-trends within the data set, as it is unlikely that the Nsuze Group data represents one source and one subsequent fractionation trend. V and Sc have pronounced scatter and the mobility of these elements is likely. As samples have been taken over a large geographic and stratigraphic range, it is important to note that while certain elements may be mobile in one area of Nsuze group sub-crop, in another area that has undergone different degrees or types of alteration and metamorphism, the same elements may be semi-mobile or relatively immobile. The observations made about the mobility of elements will be used in this chapter to establish the validity of geochemical interpretations of the data.

5.3 CLASSIFICATION

Geochemical classification has proven to be the most accurate means of determining the volcanic rock types. Fine crystal size hinders the use of IUGS petrological classification methods often associated with plutonic igneous rocks. The alteration of the mineral assemblages also renders the IUGS system invalid. The simplest form of classification involves the SiO_2 weight percent of a sample only. This type of classification is useful for establishing the distribution of data over a compositional range. The frequency graph of SiO_2 contents for the Nsuze Group data (Wagondrift Formation, Mantonga Formation, Phases 1 to 5 of the White River Section and the Nhlebela and Agatha Formations of the White Mfolozi Inlier) shows 58% of the data has an andesitic SiO_2 content (Figure 5.2). Classes used to construct the frequency graph are based on those used in Cas and Wright (1987) where ultramafic <45 wt% SiO_2, basaltic – basaltic andesite 45-52 wt% SiO_2, andesitic 52-63 wt% SiO_2, dacite – rhyodacite 63-68 wt% SiO_2 and rhyolite >68 wt% SiO_2. The rhyolitic samples are the second most abundant compositional type at 24%. Basalts – basaltic andesites and the dacite - rhyodacite proportions of the total geochemical data are both 9%. No ultramafic lithologies were identified based on SiO_2 content alone.

More complex geochemical classification schemes have been developed using fresh volcanic samples and therefore have resulted in alkali (K_2O + Na_2O) and silica wt % oxides

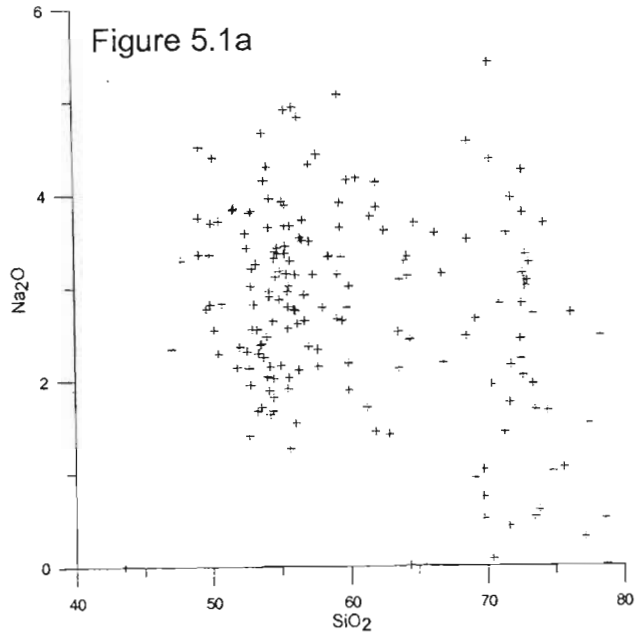

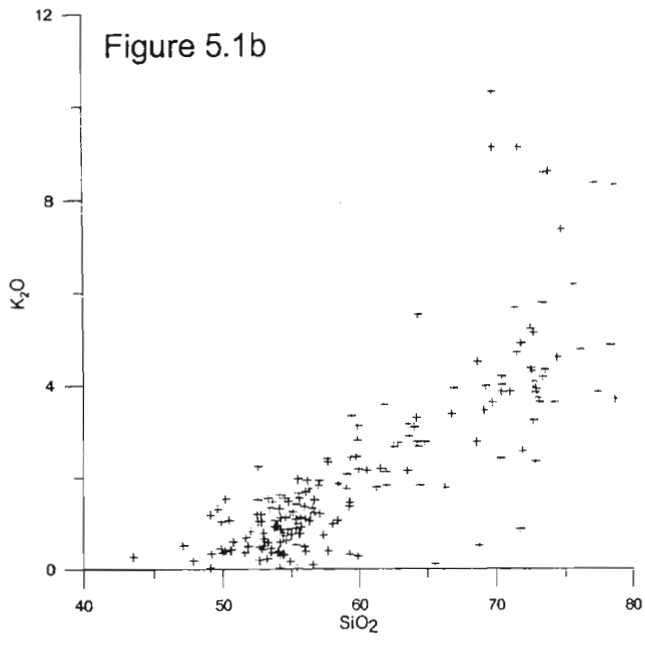

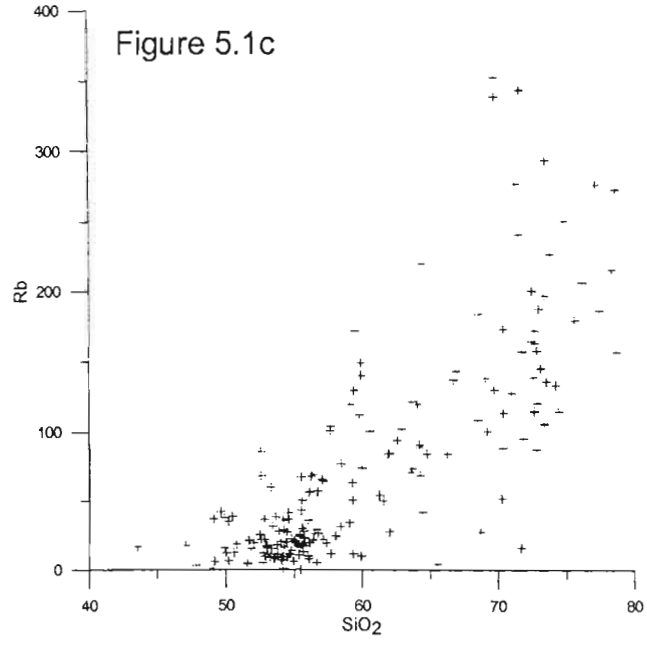

Figure 5.1a-c Harker diagrams where Na_2O, K_2O and Rb have been plotted against SiO_2 to show degree of scatter with increasing silica values. (Na_2O, K_2O and SiO_2 values in wt% oxide, Rb values in ppm)

being used as defining components i.e. total alkali-silica (TAS) diagram (Le Maitre *et al.*, 1989) (Figure 5.3). The data plots in the subalkaline and ranges from basaltic to rhyolitic. The few anomalous data points are samples that have undergone known alteration. The well-constrained nature of the TAS diagram suggests that alteration was not extensive so as to allow for large-scale mobilisation of the alkali elements. This diagram is however considered limited when working with metamorphosed and ancient volcanic rocks and other methods of classification involving traditionally less mobile elements should be investigated (Rollinson, 1993). Jensen (1976) and Winchester and Floyd (1977) have proposed alternative classification diagrams, specifically relevant to altered volcanic rocks. The relevance of these diagrams to the Nsuze Group volcanic rocks will be discussed in this section.

The Jensen Cation Diagram is a classification scheme based on the proportion of cations in a sample. It is plotted on a ternary diagram and uses the proportion of the cations (Fe^{2+} + Fe^{3+} + Ti), Al and Mg, recalculated to 100% (Jensen, 1976). The classification diagram is used specifically for subalkaline rocks, and the elements used in the diagram are considered stable under low grades of metamorphism. The version of the diagram used in this study is based on the plotting parameters of the field boundaries from Rickwood (1989).

Winchester and Floyd (1977) proposed a series of variation diagrams based on immobile elements of fresh volcanic rocks that can be used to classify subalkaline and alkaline magma series. The diagrams do not, however, distinguish between calcalkaline and tholeiite volcanic suites. These elements (SiO_2; TiO_2; Zr; Nb; Y; Ce) are generally considered to be immobile during post-consolidation alteration and metamorphic processes (Winchester and Floyd, 1977). These diagrams were tested by Floyd and Winchester (1978) using samples of metavolcanic suites that have been subjected to greenschist, amphibolite and granulite facies. Floyd and Winchester (1978) concluded that these variation diagrams provided a reliable method of characterising altered and metamorphosed volcanic rocks.

While comparing the classification schemes it is important to realise that different graphs distinguish different fields. The Jensen Cation (from here on termed "JC") plot does not differentiate between basalt and basaltic andesite or basaltic andesite and andesite. Zr/TiO_2 vs Nb/Y however does plot basaltic andesite as a separate field from basalt and andesite. The Zr/TiO_2 vs Ce binary plot does not distinguish between dacite and andesite. Interpretations must therefore be made when a field involves a range of compositions based on the data position within that field i.e. if the fields do not distinguish between basalt and basaltic andesite, a sample that plots just within the basalt boundary with andesite, can most likely be termed a basaltic andesite. Boundaries as drawn by Winchester and Floyd (1977) and Jensen (1976) are based on geochemical data sets of fresh, unaltered and unmetamorphosed volcanic rocks. These boundaries are the authors' interpretations and may not be universally definitive. Samples that plot on or near field boundaries may therefore be classified by either name on either side of the boundary.

5.3.1 Wagondrift and Mantonga Formations – White River Section

The samples of the Wagondrift Formation (sample localities shown on Appendix 1 and GPS co-ordinates given in Appendix 2), considered by Armstrong (1980) to represent the earliest phase of Nsuze Group volcanism, plot as high-Fe tholeiite basalts on the JC Diagram (Figure 5.4a). Only one sample (CG01/170) plots just within the calcalkaline basalt field, although its proximity to the field boundary suggests that it may also be a high-Fe tholeiite. This sample was taken at the same outcrop as CG01/21 and slight chemical differences may be due to localised alteration or sample processing procedures as the samples were processed in different batches.

The Wagondrift Formation samples yielded similar results when plotted on the Winchester and Floyd (1977) (from here on termed "FW") diagrams. The plot of SiO_2 – Zr/TiO_2, shows that subalkaline basalts dominate the Wagondrift Formation, although two samples (CG01/19 and CG01/20) plot very close to the andesite boundary (Figure 5.4b). The same classification results can be seen on the SiO_2 – Nb/Y graph (Figure 5.4c). Zr/TiO_2 can be used as a measure of differentiation and alkalinity, while Nb/Y can distinguish between alkaline and subalkaline suites of volcanic rocks.

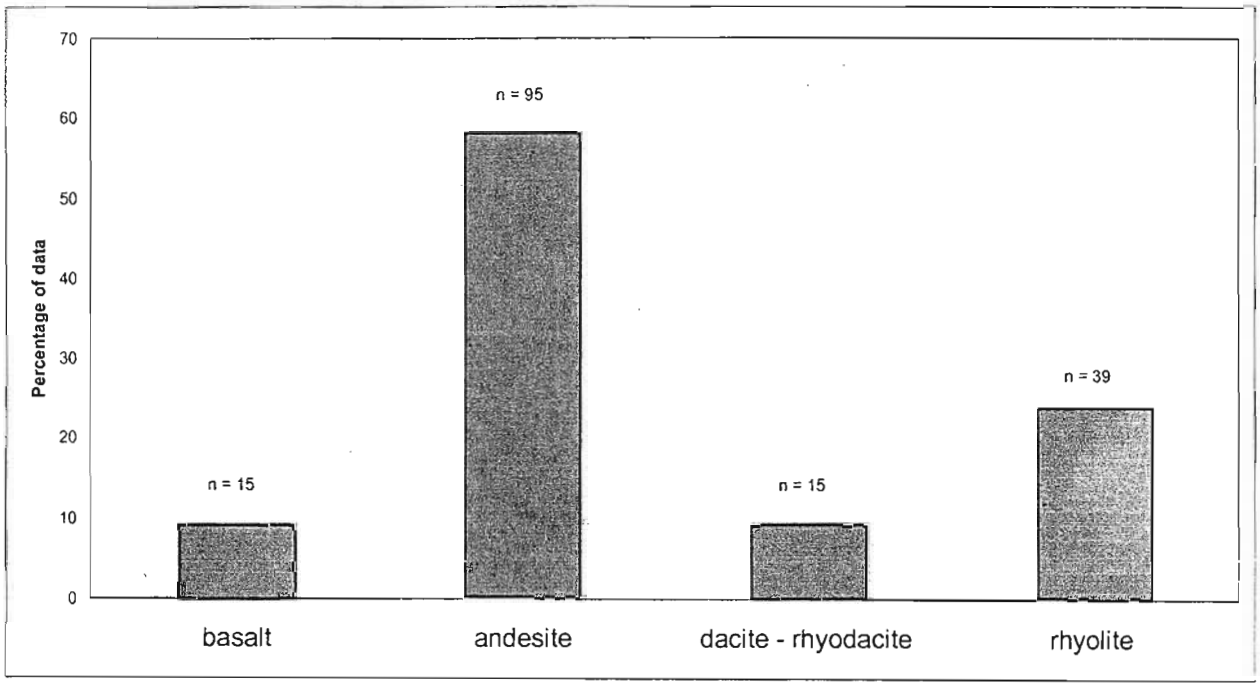

Figure 5.2 % Frequency graph showing the distribution of Nsuze Group data based on SiO_2 content. (basic 45-52 wt%SiO_2, intermediate 52-63 wt%SiO_2, dacite - rhyodacite 63-68 wt%SiO_2, rhyolite >68 wt%SiO_2)

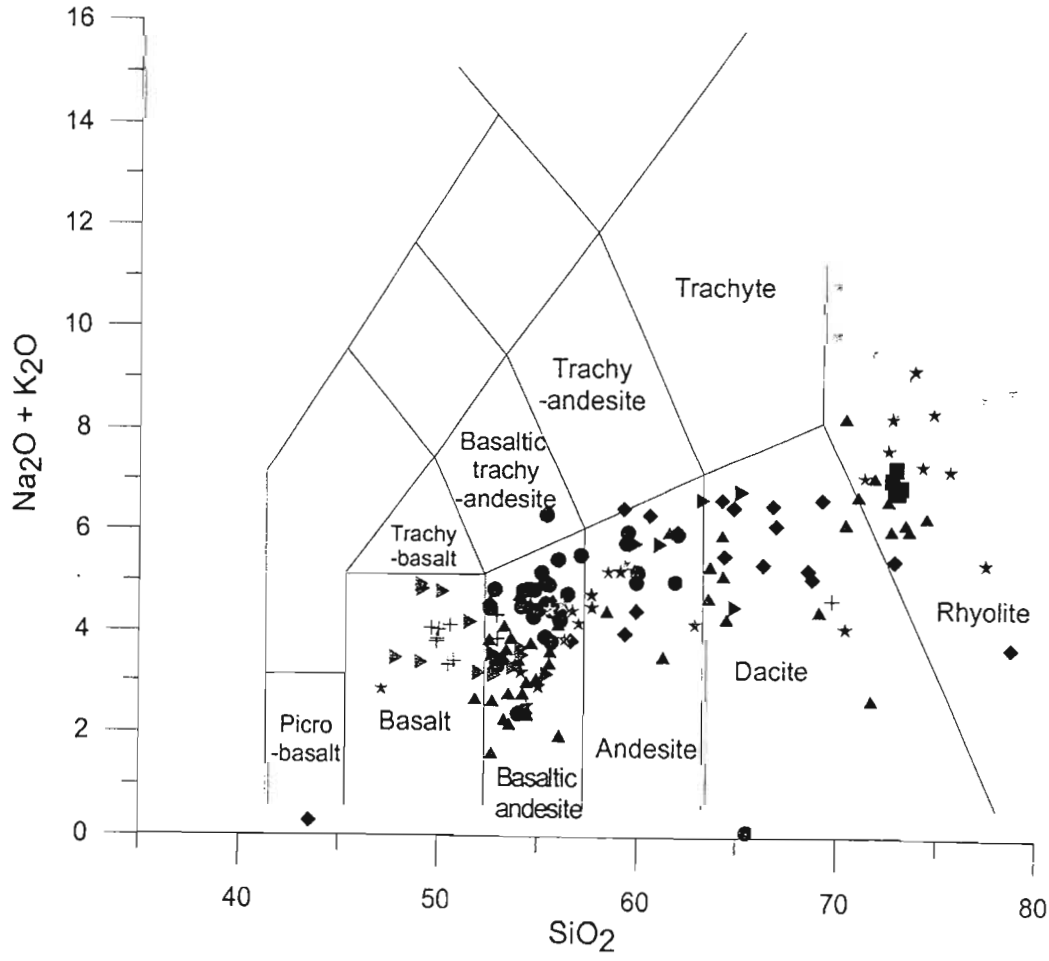

Figure 5.3 Total Alkali - Silica diagram for the classification of volcanic rocks (Le Maitre *et al.*, 1989) (Na_2O, K_2O and SiO_2 values in wt% oxide) (See Figure 5.4 for legend)

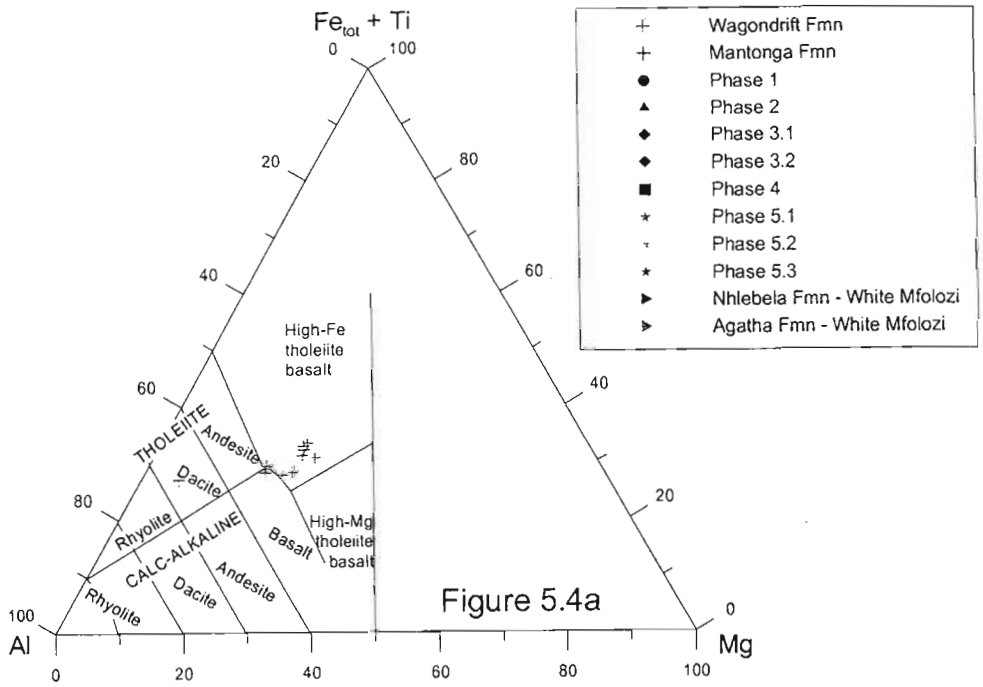

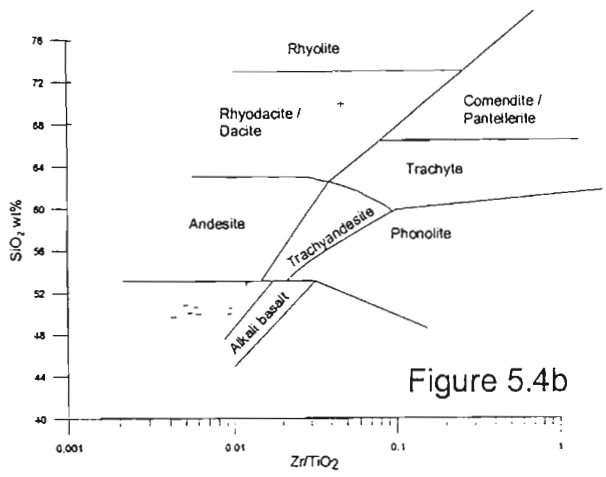

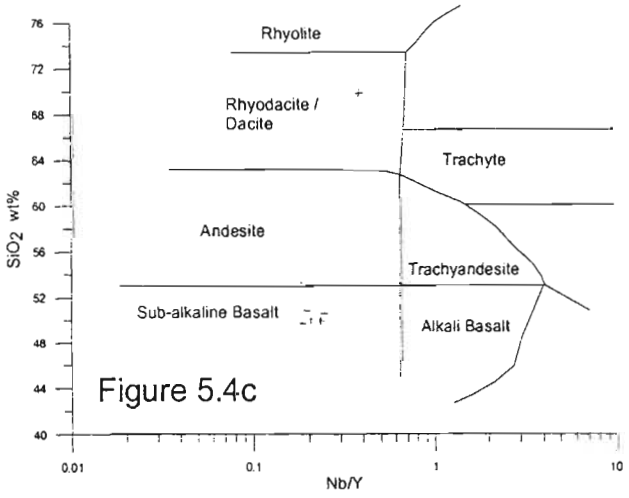

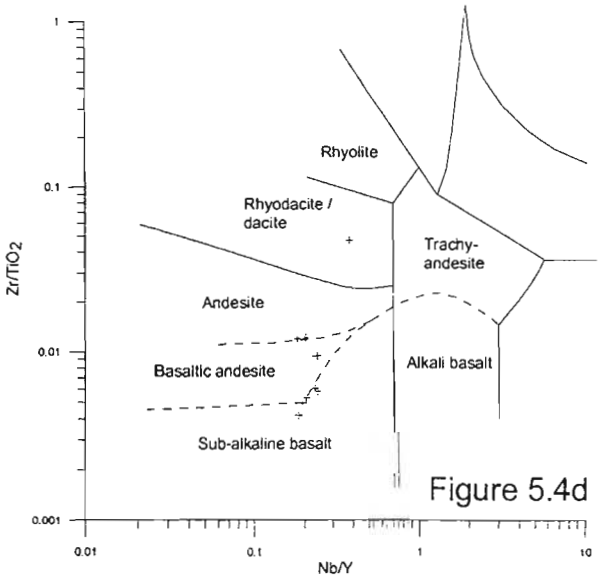

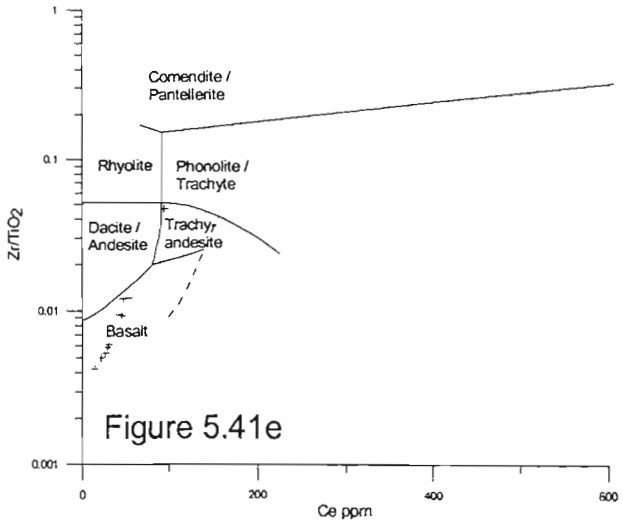

Figure 5.4 Wangondrift and Mantonga Formation Classification diagrams.
5.4a - Jensen Cation Plot (Jensen, 1976; Rickwood, 1989)
5.4b-e - Winchester and Floyd (1977)

The plot of Zr/TiO_2 against Nb/Y classifies samples CG01/13-CG01/18 being of a subalkaline basalt composition (Figure 5.4d). CG01/21 and CG01/170 plot just within the andesite field. This plot distinguishes a basaltic andesite field, in which samples CG01/19 and CG01/20 plot.

The Zr/TiO_2 – Ce graph also has samples in the subalkaline and alkaline fields. The subalkaline nature of the Wagondrift Formation is evident in the small variation in Ce values resulting in a steep linear trend on the graph (Figure 5.4e). Wagondrift Formation samples all classify as basalts, although CG01/13 is the most basic, while the two samples CG01/19 and CG01/20 plot close to the subalkaline basalt - andesite boundary. Individual sample results for all classification diagrams can be viewed in Appendix 6.

One sample was collected from the Mantonga Formation. The locality lies at the very top of the formation where lavas lie interbedded with quartzites. The sample, CG01/122, is classified as a tholeiitic dacite (Figure 5.4a), rhyodacite – dacite on the SiO_2 – Zr/TiO_2, SiO_2 – Nb/Y (Figure 5.4b-c) and Zr/TiO_2 – Nb/Y graphs (Figure 5.4d) and just within the trachy-andesite field on the Zr/TiO_2 – Ce graph (Figure 5.4e). The upper lava flow of the Mantonga Formation can therefore be classified as a dacite with slightly alkaline Ce values.

5.3.2 Phase 1, Bivane Subgroup – White River Section

Sampling data for Phase 1 identified in the White River Section of the Northern Region is plotted in Appendix 1 and described in Appendix 2. The JC ternary plot shows that the volcanic rocks of Phase 1 range in composition from tholeiitic high-Fe basalt to tholeiitic andesite (Figure 5.5a). Certain samples (CG01/1-3; CG01/6; CG01/49 and 2000/PG/20) plot just within the calcalkaline basalt field. It is clearly evident by field relationships that the volcanic units that these samples represent are closely related to the tholeiite samples. The occurrence of calcalkaline characteristics can therefore be attributed to alteration resulting in the one or more of the components of the JC plot (FeO, Fe_2O_3, TiO_2, MgO and Al_2O_3) not being representative of the original chemistry of the rock.

The FW binary plots all show samples to be of subalkaline basalt to andesitic composition (Figure 5.2b-e). Individual sample comparisons are reported in Appendix 6. Samples that deviated from the main group include CG01/5, CG01/7 and CG01/167. CG01/5 was taken in the centre of an epidote alteration patch, which is commonly associated with extensive silicification. This sample plotted as a rhyodacite / dacite on two graphs namely those including silica, SiO_2 vs Zr/TiO_2 (Figure 5.5b) and SiO_2 vs Nb/Y (Figure 5.5c). The sample however plots as an andesite on the Zr/TiO2 vs Nb/Y (Figure 5.5d) and Zr/TiO2 vs Ce (Figure 5.5e) FW graphs. CG01/7 and CG01/167 were taken from the same unit. These samples represent a volcanic unit described as a "fine-grained andesite" in Chapter 3. This unit, while markedly different in appearance in the field, is geochemically similar to the volcanic units surrounding it on the cliff section. The marked change in physical and petrological appearance may suggest that while it is geochemically similar to those units above and below it, the pinching-out unit may still represent a pyroclastic flow deposit as opposed to a lava flow or tuff, and was therefore deposited in a different manner to the rest of the volcanic units on the cliff.

5.3.3 Phase 2, Bivane Subgroup – White River Section

The localities of samples taken from Phase 2 are shown in Appendix 1 and recorded in Appendix 2. Classification results for individual samples are compared in Appendix 6. The JC plot yields three main groups of samples: a tholeiitic andesite group, an acid group that trends from tholeiitic dacite to tholeiitic rhyolite, and another dominant group that trends from high-Mg tholeiitic basalt to high-Fe tholeiitic basalt with a few samples plotting in the calcalkaline basalt field (Figure 5.6a). One sample CG01/39 plots as a calcalkaline dacite.

The FW binary plots yield similar results although certain samples show marked differences in classification from graph to graph. An acid group is identifiable on all graphs SiO_2 vs Zr/TiO_2 (dacite to rhyolite; Figure 5.6b); SiO_2 vs Nb/Y (dacite to rhyolite; Figure 5.6c); Zr/TiO_2 vs Nb/Y (dacite to rhyodacite; Figure 5.6d) and Zr/TiO_2 vs Ce (dacite to rhyolite / trachyte; Figure 5.6e). The other major group represented on these graphs is subalkaline basalt to andesite

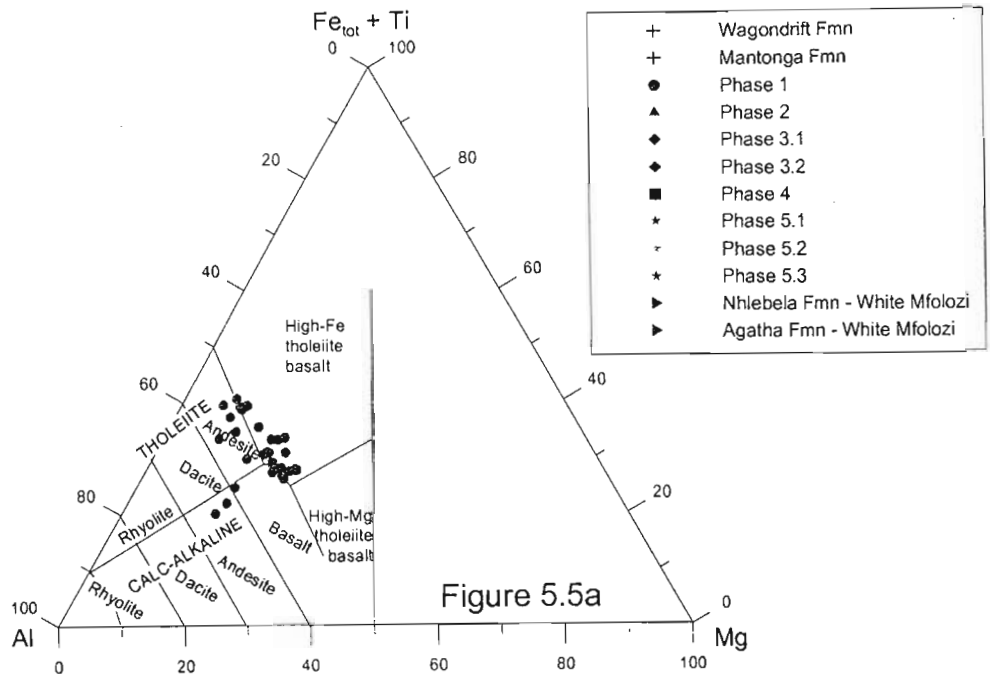

Figure 5.5a

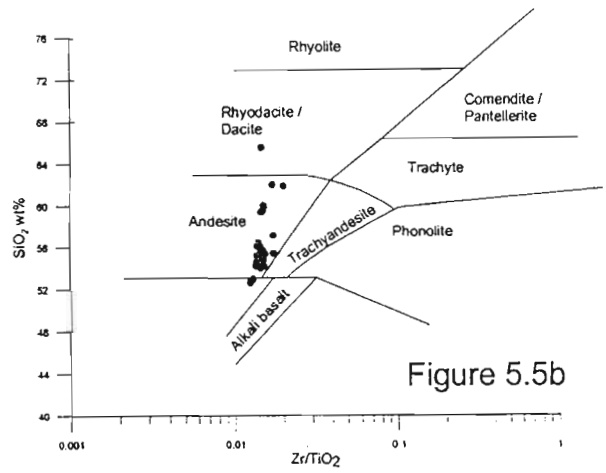

Figure 5.5b

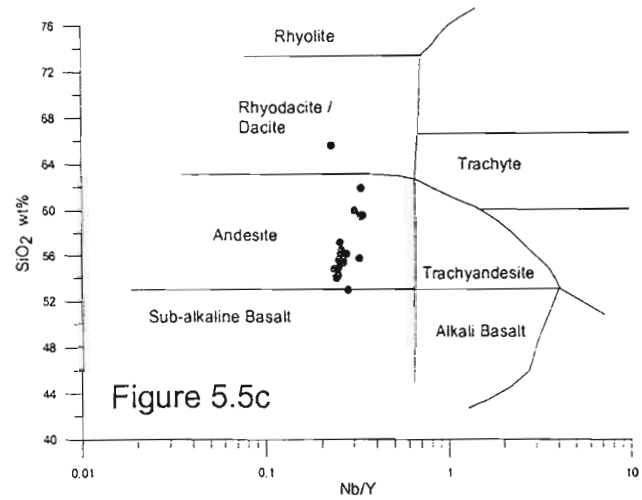

Figure 5.5c

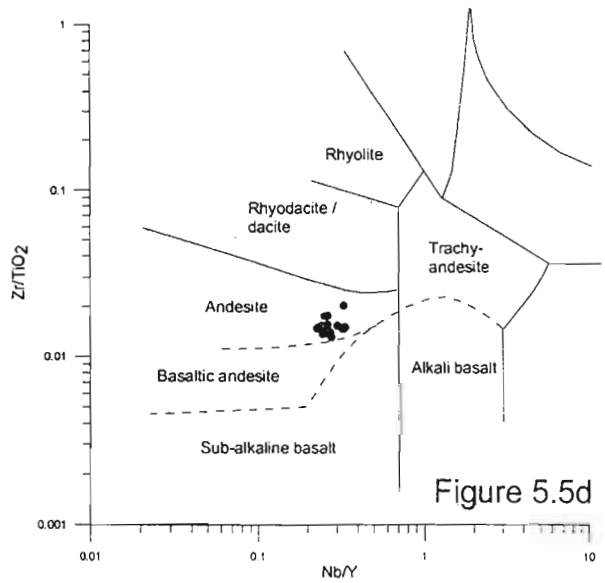

Figure 5.5d

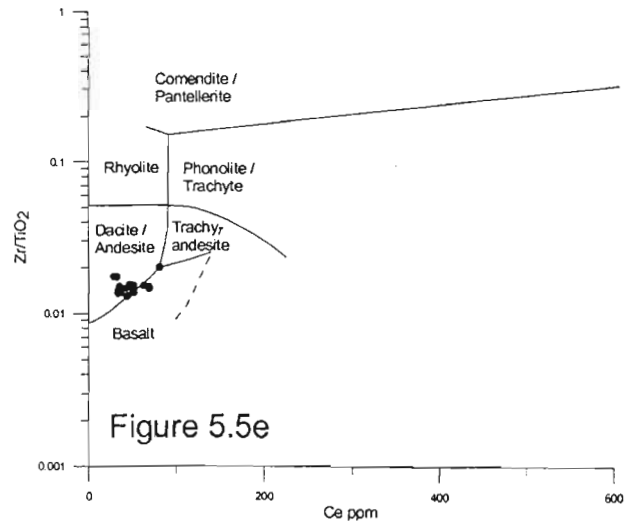

Figure 5.5e

Figure 5.5 Phase 1- White River Section Classification diagrams.
5.5a - Jensen Cation Plot (Jensen, 1976; Rickwood, 1989)
5.5b-e - Winchester and Floyd (1977)

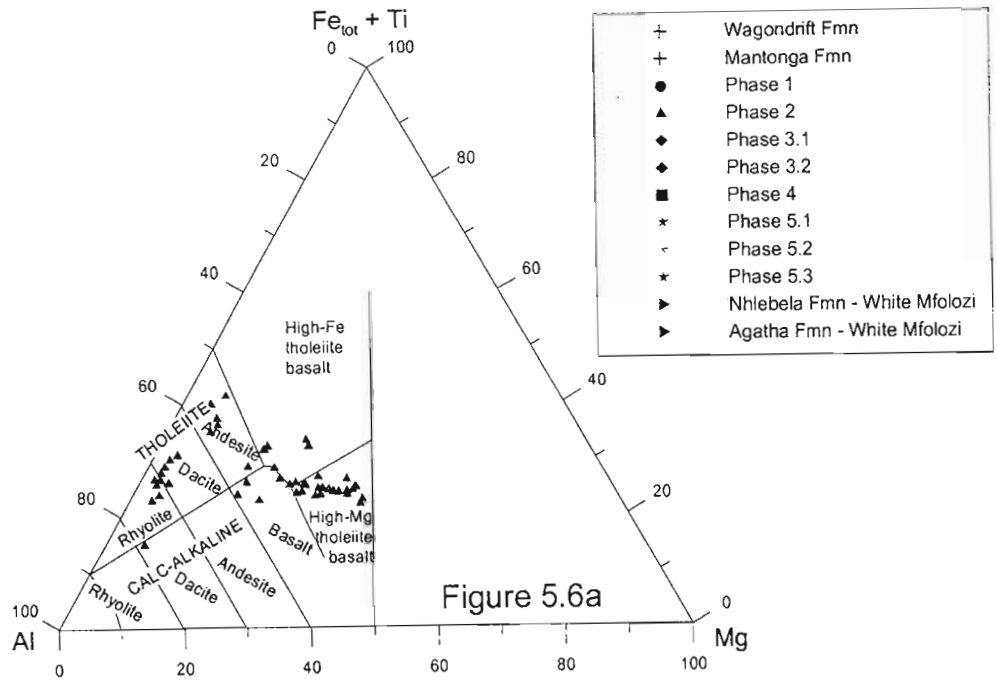

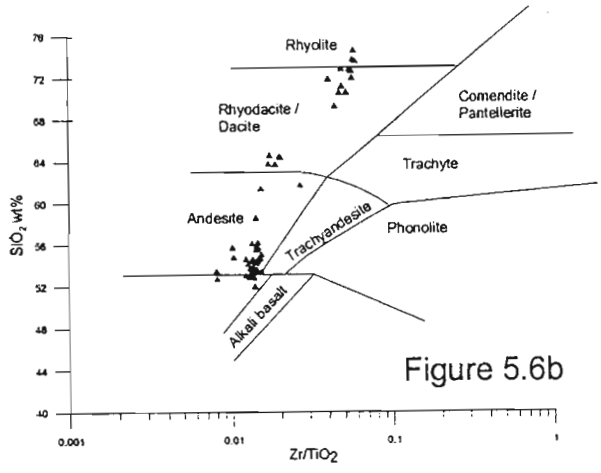

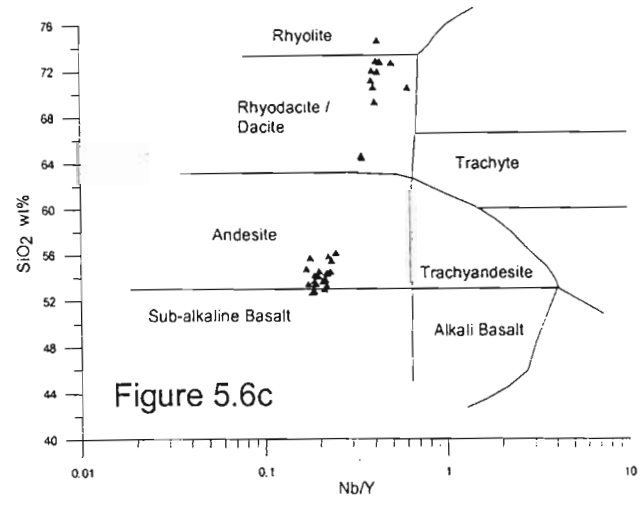

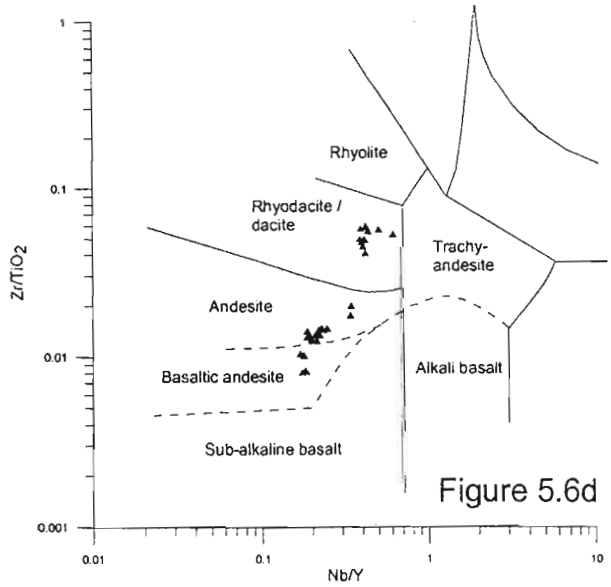

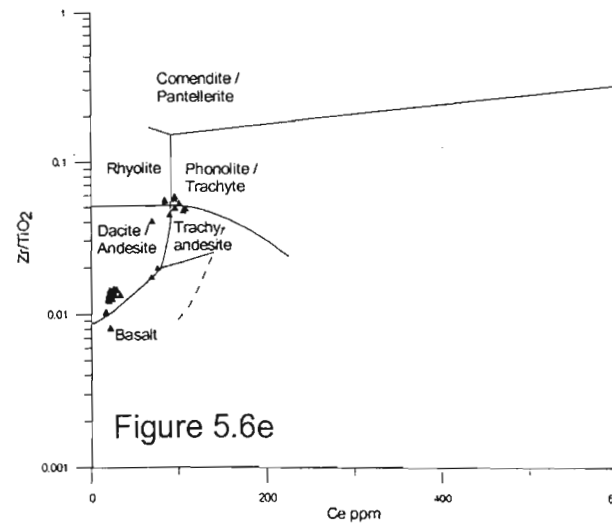

Figure 5.6 Phase 2- White River Section Classification diagrams.
5.6a - Jensen Cation Plot (Jensen, 1976; Rickwood, 1989)
5.6b-e - Winchester and Floyd (1977)

(Figure 5.6b-e). A smaller group of samples may be seen to plot between these two groups as an andesite – dacite transition composition (Figure 5.6b-e). These samples may form a legitimate classification group of their own or may have been subjected to silicification processes. This would elevate these samples' SiO_2 values so they would plot away from the main basalt – andesite group. Silica enrichment of certain volcanic rocks is supported by the fact that the samples in question plot much closer to the basalt –andesite group i.e. have a more basic composition on the Zr/TiO_2 vs Nb/Y graph (Figure 5.6d) than on the two graphs involving silica.

Phase 2 is dominated by two groups of samples: an acid group and a basic to intermediate group. A minor intermediate to acid group is also present but these samples may be affected by alteration. The FW diagrams, in contrast to the JC Plot, show the basic samples as more evolved i.e. basaltic andesite to andesite as opposed to basaltic. This may be as a result of silicification in the basic to intermediate samples or mobilisation of the components Fe_2O_3, FeO, TiO_2, Mg and Al that results in this difference. It may also be a factor of the construction of the field boundaries in the diagrams by the respective authors.

5.3.4 Phase 3, Bivane Subgroup – White River Section

Phase 3 is divided into two sub-phases based on geographic locality: Phase 3.1 in the north and Phase 3.2 in the south (Appendix 1). The samples of Phase 3.1 were collected in the Beki-Beki Tributary. As noted in the field descriptions, these outcrops are severely weathered, in particular those of basic to intermediate composition and therefore a bias may have been introduced in the sample collecting towards the acid volcanic rocks, as they were more suitable for geochemical analysis. The JC Plot for Phase 3.1 shows a trend of compositions from tholeiitic andesite to tholeiitic rhyolite (Figure 5.7a). Sample CG01/137 does not plot within this array, but instead lies deep within the high-Fe tholeiite basalt field. Compositions for specific samples can be seen in Appendix 6.

Winchester and Floyd's (1977) graph of SiO_2 vs Zr/TiO_2 used to classify samples representative of Phase 3.1 show a similar linear array from andesite through to rhyolite (Figure 5.7b). The andesite samples are closer to the andesite – dacite boundary on the FW graph than on the JC Plot. Samples CG01/117 and CG01/118 plot as trachy-andesites, indicating an alkaline affiliation. As no other samples show this affinity, disturbance of SiO_2 or Zr/TiO_2 values may be attributed to alteration. Sample CG01/137 plots below the boundary of alkali basalt and subalkaline basalt. This composition appears to be beyond the natural boundaries of primary volcanic rock compositions and its geochemical signature is therefore due to alteration. The sample appears to be severely depleted in silica, as an increase of wt% SiO_2 would result in the CG01/137 plotting in the andesite field with the other Phase 3.1 samples.

The three Winchester and Floyd (1977) graphs involving Nb/Y and Ce have a limited number of samples due to the fact that not all samples were analysed for all trace elements. Groups and trends are therefore more difficult to determine because of fewer samples. SiO_2 vs Nb/Y graph produces a linear trend from subalkaline andesite to rhyodacite (Figure 5.7c). Once again sample CG01/137 plots below the field boundary for alkali basalt and subalkaline basalt, an indication that the sample's geochemical characteristics have been subjected to alteration. A similar linear trend is not as obvious on the Zr/TiO_2 vs Nb/Y graph, but the samples still span the upper andesite field into the dacite / rhyodacite field (Figure 5.7d). CG01/137 plots as subalkaline basalt far removed from the rest of the samples of Phase 3.1. The Phase 3.1 samples cluster around the andesite / dacite – trachy-andesite border on the Zr/TiO2 vs Ce graph (Figure 5.7e). CG01/137 plots at the bottom of the andesite field and is again removed from the rest of the samples for Phase 3.1.

Sample CG01/137 plots as a different or unnatural composition in each graph (Figure 5.7a-e). This sample was noted in hand specimen to have a strange mottled appearance of light blue fine grained material in a dark blue "lava" matrix. The exact nature of this sample and its primary outcrop are unknown but the composition reflected in the geochemistry is not primary. Care must therefore be taken with this sample in future graphs.

Phase 3.2 lies to the south of the White River Section (Appendix 1). A lack of samples from within Phase 3.2 makes the identification of

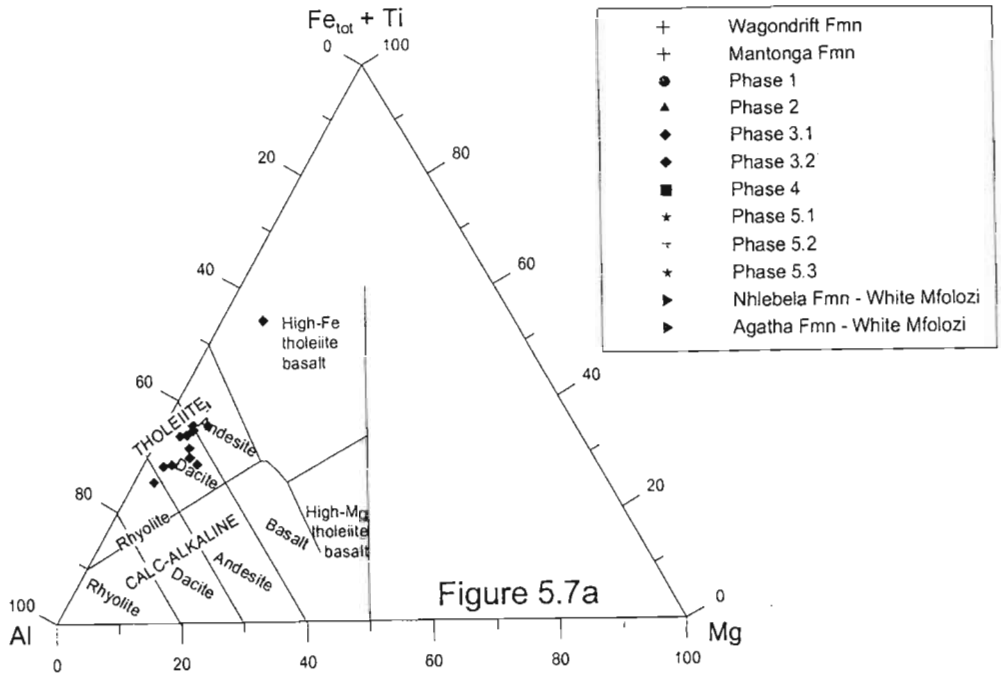

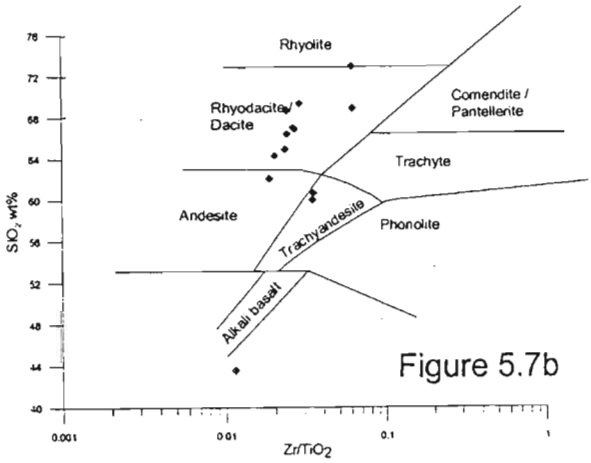

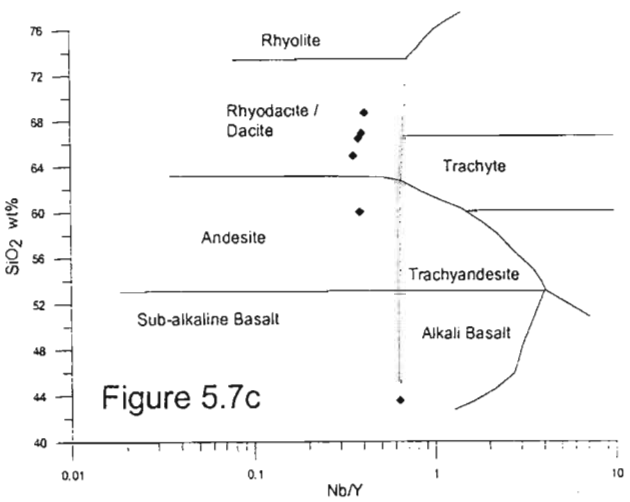

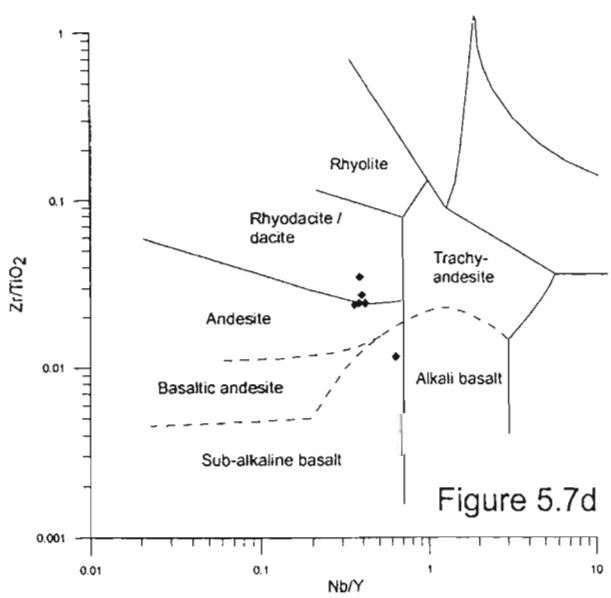

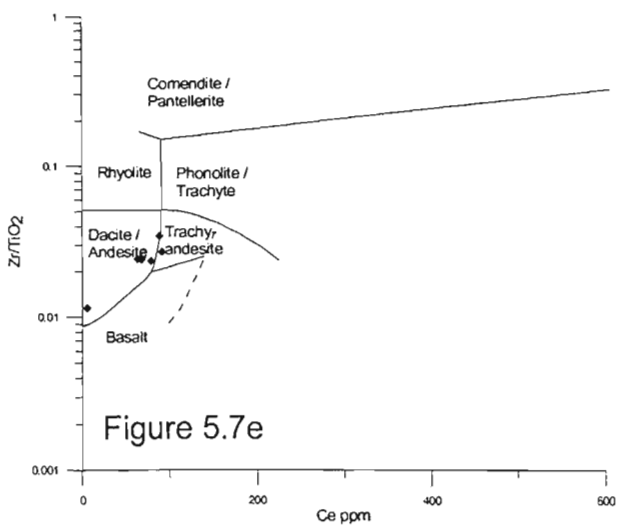

Figure 5.7 Phase 3.1 - White River Section Classification diagrams.
5.7a - Jensen Cation Plot (Jensen, 1976; Rickwood, 1989)
5.7b-e - Winchester and Floyd (1977)

trends and clusters difficult. Phase 3.2 possibly forms three groups on the JC Plot, a high-Fe tholeiitic basalt group, a tholeiitic andesite group and a tholeiitic rhyolite group (Figure 5.8a). No such groups can be interpreted from the FW graph of SiO_2 vs Zr/TiO_2. On this graph samples appear to be predominantly andesitic in composition, with two outliers. CG01/75 plots as a dacite, while CG01/78 plots as alkali basalt (Figure 5.8b). CG01/80 although still andesitic, lies close to the alkali boundary. On an individual basis samples plot as different rock types on the JC plot compared to FW SiO_2 vs Zr/TiO_2 graph i.e. CG01/79 is a high-Fe tholeiitic basalt on JC diagram and an andesite on the FW SiO2 vs Zr/TiO_2 graph, and for both graphs the sample plots convincingly within the respective fields. A comparison of sample compositions for each classification diagram can be seen in Appendix 6.

The FW diagrams of SiO_2 vs Nb/Y (Figure 5.8c), Zr/TiO_2 vs Nb/Y (Figure 5.8d) and Zr/TiO_2 vs Ce (Figure 5.8e) have fewer sample points than the previously described classification diagrams for Phase 3.2. This is as a result of fewer Phase 3.2 samples being analysed by ICP-MS for trace elements. For FW diagrams SiO_2 vs Nb/Y and Zr/TiO_2 vs Nb/Y, two samples (CG01/79 and CG01/81) are andesitic in composition. CG01/75 plots in both diagrams as a dacite (Figure 5.8c & d). CG01/79 and CG01/81 also plot as andesites on the FW Zr/TiO2 vs Ce graph, but CG01/75 has a composition of trachy-andesite (Figure 5.8e).

5.3.5 Phase 4, Bivane Subgroup – White River Section

Phase 4 outcrops on the top of a hill in the north of the White River Section (Appendix 1). Five samples (only four run for ICP-MS trace element analysis) represent this laterally extensive but stratigraphically limited unit. On all classification diagrams samples plot as a tight cluster suggesting that they represent the same stratigraphic unit. Phase 4 is classified as tholeiitic rhyolite on the JC diagram (Figure 5.9a). The FW SiO_2 vs Zr/TiO_2 graph classifies the Phase 4 samples as rhyolites, with the exception of 2000PG/30, which plots just below the lower rhyolite field boundary as a rhyodacite (Figure 5.9b). The tightly clustered nature of the samples however still suggests that they are of the same volcanic unit, but that the group spans the boundary of the rhyodacite and rhyolite fields. The Phase 4 cluster of samples plot just below the rhyolite boundary as rhyodacites on the FW SiO2 vs Nb/Y graph (Figure 5.9c). All samples for Phase 4 plot neatly into the rhyodacite / dacite field on the FW Zr/TiO2 vs Nb/Y diagram (Figure 5.9d). On the FW Zr/TiO2 vs Ce graph Phase 4 sample cluster plots on the subalkaline dacite – alkaline trachy-andesite boundary (Figure 5.9e).

5.3.6 Phase 5, Bivane Subgroup – White River Section

Phase 5 is divided into three sub-phases based on geographic locality, Phase 5.1 in the north, Phase 5.2 in the centre and Phase 5.3 in the south of the White River Section (Appendix 1). Phase 5.1 samples were collected in the Beki-Beki tributary (Appendix 1) where the outcrops are highly weathered as well as been affected by a shear zone in the north of the Phase 5.1 area. Few samples were therefore suitable for geochemical analysis and those investigated may not be fully representative of the phase as a whole. The samples of Phase 5.1 are classified as high-Fe tholeiite basalts according to the JC diagram (Figure 5.10a). Sample CG01/111 plots as a komatiitic basalt. This sample has a high-Mg content, which is not observed in other samples of the Nsuze Group data set. Whether this is a factor of true ultramafic composition or as a result of alteration must be determined by looking at the other major and trace elements. The FW SiO_2 vs Zr/TiO_2 diagram shows different classification results for the same Phase 5.1 samples. Samples classify as andesites, with only CG01/112 plotting as subalkaline basalt (Figure 5.10b). CG01/107 plots at the andesite – dacite border. Only one sample from Phase 5.1 was analysed for trace elements using ICP-MS. This sample CG01/106 plots as andesite on the FW SiO_2 vs Nb/Y (Figure 5.10c), Zr/TiO_2 vs Nb (Figure 5.10d) and Zr/TiO_2 vs Ce graphs (Figure 5.10e).

Phase 5.2 classifies as two groups of samples on the JC diagram, an acid group and a high Fe-tholeiite basalt group (Figure 5.11a). Sample CG01/43 plots as a calcalkaline rhyolite but its relationship to the other tholeiitic rhyolite samples has been observed in the field so its calcalkaline affinity may be due to alteration. The same set of samples plot as two groups, one intermediate or andesitic and the other acid on the FW SiO_2 vs Zr/TiO_2 graph (Figure 5.11b). The acid samples form an almost vertical linear

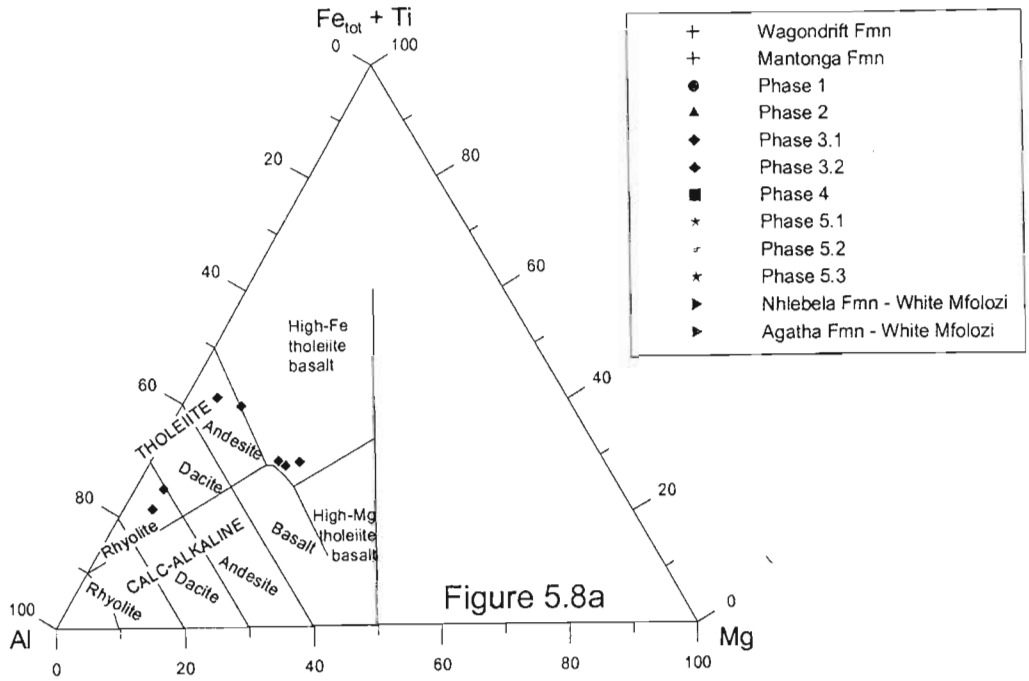

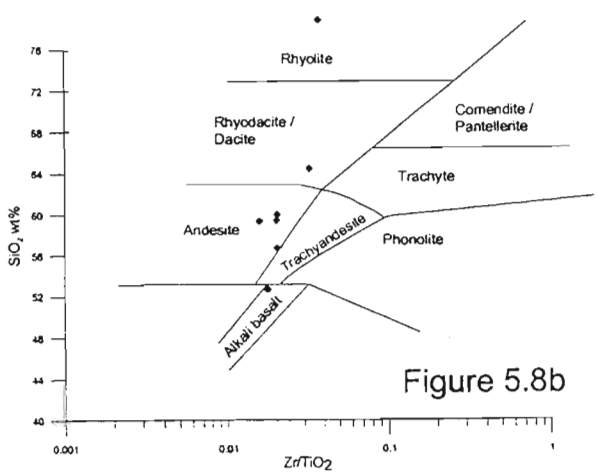

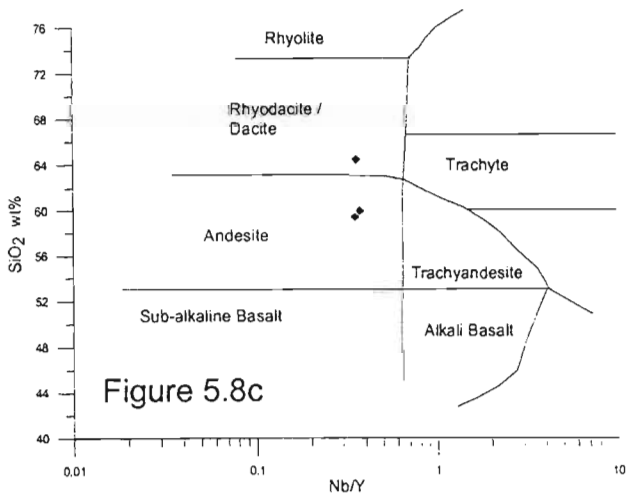

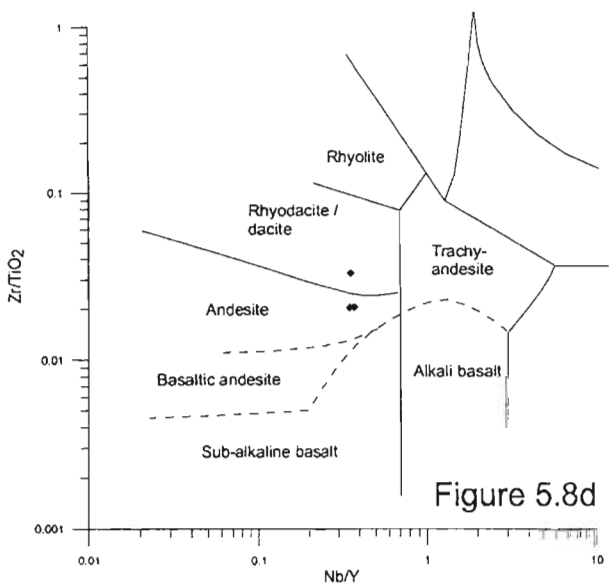

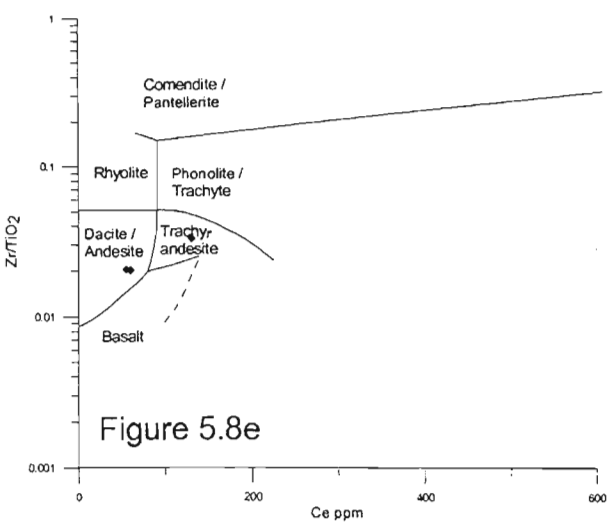

Figure 5.8 Phase 3.2 - White River Section Classification diagrams.
5.8a - Jensen Cation Plot (Jensen, 1976; Rickwood, 1989)
5.8b-e - Winchester and Floyd (1977)

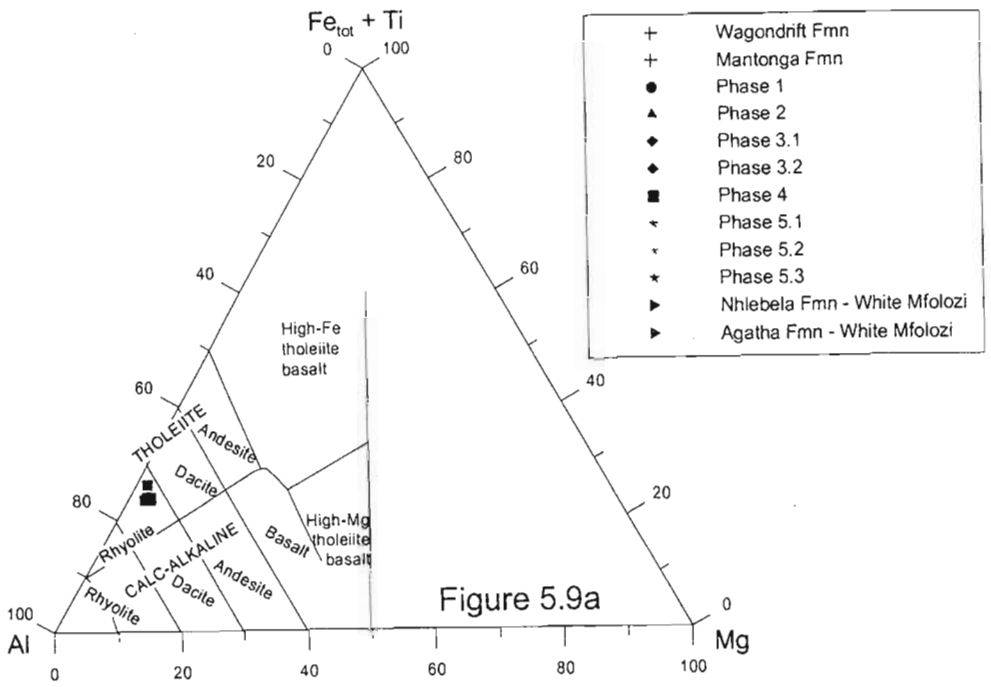

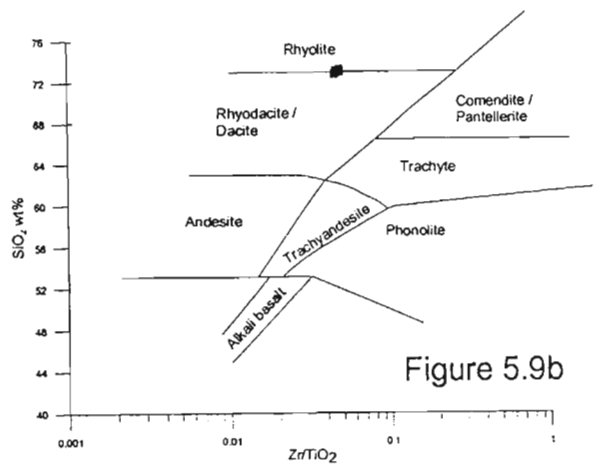

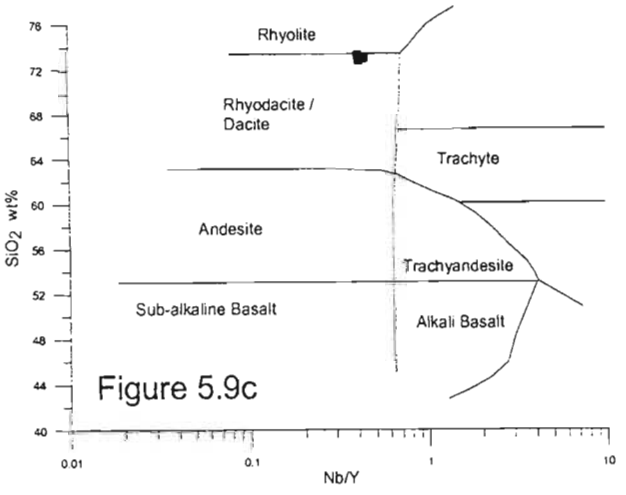

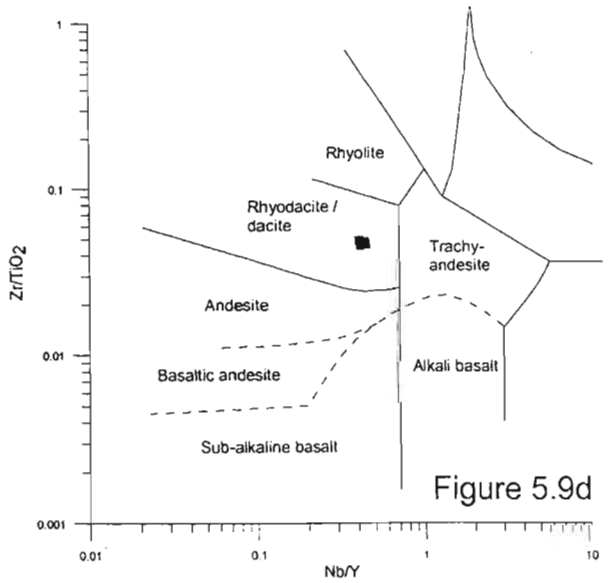

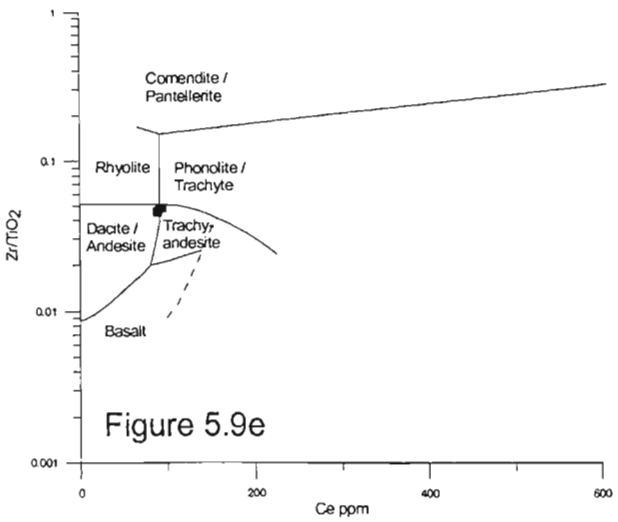

Figure 5.9 Phase 4 - White River Section Classification diagrams.
5.9a - Jensen Cation Plot (Jensen, 1976; Rickwood, 1989)
5.9b-e - Winchester and Floyd (1977)

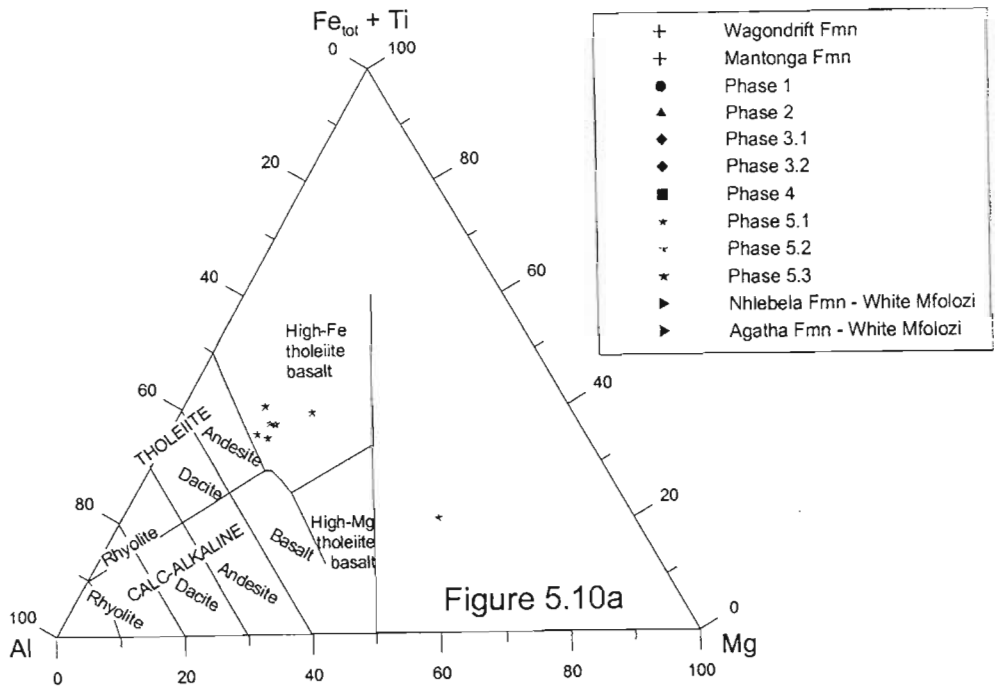

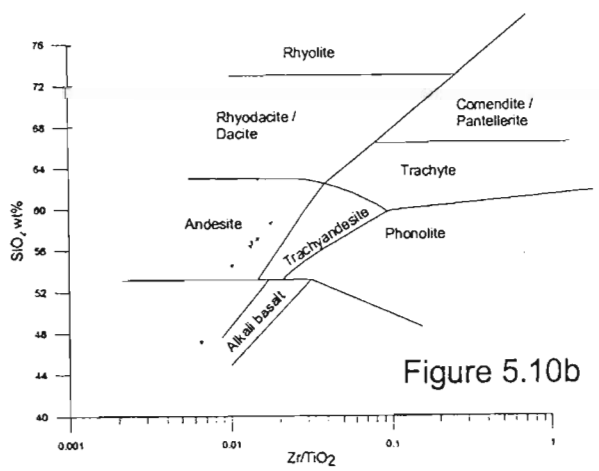

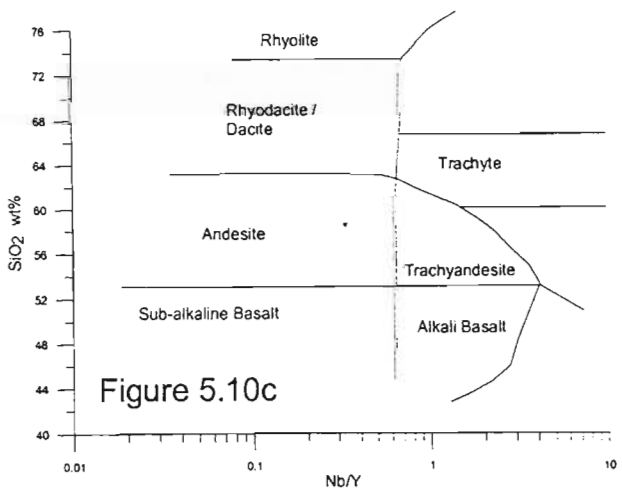

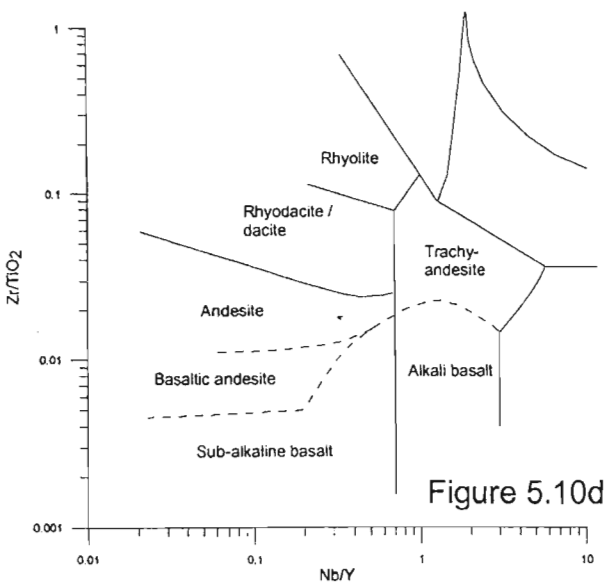

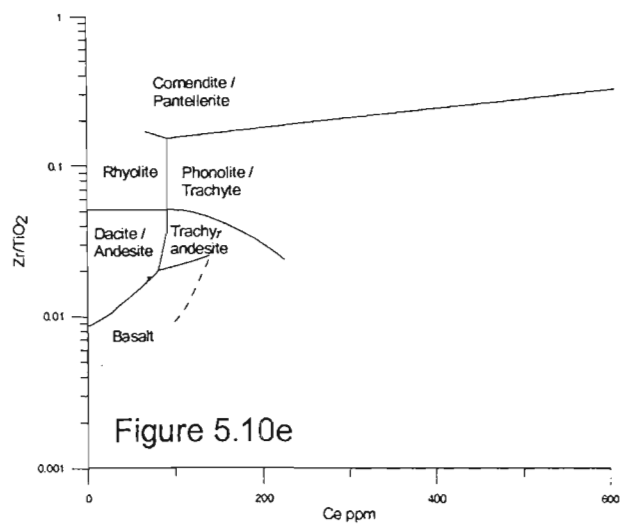

Figure 5.10 Phase 5.1 - White River Section Classification diagrams.
5.10a - Jensen Cation Plot (Jensen, 1976; Rickwood, 1989)
5.10b-e - Winchester and Floyd (1977)

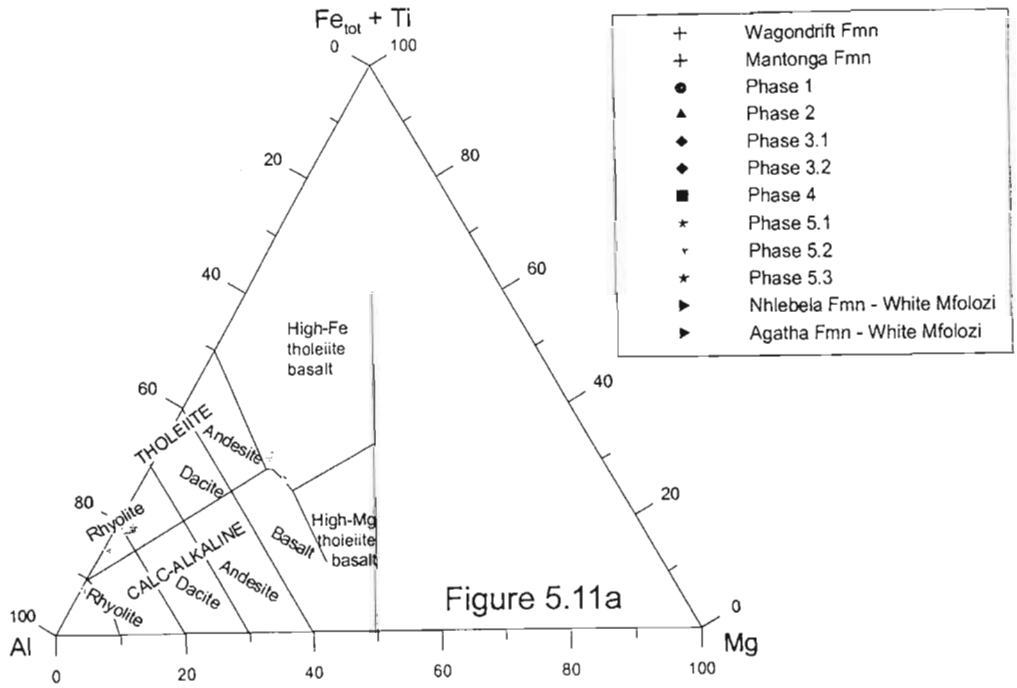

Figure 5.11a

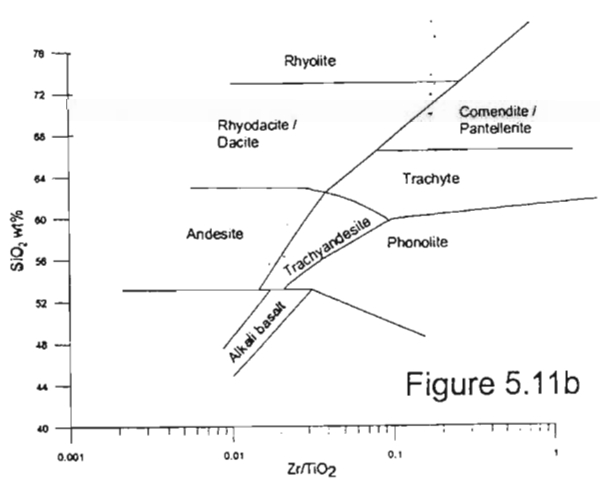

Figure 5.11b

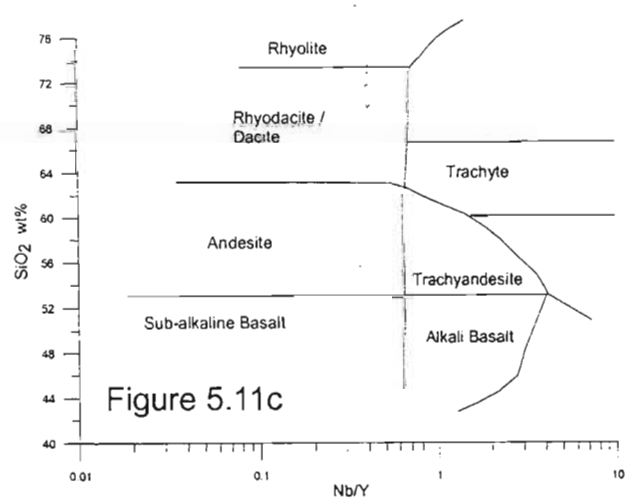

Figure 5.11c

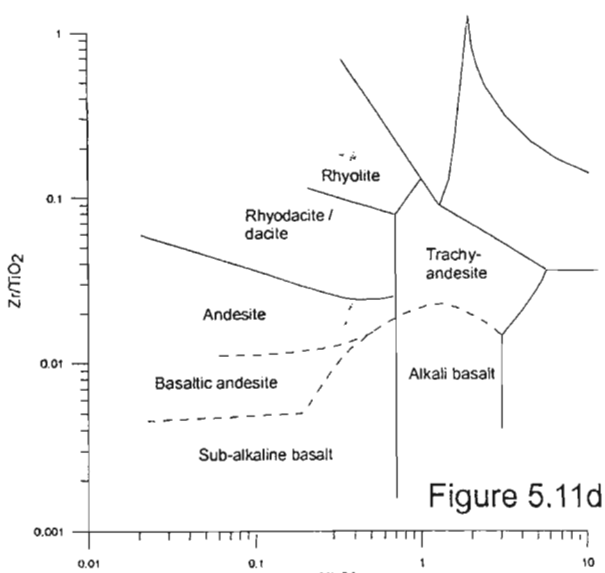

Figure 5.11d

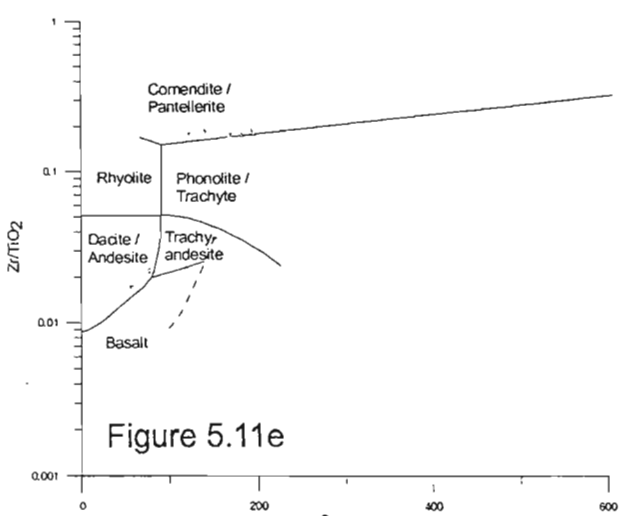

Figure 5.11e

Figure 5.11 Phase 5.2 - White River Section Classification diagrams.
5.11a - Jensen Cation Plot (Jensen, 1976; Rickwood, 1989)
5.11b-e - Winchester and Floyd (1977)

trend from alkaline pantellerite through into sub-alkaline rhyodacite and into the rhyolite field. It is debatable whether this trend is primary or secondary in nature. The occurrence of two samples (2000PG/2 and 2000PG/5) in the pantellerite field in contrast to the other PG samples (taken in the same vicinity - see Appendix 1), which plot in the subalkaline acid fields, suggests that these two samples have ether undergone SiO_2 depletion, Zr enrichment or TiO_2 depletion. Phase 5.2 also classifies into two compositional groups on the FW SiO_2 vs Nb/Y graph. The andesite group of samples is the same as that reflected in the previous classification diagrams. The acid group of samples trends in a vertical linear array across the rhyodacite – rhyolite boundary with samples plotting in both fields (Figure 5.11c). The same classification results are observed from FW Zr/TiO_2 vs N/Y diagram with samples plotting as two distinct groups of andesite or rhyolite (Figure 5.11d). The FW Zr/TiO_2 vs Ce graph shows an andesite group of samples and an acid group of samples (Figure 5.11e). The acid group, however plot entirely as alkaline acid compositions i.e. phonolite and pantellerite.

Phase 5.3 lies in the south of the White River Section (Appendix 1). Two main groups of samples can be identified in the JC diagram of Phase 5.3. The basic to intermediate group spans a wide range of compositions from high-Mg tholeiite basalt along the high-Fe tholeiite basalt and calcalkaline basalt boundary and just into the tholeiitic andesite field (Figure 5.12a). The acid group of Phase 5.3 samples plot within the tholeiitic rhyolite field. CG01/97 plots as a tholeiitic dacite away from the rest of the Phase 5.3 acid samples. This sample was observed to have well developed layering.

The FW graph of SiO_2 vs Zr/TiO_2 shows the same two groups of composition as seen on the JC plot. The intermediate group trends from the trachy-andesite field through the andesite field (Figure 5.12b). The reason for samples plotting in the alkaline field of trachy-andesite is possibly due to alteration. The acid group of samples plot from rhyodacite into the rhyolite field. CG01/97 plots away from any group as a rhyodacite / dacite.

The FW graph of SiO_2 vs Nb/Y reveals the same two compositional groups as interpreted from Figure 5.9a and 5.9b (Figure 5.12c). The andesite group has no samples plotting across the alkaline – subalkaline boundary. The acid group plots from just below the rhyodacite / rhyolite boundary into the rhyolite field. There are no outliers but this may be due to the fact that samples such as CG01/97 were not processed for trace elements using ICP-MS. The same results can be observed from the FW Zr/TiO_2 vs Nb/Y diagram, an andesite group and an acid group (which lies solely in the rhyolite field) (Figure 5.12d). While the FW Zr/TiO_2 vs Ce plot has two compositionally distinct groups, an intermediate and an acid group, the acid group lies across the alkaline – subalkaline boundary (Figure 5.12e). The intermediate andesite group plots almost entirely as andesites except for CG01/165, which plots just within the subalkaline basalt field. The acid group trends from phonolite to pantellerite, both alkaline compositions.

5.3.7 Nhlebela and Agatha Formations, Bivane Subgroup – White Mfolozi Inlier

The White Mfolozi Inlier contains two volcanic units, the Nhlebela Formation and the younger Agatha Formation. The Nhlebela Formation samples were taken in the White Mfolozi River (Figure 3.47). The comparison of individual sample compositions is recorded in Appendix 6. The Nhlebela Formation shows a spectrum of compositions from high-Fe tholeiitic basalt through tholeiitic andesite to tholeiitic dacite when plotted on the JC diagram (Figure 5.13a). It is noticeable that CG02/210 has the lowest Al content and plots well within the high-Fe tholeiite basalt field. The FW SiO_2 vs Zr/TiO_2 and FW SiO_2 vs Nb/Y graph show a similar scenario with the Nhlebela Formation samples plotting from andesite to dacite. The sample CG02/210 plots as a subalkaline basalt and is distinctly separate from rest of the data. On the FW Zr/TiO_2 vs Nb/Y diagram, the Nhlebela Formation samples plot as dacites, while CG02/210 lies on the basaltic andesite – sub-alkaline basalt boundary. The FW Zr/TiO_2 vs Ce graph also demonstrates the distinct difference between CG02/210 (basalt) and the rest of the Nhlebela Formation data (dacite / andesite). All samples show a subalkaline affinity. CG02/210 although stratigraphically located in the middle of the sequence (Figure 3.47) is different from the other Nhlebela Formation samples, which clearly form part of the same system. CG02/210 is described in hand specimen as being massive and fine-grained. The locality where the sample

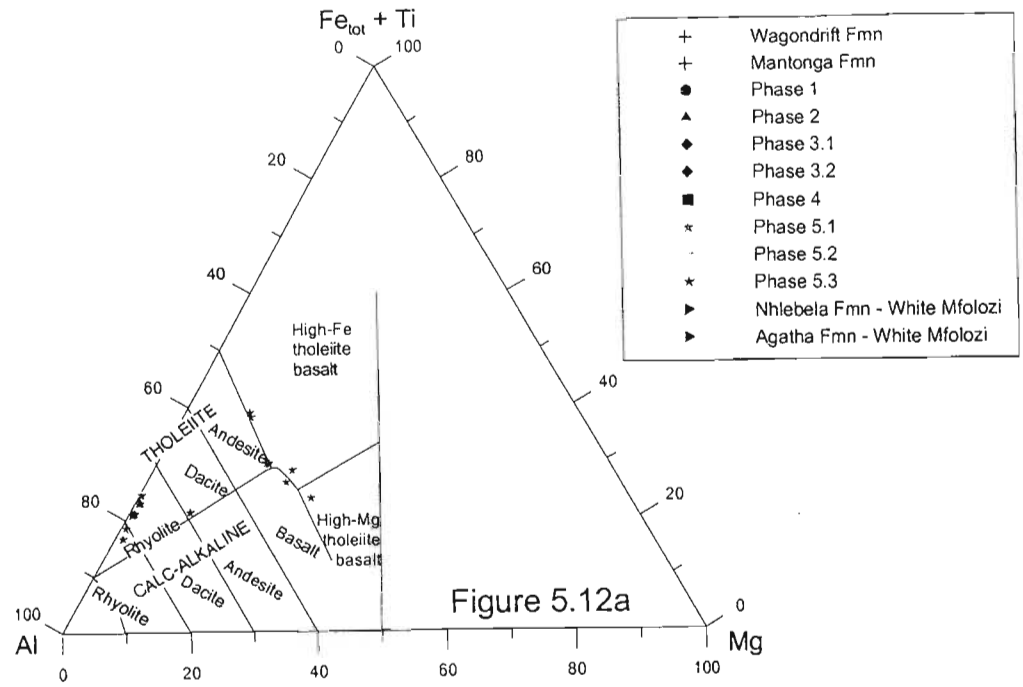

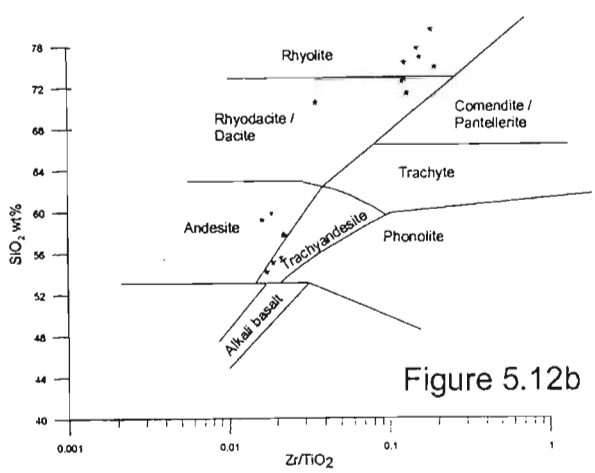

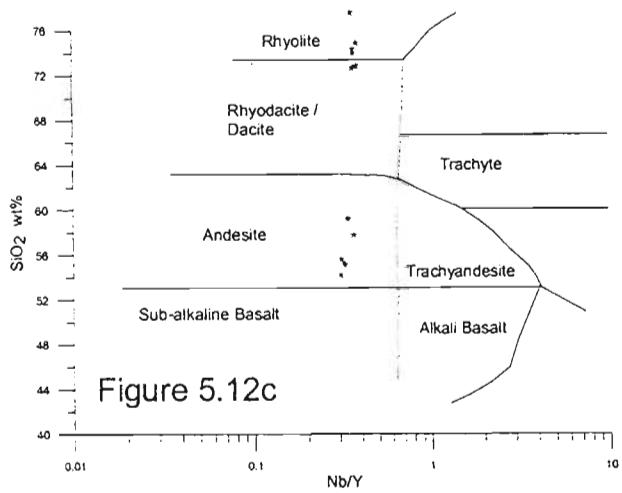

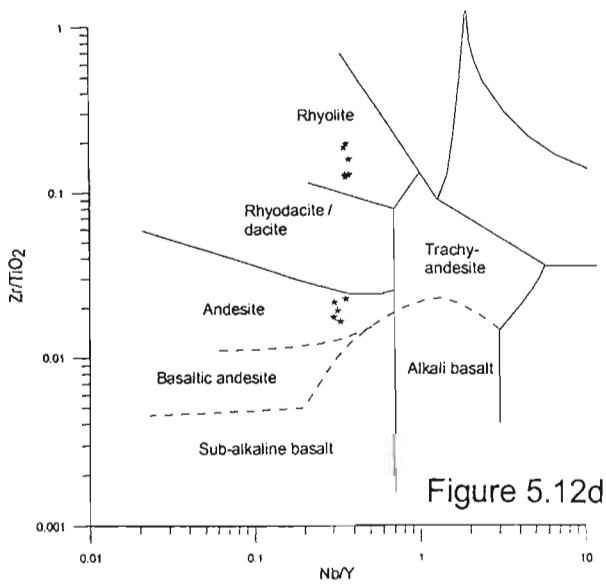

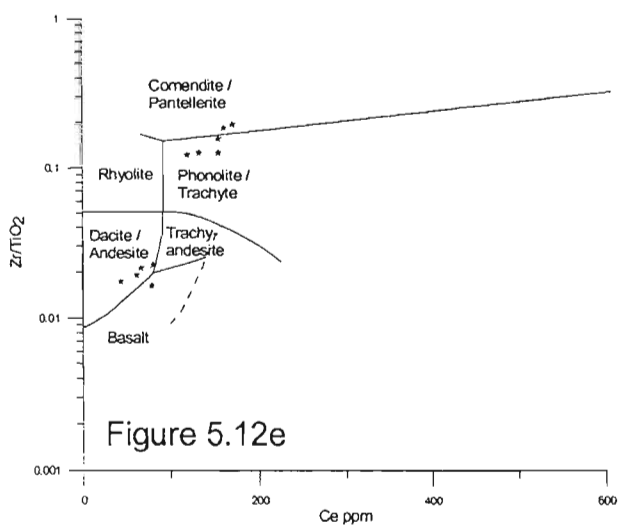

Figure 5.12 Phase 5.3 - White River Section Classification diagrams.
5.12a - Jensen Cation Plot (Jensen, 1976; Rickwood, 1989)
5.12b-e - Winchester and Floyd (1977)

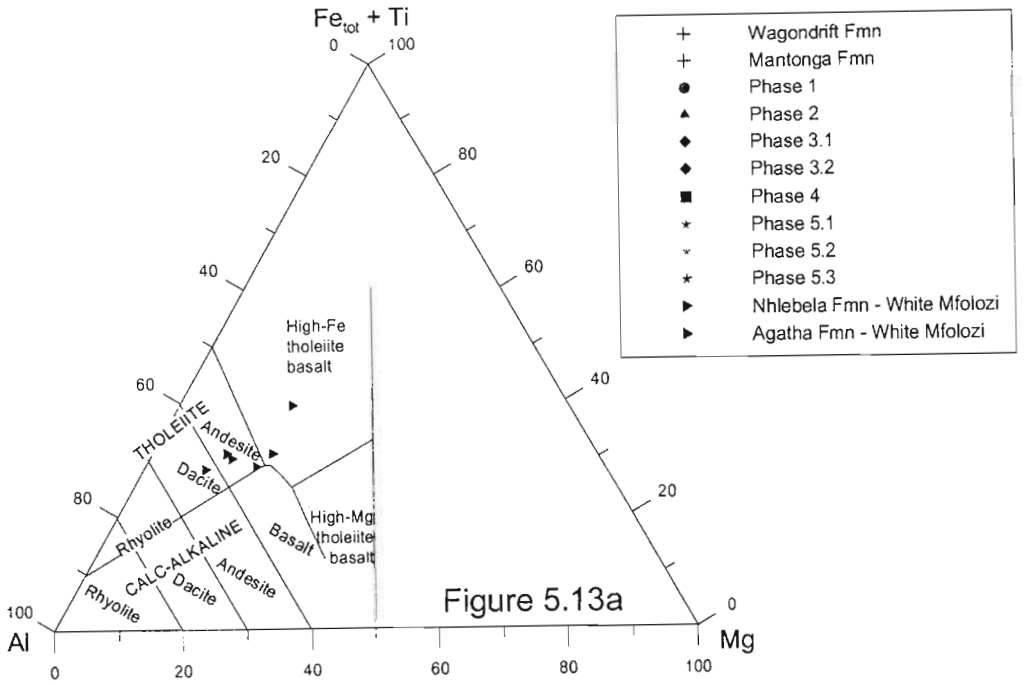

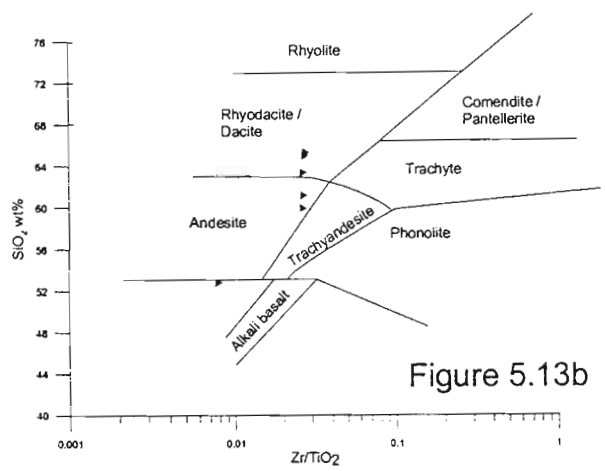

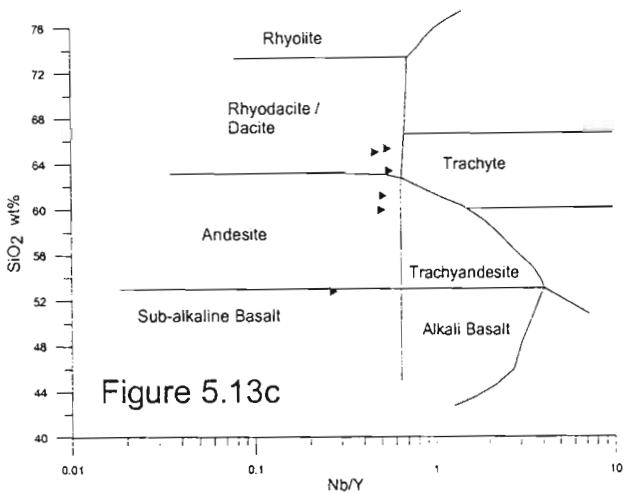

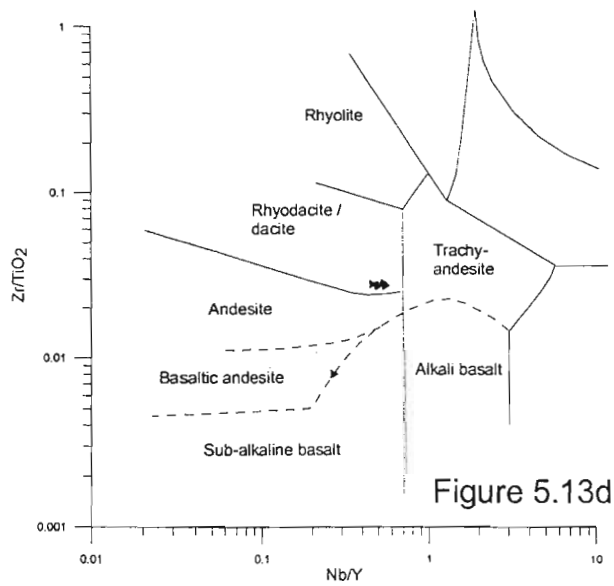

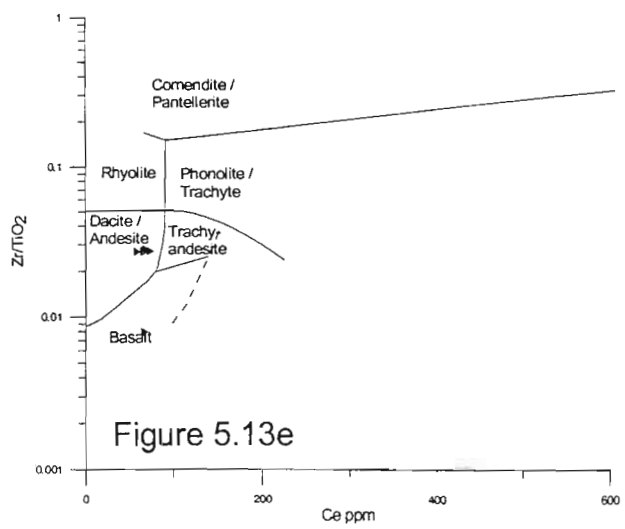

Figure 5.13 Nhlebela Formation - White Mfolozi Inlier Classification diagrams.
5.13a - Jensen Cation Plot (Jensen, 1976; Rickwood, 1989)
5.13b-e - Winchester and Floyd (1977)

was taken does, however, lack vesicles, amygdales or other common structures associated with lavas. The presence of intrusives (both sills and dykes of varying ages) in the area suggests that CG02/210 may represent a basic intrusive (probably a sill) that due to the outcrop pattern is not easily identifiable. Whether the sample represents a feeder intrusive to the Nsuze Group lavas or a later intrusive event is unknown.

The location of the Agatha Formation samples is illustrated in Figure 3.55, and described in Appendix 2. The comparison of individual sample compositions is recorded in Appendix 6. The Agatha Formation samples plot as high-Fe tholeiite basalts on the JC plot (Figure 5.14a). When samples are plotted on the FW SiO_2 vs Zr/TiO_2 graph, the form a near vertical array from alkali basalt through subalkaline basalt to andesite (Figure 5.14b). The alkaline affinity is not repeated in the FW graphs of SiO_2 vs Nb/Y – subalkali basalt to andesite (Figure 5.14c), Zr/TiO_2 vs Nb/Y – basaltic andesite to andesite (Figure 5.14d), and Zr/TiO_2 vs CE – basalt to andesite (Figure 5.14e). The fact that the Zr/TiO_2 ratio controls the alkali boundary in FW SiO_2 vs Zr/TiO_2 (and the samples plot as alkali basalts) and that the Zr/TiO_2 ratio also controls the fractionation fields in Zr/TiO_2 vs Nb/Y (no samples plot as basalts, but only basaltic andesites), suggests that the Zr/TiO_2 ratios may be elevated for certain Agatha Formation samples.

5.3.8 Discussion of compositional variation within Nsuze Group

The White River Section in the Northern Region of the Nsuze Group demonstrates a wide spectrum of lava compositions from basalt through to rhyolite. The overall geochemical affinity of the data set appears to be subalkaline. The alkaline nature of certain samples may be due to alteration, in particular the enrichment of Ce in acid compositions. The Jensen Cation incorporates the tholeiite – calcalkaline boundary and samples on this diagram appear to exhibit a tholeiitic affinity. Those samples that plot within the calcalkaline field are generally of a basaltic composition and plot at the apex of the tholeiite – calcalkaline curve. A slight change in the components Fe, Ti, Mg or Al through alteration could result in the basic samples crossing the tholeiite – calcalkaline curve.

The Wagondrift Formation is composed of sub-alkaline tholeiitic basalts to basaltic andesites, while the volcanic rock at the top of the Mantonga Formation is acid in composition. The predominantly sedimentary nature of the Mantonga Formation, with minor pyroclastics and lava flows indicates that the relative volcanic quiescence coincided at the same time with fractionation of the magma at depth. In general, the Phase 1 volcanic rocks form a suite of tholeiitic basalts, basaltic andesites and andesites. There is a distinct lack of acid compositions as seen in the lower Mantonga Formation. This would suggest that either a common magma chamber was re-injected with more primitive magma, or that the source areas of the Mantonga Formation and Phase 1 are different. Phase 2 is dominated by two groups of samples: an acid group and a basic to intermediate group. Phase 3 has a complete range of compositions from andesite to rhyolite found in both the north and south of the White River Section. Phase 4 represents a purely acid phase of volcanism, while Phase 5 is dominated by acid compositions, with a minor group of intermediate volcanic rocks. There is an overall increase in the proportion of acid compositions to basic compositions with younger phases of eruption of the Bivane Subgroup. Basic compositions are limited to the Wagondrift Formation and Phase 1, although Phase 5.1 may contain an ultramafic component. The dacite and rhyolite lithologies show increasing acidity from Phase 2 to Phase 5.

The White Mfolozi Inlier contains a complete spectrum of compositions from basic to intermediate, to acid phases. The older Nhlebela Formation contains intermediate and acid compositions, while basalts and basaltic andesites, with minor andesites, dominate the younger Agatha Formation. While all of the White Mfolozi Inlier samples are subalkaline, the Nhlebela Formation data plots closer to the subalkali – alkali boundary.

5.3.9 Discussion of classification techniques

This exercise shows that no one classification scheme can be deemed reliable for altered and metamorphosed volcanic rocks. Comparison between results for individual samples (Appendix 6) shows marked differences in composition depending on which classification scheme has been used. A marked difference between the Jensen Cation plot and the Floyd and Winchester diagrams is the basic versus

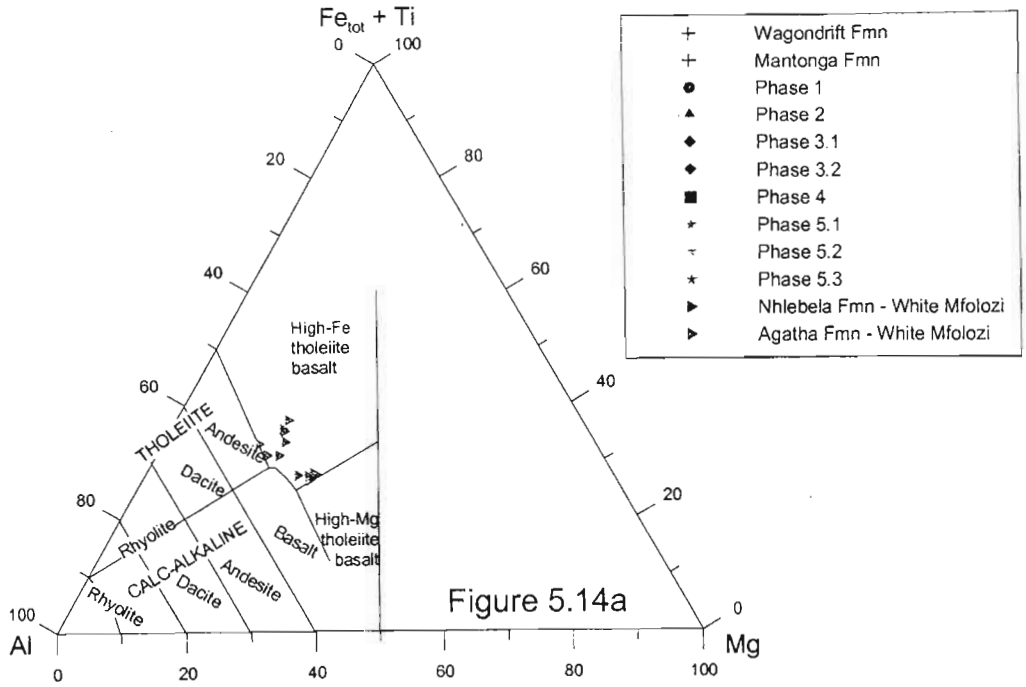

Figure 5.14a

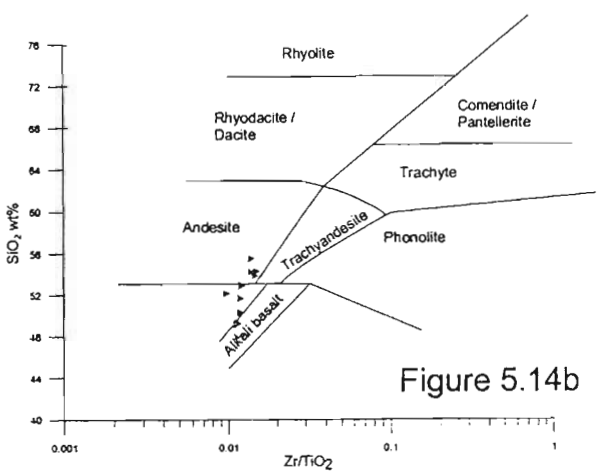

Figure 5.14b

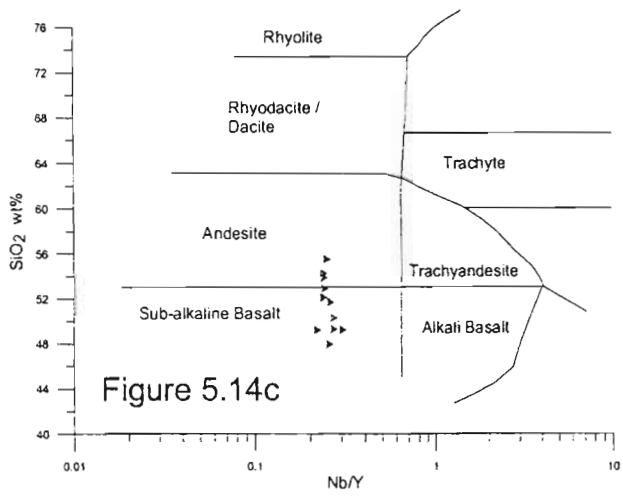

Figure 5.14c

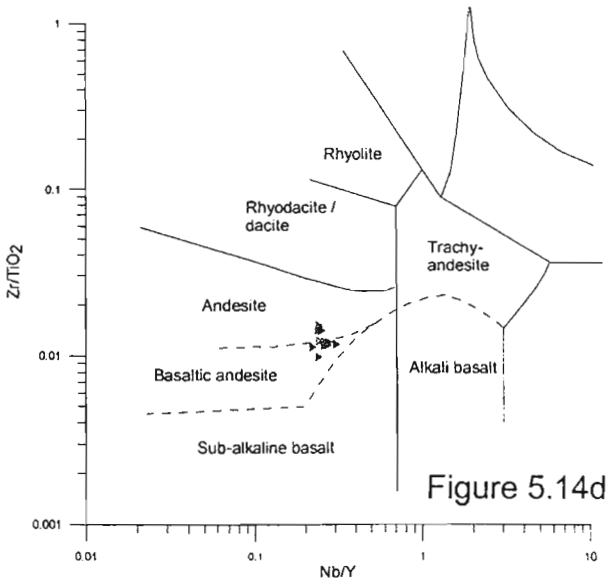

Figure 5.14d

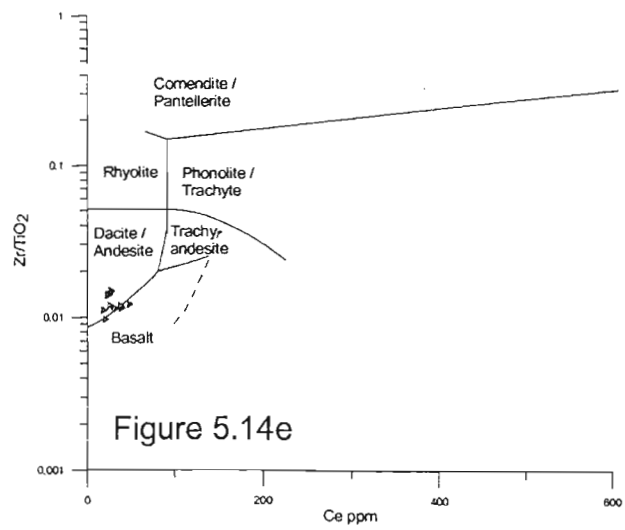

Figure 5.14e

Figure 5.14 Agatha Formation - White Mfolozi Inlier Classification diagrams.
5.14a - Jensen Cation Plot (Jensen, 1976; Rickwood, 1989)
5.14b-e - Winchester and Floyd (1977)

intermediate ratio of samples i.e. far more samples plotted as basalts on the JC graph than on the FW graphs. This may be a factor of the elements involved and the data sets used to construct the compositional fields by the respective authors. The best solution for Archaean metamorphosed and altered volcanic rocks is the collaborative interpretation of compositions based on all classification schemes available and a sound understanding of the metamorphic and alteration processes that may have affected the lithologies.

5.4 MAJOR ELEMENT INTERPRETATION

Geochemical data have not been plotted using the conventional Harker diagram format (versus SiO_2) or other variation diagram norms i.e. versus MgO. Instead all major elements have been plotted against Nb, a trace element that has proven to be immobile, yet can still be used as an indicator of fractionation.

The graph of SiO_2 vs Nb shows two possible trends (Figure 5.15a). The two trends can be divided on age of samples. The steeper array (A on Figure 5.15a) represents geochemical data from the Wagondrift Formation, the Mantonga Formation, Phase 1, Phase 2, Phase 3.1 and Phase 4. The gentler trend (B on Figure 5.15a) correlates to Phase 3.2, Phase 5.1, Phase 5.2 and Phase 5.3. Phase 5.2 exhibits a sub-trend within the acid samples, which runs perpendicular to the dominant fractionation trend of B. Trend A is less evolved than B, based on lower Nb values for increasing SiO_2, and may signify a different source magma for the early and late eruptive phases of the White River Section. Phase 5 acid volcanic rocks plot separately from the acid samples of Phase 2, Phase 3 and Phase 4. This is a factor of the high Nb concentrations of the younger acid rocks compared to the lower Nb values of the older acid rocks. A plot of SiO_2 vs MgO clearly demonstrates that the two trends are a function of the rocks' Nb concentrations as this graph shows one negative slope (Figure 5.15b). It is interesting to note the high Mg content of the Phase 2 samples, although these samples do not have the lowest SiO_2 values. The White Mfolozi Inlier samples of the Nhlebela and Agatha Formations do not fall on either trend A or B.

The graph of Al_2O_3 vs Nb shows a general trend of decreasing Al_2O_3 for increasing Nb (Figure 5.15c). Within this overall negative trend the data of each episode of eruption (where sufficient data are present) exhibits a positive sub-trend of increasing Al_2O_3 with increasing Nb. These sub-trends represent the accumulation of plagioclase, an Al-rich phase, with ongoing fractionation.

An overall trend of decreasing FeO for increasing Nb can be interpreted from Figure 5.15d. There however appears to be individual positive arrays within the different geochemical data groups, trending perpendicular to the overall negative trend. The sub-trends are again a factor of fractionation of Fe-rich phases within a compositional range.

The MgO variation graph against Nb has a strong negative trend, especially evident with the basic to intermediate sample data (Figure 5.15e). It is notable that samples of Phase 2 have higher MgO concentrations than any other group, and therefore Phase 2 represents the most mafic phase of eruption of the Bivane Subgroup.

CaO plotted against Nb for the Nsuze Group data, has a negative trend for basic and intermediate composition samples (Figure 5.15f). The data for the Wagondrift Formation, the Mantonga Formation, Phase 1, Phase 2, Phase 3 and Phase 4 appear to form a separate array to the basic and intermediate samples from Phase 5. The acid data from Phase 5 does not plot with the acid data from other samples groups but this is due to higher Nb values for the Phase 5 acid samples.

Na_2O plots as scatter against Nb and is possibility as a result of the mobility of Na during post-volcanic processes (Figure 5.15g). It can however be observed again that the acid Phase 5 samples plot as a separate group to the other volcanic phases. This is however due to their high Nb concentration rather than a factor of Na_2O. Certain Phase 5 acid samples do have considerably poor Na_2O concentrations as compared to other acid samples like Phase 4. This is most likely due to the mobility of Na. The Nhlebela Formation samples have high Na_2O values possibly due to the influence of an aqueous phase throughout the early stages of eruption.

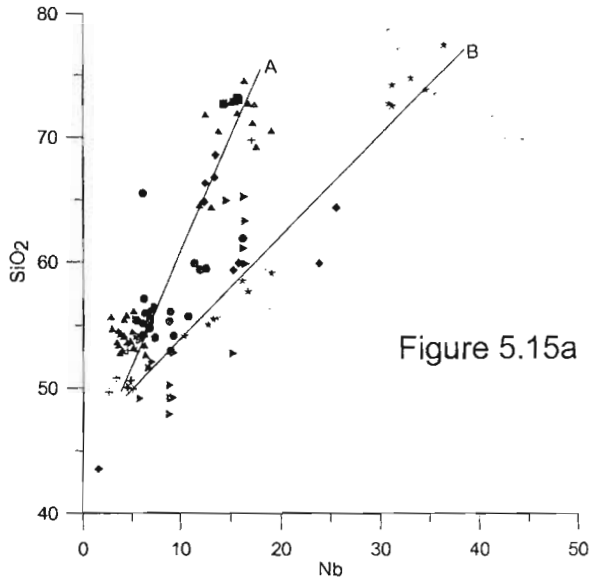

Figure 5.15a

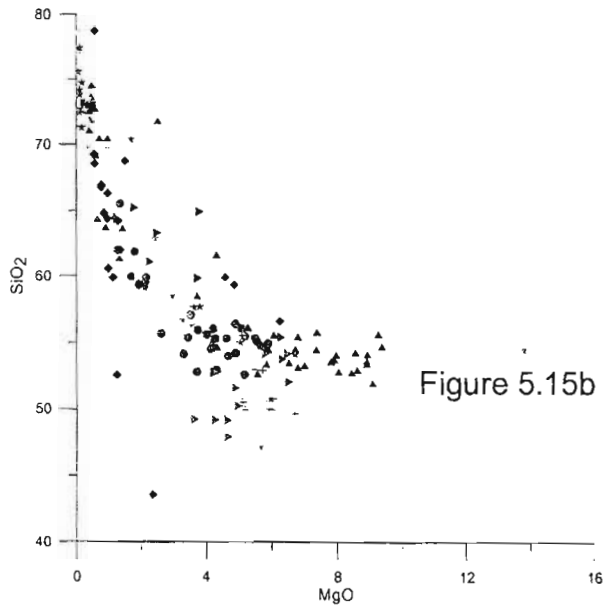

Figure 5.15b

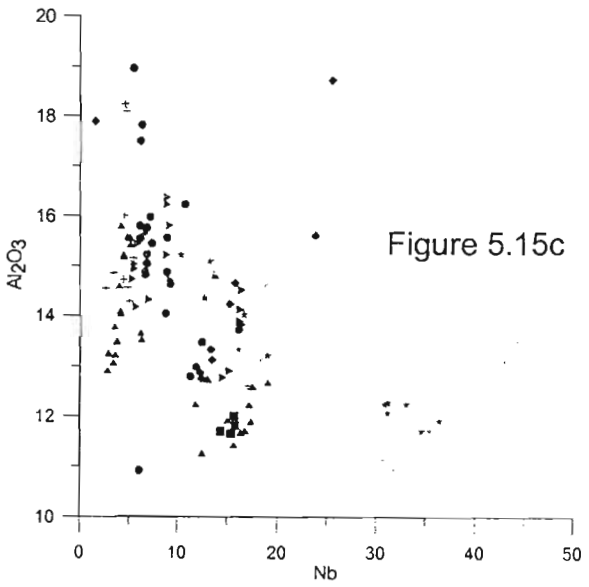

Figure 5.15c

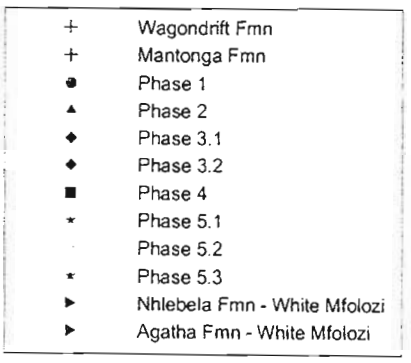

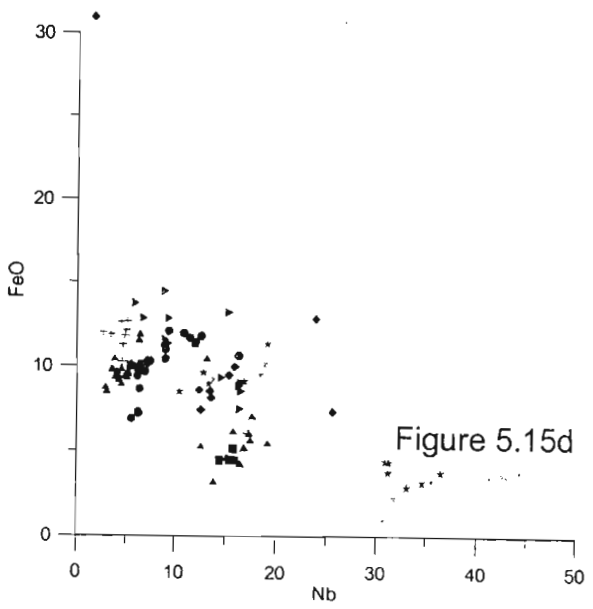

Figure 5.15d

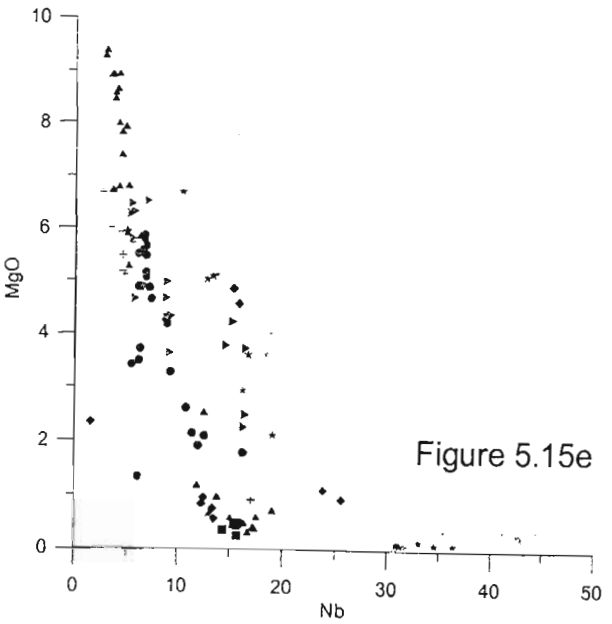

Figure 5.15e

Figure 5.15a-e Variation diagrams of major elements versus Nb
(Oxides are in weight % and Nb in ppm)

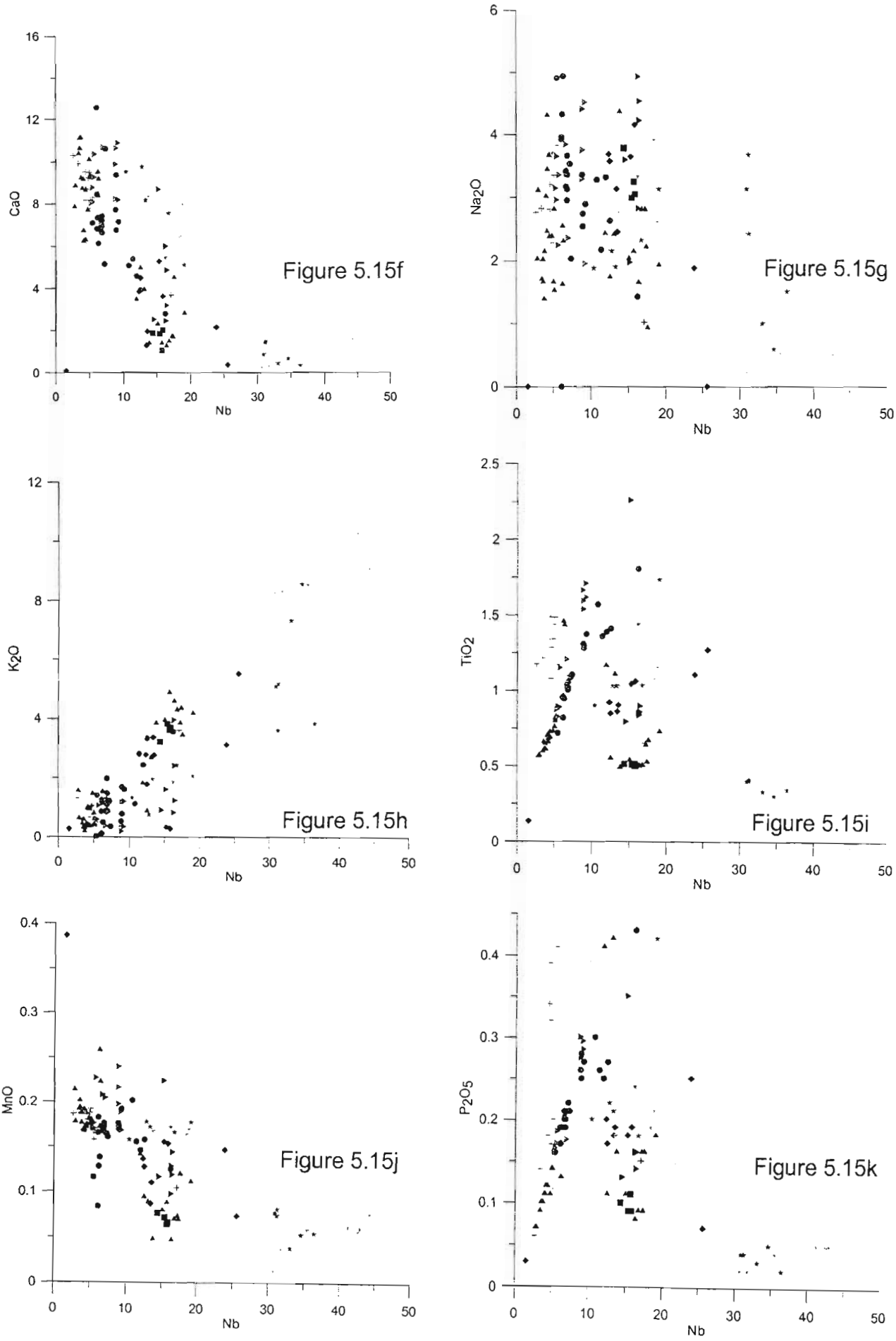

Figure 5.15f-k Variation diagrams of major elements versus Nb
(Oxides are in weight % and Nb is in ppm)

K_2O is the least mobile of the major elements. It forms a relatively well-constrained positive trend with Nb especially with respect to the Wagondrift Formation, the Mantonga Formation, Phase 1, Phase 2, Phase 3.1 and Phase 4 (Figure 5.15h). Phase 3.2 samples (those taken in the south of the White River Section – Appendix 1) plot off the main linear array, as does the data from Phase 5, both the intermediate and acid compositions. While those of Phase 3.2 plot of the main array due to higher Nb concentrations, those acid samples of Phase 5 have considerably higher K_2O than the rest of the data.

The variation diagram of TiO_2 against Nb shows a very broad negative trend, which has numerous positive sub-trends, superimposed on it (Figure 5.15i). Each phase exhibits a strong positive trend within the different compositional groups, and the compositional groups form the overall negative slope of decreasing TiO_2 with increasing Nb. The positive sub-trends are most pronounced in more basic groupings at low Nb values. These sub-trends signify fractionation processes within each compositional group where the accumulation of plagioclase phenocrysts resulted in the enrichment of Ti in the magma that was subsequently erupted.

MnO vs Nb shows a gentle negative slope from basic to acid compositions (Figure 5.15j). Only the data of Phase 1 and Phase 2 show significant positive sub-trends perpendicular to the overall negative trend. P_2O_5 vs MgO has very pronounced positive sub-trends superimposed on the overall negative slope (Figure 5.15k). These sub-trends are most pronounced at the basic spectrum of the graph and are significantly defined for the Wagondrift Formation, Phase 1, Phase 2 and the Agatha Formation of the White Mfolozi Inlier.

The data of the Nhlebela and Agatha Formations seem to be associated with the Nsuze Group data from the White River Section. The sample CG02/210 plots separate to the Nhlebela Formation data on all graphs, but is most pronounced on the graphs of SiO_2, FeO, CaO, TiO_2, MnO and P_2O_5. This again supports the fact that this sample may represent a later intrusive event.

5.5 TRACE ELEMENT INTERPRETATION

The trace element data has been plotted against Nb due to its relatively immobile nature in the Nsuze Group volcanic rocks.

The trace element Y shows a linear array that increases in concentration with increasing Nb values (Figure 5.16a). Y is considered to be an immobile element during alteration and low-grade metamorphic conditions (Floyd and Winchester, 1978). This concept of Y immobility is supported in the Nsuze Group geochemical data, with only minor scatter evident along the linear trend. Phase 5 acid samples plot separately but still along the same linear trend, as the rest of the data of the volcanic phases. These high Nb values (>30ppm) and high Y values (>80ppm) relative to other acid samples present in the data set suggest that the acid volcanic rocks of Phase 5 represent highly fractionated magma.

Zr forms a well-constrained positive linear trend with Nb that almost mimics that of Y (Figure 5.16b). Once again the acid samples of Phase 5 have high Zr values (>500ppm) compared to acid data in other data groups i.e. Phase 4 (Zr =250ppm). This is again evidence that Phase 5 acid volcanic rocks represent a highly fractionated magma.

Sr shows a moderate amount of scatter, although a general negative linear trend can be inferred (Figure 5.16c). CG01/5 shows high concentrations of Sr (1150ppm) in relation to other Phase 1 data. This sample was taken as an example of epidote alteration, which causes Sr enrichment. The abnormally high amount of apatite or plagioclase may account for the Sr-rich signature of CG01/5, where the Sr has substituted for Ca. The presence of epidote in the alteration, which is a Ca-rich mineral, would suggest that other Ca-rich minerals are also present. Low Sr values, as seen in CG01/137, are a factor of Ca-depletion and advanced albitization. Positive (near-vertical) sub-trends within each compositional group can be inferred from the basic spectrum of the graph. This is attributed to the accumulation of the dominating fractionating phase plagioclase.

Rb values form a positive linear trend with Nb with high Rb values corresponding to high Nb

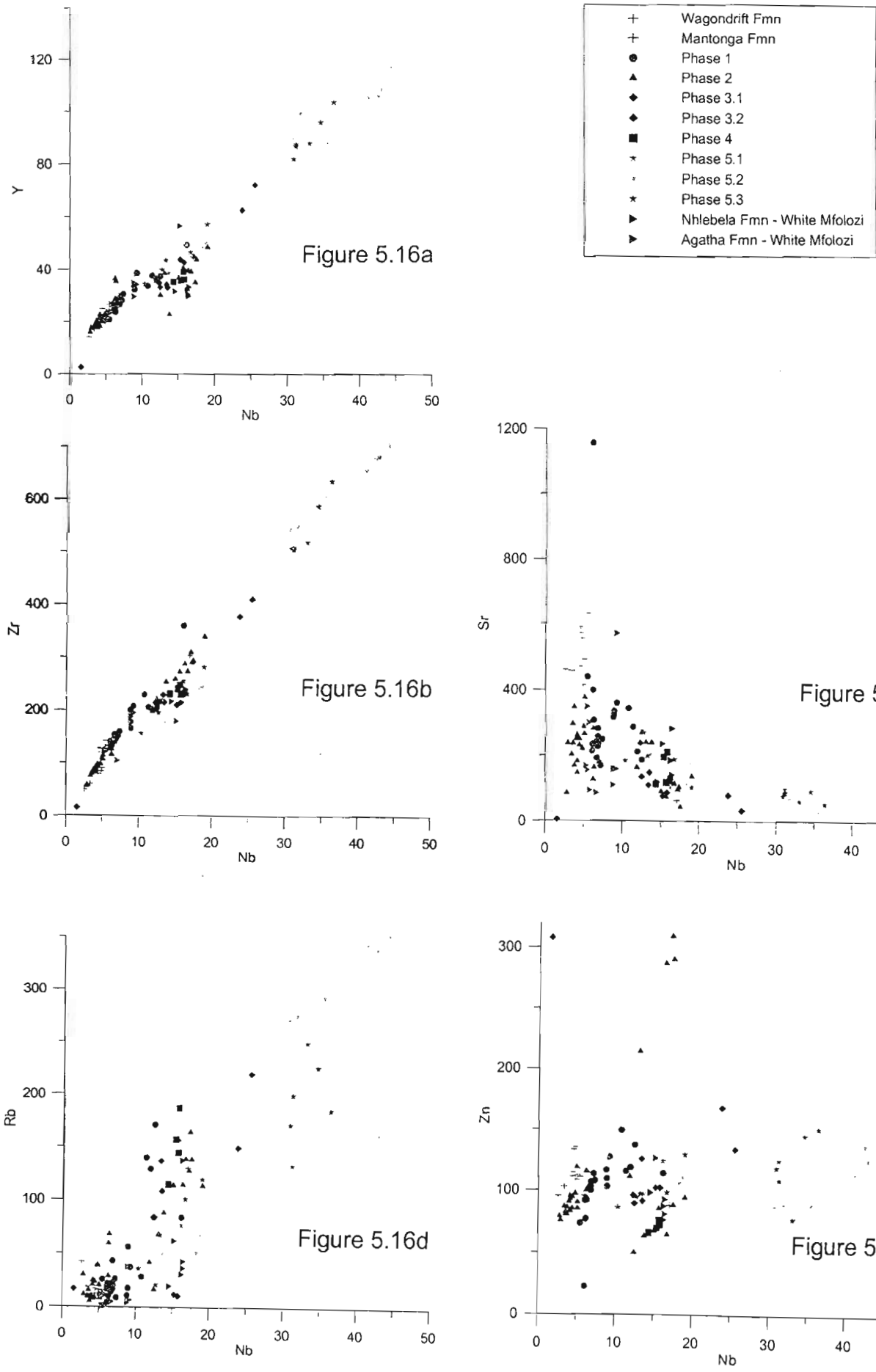

Figure 5.16a-e Variation diagrams of trace elements versus Nb
(All values in ppm)

values (Figure 5.16d). Rb is an incompatible element and therefore the concentration increases with increasing fractionation.

Zn plotted against Nb shows wide scatter (Figure 5.16e). CG/137, CG01/93, CG01/84, CG01/63 and CG01/92 (>200ppm) have anomalous high Zn concentrations, compared to the rest of the Nsuze Group data. Zn has a high degree of mobility in the Nsuze Group volcanic rocks as a result of deuteric and hydrothermal processes.

Cu data is scattered when plotted against Nb (Figure 5.16f). It can however be interpreted that basaltic samples, in particular those of the Wagondrift Formation, have been subjected to more Cu moving fluids than the acid samples. Humphris and Thompson (1978) showed that Cu is readily mobilised in metabasalts by hydrothermal fluids, and that concentrations of Cu greater than 50ppm are most often caused by late-stage sulphide growth. The Nhlebela Formation of the White Mfolozi Inlier, although comprising andesites and dacites, also has high Cu values. This may be due to the aqueous phase represented in the lower lavas of the Nhlebela Formation, which would have mobilised Cu.

Cr is often taken as an indictor of fractional crystallization. In the Nsuze Group volcanic rocks, the samples with the highest Cr values - Phase 2 have the highest MgO concentrations (Figure 5.16g). This is additional evidence that while Phase 2 does not have the lowest SiO_2 values, the phase does contain the most primitive signatures preserved in the Nsuze Group volcanics. It is evident that most intermediate to acid samples have little to no Cr present as would be expected in fractionated compositions.

The Ni versus Nb graph shows a steeply negative linear trend for basalt to basaltic andesite data (Figure 5.16h). The Ni concentrations of Phase 2 are not markedly higher than those of the Wagondrift Formation but still provide evidence that Phase 2 represents the most primitive signature of the Nsuze Group. Intermediate to acid samples have little to no Ni present.

V plots as scatter against Nb (Figure 5.16i). There appears to be a sharp contrast between the basic to intermediate data and the acid data. This may be due to the presence of V in epidote, associated with the low-grade metamorphic assemblage of basic and intermediate volcanic rocks. Linear sub-trends are evident in the basic and intermediate data and may be a factor of the accumulation of plagioclase in the magma. Epidote is a common metamorphic product of plagioclase under greenschist conditions.

Ba forms a scattered trend when plotted against Nb (Figure 5.16j). While increasing Nb values correspond to increasing Ba values, scatter increases towards the acid samples, culminating in a wide envelope for Phase 5 acid samples. Ba is mobile during weathering and metamorphism, and enrichment of Ba can often be an effect of chloritization (Cann, 1969). Ba also substitutes for K in feldspars, which would explain the generally high Ba values in the acid data.

5.6 RARE EARTH ELEMENT INTERPRETATION

The rare earth elements (REE) were analysed for selected samples using ICP-MS (See Appendix 3). REE data has been normalized using values of Boynton (1984) based upon Evensen *et al.* (1978) as recommended by Rollinson (1993). These normalization values are based on average C1 chondrite values. Nsuze Group REE data has been normalized to chondrite for ease of comparison to existing literature.

5.6.1 Wagondrift Formation – White River Section

The basalts of the Wagondrift Formation represent the oldest basic rocks of the Nsuze Group in the Northern Region (Armstrong, 1980). ∑REE values range from 34.4ppm to 110ppm, with an average of 73.3ppm. $(La/Lu)_{cn}$ ratios fall between 5.46 and 11.93, with an average of 8.54 (Table 5.1). The LREE are therefore enriched relative to the HREE. The gradient for the LREE (La/Sm_{cn}) is consistently shallower than that for the HREE (Gd/Lu_{cn}) for all Wagondrift Formation samples (Table 5.1; Figure 5.17). It is interesting to note that the least evolved sample (CG01/13) is also the youngest sample of the Wagondrift Formation, based on regional dip and strike orientations (N-S strike, eastward dipping). This trend continues, as the order of evolution according to the REE is CG01/13, CG01/15, CG01/16, CG01/17, CG01/18, CG01/20 and CG01/19. Apart from CG01/19 and CG01/20, this order is exactly the opposite of the supposed stratigraphic order if the strata dipped towards the east

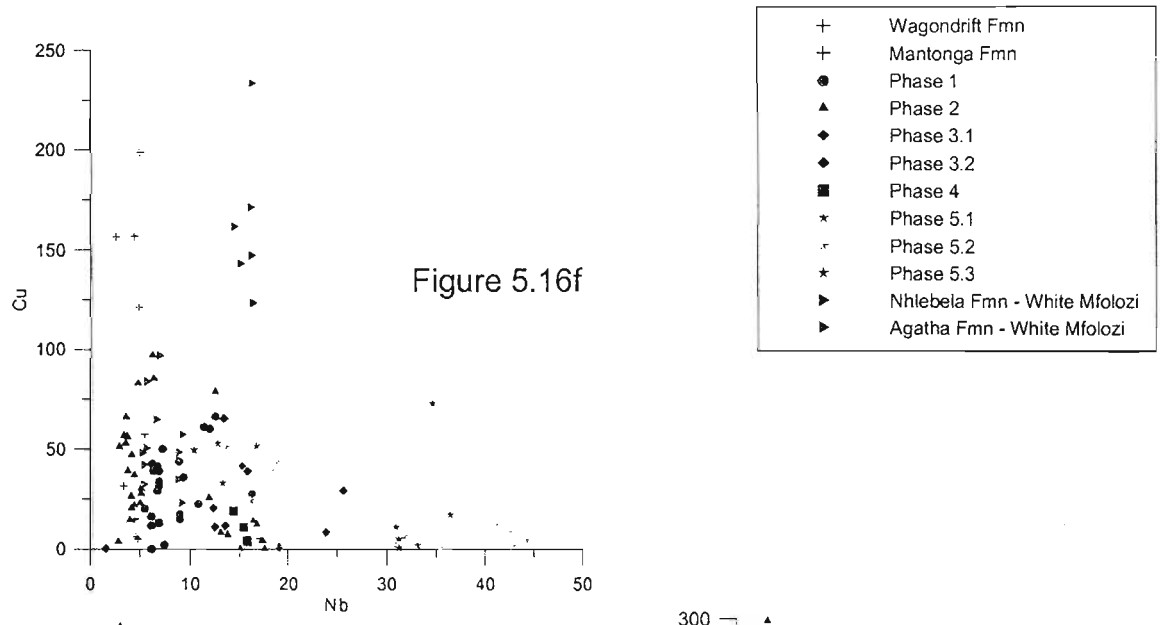

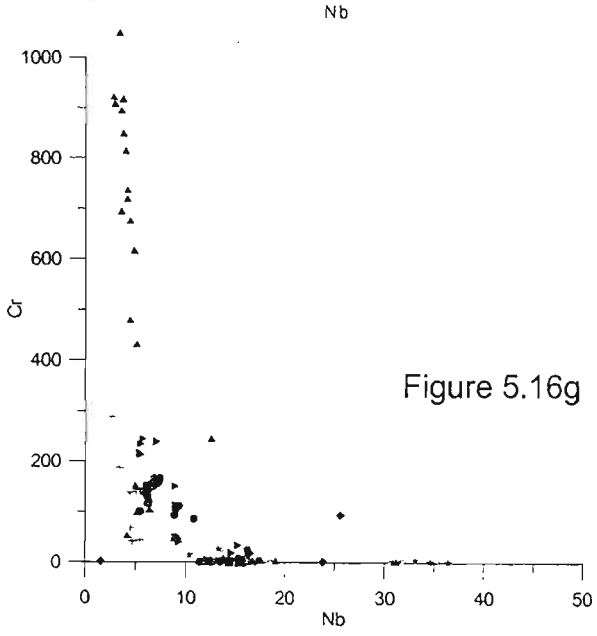

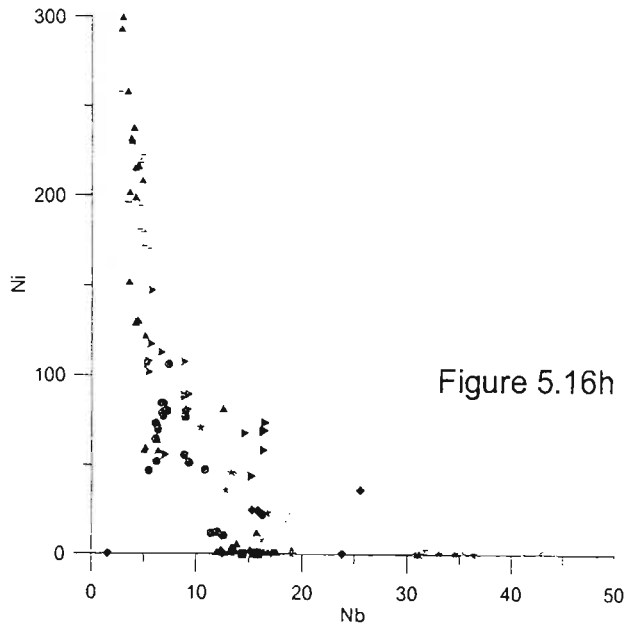

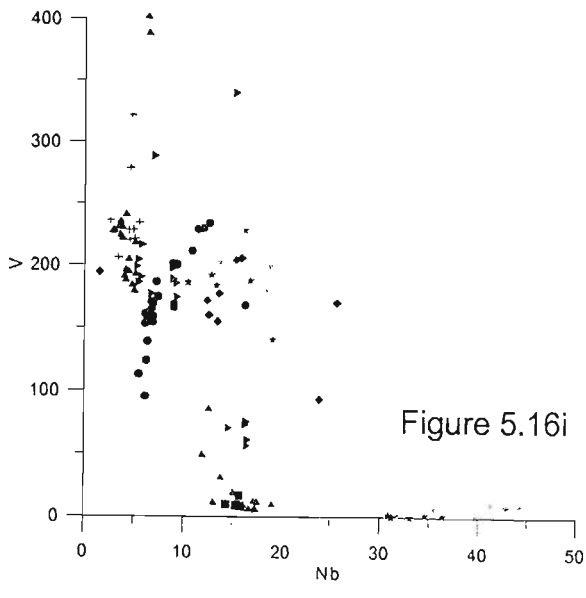

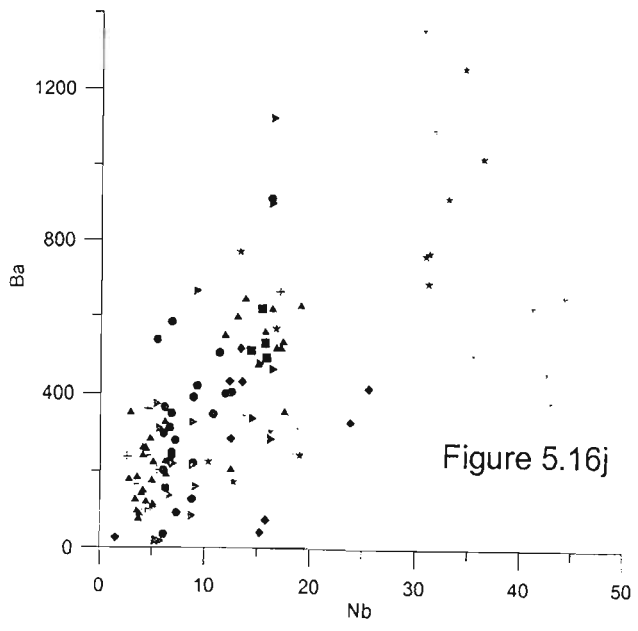

Figure 5.16f-j Variation diagrams of trace elements versus Nb
(All values in ppm)

Table 5.1 REE summary data for the Wagondrift Formation and the Mantonga Formation – White River Section

	ΣREE	$(La/Lu)_{cn}$	$(La/Sm)_{cn}$	$(Gd/Lu)_{cn}$	Eu/Eu*	$(La/Yb)_{cn}$
Wagondrift Formation						
CG01/13	34.4	5.46	1.88	2.56	1.52	4.85
CG01/15	48.6	6.99	2.19	2.80	1.35	6.08
CG01/16	59.6	6.90	2.09	2.94	1.18	6.00
CG01/17	63.5	7.32	2.27	2.86	1.18	6.45
CG01/18	67.8	7.36	2.20	2.97	1.15	6.52
CG01/19	110	10.68	2.49	3.46	0.94	9.34
CG01/20	96.2	9.99	2.39	3.32	1.01	8.80
CG01/21	91.0	11.93	2.56	3.58	1.19	10.46
CG01/170	88.2	10.21	2.38	3.30	1.18	9.04
average	73.3	8.54	2.27	3.09	1.19	7.31
Mantonga Formation						
CG01/122	620	10.27	4.53	1.93	0.48	9.35

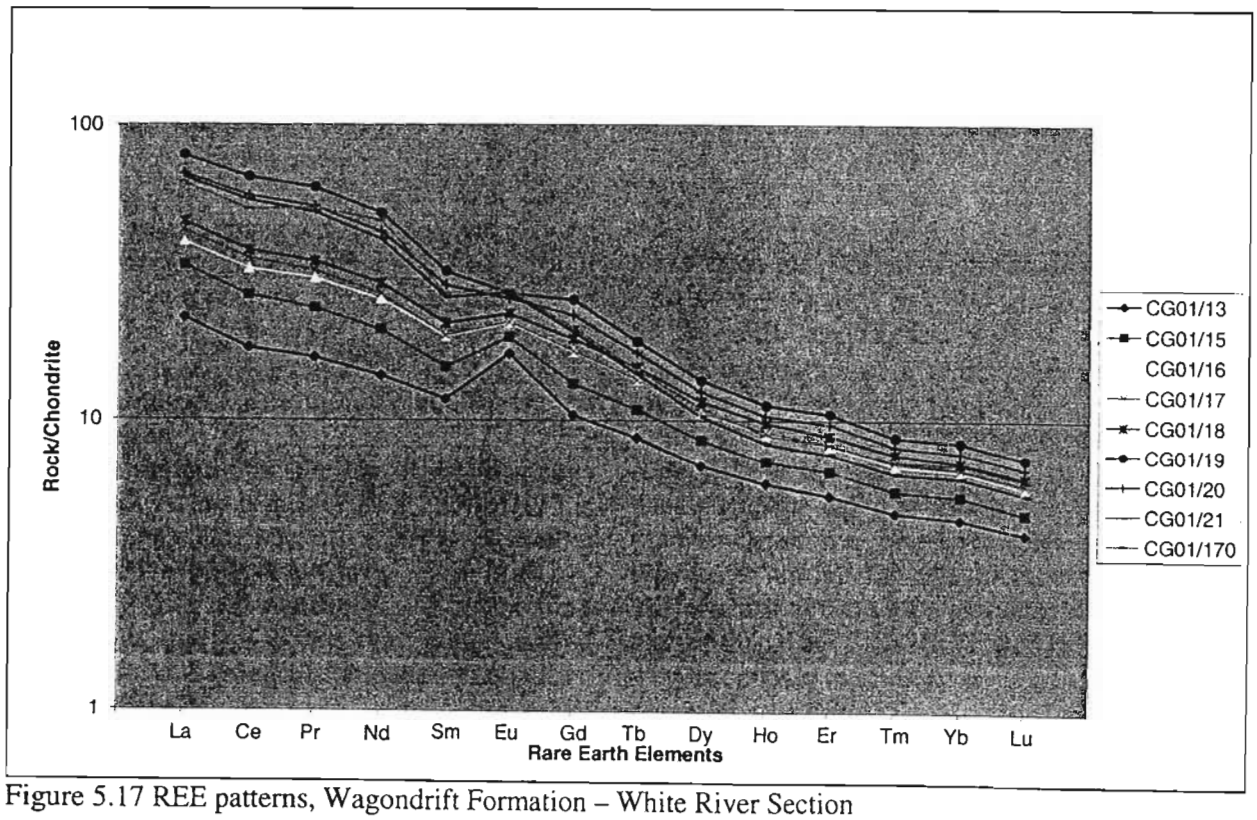

Figure 5.17 REE patterns, Wagondrift Formation – White River Section

(Appendix 1). The overall fractionation trend of the samples is controlled by plagioclase as the entire REE pattern is elevated for each sample. A less significant pyroxene fractionation has resulted in gradual LREE enrichment and continuing overall steepening of the REE patterns, with evolution of the magma. The stratigraphically oldest samples CG01/170 and CG01/21 show the most pronounced effect of pyroxene fractionation. The Eu anomaly is most pronounced and positive in the least evolved sample CG01/13 (Eu/Eu* = 1.52) and lessens progressively in the more evolved samples until the Eu anomaly for CG01/19 is slightly negative (Eu/Eu* = 0.94). This signifies that the least evolved samples were carrying entrained plagioclase, resulting in a positive anomaly and the more evolved the samples were beginning to fractionated plagioclase.

CG01/21 and CG01/170 do not appear to form the same REE pattern as the other samples. CG01/21, CG01/20 and CG01/170 were taken from the same outcrop. While CG01/21 mimics the LREE pattern of CG01/20, its Eu anomaly and HREE pattern follow that of CG01/170 (Table 5.1; Figure 5.17). CG01/170 has enriched Pr and Nd values as compared to the other Wagondrift Formation samples. The HREE for CG01/170 and CG01/21 are significantly depleted when compared to the rest of the samples of the Wagondrift Formation. Both samples have a positive Eu anomaly (Eu/Eu* = 1.18-1.19).

5.6.2 Mantonga Formation – White River Section

Only one sample from the top of the Mantonga Formation was analysed for REE. CG01/122 is classified as a dacite and is therefore representative of evolved lava. The $(La/Lu)_{cn}$ ratio (10.27) is not significantly different from that of CG01/19 (10.68), the most evolved sample of the Wagondrift Formation (Table 5.1). The difference between the Wagondrift Formation samples and the Mantonga Formation data lies in relationship between the LREE and the HREE. The LREE have a significantly steeper gradient than the HREE, i.e. $(La/Sm)_{cn}$ = 4.53 vs $(Gd/Lu)_{cn}$ = 1.93 (Table 5.1; Figure 5.18). The REE pattern also shows a pronounced negative Eu anomaly (Eu/Eu* = 0.48). The REE pattern of the Mantonga Formation does not appear to represent more evolved Wagondrift lava.

5.6.3 Phase 1, Bivane Subgroup – White River Section

Phase 1 represents the initial stage of Bivane Subgroup volcanism. The compositional range of Phase 1 is from basaltic andesite to andesite. ∑REE range from 238ppm to 635ppm, average 363ppm (Table 5.2). La/Lu_{cn} ratios fall between 6.15 and 9.39, at an average of 8.94. LREE are therefore enriched relative to HREE (Table 5.2; Figure 5.19). The slopes of the LREE ($La/Sm_{cn\ average}$ = 2.94) are steeper than the gradients of the HREE ($Gd/Lu_{cn\ average}$ = 2.30). Eu anomalies are both positive and negative (Eu/Eu* = 0.71-1.24). This may be due to the presence of feldspar phenocrysts in many of the lava flows found in Phase 1 (See Chapter 3). The negative and positive anomalies should differentiate between porphyritic and non-porphyritic volcanic units in Phase 1. This is evident from the CG01/20 and CG01/21, which contain visible phenocrysts and also have pronounced positive Eu anomalies (Eu/Eu* = 1.12 and 1.24). Other samples with positive Eu anomalies contain aphanitic feldspar phenocrysts. Samples with negative Eu anomalies must therefore represent residual melt. Three samples (CG01/7, CG01/167 and PG26/2000) are markedly different from the other Phase 1 data. These three samples were taken from the same unit at different localities. This volcanic unit is the "fine-grained andesite" of the cliff section described in Chapter 3. Classification proved that this unit was in fact andesitic in composition (Appendix 6). The data from CG01/7, CG01/167 and PG26/2000 suggests that the volcanic unit is more evolved than the other units of Phase 1. These three samples have the highest LREE enrichment relative to the HREE ($(La/Lu)_{cn}$ = 8.94-9.39). The gradient of the LREE pattern is significantly steeper than that of the HREE ($(La/Sm)_{cn}$ = 3.95-4.07 as opposed to (Gd/Lu)cn = 2.06-2.07). This provides $LREE/HREE_{average}$ ratio of 1.93 (as opposed to the $LREE/HREE_{average}$ ratio for the rest of Phase 1 data which equals 1.19). CG01/7, CG01/167 and PG26/2000 also have the most pronounced negative Eu anomalies (Eu/Eu* = 0.71-0.73). The suite of Phase 1 REE patterns appears to reflect the evolution of magma controlled by the fractionation of plagioclase. While slight changes in the gradient of the slopes are evident, the $(La/Lu)_{cn}$ ratios generally fall in a

Table 5.2 REE summary data for Phase 1, Bivane Subgroup – White River Section

	∑REE	$(La/Lu)_{cn}$	$(La/Sm)_{cn}$	$(Gd/Lu)_{cn}$	Eu/Eu*	$(La/Yb)_{cn}$
Phase 1 - Bivane Subgroup						
CG01/1	288	6.75	2.74	2.19	1.05	8.97
CG01/2	343	6.74	2.62	2.30	1.09	8.60
CG01/3	291	6.85	2.71	2.26	0.99	8.88
CG01/4	352	6.97	2.76	2.30	0.96	9.05
CG01/5	303	6.97	2.79	2.29	0.89	9.09
CG01/6	323	6.93	2.70	2.29	1.00	9.02
CG01/7	510	9.39	4.03	2.09	0.71	12.84
CG01/47	313	6.59	2.83	2.24	0.95	8.88
CG01/48	306	6.68	2.83	2.25	0.93	8.92
CG01/49	292	6.56	2.77	2.32	0.96	8.70
CG01/50	316	6.97	2.84	2.30	0.98	9.34
CG01/51	312	6.29	2.67	2.25	0.96	8.42
CG01/125	369	6.73	2.55	2.35	0.93	8.73
CG01/128	414	7.90	2.79	2.47	0.92	10.46
CG01/131	407	7.94	2.88	2.42	1.05	10.28
CG01/167	505	9.27	4.07	2.06	0.72	12.50
PG20/2000	238	7.29	2.83	2.24	1.24	9.59
PG21/2000	264	7.07	2.83	2.21	1.12	9.33
PG22/2000	394	7.88	2.91	2.61	0.88	10.10
PG23/2000	429	7.67	2.94	2.50	0.86	9.88
PG24/2000	635	8.83	2.95	2.59	0.81	11.30
PG25/2000	299	6.15	2.62	2.20	0.96	8.26
PG26/2000	455	8.94	3.95	2.07	0.73	12.08
average	363	7.36	2.94	2.30	0.94	9.71

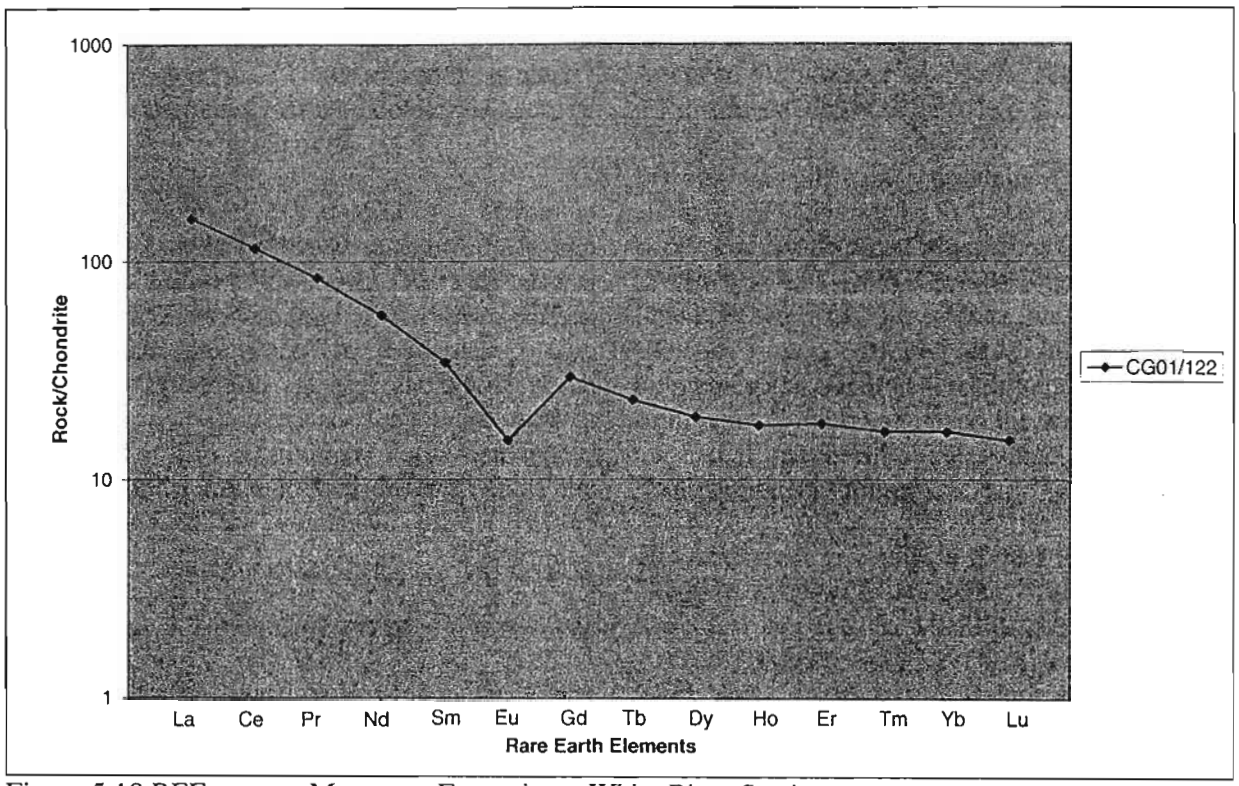

Figure 5.18 REE pattern, Mantonga Formation – White River Section

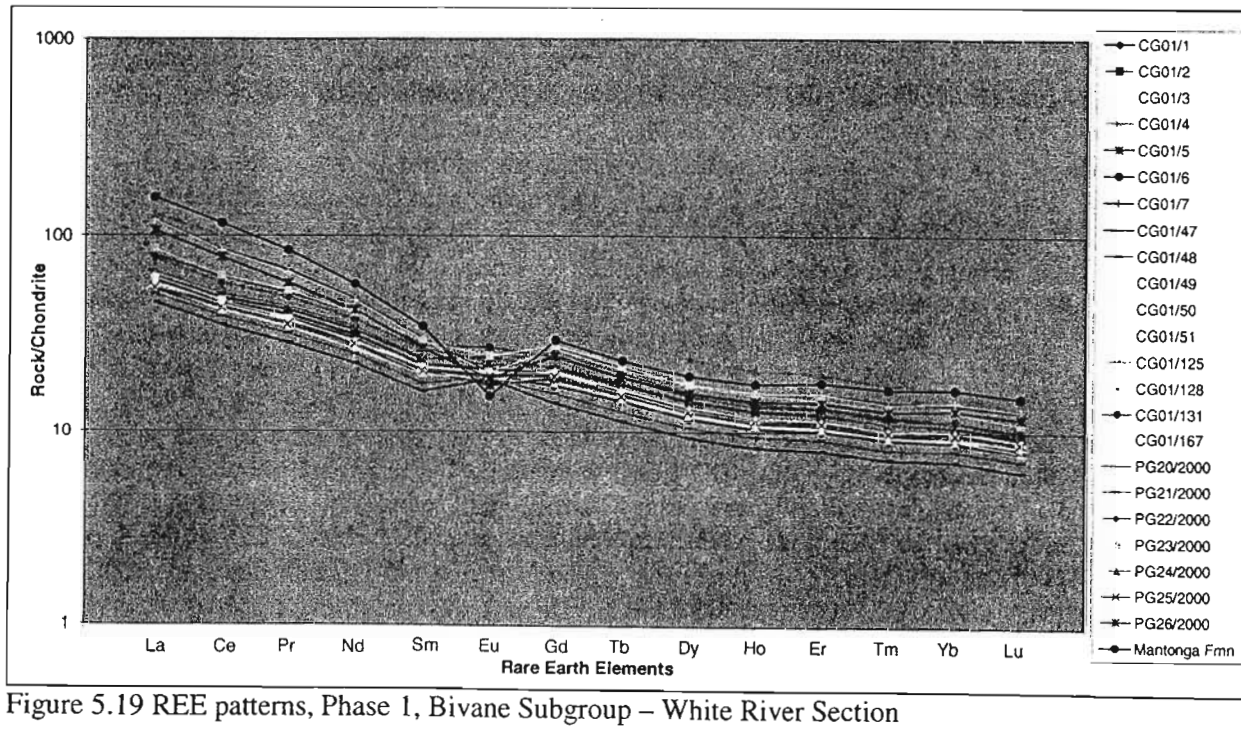

Figure 5.19 REE patterns, Phase 1, Bivane Subgroup – White River Section

limited range, resulting in a systematic enrichment of all REE (except Eu) with increasing fractionation. This plagioclase influence on the Phase 1 volcanic rocks is clearly seen in the dominance of plagioclase phenocrysts in many of the volcanic units.

A comparison of CG01/122 – Mantonga Formation sample (in black on Figure 5.19) and the Phase 1 data shows that CG01/122 has a steeper LREE pattern and a shallower HREE pattern than any Phase 1 REE data. The Mantonga Formation sample also has a much larger negative Eu anomaly than those seen in Phase 1. The Mantonga Formation upper volcanic units are therefore different from the initial stage of the volcanism in the Bivane Subgroup i.e. Phase 1.

5.6.4 Phase 2, Bivane Subgroup – White River Section

Phase 2 of the Bivane Subgroup in the White River Section of the Northern Region comprises intermediate and acid volcanic rocks. No true basalts are identified from this stage of volcanism and the least evolved lava composition is basaltic andesite. Phase 2 can be divided into two groups based on REE patterns and characteristics. These two groups correspond to the compositional groups identified using classification diagrams. The two distinct REE patterns are therefore different primarily due to fractionation. These two groups will be dealt with on separate graphs.

The basic to intermediate samples are plotted on Figure 5.20. These samples have a total REE concentration between 174 and 284ppm with an average of 214ppm (Table 5.3). $(La/Lu)_{cn}$ ratios ranges from 2.26 to 6.50, average 5.41. LREE are enriched relative to the HREE. Two samples CG01/141 and CG01/142 have the lowest $(La/Lu)_{cn}$ ratios, 2.27 and 2.26 respectively. Both CG01/141 and CG01/142 (which almost overlie each other) form relatively flat REE patterns compared to the rest of the data. There is less variation within the LREE ($(La/Sm)_{cn}$ = 1.77; 1.73) and the HREE are more enriched than for other samples in the Phase 2 data set. LREE are only slightly enriched relative to the HREE. CG01/141 and CG01/142 have the lowest negative Eu anomalies of the basic – intermediate Phase 2 data (Eu/Eu* = 0.79, 0.86 respectively). According to field interpretations CG01/141 represents a small dyke (14cm wide) found within a lava flow. CG01/142 was taken from the overlying younger lava flow. It can therefore be interpreted that the dyke was a feeder to the younger lava flow. The reason for the difference between these two samples and the rest of the Phase 2 data is unknown. CG01/26 is the only sample with a pronounced positive Eu anomaly (Eu/Eu* = 1.18). All other samples have near-flat or slightly negative Eu anomalies (Eu/Eu* = 0.88-1.06). The REE patterns of the Phase 2 basic to intermediate data (excluding CG01/141 and CG01/142) have been influenced by plagioclase fractionation, although the lack of significant Eu anomalies and the small range of the REE patterns suggest that plagioclase fractionation was minor.

The acid group of samples have $\sum$REE = 484 – 722ppm, average = 606ppm. The LREE are enriched relative to the HREE ($(La/Lu)_{cn}$ = 10.37 – 12.20, average = 11.22) (Table 5.3; Figure 5.21). All samples have a negative Eu anomaly with Eu/Eu* = 0.53 – 0.72, average = 0.58. The acid samples are clearly controlled by the fractionation of feldspar, where increasing fractionation results in the enrichment of all REE (except Eu), and therefore causes the REE patterns to stack.

CG01/31, CG01/32, CG01/34 and CG01/35 are intrusive samples taken from the Feeder Dyke System described in Chapter 3, illustrated in Figure 3.42. CG01/32 and CG01/35 represent the least evolved igneous rocks found in the Phase 2 (although they may in fact feed much younger flows representative of other phases of eruption). Their REE pattern does however appear to mimic those of the other basic to intermediate samples of Phase 2 (Table 5.3; Figure 5.22). Although CG01/32 (west dyke) and CG01/35 (east dyke) are thought to be the same intrusive that was later split by a younger acid dyke, their REE patterns, while similar, are not identical. CG01/32 is lightly more enriched in REE than CG01/35. CG01/35 has a steeper LREE pattern and a flatter HREE pattern than CG01/32. If the narrow dykes represent the same intrusion that was subsequently split by a later larger intrusion, the differences in REE patterns may be attributed to mobility of the REE caused by the thermal effect of the later acid intrusion. Thermal metamorphism can cause the enrichment or depletion of all elements (Brewer and Atkin, 1989). CG01/31 and CG01/34 represent the central acid dyke (Figure 3.42).

Table 5.3 REE summary data for Phase 2, Bivane Subgroup – White River Section

	∑REE ppm	$(La/Lu)_{cn}$	$(La/Sm)_{cn}$	$(Gd/Lu)_{cn}$	Eu/Eu*	$(La/Yb)_{cn}$
Phase 2 basic to intermediate samples - Bivane Subgroup						
CG01/162	174	4.88	2.61	1.76	1.00	4.35
CG01/33	175	5.14	2.64	1.90	0.95	4.36
CG01/27	177	5.32	2.75	1.87	0.92	4.64
CG01/88	186	5.63	2.71	1.89	0.93	5.01
CG01/30	191	5.48	2.52	2.08	0.99	4.54
CG01/26	194	5.46	2.88	1.85	1.18	4.83
CG01/22	202	6.93	3.10	2.07	0.95	6.13
CG01/148	208	4.99	2.61	1.79	0.97	4.48
CG01/29	209	5.94	2.88	1.97	0.93	5.21
CG01/38	211	5.83	2.94	1.96	1.04	5.19
CG01/90	220	6.05	2.85	1.94	1.06	5.27
CG01/151	221	6.22	2.73	2.08	0.96	5.24
CG01/160	224	5.87	2.64	2.08	0.88	4.97
CG01/23	225	6.49	3.07	1.95	1.05	5.73
CG01/41	235	6.50	3.10	1.98	0.92	5.87
CG01/142	255	2.27	1.77	1.29	0.86	2.15
CG01/141	258	2.26	1.73	1.30	0.79	2.11
CG01/36	284	6.07	2.89	2.07	0.88	5.34
average	214	5.41	2.69	1.88	0.96	4.74
Phase 2 acid samples - Bivane Subgroup						
CG01/40	513	10.37	4.07	2.29	0.66	9.44
CG01/92	547	10.64	4.05	2.27	0.72	9.68
CG01/163	577	12.11	4.76	2.18	0.56	11.04
CG01/161	591	11.06	4.58	2.08	0.54	10.22
CG01/84	603	12.20	4.65	2.24	0.53	11.00
CG01/28	630	10.53	4.51	2.15	0.56	9.57
CG01/93	636	11.32	4.52	2.18	0.57	10.13
CG01/25	639	12.10	4.97	2.10	0.55	11.23
CG01/39	722	10.65	4.34	2.17	0.56	9.69
average	606	11.22	4.49	2.19	0.58	10.22
Feeder Dyke System samples						
CG01/34	484	11.62	4.63	2.18	0.66	10.21
CG01/31	720	15.99	5.15	2.59	0.55	14.03
CG01/35	147	5.03	2.94	1.65	0.93	4.34
CG01/32	155	5.40	2.72	1.86	0.97	4.46

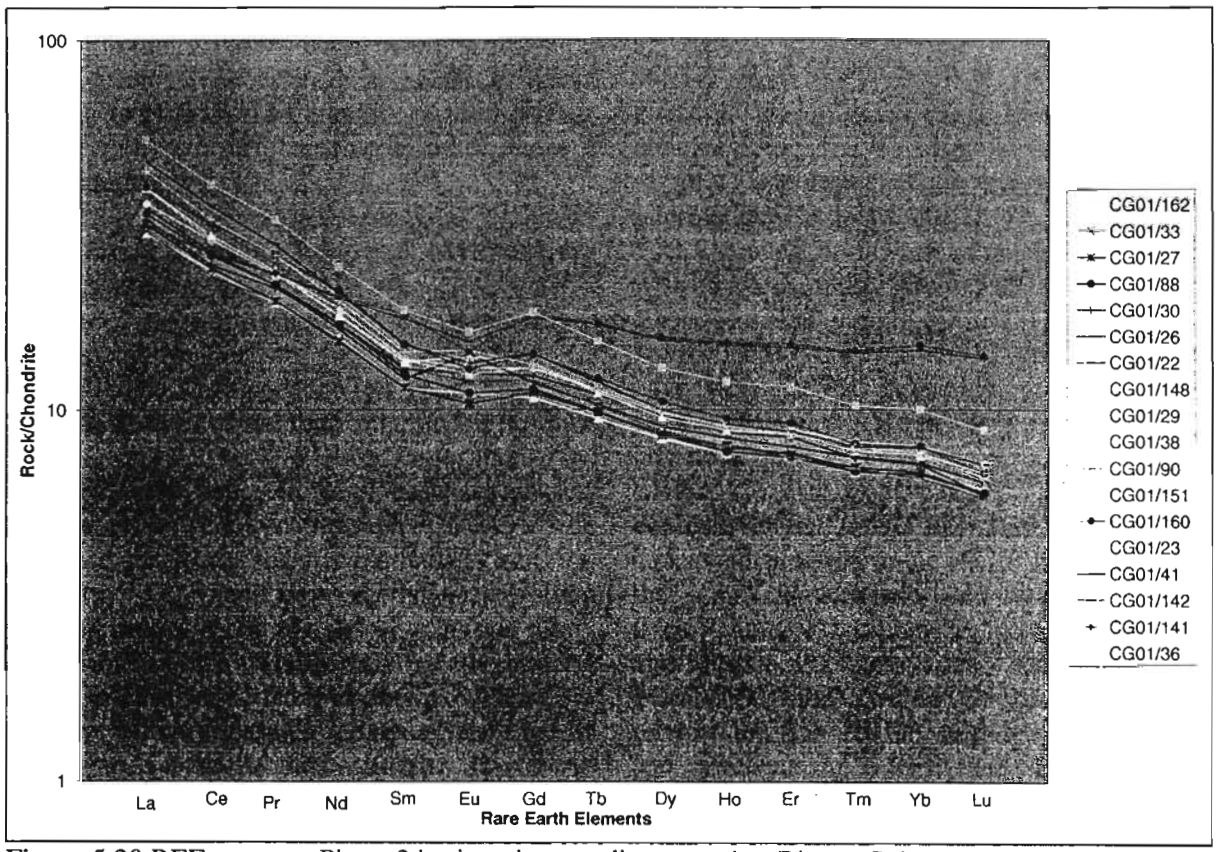

Figure 5.20 REE patterns, Phase 2 basic to intermediate samples, Bivane Subgroup - White River Section

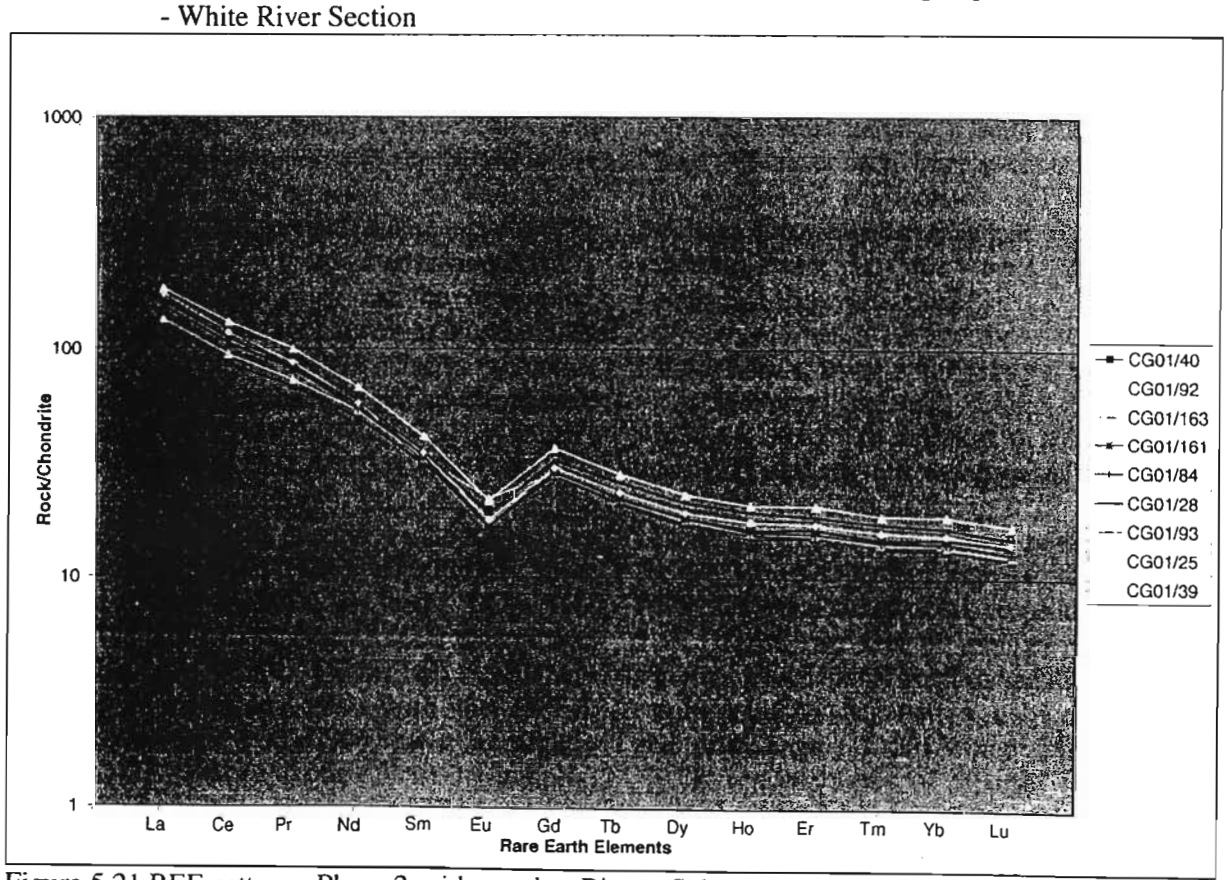

Figure 5.21 REE patterns, Phase 2 acid samples, Bivane Subgroup – White River Section

CG01/34 was taken from the eastern chill margin of the central dyke. CG01/31 has a similar REE pattern to the rest of the acid Phase 2 samples. It is however more enriched in LREE elements relative to HREE. The gradient of the LREE is considerably steeper than that of other Phase 2 acid samples.

5.6.5 Phase 3, Bivane Subgroup – White River Section

Phase 3.1 lies in the north of the White River Section of the Northern Region and Phase 3.2 lies to the south (Appendix 1). These two areas have been divided, as their relationship to each other is not known. While a large number of samples were collected from both sub-phases, few samples were sent through ICP-MS to be analysed for REE. This is particularly relevant for Phase 3.1, which is primarily located along the Beki-Beki tributary. Most outcrops along this tributary are significantly weathered and fresh samples are difficult to obtain. Phase 3.1 has no primary basaltic compositions, but is made up of dacite and andesite lavas and pyroclastics. Sampling may, however, have resulted in bias towards the more competent compositions, as basaltic samples would have been unsuitable for geochemical analysis.

The ∑REE ranges for Phase 3.1 are from 448 to 706ppm, average 557ppm (Table 5.4). The LREE are enriched relative to the HREE where $(La/Lu)_{cn}$ ratios are between 6.82 and 11.31, average 9.38. All samples show negative Eu anomalies (Eu/Eu* = 0.46 – 0.65, average 0.59). Three different groupings can be determined from the REE patterns shown in Figure 5.23. CG01/121 and CG01/136 are close to each other geographically (Appendix 1) and appear to have very similar REE patterns. CG01/121 is slightly more evolved than CG01/136 and is stratigraphically younger, implying that the samples represent the magma source undergoing fractionation. CG01/118 is significantly more evolved than CG01/121 and CG01/136. CG01/118 has a flatter overall REE pattern than CG01/121 and CG01/136, as the LREE are slightly less enriched relative to the HREE. PG29/2000 and PG30/2000 have a slightly differing REE pattern to other Phase 3.1 samples. Gd to Er appears to be enriched relative to the rest of the HREE forming a convex shape. The same elements from Gd to Er on the REE pattern for CG01/121, CG01/136 and CG01/118 are depleted relative to the rest of the HREE forming a slight concave shape. PG29/2000 and PG30/2000 both show a slight negative Pr anomaly.

Phase 3.2 is composed of intermediate and acid compositions. The REE data set comprises three samples, two intermediate and one acid. The intermediate samples' (CG01/79 and CG01/81) ∑REE concentration varies from 449 to 467ppm, with $(La/Lu)_{cn}$ ratios from 5.07 to 6.16 (Table 5.4). The acid sample (CG01/75) has ∑REE = 885ppm and $(La/Lu)_{cn}$ = 8.41. All three samples have steep LREE patterns, and relatively flat HREE patterns (Table 5.4; Figure 5.23). Negative Eu anomalies are prominent for each sample ($Eu/Eu^*_{average}$ = 0.59). Gd to Er are depleted relative to the other HREE and create a concave depression in the HREE pattern. This is the same characteristic recognised in samples from Phase 3.1. Similarities between Phase 3.1 and Phase 3.2 (excluding PG29/2000 and PG30/2000) include the Gd to Er depletion relative to other HREE, negative Eu anomalies and gradient of LREE and HREE slopes. Differences are most pronounced with the intermediate samples. Phase 3.2 intermediate samples are less enriched in LREE relative to the HREE than Phase 3.1 intermediate samples. HREE are more enriched in the Phase 3.2 samples than the Phase 3.1 samples, resulting in a flatter HREE pattern. Both Phase 3.1 and Phase 3.2 have been largely controlled by the fractionation of plagioclase. All REE (except Eu) have experienced enrichment with increasing evolution and Eu has been depleted as plagioclase has crystallized.

5.6.6 Phase 4, Bivane Subgroup – White River Section

Phase 4 is thought to represent an acid lava dome and REE patterns are therefore as a result of fractionation. Two differing REE patterns are observed in Figure 5.24. These two patterns are formed by CG01/9 and CG01/11, and PG27/2000 and PG28/2000, respectively (Table 5.5). These two sets of samples were run in different geochemical batches and differing REE results could be attributed to analytical processes and procedures. CG01/9 and CG01/11 have ∑REE concentrations of 594ppm and 634ppm respectively (Table 5.5). PG27/2000 and PG28/2000 have ∑REE = 601ppm and 587ppm. The main difference between the two groups of samples is LREE enrichment relative to HREE. $(La/Lu)_{cn}$ ratio equals 12.31 and 12.64 for

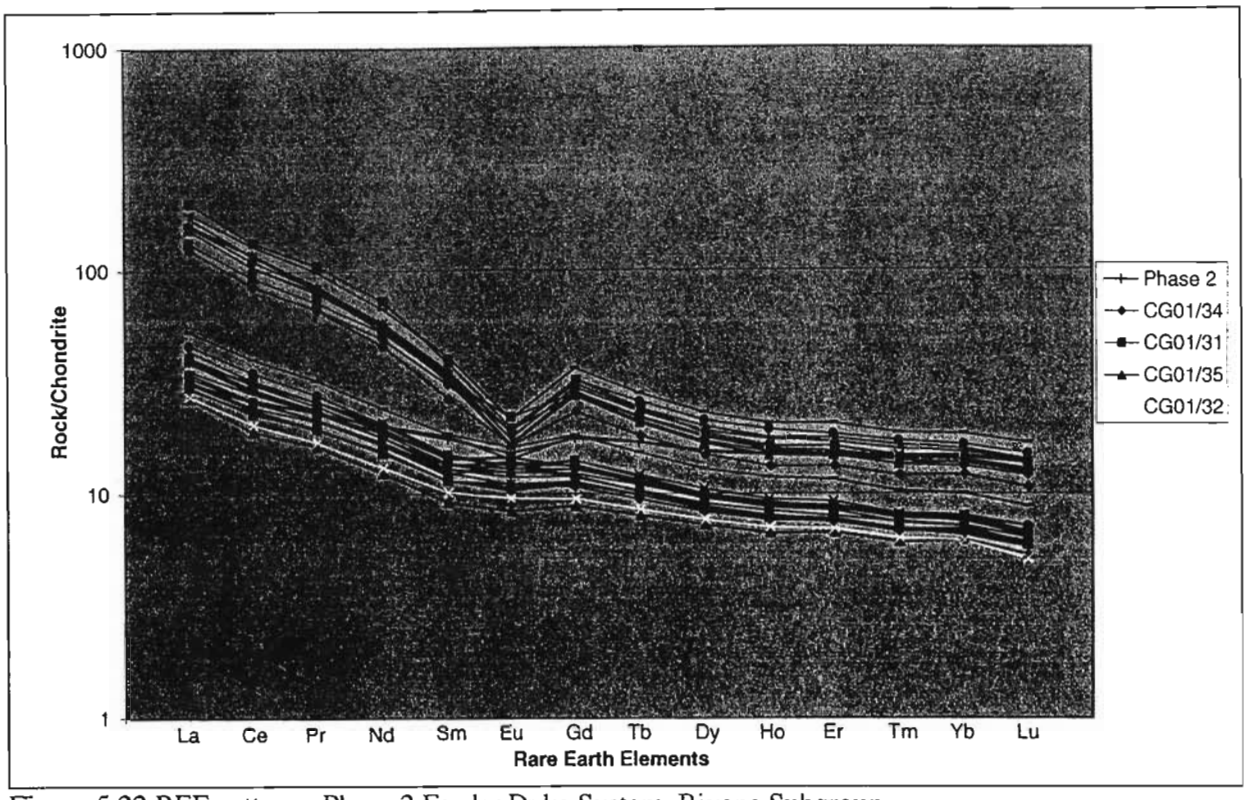

Figure 5.22 REE patterns, Phase 2 Feeder Dyke System, Bivane Subgroup
– White River Section compared to the rest of the Phase 2 data in black

Table 5.4 REE summary data for Phase 3, Bivane Subgroup – White River Section

	ΣREE ppm	$(La/Lu)_{cn}$	$(La/Sm)_{cn}$	$(Gd/Lu)_{cn}$	Eu/Eu*	$(La/Yb)_{cn}$
Phase 3.1 - Bivane Subgroup						
CG01/118	706	6.82	3.69	1.73	0.46	6.22
CG01/121	484	9.93	4.33	2.00	0.65	9.26
CG01/136	448	9.67	4.38	1.96	0.60	8.89
PG29/2000	544	9.14	4.00	1.64	0.59	8.98
PG30/2000	601	11.31	4.51	1.75	0.65	11.01
average	557	9.38	4.18	1.82	0.59	8.87
Phase 3.2 - Bivane Subgroup						
CG01/75	885	8.41	4.10	1.79	0.56	7.79
CG01/79	449	5.07	3.05	1.53	0.60	4.69
CG01/81	467	6.16	3.68	1.58	0.57	5.67
average	600	6.55	3.61	1.63	0.58	6.05

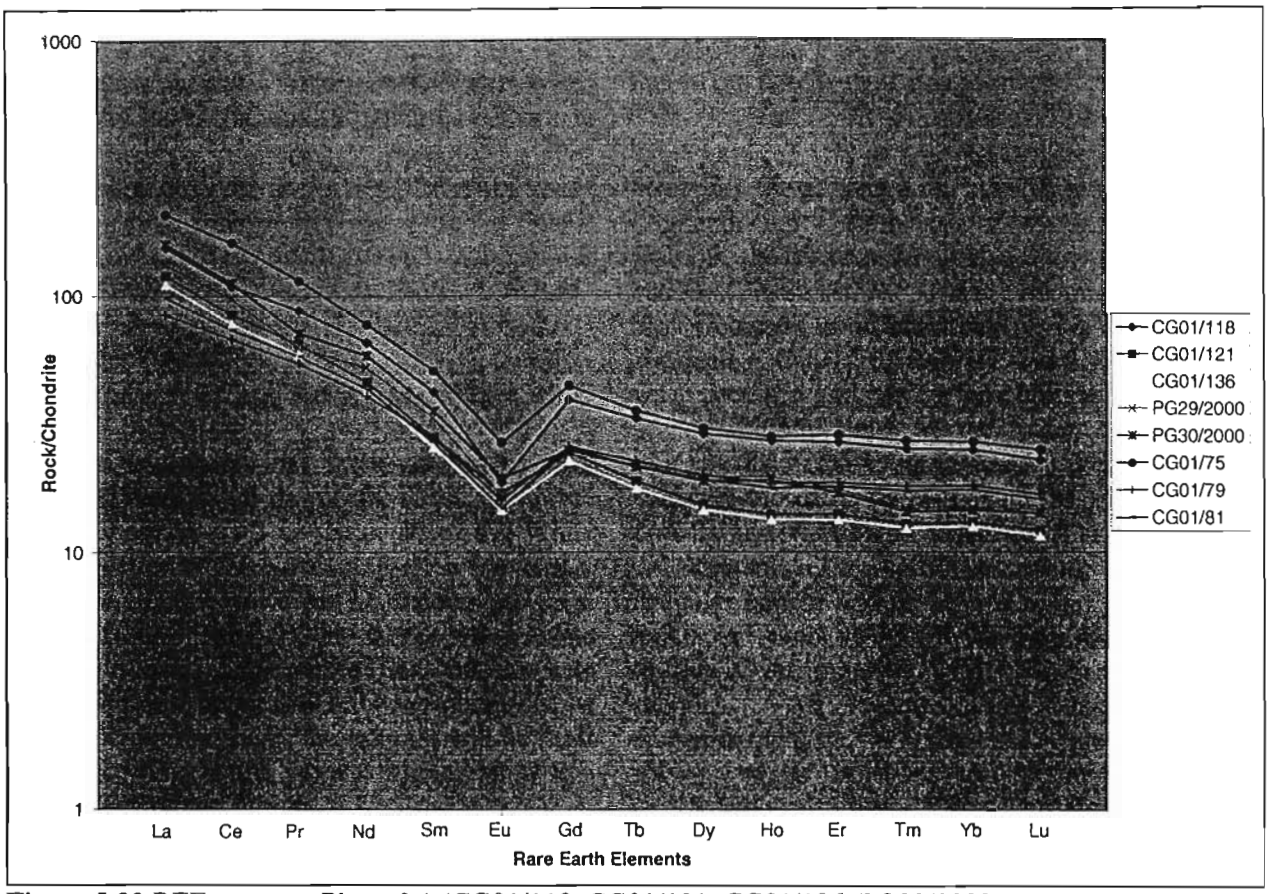

Figure 5.23 REE patterns, Phase 3.1 (CG01/118, CG01/121, CG01/136, PG29/2000, PG30/2000) and Phase 3.2 (CG01/75, CG01/79, CG01/81), Bivane Subgroup – White River Section

Table 5.5 Phase 4 REE summary data for Phase 4, Bivane Subgroup – White River Section

	ΣREE ppm	**$(La/Lu)_{cn}$**	**$(La/Sm)_{cn}$**	**$(Gd/Lu)_{cn}$**	**Eu/Eu***	**$(La/Yb)_{cn}$**
Phase 4 - Bivane Subgroup						
CG01/9	594	12.31	4.70	2.23	0.55	11.08
CG01/11	634	12.64	4.77	2.25	0.57	11.48
PG27/2000	601	10.51	4.45	1.64	0.51	10.17
PG28/2000	587	11.01	4.42	1.72	0.52	10.59
average	604	11.62	4.58	1.96	0.54	10.83

CG01/9 and CG01/11 as opposed to 10.51 and 11.01 for PG27/2000 and PG28/2000. Another difference is the HREE pattern is flatter for PG27/2000 and PG28/2000 than for CG01/9 and CG01/11. PG27/2000 and PG28/2000 both show a slight negative Pr anomaly. These two samples also do not show the steep trend from Gd to Ho that forms the concave depression on the HREE patterns of CG01/9 and CG01/11. All samples show negative Eu anomalies (Eu/Eu* = 0.51-0.57).

5.6.7 Phase 5, Bivane Subgroup – White River Section

Phase 5 is divided into three geographic sub-phases, Phase 5.1 in the north, Phase 5.2 in the centre and Phase 5.3 in the south of the White River Section of the Northern Region (Appendix 1). As a whole Phase 5 can be divided into three events (see Chapter 3), an initial intermediate stage, an acid stage and a final intermediate stage. Because compositional correlations can be drawn across the phase, the samples will be dealt with according to the three volcanic events and not by geographic subphases.

Although the initial intermediate stage is not found in Phase 5.2, CG01/106 from Phase 5.1 and CG01/96 and CG01/165 from Phase 5.3, have been plotted on the Figure 5.25. CG01/106 appears to form a similar REE pattern to CG01/96 and CG01/165 and is possibly derived from the same source. CG01/96 is the least evolved sample, followed by CG01/106 and CG01/165. CG01/165 ($\sum$REE = 636ppm) appears to be a more evolved duplicate of CG01/96 ($\sum$REE = 349ppm) (Table 5.6). This can also be seen when comparing the LREE enrichment relative to the HREE where $(La/Lu)_{cn}$ = 6.24 for CG01/96 and 6.21 for CG01/165. Their LREE patterns ($(La/Sm)_{cn}$ = 3.26 and 3.28) and HREE patterns ($(Gd/Lu)_{cn}$ = 1.79 and 1.76) are almost identical. Both samples show a negative Eu anomaly where Eu/Eu* = 0.66 and 0.62.

Evidence for the acid stage of volcanism in Phase 5 is present in Phase 5.2 and Phase 5.3. Phase 5.2 samples have $\sum$REE concentrations ranging from 944 to 1369ppm with an average of 1208ppm (Table 5.6). The $(La/Lu)_{cn}$ ratios range from 5.86 (CG01/43) to 7.9 (PG3/2000) (Figure 5.26). The Eu anomalies become increasingly negative the more evolved the sample, indicating the fractionation of plagioclase. This results in overlapping of the Eu anomalies of the evolved patterns over the less evolved patterns. All samples show a steep decline from Gd to Ho, before the HREE flatten out.

The Phase 5.3 acid data represent samples, which have all been taken in the same vicinity (Appendix 1). On the basis of two distinct REE patterns, the data can be divided into two distinct groups (Figure 5.27). These two groups were also processed in different batches i.e. the group containing CG01/98, CG01/99 and CG01/171 was processed and run for geochemical analysis at a different time to the other group of PG41/2000, PG42/2000 and PG43/2000. Whether the differing REE patterns are due to processing error or true geochemical signature is not known. The LREE appear to form an irregular pattern and no sample seems to mimic another in terms of the LREE. This may be due to the slight mobility of LREE in the acid samples. All samples show negative Eu anomalies (Eu/Eu* = 0.41 – 0.57) although no pattern exists relative to fractionation or enrichment of other REE. The fundamental difference between the PG samples and the CG samples of Phase 5.3 acid data lies between Tb and Ho. These elements (Tb, Dy and Ho) in CG01/98, CG01/99 and CG01/171 are depleted relative to the other HREE and form a steep concave slope, before it flattens into the remaining HREE (Er, Tm, Yb, Lu) (Table 5.6; Figure 5.27). This concave feature is not present in PG41/2000, PG42/2000 and PG43/2000, but instead Tb, Dy and Ho form a relative flat pattern with Er, Tm, Yb and Lu.

The final intermediate stage of Phase 5 is found in both Phase 5.2 and Phase 5.3. The REE patterns for this final stage for each phase are slightly different. Phase 5.2 has $\sum$REE from 442 to 582ppm (Table 5.6). The LREE are enriched relative to the HREE ($(La/Lu)_{cn}$ = 6.67 – 7.11) (Table 5.6; Figure 5.28). All samples have a negative Eu anomaly (Eu/Eu* = 0.55 –0.68). The samples show a distinctly steep slope from Gd to Ho before flattening. These elements are enriched relative to the rest of the HREE. $\sum$REE for Phase 5.3 ranges from 484 to 602 (Table 5.6). $(La/Lu)_{cn}$ ratios fall between 5.69 and 6.51 (Figure 5.28). Within the LREE, Phase 5.3 samples have a slight negative Pr anomaly. Gd values are noticeably less enriched relative to the other HREE. The HREE pattern from Gd to Lu is flatter than that for Phase 5.2. All samples

Table 5.6 REE summary for Phase 5, Bivane Subgroup – White River Section

	∑REE(ppm)	$(La/Lu)_{cn}$	$(La/Sm)_{cn}$	$(Gd/Lu)_{cn}$	Eu/Eu*	$(La/Yb)_{cn}$
Initial intermediate stage						
Phase 5.1						
CG01/106	559	6.55	3.53	1.71	0.61	5.94
Phase 5.3						
CG01/96	349	6.24	3.26	1.79	0.66	5.43
CG01/165	636	6.21	3.28	1.76	0.62	5.72
average	515	6.33	3.36	1.75	0.63	5.70
Acid stage						
Phase 5.2						
CG01/42	1068	6.36	3.87	1.54	0.44	5.85
CG01/43	944	5.86	3.79	1.43	0.43	5.43
PG1/2000	1273	7.82	4.13	1.67	0.31	7.26
PG2/2000	1369	7.64	4.16	1.63	0.32	7.08
PG3/2000	1176	7.90	4.18	1.61	0.30	7.44
PG4/2000	1338	7.82	4.05	1.75	0.33	7.19
PG5/2000	1288	7.52	4.08	1.61	0.31	7.06
Phase 5.3						
CG01/98	883	5.60	3.54	1.45	0.45	5.23
CG01/99	1003	6.13	3.74	1.46	0.52	5.79
CG01/171	1049	6.39	3.48	1.64	0.52	5.92
PG41/2000	1221	6.12	3.77	1.23	0.35	5.98
PG42/2000	1008	5.51	3.41	1.21	0.41	5.27
PG43/2000	1278	7.20	4.00	1.32	0.57	7.03
average	1146	6.76	3.86	1.50	0.40	6.35
Final intermediate stage						
Phase 5.2						
CG01/44	442	6.67	3.70	1.73	0.68	5.98
CG01/45	589	7.11	3.98	1.72	0.58	6.52
CG01/46	582	7.00	4.00	1.71	0.55	6.42
Phase 5.3						
PG38/2000	602	6.51	3.55	1.37	0.56	6.22
PG39/2000	521	5.75	3.20	1.34	0.62	5.63
PG40/2000	484	5.69	3.20	1.39	0.58	5.35
average	537	6.45	3.60	1.54	0.60	6.02

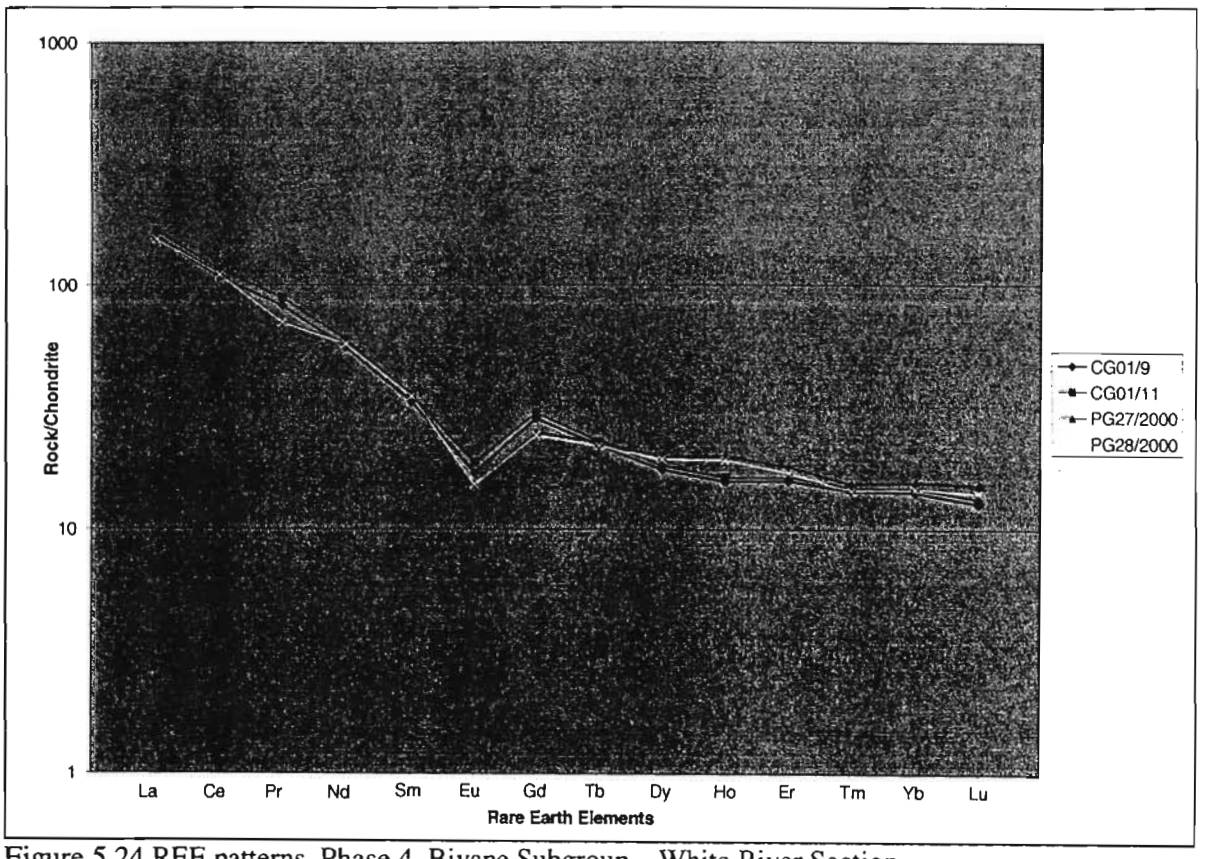

Figure 5.24 REE patterns, Phase 4, Bivane Subgroup – White River Section

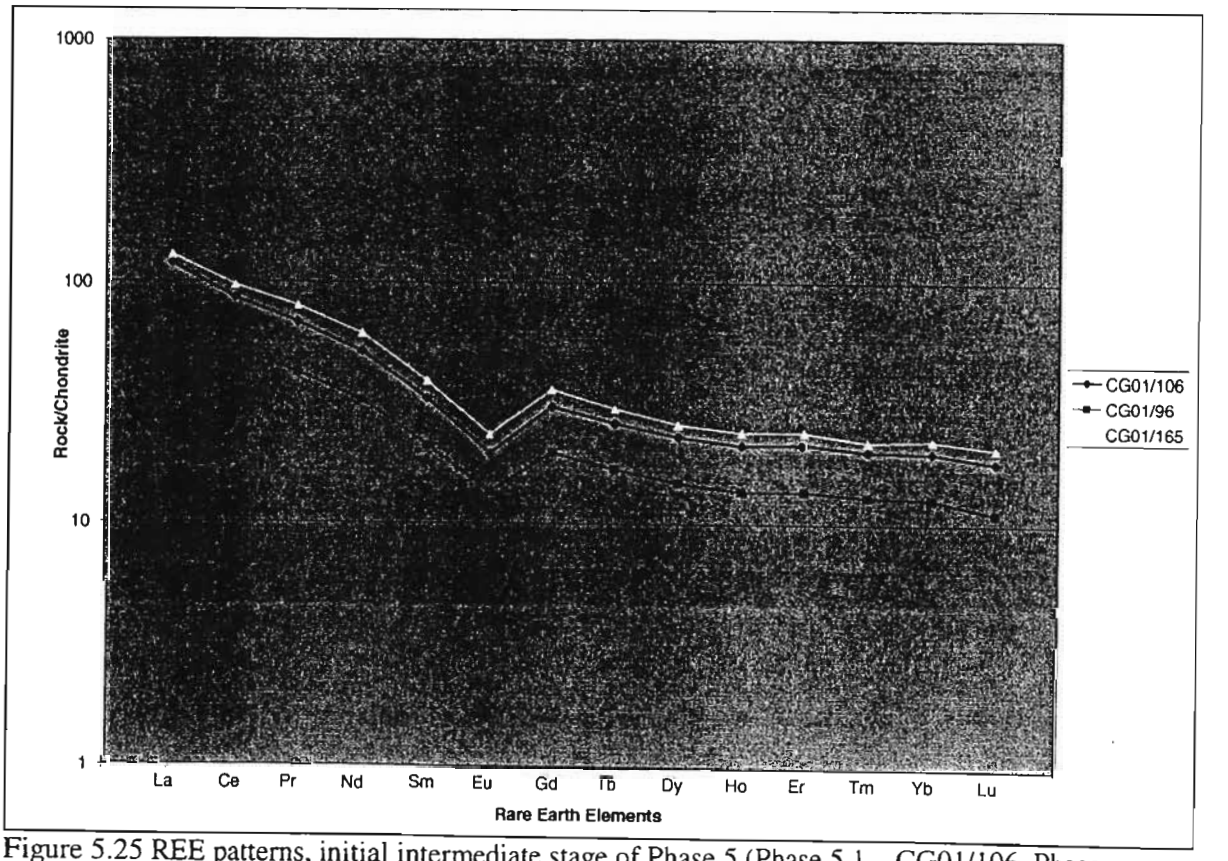

Figure 5.25 REE patterns, initial intermediate stage of Phase 5 (Phase 5.1 – CG01/106, Phase 5.2 – CG01/96, CG01/165), Bivane Subgroup – White River Section

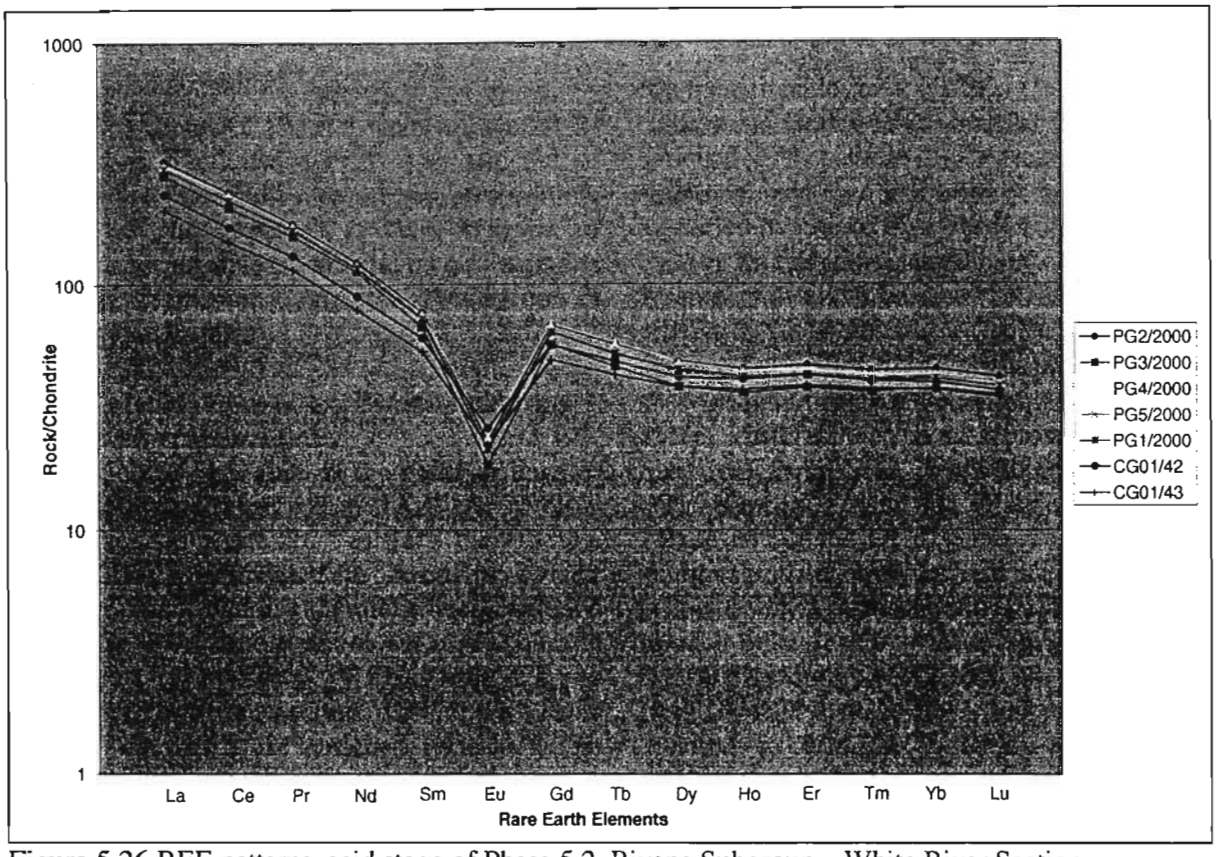

Figure 5.26 REE patterns, acid stage of Phase 5.2, Bivane Subgroup – White River Section

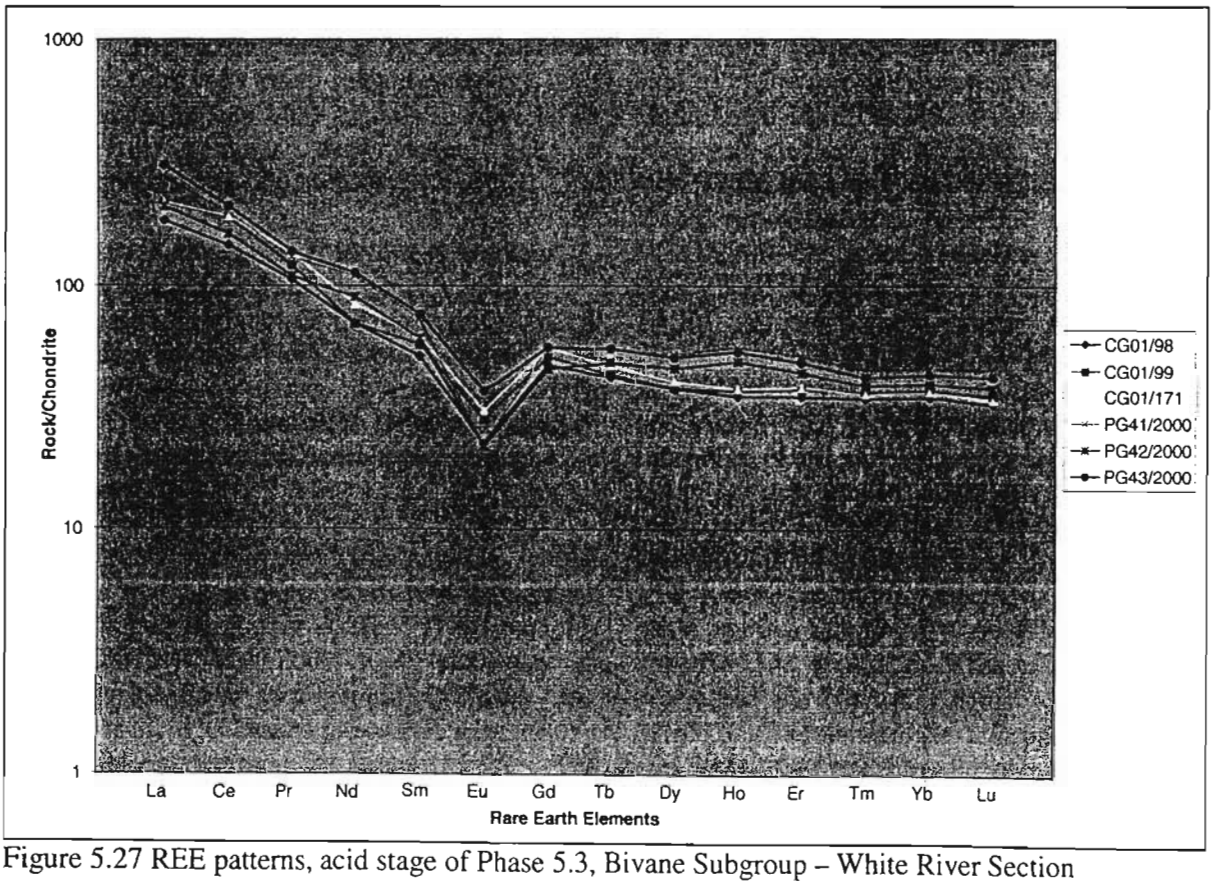

Figure 5.27 REE patterns, acid stage of Phase 5.3, Bivane Subgroup – White River Section

have a negative Eu anomaly (Eu/Eu* = 0.56 – 0.62).

All REE patterns of Phase 5 were influenced by plagioclase fractionation. As the samples of Phase 5 are intermediate to acid in composition, this is to be expected. The presence of pronounced negative Eu anomalies also supports the large degrees of plagioclase fractionation in the magma chamber.

5.6.8 Nhlebela Formation, Bivane Subgroup – White Mfolozi Inlier

The Nhlebela Formation is the older of the two volcanic events preserved in the White Mfolozi Inlier. As discussed earlier the sample CG02/210 is considered to represent a later intrusive event and has therefore been excluded from the REE interpretation of the Nhlebela Formation. The range of ∑REE is from 428ppm to 511ppm, with an average of 475ppm (Table 5.7). The LREE are enriched relative to the HREE with $(La/Lu)_{cn}$ ratios from 7.97 to 9.64, average = 8.8 (Table 5.7; Figure 5.29). The slope of the LREE is also considerably steeper ($(La/Sm)_{cn\ average}$ = 3.62) than the slope of the HREE ($(La/Sm)_{cn\ average}$ = 1.89). All samples have a negative Eu anomaly (Eu/Eu* = 0.68-0.75). The REE patterns of the Nhlebela Formation are all closely related and very little fractionation of any kind appears to have taken place (the samples were taken over a stratigraphic range (Figure 3.47)).

5.6.9 Agatha Formation, Bivane Subgroup – White Mfolozi Inlier

The Agatha Formation is the youngest volcanic succession in the White Mfolozi Inlier. The White Mfolozi River has cut a section through the tilted lavas sub-parallel to strike providing an excellent stratigraphic succession through the lava flows.

Figure 5.30 shows the REE patterns of the samples that broadly correspond to Traverse 1 (See Chapter 3, Figure 3.55). These samples (WM2/2000 – WM6/2000) were taken over an approximate 75m stratigraphic thickness and were classified as basalts to basaltic andesites by classification diagrams in Section 5.3.7. The ∑REE concentrations range from 291ppm to 422ppm, average 351ppm (Table 5.7). These total REE concentrations are comparatively high for both tholeiitic basic and intermediate volcanic rocks (continental tholeiites - ∑REE = 15.2 – 322ppm, Cullers and Graf, 1984; continental andesite - ∑REE = 67 – 341ppm, Cullers and Graf, 1984). In order to attain these enriched REE patterns, the basalts and basaltic andesites need an alkali affinity, a fact that was identified by one of the classification graphs FW SiO_2 vs Zr/TiO_2 that classed most of the Traverse 1 samples as alkali basalts. LREE are enriched relative to the HREE where $(La/Lu)_{cn}$ = 4.5 – 7.5, average 5.57. The LREE show that all samples show a slight negative Ce anomaly. All samples except WM6/2000 form an approximate straight line from Pr to Sm. WM6/2000 shows slight enrichment of Pr and Nd relative to the other LREE. While the LREE patterns appear to have similar characteristics, they are not parallel. This is due to varying concentrations of LREE relative to each other resulting in differing gradients of the LREE slopes. WM2/2000 has a particularly steep LREE pattern ($(La/Sm)_{cn}$ = 2.69) as opposed to WM3/2000, which has a gentler LREE pattern ($(La/Sm)_{cn}$ = 1.89). The differing LREE ratios cause the LREE patterns of these samples to overlap in places. The Eu anomalies are highly varied in the Traverse 1 samples. WM5/2000 is the only sample with a positive Eu anomaly (Eu/Eu* = 1.5). Negative Eu anomalies vary from virtually non-existent (WM2/2000 Eu/Eu* = 0.95) to very pronounced (WM4/2000 Eu/Eu* = 0.48). The HREE patterns are for the large part similar. WM3/2000, WM4/2000 and WM5/2000 have very similar HREE patterns and their curves almost overlay one another. WM2/2000 is more enriched in Gd and WM6/2000 is more depleted in Gd but their HREE patterns possess similar undulations as those of WM3/2000, WM4/2000 and WM5/2000. All samples have similar Lu values and their HREE patterns appear to converge at this point. All samples show a steeper pattern for Gd to Dy than for Ho to Lu, although it is most pronounced in WM6/2000. Overall WM4/2000 and WM5/2000 appear to have the most similar REE patterns apart from the fact that WM5/2000 has a positive Eu anomaly and WM4/2000 has a negative Eu anomaly. These samples may represent the same original melt, where WM5/2000 contained the feldspar phenocrysts and WM4/2000 was the residual melt.

The REE patterns for the samples related to Traverse 2 are shown on Figure 5.31. (See Figure 3.55 for sample localities). Traverse 2

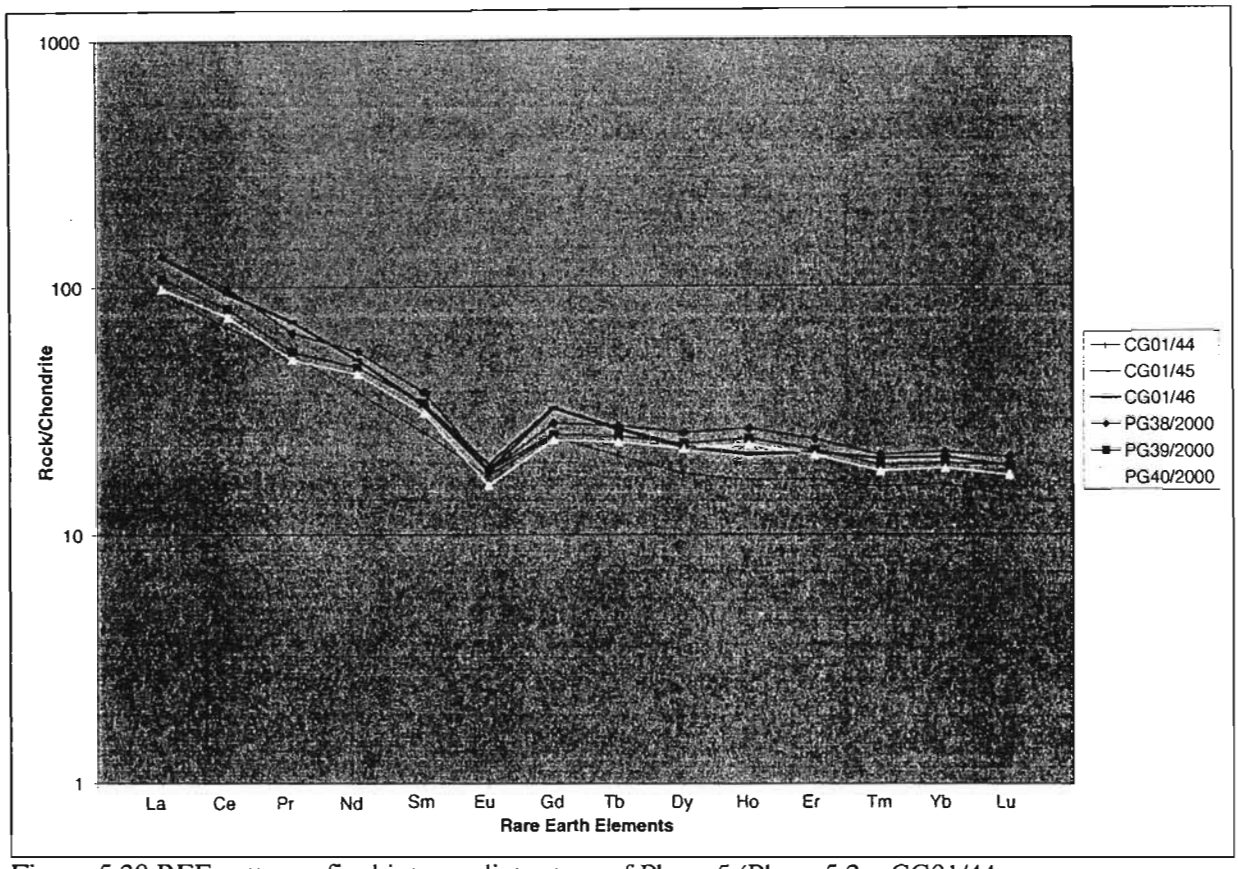

Figure 5.28 REE patterns, final intermediate stage of Phase 5 (Phase 5.2 – CG01/44, CG01/45, CG01/46; Phase 5.3 – PG38/2000, PG39/2000, PG40/2000) – White River Section

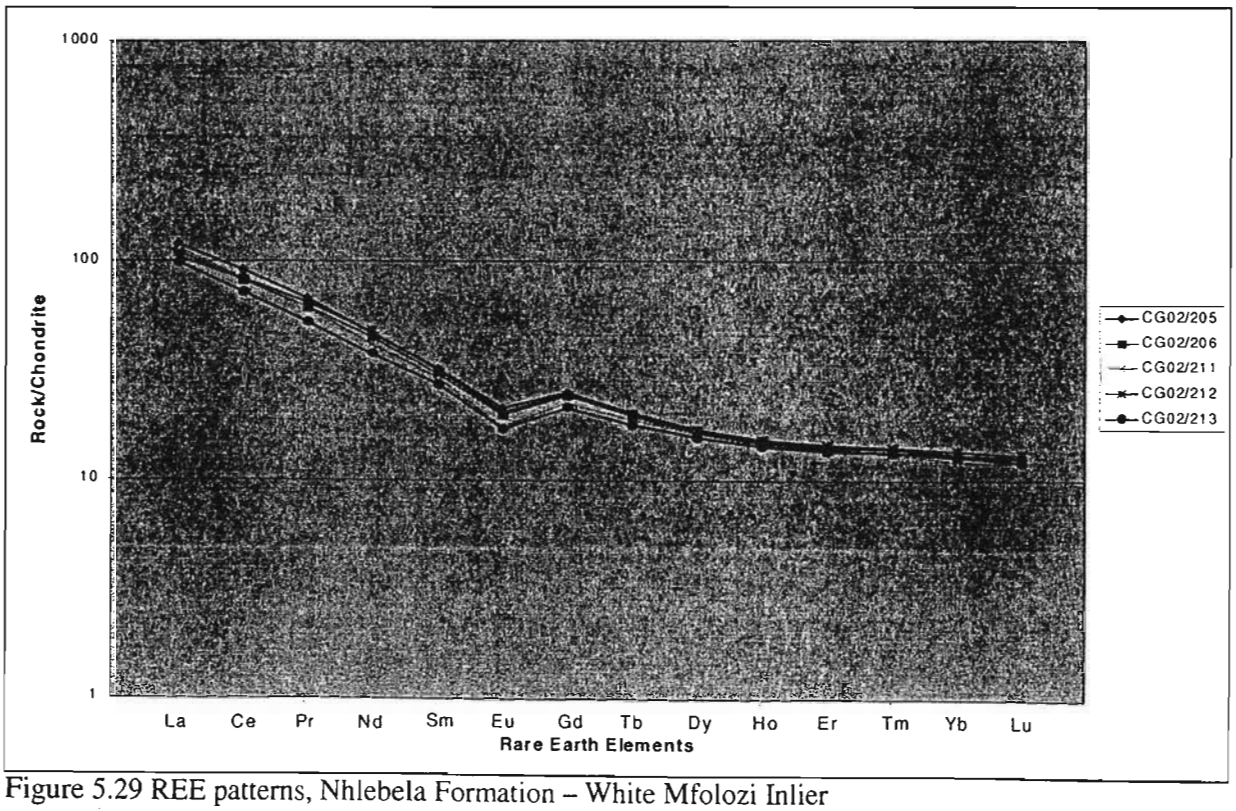

Figure 5.29 REE patterns, Nhlebela Formation – White Mfolozi Inlier

Table 5.7 REE summary data for the Nhlebela Formation and the Agatha Formation – White Mfolozi Inlier

	∑REE ppm	$(La/Lu)_{cn}$	$(La/Sm)_cn$	$(Gd/Lu)_{cn}$	Eu/Eu*	$(La/Yb)_{cn}$
Nhlebela Formation						
CG02/205	511	9.43	3.75	1.96	0.75	9.17
CG02/206	477	8.79	3.56	1.96	0.73	8.62
CG02/211	472	9.64	3.91	1.89	0.68	9.38
CG02/212	485	7.97	3.31	1.85	0.74	7.67
CG02/213	428	8.15	3.59	1.77	0.71	7.71
average	475	8.80	3.62	1.89	0.72	8.51
Agatha Formation - Traverse 1						
WM2/2000	422	7.50	2.69	2.66	0.95	6.70
WM3/2000	323	4.50	1.89	2.37	0.57	4.04
WM4/2000	347	5.63	2.39	2.29	0.48	5.09
WM5/2000	372	5.51	2.10	2.54	1.50	5.03
WM6/2000	291	4.72	2.32	1.84	0.78	4.39
average	351	5.57	2.28	2.34	0.85	5.05
Agatha Formation - Traverse 2						
WM10/2000	206	3.29	2.02	1.70	0.68	2.99
WM11/2000	212	4.88	2.41	1.97	0.88	4.41
WM12/2000	222	5.89	2.66	2.12	1.02	5.20
WM13/2000	232	5.79	2.53	2.12	0.97	5.10
WM17/2000	227	2.85	1.94	1.49	0.89	2.70
WM16/2000	242	5.93	2.58	2.15	0.99	5.18
WM15/2000	246	4.34	2.07	2.03	0.80	3.86
average	227	4.71	2.32	1.94	0.89	4.21

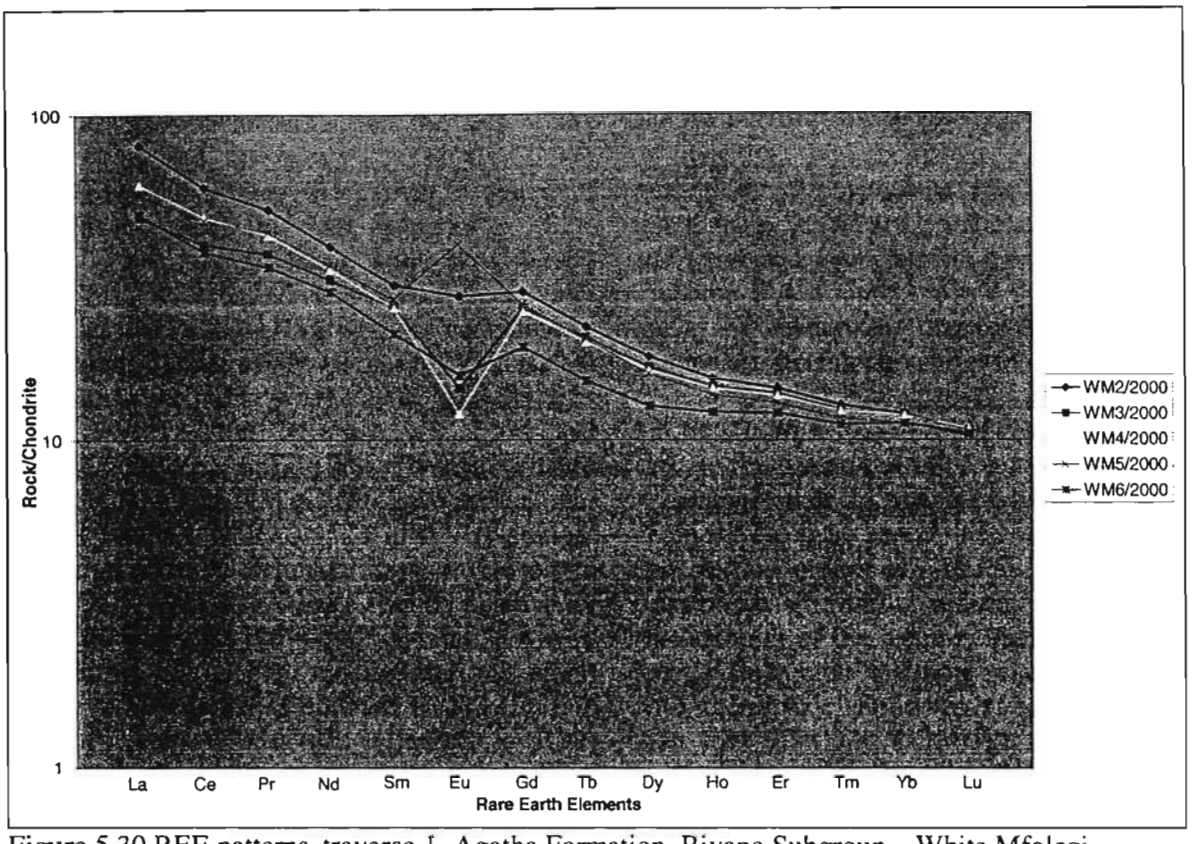

Figure 5.30 REE patterns, traverse 1, Agatha Formation, Bivane Subgroup – White Mfolozi Inlier

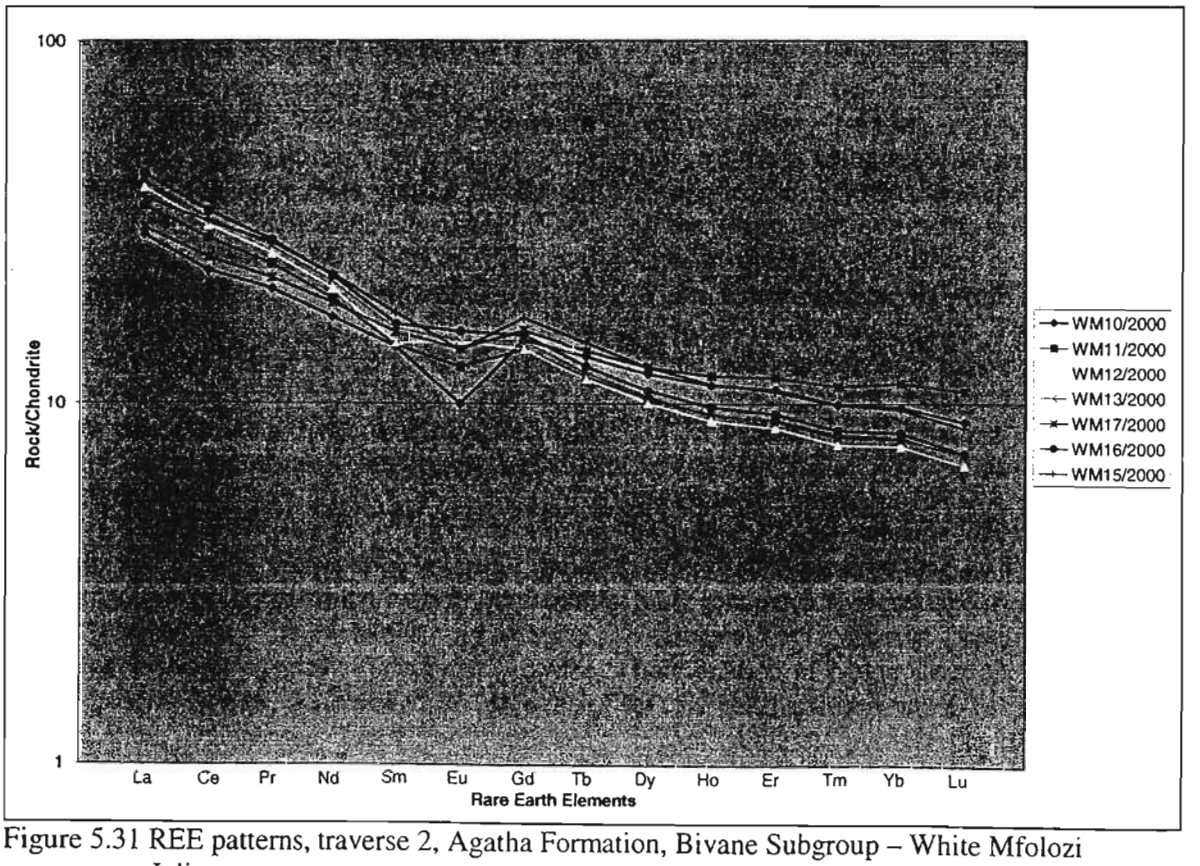

Figure 5.31 REE patterns, traverse 2, Agatha Formation, Bivane Subgroup – White Mfolozi Inlier

samples have considerably lower ∑REE concentrations than Traverse 1 samples (∑REE = 206 –246, average = 227) (Table 5.7). WM15/2000 and WM17/2000 were classified as basalts / basaltic andesites and the rest of the samples classed as andesites. The LREE are enriched relative the HREE over a range of $(La/Lu)_{cn}$ = 2.85 to 5.93, average = 4.71. WM10/2000, WM15/2000 and WM17/2000 ($(La/Sm)_{cn}$ = 2.02,2.07 and 1.94 respectively) form relatively flat LREE patterns compared to the other Traverse 2 samples WM11/2000 ($(La/Sm)_{cn}$ = 2.41), WM12/2000 ($(La/Sm)_{cn}$ = 2.66), WM13/2000 ($(La/Sm)_{cn}$ = 2.53) and WM16/2000 ($(La/Sm)_{cn}$ = 2.58). WM11/2000 to WM13/2000, and WM16/2000 have very similar LREE patterns, which form a relatively straight line from La to Nd before falling more steeply to Sm. Only WM12/2000 has a slightly positive Eu anomaly where Eu/Eu* = 1.02. Eu has, however, proven to be slightly mobile and the slight negative Eu anomalies of WM13/2000 (Eu/Eu* = 0.97) and WM16/2000 (Eu/Eu* = 0.99) suggest that the positive anomaly may be a factor of secondary processes. WM11/2000, WM15/2000 and WM17/2000 have Eu/Eu* between 0.80 and 0.89. WM10/2000 has a distinct negative Eu anomaly (Eu/Eu* = 0.68). The HREE patterns for the Traverse 2 samples show a divergent pattern from Gd to Lu (as opposed to the convergent pattern seen for Traverse 1 samples). WM15/2000 has a much steeper HREE pattern than the other samples and this results in the curve cross cutting the overall pattern. WM10/2000, WM11/2000, WM12/2000, WM13/2000, WM16/2000 and WM17/2000 all form sub-parallel HREE patterns, with varying $(Gd/Lu)_{cn}$ ratios resulting in the divergent nature of the pattern. Overall WM10/2000 and WM17/2000 have flatter REE patterns than the other Traverse 2 samples, with lower LREE abundances but higher HREE concentrations.

Overall the Agatha Formation volcanic rocks appear to have been controlled by both pyroxene and plagioclase fractionation processes. Traverse 1 shows systematic steepening of the REE pattern slopes, indicative of pyroxene fractionation, where the LREE are enriched while the HREE are depleted. The presence of Eu anomalies, both negative and positive, and the pivot point of steepening at Lu and not Gd, suggests that plagioclase fractionation was also a factor in the source magma that these lavas represent. Traverse 2 samples show the influence of pyroxene fractionation in the melt, prior to eruption, with the pivot point appearing to lie at Gd, where the LREE have been enriched and the HREE have been depleted. The presence of negative Eu anomalies is also a clear indication of plagioclase fractionation. The relationship between the samples of Traverse 1 and Traverse 2 is unclear but it would appear that Traverse 1 is a more evolved suite of volcanic rocks that underwent extensive pyroxene and plagioclase fractionation prior to eruption.

5.6.10 Comparison of basic volcanic rocks of the Nsuze Group

A comparison of the samples with the most basic compositions can reveal differences in source and melting processes. The flatness of a REE pattern i.e. $(La/Lu)_{cn}$, reflects the degree of fractionation of the magma, therefore the lower the $(La/Lu)_{cn}$ ratio, the more primitive compared with chondrite. The lowest $(La/Lu)_{cn}$ ratios are 2.26 and 2.27 for CG01/141 and CG01/142 respectively. These samples form part of Phase 2. Phase 2 is also the phase with the lowest $(La/Lu)_{cn}$ ratios for basic compositions. Phase 2 also has the lowest ∑REE concentrations. Phase 2 is therefore considered to reflect the most primitive i.e. least evolved magma of the White River Section of the Nsuze Group. The Agatha Formation of the White Mfolozi Inlier has relatively low $(La/Lu)_{cn}$ ratios with lowest at 2.85, which is comparable to the ratios of Phase 2. Figure 5.32 shows the average REE patterns of the Wagondrift Formation and the basalts and basaltic andesites of Phase 1 and Phase 2 of the White River Section, as well as the Nhlebela Formation and the Agatha Formation of the White Mfolozi Section. It is significant to note that the Wagondrift Formation has a steeper HREE pattern than LREE pattern ($(Gd/Lu)_{cn}$ = 3.09 vs $(La/Sm)_{cn}$ = 2.27). This does not occur in the Agatha Formation, Phase 1 or Phase 2 (or in any other of the volcanic phases), which have flatter HREE patterns than LREE patterns. The REE geochemical signature of the Nsuze Group volcanics are largely controlled by the fractionation of plagioclase, the initial steepness of the REE patterns must be attributed to the crystallization of pyroxene in the earliest stages of evolution of the magma. The steeper HREE patterns of the Wagondrift Formation may be explained by different magma sources. The Wagondrift Formation may have tapped a source in which the HREE had been depleted by an

earlier partial melting event. Alternatively pyroxene fractionation may have taken place resulting in LREE enrichment and HREE depletion, although pyroxene is not present in the Wagondrift Formation as a phenocryst phase. The subsequent phase of plagioclase fractionation is however recorded.

5.7 GEOCHEMICAL AFFINITY

The classification diagrams used in Section 5.3 of this chapter distinguish different geochemical affinities. While the Winchester and Floyd (1977) diagrams distinguish between alkaline and subalkaline compositions, the Jensen Cation diagram uses Rickwood (1989) corrected values to divide tholeiitic and calcalkaline compositions. Results from Winchester and Floyd graphs show that the Nsuze Group data is predominantly subalkaline. There are samples that plot within the alkali fields, commonly on the alkali – subalkali boundary. The Winchester and Floyd diagrams are not entirely reliable for determining the geochemical affinity of the Nsuze Group due to the fact the field boundaries are based on actual data sets and are therefore relatively subjective. In general it can be said that the data is predominantly subalkaline, with certain alkali tendencies in more acid compositions. Jensen Cation diagrams show that the majority of data plots as tholeiitic compositions. Calcalkaline signatures are preserved in particular at the basic end of the compositional spectrum.

The most common method of determining general geochemical affinity of data is by using an AFM plot based on Irvine and Baragar (1971). This diagram (Figure 5.33) shows that the approximately 50% of samples plot as tholeiites, with the other 50% found in the calcalkaline field. The alkali elements are known for their mobility during metamorphic events and the AFM diagram cannot be relied on for an accurate assessment of geochemical affinity of the Nsuze Group data.

Two methods of determining geochemical affinity using immobile trace elements have been applied to the Nsuze Group data. The first is a binary plot of Zr versus Y, where the ratio between the two components can differentiate between tholeiitic, transitional and calcalkaline compositions (Barrett and MacLean, 1997) (Figure 5.34). The Nsuze Group data plots within the transitional field ($4<Zr/Y<7$), with moderate scatter into the tholeiitic field ($Zr/Y<4$) and the calcalkaline field ($Zr/Y>7$). The second method of using immobile trace elements to determine geochemical affinity is to use REE ratios. Barrett and MacLean (1997) suggested that $(La/Yb)_{cn}$ ratios could be used to determine the affinity of a data set. $(La/Yb)_{cn}$ = 1-3 is tholeiitic, $(La/Yb)_{cn}$ = 3-6 is transitional and $(La/Yb)_{cn} \geq 6$ is calcalkaline. Most phases of eruption from the White River Section show average calcalkaline $(La/Yb)_{cn}$ ratios, with only Phase 5.1 and Phase 5.3 averaging below 6, to show a transitional affinity (Table 5.8) (for individual sample ratios, see Tables 5.1 to 5.7). The Nhlebela Formation of the White Mfolozi Inlier has a calcalkaline affinity while the Agatha Formation has an overall transitional affinity.

The subjectivity of constructed diagrams to determine the geochemical affinity of a dataset results in no one diagram proving accurate. An overall determination has been derived from results drawn from all methods tested. It therefore appears that the Nsuze Group data has a general transitional trending towards calcalkaline geochemical affinity.

5.8 INCOMPATIBLE ELEMENT DIAGRAMS (SPIDER DIAGRAMS)

Trace elements spider diagrams have been normalized to MORB using the normalization values and trace element order of Pearce (1983). MORB-normalized spider diagrams are most appropriate for evolved basalts and andesites and are therefore most suited to the Nsuze Group suite of volcanic rocks. Pearce (1983) divided the graph into mobile elements (Sr, K, Rb, Ba) on the left and immobile elements (Th, Ta, Nb, Ce, P, Zr, Hf, Sm, Ti, Y, Yb) on the right of the diagram. The elements are arranged so that the incompatibility of the mobile and immobile elements increases from the outside towards the centre of the pattern. Pearce (1983) stated that fractional crystallization and variable degrees of partial melting are unlikely to affect the shape of the trace element patterns. As a result these diagrams can be used to interpret source characteristics.

The Wagondrift Formation is composed predominantly of basalts through to basaltic andesites. The incompatible element plot for the Wagondrift Formation data is shown in Figure

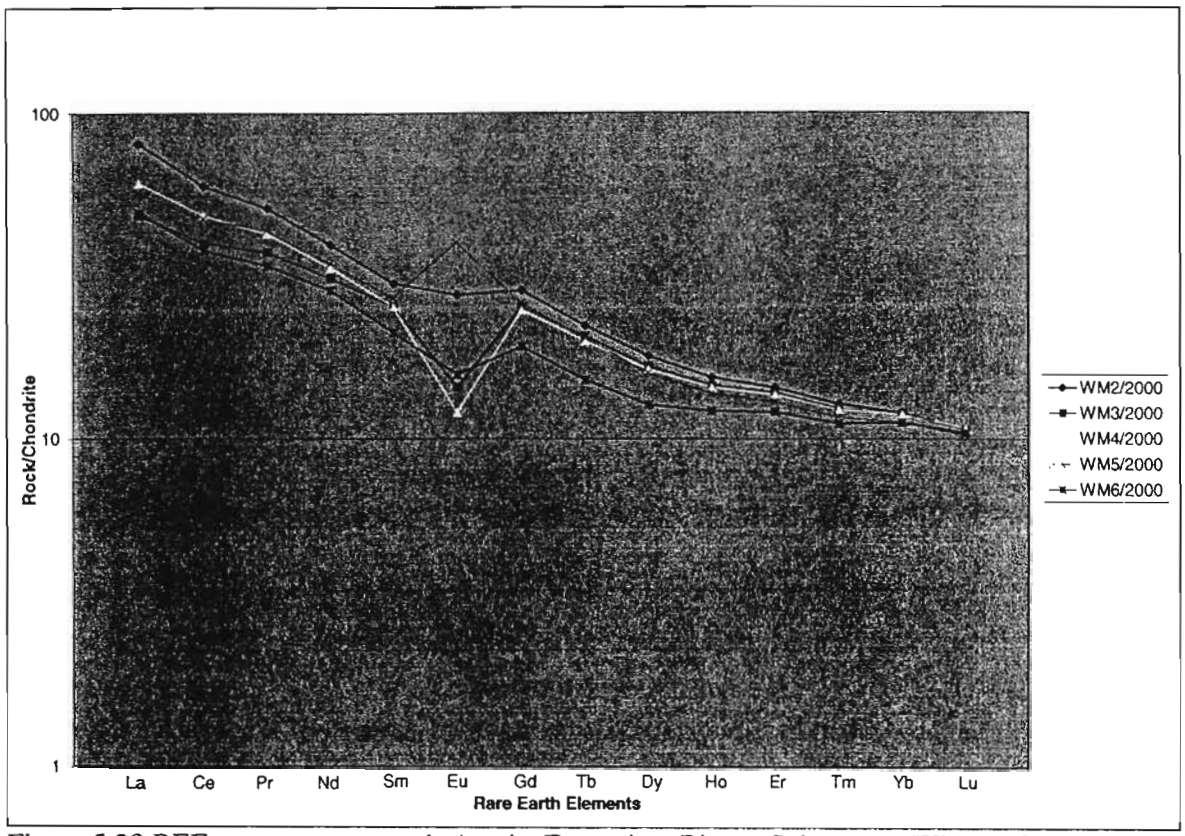

Figure 5.30 REE patterns, traverse 1, Agatha Formation, Bivane Subgroup – White Mfolozi Inlier

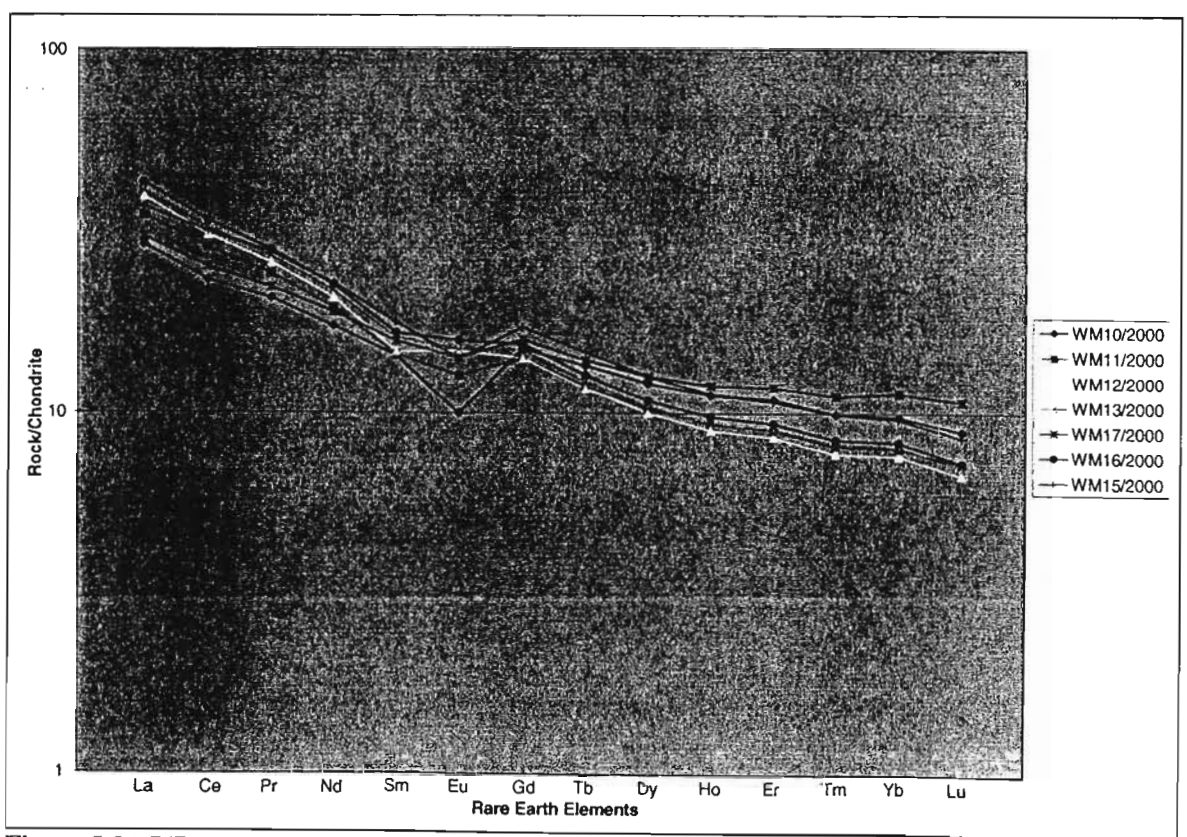

Figure 5.31 REE patterns, traverse 2, Agatha Formation, Bivane Subgroup – White Mfolozi Inlier

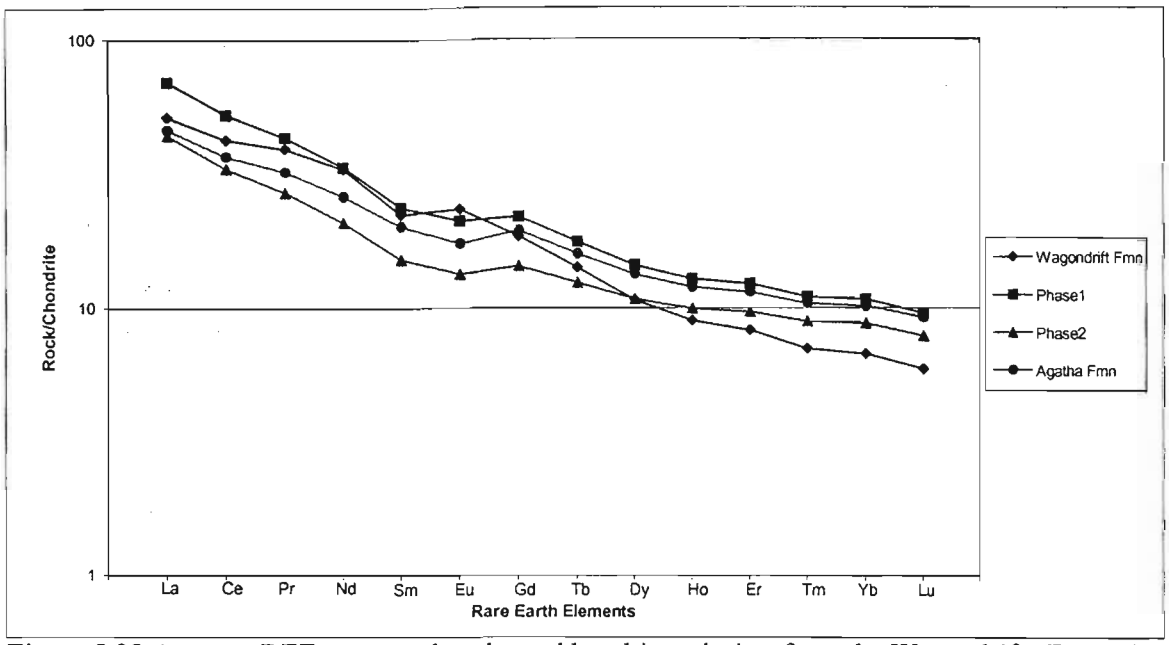

Figure 5.32 Average REE patterns, basalts and basaltic andesites from the Wagondrift Formation, Phase 1 and Phase 2, Bivane Subgroup – White River Section and the Agatha Formation, Bivane Subgroup – White Mfolozi Inlier

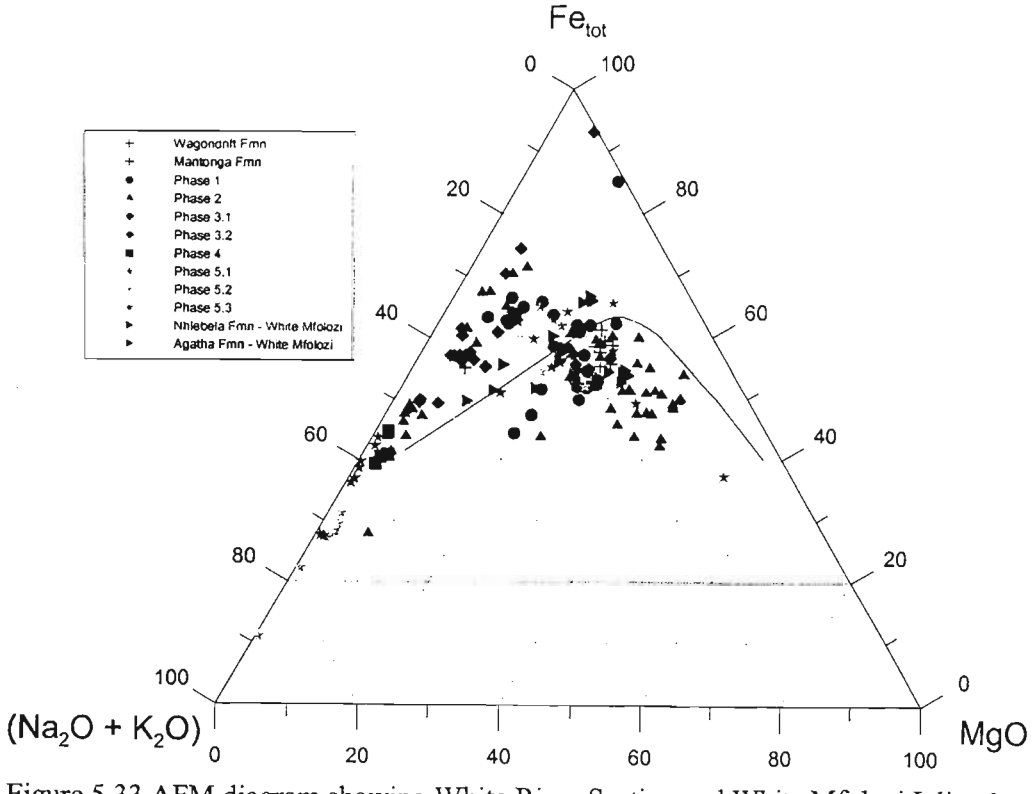

Figure 5.33 AFM diagram showing White River Section and White Mfolozi Inlier data. Tholeiite – calc-alkaline boundary is based on Irvine and Baragar (1971).

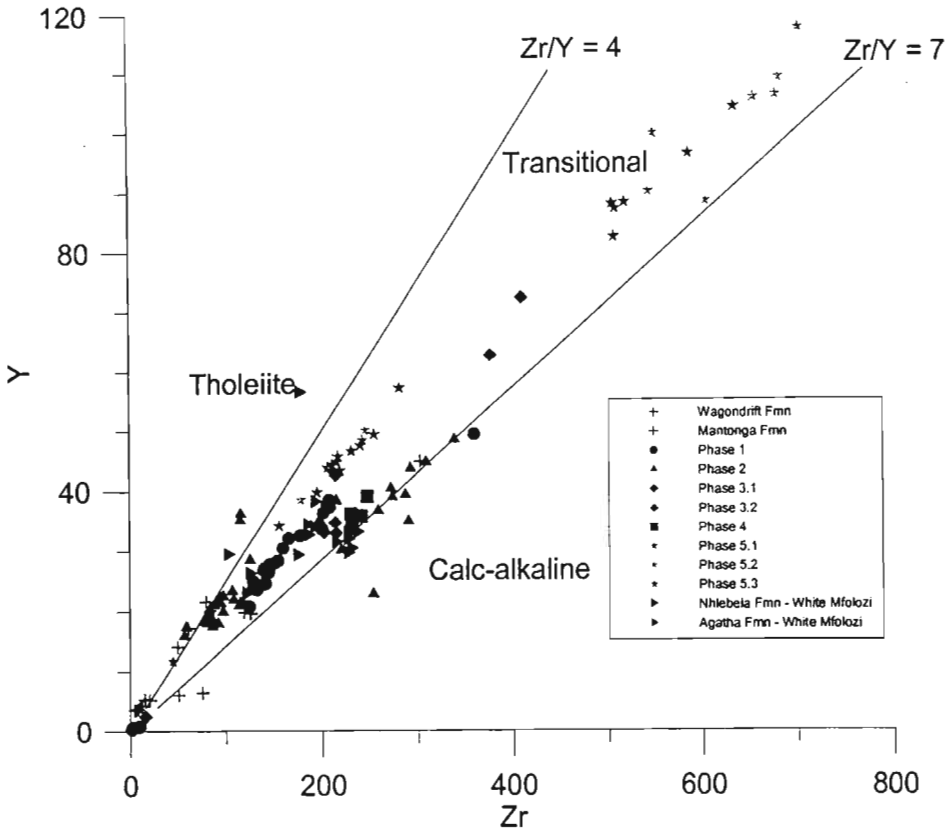

Figure 5.34 Zr/Y affinity plot where Zr/Y <4 = tholeiite, 4< Zr/Y <7 = transitional and Zr/Y >7 = calc-alkaline (Barrett and MacLean, 1997)

Table 5.8 $(La/Yb)_{cn}$ ratios show geochemical affinity where $(La/Yb)_{cn}$ = 1-3 is tholeiitic, $(La/Yb)_{cn}$ = 3-6 is transitional and $(La/Yb)_{cn}$ ≥6 is calc-alkaline. (Barrett and MacLean, 1997)

	$(La/Yb)_{cn}$ average	Affinity
White Mfolozi Inlier		
Nhlebela Formation	8.51	calc-alkaline
Agatha Formation	4.56	transitional
White River Section		
Wagondrift Formation	7.50	calc-alkaline
Mantonga Formation	9.35	calc-alkaline
Phase 1	6.54	calc-alkaline
Phase 2	7.50	calc-alkaline
Phase 3.1	8.87	calc-alkaline
Phase 3.2	6.05	calc-alkaline
Phase 4	10.83	calc-alkaline
Phase 5.1	5.94	transitional
Phase 5.2	6.62	calc-alkaline
Phase 5.3	5.78	transitional

5.35. All samples show a similar overall pattern. The graph peaks at Rb-Ba and Ce-P. Sm forms a small peak. A trough incorporating Th-Nb is found between the peaks of Ba and Ce. Hf is distinctly depleted in the Wagondrift Formation data.

The Mantonga Formation has low Sr values but enriched K to Ba concentrations (Figure 5.36). The incompatible element pattern shows a Ta-Nb negative anomaly, as well as negative troughs at P and Ti. The lack of a negative anomaly at Hf, presence of P anomaly and enriched Th concentrations suggests that simple fractionation processes do not relate the Mantonga Formation to the Wagondrift Formation.

Phase 1 shows enrichment of Rb-Th (Figure 5.37). Another peak is found at Ce. In between Th and Ce, a distinct Ta-Nb trough is present. The data from P to Yb has an overall negative slope. P, Hf, Ti and Yb show slight depletion relative to Zr, Sm and Y. The Ti trough is the most distinct of these.

The incompatible element patterns for Phase 2 show the two compositional groupings – basic to intermediate and acid, as identified by the classification diagrams and the REE plots (Figure 5.38). The data shows enrichment in the mobile elements K, Rb, Ba (although in more acid samples Ba forms a negative spike relative to Rb and Th) and Th. Ta and Nb form a distinctive trough, followed by a Ce peak. P is depleted relative to Ce and Zr. Zr – Sm forms an enriched plateau in the acid samples. The intermediate data shows slight Hf depletion relative to Zr and Sm. Ti forms a trough between the enriched Sm and Y values.

Although little data for Phase 3 exists, certain key features can still be identified in incompatible element patterns (Figure 5.39). K-Th forms a peak relative to the rest of the data, with a slight negative spike for Ba. Ta-Nb forms a small trough before Ce peaks. P and Ti form distinctive depletion spikes.

Phase 4 is an acid only group. Again K, Rb and Th are enriched, while Ba shows a slightly negative spike (Figure 5.40). Ta is enriched, while Nb is severely depleted, resulting in a severely negative Nb spike. This is significant as all other phases show a Ta-Nb trough of similar normalized value. Ce is enriched while P and Ti form depletion spikes.

Phase 5 incompatible elements form a similar pattern to Phases 1, 2 and 3 (Figure 5.41). K, Rb and Th are enriched, while Ba forms a negative spike between them. Ta-Nb forms a slight trough between enriched Th and the smaller peak of Ce. Both P and Ti form distinct negative spikes.

The Nhlebela Formation incompatible element patterns show correlation from Th to Yb, but not from Sr to Ba (Figure 5.42). This is explained by the mobility of Sr, K, Rb and Ba, as the Nhlebela Formation was subjected to a prominent aqueous component during its initial stages of eruption. The pattern shows a trough at Ta-Nb and negative anomalies at P and Ti.

The Sr-Th normalized values of the Agatha Formation data from the White Mfolozi Section show little correlation with each other. As these elements are considered mobile, these samples must be identified as having undergone extensive alteration (Figure 5.43). Data from Ta to Yb can only be considered for interpretation. Two patterns are evident, the first involving WM6/2000, WM10/2000, WM15/2000 and WM17/2000 and the second involving WM2/2000 to WM5/2000, WM11/2000, WM12/2000, WM13/2000 and WM16/2000. While both patterns identify a Ta-Nb trough and a slight Ce peak, their differences are seen from P to Ti. The first group forms a relatively straight pattern from P to Ti, with no defining peaks or troughs. The second group has a slight P, Hf and Ti depletion spike relative to Ce, Zr and Sm and therefore forms a gentle zigzag pattern. These groups are the same as those identified using REE patterns.

The White River Section data, represented by the Bivane Subgroup Phases 1 to 5, show distinct P and Ti negative anomalies, which increase with increasing fractionation. Phase 1, Phase 2, Phase 3, Phase 4 and Phase 5 all show a Ta-Nb trough between enriched Th and Ce normalized values. The Wagondrift Formation samples do not show the same Th enrichment as the Bivane Subgroup data, which results in a Th-Ta-Nb trough. The presence of a distinctive Hf negative anomaly, which has not been identified for any of the Bivane Subgroup phases, suggests that the source

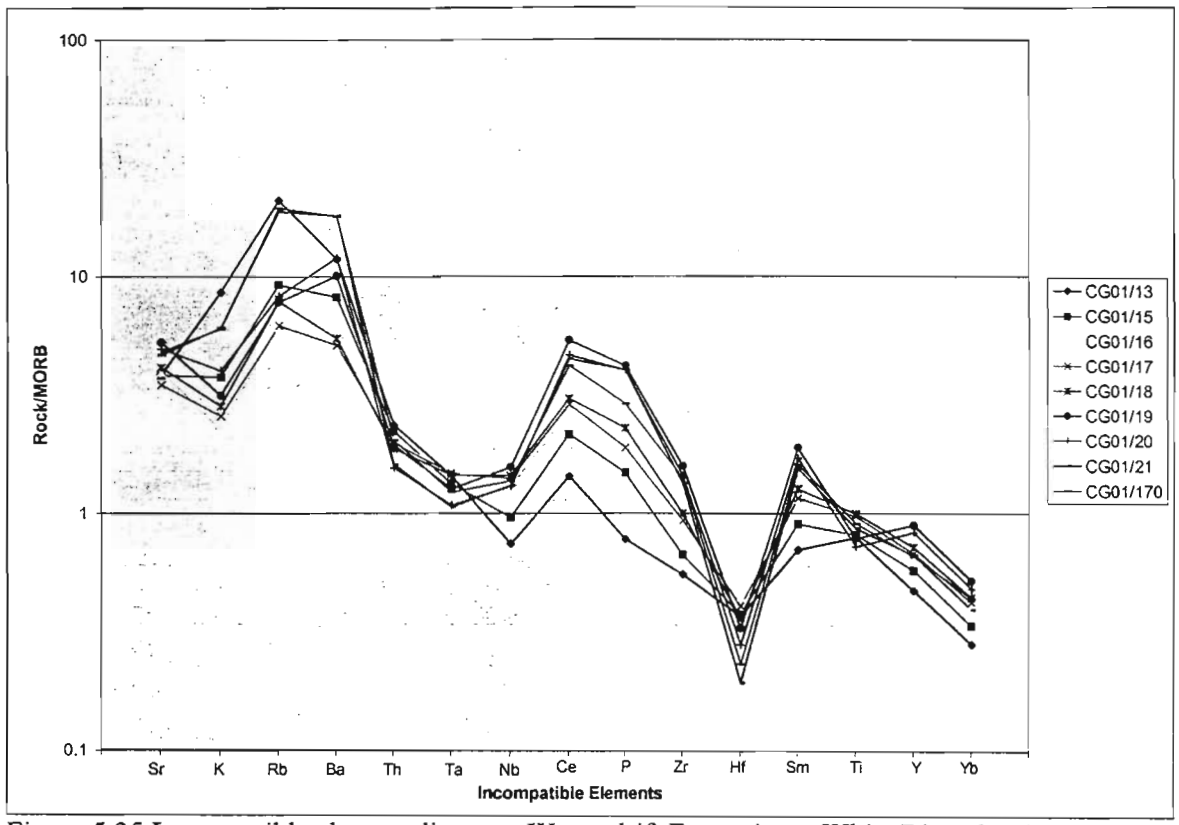

Figure 5.35 Incompatible element diagram, Wagondrift Formation - White River Section (after Pearce, 1983)

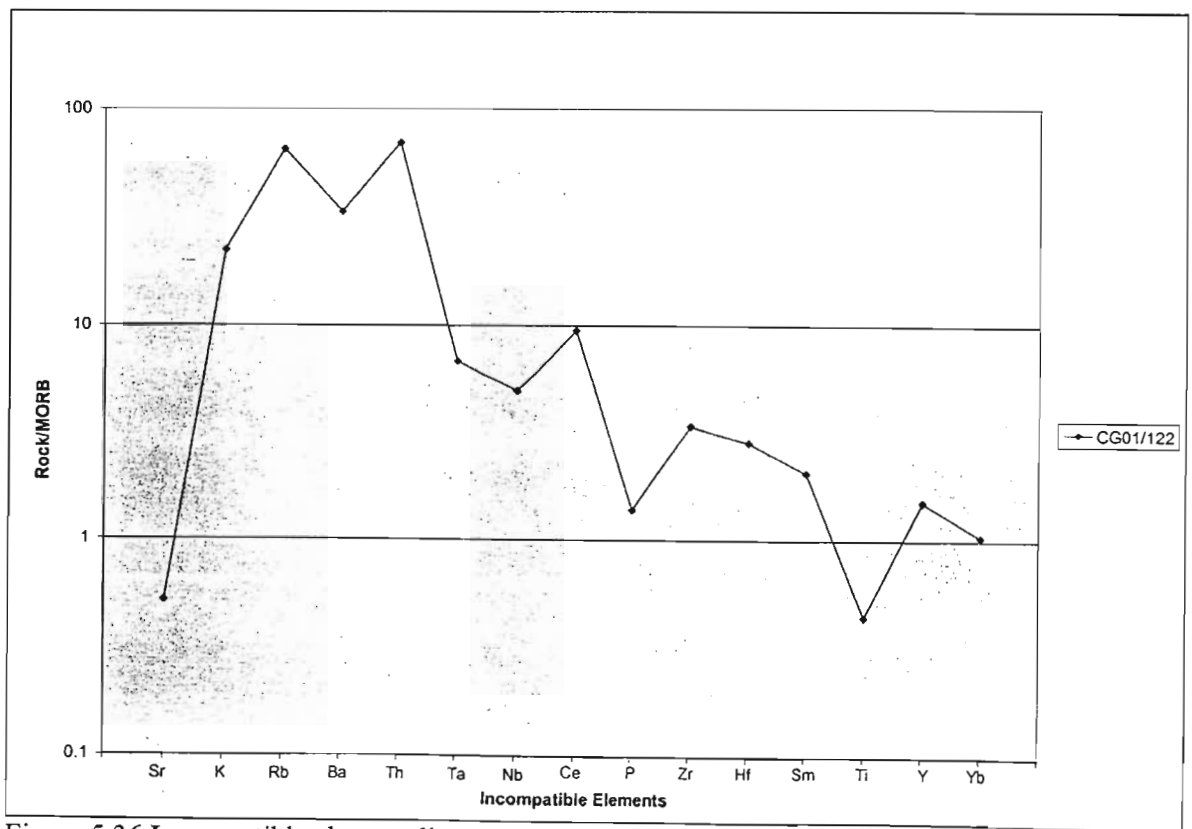

Figure 5.36 Incompatible element diagram, Mantonga Formation – White River Section (after Pearce, 1983).

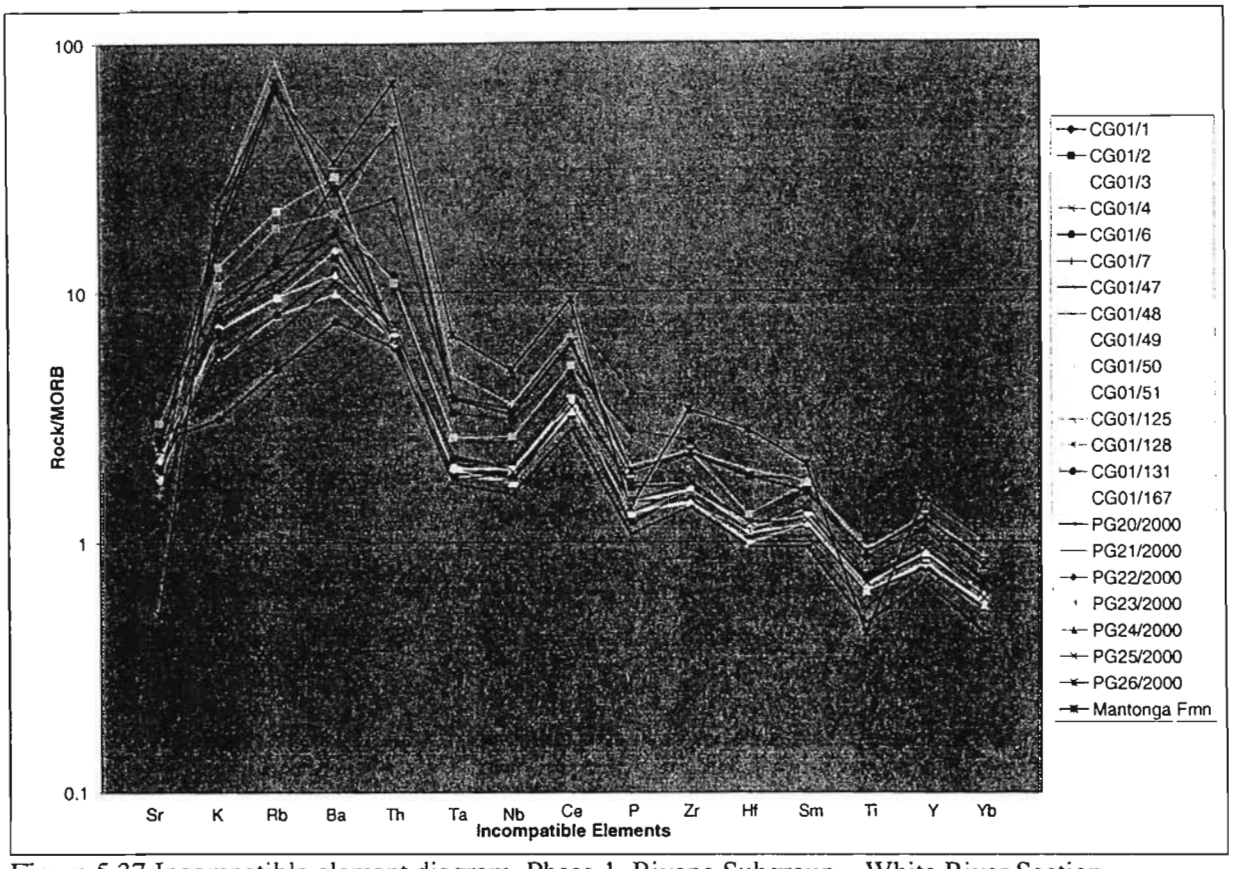

Figure 5.37 Incompatible element diagram, Phase 1, Bivane Subgroup – White River Section (after Pearce, 1983)

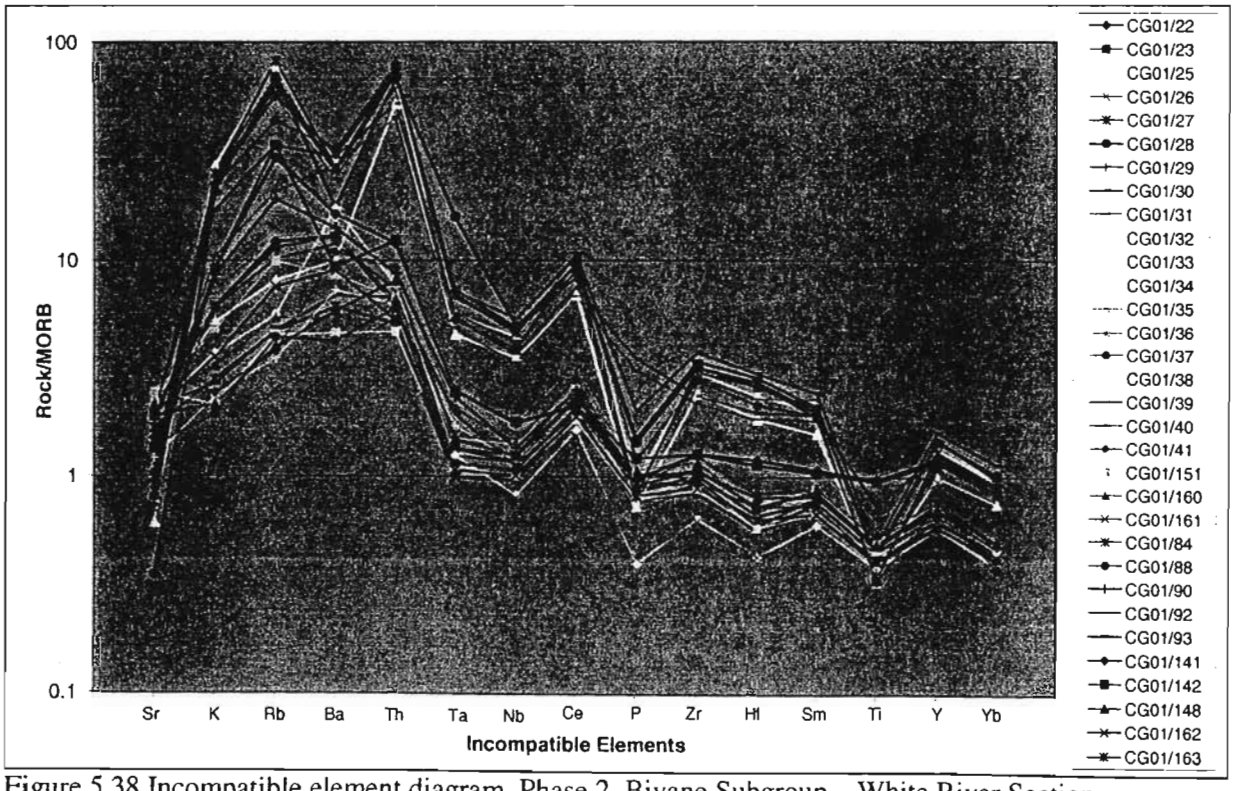

Figure 5.38 Incompatible element diagram, Phase 2, Bivane Subgroup – White River Section (after Pearce, 1983)

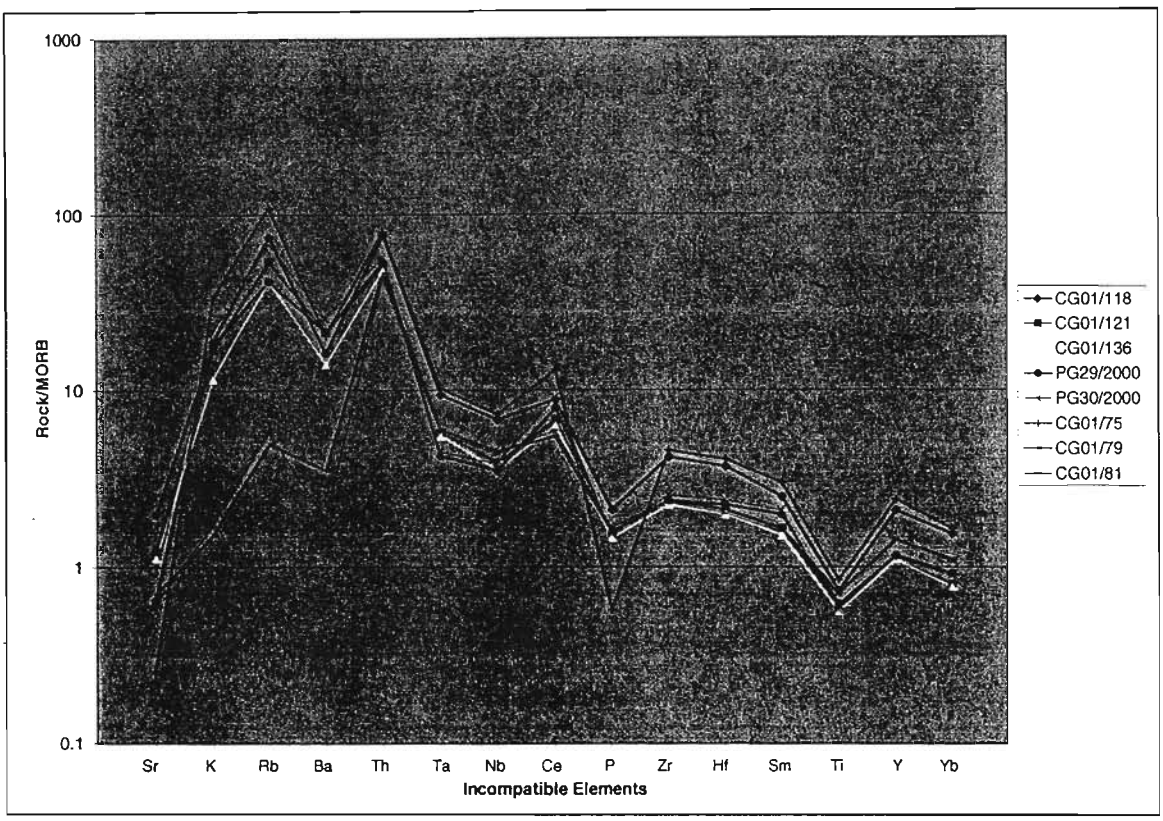

Figure 5.39 Incompatible element diagram, Phase 3 (Phase 3.1 – CG01/118, CG01/121, CG01/136, PG29/2000, PG30/2000; Phase 3.2 – CG01/75, CG01/79, CG01/81), Bivane Subgroup – White River Section (after Pearce, 1983)

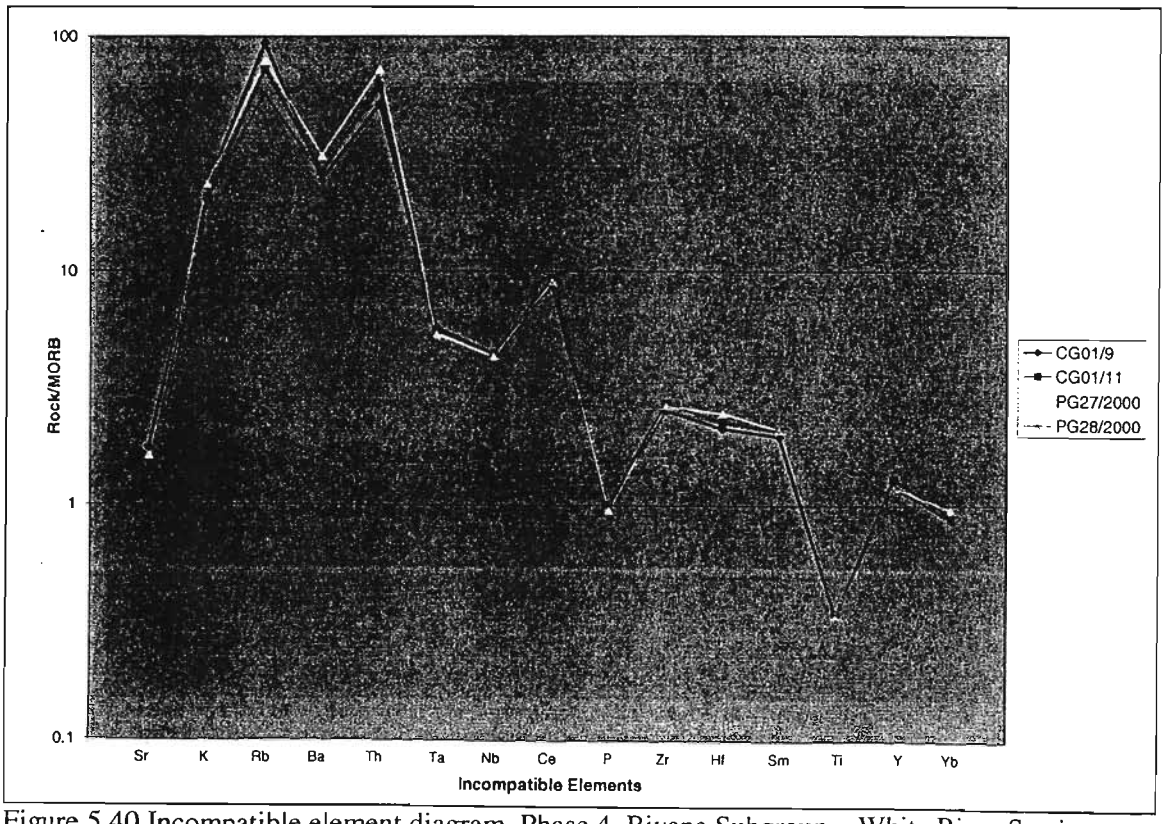

Figure 5.40 Incompatible element diagram, Phase 4, Bivane Subgroup – White River Section (after Pearce, 1983)

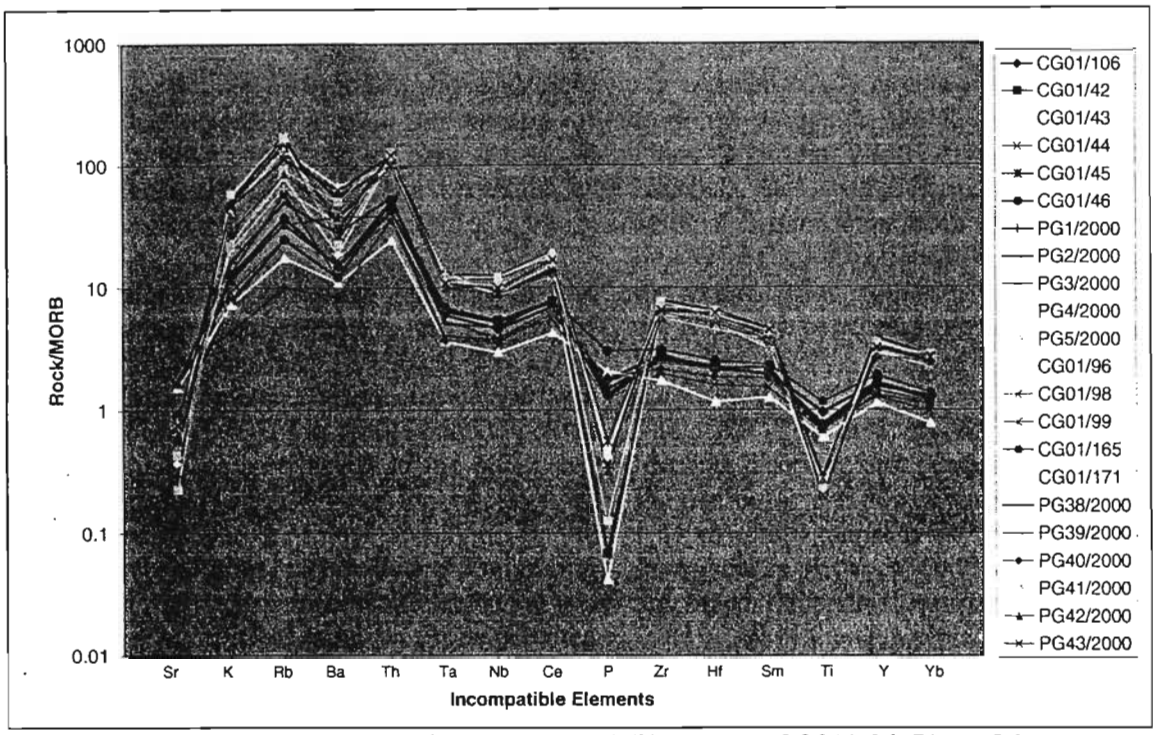

Figure 5.41 Incompatible element diagram, Phase 5 (Phase 5.1 – CG01/106; Phase 5.2 – CG01/42, CG01/43, CG01/44, CG01/45, PG1/2000, PG2/2000, PG3/2000, PG4/2000, PG5/2000; Phase 5.3 – CG01/96, CG01/98, CG01/99, CG01/165, CG10/171, PG38/2000, PG39/2000, PG40/2000, PG41/2000, PG42/2000, PG43/2000), Bivane Subgroup – White River Section (after Pearce, 1983)

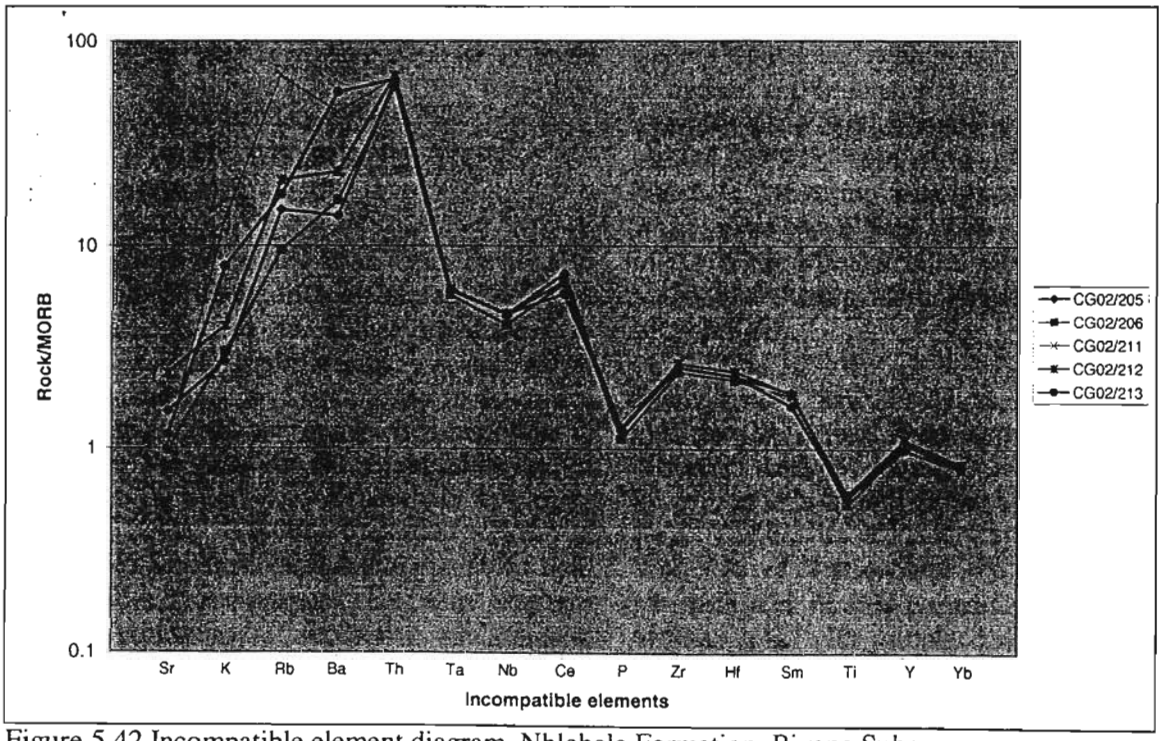

Figure 5.42 Incompatible element diagram, Nhlebela Formation, Bivane Subgroup – White Mfolozi Inlier (after Pearce, 1983)

of the Wagondrift Formation is not the same as that for the large volcanic succession of the Bivane Subgroup. The Agatha Formation (of the White Mfolozi Inlier) has incompatible element patterns that resemble a smoother version of Phase 1, although the lack of large Ti and P negative anomalies suggests the operation of different processes.

The prominent Ta-Nb trough identified in the incompatible element patterns is characteristic of convergent plate tectonics (Wilson, 1989). Low Ta and Nb normalized abundances may be as a result of the retention of insoluble mineral phases (rutile, titanite or perovskite) in the subducted slab (Brenan *et al.*, 1994) or the retention of orthopyroxene, garnet, spinel or olivine in the mantle wedge during reaction between migrating melts and the upper mantle (Keleman *et al.*, 1993). The same effect can however be obtained by crustal contamination of the basaltic melt (Wilson, 1989). A negative Ti anomaly is also commonly associated with convergent continental settings as it may be retained in minerals like rutile and ilmenite in the subducted slab (Wilson, 1989, Rollinson, 1993). Negative Nb values are also characteristic of continental crust and may indicate crustal contamination (Rollinson, 1993). The high normalized abundances of Rb, K and Ba relative to the other incompatible elements also suggests that crustal contamination may have been a factor in these lavas.

5.9 TECTONIC DISCRIMINATION DIAGRAMS

Discrimination diagrams have been devised to distinguish between different tectonic settings, using elements and ratios that are distinct to different tectonic environments. A number of different diagrams have been tested to determine a geochemical tectonic setting. It is important to remember the mobility of certain elements, in particular Ti, which may cause data to plot in incorrect fields. It is also important to keep in mind field observations and interpretations both volcanic and sedimentary i.e. the Northern Region represents a sub-aerial environment, while the Central Region has a combination of sub-aerial and sub-aqueous deposits. The majority of tectonic discrimination diagrams use basalts and basaltic andesites only. This presents a problem with the Nsuze Group data set, especially in the White River Section of the Northern Region where units of basic composition are few, and those present are highly altered and weathered and as a result were not sampled. Only basalts and basaltic andesites from the Wagondrift Formation, Phase 1 and Phase 2 of the White River Section and the Nhlebela and Agatha Formations of the White Mfolozi Section have been used. Even though the Nhlebela Formation is andesitic to dacitic, the data has been used as it is all that represents the first stage of volcanism in the White Mfolozi Inlier.

Table 5.9 is a summary of results from each tectonic discrimination diagram represented in Figures 5.44 to 5.50. Figure 5.44 and Figure 5.45 are two versions of Zr/Y vs Zr. Figure 5.44 distinguishes between continental and oceanic arc based on a Zr/Y ratio equal to 3 (Pearce, 1983). All of the data plots above the line, with Zr/Y ratios greater than 3 and is therefore classed as representing a continental arc tectonic setting. The Wagondrift Formation data plots separately from the Phase 1, Phase 2 and White Mfolozi Inlier data, with Zr/Y ratios closer to 3. Phase 2 plots between Phase 1 and White Mfolozi Inlier data and the data of the Wagondrift Formation. The boundaries denoted by Pearce and Norry (1979) on Figure 5.45 distinguish between volcanic arc basalts, MORB and within-plate basalts. The Wagondrift Formation plots in two fields (MORB and within-plate basalts) as well as outside any denoted field. Phase 1 data plots as within-plate basalts, while Phase 2 basalts are classed as MORB and within-plate basalts. The Nhlebela Formation data plots entirely in the within-plate basalt field. The Agatha Formation of the White Mfolozi Inlier plots dominantly as within-plate basalts although data is found in the MORB fields.

Pearce and Cann (1973) used the immobile elements Ti, Zr and Y to identify basalts from different tectonic settings. The Wagondrift Formation falls entirely in the within-plate basalt field. The basalts of Phase 1 and Phase 2 of the White River Section and the samples of the Nhelbela and Agatha Formations of the White Mfolozi Inlier plot as calcalkali basalts (Figure 5.46). The data of the Wagondrift Formation is clearly different to the other basalts of the Bivane Subgroup.

Pearce and Gale (1977) use Zr/Y and Ti/Y ratios to identify plate margin and within-plate basalts.

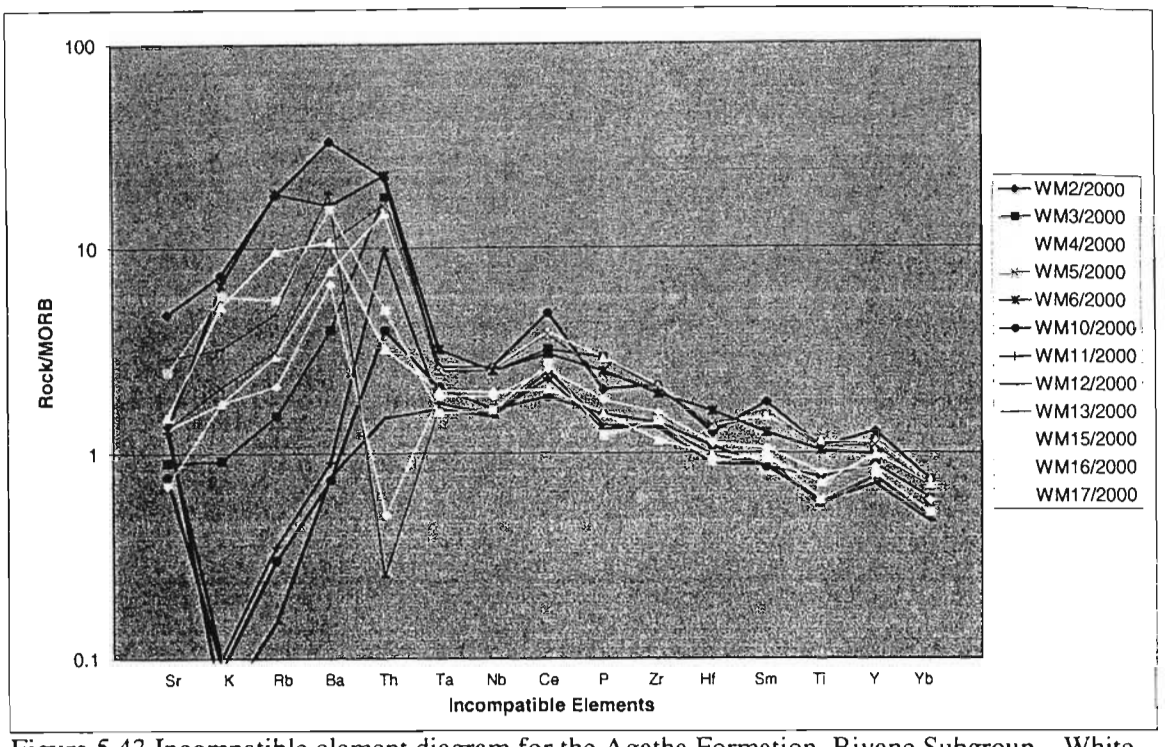

Figure 5.43 Incompatible element diagram for the Agatha Formation, Bivane Subgroup – White Mfolozi Inlier (after Pearce, 1983)

Table 5.9 Summary of results of tectonic discrimination diagrams

Diagram	Result	Figure
Zr/Y - Zr	All - Continental Arc	5.44
	Wagondrift – MORB, within-plate basalts Phase 1 – within-plate basalts Phase 2 – within-plate basalts, MORB Nhlebela – within-plate basalts Agatha – MORB, within-plate basalts	5.45
Ti-Zr-Y	Wagondrift – within-plate basalts, calc-alkali basalts Phase 1 – calc-alkali basalts Phase 2 – calc-alkali basalts Nhlebela – calc-alkali basalts Agatha – calc-alkali basalts	5.46
Zr/Y - Ti/Y	Wagondrift – within-plate basalt, plate margin basalt Phase 1 – plate margin basalt Phase 2 – plate margin basalt Nhlebela – plate margin basalt Agatha – plate margin basalt	5.47
Th/Yb - Ta/Yb	Wagondrift – tholeiite – calc-alkaline, plots between all fields Phase 1 – calc-alkaline active continental margin, enriched mantle source Phase 2 – calc-alkaline active continental margin, enriched mantle source Nhlebela – shoshonitic active continental margin, enriched mantle source Agatha – calc-alkaline active continental margin, enriched mantle source	5.48
Th - Hf - Ta	Wagondrift – alkaline within-plate basalts Everything else – calc-alkaline island arc	5.49
Zr - Nb - Y	Wagondrift – within-plate tholeiites, volcanic arc basalts, N –type MORB Phase 1 – within-plate tholeiites, volcanic-arc basalts Phase 2 – within-plate tholeiites, volcanic-arc basalts Nhlebela – within-plate alkali basalts, within-plate tholeiites Agatha – within-plate tholeiites, volcanic-arc basalts	5.50

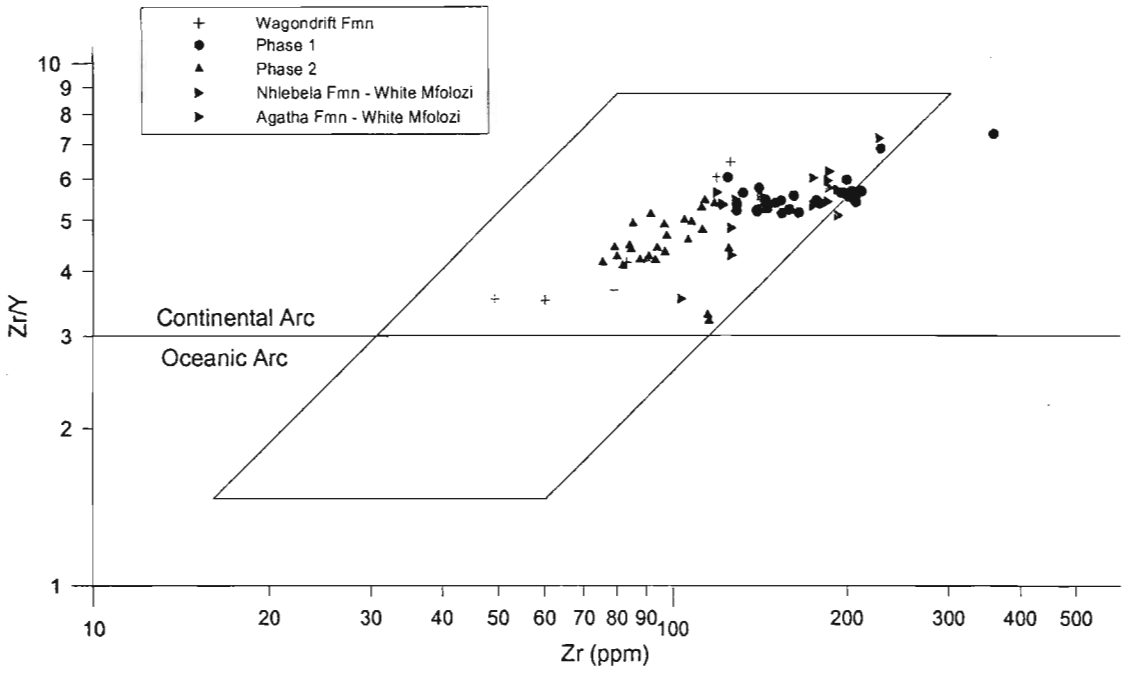

Figure 5.44 Zr/Y - Y discrimination diagram for basalts where the ratio of Zr/Y = 3 separates continental arc basalts from oceanic arc basalts (after Pearce, 1983)

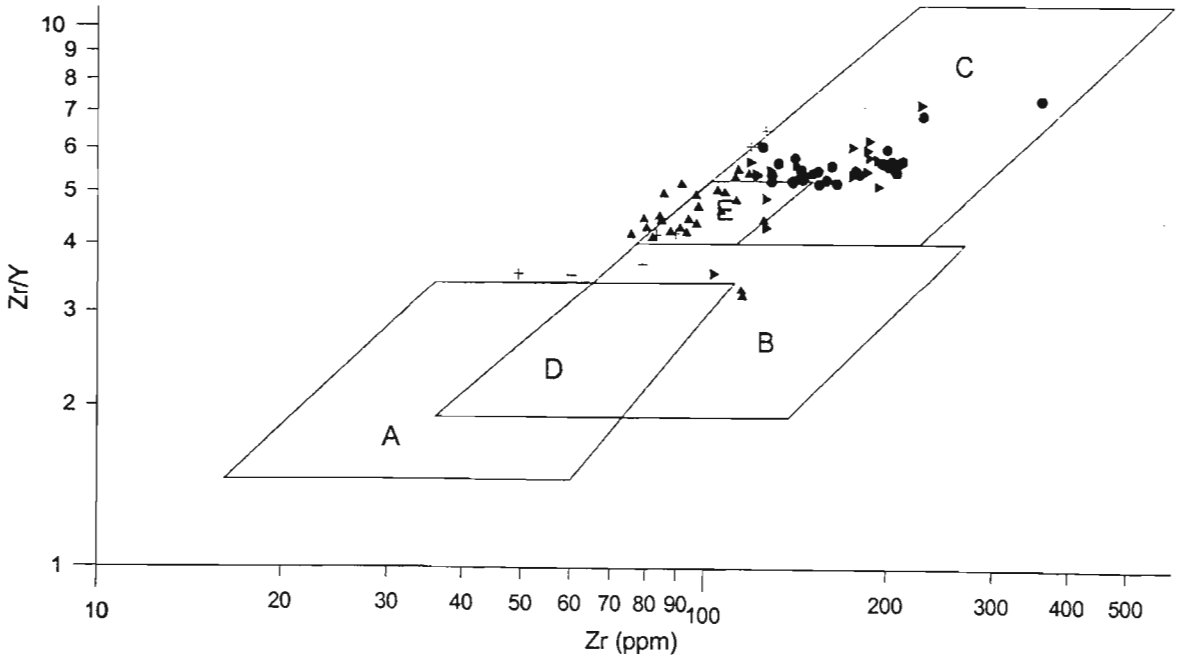

Figure 5.45 Zr/Y - Y discrimination diagram for basalts where A - volcanic - arc basalts B - MORB, C - within-plate basalts, D - MORB & volcanic -arc basalts, E - MORB & within - plate basalt (after Pearce and Norry, 1979)

The Wagondrift Formation basalts have higher Ti/Y ratios and as a result plot in the within-plate basalt field (Figure 5.47). All basalt data from Phase 1, Phase 2 and the White Mfolozi Inlier plots in the plate margin basalt field. Again it is clearly evident that the Wagondrift Formation basalts are distinctly different from the Bivane Subgroup data.

The incompatible elements Th, Yb and Ta can be used to identify tectonic setting, geochemical affinity and the nature of the mantle source (Pearce, 1983). The Wagondrift Formation basalts do not plot in any distinguished field but can be interpreted from the graph that they represent tholeiitic to calcalkaline magmas derived from a slightly depleted mantle source (Figure 5.48). These basalts plot closest to the oceanic island arc tectonic setting. Phase 1 and Phase 2 of the White River Section, as well as the Agatha Formation of the White Mfolozi Inlier plot within the calcalkaline active continental margin field and were derived from an enriched mantle source. The Nhlebela Formation is characterised on this diagram as a shoshonitic active continental margin from an enriched source. This may be a factor of fractionation, as the Nhlebela Formation samples are more evolved than the rest of the data considered. Pronounced differences are again evident between the Wagondrift Formation and the basalts of the Bivane Subgroup.

Wood (1980) used the incompatible elements Hf, Th and Ta to distinguish between different tectonic settings. This ternary diagram is suitable for all compositions from basalts to rhyolites and the all data has been used. The Wagondrift Formation plots as calcalkaline within-plate basalts, but trends towards and just into the tholeiitic within-plate field (Figure 5.49). All other data, which is representative of the Bivane Subgroup both in the White River Section and the White Mfolozi Inlier, plots as calcalkaline volcanic arc setting. The Bivane Subgroup and the Wagondrift Formation data are clearly related to different tectonic settings.

The immobile elements Zr, Nb, and Y are used to identify the tectonic setting of basalts (Meschede, 1986). The Wagondrift Formation plots in the within-plate tholeiite and volcanic-arc basalt field, although data trends into the N-type MORB – volcanic-arc basalt field (Figure 5.50). Phase 1 and the Agatha Formation basalts plot as within-plate tholeiites and volcanic-arc basalts. Phase 2 basalts also plot in the within-plate tholeiite and volcanic-arc basalts but like the Wagondrift Formation trends into the N-type MORB – volcanic-arc basalt field. The Nhlebela Formation plots as within-plate alkali basalts and within-plate tholeiites. This again may be a factor of the higher level of fractionation of these samples and would be reflected by elevated Nb and Zr values. The Wagondrift Formation does not plot differently from the Bivane Subgroup data on this diagram but this may be due to the fact that the diagram does not distinguish between within-plate basalts and volcanic-arc basalts, which is where the difference appears to lie.

It is clear that the Wagondrift Formation is distinctly different from the Phase 1, Phase 2, Nhlebela Formation and Agatha Formation data. The Wagondrift Formation has a within-plate basalt signature while the rest of the Nsuze Group data is characteristic of volcanic-arc environments. It is also apparent that the Phase 1 data from the north is tectonically similar to that in the Central Region of the White Mfolozi Inlier. As field evidence indicates us that the Bivane Subgroup is predominantly representative of a sub-aerial depositional environment, and certain tectonic discrimination diagrams have distinguished the data as continental arc, it can be interpreted that the Bivane Subgroup volcano-sedimentary succession was formed at an active continental margin. The Wagondrift Formation may represent an unrelated volcanic event prior to the formation of the subduction zone responsible for the Bivane Subgroup volcanism.

5.10 CONCLUSION

The volcanic rocks of the Nsuze Group range in composition from basalt to rhyolite, with a minor picritic basalt phase. The volcanic rocks show a transitional to calcalkaline affinity. Alteration and metamorphism of these rocks has caused the mobilisation of Na_2O but not K_2O. All other elements (except perhaps V and Sc) appear to be semi- to completely immobile allowing a considerably high degree of confidence in the geochemical data for 3Ga rocks. Overall trends are evident within the Major elements, although superimposed sub-trends are evident within each grouping of samples. These sub-trends formed as a result of fractionation processes involving specific key minerals i.e. plagioclase and

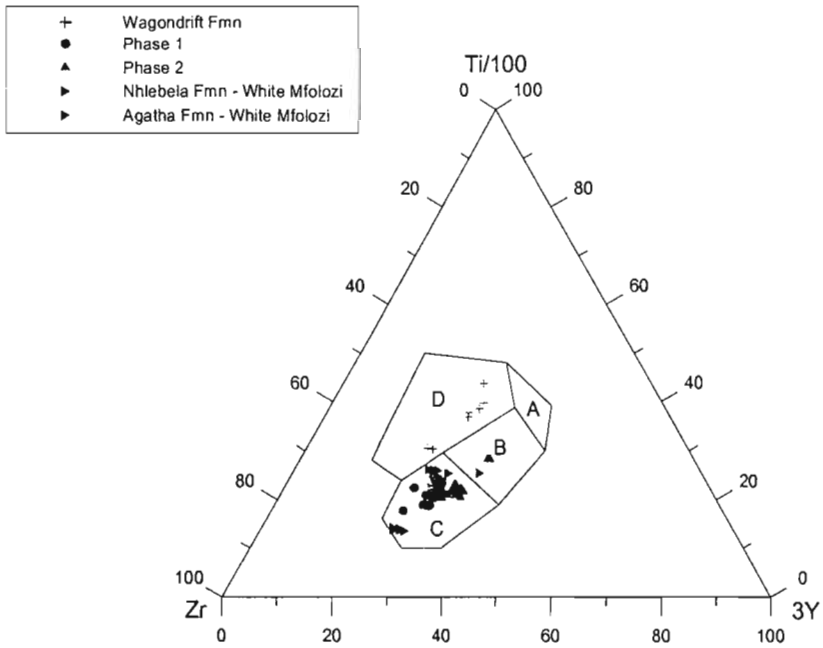

Figure 5.46 Ti-Zr-Y discrimination diagram for basalts where A - island - arc tholeiites B - MORB, island - arc tholeiites & calc-alkali basalts, C - calc-alkali basalts, D - within-plate basalts (after Pearce and Cann, 1973)

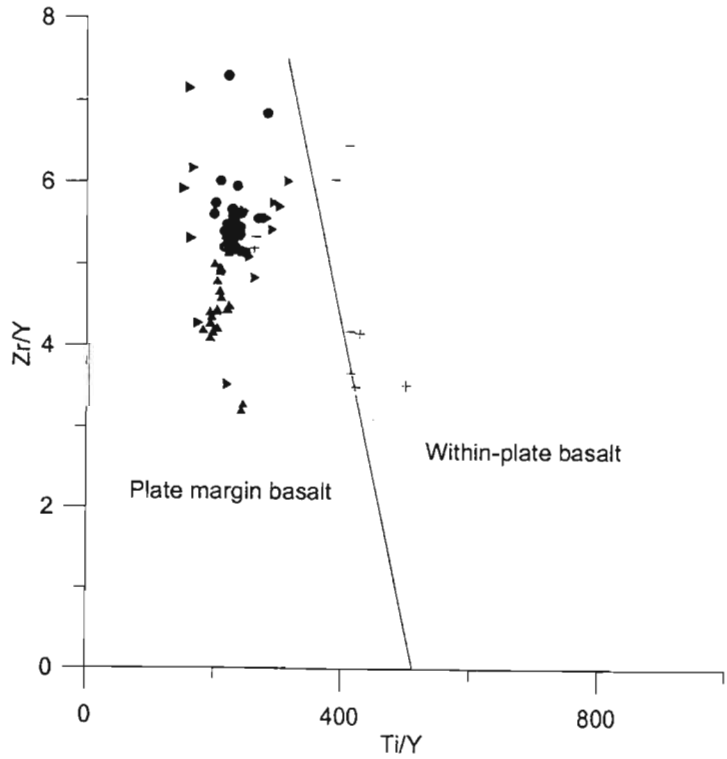

Figure 5.47 Zr/Y - Ti/Y discrimination diagram for basalts distinguishing between within - plate basalts and plate margin basalts (after Pearce and Gale, 1977)

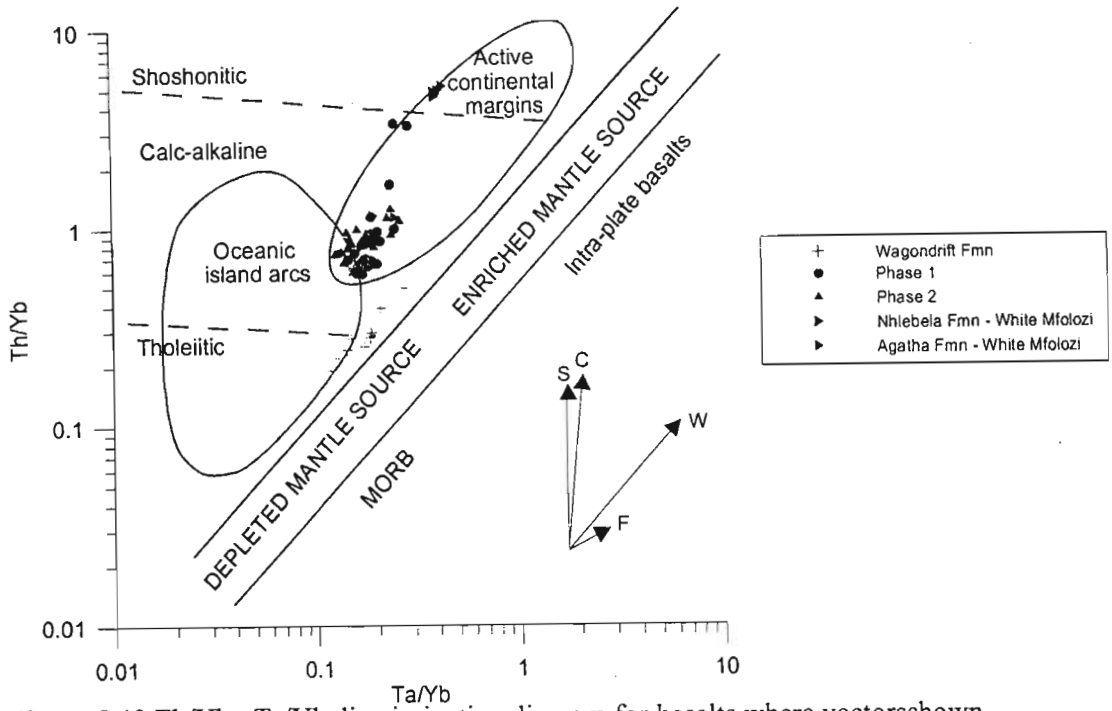

Figure 5.48 Th/Yb - Ta/Yb discrimination diagram for basalts where vectorsshown indicate the influence of S- subduction component, W - within - plate enrichment, C - crustal contamination, F - fractional crystallization (after Pearce, 1983)

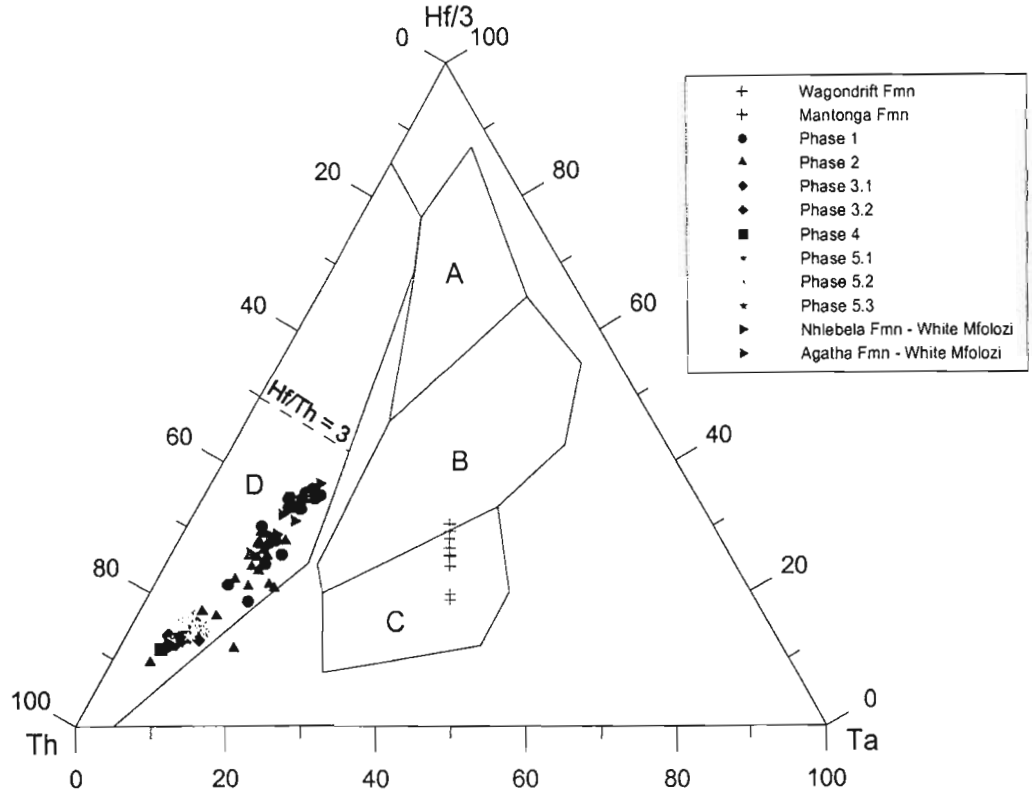

Figure 5.49 Th-Hf-Ta discrimination diagram for all compositions of volcanic rocks where A - N-type MORB, B - E-type MORB & within - plate tholeiites, C - alkaline within - plate basalts, D - volcanic - arc basalts if Hf/Th >3 tholeiitic or Hf/Th <3 calc-alkaline (after Wood, 1980)

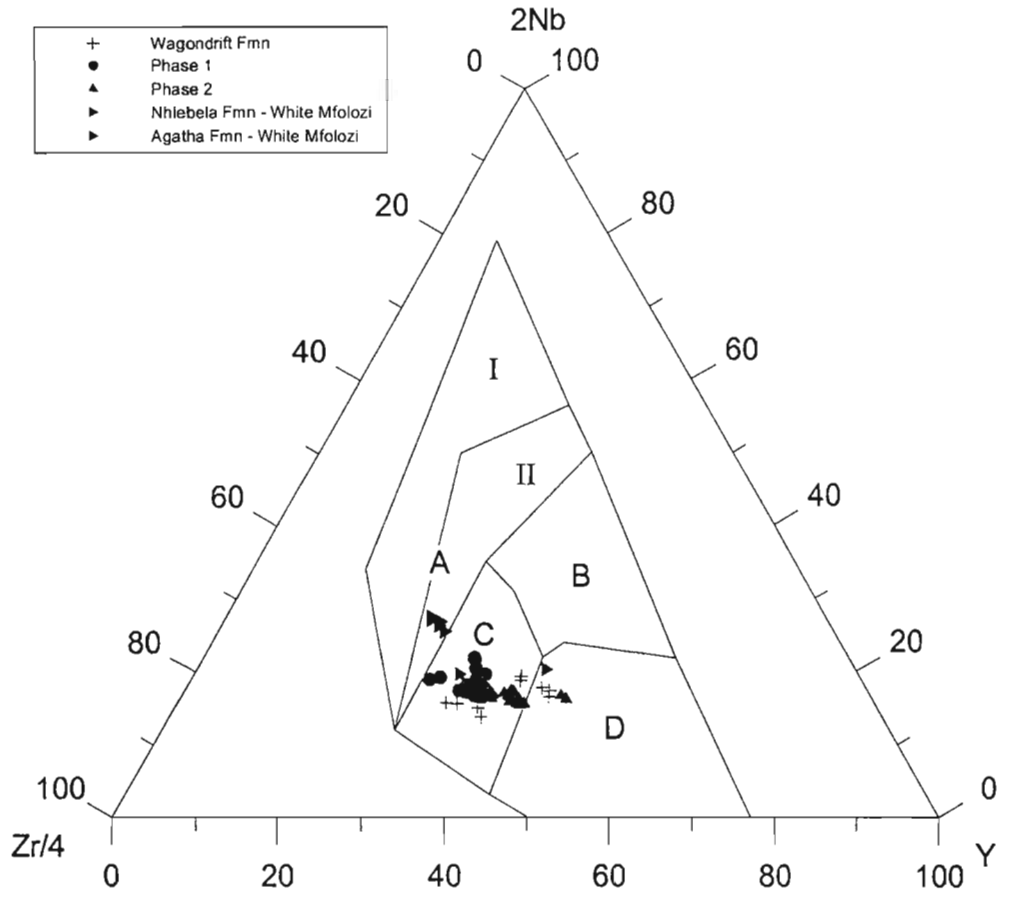

Figure 5.50 Zr-Nb-Y discrimination diagram for basalts where AI - within - plate alkali basalts, AII - within - plate alkali basalts & within - plate tholeiites, B - E-type MORB, C - within - plate tholeiites & volcanic - arc basalts, D - N-type MORB & volcanic - arc basalts (after Meschede, 1986)

pyroxene, which would allow considerable changes in bulk major element but not trace element concentrations. REE patterns show that the evolution of the Bivane Subgroup lavas was largely controlled by the fractionation of plagioclase. The phases of the Bivane Subgroup in the White River Section and the Nhlebela and Agatha Formations in the White Mfolozi Section do appear to be related. The Nhlebela Formation represents a more evolved magmatic suite than the younger Agatha Formation. The close correlation of the Nhlebela Formation samples suggests one source erupting sufficient lava to form a complex flow field. In contrast the Agatha Formation seems to have been formed by two or more vents, as two distinct sample groups can be determined by geochemical interpretation. The increasingly basic nature of the lavas with younging stratigraphy (from Nhlebela Formation to Agatha Formation and within the Agatha Formation itself) is not fully understood.

The Wagondrift Formation is geochemically distinct from the Bivane Subgroup data (Phases 1 to 5). It appears that the source of the Wagondrift Formation may have been more depleted than the source of the Bivane Subgroup. It is therefore contestable whether the Wagondrift Formation should be considered part of the Nsuze Group.

Based on Mg, Cr, Ni concentrations and REE patterns, Phase 2 represents the most primitive stage of Nsuze Group volcanism. Phase 5.2 is the only phase to have an ultramafic lava component identified.

The tectonic setting of the Wagondrift Formation is within-plate basalt from a depleted source. The tectonic setting of the Bivane Subgroup is an active continental margin tapping an enriched source. The Wagondrift Formation may signify an initial phase of volcanism prior to the formation of the subduction zone. The mantle source for the Wagondrift Formation may have been previously depleted by numerous eruptions that form the volcanic rocks of the greenstone belts of the basement. The formation of a subduction zone would have resulted in the enriched mantle from which large amounts of magma were produced.

CHAPTER 6
DISCUSSION

This study focuses on the volcanic rocks preserved as the Nsuze Group in northern KwaZulu Natal and southeastern Mpumalanga. These volcanic rocks form the Bivane Subgroup and were studied in the White River area in the Northern Region and the White Mfolozi Inlier of the Central Region. A minor volcanic event preserved as a wedge at the base of the Nsuze Group in the Northern Region, the Wagondrift Formation, is also included in the study. The volcanic sequence of the Bivane Subgroup in the Northern Region has been divided into five phases in this study, based on aspects of the physical volcanology and geochemistry.

The age of the Nsuze Group volcanic sequence has been reasonably constrained by recent isotopic dating. Griffin (2002) calculated an age for the basal Wagondrift Formation of 2980±10Ma (U-Pb zircon) and an age for a rhyolite in Phase 5 of the Bivane Subgroup of 2968±6Ma (U-Pb zircon). While the Phase 5 is the final volcanic phase of the Bivane Subgroup, it does not mark the end of volcanism in the Nsuze Group as the overlying Ozwana Subgroup is characterised by dominant sedimentary and subordinate volcanic processes. Phase 5 of the Bivane Subgroup does, however, signify the conclusion in the production of large volumes of effusive magma. The period of time over which the main episode of Nsuze Group volcanism is considered to have occurred is approximately 10-14Ma.

The Nsuze Group represents a complex history of melting, magma storage, fractionation and eruption, resulting in a vast sequence of transitional to calc-alkaline basalts, andesites and rhyolites. The rock record includes both lavas and pyroclastics in the northern region, but is primarily lavas in the central region. The volcanological history of the rocks in the Northern Region suggests that the initial phases of volcanism were predominantly basaltic and volatile-poor, and low effusion rates resulted in a laterally limited outcrop pattern. Clastic sediments, derived from the granite-gneiss basement, were deposited contemporaneously in a complex fluvial system. These fluvial sediments, known as the Mantonga Formation does contain of volcanic components, although minor in volume. The onset of the Bivane Subgroup represents a marked increase in volcanic activity, resulting in the end of sedimentary processes.

The Bivane Subgroup volcanic rocks of the Northern Region represent a maturing volcanic crater field, underlain by a fractionating complex system of magma chambers. The dominance of andesitic compositions, especially plagioclase porphyritic varieties, suggests high-level fractionation. Where surface vents became plugged by high-viscosity magma, further fractionation took place. The resultant volatile-rich acid magma exploded violently through the blocked eruption vents causing huge eruption columns. The resultant deposits are ash fall and flow deposits that are recorded throughout the Bivane Subgroup volcanic pile. A constant supply of magma resulted in the development of new vents and fissures, which constantly allowed for less fractionated magmas to erupt onto the surface. The development of chambers beneath these new vents meant that the cycle was repeated.

Geochemically, the White Mfolozi Inlier did not experience the same degree of fractionation, and therefore explosive volcanism did not develop. Basaltic to andesitic lavas quietly poured out of the eruptive vents. The development of multi-level magma chambers therefore did not occur.

Geochemically the White Mfolozi Inlier volcanic rocks and those for the White River Section are related. Both suites of rocks have transitional to calc-alkaline affinities, enriched LREE relative to HREE and Ta-Nb depletion. The inferred geochemical tectonic environment is an arc setting. Based on the subaerial nature of the physical volcanology and dominance of andesitic compositions, it is suggested that the tectonic setting of the Nsuze Group was a continental arc. For this conclusion to be valid, it must be ascertained whether plate tectonic processes, in particular subduction, were operational at 2.9Ga. Numerous arguments have been made for and against the presence of plate tectonics during the Archaean. These debates centre on the nature of the Archaean oceanic crust and the thermal regime of the mantle at that time.

Sun (1984) stated that some Archaean basalts are characterised by LREE enrichment and depletion of Ta, Nb and the HREE. This suggests a mantle enrichment process related to eclogitic melting. Eclogite is generally formed by metasomatism of basalt through subduction processes. Green (1981), however, was of the opinion that oceanic crust subduction could not have taken place in the Archaean due to the lack of gabbro to eclogite transformation. Sleep and Windley (1982) argued, however, that the Archaean oceanic crust was far thicker than modern oceanic crust and therefore subduction could well have taken place.

Lowe (1994) interpreted Archaean tectonics as involving thickened oceanic crust, which is underplated along a convergent plate boundary rather than typically subducted. This would have prevented the recycling of oceanic crust back into the mantle but would have still allowed for a subduction zone component to be added to the source of the melt. Arndt (1993) was of the opinion that Archaean oceanic crust was predominantly komatiitic with minor basaltic components. The higher Archaean temperatures would have resulted in pressure release melting starting deeper in the mantle resulting in thicker oceanic crust.

Although elements such as LREE enrichment and Nb-Ta relative depletion resemble those indicative of a subduction zone component, Archaean volcanic rocks most often do not exhibit an over abundance of Sr, which is also a known subduction zone component (Sun, 1984). This is the case for the Nsuze Group volcanic suite, which is relatively depleted in Sr (Figure 5.35 to 5.43). An opposing view offered by Fyfe (1978) is that extensive underplating of the continental crust takes place by komatiitic magmas due to their density differences. The underplated komatiitic material would be eclogitised and therefore would detach and sink back into the mantle. Melts produced from this material would have a subduction zone component due to the influence of the eclogite. It is however speculative whether metasomatic enrichment processes can occur under the subcontinental crust without the influence of true subduction (Sun, 1984).

Bickle *et al.* (1994) have stated that the higher density of komatiite compared to basalt would have resulted in sinking and remelting of all Archaean oceanic crust, which would explain the lack of Archaean crust preserved in the rock record. As the earth cooled degrees of partial melting would have decreased giving rise to more prominent basalts at mid-ocean ridges (Condie, 1980). Baer (1977) suggested that deep subduction could not have occurred prior to 1000Ma because eclogite was not stable in the oceanic crust until then. A deep sinking component like eclogite must initiate subduction and a raised geothermal gradient would have prevented eclogite from forming. McCall (1981) stated that calc-alkaline volcanic suites of the Archaean mark the areas of downgoing convection in narrow convection cells and recycling of basalt through the mantle. According to McCulloch (1993) as the earth cooled, the oceanic lithosphere following a normal cooling process would have become negatively buoyant and suitable for subduction when the mantle was only 50°C hotter than at present – a scenario that only occurred 1.4 to 0.9Ga ago and only then could modern day plate tectonics have developed.

Giles (1981) has suggested that calc-alkaline magmatism that was unlikely to be caused by subduction of an oceanic plate. Based on the work of Green (1973), Giles (1981) has explained that melting in the upper mantle could have been induced by introduction of localised water from a zone of incipient melting at greater depths. For this to occur, the input of water and resultant depression of the mantle solidus must be sufficient and faults and other zones of weakness must have played a role in the transportation of the water-rich component from the zone of incipient melting to higher levels. A high geothermal gradient, like that which existed in the Archaean, is required for this zone of incipient melting to develop. This model which Giles (1981) related to the Eastern Goldfields Province in Western Australia, is however based on the fact that the calc-alkaline lithologies are localised and sporadic, and involve relatively small volumes of magma. This is in contrast to the Nsuze Group, which involves a large geographic area of a substantial thickness of transitional to calc-alkaline volcanic rocks.

The Superior Province has been interpreted using plate tectonic processes (Card, 1990; Williams *et al.*, 1992). There is, however, controversy in terms of tectonic setting with regards the two aspects of the Superior Province that correlate

most closely to the Nsuze Group – late unconformable basins and continental-style volcanism. The Nsuze Group appears to consist of elements of both of these assemblages. Those aspects of the late unconformable basins described by Thurston (1994) that apply to the Nsuze Group are alluvial-fluvial sedimentary environments and calc-alkaline volcanism. These assemblages also unconformably overly older greenstone belts, as seen with the Nsuze Group which unconformably overlies the Nondweni Greenstone Belt and is associated with the Commondale Greenstone Belt (Hunter and Wilson, 1988). Thurston (1994) suggested that the orderly sequence of depositional facies represents the more or less preserved extent of the basin. Such is the case with the Nsuze Group. The late unconformable basins are thought to have developed after early deformation of the greenstone belts, unroofing of the undeformed granitic rocks and before late deformation involving shear zones (Thurston, 1994). The shear zones discussed by Gold (1993) and Matthews (1990) are considered to be post-Nsuze Group in age but pre- or syn-Mozaan sedimentary deposition. The geochemical signature of late unconformable basins is calc-alkaline to shoshonitic, enriched in LIL elements and depleted in Ti, Ta and Nb, much like the Nsuze Group volcanic rocks. A variety of tectonic settings are, however, proposed including a mature arc, pull-apart basin, piggy-back basin and a late rift-related flysch basin.

The Continental Style volcanism described by Thurston (1994) simply involves a subaerial assemblage of andesite to rhyolite volcanic rocks with related sedimentary units. Geochemical data suggests a magmatic arc setting (Hallberg *et al.*, 1976). Again controversy surrounds the origin of these continental style assemblages. Interpretations include a subaerial equivalent of the late unconformable basins and rift-related volcanism. If the Nsuze Group is to be compared on this basis it may represent a combination of continental style volcanism in the northern and central regions and a late unconformable basin in the southern region.

Condie (1994) stated that Proterozoic greenstone belts have small proportions of basalt, little to no komatiitic material and 20-50% intermediate to acid material and are therefore analogous with continental-margin arc systems. Condie (1994) used Th/Ta vs La/Yb to distinguish between different generations of greenstone belts and modern day analogies. These elements have been used for tectonic discrimination in Chapter 5 and consistently indicate the presence of a subduction zone component. Condie (1994) has related Proterozoic greenstone belts to modern continental-arc zones using these ratios. Although the Nsuze Group is clearly Archaean, the early maturity of the Kaapvaal Craton may have allowed for more "Proterozoic type" environments to form far earlier than those sequences related to other less developed cratons e.g. Zimbabwe.

Hamilton (1993) discussed how features such as accretionary wedges, fore-arc, and back-arc basins and magmatic wedges did exist in the Proterozoic although they are manifested in different ways to their modern equivalents. Hamilton (1998) stated that these features of modern continental arc settings have no analogues in Archaean terranes and only resemble Phanerozoic convergent-plate systems when seen in isolation from their spatial association and structure. The Nsuze Group, while being Archaean in age, has already proven itself to show greater similarity to early Proterozoic sequences than Archaean greenstone belts. Therefore according to Hamilton (1993, 1998) Archaean plate tectonics did not exist, although Proterozoic sequences may resemble Phanerozoic and modern-day equivalents although the processes of formation were different.

Foley *et al.* (2003) discussed thicker oceanic crust in the Archaean, due to higher heat flow and therefore higher degrees of partial melting at the mid-ocean ridges, was most likely Mg-rich picrite. The oceanic crust was divided into basalt, gabbro, ultramafic cumulates and picrites similar to modern day oceanic crust sections. Foley *et al.* (2003) clearly stated that it is unclear as to what effect the different oceanic crust type would have on subduction and crustal recycling processes. It is considered, through experimental data, that due to the thick nature of the oceanic crust in the Early Archaean, it could not be subducted as a coherent unit. This resulted in the lower ultramafic cumulates and picrites decoupling from the upper basaltic layer and subducting beneath the continental crust. Subsequent metamorphism of the ultramafic cumulates and picrites produced pyroxenites, which is inferred to delaminate and melt to

produce basaltic compositions. This is in opposition to the consideration that the melt should produce continental crust or tonalite-trondhjemite-granodiorite (TTG) rocks. Foley *et al.* (2003) suggested that the creation of continental crust (TTG) requires the subduction and melting of garnet-amphibolite which is thought to have first developed in the late Archaean (Foley *et al.*, 1998, defined the late Archaean as >3.3Ga). Garnet-amphibolite is thought to only form by metamorphism of the upper oceanic crust i.e. full subduction of the oceanic plate.

Dating of eclogitic diamonds from various kimberlite occurrences in the Kimberly region by Richardson *et al.* (2001) have produced an age of 2.9Ga. The Os-Re ages produced from sulphide inclusions within these eclogitic diamonds provide evidence for basalt to eclogite transformation at 2.9Ga. This supports the development of eclogite in the subcontinental mantle lithosphere of the Kaapvaal Craton at the time of Nsuze melting and eruption.

According to parameters established by Kamber *et al.* (2002), the Nsuze Group suite may be dominated by adakitic magmas. Adakitic magmas are those derived directly from the melting of a subducted slab without influence from the depleted mantle wedge. Characteristics of adakitic melts include compositional ranges from andesites to dacites, strongly fractionated REE patterns, with HREE being heavily depleted relative to LREE. The source is considered to a garnet amphibolite or eclogite facies MORB (Kamber *et al.*, 2002). Adakitic melts may be affected by a number of processes that may alter the primary composition of the melting subducted slab. These processes include contamination of the melt by peridotites located in the mantle wedge, contamination by the melting of the thin accumulation of oceanic sediment on top of the slab, and contamination by the continental crust through which the melt must pass to reach the surface (Kamber *et al.*, 2002). Kamber *et al.* (2002) stated that higher Nb/Ta and lower Pd/Nd ratios are present in melts derived directly from the subducting slab, than in those from the wedge-derived arc magmas and continental crust. The Nb/Ta and Pb/Nd ratios quoted by Kamber *et al.* (2002) for adakitic melts are median ratios from existing literature concerning both continental arc and island arc adakitic magmas. Kamber *et al.* (2002) considered Nb/Ta $\geq$1.6 to be a high ratio and Pb/Nd $\leq$0.4 to be a low ratio indicative of adakitic magmas. 40.6% of the Nsuze Group data fulfils both of these criteria. Of the individual phases, however, only the medians of the Wagondrift Formation (median Nb/Ta = 19.3, median Pb/Nd = 0.19), Phase 1 (median Nb/Ta = 18.8, median Pb/Nd = 0. 34), Phase 5 (median Nb/Ta = 16.7, median Pb/Nd = 0.37) and the Agatha Formation of the White Mfolozi Formation (median Nb/Ta = 19.2, median Pb/Nd = 0.19) are adakitic in character. While this does not prove or disprove that the Nsuze Group volcanic rocks are adakitic, it suggests that the influence of the mantle wedge was limited. It may therefore be deduced that due to the adakitic component present through the time of Nsuze Group volcanism, the angle of subduction was shallow and the mantle wedge was therefore relatively narrow. Limited contamination would have resulted through the influence of the mantle wedge and contamination due to the crustal rocks may have been more predominant.

In terms of a modern continental margin, subduction principles as illustrated by the west coast of South America, two end member types of subduction may take place (Condie, 1989). A low-stress type, which involves deep subduction of the oceanic plate, and a high-stress type, which is characterised by, shallow subduction of the oceanic plate. It has already been discussed that deep subduction was most likely not possible in the Archaean due to the nature of the oceanic crust and high mantle geotherms. Modification of the high-stress type of continental margin subduction may be a feasible scenario as an origin for the Nsuze Group. Characteristics of a high-stress type subduction zone is a large accretionary prism, pronounced bulge of the descending slab, shallow dip of the relatively young descending plate and a wide range in compositions of calc-alkaline and tholeiitic volcanic rocks. There is a strong coupling of the overlying and descending plate, which results in accretionary growth. This stronger coupling is also responsible for the very shallow angle of subduction. Back-arc spreading is not common in high-stress type subduction zones due to the overriding plate retreating from the descending plate very slowly and therefore not allowing the development of extension stress or the overriding plate actually converges with the descending plate. The development of these high-stress subduction zones therefore relies on the relative

motions of the two plates and the age and temperature of the descending plate.

The Nsuze Group fits this model in terms of the compositional range of the volcanic rocks. A combination of an underplating and high-stress type subducting model would result in ultramafic to mafic compositions beneath the continental crust resulting in the formation of eclogite. This would then result in a subduction zone component being assimilated with the melt from the mantle when partial melting occurred.

The lack of large-scale sediments in the Nsuze Group, especially in the northern region would support the assumption that retro-arc spreading did not occur. (Whether the Mozaan Group represents a foreland basin is beyond the scope of this project, although the contemporaneous Witwatersrand Supergroup is considered to have been formed in a foreland basin (Catuneanu and Biddulph, 2001). It is speculated that a possible subducting front was likely to have been situated to the south - southeast of the present eastern margin of the Kaapvaal Craton. The southern region may therefore represent the equivalent of an accretionary prism. This is supported by the presence of deformation formed by thrusting that is considered to be pre-Ntingwe Group and therefore pre-Natal Mobile belt (Matthews, 1959 and Matthews, 1990). The Central Region may therefore represent a weakly developed fore-arc basin due to the presence of littoral sediments, combined with the influence of the volcanic front. The main body of the Nsuze Group i.e. the northern region may then reflect the remnants of the continental arc itself. If modern-type subduction did not occur, the Nsuze Group volcanic rocks may be best explained by the assemblages of eclogitic material under the continental lithosphere either by underplating or low-angle subduction-like processes.

CHAPTER 7
CONCLUSIONS

The Nsuze Group is a 2.9Ga volcano-sedimentary sequence that outcrops in southeastern Mpumalanga, northern KwaZulu-Natal and Swaziland. The areas of focus in this study were the White River Section in the Northern Region and the White Mfolozi Inlier in the Central Region. The conclusions of this study are as follows:

- The Nsuze Group consists of basalt, basaltic andesite, andesite, dacite and rhyolite lavas and pyroclastic rocks.
- The oldest Nsuze Group volcanism is represented by the basaltic to basaltic andesite lavas of the Wagondrift Formation in the White River Section.
- The Bivane Subgroup represents the main volcanism of the Nsuze Group. The Bivane Subgroup is divided into five phases of eruption based on physical volcanology and stratigraphy.
- Phase 1 comprises basaltic andesites and andesites. A prominent phase of porphyritic andesite volcanism, an aqueous phase resulting in pillow lava structures, as well as a pyroclastic flow deposit are preserved. The volcanic rocks are predominantly lavas although minor tuffaceous deposits are present.
- Phase 2 comprises andesites to rhyolites. Features include pyroclastic flow deposits, highly vesicular lavas with pahoehoe flow surfaces, air-fall tuffs and spheroidal structures formed as a result of non-mixing of felsic and mafic components.
- Basaltic andesites to rhyolites were formed by the Phase 3 volcanic event. Pyroclastic flow deposits, including pyroclastic breccias, as well as highly vesicular lavas characterise this stage.
- Phase 4 represents a rhyolitic lava dome and therefore signifies a proximal volcanic source.
- Phase 5 is dominated by andesites and rhyolites. The andesites form massive and vesicular lava flows as well as tuff deposits. The rhyolites were formed by pyroclastic flows and exhibit extensive flow banding.
- The Bivane Subgroup rocks represent a complex volcanic history of magma storage, fractionation and eruption, leading to the development of a maturing volcanic crater field, supplied by a multi-level system of magma chambers.
- The White Mfolozi Inlier comprises the lower Nhlebela Formation and the upper Agatha Formation.
- A lower hydroclastic lava type and an upper amygdaloidal lava type form the basaltic to andesitic Nhlebela Formation. The hydroclastic lava type was formed by the interaction of the lava with a fluvial system and waterlogged sediments. The Nhlebela Formation represents the steady and non-violent eruption of lava from one volcanic centre.
- The Agatha Formation comprises lavas of basaltic to basaltic andesitic composition. Features of the lava flows include hydroclastic breccias, aa lava and well preserved ropey pahoehoe surface textures. Localised pillow lava structures are also present in the upper Agatha Formation. The Agatha Formation represents eruption from multiple eruptive centres at initially high effusion rates, later decreasing to allow for the development of compound pahoehoe lava flows over a shallow gradient.
- The basaltic to andesitic rocks of the Nsuze Group have been metamorphosed to greenschist facies. The low-grade metamorphic mineral assemblage includes chlorite, epidote, actinolite, quartz, albite (sericite) as well as minor calcite, biotite, K-feldspar and sphene. The development of the metamorphic assemblage is due to burial metamorphism under high heat flow conditions.
- Geochemically most elements exhibit well-defined fractionation trends, as well as sub-trends within each phase group of samples. These sub-trends are formed as a result of fractionation of specific key minerals e.g. plagioclase.
- REE patterns show that the evolution of the Bivane Subgroup was largely controlled by the fractionation of plagioclase. REE patterns are enriched in LREE relative to HREE.
- The Wagondrift Formation is geochemically distinct from basaltic samples from the Bivane Subgroup and the White Mfolozi

Inlier. The Wagondrift Formation was generated from a more depleted source than the younger volcanic rocks of the Bivane Subgroup and has a within-plate tectonic signature.

- The volcanic rocks of the White River Section and the White Mfolozi Inlier are geochemically similar.
- The volcanic rocks of Phase 2 of the Bivane Subgroup have the most primitive compositions, based on Mg, Cr and Ni concentrations.
- The volcanic rocks of the Bivane Subgroup, of both the White River Section and White Mfolozi Inlier, have a subduction zone geochemical signature (Ta-Nb depletion). Tectonic discrimination diagrams suggest a continental-arc subduction setting.
- It is clear that the melting of eclogitic material provided the main source of melt for the Nsuze Group volcanic field. The formation of eclogite requires the metamorphism of basaltic material, and in the mantle this involves some form of subduction process. It is debatable whether modern-day subduction occurred in the Archaean. Archaean models of subduction-like processes include underplating of the sub-continental lithosphere and low-angle subduction, which minimises the effect of the mantle wedge.

REFERENCES

Armstrong, N.V. (1980). *Geology and geochemistry of the Nsuze Group in northern Natal and southeastern Transvaal.* Ph.D. thesis (Unpubl.), Univ. Natal, Pietermaritzburg, 386p.

Armstrong, N.V., Hunter, D.R. and Wilson, A.H. (1982). Stratigraphy and petrology of the Archaean Nsuze Group, northern Natal and southeastern Transvaal, South Africa. *Precam. Res.*, **19**, 75-107.

Armstrong, N.V., Wilson, A.H. and Hunter, D.R. (1986). The Nsuze Group, Pongola Sequence, South Africa: geochemical evidence for Archaean volcanism in a continental setting. *Precam. Res.*, **34**, 175-203.

Arndt, N.T. (1983). Role of a thin, komatiite-rich oceanic crust in the Archean plate-tectonic process. *Geology*, **11**, 372-375.

Aubele, J.C., Crumpler, L.S. and Elston, W.E. (1988). Vesicle zonation and vertical structure of basalt flows. *J. Volcanol. Geotherm. Res.*, **35**, 349-374.

Barrett, T.J. and MacLean, W.H. (1997). Volcanic sequences, lithogeochemistry and hydrothermal alteration in some bimodal VMS systems. *In*: Barrie, C.T. and Hannington, M.D. (eds.), *Volcanic-associated massive sulphide deposits: processes and examples in modern and ancient settings*. Geol. Assoc. Can. Short Course Notes, Carleton University, Ottawa, 105-133.

Barton, J.M., Hunter, D.R., Jackson, M.P.A. and Wilson, A.C. (1983). Geochronologic and Sr-isotopic studies of certain units in the Barberton granite-greenstone terrain, Swaziland. *Trans. Geol. Soc. S. Afr.*, **86**, 71-80.

Batiza, R. and White, J.D.L. (2000). Submarine lava and hyaloclastite. *In*: Sigurdsson, H. (ed.), *Encyclopaedia of Volcanoes*. Academic Press, San Diego, 361-381.

Baer, A.J. (1977). Speculations on the evolution of the lithosphere. *Precam. Res.*, **5**, 249-260.

Beukes, N.J. and Cairncross, B. (1991). A lithostratigraphic – sedimentological reference profile for the late Archaean Mozaan Group, Pongola Sequence: application to sequence stratigraphy and correlation with the Witwatersrand Supergroup. *S. Afr. J. Geol.*, **94**, 44-69.

Beukes, N.J. and Lowe, D.R. (1989). Environmental control on diverse stromatilites morphologies in the 3000Myr Pongola Supergroup, South Africa. *Sedimentology*, **36**, 383-397.

Bickle, M.J., Nisbet, E.G. and Martin, A. (1994). Archaean greenstone belts are not oceanic crust. *J. Geol.*, **102**, 121-138.

Boynton, W.V. (1984). Cosmochemistry of the rare earth elements: meteorite studies. *In*: Henderson, P. (ed.), *Rare earth element geochemistry*. Elsevier, Amsterdam, 63-114.

Brenan, J.M., Shaw, H.F., Phinney, D.L. and Ryerson, F.J. (1994). Rutile-aqueous fluid partitioning of Nb, Ta, Hf, Zr, U and Th: implications for high field strength element depletions in island-arc basalts. *Earth Planet. Sci. Lett.*, **128**, 327-339.

Brewer, T.S. and Atkin, B.P. (1989). Elemental Mobilities produced by low-grade metamorphic events. A case study from the Proterozoic supercrustals of southern Norway. *Precam. Res.*, **45**, 143-158.

Burger, A.J. and Coertze, F.J. (1973). Radiometric age measurements on rocks from southern Africa to the end of 1971. *Bull. Geol. Surv. Afr.*, **58**, 46p.

Burke, K, Kidd, W.S.F. and Kusky, T.M. (1985). The Pongola structure of the southeastern Africa: The World's oldest preserved rift? *J. Geodynamics*, **2**, 35-49.

Cann, J.R. (1969). Spilites from the Carlsberg Ridge, Indian Ocean. *J. Petrol.*, **10**, 1-19.

Cann, J.R. (1970). Rb, Sr, Y, Zr, Nb in some oceanic floor basaltic rocks. *Earth Planet. Sci. Lett.*, **10**, 7-11.

Card, K.D. (1990). A review of the Superior Province of the Canadian Shield, a product of Archean accretion. *Precam. Res.*, **48**, 99-156.

Carlson, R.W., Hunter, D.R, and Barker, F. (1983). Sm-Nd age and isotopic systematics of the Bimodal Suite, Ancient Gneiss Complex, Swaziland. *Nature*, **305**, 701-704.

Carr, P.F. and Jones, B.G. (2001). The influence of palaeoenvironment and lava flux on the emplacement of submarine, near-shore Late Permian basalt lavas, Sydney Basin (Australia). *J. Volcanol. Geotherm. Res.*, **112**, 247-266.

Cas, R.A.F. and Wright, J.V. (1987). *Volcanic Successions: Modern and Ancient.* Allen and Unwin, London, 528p.

Cashman, K.V. and Kauahikaua, J.P. (1997). Reevaluation of vesicle distributions in basaltic flows. *Geology*, **25:5**, 419-422.

Catuneanu, O. and Biddulph, M.N. (2001). Sequence stratigraphy of the Vaal Reef facies associations in the Witwatersrand foredeep, South Africa. *Sediment. Geol.*, **141**, 113-130.

Cole, E.G. (1994). *Lithostratigraphy and depositional environment of the Archaean Nsuze Group, Pongola Supergroup.* M.Sc. thesis (Unpubl.), Rand Afrikaans University, Johannesburg, 166p.

Condie, K.C. (1980). Origin and early development of the earth's crust. *Precam. Res.*, **11**, 183-197.

Condie, K.C. (1989). *Plate Tectonics and Crustal Evolution, 3rd ed.* Pergamon Press, Oxford, 476p.

Condie, K.C. (1994). Greenstones through time. *In*: Condie K.C. (ed.), *Archean Crustal Evolution*. Elsevier, Amsterdam, 85-120.

Condie, K.C., Viljoen, M.J. and Kable, E.T.D. (1977). Effects of alteration on element distributions in Archaean tholeiites from the Barberton Greenstone Belt, South Africa. *Contrib. Mineral. Petrol.*, **64**, 75-89.

Crow, C., Condie, K.C., Hunter, D.R. and Wilson, A.H. (1989). Geochemistry of volcanic rocks from the Nsuze Group, South Africa: arc-like volcanics in a 3.0Ga intracratonic rift. *J. Afr. Earth Sci.*, **9**, 589-597.

Cullers, R.L. and Graf, J.L. (1984). Rare earth elements in igneous rocks of the continental crust: predominantly basic and ultrabasic rocks. *In*: Henderson, P. (ed.). *Rare earth element geochemistry*. Elsevier, Amsterdam, 237-274.

Deer, W.A., Howie, R.A. and Zussman, J. (1992). *The rock-forming minerals, 2nd ed.* Pearson Education Limited, Essex, 696p.

Du Toit, A.L. (1931). The geology of the country surrounding Nkandla, Natal. *Explanation sheet 109*, Geol. Surv. S. Afr., 111p.

Evensen, N.M., Hamilton, P.J. and O'Nions, R.K. (1978). Rare earth element abundances on chondritic meteorites. *Geochim. Cosmochim. Acta*, **42**, 1199-1212.

Fisher, R.V. and Schmincke, H.-U. (1984). *Pyroclastic Rocks*. Springer-Verlag, Heidelberg, 472p.

Floyd, P.A. and Winchester, J.A. (1978). Identification and discrimination of altered and metamorphosed volcanic rocks using immobile elements. *Chem. Geol.*, **21**, 291-306.

Foley, S.F., Buhre, S. and Jacob, D.E. (2003). Evolution of the Archaean crust by delamination and shallow subduction. *Nature*, **421**, 249-252.

Francis, P. (1993). *Volcanoes – A planetary perspective*. Oxford University Press, Oxford, 443p.

Freundt, A., Wilson, C.J.N. and Carey, S.N. (2000). Ignimbrites and black-and-ash flow deposits. *In*: Sigurdsson, H. (ed.), *Encyclopaedia of Volcanoes*. Academic Press, San Diego, 581-599.

Fyfe, W.S. (1978). The evolution of the Earth's crust: modern plate tectonics to ancient hot spot tectonics? *Chem. Geol.*, **23**, 89-114.

Giles, C.W. (1981) Archaean calc-alkaline volcanism in Eastern Goldfields Province, Western Australia. *In*: Glover, J.E. and Groves, D.I. (eds.), *Archaean Geology, 2nd Int. Sym., Spec. Pub. 7*. Geol. Soc. Aus., Perth, 275-286.

Gold, D.J.C. (1993). *The geological evolution of a part of the Pongola basin, southeastern Kaapvaal Craton*. Ph.D. thesis (Unpubl.), Univ. Natal, Pietermaritzburg, 168p.

Gold, D.J.C. and von Veh, M.W. (1995). Tectonic evolution of the late Archaean Pongola – Mozaan basin, South Africa. *J. Afr. Earth Sci.*, **21**, 203-212.

Grandstaff, D.E., Edelman, M.J., Foster, R.W., Zbinden, E. and Kimberley, M.M. (1986). Chemistry and mineralogy of Precambrian palaeosols at the base of the Dominion and Pongola Groups (Transvaal, South Africa). *Precam. Res.*, **32**, 97-131.

Green, D.H. (1973). Experimental melting studies on a model of upper mantel composition at high pressure under water-saturated and water-undersaturated conditions. *Earth Plant. Sci. Lett.*, **19**, 37-53.

Green, D.H. (1981). Petrogenesis of Archaean ultramafic magmas and implications for Archaean tectonics. *In*: Kroner, A. (ed.), *Precambrian Plate Tectonics*. Elsevier, Amsterdam, 469-489.

Gregg, T.K.P. and Fink, J.H. (1995). Quantification of submarine lava-flow morphology through analog experiments. *Geology*, **23:1**, 73-76.

Griffin, K.R. (2002). *Magmatic and tectonic development of the Pongola Supergroup and post-Pongola Granitoids, Kaapvaal Craton, South Africa*. M.Sc. thesis (Unpubl.), Univ. Michigan. 58p.

Groenewald, P.B. (1984). *The lithostratigraphy and petrogenesis of the Nsuze Group, northwest of Nkandla, Natal*. M.Sc. thesis (Unpubl.), Univ. Natal, Pietermaritzburg, 333p.

Gunn, B.M. (1976). A comparison of modern and Archaean oceanic crust and island-arc petrochemistry. *In*: Windley, B.F. (ed.), *The early history of the earth*. John Wiley and Sons, London, 389-403.

Hall, A. (1987) *Igneous Petrology*. Longman Scientific and Technical, Essex, 573p.

Hallberg, J.A., Carter, D.N. and West, K.N. (1976). Archaean volcanism and sedimentation near Meekatharra, Western Australia. *Precam. Res.*, **3**, 577-595.

Hamilton, W.B. (1993). Evolution of the Archaean mantle and crust. *In*: Reed, J.C. Jr., Bickford, M.E., Houston, R.S., Link, P.K., Rankin, D.W., Sims, P.K., and Van Schmus, W.R., (eds.), *Precambrian: Conterminous*. Geol. Soc. Am, The Geology of North America, **C2**, 597-614.

Hamilton, W.B. (1998). Archean magmatism and deformation were not products of plate tectonics. *Precam. Res.*, **91**, 143-179.

Hammerbeck, E.C.I. (1977). *The Usushwana Complex in the southeastern Transvaal, with special reference to its mineral potential*. D.Sc. (Unpubl.), Univ. Pretoria, Pretoria, 226p.

Hammerbeck, E.C.I. (1982). The Usushwana Complex in the southeastern Transvaal with special reference to its economic potential. *Mem. Geol. Surv. S. Afr.*, **70**,119p.

Hatch, F.H. (1910). *Report on the mines and minerals of Natal*. Clay, London, 155p.

Hatfield, R.A. (1990). *The geology and structure of the Pongola Sequence east of Piet Retief, southeastern Transvaal.* M.Sc. thesis (Unpubl.), Univ. Natal, Pietermaritzburg, 109p.

Hegner, E., Kröner, A. and Hoffman, A.W. (1984). Age and isotope geochemistry of the Archaean Pongola and Usushwana suites in Swaziland, southern Africa: a case for crustal contamination of the mantle-derived magma. *Earth Planet. Sci. Lett.*, **70**, 267-279.

Hegner, E., Kröner, A. and Hunt, P. (1994). A precise U-Pb zircon age for the Archaean Pongola Supergroup volcanics in Swaziland. *J. Afr. Earth Sci.*, **18**, 339-341.

Humphrey, W.A. (1912). The geology of a portion of northern Natal between Vryheid and the Pongola River. *Ann. Rep. Geol. Surv. Union of South Africa*, 19-23.

Humphris, S.E. and Thompson, G. (1978). Trace element mobility during hydrothermal alteration of oceanic basalts. *Geochim. Cosmochim. Acta*, **42**, 127-136.

Hunter, D.R. (1961). The geology of Swaziland. *Explanation of the 1:125000 geological map.* Geol. Surv. Mines Dept. Swaziland, 104p.

Hunter, D.R. (1974). Crustal development in the Kaapvaal Craton, I. The Proterozoic. *Precam. Res.*, **1**, 295-326.

Hunter, D.R. and Wilson, A.H. (1988). A continuous record of Archaean evolution from 3.5Ga to 2.6Ga in Swaziland and northern Natal. *S. Afri. J. Geol.*, **91**, 57-74.

Irvine. T.N. and Baragar, W.R.A. (1971). A guide to the geochemical classification of the common volcanic rocks. *Can. J. Earth Sci.*, **8**, 523-548.

Jensen, L.S. (1976). *A new cation plot for classifying subalkalic volcanic rocks.* Ontario Div. Mines. Misc. Pap. 66p.

Kamber, B.S., Ewart, A. Collerson, K.D., Bruce, M.C. and McDonald, G.D. (2002). Fluid-mobile trace element constraints on the role of slab melting and implications for Archaean crustal growth models. *Contrib. Mineral. Petrol.*, **144**, 38-56.

Kamo, S.L., Davis, D.W. and de Witt, M.J. (1990). U-Pb geochronology of Archaean plutonism in the Barberton region, S. Africa: 800Ma of crustal evolution. *Abstr. 7th Int. Conf. On Geochronology, Cosmochronology and Isotope Geology*, Canberra, Australia, 53.

Keleman, P.B., Shimizu, N. and Dunn, T. (1993). Relative depletion of niobium in some arc magmas and the continental crust: partitioning of K, Nb, La and Ce during melt/rock reaction in the upper mantle. *Earth Planet. Sci. Lett.*, **120**, 111-134.

Kilburn, C. (1990). Surface of aa flow-fields on Mount Etna, Sicily: Morphology, rheology, crystallization and scaling phenomena. *In*: Fink, J.H. (ed.), *Lava flows and domes, IAVCEI Proceedings in Volcanology 2.* Springer-Verlag, Berlin, 129-156.

Krige, L.J. (1931). *In*: Humphrey, W.A. and Krige, L.J. (1931). The geology of the country south of Piet Retief. *Explanation of Sheet 102 (Vryheid),* Geol. Surv. S. Afr., 18-28.

Le Maitre, R.W., Bateman, P, Dudek, A., Keller, J. Lameyre Le Bas, M.J., Sabine, P.A., Schmid, R., Sorensen, H., Streckeisen, A., Woolley, A.R. and Zanettin, B. (1989). *A classification of igneous rocks and glossary of terms.* Blackwell, Oxford, 193p.

Linström, W. (1987). The geology of the Dundee area. *Expl. of sheet 2830*, Geol. Surv. S. Afr., 52p.

Linström, W. and Matthews, P.E. (1990a). Hlathini Formation. Catalogue of South African lithostratigraphic units. M.R. Johnson (ed.), *SACS*, **2**, 21-22.

Linström, W. and Matthews, P.E. (1990b). Mabaleni Formation. Catalogue of South African lithostratigraphic units. M.R. Johnson (ed.), *SACS*, **2**, 27-28.

Linström, W. and Matthews, P.E. (1990c). Mome Formation. Catalogue of South African lithostratigraphic units. M.R. Johnson (ed.), *SACS*, **2**, 31-32.

Lofgren, G, (1971). Experimentally produced devitrification textures in natural rhyolitic glass. *Geol. Soc. Am. Bull.*, **82**, 111-124.

Lowe, D.R. (1994). Accretionary history of the Archaean Barberton Greenstone Belt (3.55-3.22Ga), southern Africa. *Geology*, **22**, 1099-1102.

Mabuza, M.B. (1993*). The geology and geochemistry of the volcanic rocks of the Pongola Sequence in southern Swaziland.* M.Sc. thesis. (Unpubl.), Univ. Natal, Pietermaritzburg, 136p.

MacLean, W.H. and Kranidotis, P. (1987). Immobile elements as monitors of mass transfer in hydrothermal alteration: Phelps Dodge Massive Sulphide Deposit, Matagami, Quebec. *Econ. Geol.*, **82**, 951-962.

Mason, T.R. and von Brunn, V. (1977). 3G-yr old stromatilites from South Africa. *Nature*, **266**, 47-69.

Matthews, P.E. (1959). The metamorphism and tectonics of the Pre-Cape formations in the post-Ntingwe thrust belt, S.W. Zululand, Natal. *Trans. Geol. Soc. S. Afr.*, **62**, 257-322.

Matthews, P.E. (1967). The Pre-Karroo Formation of the White Umfolozi Inlier, Northern Natal. *Trans. Geol. Soc. S. Afr.*, **70**, 39-63.

Matthews, P.E. (1979a). Unpublished mapping of the Nkandla District. Univ. Natal, Durban.

Matthews, P.E. (1979b). Unpublished mapping of the Pongola District. Univ. Natal, Durban.

Matthews, P.E. (1990). A plate tectonic model for the late Archaean Pongola Supergroup in Southeastern Africa. *In*: Sychanthavong, S.P.H. (ed.), *Crustal evolution and orogeny*. Oxford Publ., New Delhi, 41-72.

Matthews, P.E. and Scharrer, R.H. (1968). A graded unconformity at the base of the early Precambrian Pongola System. *Trans. Geol. Soc. S. Afr.*, **71**, 257-272.

Matthews, P.E., Charlesworth, E.G., Eglington, B.M. and Harmer, R.E. (1989). A minimum 3.29Ga age for the Nondweni greenstone complex in the south-eastern Kaapvaal craton. *S. Afr. J. Geol.*, **92**, 272-278.

McCall, G.J.H. (1981) Progress in Research, 1970-1980. *In*: Glover, J.E. and Groves, D.I. (eds.), *Archaean Geology, 2nd Int. Sym., Spec. Pub. 7*. Geol. Soc. Aus., Perth, 3-18.

McCulloch, M.T. (1993). The role of subducting slabs in an evolving earth. *Earth Planet. Sci. Lett.*, **115**, 89-100.

McMillan, K., Cross, R.W. and Long, P.E. (1987). Two-stage vesiculation in the Cohassett flow of the Grande Ronde Basalt, south-central Washington. *Geology*, **15**, 809-812.

Meschede, M. (1986). A method of discriminating between different types of mid-ocean ridge basalts and continental tholeiites with the Nb-Zr-Y diagram. *Chem. Geol.*, **56**, 207-218.

Meyer, F.M., Reimold, W.U. and Walraven, F. (1993). The evolution of the Archaean granitic crust in the southwestern Kaapvaal Craton, South Africa. *European Union Geosciences VII, 4-8 April 1993*, 319p.

Mueller, W., Chown, E.H. and Thurston, P.C. (2000). Processes in physical volcanology and volcaniclastic sedimentation: modern and ancient. *Precam. Res.*, **101**, 81-95.

Nhleko, N. (1998). *Stratigraphy of the Archaean Mozaan Group in the Kubuta-Mooihoek area, Swaziland*. M.Sc. thesis (Unpubl.), Rand Afrikaans University, Johannesburg, 133p.

Nhleko, N., Beukes, N.J. and Gutzmer, J. (2002). High-latitude setting for the oldest known glacial deposit from the ~2.9Ga Mozaan Group, southern Africa. *16th International Sedimentological Congress Abstract Volume*. Rand Afrikaans University, Johannesburg, 278-279.

Norrish, K. and Hutton, J. T. (1969). An accurate X-ray spectrographic method for the analysis of a wide range of geological samples. *Geochim. Cosmochim. Acta*, **33**, 431-435.

Pearce, J.A. (1983). Role of sub-continental lithosphere in magma genesis at active plate margins. *In*: Hawkesworth, C.J. and Norry, M.J. (eds.), *Continental basalts and mantle xenoliths*. Shiva, Nantwich, 230-249.

Pearce, J.A. and Cann, J.R. (1973). Tectonic setting of basic volcanic rocks determined using trace element analysis. *Earth Plant. Sci. Lett.*, **24**, 419-426.

Pearce, J.A. and Gale, G.H. (1977). Identification of ore-deposition environment from trace element geochemistry of associated igneous host rocks. *Geol. Soc. Spec. Publ.*, **7**, 14-24.

Pearce, J.A. and Norry, M.J. (1979). Petrogenetic implications of Ti, Zr, Y and Nb variations in volcanic rocks. *Contrib. Mineral. Petrol.*, **69**, 33-47.

Preston, V.A. (1987). *The geology and geochemistry of the Mpongoza inlier, northern Natal*. M.Sc. thesis (Unpubl.), Univ. Natal, Pietermaritzburg, 282p.

Richardson, S.H., Shirey, S.B., Harris, J.W. and Carlson, R.W. (2001). Archean subduction recorded by Re-Os isotopes in eclogitic sulfide inclusions in Kimberley diamonds. *Earth Planet. Sci. Lett.*, **191**, 257-266

Rickwood, P.C. (1989). Boundary lines within petrologic diagrams which use oxides of major and minor elements. *Lithos*, **22**, 247-263.

Rollinson, H.R. (1993). *Using geochemical data*. Longman Scientific & Technical, Singapore, 352p.

Rowland, S.K. and Walker, G.P.L. (1987). Toothpaste lava: Characteristics and origin of a lava structural type transitional between pahoehoe and aa. *Bull. Volcanol.*, **49**, 631-641.

Rowland, S.K. and Walker, G.P.L. (1988). Mafic-crystal distributions, viscosities, and lava structures of some Hawaiian lava flows. *J. Volcanol. Geotherm. Res.*, **35**, 55-66.

Sahagain, D. (1985). Bubble migration and coalescence during the solidification of basaltic lava flows. *J. Geol.*, **93**, 205-211.

Schmid, R. (1981). Descriptive nomenclature and classification of pyroclastic deposits and fragments: Recommendations of the IUGS Subcommission on the Systematics of Igneous Rocks. *Geology*, **9**, 41-43.

Sleep, N.H. and Windley, B.F. (1982) Archaean plate tectonics: constraints and inferences. *J. Geol*, **90**, 363-379.

South African Committee for Stratigraphy (SACS) (1980). Stratigraphy of South Africa. Part 1. *In:* Kent, L.E. (ed.), *Lithostratigraphy of the Republic of South Africa, South West Africa/Namibia, and the Republics of Bophuthatswana, Transkei and Venda*, **8**, Handbk Geol. Surv. S. Afr., 690p.

Sun, S-S. (1984). Geochemical characteristics of Archaean ultramafic and mafic volcanic rocks: Implications for mantle composition and evolution. *In*: Kroner, A., Hanson, G.N. and Goodwin, A.M. (eds.), *Archaean Geochemistry*. Springer-Verlag, Berlin, 25-46.

Tankard, A.J., Jackson, M.P.A., Eriksson, K.A., Hobday, D.K., Hunter, D.R. and Minter, W.E.L. (1982). *Crustal evolution of Southern Africa*. Springer-Verlag, New York, 523p.

Thurston, P. C. (1994). Archean volcanic patterns. *In*: Condie K. C. (ed.), *Archean Crustal Evolution*. Elsevier, Amsterdam, 35-74.

Truter, F.C. (1950). A review of vulcanism in the Geological history of South Africa. *Proc. Geol. Soc. S. Afr.*, **52**, XXIX-LXXXIX.

Van Vuuren, C.J. (1965). *Die geologie van 'n gebied suid van Amsterdam, oos-Transvaal*. M.Sc (Unpubl.), Univ. Free State, 93p.

Visser, H. N., Krige, L.J. and Truter, M.A. (1947). *The geology of the country south of Ermelo. Explanation sheet 64*. Geol. Surv, S. Afr.

Von Brunn, V. (1974). Tidalites of the Pongola Supergroup (early Precambrian) in the Swart Mfolozi area, northern Natal. *Bull. Precam. Res. Unit., Univ. Cape Town*, **15**, 107-122.

Von Brunn, V. and Mason, T.R. (1977). Siliciclastic – carbonate tidal deposits from the 3000Ma Pongola Supergroup, South Africa. *Sedim. Geol.*, **18**, 245-255.

Walker, G.P.L. (1971). Compound and simple lava flows and flood basalts. *Bull. Volcanol.*, **35**, 579-590.

Walker, G.P.L. (1991). Structure and origin by injection of lava under surface crust, of tumuli, "lava rises", "lava-rise pits", and "lava-inflation clefts" in Hawaii. *Bull. Volcanol.*, **53**, 546-558.

Walraven, F. and Pape, J. (1994). Pb-Pb whole-rock ages for the Pongola Supergroup and the Usushwana Complex, South Africa. *J. Afr. Earth Sci.*, **18**, 297-308.

Watchorn, M.B. (1978). *Sedimentology of the Mozaan Group in the southeastern Transvaal and northern Natal.* M.Sc. thesis (Unpubl.), Univ. Natal, Pietermaritzburg, 111p.

Watchorn, M.B. (1980). Fluvial and tidal sedimentation in the 3000Ma Mozaan basin, South Africa. *Trans. Geol. Soc. S. Afr.*,**13**, 27-42.

Watchorn, M.B. and Armstrong, N.V. (1980). Contemporaneous sedimentation and volcanism at the base of the early Precambrian Nsuze Group, South Africa. *Trans. Geol. Soc. S. Afri.*, **83**, 231-238.

Williams, H. and McBirney, A.R. (1979). *Volcanology*. Freeman, Cooper & Co., San Francisco, 379p.

Wilmoth, R.A. and Walker, G.P.L. (1993). P-type and S-type pahoehoe: a study of vesicle distribution patterns in Hawaiian lava flows. *J. Volcanol. Geotherm. Res.*, **55**, 129-142.

Wilson, A.H. and Versfeld, J.A. (1994). The early Archaean Nondweni greenstone belt, southern Kaapvaal Craton, South Africa, Part 1. Stratigraphy, sedimentology, mineralization and depositional environment. *Precam. Res.*, **67**, 243-276.

Wilson, M. (1989). *Igneous Petrology*. Unwin Hyman, London, 466p.

Winchester, J.A. and Floyd, P.A. (1977). Geochemical discrimination of different magma series and their differentiation products using immobile elements. *Chem. Geol.*, **20**, 325-343.

Wood, D.A. (1980). The application of a Th-Hf-Ta diagram to problems of tectonomagmatic classification and to establishing the nature if crustal contamination of basaltic lavas of the British Tertiary volcanic province. *Earth Plant. Sci. Lett.*, **50**, 11-30.

Yardley, B.W. (1989). *An Introduction to Metamorphic Petrology*. Longman Scientific & Technical, New York, 248p.

Young, G.M., von Brunn, V., Gold, D.J.C. and Minter, W.E.L. (1998). Earth's oldest reported glaciation: physical and chemical evidence from the Archean Mozaan Group (~2.9Ga) of South Africa. *J. Geol.*, **106**, 523-538.

ACKNOWLEDGEMENTS

This project was funded through the National Research Foundation (NRF) in the interest of developing South Africa's natural heritage. I wish to thank the shareholders of the Mkhunyane Eco-reserve, in particular, JC and Ina van Rooyen, for their constant hospitality and interest in this project. I would also like to thank Willie, Chris and Barbara of Matatane Camp in the White Mfolozi Inlier for their hospitality and keen enthusiasm for the geology of the area.

I would like to thank my supervisor, Prof. Allan Wilson for his guidance, advice and constant patience. Thanks must also go to the technical staff of the geology department, Mukesh Seyambu, Pat Suthan, Roy Seyambu and Ilse Wells, for their assistance during sample preparation and processing. I greatly appreciate the logistical and administration work done by Debbie Mackrory.

Over the past three months, I have received much support and advice from the staff at the De Beers GeoScience Centre. In particular I would like to thank Ferdi Winter, Craig Smith and the staff of the Databank, who have made this project easier to complete whilst working.

I am deeply indebted to Samantha Perritt, not only for her enthusiastic assistance in the field, but for technical, emotional and mental support throughout the duration of this project. I greatly appreciate the support of Benardo Bene, who can always be relied upon to offer a light-hearted look at post-graduate work. Vasna Ramasar provided ongoing motivation to complete this work and for this I am grateful. Thanks must also go to the staff of the Marine Geoscience Unit, for providing me with a sanctuary to vent my frustrations and drink tea. I am eternally grateful to Jason Palmer for listening to countless hypotheses, scanning slides, fixing my graphics problems and assisting on a few fieldtrips. Lastly, I wish to thank my parents for supporting me during my time as a post-graduate student. Without them, I would never have embarked on this study.

APPENDIX 1
WHITE RIVER SECTION MAP

APPENDIX 2a
LOCALITY DATA AND FIELD DESCRIPTIONS

Appendix 2a Locality data and field descriptions for White River Section and White Mfolozi Inlier samples

Sample No.	Latitude (S)	Longitude (E)	Date	Field ID Rock Type	Comments	XRF	ICP-MS	Petrography
				White River Section, Northern Region				
2000/PG/1	27.2776	31.1077	7/2000	Rhyolite	Phase 5.2	x	x	
2000/PG/2	27.2778	31.1081	7/2000	Rhyolite	Phase 5.2	x	x	
2000/PG/3	27.2781	31.1083	7/2000	Rhyolite	Phase 5.2	x	x	
2000/PG/4	27.2780	31.1092	7/2000	Rhyolite	Phase 5.2	x	x	
2000/PG/5	27.2781	31.1093	7/2000	Rhyolite	Phase 5.2	x	x	
2000/PG/20	27.2740	31.0846	7/2000	Porphyritic Andesite	Phase 1	x	x	
2000/PG/21	27.2740	31.0846	7/2000	Porphyritic Andesite	Phase 1	x	x	
2000/PG/22	27.2740	31.0846	7/2000	Porphyritic Andesite	Phase 1	x	x	
2000/PG/23	27.2740	31.0846	7/2000	Aphyric Basalt	Phase 1	x	x	
2000/PG/24	27.2723	31.0888	7/2000	Basalt tuff	Phase 1	x	x	
2000/PG/25	27.2723	31.0888	7/2000	Basalt	Phase 1	x	x	
2000/PG/26	27.2723	31.0888	7/2000	Dacite	Phase 1	x	x	
2000/PG/27	27.2592	31.0918	7/2000	Porphyritic rhyolite	Phase 4	x	x	
2000/PG/28	27.2592	31.0918	7/2000	Porphyritic rhyolite	Phase 4	x	x	
2000/PG/29	27.2486	31.1012	7/2000	Rhyolite	Phase 3.1	x	x	
2000/PG/30	27.2474	31.1041	7/2000	Basalt	Phase 3.1	x	x	
2000/PG/38	27.3124	31.1281	7/2000	Andesite	Phase 5.3	x	x	
2000/PG/39	27.3137	31.1383	7/2000	Andesite	Phase 5.3	x	x	
2000/PG/40	27.3135	31.1340	7/2000	Andesite	Phase 5.3	x	x	
2000/PG/41	27.3120	31.1244	7/2000	Dacite	Phase 5.3	x	x	
2000/PG/42	27.3104	31.1226	7/2000	Porphyritic rhyolite	Phase 5.3	x	x	
2000/PG/43	27.3091	31.1210	7/2000	Rhyolite	Phase 5.3	x	x	
CG 01/1	27.2729	31.0897	11/5/2001	Basaltic Andesite	Phase 1 - Cliff section	x	x	x
CG 01/2	27.2729	31.0897	11/5/2001	Tuff	Phase 1 - Cliff section	x	x	x
CG 01/3	27.2729	31.0897	11/5/2001	Basaltic Andesite Tuff	Phase 1 - Cliff section	x	x	x
CG 01/4	27.2731	31.0891	11/5/2001	Epidotized Basaltic Andesite	Phase 1 - Cliff section	x	x	x
CG 01/5	27.2731	31.0891	11/5/2001	Epidotized Basaltic Andesite	Phase 1 - Cliff section	x	x	
CG 01/6	27.2731	31.0891	11/5/2001	Basaltic Andesite	Phase 1 - Cliff section	x	x	x
CG 01/7	27.2732	31.0898	11/5/2001	Rhyolite	Phase 1 - Cliff section	x	x	x
CG 01/9	27.2597	31.0922	11/5/2001	Porphyritic Rhyolite	Phase 4	x	x	x
CG 01/10	27.2596	31.0923	11/5/2001	Porphyritic Rhyolite	Phase 4 - 150m NE of CG 01/9	x		
CG 01/11	27.2383	31.0912	11/5/2001	Rhyolite	Phase 4	x	x	x
CG 01/12	27.2432	31.0622	12/5/2001	Basalt	Wagondrift Fmn			x

Co-ordinates - WGS84 Lat Long

Appendix 2a Locality data and field descriptions for White River Section and White Mfolozi Inlier samples

Sample No.	Latitude (S)	Longitude (E)	Date	Field ID Rock Type	Comments	XRF	ICP-MS	Petrography
CG 01/13	27.2439	31.0598	12/5/2001	Basalt	Wagondrift Fmn	x	x	x
CG 01/15	27.2440	31.0590	12/5/2001	Basalt	Wagondrift Fmn	x	x	
CG 01/16	27.2441	31.0579	12/5/2001	Basalt	Wagondrift Fmn	x	x	
CG 01/17	27.2442	31.0578	12/5/2001	Basalt	Wagondrift Fmn	x	x	
CG 01/18	27.2442	31.0578	12/5/2001	Basalt	Wagondrift Fmn	x	x	x
CG 01/19	27.2445	31.0562	12/5/2001	Basalt	Wagondrift Fmn	x	x	
CG 01/20	27.2446	31.0554	12/5/2001	Dacite	Wagondrift Fmn	x	x	x
CG 01/21	27.2446	31.0554	12/5/2001	Dacite	Wagondrift Fmn	x	x	x
CG 01/22	27.2887	31.0913	13/5/2001	Andesite / Basalt	Phase 2	x	x	
CG 01/23	27.2887	31.0913	13/5/2001	Andesite / Basalt	Phase 2	x	x	
CG 01/24	27.2887	31.0913	13/5/2001	Andesite / Basalt	Phase 2			x
CG 01/25	27.2890	31.0928	13/5/2001	Basaltic Andesite	Phase 2	x	x	
CG 01/26	27.2954	31.0897	13/5/2001	Basalt	Phase 2	x	x	
CG 01/27	27.2968	31.0878	13/5/2001	Basalt	Phase 2	x	x	
CG 01/28	27.2977	31.0865	13/5/2001	Dacite / Basalt	Phase 2	x	x	
CG 01/29	27.2979	31.0865	13/5/2001	Basaltic Andesite	Phase 2	x	x	
CG 01/30	27.2978	31.0867	13/5/2001	Andesite / Basalt	Phase 2	x	x	x
CG 01/31	27.2987	31.0861	13/5/2001	Intrusive	Phase 2 - Central dyke	x	x	x
CG 01/32	27.2979	31.0865	13/5/2001	Intrusive	Phase 2 - West dyke	x	x	x
CG 01/33	27.2957	31.0906	13/5/2001	Basalt	Phase 2	x	x	
CG 01/34	27.2987	31.0860	5/7/2001	Intrusive	Phase 2 - E chill margin of central dyke	x	x	x
CG 01/35	27.2987	31.0860	5/7/2001	Intrusive	Phase 2 - Eastern dyke	x	x	x
CG 01/36	27.2987	31.0860	5/7/2001	Andesite	Phase 2 - Lava on west of dykes	x	x	x
CG 01/37	27.3002	31.0839	5/7/2001	Andesite	Phase 2 - Subvolcanic intrusion	x	x	
CG 01/38	27.3007	31.0840	5/7/2001	Andesite	Phase 2	x	x	
CG 01/39	27.3007	31.0840	5/7/2001	Andesite	Phase 2	x	x	
CG 01/40	27.3028	31.0876	5/7/2001	Basalt	Phase 2	x	x	
CG 01/41	27.3038	31.0915	5/7/2001	Aphyric Andesite	Phase 2	x	x	
CG 01/42	27.2715	31.1186	6/7/2001	Rhyolite / Perlite	Phase 5.2	x	x	x
CG 01/43	27.2711	31.1192	6/7/2001	Rhyolite / Perlite	Phase 5.2 - Flow banding	x	x	x
CG 01/44	27.2707	31.1197	6/7/2001	Aphyric Andesite	Phase 5.2	x	x	
CG 01/45	27.2713	31.1213	6/7/2001	Andesite	Phase 5.2	x	x	
CG 01/46	27.2736	31.1213	6/7/2001	Andesite	Phase 5.2	x	x	
CG 01/47	27.2724	31.0900	13/7/2001	Basaltic Andesite	Phase 1 - Cliff section	x	x	x

Co-ordinates - WGS84 Lat Long

Appendix 2a Locality data and field descriptions for White River Section and White Mfolozi Inlier samples

Sample No.	Latitude (S)	Longitude (E)	Date	Field ID Rock Type	Comments	XRF	ICP-MS	Petrography
CG 01/48	27.2724	31.0900	13/7/2001	Basaltic Andesite	Phase 1 - Cliff section	x	x	x
CG 01/49	27.2724	31.0900	13/7/2001	Basaltic Andesite	Phase 1 - Cliff section	x	x	x
CG 01/50	27.2726	31.0893	13/7/2001	Basaltic Andesite	Phase 1 - Cliff section	x	x	x
CG 01/51	27.2726	31.0893	13/7/2001	Basaltic Andesite	Phase 1 - Cliff section	x	x	x
CG 01/74	27.2930	31.0930	8/9/2001	Andesitic tuff	Phase 3.1 - Layering with nodules	x		
CG 01/75	27.2930	31.0940	8/9/2001	Massive Andesite	Phase 3.1	x	x	
CG 01/76	27.2930	31.0940	8/9/2001	Amygdaloidal Andesite	Phase 3.1			x
CG 01/77	27.2990	31.0960	8/9/2001	Massive Andesite	Phase 3.1	x		
CG 01/78	27.2990	31.0960	8/9/2001	Amygdaloidal Andesite	Phase 3.1	x		
CG 01/79	27.3000	31.0960	8/9/2001	Basalt	Phase 3.1 - Possible pillows	x	x	
CG 01/80	27.3050	31.0990	8/9/2001	Basaltic Andesite - tuff	Phase 3.1 - Well defined layering	x		
CG 01/81	27.3050	31.0990	8/9/2001	Basaltic Andesite	Phase 3.1 - Older flow below CG01/80	x	x	
CG 01/82	27.2782	31.0958	9/9/2001	Lapilli tuff: andesite - dacite	Phase 2	x		x
CG 01/83	27.2782	31.0958	9/9/2001	Andesitic tuff	Phase 2	x		
CG 01/84	27.2782	31.0958	9/9/2001	Tuffaceous andesite (lava?)	Phase 2	x	x	x
CG 01/85	27.2782	31.0958	9/9/2001	Vesicular dacite (froth flow?)	Phase 2	x		x
CG 01/86	27.2782	31.0958	9/9/2001	Massive Rhyolite	Phase 2	x		x
CG 01/87	27.2785	31.0952	9/9/2001	Dacite	Phase 2	x		
CG 01/88	27.2807	31.0938	9/9/2001	Andesite	Phase 2	x	x	
CG 01/89	27.2822	31.0923	9/9/2001	Massive Andesite	Phase 2	x		
CG 01/90	27.2797	31.0886	9/9/2001	Rhyolitic tuff	Phase 2	x	x	x
CG 01/91	27.2797	31.0886	9/9/2001	Dacite - Rhyolite	Phase 2	x		
CG 01/92	27.2797	31.0886	9/9/2001	Andesite	Phase 2	x	x	
CG 01/93	27.2835	31.0900	9/9/2001	Andesite	Phase 2	x	x	
CG 01/94	27.2838	31.0910	9/9/2001	Basaltic Andesite - pyroclastic	Phase 2 - Layering and nodules	x		x
CG 01/96	27.3088	31.1205	10/9/2001	Mafic intrusive	Phase 5.3	x	x	
CG 01/97	27.3090	31.1210	10/9/2001	Basaltic tuff	Phase 5.3 - Well developed layering	x		
CG 01/98	27.3093	31.1215	10/9/2001	Andesite	Phase 5.3	x	x	x
CG 01/99	27.3110	31.1230	10/9/2001	Rhyolite (perthite)	Phase 5.3	x	x	
CG 01/100	27.3110	31.1230	10/9/2001	Rhyolite (perthite)	Phase 5.3 - Flow banded			x
CG 01/101	27.3117	31.1238	10/9/2001	Porphyritic rhyolite / dacite	Phase 5.3	x		
CG 01/102	27.3115	31.1247	10/9/2001	Dacite	Phase 5.3	x		
CG 01/103	27.3122	31.1288	10/9/2001	Andesite	Phase 5.3 - Varies from massive to pyroclastic	x		x
CG 01/106	27.2524	31.1169	11/9/2001	Andesite	Phase 5.1	x	x	

Co-ordinates - WGS84 Lat Long

Appendix 2a Locality data and field descriptions for White River Section and White Mfolozi Inlier samples

Sample No.	Latitude (S)	Longitude (E)	Date	Field ID Rock Type	Comments	XRF	ICP-MS	Petrography
CG 01/107	27.2555	31.1240	11/9/2001	Andesite	Phase 5.1	x		x
CG 01/108	27.2524	31.1169	11/9/2001	Andesite	Phase 5.1 - Nodular	x		
CG 01/109	27.2522	31.1182	11/9/2001	Andesite	Phase 5.1 - Nodular	x		x
CG 01/110	27.2525	31.1155	11/9/2001	Andesite	Phase 5.1 - Vesicular	x		
CG 01/111	27.2528	31.1158	11/9/2001	Andesite	Phase 5.1 - Massive			
CG 01/112	27.2542	31.1141	11/9/2001	Basalt	Phase 5.1 - Vesicular surfaces			
CG 01/114	27.2562	31.1100	11/9/2001	Dacite	Phase 3.1	x		
CG 01/115	27.2557	31.1093	11/9/2001	Dacite	Phase 3.1	x		
CG 01/116	27.2557	31.1091	12/9/2001	Andesite	Phase 3.1	x		
CG 01/117	27.2555	31.1088	12/9/2001	Andesite	Phase 3.1 - Fine scale layering	x		
CG 01/118	27.2554	31.1085	12/9/2001	Andesite	Phase 3.1	x	x	
CG 01/119	27.2553	31.1080	12/9/2001	Tuffaceous Dacite	Phase 3.1	x		
CG 01/120	27.2552	31.1079	12/9/2001	Dacite	Phase 3.1	x		
CG 01/121	27.2552	31.1065	12/9/2001	Dacite	Phase 3.1	x	x	x
CG 01/122	27.2635	31.0785	14/9/2001	Basaltic Andesite	Mantonga Fmn - Intercalated with quartzites	x	x	x
CG 01/123	27.2627	31.0818	14/9/2001	Basalt	Phase 1	x		x
CG 01/125	27.2628	31.0832	14/9/2001	Andesite	Phase 1	x	x	x
CG 01/126	27.2626	31.0818	14/9/2001	Andesite	Phase 1	x		x
CG 01/127	27.2627	31.0823	14/9/2001	Andesite	Phase 1 - Close to epidote alteration	x		
CG 01/128	27.2633	31.0836	14/9/2001	Andesite	Phase 1 - Glomeroporphyritic	x	x	
CG 01/129	27.2630	31.0850	14/9/2001	Andesite	Phase 1 - Tuffaceous			x
CG 01/130	27.2661	31.0865	14/9/2001	Porphyritic andesite	Phase 1 - Glomeroppophyritic			x
CG 01/131	27.2669	31.0866	14/9/2001	Basaltic andesite	Phase 1 - Massive	x	x	x
CG 01/132	27.2683	31.0863	14/9/2001	Andesite	Phase 1 - Amygdaloidal	x		
CG 01/133	27.2706	31.0848	14/9/2001	Dacite	Phase 1	x		x
CG 01/134	27.2738	31.0845	14/9/2001	Andesite	Phase 1	x		
CG 01/135	27.2760	31.0897	14/9/2001	Andesite	Phase 1	x		x
CG 01/136	27.2553	31.1073	15/9/2001	Dacite	Phase 3.1 - Fine scale layering	x	x	x
CG 01/137	27.2580	31.1043	15/9/2001	Basalt	Phase 3.1 - Strange mottled appearance	x	x	x
CG 01/139	27.2580	31.1043	15/9/2001	Dacite	Phase 3.1	x		
CG 01/140	27.2630	31.1015	15/9/2001	Tuffaceous andesite	Phase 2	x		
CG 01/141	27.2657	31.0992	15/9/2001	Small dyke	Phase 2	x	x	x
CG 01/142	27.2657	31.0992	15/9/2001	Dacite	Phase 2	x	x	
CG 01/143	27.2657	31.0992	15/9/2001	Andesite	Phase 2	x		

Co-ordinates - WGS84 Lat Long

Appendix 2a Locality data and field descriptions for White River Section and White Mfolozi Inlier samples

Sample No.	Latitude (S)	Longitude (E)	Date	Field ID Rock Type	Comments	XRF	ICP-MS	Petrography
CG 01/144	27.2657	31.0992	15/9/2001	Tuffaceous andesite	Phase 2 - Below CG01/143	x		
CG 01/146	27.2695	31.0968	15/9/2001	Porphyritic andesite	Phase 2			x
CG 01/147	27.2695	31.0968	15/9/2001	Massive andesite	Phase 2	x		
CG 01/148	27.2702	31.0950	15/9/2001	Basalt	Phase 2	x	x	
CG 01/149	27.2742	31.0937	15/9/2001	Basalt	Phase 2 - Epidotization	x		
CG 01/150	27.2768	31.0947	15/9/2001	Basaltic andesite	Phase 2 - Epidotized and weathered	x		
CG 01/151	27.2910	31.0888	16/9/2001	Basaltic andesite	Phase 2 - Very vesicular and amygdaloidal	x	x	
CG 01/153	27.2902	31.0886	16/9/2001	Andesite	Phase 2	x		
CG 01/154	27.2898	31.0883	16/9/2001	Basaltic andesite	Phase 2 - Massive	x		
CG 01/157	27.2895	31.0885	16/9/2001	Porphyritic andesite	Phase 2 - Glomeroporphyritic			x
CG 01/158	27.2895	31.0885	16/9/2001	Massive andesite	Phase 2	x		
CG 01/160	27.2892	31.0887	16/9/2001	Massive andesite	Phase 2	x	x	
CG 01/161	27.2892	31.0930	16/9/2001	Rhyolite	Phase 2	x	x	x
CG 01/162	27.2837	31.0966	16/9/2001	Andesite	Phase 2	x	x	
CG 01/163	27.2837	31.0966	16/9/2001	Dacite	Phase 2 - Duplicate of CG01/161	x	x	
CG 01/165	27.3153	31.1183	17/9/2001	andesite - dacite	Phase 5.3	x	x	
CG 01/166	27.3158	31.1172	17/9/2001	basaltic andesite	Phase 5.3 - Alteration and shearing	x		x
CG 01/167	27.2742	31.0898	17/9/2001	Andesite	Phase 1 - Cliff section, duplicate of CG01/7	x	x	x
CG 01/168	27.2742	31.0898	17/9/2001	Porphyritic Andesite	Phase 1 - Cliff section			x
CG 01/170	27.2446	31.0554	24/10/2001	Andesite	Wagondrift Fmn - CG01/20 & 21	x	x	
CG 01/171	27.3104	31.1226	24/10/2001	Porphyritic Rhyolite	Phase 5.3	x	x	
				White Mfolozi Inlier, Central Region				
WM/2/2000	28.2356	31.1795	6/2000	Basalt	Agatha Fmn	x	x	x
WM/3/2000	28.2355	31.1797	6/2000	Basalt	Agatha Fmn	x	x	x
WM/4/2000	28.2354	31.1800	6/2000	Basalt	Agatha Fmn	x	x	
WM/5/2000	28.2353	31.1807	6/2000	Basalt	Agatha Fmn	x	x	x
WM/6/2000	28.2349	31.1814	6/2000	Basalt	Agatha Fmn	x	x	
WM/10/2000	28.2326	31.1889	6/2000	Basalt	Agatha Fmn	x	x	x
WM/11/2000	28.2322	31.1884	6/2000	Basalt	Agatha Fmn	x	x	
WM/12/2000	28.2322	31.1880	6/2000	Basalt	Agatha Fmn	x	x	
WM/13/2000	28.2323	31.1874	6/2000	Basalt	Agatha Fmn	x	x	x
WM/15/2000	28.2331	31.1861	6/2000	Basalt	Agatha Fmn	x	x	
WM/16/2000	28.2330	31.1862	6/2000	Basalt	Agatha Fmn	x	x	
WM/17/2000	28.2329	31.1863	6/2000	Basalt	Agatha Fmn	x	x	

Co-ordinates - WGS84 Lat Long

Appendix 2a Locality data and field descriptions for White River Section and White Mfolozi Inlier samples

Sample No.	Latitude (S)	Longitude (E)	Date	Field ID Rock Type	Comments	XRF	ICP-MS	Petrography
CG02/200	28.2365	31.1620	27/6/2002	basaltic andesite	Nhlebela Fmn			x
CG02/205	28.2421	31.1621	27/6/2002	andesite	Nhlebela Fmn	x	x	
CG02/206	28.2423	31.1619	27/6/2002	porphyritic andesite	Nhlebela Fmn	x	x	x
CG02/207	28.2571	31.1728	28/6/2002	lava with orientated feldspars	Nhlebela Fmn			x
CG02/210	28.2499	31.1621	28/6/2002	andesite - dacite	Nhlebela Fmn	x	x	
CG02/211	28.2472	31.1619	28/6/2002	basalt - basaltic andesite	Nhlebela Fmn	x	x	x
CG02/212	28.2452	31.1619	28/6/2002	basaltic andesite	Nhlebela Fmn	x	x	
CG02/213	28.2452	31.1620	28/6/2002	andesite	Nhlebela Fmn	x	x	x

Co-ordinates - WGS84 Lat Long

APPENDIX 2b
PETROGRAPHIC DESCRIPTIONS

Appendix 2b Petrographic descriptions for White River Section and White Mfolozi Inlier samples

Sample	Mineralogy	Textures	Comments
		Basalts – White River Section, Northern Region	
CG01/12 Wagondrift Formation	Epidote, chlorite, plagioclase (sericite), devitrified basaltic glass, actinolite, quartz, biotite, leucoxene / sphene	Microcrystalline Spherulitic high relief structures – basaltic glass Scattered vesicles – filled with quartz, overprinted along edges by epidote, chlorite and actinolite elongated crystal growth into vesicles Vague preferred orientation of sericite patches – original plagioclase crystals aligned	
CG01/13 Wagondrift Formation	Chlorite, epidote, devitrified basaltic glass, plagioclase (sericite), quartz, opaque minerals	Coarser grained than CG01/12 Relict clinopyroxene phenocrysts Devitrified basaltic glass – spherulitic high relief	
CG01/18 Wagondrift Formation	Chlorite, epidote, devitrified basaltic glass, plagioclase (sericite), quartz, leucoxene / sphene	Coarser grained than CG01/13	
CG01/137 Phase 3.1	Chlorite, epidote, biotite, plagioclase, quartz, opaque minerals	Two distinct areas – one has matrix >95% chlorite and other has matrix of biotite, chlorite and epidote	Extensive veining – zeolite, quartz
		Basaltic andesites – White River Section, Northern Region	
CG01/30 Phase 2	Biotite, actinolite, chlorite, epidote, quartz, plagioclase, opaque minerals	Very fine grained Needle like intergrowths of actinolite, chlorite and plagioclase	
CG01/123 Phase 1	Chlorite, epidote, quartz, devitrified glass, plagioclase, opaque minerals		
CG01/126 Phase 1	Chlorite, actinolite, epidote, leucoxene / sphene, haematite Quartz, plagioclase, k-feldspar aggregates	Remnant albite phenocrysts varying sizes from <10microns to 1mm	Veining - epidote
CG01/129 Phase 1	Chlorite, actinolite, epidote, leucoxene / sphene	Very fine grained matrix Equigranular	Veining - epidote
		Andesites – White River Section, Northern Region	
CG01/1 Phase 1	Chlorite, actinolite, plagioclase, quartz	Plagioclase phenocrysts – glomeroporphyritic 5-10mm No preferred orientation	
CG01/2 Phase 1	Chlorite, epidote, quartz, plagioclase, hornblende, biotite	Amygdales – calcite and quartz infilling	
CG01/3 Phase 1	Chlorite, epidote, actinolite, plagioclase, quartz	Vague preferred orientation of acicular crystals in matrix Amygdales – calcite and quartz	
CG01/4 Phase 1	Epidote, chlorite, plagioclase, quartz, actinolite, opaque minerals	High proprtion of plagioclase but as part of matrix No plagioclase phenocrysts No preferred orientation of plagioclase	
CG01/6 Phase 1	Chlorite, epidote, fluorite, quartz, plagioclase	Amygdales – calcite and quartz Acicular opaque minerals with random orientation	
CG01/7 Phase 1	Calcite, quartz, biotite, plagioclase, minor chlorite, actinolite, epidote	Very fine grained Matrix – quartz, plagioclase, epidote, chlorite Overprinting of biotite and opaque minerals	

Sample	Mineralogy	Textures	Comments
CG01/20 Wagondrift Formation	Epidote, chlorite, actinolite, opaque minerals, quartz, plagioclase, zircon	Opaque minerals found within rim of fine-grained mineral aggregate	
CG01/21 Wagondrift Formation	Epidote, chlorite, actinolite, opaque minerals, quartz, plagioclase, biotite, zircon	Opaque minerals found within rim of fine-grained mineral aggregate	
CG01/24 Phase 2	Biotite, quartz, plagioclase, epidote	Amygdales – quartz Epidote, quartz and plagioclase aggregate surrounded by biotite dominated rims forming generally spheroidal shapes Not all spheroidal structures are complete	Possible non mixing of mafic and acid liquids
CG01/36 Phase 2	Chlorite, biotite, quartz, plagioclase, epidote	Amygdales – calcite and quartz	
CG01/47 Phase 1	Chlorite, epidote, quartz, biotite, plagioclase, actinolite	Porphyritic – plagioclase phenocrysts Amygdales - quartz	
CG01/48 Phase 1	Chlorite, epidote, plagioclase, quartz, biotite, actinolite	Plagioclase phenocrysts Well rounded amygdales - quartz	
CG01/49 Phase 1	Chlorite, epidote, biotite, plagioclase, quartz	Amygdales – quartz and calcite Remnant plagioclase phenocrysts	
CG01/50 Phase 1	Chlorite, epidote, actinolite, biotite, plagioclase, quartz, hornblende, calcite	Well rounded amygdales – quartz and calcite Remnant plagioclase phenocrysts	
CG01/51 Phase 1	Chlorite, biotite, epidote, quartz, plagioclase, actinolite, biotite, hornblende	Small amygdales – quartz Remnant plagioclase phenocrysts	
CG01/76 Phase 3.2	Chlorite, hornblende, plagioclase, haematite, quartz, calcite	Amygdales – two stage growth – calcite rim with quartz core.	
CG01/90 Phase 2	Chlorite, epidote, biotite, quartz, k-feldspar, biotite	Very fine grained Quartz and k-feldspar intergrowths	
CG01/94 Phase 2	Chlorite, epidote, calcite, quartz, plagioclase, biotite, sphene, haematite	Generally Equigranular but areas of large quartz aggregates	Veining – quartz, calcite and chlorite
CG01/103 Phase 5.3	Quartz, plagioclase, epidote, chlorite, biotite, devitrified glass	Acicular growth of minerals Amygdales – quartz, zeolite Remnant plagioclase phenocrysts	
CG01/107 Phase 5.1	Chlorite, epidote, devitrified glass, quartz, plagioclase	Sheared amygdales – quartz, calcite and zeolites	Sheared nature of amygdales creates porphyroblastic appearance
CG01/109 Phase 5.2	Chlorite, epidote, devitrified glass, quartz, plagioclase	Acicular growth of minerals	
CG01/125 Phase 1	Epidote, chlorite, quartz, actinolite, hornblende	Very fine grained	Veining – quartz, epidote, chlorite
CG01/130 Phase 1	Epidote, quartz, chlorite, actinolite, plagioclase, zircon, opaque minerals	Remnant plagioclase phenocrysts Pseudomorphs of phenocrysts made up of epidote, quartz, chlorite, actinolite and plagioclase Pseudomorphs maintain initial crystal shape	Extensive saussuritisation

Sample	Mineralogy	Textures	Comments
CG01/131 Phase 1	Chlorite, epidote, biotite, quartz, plagioclase, actinolite, opaque minerals	Amygdales – quartz aggregates	
CG01/135 Phase 1	Chlorite, epidote, quartz, actinolite, plagioclase	Actinolite forms acicular crystals radiating from central point Plagioclase forms acicular laths	
CG01/146 Phase 2	Chlorite, biotite, epidote, calcite, plagioclase, quartz	Plagioclase phenocrysts – glomeroporphyritic, albite twinning	
CG01/166 Phase 5.3	Epidote, biotite, chlorite, calcite, devitrified glass	Quenching texture Very fine grained matrix	
CG01/167 Phase 1	Biotite, chlorite, quartz, plagioclase, opaque minerals	Very fine grained Elongated opaque minerals	Veining - epidote
CG01/168 Phase 5.3	Epidote, biotite, chlorite, quartz	Remnant plagioclase phenocrysts Amygdales – quartz rim, epidote core	
		Dacites to rhyolites – White River Section, Northern Region	
CG01/9 Phase 4	Chlorite, epidote, quartz, k-feldspar, plagioclase, hornblende, biotite	Granophyric texture – equidimensional recrystallized aggregates of quartz and k-feldspar intergrowths	4th stage devitrification of acid volcanic glass (Lofgren, 1971)
CG01/11 Phase 4	Quartz, calcite, k-feldspar, biotite, chlorite	Albite and k-feldspar phenocrysts Biotite and chlorite pseudomorph grain boundaries of original phenocrysts Spherulitic textures of quartz and k-feldspar	3rd stage devitrification of acid volcanic glass (Lofgren, 1971)
CG01/42 Phase 5.2	Quartz, k-feldspar, plagioclase, biotite, hornblende	Hydration cracks radiating from vein – perlitic Devitrification needles	Veining - epidote
CG01/43 Phase 5.2	Quartz, k-feldspar, plagioclase, biotite, calcite	Quartz patches and murky grey mineral intergrowths form flow banding	
CG01/84 Phase 2	Quartz, k-feldspar, plagioclase, fluorite	Foliation with microfaults	Foliation due to flow movement after deposition – no shearing evident in surrounding outcrops
CG01/85 Phase 2	Quartz, k-feldspar, biotite, epidote, chlorite	Fibrous intergrowths of k-feldspar and quartz Biotite pseudomorphs outline of remnant phenocryst	
CG01/86 Phase 2	Biotite, quartz, epidote, calcite, chlorite	Massive	
CG01/98 Phase 5.3	Plagioclase, quartz, k-feldspar, calcite, biotite, leucoxene / sphene	Remnant plagioclase phenocrysts	
CG01/100 Phase 5.3	Quartz, k-feldspar, plagioclase, calcite, zircon, grey murky aggregates, glass	Flow banded Feldspar phenocrysts Highly vesicular fragments Feldspars form woven effect with acicular crystal growth	Flow banding between glass and collapsed remnant pumice (grey murky aggregates)
CG01/121 Phase 3.1	Quartz, k-feldspar, albite, biotite, high proportion of opaque minerals	K-feldspar and albite phenocrysts	
CG01/122 Mantonga Formation	Quartz, k-feldspar, plagioclase, <0.5% mafic minerals, zircon	Feldspars form woven texture	

Sample	Mineralogy	Textures	Comments
CG01/133 Phase 1	Quartz, plagioclase, epidote, biotite, chlorite, opaque minerals	Radial spherulitic structures formed by chlorite and biotite Plagioclase forms acicular laths	
CG01/136 Phase 3.1	Plagioclase, biotite, calcite, quartz, chlorite	Amygdales – calcite Preferred orientation of biotite	
CG01/157 Phase 2	Actinolite, biotite, plagioclase, grey murky aggregate, quartz	Plagioclase phenocrysts – glomeroporphyritic Matrix –fine grained needle like intergrowths	
CG01/161 Phase 2	Quartz, k-feldspar, epidote, biotite, chlorite	Quartz and k-feldspar intergrowths in places – spherulitic and granophyric	3rd to 4th stage devitrification of acid volcanic glass
		Nhlebela Formation – White Mfolozi Inlier, Central Region	
CG02/200	Chlorite, actinolite, opaque minerals, calcite	Irregular amygdales - chlorite	
CG02/206	Actinolite, plagioclase, chlorite, quartz	Irregular amygdales – quartz rim and chlorite core Irregular shape looks like filled in spaces between growing aggregates	
CG02/207	Chlorite, calcite, quartz, plagioclase, devitrified glass, epidote, actinolite, opaque minerals	Irregular amygdales – calcite and quartz Vague preferred orientation of chlorite, epidote and actinolite	
CG02/211	Chlorite, plagioclase, actinolite, epidote, opaque minerals	Bladed opaque minerals	
CG02/213	Chlorite, plagioclase (albite), quartz, opaque minerals, leucoxene / sphene	Plagioclase phenocrysts	
		Agatha Formation – White Mfolozi Inlier, Central Region	
WM2/2000	Epidote, chlorite, plagioclase, devitrified glass, calcite, quartz	Granular texture Remnants of plagioclase phenocrysts	
WM3/2000	Chlorite, opaque minerals, calcite, actinolite, sphene	Remnants of plagioclase phenocrysts Amygdales – quartz and minor calcite	
WM5/2000	Chlorite, calcite, epidote, plagioclase actinolite, haematite, opaque minerals	Remnants of plagioclase phenocrysts	
WM10/2000	Chlorite, actinolite, plagioclase, calcite, epidote, devitrified glass	Remnants of plagioclase phenocrysts	
WM13/2000	Chlorite, epidote, calcite, quartz, devitrified glass, actinolite	No phenocrysts Fine and coarse grained areas with no apparent change in mineralogy Amygdales – chlorite, epidote, calcite	

APPENDIX 3
ANALYTICAL PROCEDURES

APPENDIX 3
ANALYTICAL PROCEDURES

Samples for this study were collected from the Nsuze Group and associated lithologies throughout the Pongola Supergroup subcrop area. Care was taken to select fresh, non-weathered samples for geochemical analysis. Samples were processed using X-ray Fluorescence (XRF) for whole-rock major and minor elements. Samples were then selected for Inductively Coupled Plasma Mass Spectrometry (ICP-MS) to determine whole-rock trace elements and rare earth element concentrations.

SAMPLE PREPARATION

Samples were cleaned of all weathered and altered surfaces. They were subsequently cut into blocks approximately 2x3x3cm using a diamond rock cutting saw. Samples blocks were then scrubbed under running water followed by cleaning in an ultrasonic cleaner for 1 minute. Once they were rinsed again, the samples were then dried in an oven at 100°C.

The block samples were crushed using a low molybdenum carbon steel jaw crusher to obtain fragments of <1cm. The crush was statistically split to 100g using the cone-and –quartering technique and then milled using high purity carbon steel mills. The remainder of the crushed samples have been stored for future use. The milled fraction was used to prepare fusion discs and pressed powder pellets for XRF and dissolved sample for ICP-MS analysis. The balance has been stored for future use. Samples were processed in order from the mafic to acid to minimize the possibility of contamination.

X-RAY FLUORESCENCE

XRF analysis was performed at the University of Natal, Durban's School of Geological and Computer Sciences using a Philips PW1404 spectrometer. Instrument calibration was controlled with international standards and internal synthetic standards and blanks. The following international standards were used: BCR-1, AGV-10 and BHVO-1, in addition to in-house control standards and blanks. Batch control standards were CG01/18 – basic, CG01/2 – intermediate, CG0/11 – acid. Prof. A.H. Wilson of the Department of Geology, University of Natal, Durban compiled the computer programs for reduction of count data and calculation of mass absorption coefficients. Major elements were analysed using the lithium tetraborate fusion method of Norrish and Hutton (1969), while minor elements were measured using pressed powder pellets.

Preparation of Norrish Fusion Discs

Approximately 0.5g of sample was weighed into silica crucibles that had been cleaned in a diluted solution of HCl. The crucibles with sample were placed in a furnace at 1000^{0}C for 4 hrs, then removed and allowed to cool in a desiccator. The Johnson Matthey Spectroflux 105 used for the fusion discs was preheated in Pt crucibles at 1000^{0}C, and approximately 0.4g of the ashed sample was added as close to the ratio weight sample : weight flux = 2.2 as possible. The samples were fused at 1000^{0}C and the product cast in a brass die maintained at 250^{0}C. Discs annealed for 3 hours on a heated asbestos plate and then allowed to cool gradually.

Pressed Powder Pellets

Approximately 10g of finely milled sample was mixed with 0.6 Mowiol in an agate mortar. The mixture was compressed to 10 tonnes in a position cylinder. The resultant pellets are approximately 5mm thick. The pellets were hardened in an oven at 120^{0}C for 3-4 hours.

INDUCTIVELY COUPLED PLASMA MASS SPECTROMETRY

Trace elements, including the rare earth elements, were analysed using ICP-MS at the University of Natal, Durban's School of Geological and Computer Sciences using a Perkin Elmer 6100 ICP-MS.

Laboratory Procedures

Sample preparation involved digesting 50mg of sample powder using HF and HNO_3. BCR-1 and BHVO-1 were used as controls and certified reference standard RGM-1 was run as an unknown. Primary calibration was done against certified Perkin Elmer standard solutions.

APPENDIX 4
MAJOR, MINOR AND TRACE
ELEMENT GEOCHEMISTRY DATA

Appendix 4 Major, minor and trace element geochemistry data										
Wagondrift Formation - White River Section, Northern Region										
XRF		CG01/13	CG01/15	CG01/16	CG01/17	CG01/18	CG01/19	CG01/20	CG01/21	CG01/170
wt%	SiO_2	49.63	50.77	50	50.58	49.89	52.92	52.95	49.9	50.47
	Al_2O_3	14.54	14.85	14.71	14.56	14.28	15.15	16.01	18.24	18.09
	Fe_2O_3	1.48	1.47	1.55	1.5	1.56	1.26	1.26	1.39	1.46
	FeO	11.96	11.87	12.58	12.11	12.64	10.18	10.23	11.26	11.79
	MnO	0.186	0.187	0.1878	0.1874	0.1917	0.1571	0.1859	0.1797	0.173
	MgO	6.67	6	5.91	5.93	5.96	5.71	5.47	5.17	5.1
	CaO	10.28	9.89	9.51	9.24	9.48	8.29	8.7	8.17	7.76
	Na_2O	2.76	2.82	3.69	3.71	3.35	3.82	3.2	2.81	2.28
	K_2O	1.3	0.59	0.34	0.41	0.44	0.5	0.65	1.03	1.05
	TiO_2	1.1715	1.2101	1.4837	1.4352	1.4806	1.1688	1.075	1.2817	1.3375
	P_2O_5	0.06	0.14	0.18	0.17	0.2	0.41	0.34	0.39	0.32
	Cr_2O_3	0.0293	0.0161	0.0131	0.018	0.016	-0.0024	-0.0005	-0.0024	0.0146
	NiO	0.0346	0.027	0.0244	0.0223	0.0245	0.0223	0.026	0.0282	0.0274
ppm	Y	14.05	17.2	21.55	20.1	21.5	26.6	24.7	19.8	19.55
	Rb	41.75	18.4	12.05	12.35	15.6	15.55	16.45	37.45	38.6
	Zr	49.35	60.1	78.8	83.15	89.45	141.4	128	119	125.7
	Sr	460.65	456.8	470.25	414.75	492.6	631.25	590.8	571.05	555.6
	Zn	95.2	102.9	110.8	108.2	112	110.5	114	133.1	134.9
	Cu	156.3	31.2	156.6	120.9	198.3	57.1	14.8	5.8	5
	Ni	257.8	196	180.9	171.6	179.4	170.1	194	217.9	222
	Cr	288.1	187.2	137.3	150	139.5	42.2	67	41.2	40.5
	V	236	206.2	228.4	228.5	221.2	234.1	220.3	278.6	321.8
	Sc	29.7	27	30.6	30.1	29.4	23.9	23.3	29.6	29.4
	K	10632.9	4657.7	2755.8	3163.7	3500.5	3885.4	4957.1	7494.1	7534.4
	S	324.2	112.1	374.3	316.9	385.2	115.3	88.4	59	31
	P	403.8	770.8	1105.5	978	1189.4	2188.3	2095.3	2100.1	1504.2
	Co	65.1	127.1	57	63	56.2	43.3	49.8	48.2	54.3
ICP-MS		CG01/13	CG01/15	CG01/16	CG01/17	CG01/18	CG01/19	CG01/20	CG01/21	CG01/170
ppm	Nb	2.588	3.357	4.424	4.872	5.021	5.444	4.501	4.554	4.731
	Ba	235.648	162.816	97.839	102.006	109.588	200.285	238.361	359.913	356.940
	La	6.865	10.301	12.407	13.606	14.478	24.398	21.143	20.592	19.749
	Ce	14.194	21.389	26.173	28.510	30.220	53.602	46.408	44.795	41.692
	Pr	1.987	2.924	3.677	3.903	4.199	7.477	6.436	6.152	6.387
	Nd	8.495	12.153	15.382	16.020	17.394	30.077	25.900	24.446	28.388
	Sm	2.292	2.956	3.737	3.775	4.137	6.175	5.558	5.067	5.216
	Eu	1.234	1.406	1.565	1.575	1.684	1.973	1.896	1.984	2.035
	Gd	2.690	3.445	4.412	4.445	4.883	6.616	5.872	5.167	5.328
	Tb	0.413	0.514	0.649	0.652	0.715	0.877	0.803	0.680	0.705
	Dy	2.256	2.755	3.418	3.433	3.725	4.394	4.028	3.322	3.550
	Ho	0.436	0.519	0.645	0.654	0.704	0.808	0.743	0.598	0.641
	Er	1.160	1.405	1.724	1.745	1.862	2.209	2.034	1.613	1.732
	Tm	0.156	0.185	0.226	0.233	0.249	0.284	0.264	0.214	0.234
	Yb	0.954	1.142	1.393	1.423	1.497	1.761	1.620	1.328	1.474
	Lu	0.131	0.153	0.187	0.193	0.204	0.237	0.220	0.179	0.201
	Hf	0.878	0.900	1.055	0.965	0.867	0.788	0.668	0.464	0.555
	Ta	0.256	0.238	0.261	0.263	0.260	0.227	0.193	0.190	0.219
	W	0.401	0.325	0.218	0.258	0.321	0.204	0.184	0.220	0.214
	Pb	6.468	3.691	2.713	2.859	3.222	3.399	4.684	7.465	7.459
	Th	0.466	0.441	0.406	0.390	0.372	0.383	0.307	0.317	0.402
	U	0.109	0.094	0.083	0.086	0.078	0.093	0.077	0.092	0.092

Appendix 4 Major, minor and trace element geochemistry data									
Mantonga Fmn		Phase 1, Bivane Subgroup - White River Section, Northern Region							
	XRF	CG01/122	CG01/1	CG01/2	CG01/3	CG01/4	CG01/5	CG01/6	CG01/7
wt%	SiO_2	69.73	55.95	56.42	54.22	53.99	65.51	55.34	59.38
	Al_2O_3	12.6	17.82	15.98	15.81	15.45	10.91	15.77	12.97
	Fe_2O_3	0.74	1.07	1.27	1.21	1.27	0.9	1.19	1.41
	FeO	6	8.66	10.31	9.77	10.28	7.28	9.67	11.42
	MnO	0.104	0.138	0.1642	0.1825	0.1606	0.084	0.1759	0.1457
	MgO	0.9	3.72	4.86	4.88	4.65	1.32	5.47	1.9
	CaO	3.68	6.13	5.16	8.46	10.59	12.54	6.63	4.59
	Na_2O	1.02	4.93	3.53	3.95	2.03	0	3.66	3.32
	K_2O	3.6	0.49	1.21	0.86	0.35	0.11	0.89	2.43
	TiO_2	0.6501	0.9432	1.0841	0.954	1.103	0.9528	1.0111	1.3872
	P_2O_5	0.15	0.19	0.22	0.19	0.21	0.19	0.2	0.25
	Cr_2O_3	0.0043	0.0122	0.0154	0.0134	0.0174	0.0123	0.0143	-0.0075
	NiO	0	0.0079	0.0102	0.0106	0.0134	0.01	0.0094	0.0018
ppm	Y	44.8	23.55	28.05	24.8	30.45	26.8	26.45	36.35
	Rb	129	9.9	25.95	16.25	8.55	3.95	16.45	128.7
	Zr	302.7	132.05	150.7	128.6	158.85	139.15	144.15	200.8
	Sr	61.6	307	168.25	233.65	249.1	1156.1	235	211.1
	Zn	87.4	91.9	113.2	93.7	107.7	22.1	106.6	118.4
	Cu	5.1	38.9	49.8	16.1	2	0	13	60
	Ni	0	69.4	79.9	72.9	105.9	64.3	80.4	12.1
	Cr	0	151.6	157.1	151.8	165.2	131.4	158.2	0.6
	V	4.7	138.9	186.4	160.8	174.3	95.5	158.6	229.6
	Sc	9.2	22.2	25.3	24.9	26.3	23.4	25.9	21.5
	K	27485.5	3895.3	10117.9	6566.2	3163.9	930.1	7343.4	19923.6
	S	752.7	176.3	177.5	88.2	61.3	38.2	91.6	244.8
	P	717.2	763.1	866.4	702.9	899.1	1007.3	686.1	996.9
	Co	6.1	43.2	47.5	42.3	57.4	16.7	44.1	34.7
	ICP-MS	CG01/122	CG01/1	CG01/2	CG01/3	CG01/4	CG01/5	CG01/6	CG01/7
ppm	Nb	17.044	6.277	7.160	6.066	7.337	6.066	6.817	11.908
	Ba	662.995	153.395	277.926	199.809	89.865	35.195	246.696	398.752
	La	48.446	16.621	19.210	16.833	20.482	17.749	18.612	37.435
	Ce	93.450	33.505	39.105	33.431	41.030	35.483	37.242	68.730
	Pr	10.307	4.375	5.139	4.355	5.347	4.632	4.861	8.173
	Nd	34.104	16.904	19.910	16.949	20.669	17.926	18.762	28.538
	Sm	6.727	3.823	4.615	3.907	4.664	4.006	4.331	5.846
	Eu	1.121	1.433	1.787	1.383	1.617	1.280	1.546	1.483
	Gd	7.628	4.514	5.479	4.644	5.655	4.863	5.144	6.963
	Tb	1.102	0.688	0.834	0.703	0.850	0.736	0.784	1.023
	Dy	6.289	3.795	4.651	3.946	4.716	4.068	4.335	5.699
	Ho	1.280	0.750	0.922	0.773	0.934	0.795	0.858	1.150
	Er	3.802	2.121	2.592	2.174	2.632	2.249	2.402	3.329
	Tm	0.542	0.297	0.360	0.301	0.360	0.310	0.334	0.466
	Yb	3.492	1.853	2.235	1.895	2.264	1.952	2.063	2.916
	Lu	0.490	0.256	0.296	0.255	0.305	0.264	0.279	0.414
	Hf	6.740	2.518	2.618	2.362	2.795	2.522	2.613	4.371
	Ta	1.217	0.372	0.381	0.335	0.363	0.285	0.333	0.684
	W	0.675	0.572	0.355	0.293	0.299	0.279	0.257	0.391
	Pb	11.670	5.459	3.884	5.010	7.242	13.332	4.023	13.291
	Th	13.791	1.204	1.296	1.290	1.316	1.339	1.268	4.773
	U	3.041	0.205	0.219	0.216	0.220	0.225	0.214	1.033

Appendix 4 Major, minor and trace element geochemistry data									
Phase 1, Bivane Subgroup - White River Section, Northern Region									
	XRF	CG01/47	CG01/48	CG01/49	CG01/50	CG01/51	CG01/123	CG01/125	CG01/126
wt%	SiO_2	54.77	54.95	55.13	55.49	56.06	52.58	52.95	52.81
	Al_2O_3	15.23	14.82	15.55	15.05	15.04	15.18	15.57	16.98
	Fe_2O_3	1.24	1.24	1.16	1.2	1.22	1.4	1.36	1.32
	FeO	10.01	10.06	9.41	9.68	9.88	11.35	10.98	10.66
	MnO	0.1714	0.1695	0.1652	0.1667	0.1742	0.1858	0.172	0.1647
	MgO	5.65	5.86	5.51	5.15	5.06	5.15	4.29	3.69
	CaO	6.97	6.75	6.83	7.42	7.21	8	9.37	8.04
	Na_2O	3.36	3.17	3.92	2.95	3.13	3.42	2.54	3.8
	K_2O	1.46	1.25	1.24	1.97	1.09	1.03	0.78	1.03
	TiO_2	1.0503	1.0272	0.9508	1.0026	1.0175	1.2398	1.2786	1.2985
	P_2O_5	0.21	0.2	0.19	0.19	0.21	0.24	0.25	0.24
	Cr_2O_3	0.0224	0.0132	0.0165	0.0166	0.0155	0.0159	0.0154	0.0146
	NiO	0.0118	0.0106	0.0104	0.0116	0.0117	0.0073	0.0088	0.0056
ppm	Y	27.8	27.05	24.15	27.55	27.05	30.1	32.1	29.2
	Rb	22.2	20.55	19.25	42.65	19.3	21.7	17.3	21.8
	Zr	145.55	139.65	128.75	144.3	144.7	154.2	165	161.8
	Sr	227.25	191.65	213.55	281.45	256.6	290.4	334.7	395.2
	Zn	99.7	101.7	91.7	102.7	104.3	115.6	103	110.8
	Cu	33.6	29.1	11.6	38.7	31.6	45.6	17.2	2.5
	Ni	77.3	78.7	73	79	84.1	76.6	76.6	55.2
	Cr	154.9	157.2	137.7	158.6	165.7	53.9	47.5	33.1
	V	169	164.2	153.1	155.3	154.3	169.3	165.6	144.7
	Sc	26.1	25.9	24.3	23.7	23	26.8	29	23
	K	10850.5	9442.2	9130.5	15872.6	8851.8	8468.1	6245.7	8074.5
	S	59.2	65.2	25.1	92.3	63.2	130.3	72.7	36.8
	P	614.1	685.5	684.4	677.8	756.8	996.9	1121.2	1085.4
	Co	53.9	51.1	54.8	55.4	52.3	64	57.6	52.7
	ICP-MS	CG01/47	CG01/48	CG01/49	CG01/50	CG01/51	CG01/123	CG0/125	CG0/126
ppm	Nb	6.808	6.654	6.060	6.800	6.815	n.p.	8.904	n.p.
	Ba	347.597	311.346	296.446	584.121	238.452	n.p.	218.016	n.p.
	La	18.448	18.116	16.920	18.897	17.632	n.p.	20.561	n.p.
	Ce	36.549	35.871	34.031	37.523	36.084	n.p.	43.384	n.p.
	Pr	4.521	4.405	4.184	4.607	4.522	n.p.	5.535	n.p.
	Nd	17.031	16.747	15.913	17.115	17.453	n.p.	22.283	n.p.
	Sm	4.104	4.027	3.844	4.178	4.151	n.p.	5.078	n.p.
	Eu	1.434	1.382	1.379	1.495	1.460	n.p.	1.682	n.p.
	Gd	5.239	5.107	4.998	5.205	5.257	n.p.	6.000	n.p.
	Tb	0.769	0.753	0.720	0.759	0.785	n.p.	0.902	n.p.
	Dy	4.248	4.167	4.005	4.183	4.334	n.p.	5.048	n.p.
	Ho	0.841	0.835	0.789	0.830	0.854	n.p.	0.978	n.p.
	Er	2.389	2.336	2.220	2.344	2.408	n.p.	2.728	n.p.
	Tm	0.330	0.318	0.306	0.324	0.331	n.p.	0.372	n.p.
	Yb	2.076	2.031	1.945	2.023	2.093	n.p.	2.355	n.p.
	Lu	0.291	0.282	0.268	0.282	0.291	n.p.	0.317	n.p.
	Hf	2.878	2.722	2.610	2.721	2.834	n.p.	1.797	n.p.
	Ta	0.396	0.376	0.349	0.354	0.358	n.p.	0.449	n.p.
	W	0.350	0.297	0.280	0.268	0.303	n.p.	0.216	n.p.
	Pb	4.825	3.917	4.066	5.758	5.181	n.p.	6.883	n.p.
	Th	1.389	1.355	1.249	1.388	1.392	n.p.	2.185	n.p.
	U	0.218	0.211	0.199	0.219	0.222	n.p.	0.328	n.p.

Appendix 4 Major, minor and trace element geochemistry data

Phase 1, Bivane Subgroup - White River Section, Northern Region

XRF		CG01/127	CG01/128	CG01/131	CG01/132	CG01/133	CG01/134	CG01/135	CG01/167
wt%	SiO_2	54.52	56.06	55.68	55.61	61.98	55.33	59.96	59.45
	Al_2O_3	15.5	14.87	16.24	14.38	12.76	14.14	13.02	13.47
	Fe_2O_3	1.3	1.29	1.47	1.39	1.35	1.45	1.48	1.45
	FeO	10.55	10.43	11.93	11.26	10.94	11.75	11.99	11.77
	MnO	0.1641	0.1689	0.2013	0.1789	0.1423	0.1812	0.1393	0.1573
	MgO	4.12	4.18	2.6	3.99	1.24	4.6	1.66	2.08
	CaO	7.44	6.76	5.09	7.82	3.7	5.69	4.44	3.93
	Na_2O	3.31	2.74	3.28	3.01	4.11	3.88	3	2.63
	K_2O	1.53	1.68	1.12	0.78	1.81	1.08	2.17	3.33
	TiO_2	1.3316	1.2926	1.5685	1.3172	1.1626	1.3518	1.416	1.4082
	P_2O_5	0.28	0.28	0.3	0.26	0.4	0.26	0.28	0.27
	Cr_2O_3	0.0241	0.024	0.0194	0.022	0.0086	0.0219	0.0059	0.0065
	NiO	0.008	0.0085	0.0039	0.0074	0	0.0064	0	0.0006
ppm	Y	33.55	32.55	33.5	34.85	35.3	36	37.45	37.3
	Rb	40.9	55.55	27.8	17.15	27.3	18.75	72.75	170.8
	Zr	179.55	176.85	228.7	195.4	197.6	203.4	211.55	207.5
	Sr	355.9	326.1	343.4	289.45	153.5	205	227.95	186
	Zn	113	109.3	149.4	116.4	155.7	129.4	117.4	136.9
	Cu	26.2	14.8	22.4	26.5	52.5	41.1	51.3	66.1
	Ni	76	79.3	47.1	57.8	0.8	55.9	12.7	10.2
	Cr	114.4	103.2	85.5	88.3	0	92.7	0	0
	V	174.7	168.3	211	198.8	74.1	203.4	230	233.7
	Sc	24.1	24.1	26.3	27.7	19.9	27.5	21.3	21.8
	K	12586.1	13675.8	8732	6360.1	15124.7	8917.7	18420.9	26902.9
	S	104.4	51.8	103.7	89.1	392.8	144.1	726.6	235.7
	P	1399	1373.5	1459.6	1037	1782.7	842.6	1243	1056.8
	Co	48.5	52.2	51.7	57.3	45.2	63.6	49.7	37.6
ICP-MS		CG0/127	CG0/128	CG01/131	CG01/132	CG01/133	CG01/134	CG01/135	CG01/167
ppm	Nb	n.p.	8.892	10.750	n.p.	n.p.	n.p.	n.p.	12.481
	Ba	n.p.	388.822	345.472	n.p.	n.p.	n.p.	n.p.	402.363
	La	n.p.	24.970	24.706	n.p.	n.p.	n.p.	n.p.	37.194
	Ce	n.p.	50.644	49.722	n.p.	n.p.	n.p.	n.p.	68.283
	Pr	n.p.	6.367	6.248	n.p.	n.p.	n.p.	n.p.	7.952
	Nd	n.p.	24.822	24.317	n.p.	n.p.	n.p.	n.p.	28.202
	Sm	n.p.	5.635	5.387	n.p.	n.p.	n.p.	n.p.	5.752
	Eu	n.p.	1.824	1.990	n.p.	n.p.	n.p.	n.p.	1.475
	Gd	n.p.	6.529	6.283	n.p.	n.p.	n.p.	n.p.	6.919
	Tb	n.p.	0.964	0.917	n.p.	n.p.	n.p.	n.p.	0.999
	Dy	n.p.	5.326	4.966	n.p.	n.p.	n.p.	n.p.	5.723
	Ho	n.p.	1.020	0.980	n.p.	n.p.	n.p.	n.p.	1.152
	Er	n.p.	2.844	2.790	n.p.	n.p.	n.p.	n.p.	3.319
	Tm	n.p.	0.383	0.387	n.p.	n.p.	n.p.	n.p.	0.458
	Yb	n.p.	2.388	2.402	n.p.	n.p.	n.p.	n.p.	2.977
	Lu	n.p.	0.328	0.323	n.p.	n.p.	n.p.	n.p.	0.417
	Hf	n.p.	2.651	3.057	n.p.	n.p.	n.p.	n.p.	4.635
	Ta	n.p.	0.484	0.589	n.p.	n.p.	n.p.	n.p.	0.857
	W	n.p.	0.233	0.617	n.p.	n.p.	n.p.	n.p.	0.238
	Pb	n.p.	7.307	9.101	n.p.	n.p.	n.p.	n.p.	12.167
	Th	n.p.	2.270	2.362	n.p.	n.p.	n.p.	n.p.	9.542
	U	n.p.	0.364	0.377	n.p.	n.p.	n.p.	n.p.	2.035

Appendix 4 Major, minor and trace element geochemistry data								
Phase 1, Bivane Subgroup - White River Section, Northern Region								
	XRF	PG20/2000	PG21/2000	PG22/2000	PG23/2000	PG24/2000	PG25/2000	PG26/2000
wt%	SiO_2	55.37	57.09	55.31	54.14	61.84	54.74	59.88
	Al_2O_3	18.96	17.5	14.04	14.63	13.72	14.87	12.79
	Fe_2O_3	0.85	0.89	1.39	1.49	1.31	1.25	1.44
	FeO	6.87	7.19	11.23	12.06	10.62	10.12	11.66
	MnO	0.1162	0.1279	0.1758	0.1919	0.1246	0.1726	0.155
	MgO	3.42	3.5	4.25	3.28	1.77	5.79	2.13
	CaO	7.1	7.34	7.72	7.15	2.8	6.86	5.39
	Na_2O	4.9	4.31	3.36	2.89	1.43	3.42	2.17
	K_2O	1.4	1.2	0.53	1.6	3.56	0.87	2.81
	TiO_2	0.7168	0.818	1.3067	1.3709	1.803	1.0324	1.358
	P_2O_5	0.16	0.17	0.26	0.27	0.43	0.21	0.26
	Cr_2O_3	0.0195	0.0235	0.0191	0.0202	0.0088	0.029	0.0022
	NiO	0.0065	0.0076	0.0093	0.008	0.0039	0.0115	0.0033
ppm	Y	20.7	24.55	33.6	38.45	49.3	28.35	37.5
	Rb	25.5	21.55	10.6	36.5	83.15	13.8	139.3
	Zr	124.25	140.7	199.55	207	359.3	153.75	205.05
	Sr	439.4	399.1	315.8	359.7	132.25	241.7	286.2
	Zn	73.2	76.8	116.3	126.9	113.6	101.7	115.3
	Cu	20	42.3	43.6	35.7	27.6	41.1	60.9
	Ni	46.6	51.7	55.3	50.9	21.9	84.4	11.5
	Cr	100.1	115.8	93	110.5	23.5	157.3	0
	V	113.1	123.9	200.9	200.2	167.4	170.1	229
	Sc	12.7	15.8	29.5	25.8	23.5	26	23.1
	K	11622.6	9728.2	4590	13341.8	28841.1	6555.4	22479.6
	S	61.6	91.6	229	1539.5	100.2	97.5	435
	P	563.3	641.2	965.7	976.6	2074.3	762.8	1002.6
	Co	39.1	34.1	59.2	50.9	33.3	58.1	39
	ICP-MS	PG20/2000	PG21/2000	PG2000/22	PG2000/23	PG2000/24	PG2000/25	PG2000/26
ppm	Nb	5.427	6.160	8.800	9.241	16.171	6.633	11.336
	Ba	538.601	363.444	124.569	418.835	910.282	222.829	503.492
	La	14.177	15.620	23.989	26.389	40.274	16.737	32.936
	Ce	28.363	31.494	46.400	50.585	80.392	34.769	62.576
	Pr	3.478	3.878	5.953	6.446	9.989	4.312	7.018
	Nd	13.461	15.110	22.512	24.210	38.353	16.944	25.119
	Sm	3.155	3.475	5.191	5.655	8.574	4.024	5.251
	Eu	1.373	1.380	1.699	1.791	2.441	1.410	1.376
	Gd	3.646	4.087	6.646	7.196	9.856	4.994	6.376
	Tb	0.540	0.604	0.965	1.036	1.418	0.729	0.906
	Dy	2.987	3.395	5.185	5.625	7.697	4.117	5.132
	Ho	0.597	0.675	1.016	1.114	1.508	0.822	1.040
	Er	1.678	1.911	2.830	3.090	4.217	2.343	2.995
	Tm	0.234	0.261	0.391	0.431	0.573	0.321	0.418
	Yb	1.478	1.674	2.374	2.671	3.565	2.027	2.726
	Lu	0.202	0.229	0.316	0.357	0.474	0.282	0.383
	Hf	2.298	2.524	2.940	3.088	6.035	2.851	4.367
	Ta	0.308	0.312	0.456	0.471	0.673	0.318	0.671
	W	0.226	0.260	0.232	0.221	0.876	0.412	0.445
	Pb	4.926	4.401	5.884	6.417	8.732	4.887	12.533
	Th	1.254	1.405	2.087	2.204	4.022	1.490	8.993
	U	0.208	0.232	0.325	0.345	0.597	0.236	1.881

Appendix 4 Major, minor and trace element geochemistry data									
Phase 2, Bivane Subgroup - White River Section, Northern Region									
	XRF	CG01/22	CG01/23	CG01/25	CG01/26	CG01/27	CG01/28	CG01/29	CG01/30
wt%	SiO_2	55.35	55.7	71.8	52.68	53.55	69.09	53.98	52.85
	Al_2O_3	15.78	15.15	11.38	13.45	13.03	12.55	14.06	14.56
	Fe_2O_3	1.14	1.1	0.75	1.28	1.2	0.86	1.13	1.19
	FeO	9.25	8.88	6.07	10.37	9.75	6.95	9.13	9.61
	MnO	0.1905	0.1714	0.0874	0.1871	0.1916	0.119	0.1667	0.1684
	MgO	6.76	7.35	0.38	8.42	8.88	0.56	7.94	8.6
	CaO	6.22	6.28	1.38	11.11	10.36	4.5	9.14	8.71
	Na_2O	3.44	3.66	2.14	1.39	1.7	0.93	2.46	3.01
	K_2O	0.99	0.92	4.87	0.19	0.44	3.44	0.94	0.43
	TiO_2	0.6569	0.6856	0.4881	0.6438	0.5965	0.6701	0.7093	0.697
	P_2O_5	0.12	0.12	0.09	0.1	0.09	0.16	0.11	0.11
	Cr_2O_3	0.0569	0.0525	-0.0087	0.1114	0.1296	-0.0068	0.0858	0.0953
	NiO	0.0162	0.017	0.0034	0.0307	0.0336	-0.0004	0.0279	0.0323
ppm	Y	17.9	19.8	40.3	20.1	18.25	43.65	20.95	18.85
	Rb	24.3	22.9	156.2	5.05	9.45	137.4	20.3	9.55
	Zr	91.55	96.65	271.45	81.9	75.55	292.15	87.7	84.1
	Sr	180.65	248.85	73	347.2	201.45	41.9	261	248.85
	Zn	92.8	84.9	84.7	79.9	86.5	87.5	83	90.1
	Cu	20.2	36.7	3.5	55.7	56.3	0	26.1	14.2
	Ni	128.7	129.5	11	231.1	257.2	0	214.5	236.9
	Cr	49.9	476.1	1.2	914.4	1045.6	0	715.8	811.1
	V	195.9	204.1	9.6	230.5	230.4	10.8	187.8	191
	Sc	28.9	31.2	7.7	39	36.6	10.5	28.5	31.8
	K	7631.2	7607.7	33960.5	1498.7	3517.4	25711.2	7577.1	3328.7
	S	107.8	127.4	524	398.7	245.6	85.2	146.3	293
	P	446.8	516.2	508.8	360.8	414.4	761.4	477.7	397
	Co	46.4	53	9.1	50.3	54.8	7.5	49.4	54.5
	ICP-MS	CG01/22	CG01/23	CG01/25	CG01/26	CG01/27	CG01/28	CG01/29	CG01/30
ppm	Nb	4.115	4.385	15.649	3.695	3.377	17.497	4.091	3.957
	Ba	258.672	255.704	554.421	73.169	122.668	349.249	237.804	138.319
	La	12.464	13.620	53.500	10.798	9.765	49.134	12.143	10.045
	Ce	23.980	26.168	94.142	21.358	19.394	89.351	23.224	19.806
	Pr	2.914	3.179	10.524	2.641	2.398	10.181	2.832	2.598
	Nd	10.752	11.811	34.625	9.913	9.153	34.431	10.770	10.233
	Sm	2.532	2.788	6.769	2.360	2.232	6.849	2.649	2.506
	Eu	0.874	1.063	1.307	1.035	0.763	1.397	0.912	0.918
	Gd	3.109	3.420	7.771	3.051	2.873	8.387	3.364	3.188
	Tb	0.485	0.534	1.111	0.489	0.467	1.228	0.542	0.520
	Dy	2.822	3.147	6.183	2.903	2.752	6.861	3.211	3.108
	Ho	0.573	0.650	1.267	0.603	0.574	1.395	0.660	0.625
	Er	1.568	1.801	3.596	1.670	1.589	3.878	1.805	1.772
	Tm	0.225	0.259	0.516	0.242	0.227	0.559	0.258	0.241
	Yb	1.370	1.603	3.211	1.507	1.420	3.461	1.573	1.493
	Lu	0.187	0.218	0.459	0.205	0.191	0.484	0.212	0.190
	Hf	1.586	1.743	5.684	1.479	1.358	6.297	1.426	1.320
	Ta	0.244	0.244	1.016	0.196	0.179	2.845	0.226	0.353
	W	0.213	0.214	0.444	0.220	0.200	0.604	0.196	0.234
	Pb	4.187	3.709	15.897	4.372	2.716	13.455	3.381	3.859
	Th	1.237	1.317	13.646	1.100	1.025	13.470	1.467	1.357
	U	0.223	0.244	3.334	0.212	0.195	3.018	0.366	0.328

Appendix 4 Major, minor and trace element geochemistry data									
Phase 2, Bivane Subgroup - White River Section, Northern Region									
XRF		CG01/31	CG01/32	CG01/33	CG01/34	CG01/35	CG01/36	CG01/37	CG01/38
wt%	SiO_2	72.65	54.62	54.44	71.69	55.56	54.21	70.36	54.04
	Al_2O_3	11.88	13.22	13.75	11.22	12.88	15.56	14.78	14.01
	Fe_2O_3	0.56	1.04	1.2	0.64	1.07	1.25	0.39	1.15
	FeO	4.52	8.46	9.72	5.19	8.69	10.1	3.12	9.32
	MnO	0.0793	0.1776	0.2011	0.0939	0.2135	0.1713	0.0476	0.1689
	MgO	0.55	9.35	6.69	2.49	9.25	4.84	0.93	8.9
	CaO	2.3	8.84	11.07	4.97	7.84	9.48	1.38	6.71
	Na_2O	2.03	3.11	2.01	1.74	2.02	1.62	4.35	4.29
	K_2O	3.94	0.62	0.31	0.87	1.54	1.11	3.84	0.39
	TiO_2	0.5385	0.5692	0.6562	0.5514	0.562	0.9597	0.4904	0.6773
	P_2O_5	0.11	0.07	0.1	0.11	0.07	0.17	0.16	0.12
	Cr_2O_3	-0.0077	0.1015	0.0703	0.0175	0.1044	0.0139	0	0.0861
	NiO	-0.0002	0.0381	0.0198	0.0103	0.0384	0.0109	0.0018	0.0276
ppm	Y	36.65	17.3	17.95	30.05	15.85	28.45	22.7	22.35
	Rb	113.1	11.3	9.15	16.15	29.75	28.45	87.35	7.1
	Zr	258.25	57.8	79.3	219.6	55.8	124.9	252.75	93.15
	Sr	88.5	237.05	295	268.95	84.75	280.8	237.65	145.65
	Zn	66.8	75.4	81.9	49.1	78.5	99.7	62.6	95.1
	Cu	0	50.8	52.4	78.5	3.4	42.1	6.8	46.8
	Ni	1.2	298.6	151.2	80.5	292.1	72.5	4.8	197.8
	Cr	4.1	904.9	690.8	242.1	918.8	123.6	5.7	732.9
	V	18.6	227.8	223.7	85	227	157.4	30.4	240.5
	Sc	10.5	45.9	37.7	16.1	44.3	20.3	6.4	38.8
	K	27783.3	4666.3	2684.3	6469.5	9864.9	8683	27209.5	2915.7
	S	1476.7	176.8	82.9	254.9	15.3	1519.6	4.6	135.2
	P	449.7	208.5	409.3	382.4	220.7	585	628.7	403
	Co	3.6	54	54.5	21.6	60.2	73.1	5.2	66.6
ICP-MS		CG01/31	CG01/32	CG01/33	CG01/34	CG01/35	CG01/36	CG01/37	CG01/38
ppm	Nb	15.017	2.890	3.527	12.467	2.776	6.209	13.742	4.119
	Ba	472.205	349.028	92.672	198.864	175.562	221.232	641.281	145.962
	La	62.024	8.550	9.362	38.454	8.355	16.580	55.643	12.244
	Ce	107.857	16.579	18.499	69.394	15.410	32.659	100.300	23.767
	Pr	12.881	2.089	2.408	8.188	1.996	3.966	11.195	2.889
	Nd	43.856	7.867	9.296	27.632	7.425	14.555	36.092	10.750
	Sm	7.575	1.980	2.228	5.228	1.785	3.615	6.384	2.616
	Eu	1.439	0.704	0.785	1.213	0.616	1.187	1.295	1.019
	Gd	8.399	2.464	2.891	6.031	2.293	4.734	6.514	3.444
	Tb	1.145	0.403	0.467	0.860	0.380	0.725	0.785	0.525
	Dy	6.020	2.464	2.796	4.828	2.340	4.160	3.763	3.070
	Ho	1.174	0.508	0.565	0.953	0.480	0.852	0.664	0.631
	Er	3.423	1.464	1.618	2.784	1.410	2.422	1.754	1.817
	Tm	0.466	0.205	0.225	0.390	0.197	0.333	0.211	0.252
	Yb	2.981	1.293	1.447	2.538	1.299	2.094	1.269	1.591
	Lu	0.403	0.164	0.189	0.344	0.172	0.284	0.174	0.218
	Hf	5.525	1.026	1.383	4.439	1.029	2.417	5.147	1.800
	Ta	1.025	0.227	0.201	0.822	0.172	0.495	0.964	0.310
	W	0.565	0.236	0.405	0.307	0.168	0.401	0.447	0.288
	Pb	21.488	5.013	2.690	11.924	5.500	6.230	21.514	3.331
	Th	12.359	1.536	0.946	10.398	1.501	2.569	15.560	1.254
	U	3.378	0.283	0.162	2.817	0.261	0.678	1.851	0.210

Appendix 4 Major, minor and trace element geochemistry data

Phase 2, Bivane Subgroup - White River Section, Northern Region

XRF		CG01/39	CG01/40	CG01/41	CG01/82	CG01/83	CG01/84	CG01/85	CG01/86
wt%	SiO_2	70.38	64.44	56.03	73.54	73.37	74.42	61.53	61.24
	Al_2O_3	12.64	12.2	15.54	12.02	11.79	11.64	14.87	13.55
	Fe_2O_3	0.66	1.39	1.17	0.65	0.61	0.52	0.87	1.3
	FeO	5.38	11.25	9.47	5.3	4.94	4.17	7.01	10.51
	MnO	0.1104	0.1409	0.1794	0.0694	0.0678	0.0465	0.1276	0.1542
	MgO	0.68	1.14	5.25	0.42	0.38	0.44	4.28	1.29
	CaO	2.82	3.5	9.32	1.36	1.46	1.25	4.18	6.52
	Na_2O	1.93	2.42	1.53	1.66	1.94	1.65	3.75	1.69
	K_2O	4.17	1.81	0.39	4.31	4.15	4.57	2.18	1.78
	TiO_2	0.7272	1.1608	0.7972	0.5118	0.4973	0.499	0.6514	1.1869
	P_2O_5	0.18	0.41	0.14	0.08	0.08	0.08	0.16	0.23
	Cr_2O_3	0	0	0.0133	0.008	0.0059	0.006	0.0234	0
	NiO	0.0021	0.0004	0.0095	0.0002	0.0015	0.0003	0.005	0
ppm	Y	48.35	35.15	20.9	43.45	42.5	39.25	23.75	32.1
	Rb	112.5	41.15	7.6	134.75	104.9	113.5	49.1	53.3
	Zr	338.3	196.8	113.5	288.4	290.9	286.85	170.8	177.7
	Sr	135.05	161.8	376.2	100.35	100.7	116.5	164.6	355.2
	Zn	93.6	110.5	89.8	97.3	78.4	58.5	89.8	102.5
	Cu	1.1	25.4	27.3	10.2	7.5	13.9	0	75.4
	Ni	1.2	0.1	58.8	0	4.3	0	38.5	7
	Cr	0	3.4	95.6	0	0.2	0	118	12.5
	V	9.2	48.3	192.2	8.1	1.8	5.9	135.9	193.4
	Sc	10.3	24.2	25.5	9.6	8.1	7.5	21	26.4
	K	30798.8	12939.5	3049.3	30197.2	29266.7	31265.2	17274.2	14278.5
	S	36.3	919.5	60.8	70.5	141.7	566.2	7.2	218.8
	P	1066.9	1632.7	482	391.5	413.4	431.4	647.6	901.9
	Co	7.1	24	56.7	1	10	1.1	39.1	41.5
ICP-MS		CG01/39	CG01/40	CG01/41	CG01/82	CG01/83	CG01/84	CG01/85	CG01/86
ppm	Nb	19.019	11.853	5.077	n.p.	n.p.	16.327	n.p.	n.p.
	Ba	623.768	546.281	218.486	n.p.	n.p.	614.337	n.p.	n.p.
	La	55.725	38.850	14.392	n.p.	n.p.	48.605	n.p.	n.p.
	Ce	104.671	68.709	28.453	n.p.	n.p.	95.546	n.p.	n.p.
	Pr	12.079	8.287	3.400	n.p.	n.p.	10.017	n.p.	n.p.
	Nd	40.542	29.779	12.355	n.p.	n.p.	32.440	n.p.	n.p.
	Sm	8.070	6.012	2.925	n.p.	n.p.	6.582	n.p.	n.p.
	Eu	1.591	1.421	0.980	n.p.	n.p.	1.223	n.p.	n.p.
	Gd	9.489	7.176	3.659	n.p.	n.p.	7.453	n.p.	n.p.
	Tb	1.339	1.002	0.561	n.p.	n.p.	1.037	n.p.	n.p.
	Dy	7.445	5.534	3.209	n.p.	n.p.	5.851	n.p.	n.p.
	Ho	1.489	1.109	0.655	n.p.	n.p.	1.140	n.p.	n.p.
	Er	4.323	3.146	1.838	n.p.	n.p.	3.270	n.p.	n.p.
	Tm	0.606	0.437	0.258	n.p.	n.p.	0.466	n.p.	n.p.
	Yb	3.877	2.773	1.654	n.p.	n.p.	2.979	n.p.	n.p.
	Lu	0.543	0.389	0.230	n.p.	n.p.	0.414	n.p.	n.p.
	Hf	7.236	4.445	2.000	n.p.	n.p.	6.598	n.p.	n.p.
	Ta	1.297	0.882	0.375	n.p.	n.p.	1.251	n.p.	n.p.
	W	0.448	0.679	0.279	n.p.	n.p.	0.481	n.p.	n.p.
	Pb	18.271	13.231	5.465	n.p.	n.p.	27.530	n.p.	n.p.
	Th	14.843	9.003	1.839	n.p.	n.p.	14.352	n.p.	n.p.
	U	3.241	2.097	0.248	n.p.	n.p.	3.420	n.p.	n.p.

Appendix 4 Major, minor and trace element geochemistry data									
Phase 2, Bivane Subgroup - White River Section, Northern Region									
	XRF	CG01/87	CG01/88	CG01/89	CG01/90	CG01/91	CG01/92	CG01/93	CG01/94
wt%	SiO_2	53.21	54.19	52.71	53.62	58.41	64.27	70.98	55.96
	Al_2O_3	17.07	13.47	14.83	15.56	16.26	12.7	12.19	15.36
	Fe_2O_3	1.2	1.15	1.19	1.16	1.23	1.28	0.74	1.42
	FeO	9.72	9.33	9.65	9.39	9.97	10.37	5.97	11.5
	MnO	0.171	0.1759	0.1716	0.1807	0.1619	0.0881	0.0725	0.1904
	MgO	6.97	8.53	8.02	7.88	3.7	0.62	0.37	4.15
	CaO	7.42	9.21	9.54	7.69	4.56	3.94	1.71	5.5
	Na_2O	3.25	2.14	2.12	2.38	3.32	2.41	2.8	2.75
	K_2O	0.22	0.29	0.47	1.45	1.05	2.67	3.84	1.35
	TiO_2	0.7007	0.6086	0.7259	0.7252	0.8504	1.105	0.64	1.1487
	P_2O_5	0.13	0.1	0.12	0.11	0.17	0.42	0.16	0.2
	Cr_2O_3	0.0627	0.1224	0.0953	0.087	0.019	0.007	0.0047	0.0345
	NiO	0.0141	0.0269	0.0271	0.0244	0.0108	0	0	0.0085
ppm	Y	21.05	17.4	21	22.4	22.1	38.3	44.6	34.6
	Rb	8.8	8.9	12.2	38.1	30.9	67.35	126.6	35.5
	Zr	104.8	85.4	97.5	96.9	118.1	214.2	308.8	150.8
	Sr	180.6	167.3	208.1	220	241.2	238.3	94.75	249.9
	Zn	97.5	83	85.9	84	102.6	115.8	84.5	116.7
	Cu	6	38.7	48.2	82.5	47.1	8	3.8	47.9
	Ni	121.8	229.5	218.3	207.6	94	0	0	80.8
	Cr	405.4	845.9	679.3	613.6	116.1	0	0	166.2
	V	223.2	221.2	183.3	183.5	143.5	10.9	11.6	184.4
	Sc	32.7	35.3	28.2	30.7	20.7	20.7	11.6	24.3
	K	1790.5	2399.6	3748.8	10679.8	7983.3	21216.3	28021.5	9628.3
	S	18.4	96.3	92.6	151.1	69.2	322	113.7	13.8
	P	556.4	466.1	577.4	481.4	679.7	1849.7	789.2	883.4
	Co	63.7	64.5	58.4	62.2	52.9	30.9	3.6	60.5
	ICP-MS	CG01/87	CG01/88	CG01/89	CG01/90	CG01/91	CG01/92	CG01/93	CG01/94
ppm	Nb	n.p.	3.752	n.p.	4.769	n.p.	13.017	17.159	n.p.
	Ba	n.p.	85.735	n.p.	280.556	n.p.	594.631	512.452	n.p.
	La	n.p.	10.429	n.p.	12.746	n.p.	41.184	50.010	n.p.
	Ce	n.p.	20.984	n.p.	25.258	n.p.	75.578	95.671	n.p.
	Pr	n.p.	2.646	n.p.	3.035	n.p.	8.820	10.417	n.p.
	Nd	n.p.	10.212	n.p.	11.509	n.p.	31.961	34.951	n.p.
	Sm	n.p.	2.422	n.p.	2.808	n.p.	6.399	6.964	n.p.
	Eu	n.p.	0.815	n.p.	1.074	n.p.	1.622	1.404	n.p.
	Gd	n.p.	2.933	n.p.	3.414	n.p.	7.329	8.063	n.p.
	Tb	n.p.	0.467	n.p.	0.542	n.p.	1.041	1.137	n.p.
	Dy	n.p.	2.750	n.p.	3.164	n.p.	5.802	6.469	n.p.
	Ho	n.p.	0.554	n.p.	0.652	n.p.	1.135	1.283	n.p.
	Er	n.p.	1.571	n.p.	1.828	n.p.	3.245	3.727	n.p.
	Tm	n.p.	0.222	n.p.	0.255	n.p.	0.456	0.535	n.p.
	Yb	n.p.	1.403	n.p.	1.631	n.p.	2.868	3.327	n.p.
	Lu	n.p.	0.193	n.p.	0.219	n.p.	0.402	0.459	n.p.
	Hf	n.p.	1.748	n.p.	1.743	n.p.	4.774	6.878	n.p.
	Ta	n.p.	0.208	n.p.	0.424	n.p.	0.993	1.213	n.p.
	W	n.p.	0.166	n.p.	0.137	n.p.	0.367	0.553	n.p.
	Pb	n.p.	3.141	n.p.	5.467	n.p.	10.404	16.425	n.p.
	Th	n.p.	1.212	n.p.	1.744	n.p.	10.440	14.225	n.p.
	U	n.p.	0.218	n.p.	0.400	n.p.	2.509	3.120	n.p.

Appendix 4 Major, minor and trace element geochemistry data									
Phase 2, Bivane Subgroup - White River Section, Northern Region									
	XRF	CG01/140	CG01/141	CG01/142	CG01/143	CG01/144	CG01/147	CG01/148	CG01/149
wt%	SiO_2	64.22	53.29	52.55	54.9	54.57	63.61	53.51	54.4
	Al_2O_3	12.89	13.63	13.5	17.5	16.47	13.46	15.19	14.85
	Fe_2O_3	1.11	1.42	1.46	1.15	1.47	1.38	1.21	1.17
	FeO	9.02	11.47	11.82	9.31	11.94	11.19	9.78	9.47
	MnO	0.1392	0.2578	0.2221	0.1519	0.173	0.1242	0.1738	0.1987
	MgO	1.2	5.81	5.55	4.15	4.31	0.87	7.78	7.33
	CaO	3.76	8.36	9.17	8.52	4.77	2.04	8.62	8.35
	Na_2O	3.11	2.54	2.3	2.86	3.38	2.11	2.37	2.63
	K_2O	2.77	1.53	1.5	0.16	1.12	3.14	0.36	0.32
	TiO_2	0.9754	1.4548	1.4305	0.9295	1.1247	1.2873	0.7224	0.6862
	P_2O_5	0.22	0.13	0.13	0.19	0.21	0.4	0.12	0.12
	Cr_2O_3	0.0059	0.0256	0.0236	0.028	0.027	0.006	0.0911	0.0923
	NiO	0.0009	0.0063	0.006	0.0104	0.0125	0	0.0255	0.0251
ppm	Y	31.75	36.2	35.1	23.6	29.75	38.75	21.3	21.4
	Rb	89.55	58.9	67.5	6.05	36	120.65	8	8.9
	Zr	193.8	115.35	114.8	138.65	165.35	215.15	94	90.9
	Sr	185.3	124.9	161.8	390.75	275.4	79.45	229.3	201.6
	Zn	96.1	208.2	112.2	110	121.9	94.3	92.9	92.6
	Cu	16.6	96.5	84.9	0	15.6	7.4	21.7	38.3
	Ni	0	62.9	57	87.6	100.9	8.2	215.4	217.6
	Cr	0	112.7	100.7	152.7	168.2	0	672	682.9
	V	210.2	400.7	387.9	154.7	185.4	89.9	194.2	187.3
	Sc	28	50.2	48.6	24.3	26.6	26.4	30.9	30.5
	K	21567.5	11433	11308.6	1229.4	8442.3	24808.7	2682.7	2553.9
	S	93.6	1591.8	1174.9	10	51.7	44.5	43.8	0
	P	951.5	510.6	642.8	859.8	967.8	1905.5	537.3	540.6
	Co	36.4	46.9	43.7	54.1	62.2	30.9	67.3	62.7
	ICP-MS	CG01/140	CG01/141	CG01/142	CG01/143	CG01/144	CG01/147	CG01/148	CG01/149
ppm	Nb	n.p.	6.205	6.312	n.p.	n.p.	n.p.	4.395	n.p.
	Ba	n.p.	325.487	187.164	n.p.	n.p.	n.p.	116.857	n.p.
	La	n.p.	9.748	9.658	n.p.	n.p.	n.p.	11.090	n.p.
	Ce	n.p.	21.471	21.214	n.p.	n.p.	n.p.	23.039	n.p.
	Pr	n.p.	2.850	2.834	n.p.	n.p.	n.p.	2.851	n.p.
	Nd	n.p.	12.146	11.997	n.p.	n.p.	n.p.	11.265	n.p.
	Sm	n.p.	3.535	3.432	n.p.	n.p.	n.p.	2.677	n.p.
	Eu	n.p.	1.051	1.120	n.p.	n.p.	n.p.	0.951	n.p.
	Gd	n.p.	4.679	4.577	n.p.	n.p.	n.p.	3.328	n.p.
	Tb	n.p.	0.805	0.805	n.p.	n.p.	n.p.	0.534	n.p.
	Dy	n.p.	5.028	4.946	n.p.	n.p.	n.p.	3.201	n.p.
	Ho	n.p.	1.084	1.070	n.p.	n.p.	n.p.	0.647	n.p.
	Er	n.p.	3.149	3.084	n.p.	n.p.	n.p.	1.857	n.p.
	Tm	n.p.	0.467	0.461	n.p.	n.p.	n.p.	0.265	n.p.
	Yb	n.p.	3.111	3.027	n.p.	n.p.	n.p.	1.668	n.p.
	Lu	n.p.	0.449	0.442	n.p.	n.p.	n.p.	0.231	n.p.
	Hf	n.p.	2.886	2.726	n.p.	n.p.	n.p.	1.931	n.p.
	Ta	n.p.	0.454	0.450	n.p.	n.p.	n.p.	0.269	n.p.
	W	n.p.	0.252	0.198	n.p.	n.p.	n.p.	0.202	n.p.
	Pb	n.p.	7.683	8.028	n.p.	n.p.	n.p.	3.590	n.p.
	Th	n.p.	2.402	2.457	n.p.	n.p.	n.p.	1.620	n.p.
	U	n.p.	0.602	0.621	n.p.	n.p.	n.p.	0.381	n.p.

Appendix 4 Major, minor and trace element geochemistry data										
Phase 2, Bivane Subgroup - White River Section, Northern Region										
XRF		CG01/150	CG01/151	CG01/153	CG01/154	CG01/158	CG01/160	CG01/161	CG01/162	CG01/163
wt%	SiO_2	51.84	54.39	55.53	53.4	63.54	53.07	72.58	53.29	72.49
	Al_2O_3	13.7	15.53	15.16	15.08	13.31	15.4	11.67	13.19	11.86
	Fe_2O_3	1.2	1.14	1.16	1.16	1.22	1.18	0.63	1.2	0.69
	FeO	9.74	9.26	9.37	9.38	9.88	9.58	5.09	9.72	5.55
	MnO	0.1903	0.1749	0.1601	0.1732	0.1313	0.178	0.0693	0.1931	0.0687
	MgO	9.07	5.87	6.04	6.49	1.39	6.77	0.28	8.89	0.35
	CaO	10.3	10.08	8.5	9.65	4.25	9.24	1.48	10.59	1.68
	Na_2O	2.13	1.66	2.55	2.28	2.5	2.81	2.8	1.66	2.21
	K_2O	0.49	0.79	0.77	1.32	2.13	0.6	4.28	0.57	4.34
	TiO_2	0.6188	0.7556	0.7811	0.7991	1.1453	0.8131	0.5056	0.6073	0.526
	P_2O_5	0.1	0.14	0.14	0.14	0.35	0.14	0.09	0.1	0.09
	Cr_2O_3	0.1309	0.0246	0.0297	0.0549	0.0069	0.062	0.0045	0.1235	0.0052
	NiO	0.0288	0.0054	0.0065	0.014	0	0.0169	0.0003	0.0248	0.0007
ppm	Y	19.3	21.9	21.35	23.6	35.15	23.3	38.9	18.85	34.9
	Rb	15.3	19.8	18.2	31.1	69.9	10.95	137.8	15.15	163.5
	Zr	84.7	107.9	112.15	112.5	211.15	106.3	273.1	80.1	289.9
	Sr	207.4	286.3	221	294.6	251.85	264.05	111.9	235.45	102.4
	Zn	87.4	118.3	90.5	84.9	108.1	84.6	63.7	84	77
	Cu	57.9	22.6	3.1	36.1	1.7	30	12.1	65.7	3.7
	Ni	244.1	57.3	59	116.5	2.3	121.1	0	201	0
	Cr	920.5	147.2	140.1	376.1	0	428.4	0	891.2	0
	V	234.4	178.6	183.7	194.3	88.7	217.7	5.3	234.9	5.2
	Sc	37	28.9	30.7	28.2	16.4	31.8	8.7	37.9	8.9
	K	4117.9	5984.4	5967.3	10442.7	17269.9	4073.6	30958.3	4466.5	30992.2
	S	14.7	566.1	96.8	36	480.6	71.5	551.6	71.9	184.3
	P	513.7	550.9	650.1	542.8	1473	565.8	450.1	427.8	427.5
	Co	69.3	56.3	53	57.4	37.9	58.7	4.1	64.7	2
ICP-MS		CG01/150	CG01/151	CG01/153	CG01/154	CG01/158	CG01/160	CG01/161	CG01/162	CG01/163
ppm	Nb	n.p.	4.959	n.p.	n.p.	n.p.	5.062	16.717	3.556	17.322
	Ba	n.p.	170.955	n.p.	n.p.	n.p.	108.314	513.233	180.074	529.802
	La	n.p.	12.408	n.p.	n.p.	n.p.	12.279	47.147	9.224	47.406
	Ce	n.p.	25.667	n.p.	n.p.	n.p.	25.505	84.487	19.034	83.855
	Pr	n.p.	3.160	n.p.	n.p.	n.p.	3.182	9.915	2.369	9.751
	Nd	n.p.	12.240	n.p.	n.p.	n.p.	12.545	34.992	9.368	33.837
	Sm	n.p.	2.863	n.p.	n.p.	n.p.	2.931	6.473	2.226	6.267
	Eu	n.p.	0.992	n.p.	n.p.	n.p.	0.942	1.221	0.813	1.218
	Gd	n.p.	3.470	n.p.	n.p.	n.p.	3.640	7.415	2.784	7.134
	Tb	n.p.	0.546	n.p.	n.p.	n.p.	0.574	1.053	0.449	0.987
	Dy	n.p.	3.199	n.p.	n.p.	n.p.	3.384	5.866	2.684	5.416
	Ho	n.p.	0.642	n.p.	n.p.	n.p.	0.680	1.165	0.549	1.069
	Er	n.p.	1.810	n.p.	n.p.	n.p.	1.936	3.423	1.588	3.118
	Tm	n.p.	0.253	n.p.	n.p.	n.p.	0.263	0.478	0.220	0.438
	Yb	n.p.	1.598	n.p.	n.p.	n.p.	1.665	3.109	1.431	2.896
	Lu	n.p.	0.207	n.p.	n.p.	n.p.	0.217	0.443	0.196	0.407
	Hf	n.p.	1.816	n.p.	n.p.	n.p.	1.657	6.334	1.523	6.580
	Ta	n.p.	0.272	n.p.	n.p.	n.p.	0.284	1.263	0.193	1.315
	W	n.p.	0.177	n.p.	n.p.	n.p.	0.242	0.257	0.166	0.276
	Pb	n.p.	56.578	n.p.	n.p.	n.p.	3.777	24.523	3.842	17.096
	Th	n.p.	1.350	n.p.	n.p.	n.p.	1.336	14.210	1.062	14.706
	U	n.p.	0.206	n.p.	n.p.	n.p.	0.205	3.343	0.168	3.466

Appendix 4 Major, minor and trace element geochemistry data									
Phase 3.1, Bivane Subgroup - White River Section, Northern Region									
	XRF	CG01/114	CG01/115	CG01/116	CG01/117	CG01/118	CG01/119	CG01/120	CG01/121
wt%	SiO_2	68.73	72.81	61.97	60.55	59.89	69.21	66.91	68.54
	Al_2O_3	13.78	12.41	15.8	17.77	15.61	13.4	13.18	13.11
	Fe_2O_3	0.88	0.63	1.03	1.05	1.58	0.78	1.14	1
	FeO	7.12	5.07	8.32	8.54	12.77	6.31	9.19	8.12
	MnO	0.113	0.0711	0.1406	0.1259	0.146	0.084	0.112	0.1098
	MgO	1.47	0.44	1.32	0.95	1.09	0.52	0.74	0.54
	CaO	1.2	2.18	3.82	2.72	2.15	1.43	1.21	1.96
	Na_2O	4.54	3.05	3.85	4.16	1.88	2.64	2.17	2.45
	K_2O	0.51	2.34	2.11	2.14	3.11	3.96	3.92	2.76
	TiO_2	0.937	0.6233	1.271	1.2692	1.1008	0.8336	0.8462	0.9006
	P_2O_5	0.21	0.15	0.31	0.27	0.25	0.19	0.19	0.19
	Cr_2O_3	0.0032	0.0014	0.0091	0.0106	0.0086	0.0073	0.004	0.0047
	NiO	0.0015	0.001	0.0021	0	0	0.0021	0	0.0001
ppm	Y	73.6	57.35	44.05	64.85	62.5	36.2	35.35	32.9
	Rb	27.25	86.25	83.4	99.8	148.45	99.5	142.15	107.6
	Zr	576.65	379.15	234.75	438.95	376.45	238.5	221.15	214.3
	Sr	93.25	199.6	170.2	152.3	77.85	161.95	107.15	146.9
	Zn	57.6	35.4	124.8	105.8	167.3	90	103.3	90.9
	Cu	0	13.5	39.2	0	8.2	16.4	0	11.5
	Ni	3.7	0.3	24.4	0	0	0	0	1
	Cr	0	0	14.2	0	0	0	0	0
	V	35.7	37	315.6	117.4	93	97.6	140.2	176.6
	Sc	16.5	10.2	30.2	22.2	20.2	20.8	22.4	24.2
	K	3755.8	17736.7	16391.5	16455.1	23486.9	29545.6	29755	20955
	S	587.4	864.1	130.4	126.6	110.3	101.3	64.6	81.3
	P	1017.5	758.2	1298.5	1310.1	1104.3	822.3	801.7	809.2
	Co	21.4	12.4	58.4	23.7	33.4	26.6	26.8	30.7
	ICP-MS	CG01/114	CG01/115	CG01/116	CG01/117	CG01/118	CG01/119	CG01/120	CG01/121
ppm	Nb	n.p.	n.p.	n.p.	n.p.	23.805	n.p.	n.p.	13.471
	Ba	n.p.	n.p.	n.p.	n.p.	324.951	n.p.	n.p.	428.538
	La	n.p.	n.p.	n.p.	n.p.	48.012	n.p.	n.p.	37.312
	Ce	n.p.	n.p.	n.p.	n.p.	88.707	n.p.	n.p.	68.247
	Pr	n.p.	n.p.	n.p.	n.p.	10.749	n.p.	n.p.	7.905
	Nd	n.p.	n.p.	n.p.	n.p.	39.470	n.p.	n.p.	27.473
	Sm	n.p.	n.p.	n.p.	n.p.	8.189	n.p.	n.p.	5.424
	Eu	n.p.	n.p.	n.p.	n.p.	1.371	n.p.	n.p.	1.245
	Gd	n.p.	n.p.	n.p.	n.p.	10.144	n.p.	n.p.	6.293
	Tb	n.p.	n.p.	n.p.	n.p.	1.566	n.p.	n.p.	0.891
	Dy	n.p.	n.p.	n.p.	n.p.	9.276	n.p.	n.p.	4.884
	Ho	n.p.	n.p.	n.p.	n.p.	1.934	n.p.	n.p.	0.999
	Er	n.p.	n.p.	n.p.	n.p.	5.590	n.p.	n.p.	2.927
	Tm	n.p.	n.p.	n.p.	n.p.	0.812	n.p.	n.p.	0.415
	Yb	n.p.	n.p.	n.p.	n.p.	5.201	n.p.	n.p.	2.718
	Lu	n.p.	n.p.	n.p.	n.p.	0.731	n.p.	n.p.	0.390
	Hf	n.p.	n.p.	n.p.	n.p.	8.870	n.p.	n.p.	5.017
	Ta	n.p.	n.p.	n.p.	n.p.	1.692	n.p.	n.p.	1.035
	W	n.p.	n.p.	n.p.	n.p.	1.029	n.p.	n.p.	0.875
	Pb	n.p.	n.p.	n.p.	n.p.	17.335	n.p.	n.p.	14.216
	Th	n.p.	n.p.	n.p.	n.p.	15.403	n.p.	n.p.	10.277
	U	n.p.	n.p.	n.p.	n.p.	3.841	n.p.	n.p.	2.542

Appendix 4 Major, minor and trace element geochemistry data						
Phase 3.1, Bivane Subgroup - White River Section, Northern Region						
XRF		CG01/136	CG01/137	CG01/139	PG29/2000	PG30/2000
wt%	SiO_2	66.28	43.53	64.19	64.79	66.76
	Al_2O_3	12.74	17.88	13.2	12.85	13.32
	Fe_2O_3	0.91	3.81	1.17	1.06	1.05
	FeO	7.39	30.89	9.44	8.57	8.51
	MnO	0.1268	0.3868	0.1514	0.1359	0.0863
	MgO	0.93	2.34	1.25	0.82	0.73
	CaO	4.49	0.09	2.57	3.86	1.29
	Na_2O	3.57	0	3.32	3.68	3.13
	K_2O	1.76	0.27	3.28	2.77	3.36
	TiO_2	0.8448	0.134	0.9851	0.9174	0.8589
	P_2O_5	0.17	0.03	0.2	0.2	0.18
	Cr_2O_3	0.0053	0.0085	0.0012	0.0038	0.0065
	NiO	0.0004	0	0	0.0003	0.0024
ppm	Y	33	2.4	35.4	34.65	34
	Rb	83.05	16.5	87.8	83.05	136.15
	Zr	201.75	15.2	196.9	213.35	228.6
	Sr	134.2	3.6	208.7	236.85	108.05
	Zn	88.8	307.4	100.5	95.5	125.1
	Cu	10.8	0	12.3	20.3	65.1
	Ni	0	0	0.9	1.2	2.7
	Cr	0	0	0	0	0
	V	159.5	194.1	202.7	170.9	154.5
	Sc	25.6	18.4	26.7	24	25.3
	K	14377.7	1881.4	24543.6	22267.5	26897.1
	S	277.7	37.8	83.1	497.1	632.4
	P	763.2	74.6	862.5	823.2	795.5
	Co	28.9	50.5	38.5	34.5	28.1
ICP-MS		CG01/136	CG01/137	CG01/139	PG29/2000	PG30/2000
ppm	Nb	12.443	1.503	n.p.	12.282	13.338
	Ba	281.275	24.988	n.p.	429.454	513.312
	La	34.530	2.875	n.p.	41.403	49.565
	Ce	62.722	5.349	n.p.	79.169	90.863
	Pr	7.174	0.588	n.p.	7.684	8.706
	Nd	25.281	2.074	n.p.	31.479	34.997
	Sm	4.965	0.427	n.p.	6.513	6.907
	Eu	1.065	0.089	n.p.	1.226	1.423
	Gd	5.841	0.546	n.p.	6.199	6.417
	Tb	0.834	0.083	n.p.	1.039	1.017
	Dy	4.691	0.493	n.p.	6.293	6.069
	Ho	0.956	0.099	n.p.	1.404	1.357
	Er	2.790	0.295	n.p.	3.664	3.552
	Tm	0.399	0.041	n.p.	0.478	0.462
	Yb	2.620	0.269	n.p.	3.110	3.035
	Lu	0.371	0.038	n.p.	0.471	0.455
	Hf	4.736	0.452	n.p.	5.372	5.760
	Ta	0.991	0.121	n.p.	0.765	0.808
	W	0.459	0.069	n.p.	0.832	4.895
	Pb	14.391	1.687	n.p.	14.474	18.963
	Th	9.674	0.916	n.p.	10.685	11.601
	U	2.571	0.258	n.p.	2.624	2.859

Appendix 4 Major, minor and trace element geochemistry data								
Phase 3.2, Bivane Subgroup - White River Section, Northern Region								
	XRF	CG01/74	CG01/75	CG01/77	CG01/78	CG01/79	CGO1/80	CG01/81
wt%	SiO_2	59.25	64.34	78.7	52.56	59.88	56.6	59.32
	Al_2O_3	13.28	18.7	11.51	17.25	14.64	16.04	14.22
	Fe_2O_3	1.41	0.9	0.45	1.83	1.23	1.43	1.17
	FeO	11.44	7.28	3.64	14.78	9.94	11.56	9.45
	MnO	0.1785	0.0728	0.0274	0.2758	0.1523	0.1645	0.1543
	MgO	1.91	0.92	0.54	1.21	4.55	6.22	4.83
	CaO	3.14	0.36	0.09	4.7	3.62	2.3	5.26
	Na_2O	5.06	0	0.01	2.3	4.14	3.72	3.64
	K_2O	1.36	5.5	3.67	2.24	0.27	0.09	0.32
	TiO_2	1.7625	1.264	0.6338	2.0829	1.0577	1.1723	1.0393
	P_2O_5	0.41	0.07	0.05	0.55	0.19	0.21	0.18
	Cr_2O_3	0.0098	0.0231	0.018	0.0118	0.0109	0.0112	0.0127
	NiO	0	0.0054	0.0027	0	0.0021	0.0028	0.002
ppm	Y	56.2	72.1	36.3	75.3	42.5	46.4	43.6
	Rb	62.3	219	155.4	85.2	9.9	4.9	11.5
	Zr	275.1	409.2	237.6	367.2	213.9	237	209
	Sr	221.9	30.8	13.8	105.9	84.7	51.8	74.2
	Zn	131.1	133	67.2	164.2	101.5	125.1	101.6
	Cu	5.7	29	29.5	0	38.5	63.9	41.2
	Ni	0	35.7	15.3	0	23.9	27.7	24.2
	Cr	0	92.4	77	0	0.8	1.8	5.8
	V	181.4	169.4	84.9	329.5	205.3	239.7	203.7
	Sc	33.1	30.9	17.7	44.6	35.5	36.2	34.2
	K	9962.4	41193.3	27337.2	17377.4	1876.5	648.3	2131.8
	S	794.8	179.5	161.4	464.2	93	106.7	16.4
	P	1634.7	301.4	213.4	2632.7	822.9	888.5	875.1
	Co	31.3	33.6	7.6	40.3	46.4	58.7	42.3
	ICP-MS	CG01/74	CG01/75	CG01/77	CG01/78	CG01/79	CGO1/80	CG01/81
ppm	Nb	n.p.	25.539	n.p.	n.p.	n.p.	15.762	15.213
	Ba	n.p.	410.893	n.p.	n.p.	n.p.	70.089	37.592
	La	n.p.	64.605	n.p.	n.p.	n.p.	26.213	30.570
	Ce	n.p.	130.404	n.p.	n.p.	n.p.	54.872	59.542
	Pr	n.p.	14.066	n.p.	n.p.	n.p.	6.634	7.092
	Nd	n.p.	46.439	n.p.	n.p.	n.p.	24.393	25.852
	Sm	n.p.	9.916	n.p.	n.p.	n.p.	5.412	5.221
	Eu	n.p.	1.956	n.p.	n.p.	n.p.	1.170	1.088
	Gd	n.p.	11.504	n.p.	n.p.	n.p.	6.628	6.539
	Tb	n.p.	1.678	n.p.	n.p.	n.p.	1.066	1.016
	Dy	n.p.	9.749	n.p.	n.p.	n.p.	6.406	6.150
	Ho	n.p.	2.008	n.p.	n.p.	n.p.	1.327	1.269
	Er	n.p.	5.958	n.p.	n.p.	n.p.	3.885	3.760
	Tm	n.p.	0.870	n.p.	n.p.	n.p.	0.580	0.557
	Yb	n.p.	5.588	n.p.	n.p.	n.p.	3.770	3.632
	Lu	n.p.	0.798	n.p.	n.p.	n.p.	0.537	0.515
	Hf	n.p.	9.709	n.p.	n.p.	n.p.	5.076	4.803
	Ta	n.p.	1.843	n.p.	n.p.	n.p.	1.077	1.032
	W	n.p.	3.119	n.p.	n.p.	n.p.	1.167	0.720
	Pb	n.p.	16.246	n.p.	n.p.	n.p.	15.462	10.648
	Th	n.p.	16.081	n.p.	n.p.	n.p.	9.347	8.713
	U	n.p.	3.767	n.p.	n.p.	n.p.	1.986	1.877

Appendix 4 Major, minor and trace element geochemistry data						
Phase 4, Bivane Subgroup - White River Section, Northern Region						
	XRF	CG01/9	CG01/10	CG01/11	PG27/2000	PG28/2000
wt%	SiO_2	72.99	72.87	73.12	72.84	72.67
	Al_2O_3	11.8	11.86	11.99	11.64	11.69
	Fe_2O_3	0.55	0.54	0.63	0.55	0.55
	FeO	4.42	4.36	5.1	4.45	4.44
	MnO	0.0658	0.0684	0.0641	0.0713	0.0765
	MgO	0.46	0.32	0.23	0.44	0.34
	CaO	2.02	1.4	1.06	1.84	1.86
	Na_2O	3.05	3.33	3.25	2.99	3.78
	K_2O	3.7	3.9	3.61	3.82	3.22
	TiO_2	0.5022	0.5153	0.513	0.508	0.5135
	P_2O_5	0.09	0.09	0.11	0.09	0.1
	Cr_2O_3	-0.0089	-0.0107	-0.0078	0.0055	0.0073
	NiO	-0.0009	-0.0003	-0.0003	0.001	0.0026
ppm	Y	36.15	37	39.05	35.8	35.2
	Rb	186.35	119.45	144	156.65	113.8
	Zr	229.75	250.8	247.1	240.5	230.8
	Sr	210.6	107.7	117.7	194.55	112.9
	Zn	71.8	68.5	75.2	69.2	65.5
	Cu	3.4	3.1	4.4	10.8	18.9
	Ni	0	0.5	0.8	0.5	0
	Cr	4.7	1.2	0.2	0	0
	V	8.5	12.5	16.9	9.3	10.2
	Sc	6.5	11.6	10.6	6.3	10.4
	K	28167.5	29065.4	25703.3	29077.6	24833.6
	S	198.1	152	229	95.3	51.4
	P	518.2	522.4	530	501.8	536.4
	Co	6.3	4.5	7.8	4.8	7.5
	ICP-MS	CG01/9	CG01/10	CG01/11	PG27/2000	PG28/2000
ppm	Nb	15.792	n.p.	15.678	15.363	14.327
	Ba	490.488	n.p.	528.671	618.515	508.978
	La	48.578	n.p.	52.213	49.087	47.922
	Ce	87.387	n.p.	93.766	90.676	89.234
	Pr	10.051	n.p.	10.841	8.661	8.565
	Nd	33.438	n.p.	36.040	34.751	34.385
	Sm	6.508	n.p.	6.884	6.939	6.819
	Eu	1.250	n.p.	1.372	1.115	1.115
	Gd	7.340	n.p.	7.749	6.408	6.255
	Tb	1.040	n.p.	1.080	1.073	1.030
	Dy	5.651	n.p.	5.882	6.377	6.213
	Ho	1.123	n.p.	1.168	1.433	1.375
	Er	3.307	n.p.	3.424	3.783	3.575
	Tm	0.464	n.p.	0.479	0.496	0.465
	Yb	2.957	n.p.	3.066	3.254	3.050
	Lu	0.410	n.p.	0.429	0.485	0.452
	Hf	5.134	n.p.	5.465	5.958	5.408
	Ta	1.042	n.p.	1.019	0.977	0.912
	W	0.521	n.p.	1.366	0.628	0.451
	Pb	23.914	n.p.	18.046	19.274	19.621
	Th	10.235	n.p.	12.113	14.427	13.036
	U	2.717	n.p.	3.539	3.986	3.544

Appendix 4 Major, minor and trace element geochemistry data								
Phase 5.1, Bivane Subgroup - White River Section, Northern Region								
	XRF	CG01/106	CG01/107	CG01/108	CG01/109	CG01/110	CG01/111	CG01/112
wt%	SiO_2	58.47	62.85	56.99	56.68	56.29	54.43	47.1
	Al_2O_3	13.32	11.04	13.58	12.85	12.89	10.62	13.77
	Fe_2O_3	1.32	1.33	1.36	1.42	1.44	1.07	1.77
	FeO	10.67	10.78	10.98	11.49	11.66	8.65	14.32
	MnO	0.1714	0.1539	0.1776	0.1939	0.1803	0.2651	0.2282
	MgO	2.93	2.41	3.49	3.24	3.51	13.79	5.64
	CaO	5.45	4.87	7.59	7.64	8.22	7.49	9.73
	Na_2O	3.33	1.4	2.35	2.91	2.1	1.81	2.33
	K_2O	1.85	2.75	1.81	1.5	1.74	0.72	0.51
	TiO_2	1.4372	1.6136	1.3985	1.5877	1.5881	0.434	3.3319
	P_2O_5	0.24	0.28	0.22	0.23	0.23	0.06	0.34
	Cr_2O_3	0.0106	0.0099	0.0078	0.0102	0.011	0.2364	0.0383
	NiO	0	0	0	0	0	0.0505	0.0096
ppm	Y	49.35	47.5	43.8	44.75	44.35	11.7	45.65
	Rb	75.85	101.15	64.9	56.1	68.25	27.1	17.65
	Zr	254.25	239.9	205.7	214.85	210.4	44.2	216.45
	Sr	101.45	132.3	198.1	153.35	197.15	128.2	235.05
	Zn	123.5	123.9	120.3	121.6	118	67.5	119.1
	Cu	24.2	0	24.2	2.2	8.2	27.5	394.5
	Ni	7.8	0	12.9	7.7	9	385.4	92.8
	Cr	0	0	0	0	0	1627.9	141.2
	V	227.8	219	250.5	296.4	295.2	164.1	430
	Sc	30.1	21.3	33.6	31.5	30.2	31.5	26
	K	15436.4	22325.2	15044.6	12112.3	15117.2	5091.5	4045
	S	2195.3	109.3	241.1	565.5	302.7	75.4	1335
	P	909	1345.1	813.3	881	764.4	239.6	1728.6
	Co	32.9	37.1	41.1	44.6	44.5	69.7	43.9
	ICP-MS	CG01/106	CG01/107	CG01/108	CG01/109	CG01/110	CG01/111	CG01/112
ppm	Nb	16.131	n.p.	n.p.	n.p.	n.p.	n.p.	n.p.
	Ba	300.864	n.p.	n.p.	n.p.	n.p.	n.p.	n.p.
	La	36.722	n.p.	n.p.	n.p.	n.p.	n.p.	n.p.
	Ce	69.395	n.p.	n.p.	n.p.	n.p.	n.p.	n.p.
	Pr	8.356	n.p.	n.p.	n.p.	n.p.	n.p.	n.p.
	Nd	31.138	n.p.	n.p.	n.p.	n.p.	n.p.	n.p.
	Sm	6.536	n.p.	n.p.	n.p.	n.p.	n.p.	n.p.
	Eu	1.444	n.p.	n.p.	n.p.	n.p.	n.p.	n.p.
	Gd	7.998	n.p.	n.p.	n.p.	n.p.	n.p.	n.p.
	Tb	1.249	n.p.	n.p.	n.p.	n.p.	n.p.	n.p.
	Dy	7.463	n.p.	n.p.	n.p.	n.p.	n.p.	n.p.
	Ho	1.531	n.p.	n.p.	n.p.	n.p.	n.p.	n.p.
	Er	4.524	n.p.	n.p.	n.p.	n.p.	n.p.	n.p.
	Tm	0.654	n.p.	n.p.	n.p.	n.p.	n.p.	n.p.
	Yb	4.169	n.p.	n.p.	n.p.	n.p.	n.p.	n.p.
	Lu	0.582	n.p.	n.p.	n.p.	n.p.	n.p.	n.p.
	Hf	5.151	n.p.	n.p.	n.p.	n.p.	n.p.	n.p.
	Ta	1.080	n.p.	n.p.	n.p.	n.p.	n.p.	n.p.
	W	1.232	n.p.	n.p.	n.p.	n.p.	n.p.	n.p.
	Pb	9.325	n.p.	n.p.	n.p.	n.p.	n.p.	n.p.
	Th	8.596	n.p.	n.p.	n.p.	n.p.	n.p.	n.p.
	U	1.778	n.p.	n.p.	n.p.	n.p.	n.p.	n.p.

Appendix 4 Major, minor and trace element geochemistry data											
Phase 5.2, Bivane Subgroup - White River Section, Northern Region											
XRF		CG01/42	CG01/43	CG01/44	CG01/45	CG01/46	PG1/2000	PG2/2000	PG3/2000	PG4/2000	PG5/2000
wt%	SiO_2	77.14	78.64	55.54	56.19	59.3	71.6	69.74	73.45	72.67	69.77
	Al_2O_3	10.9	11.11	14.86	14.6	13.11	12.8	13.48	11.69	13.09	13.63
	Fe_2O_3	0.27	0.12	1.14	1.25	1.17	0.43	0.46	0.4	0.42	0.45
	FeO	2.21	0.96	9.21	10.09	9.48	3.46	3.75	3.24	3.44	3.66
	MnO	0.0375	0.0128	0.1667	0.1693	0.1631	0.0619	0.0764	0.0585	0.0604	0.0571
	MgO	0.07	0.04	5.11	4	3.61	0.34	0.34	0.33	0.23	0.27
	CaO	0.31	0.2	8.33	7.95	6.44	0.96	1.61	1.06	1.31	0.59
	Na_2O	0.3	0.5	2.78	2.6	3.9	0.42	0.73	0.52	4.23	0.5
	K_2O	8.31	8.26	1.65	1.93	1.44	9.08	9.08	8.53	4.05	10.27
	TiO_2	0.2986	0.3061	1.0335	1.1517	1.0756	0.3798	0.4139	0.348	0.3715	0.3909
	P_2O_5	0.02	0.02	0.18	0.21	0.19	0.05	0.05	0.04	0.05	0.05
	Cr_2O_3	0	0	0.0028	0	0	0.0091	0.0029	0.0047	0.0051	0.0091
	NiO	0.0001	0	0.0062	0.0035	0.004	0.001	0.0019	0.0015	0.0009	0.0011
ppm	Y	99.4	89.75	38.5	50.05	48.3	105.3	117	88.1	108.55	105.7
	Rb	274.95	271.3	49.6	66.8	49.85	342.2	351.25	291.95	161.9	337.5
	Zr	548.65	543.65	177.8	244.85	242.3	654.95	702.5	604.25	681.2	677.85
	Sr	66.85	84	203.4	178.2	110.5	35.35	47.2	27.5	44.75	27.25
	Zn	88.6	86.8	96.7	110.2	105.8	113.5	84	88.9	125	137
	Cu	6.2	2.3	50.5	43.6	39.2	12	4.3	0.7	1.4	8.2
	Ni	2.2	0.3	44.6	22.8	17.5	0.9	0.2	0.9	1.7	0.6
	Cr	3	0.3	21.3	0.1	2.9	0	0	0	0	0
	V	1.5	1.5	202	198.3	178.9	9.4	9.6	7.1	8.6	9.2
	Sc	4.2	4.1	31.3	25.9	27	3.2	4.2	2.3	3	2.3
	K	53508.1	54112	11529.3	14468.9	9745.7	62641.1	62740.8	59496.7	28599.9	73169.8
	S	86.2	90.6	169.5	218.4	456.9	172.1	435.9	52.7	56.1	326.6
	P	35.9	22	637.5	768.4	693.1	176.8	220.7	200.2	218.3	237.8
	Co	0.9	1.5	43.4	39.9	36.5	0	3.8	1.9	2.1	0.9
ICP-MS		CG01/42	CG01/43	CG01/44	CG01/45	CG01/46	PG1/2000	PG2/2000	PG3/2000	PG4/2000	PG5/2000
ppm	Nb	31.704	30.592	13.591	18.708	18.282	41.151	44.216	35.404	42.913	42.516
	Ba	1087.828	1354.736	341.707	306.780	242.939	623.980	651.946	501.806	379.892	455.293
	La	72.957	63.199	29.663	41.425	40.774	93.368	100.002	87.400	96.205	93.605
	Ce	139.822	121.696	55.706	76.647	76.026	181.066	194.762	168.238	191.907	180.743
	Pr	16.093	14.108	6.568	8.911	8.836	20.540	21.872	19.445	21.493	20.945
	Nd	54.166	47.771	22.621	30.673	30.571	70.124	74.366	68.055	72.937	73.540
	Sm	11.873	10.486	5.042	6.548	6.418	14.209	15.111	13.147	14.948	14.423
	Eu	1.912	1.651	1.266	1.407	1.323	1.568	1.696	1.350	1.750	1.601
	Gd	14.730	12.850	6.419	8.391	8.301	16.678	17.875	14.857	18.005	16.783
	Tb	2.320	2.044	0.984	1.268	1.254	2.490	2.729	2.206	2.762	2.520
	Dy	13.590	12.398	5.688	7.310	7.172	14.648	15.796	12.409	15.723	14.376
	Ho	2.964	2.693	1.190	1.519	1.506	3.038	3.281	2.601	3.212	2.993
	Er	9.015	8.191	3.527	4.502	4.475	9.004	9.924	8.026	9.462	9.148
	Tm	1.319	1.223	0.504	0.655	0.652	1.334	1.456	1.193	1.393	1.352
	Yb	8.404	7.849	3.342	4.280	4.283	8.669	9.517	7.925	9.027	8.933
	Lu	1.192	1.120	0.462	0.605	0.605	1.240	1.360	1.148	1.278	1.292
	Hf	12.024	11.752	3.847	5.316	5.394	13.882	15.542	14.470	14.263	14.314
	Ta	2.259	2.226	0.975	1.190	1.142	2.116	2.320	1.941	2.202	2.152
	W	1.184	1.444	0.559	0.582	0.606	1.256	1.238	1.067	1.175	1.714
	Pb	48.697	27.174	8.057	10.958	9.729	27.224	18.017	12.067	30.518	35.291
	Th	20.332	20.250	7.069	10.319	10.540	22.898	24.815	22.785	23.524	24.104
	U	5.238	5.010	1.471	2.159	2.179	4.449	4.908	4.464	4.584	4.637

Appendix 4 Major, minor and trace element geochemistry data									
Phase 5.3, Bivane Subgroup - White River Section, Northern Region									
XRF		CG01/96	CG01/97	CG01/98	CG01/99	CG01/101	CG01/102	CG01/103	CG01/165
wt%	SiO_2	54.12	70.39	72.48	74.74	75.6	71.3	57.67	59.09
	Al_2O_3	15.22	15.53	12.26	12.23	10.96	14.78	14.22	13.2
	Fe_2O_3	1.05	0.65	0.53	0.35	0.52	0.58	1.15	1.4
	FeO	8.49	5.3	4.31	2.86	4.24	4.69	9.32	11.31
	MnO	0.1573	0.0606	0.0808	0.0384	0.0699	0.0505	0.1595	0.1769
	MgO	6.68	1.67	0.08	0.15	0.04	0.14	3.78	2.1
	CaO	9.51	0.86	1.42	0.45	0.73	0.41	7.75	5.11
	Na_2O	1.88	0.07	2.42	1	1.04	1.42	2.14	3.13
	K_2O	1.31	3.99	5.19	7.33	6.14	5.63	2.34	2.06
	TiO_2	0.899	0.8629	0.413	0.3321	0.3178	0.4345	1.0441	1.7319
	P_2O_5	0.2	0.04	0.04	0.03	0.02	0.03	0.18	0.42
	Cr_2O_3	0.0072	0.0271	0.0057	0.0086	0.0072	0.0037	0.0061	0.0098
	NiO	0.0067	0.0087	0.0009	0.0013	0.0008	0.0007	0.0022	0
ppm	Y	34.2	48.5	87.75	88	85.3	110.3	47.95	57.15
	Rb	35.3	171.8	199	249.1	178	275.85	103.35	118.7
	Zr	155.3	307.8	504.85	518.4	478.3	566.9	228.4	281.05
	Sr	183.2	13.1	85.7	60.5	68.9	53.6	200.45	102.5
	Zn	85.9	100.6	108.6	77.2	147.6	142.3	100.6	129
	Cu	49.2	43.9	0.6	1.7	3.4	0	37	0
	Ni	70.5	63.7	0	0.6	0	0	21.4	0
	Cr	13.3	191.5	0	3.4	0	0	0	0
	V	185.7	137.2	0.3	0	0	0.7	189.5	140.1
	Sc	35.2	26.4	4.7	4.7	3	5.9	26.5	27.8
	K	9144.2	29981.2	35618.2	48920.5	40004.9	40330	19452.9	16337.6
	S	94.4	11.7	39.3	62.1	168.6	132.1	474.6	377.4
	P	1076.7	173.6	154.7	147.8	72.8	166.4	667.5	1587.7
	Co	46.2	14.6	0	2.6	0	0	37.3	37
ICP-MS		CG01/96	CG01/97	CG01/98	CG01/99	CG01/101	CG01/102	CG01/103	CG01/165
ppm	Nb	10.350	31.200	n.p.	33.055	n.p.	n.p.	n.p.	19.005
	Ba	221.242	764.405	n.p.	909.462	n.p.	n.p.	n.p.	240.686
	La	21.500	56.994	n.p.	67.156	n.p.	n.p.	n.p.	39.863
	Ce	42.903	118.300	n.p.	153.535	n.p.	n.p.	n.p.	78.420
	Pr	5.188	12.946	n.p.	14.836	n.p.	n.p.	n.p.	9.727
	Nd	19.685	42.319	n.p.	42.289	n.p.	n.p.	n.p.	36.850
	Sm	4.153	10.123	n.p.	11.306	n.p.	n.p.	n.p.	7.656
	Eu	0.998	1.656	n.p.	2.074	n.p.	n.p.	n.p.	1.736
	Gd	5.151	12.365	n.p.	13.393	n.p.	n.p.	n.p.	9.450
	Tb	0.800	2.027	n.p.	2.084	n.p.	n.p.	n.p.	1.439
	Dy	4.793	12.217	n.p.	12.296	n.p.	n.p.	n.p.	8.409
	Ho	0.981	2.535	n.p.	2.647	n.p.	n.p.	n.p.	1.731
	Er	2.866	7.384	n.p.	7.899	n.p.	n.p.	n.p.	5.086
	Tm	0.422	1.120	n.p.	1.186	n.p.	n.p.	n.p.	0.716
	Yb	2.668	7.342	n.p.	7.820	n.p.	n.p.	n.p.	4.695
	Lu	0.358	1.058	n.p.	1.139	n.p.	n.p.	n.p.	0.667
	Hf	2.785	11.814	n.p.	12.152	n.p.	n.p.	n.p.	6.063
	Ta	0.658	2.337	n.p.	2.445	n.p.	n.p.	n.p.	1.249
	W	0.516	0.799	n.p.	0.856	n.p.	n.p.	n.p.	0.515
	Pb	6.735	14.637	n.p.	25.716	n.p.	n.p.	n.p.	12.839
	Th	4.911	20.034	n.p.	21.147	n.p.	n.p.	n.p.	10.030
	U	1.030	5.561	n.p.	5.497	n.p.	n.p.	n.p.	2.104

Appendix 4 Major, minor and trace element geochemistry data									
Phase 5.3, Bivane Subgroup - White River Section, Northern Region									
XRF		CG01/166	CG01/171	PG38/2000	PG39/2000	PG40/2000	PG41/2000	PG42/2000	PG43/2000
wt%	SiO_2	59.79	74.2	57.64	55.48	55	77.43	72.68	73.8
	Al_2O_3	12.94	12.05	14.01	15.09	14.35	11.89	12.23	11.68
	Fe_2O_3	1.35	0.46	1.13	1.1	1.19	0.46	0.54	0.39
	FeO	10.92	3.72	9.11	8.94	9.61	3.74	4.34	3.13
	MnO	0.1564	0.074	0.1655	0.1716	0.1773	0.0546	0.0773	0.0528
	MgO	2.16	0.08	3.6	5.08	5.02	0.08	0.11	0.09
	CaO	4.87	1.48	7.54	8.16	9.74	0.35	0.86	0.68
	Na_2O	2.77	3.67	2.32	1.9	2.15	1.51	3.13	0.59
	K_2O	2.45	3.6	2.41	1.95	0.75	3.83	5.09	8.56
	TiO_2	1.5489	0.4033	1.032	1.0292	1.0281	0.3437	0.4023	0.3025
	P_2O_5	0.28	0.04	0.18	0.21	0.22	0.02	0.04	0.05
	Cr_2O_3	0.0067	0.0086	0.0019	0.0146	0.006	0	0.0051	0.0028
	NiO	0	0.0014	0.0043	0.0074	0.0055	0	0.0015	0.0017
ppm	Y	57	86.9	46.55	43.35	39.75	103.75	82.15	96.05
	Rb	111.2	132.2	100.1	66.55	20.35	184.8	171	225.55
	Zr	287.1	508	230.55	218.45	194.7	634.3	506.7	586.3
	Sr	124.2	97.9	187.8	198.15	269	52	75.9	92.1
	Zn	120.5	124.6	97.9	96.8	94.1	150.6	118.5	144.9
	Cu	9.1	5	51.4	33	52.6	17.1	10.9	72.7
	Ni	0	0	22.7	45.5	35.7	0	0	0.4
	Cr	0	0	0	25.3	0	0	0	0.5
	V	247.5	0	187.2	183.2	191.7	1.2	1.5	1.9
	Sc	27.5	4.5	27.1	28.8	34.2	3.7	5	2.8
	K	19552.9	24995.1	20284.9	13959.1	5390.2	27522.5	35716.1	57640
	S	771.4	76.4	1171.4	91.4	479.7	285.1	55.8	314.4
	P	1014.9	163	652.8	881	967.7	66	166.1	290.7
	Co	33	0.4	40.7	46.7	45.7	0	3.1	0
ICP-MS		CG01/166	CG01/171	PG38/2000	PG39/2000	PG40/2000	PG41/2000	PG42/2000	PG43/2000
ppm	Nb	n.p.	31.157	16.682	13.241	12.723	36.379	30.867	34.583
	Ba	n.p.	684.722	565.239	768.464	168.864	1015.508	757.754	1255.328
	La	n.p.	67.616	41.228	33.610	30.566	86.287	65.105	95.407
	Ce	n.p.	153.681	80.046	66.258	61.306	159.732	131.571	169.521
	Pr	n.p.	16.547	7.957	6.672	6.229	15.894	13.389	16.840
	Nd	n.p.	50.561	33.034	28.388	26.727	65.951	54.018	67.964
	Sm	n.p.	12.237	7.312	6.603	6.005	14.414	12.006	14.997
	Eu	n.p.	2.258	1.334	1.335	1.161	1.628	1.609	2.739
	Gd	n.p.	14.483	7.246	6.547	6.222	14.420	11.915	14.610
	Tb	n.p.	2.254	1.297	1.179	1.114	2.612	2.327	2.638
	Dy	n.p.	13.116	8.240	7.477	7.141	16.876	14.886	16.540
	Ho	n.p.	2.715	1.919	1.741	1.653	4.047	3.541	3.884
	Er	n.p.	8.032	5.060	4.581	4.372	10.887	9.336	10.246
	Tm	n.p.	1.173	0.676	0.615	0.582	1.480	1.264	1.381
	Yb	n.p.	7.701	4.469	4.024	3.851	9.720	8.330	9.151
	Lu	n.p.	1.100	0.658	0.608	0.558	1.463	1.228	1.376
	Hf	n.p.	10.969	5.300	5.214	4.499	15.471	13.029	14.787
	Ta	n.p.	2.356	0.908	0.726	0.670	2.000	1.779	1.952
	W	n.p.	0.915	0.896	0.453	0.459	1.917	0.849	1.628
	Pb	n.p.	36.223	14.163	7.039	8.861	31.628	20.905	38.716
	Th	n.p.	20.159	11.022	7.794	7.283	25.935	20.058	24.306
	U	n.p.	5.617	2.317	1.773	1.530	6.556	5.863	5.950

Appendix 4 Major, minor and trace element geochemistry data							
Nhlebela Formation, Bivane Subgroup - White Mfolozi Inlier, Central Region							
XRF		CG02/205	CG02/206	CG02/210	CG02/211	CG02/212	CG02/213
wt%	SiO_2	61.06	64.87	52.73	65.18	59.82	63.24
	Al_2O_3	13.88	12.76	12.89	14.11	14.50	13.81
	Fe_2O_3	1.09	1.15	1.62	0.92	1.11	1.05
	FeO	8.82	9.30	13.15	7.44	8.98	8.51
	MnO	0.1276	0.1160	0.2234	0.0969	0.1432	0.1182
	MgO	2.24	3.77	4.21	1.76	3.71	2.47
	CaO	5.97	2.52	8.66	2.44	4.86	3.18
	Na_2O	4.92	3.59	1.97	2.82	4.52	4.21
	K_2O	0.81	0.90	1.59	3.94	1.22	2.39
	TiO_2	0.8485	0.7916	2.2573	0.8355	0.8940	0.8553
	P_2O_5	0.16	0.13	0.35	0.16	0.16	0.14
	Cr_2O_3	0.0025	0.0040	0.0005	0.0016	-0.0035	0.0044
	NiO	0.0090	0.0084	0.0062	0.0077	0.0098	0.0088
ppm	Y	31.93	31.44	56.46	30.37	33.10	29.63
	Rb	30.06	19.09	61.26	136.42	41.83	35.58
	Zr	228.16	215.46	178.22	231.56	237.96	227.85
	Sr	183.27	117.22	234.16	125.12	281.25	140.06
	Zn	75.50	97.48	125.74	86.60	92.02	80.14
	Cu	170.82	161.26	142.60	146.68	122.88	233.00
	Ni	68.08	67.28	43.31	57.83	73.35	68.82
	Cr	17.39	16.47	31.72	18.88	14.52	16.19
	V	72.67	69.98	339.24	75.31	60.48	56.00
	Sc	11.19	10.27	37.82	11.03	11.86	11.34
	K	-	-	-	-	-	-
	S	-	-	-	-	-	-
	P	647.32	583.28	1552.87	707.13	666.98	658.11
	Co	37.25	37.80	42.93	32.16	39.44	35.47
ICP-MS		CG02/205	CG02/206	CG02/210	CG02/211	CG02/212	CG02/213
ppm	Nb	16.23	14.52	15.17	16.29	16.43	16.38
	Ba	280.02	333.49	475.09	896.40	459.94	1122.02
	La	37.17	33.87	30.85	35.58	32.41	30.56
	Ce	73.37	65.91	66.43	67.87	67.07	58.66
	Pr	8.29	7.60	8.35	7.53	7.96	6.52
	Nd	28.54	27.31	33.30	25.18	28.94	22.82
	Sm	6.24	5.98	7.97	5.72	6.16	5.35
	Eu	1.57	1.47	2.04	1.28	1.51	1.27
	Gd	6.46	6.30	8.91	5.84	6.30	5.54
	Tb	0.96	0.93	1.47	0.89	0.95	0.85
	Dy	5.49	5.34	9.18	5.21	5.48	5.05
	Ho	1.09	1.06	1.92	1.04	1.09	1.03
	Er	2.97	2.89	5.42	2.86	3.04	2.84
	Tm	0.45	0.43	0.84	0.43	0.46	0.43
	Yb	2.73	2.65	5.23	2.56	2.85	2.67
	Lu	0.41	0.40	0.77	0.38	0.42	0.39
	Hf	5.46	5.24	4.65	5.54	5.79	5.48
	Ta	1.09	1.04	0.99	1.10	1.12	1.10
	W	1.38	0.94	1.08	2.51	1.68	1.48
	Pb	5.56	5.55	11.96	10.61	6.05	8.62
	Th	12.62	11.87	6.49	12.97	13.49	12.93
	U	3.24	3.05	1.87	3.30	3.44	3.27

Appendix 4 Major, minor and trace element geochemistry data								
Agatha Formation, Bivane Subgroup - White Mfolozi Inlier, Central Region								
	XRF	WM2/2000	WM3/2000	WM4/2000	WM5/2000	WM6/2000	WM10/2000	WM11/2000
wt%	SiO_2	52.8	47.85	49.185	50.19	49.13	49.11	54.14
	Al_2O_3	14.7	15.21	15.805	16.365	16.23	15.435	15.02
	Fe_2O_3	1.58	1.775	1.4	1.425	1.365	1.695	1.23
	FeO	12.795	14.41	11.32	11.545	11.04	13.7	9.975
	MnO	0.16735	0.21585	0.1882	0.197	0.23915	0.22675	0.1757
	MgO	4.315	4.655	3.635	4.96	4.265	4.645	5.785
	CaO	8.16	9.865	10.865	8.215	10.62	10.345	8.765
	Na_2O	1.945	3.285	4.5	4.39	3.745	3.35	3.645
	K_2O	1.185	0.175	0.33	0.395	1.175	0.02	0.02
	TiO_2	1.6134	1.659	1.70585	1.58925	1.53525	1.1457	0.88685
	P_2O_5	0.285	0.3	0.295	0.275	0.26	0.185	0.165
	Cr_2O_3	0.0149	0.0152	0.0154	0.0191	0.0164	0.0187	0.0333
	NiO	0.0127	0.014	0.01305	0.0165	0.01315	0.0227	0.0153
ppm	Y	38.2	34.4	34	32.65	29.3	26.25	23.05
	Rb	36.2	3.05	6	6.25	36.9	0.6	0.7
	Zr	193.75	185.8	193.15	187.05	175.55	126.35	122.55
	Sr	570.7	108.05	157.7	157.45	157.25	92.2	153.35
	Zn	125.4	129	97.4	123.1	100.2	118.6	104.2
	Cu	56.8	34.4	22.8	43.8	47.9	83.4	41.8
	Ni	88.9	88.4	80.7	107.1	87.9	146.9	101.4
	Cr	38.7	46.8	44.5	148.9	111.8	138.8	212.2
	V	173.70	197.90	184.70	197.20	188.20	216.20	204.10
	Sc	21.50	29.70	31.80	26.80	31.30	39.30	30.50
	K	9215.10	1144.50	2184.30	2598.20	8269.00	111.00	124.20
	S	710.40	322.40	712.60	10.70	11.50	14.30	110.80
	P	1071.80	1536.10	1526.40	1268.50	1314.30	808.30	682.90
	Co	52.80	68.10	51.30	61.50	43.70	66.80	63.00
	ICP-MS	WM2/2000	WM3/2000	WM4/2000	WM5/2000	WM6/2000	WM10/2000	WM11/2000
ppm	Nb	9.216	8.801	9.158	8.845	8.857	5.740	5.439
	Ba	664.953	80.322	155.110	210.943	323.840	14.879	18.141
	La	24.982	14.943	18.849	17.596	15.290	9.040	10.853
	Ce	48.181	32.117	39.117	38.194	30.512	18.819	23.103
	Pr	6.228	4.554	5.181	5.315	4.142	2.531	2.953
	Nd	23.599	18.637	20.064	20.698	17.120	10.429	11.716
	Sm	5.841	4.985	4.962	5.280	4.139	2.814	2.834
	Eu	2.032	1.059	0.886	2.937	1.160	0.732	0.933
	Gd	7.386	6.586	6.413	6.765	4.983	3.891	3.665
	Tb	1.052	0.977	0.946	0.966	0.719	0.641	0.564
	Dy	5.786	5.381	5.268	5.138	4.099	3.907	3.313
	Ho	1.108	1.049	1.035	0.990	0.874	0.807	0.667
	Er	3.022	2.918	2.872	2.725	2.544	2.293	1.877
	Tm	0.415	0.401	0.399	0.379	0.362	0.321	0.262
	Yb	2.512	2.494	2.496	2.357	2.347	2.035	1.658
	Lu	0.346	0.345	0.348	0.331	0.337	0.285	0.231
	Hf	3.011	3.191	3.263	3.303	3.861	2.586	2.347
	Ta	0.473	0.452	0.466	0.459	0.580	0.377	0.316
	W	0.189	0.174	0.276	0.208	0.274	0.127	0.190
	Pb	10.205	2.130	1.128	1.819	1.536	2.041	2.311
	Th	2.231	2.211	2.292	2.702	2.621	1.409	1.045
	U	0.337	0.343	0.349	0.444	0.441	0.294	0.186

Appendix 4 Major, minor and trace element geochemistry data						
Agatha Formation, Bivane Subgroup - White Mfolozi Inlier, Central Region						
	XRF	WM12/2000	WM13/2000	WM15/2000	WM16/2000	WM17/2000
wt%	SiO_2	55.41	54.16	51.58	53.76	52.03
	Al_2O_3	14.72	14.935	15.64	14.165	14.31
	Fe_2O_3	1.24	1.22	1.585	1.245	1.23
	FeO	10.04	9.865	12.805	10.055	10
	MnO	0.17	0.1699	0.2075	0.16585	0.204
	MgO	6.26	6.45	4.88	6.295	6.5
	CaO	8.01	8.085	7.04	9.245	10.65
	Na_2O	3.14	2.95	3.83	2.235	2.35
	K_2O	0.01	0.58	0.355	1.055	0.825
	TiO_2	0.8685	0.823	1.20185	0.88465	1.0772
	P_2O_5	0.16	0.16	0.205	0.17	0.175
	Cr_2O_3	0.0379	0.0377	0.0264	0.0395	0.0482
	NiO	0.0164	0.01505	0.01685	0.0161	0.00835
ppm	Y	21.25	22.85	25.65	23.65	29.45
	Rb	0.3	9.5	4.25	11.2	19.35
	Zr	119.5	122.15	142.1	128.6	103.65
	Sr	166.8	347.85	84	299.65	180.75
	Zn	124.2	94.3	117.9	94.4	87.8
	Cu	47.7	32	64.4	50.1	96.4
	Ni	105.7	107.6	112.4	117.2	55.2
	Cr	216.1	233	145.6	243.2	237.6
	V	198.7	185.9	176.4	190.3	288.2
	Sc	32.7	29.3	20.4	28.9	39.8
	K	71.6	4015.9	2207.5	7284.5	6532.8
	S	13	337.1	77.9	946.4	415.3
	P	719.1	723.1	953.6	641	814.8
	Co	56.7	60.1	60	59.3	41.7
	ICP-MS	WM12/2000	WM13/2000	WM15/2000	WM16/2000	WM17/2000
ppm	Nb	5.265	5.421	6.640	5.657	6.988
	Ba	15.448	372.376	133.615	309.142	214.735
	La	12.194	12.666	11.470	13.304	9.495
	Ce	24.997	26.238	25.590	27.370	20.447
	Pr	3.170	3.302	3.376	3.438	2.716
	Nd	12.491	13.049	13.673	13.538	11.425
	Sm	2.882	3.154	3.486	3.242	3.079
	Eu	1.091	1.104	1.039	1.167	1.044
	Gd	3.677	3.865	4.477	4.021	4.142
	Tb	0.557	0.579	0.700	0.604	0.663
	Dy	3.223	3.366	4.078	3.495	4.078
	Ho	0.641	0.664	0.813	0.701	0.858
	Er	1.794	1.885	2.260	1.963	2.483
	Tm	0.248	0.265	0.321	0.273	0.361
	Yb	1.581	1.676	2.004	1.731	2.371
	Lu	0.215	0.227	0.275	0.233	0.346
	Hf	2.131	2.120	2.665	2.172	2.359
	Ta	0.295	0.290	0.340	0.283	0.364
	W	0.187	0.175	0.224	0.163	0.166
	Pb	7.038	3.405	1.507	3.497	2.261
	Th	0.998	1.048	1.573	1.071	1.407
	U	0.229	0.175	0.244	0.182	0.308

APPENDIX 5
MOBILITY OF ELEMENTS

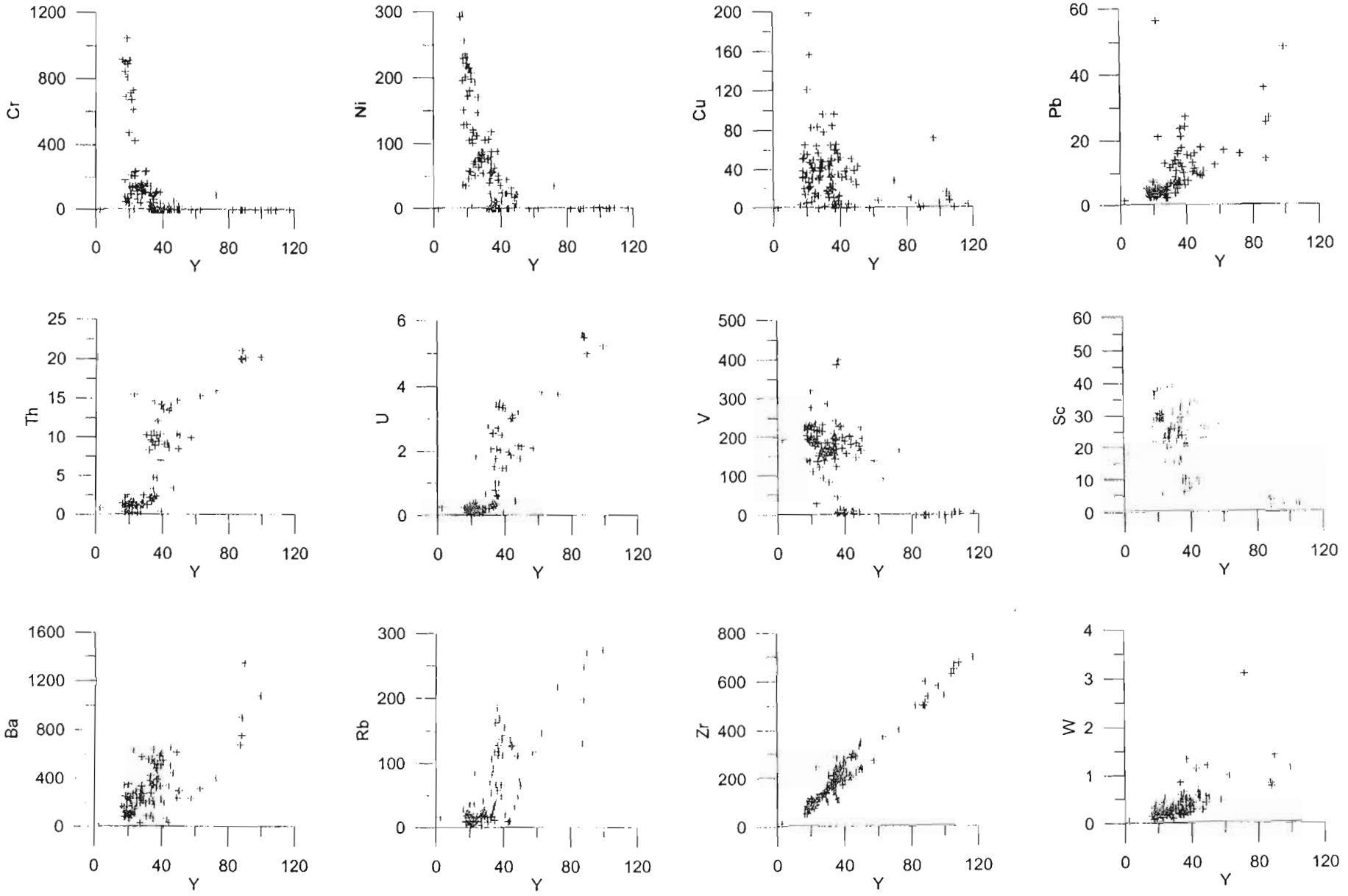

Appendix 5 Immobile element Y used to determine mobility of other trace elements.
(all values in ppm)

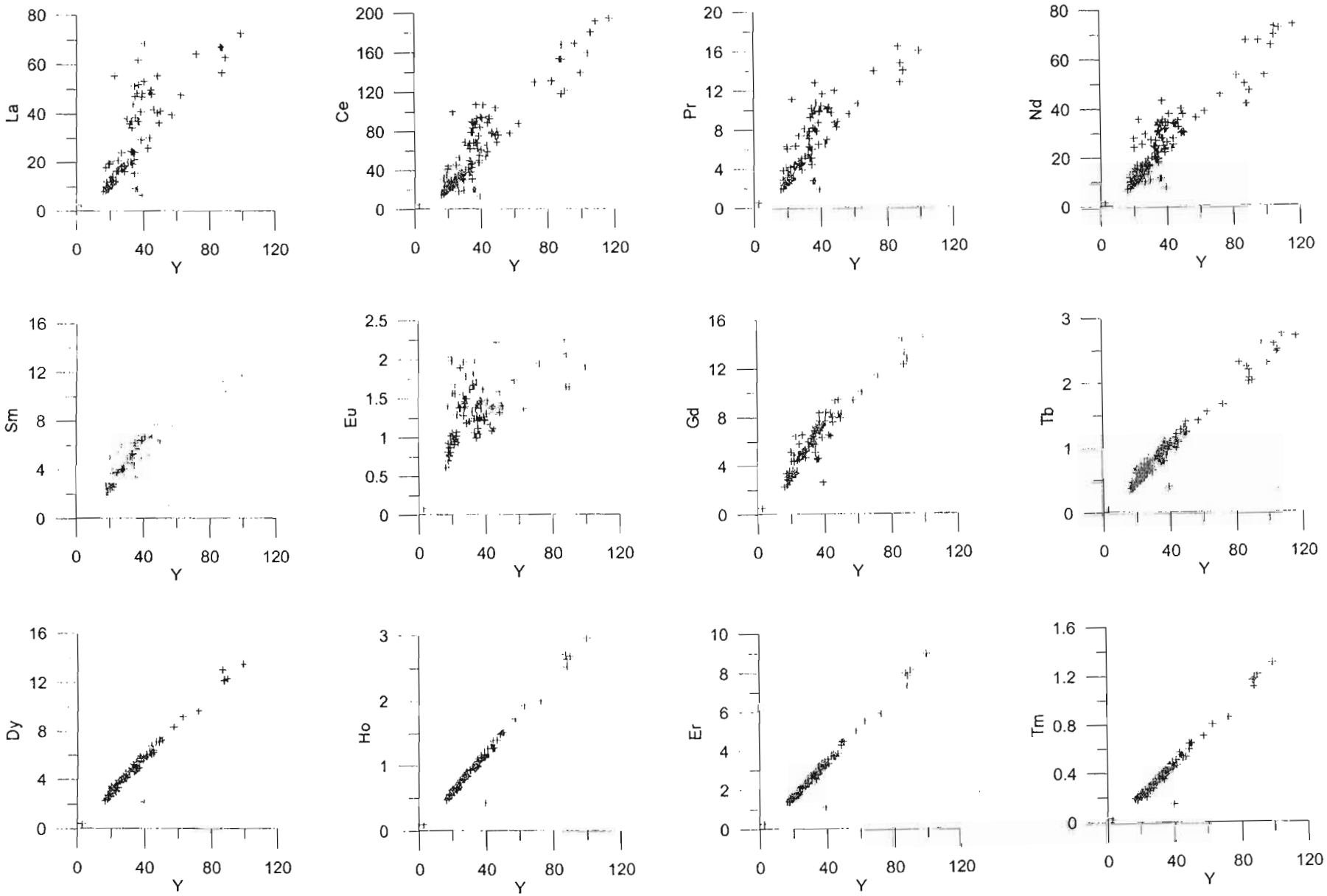

Appendix 5 Immobile element Y used to determine mobility of other trace elements.
(all values in ppm)

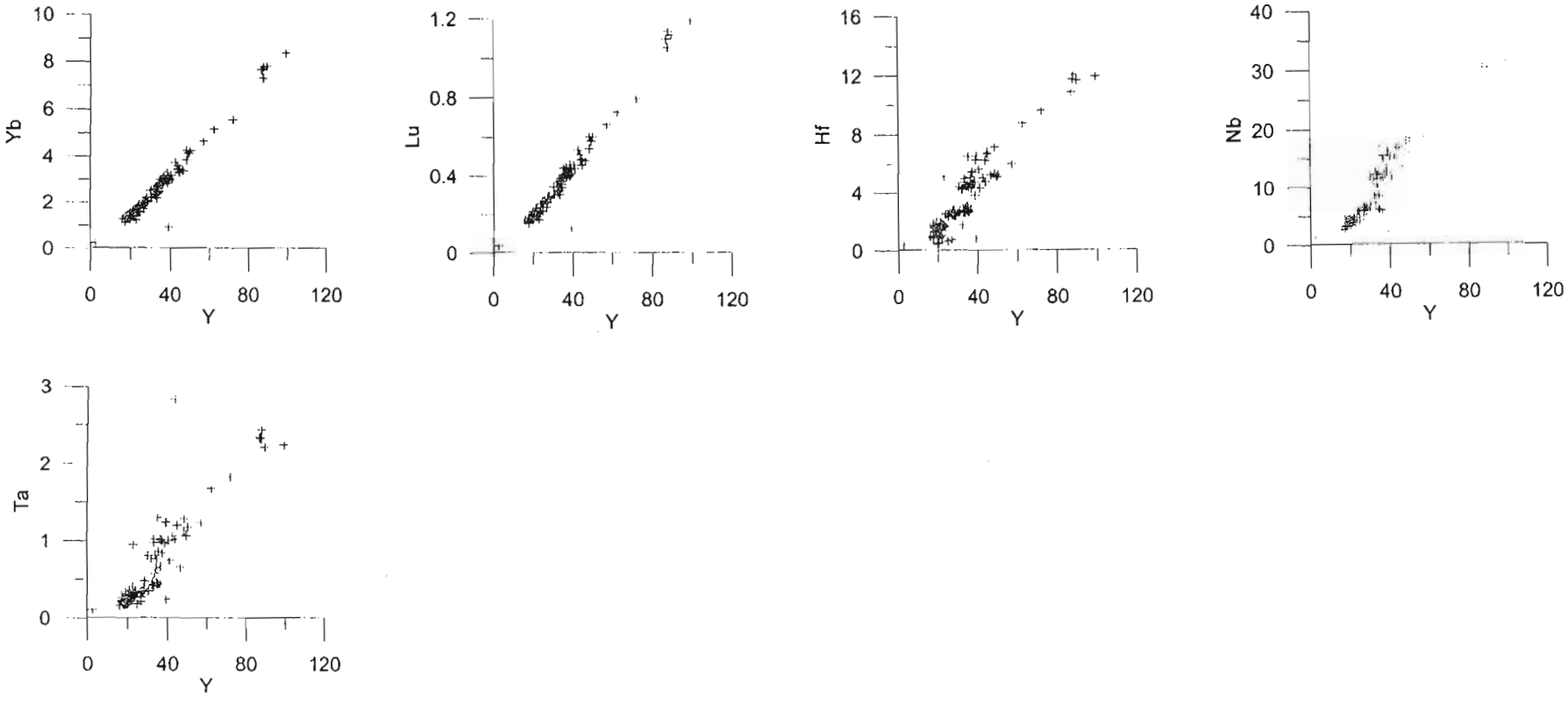

Appendix 5 Immobile element Y used to determine mobility of other trace elements.
(all values in ppm)

APPENDIX 6
CLASSIFICATION COMPARISONS

Appendix 6. Comparison of results of classification diagrams for individual volcanic samples (WR White River Section; WM White Mfolozi Inlier)

Phase / Fmn	Sample No.	Jensen Cation	SiO_2 vs Zr/TiO_2	SiO_2 vs Nb/Y	Zr/TiO_2 vs Nb/Y	Zr/TiO_2 vs Ce
WR - Phase 5.2	CG 01/46	high-Fe tholeiite basalt	andesite	andesite	andesite	andesite
WR - Phase 5.3	2000/PG/38	tholeiitic andesite	andesite	andesite	andesite	andesite
WR - Phase 5.3	2000/PG/39	calcalkaline basalt	trachyandesite	andesite	andesite	andesite
WR - Phase 5.3	2000/PG/40	high-Fe tholeiite basalt	trachyandesite	andesite	andesite	andesite
WR - Phase 5.3	2000/PG/41	tholeiitic rhyolite	rhyolite	rhyolite	rhyolite	pantellerite
WR - Phase 5.3	2000/PG/42	tholeiitic rhyolite	rhyodacite	rhyodacite	rhyolite	phonolite
WR - Phase 5.3	2000/PG/43	tholeiitic rhyolite	rhyolite	rhyolite	rhyolite	pantellerite
WR - Phase 5.3	CG 01/96	high-Mg tholeiite basalt	trachyandesite	andesite	andesite	andesite
WR - Phase 5.3	CG 01/97	tholeiitic dacite	rhyodacite	-	-	-
WR - Phase 5.3	CG 01/98	tholeiitic rhyolite	rhyodacite	rhyodacite	rhyolite	phonolite
WR - Phase 5.3	CG 01/99	tholeiitic rhyolite	rhyolite	rhyolite	rhyolite	phonolite
WR - Phase 5.3	CG 01/101	tholeiitic rhyolite	rhyolite	-	-	-
WR - Phase 5.3	CG 01/102	tholeiitic rhyolite	rhyodacite	-	-	-
WR - Phase 5.3	CG 01/103	tholeiitic andesite	andesite	-	-	-
WR - Phase 5.3	CG 01/165	high-Fe tholeiite basalt	andesite	andesite	andesite	basalt
WR - Phase 5.3	CG 01/166	high-Fe tholeiite basalt	andesite	-	-	-
WR - Phase 5.3	CG 01/171	tholeiitic rhyolite	rhyolite	rhyolite	rhyolite	rhyolite
WM - Nhlebela Fmn	CG02/205	tholeiitic andesite	andesite	andesite	rhyodacite / dacite	andesite
WM - Nhlebela Fmn	CG02/206	high-Fe tholeiite basalt	rhyodacite / dacite	rhyodacite / dacite	rhyodacite / dacite	andesite
WM - Nhlebela Fmn	CG02/210	high-Fe tholeiite basalt	subalkaline basalt	subalkaline basalt	subalkaline basalt	subalkaline basalt
WM - Nhlebela Fmn	CG02/211	tholeiitic dacite	rhyodacite / dacite	rhyodacite / dacite	rhyodacite / dacite	andesite
WM - Nhlebela Fmn	CG02/212	tholeiitic andesite	andesite	andesite	rhyodacite / dacite	andesite
WM - Nhlebela Fmn	CG02/213	tholeiitic andesite	rhyodacite / dacite	rhyodacite / dacite	rhyodacite / dacite	andesite
WM - Agatha Fmn	WM/2/2000	high-Fe tholeiite basalt	subalkaline basalt	subalkaline basalt	basaltic andesite	basalt
WM - Agatha Fmn	WM/3/2000	high-Fe tholeiite basalt	alkali basalt	subalkaline basalt	basaltic andesite	basalt
WM - Agatha Fmn	WM/4/2000	high-Fe tholeiite basalt	alkali basalt	subalkaline basalt	basaltic andesite	basalt
WM - Agatha Fmn	WM/5/2000	high-Fe tholeiite basalt	alkali basalt	subalkaline basalt	basaltic andesite	basalt
WM - Agatha Fmn	WM/6/2000	high-Fe tholeiite basalt	alkali basalt	subalkaline basalt	basaltic andesite	basalt
WM - Agatha Fmn	WM/10/2000	high-Fe tholeiite basalt	alkali basalt	subalkaline basalt	basaltic andesite	basalt
WM - Agatha Fmn	WM/11/2000	high-Fe tholeiite basalt	andesite	andesite	andesite	andesite
WM - Agatha Fmn	WM/12/2000	high-Fe tholeiite basalt	andesite	andesite	andesite	andesite
WM - Agatha Fmn	WM/13/2000	high-Fe tholeiite basalt	andesite	andesite	andesite	andesite
WM - Agatha Fmn	WM/15/2000	high-Fe tholeiite basalt	subalkaline basalt	subalkaline basalt	basaltic andesite	andesite
WM - Agatha Fmn	WM/16/2000	high-Fe tholeiite basalt	andesite	andesite	andesite	andesite
WM - Agatha Fmn	WM/17/2000	high-Fe tholeiite basalt	subalkaline basalt	subalkaline basalt	basaltic andesite	basalt

Appendix 6. Comparison of results of classification diagrams for individual volcanic samples (WR White River Section; WM White Mfolozi Inlier)

Phase / Fmn	Sample No.	Jensen Cation	SiO_2 vs Zr/TiO_2	SiO_2 vs Nb/Y	Zr/TiO_2 vs Nb/Y	Zr/TiO_2 vs Ce
WR - Phase 2	CG 01/92	tholeiitic andesite	dacite	dacite	andesite	andesite
WR - Phase 2	CG 01/93	tholeiitic dacite	dacite	rhyodacite	rhyodacite	trachyandesite
WR - Phase 2	CG 01/94	high-Fe tholeiite basalt	andesite	-	-	-
WR - Phase 3.1	CG 01/114	tholeiitic andesite	rhyodacite	-	-	-
WR - Phase 3.1	CG 01/115	tholeiitic dacite	rhyodacite	-	-	-
WR - Phase 3.1	CG 01/116	tholeiitic andesite	andesite	-	-	-
WR - Phase 3.1	CG 01/117	tholeiitic andesite	trachyandesite	-	-	-
WR - Phase 3.1	CG 01/118	high-Fe tholeiite basalt	trachyandesite	andesite	dacite	dacite
WR - Phase 3.1	CG 01/119	tholeiitic andesite	dacite	-	-	-
WR - Phase 3.1	CG 01/120	tholeiitic basaltic andesite	dacite	-	-	-
WR - Phase 3.1	CG 01/121	tholeiitic andesite	rhyodacite	dacite	dacite	dacite
WR - Phase 3.1	CG 01/136	tholeiitic andesite	dacite	dacite	andesite	dacite
WR - Phase 3.1	CG 01/137	high-Fe tholeiite basalt	alkali basalt	subalkaline basalt	subalkaline basalt	andesite
WR - Phase 3.1	CG 01/139	high-Fe tholeiite basalt	dacite	-	-	-
WR - Phase 3.1	2000/PG/29	tholeiitic andesite	dacite	dacite	andesite - dacite	dacite
WR - Phase 3.1	2000/PG/30	tholeiitic andesite	dacite	dacite	dacite	trachyandesite
WR - Phase 3.2	CG 01/74	tholeiitic basaltic andesite	andesite	-	-	-
WR - Phase 3.2	CG 01/75	tholeiitic rhyolite	dacite	dacite	dacite	dacite
WR - Phase 3.2	CG 01/77	tholeiitic rhyolite	rhyolite	-	-	-
WR - Phase 3.2	CG 01/78	tholeiitic andesite	alkali basalt	-	-	-
WR - Phase 3.2	CG 01/79	high-Fe tholeiite basalt	andesite	andesite	andesite	andesite
WR - Phase 3.2	CG 01/80	high-Fe tholeiite basalt	andesite	-	-	-
WR - Phase 3.2	CG 01/81	high-Fe tholeiite basalt	andesite	-	-	-
WR - Phase 4	2000/PG/27	tholeiitic rhyolite	rhyolite	rhyodacite - rhyolite boundary	dacite - rhyodacite	dacite - trachyandesite boundary
WR - Phase 4	2000/PG/28	tholeiitic rhyolite	rhyodacite boundary	rhyodacite	dacite - rhyodacite	dacite - trachyandesite boundary
WR - Phase 4	CG 01/9	tholeiitic rhyolite	rhyolite	rhyodacite	dacite - rhyodacite	dacite - trachyandesite boundary
WR - Phase 4	CG 01/10	tholeiitic rhyolite	rhyolite	-	-	-
WR - Phase 4	CG 01/11	tholeiitic rhyolite	rhyolite	rhyodacite	dacite - rhyodacite	dacite - trachyandesite boundary
WR - Phase 5.1	CG 01/106	high-Fe tholeiite basalt	andesite	andesite	andesite	andesite
WR - Phase 5.1	CG 01/107	high-Fe tholeiite basalt	andesite	-	-	-
WR - Phase 5.1	CG 01/108	high-Fe tholeiite basalt	andesite	-	-	-
WR - Phase 5.1	CG 01/109	high-Fe tholeiite basalt	andesite	-	-	-
WR - Phase 5.1	CG 01/110	high-Fe tholeiite basalt	andesite	-	-	-
WR - Phase 5.1	CG 01/111	komatiitic basalt	andesite	-	-	-
WR - Phase 5.1	CG 01/112	high-Fe tholeiite basalt	subalkaline basalt	-	-	-
WR - Phase 5.2	2000/PG/1	tholeiitic rhyolite	rhyolite	rhyodacite	rhyolite	pantellerite
WR - Phase 5.2	2000/PG/2	tholeiitic rhyolite	pantellerite	rhyodacite	rhyolite	phonolite boundary
WR - Phase 5.2	2000/PG/3	tholeiitic rhyolite	rhyolite	rhyolite	rhyolite	pantellerite
WR - Phase 5.2	2000/PG/4	tholeiitic rhyolite	rhyolite	rhyodacite	rhyolite	pantellerite
WR - Phase 5.2	2000/PG/5	tholeiitic rhyolite	pantellerite	rhyodacite	rhyolite	pantellerite
WR - Phase 5.2	CG 01/42	tholeiitic rhyolite	rhyolite	rhyolite	rhyolite	pantellerite
WR - Phase 5.2	CG 01/43	calcalkaline rhyolite	rhyolite	rhyolite	rhyolite	pantellerite
WR - Phase 5.2	CG 01/44	high-Fe tholeiite basalt	andesite	andesite	andesite	andesite
WR - Phase 5.2	CG 01/45	high-Fe tholeiite basalt	trachyandesite	andesite	andesite	andesite

Appendix 6. Comparison of results of classification diagrams for individual volcanic samples (WR White River Section; WM White Mfolozi Inlier)

Phase / Fmn	Sample No.	Jensen Cation	SiO_2 vs Zr/TiO_2	SiO_2 vs Nb/Y	Zr/TiO_2 vs Nb/Y	Zr/TiO_2 vs Ce
WR - Phase 2	CG 01/25	tholeiitic dacite	rhyodacite	rhyodacite	rhyodacite	trachyte
WR - Phase 2	CG 01/26	high-Mg tholeiite basalt	subalkaline basalt	subalkaline basalt	andesite	andesite
WR - Phase 2	CG 01/27	high-Mg tholeiite basalt	andesite	andesite	andesite	andesite
WR - Phase 2	CG 01/28	tholeiitic dacite	rhyodacite	rhyodacite	rhyodacite	dacite
WR - Phase 2	CG 01/29	high-Mg tholeiite basalt	andesite	andesite	andesite	andesite
WR - Phase 2	CG 01/30	high-Mg tholeiite basalt	subalkaline basalt	subalkaline basalt	andesite	andesite
WR - Phase 2	CG 01/31	tholeiitic rhyolite	rhyodacite	rhyodacite	rhyodacite	trachyandesite
WR - Phase 2	CG 01/32	high-Mg tholeiite basalt	andesite	andesite	basaltic andesite	basaltic andesite
WR - Phase 2	CG 01/33	high-Mg tholeiite basalt	andesite	andesite	andesite	andesite
WR - Phase 2	CG 01/34	calcalkaline basalt	rhyodacite	rhyodacite	rhyodacite	dacite
WR - Phase 2	CG 01/35	high-Mg tholeiite basalt	andesite	andesite	basaltic andesite	basaltic andesite
WR - Phase 2	CG 01/36	boundary calc-alk basalt & high-	andesite	andesite	andesite	andesite
WR - Phase 2	CG 01/37	calcalkaline dacite	rhyodacite	rhyodacite	rhyodacite	trachyte
WR - Phase 2	CG 01/38	high-Mg tholeiite basalt	andesite	andesite	andesite	andesite
WR - Phase 2	CG 01/39	tholeiitic dacite	rhyodacite	rhyodacite	rhyodacite	trachyandesite
WR - Phase 2	CG 01/40	tholeiitic andesite	dacite	dacite	andesite	andesite
WR - Phase 2	CG 01/41	calcalkaline basalt	andesite	andesite	andesite	andesite
WR - Phase 2	CG 01/140	tholeiitic andesite	dacite	-	-	-
WR - Phase 2	CG 01/141	high-Fe tholeiite basalt	andesite	andesite	basaltic andesite	basalt
WR - Phase 2	CG 01/142	high-Fe tholeiite basalt	subalkaline basalt	subalkaline basalt	basaltic andesite	basalt
WR - Phase 2	CG 01/143	calcalkaline basalt	andesite	-	-	-
WR - Phase 2	CG 01/144	high-Fe tholeiite basalt	andesite	-	-	-
WR - Phase 2	CG 01/147	tholeiitic andesite	dacite	-	-	-
WR - Phase 2	CG 01/148	high-Mg tholeiite basalt	andesite	andesite	andesite	andesite
WR - Phase 2	CG 01/149	high-Mg tholeiite basalt	andesite	-	-	-
WR - Phase 2	CG 01/150	high-Mg tholeiite basalt	subalkaline basalt	-	-	-
WR - Phase 2	CG 01/151	calcalkaline basalt	andesite	andesite	andesite	andesite
WR - Phase 2	CG 01/153	high-Fe tholeiite basalt	andesite	-	-	-
WR - Phase 2	CG 01/154	high-Mg tholeiite basalt	andesite	-	-	-
WR - Phase 2	CG 01/158	tholeiitic andesite	dacite	-	-	-
WR - Phase 2	CG 01/160	high-Mg tholeiite basalt	subalkaline basalt	-	-	-
WR - Phase 2	CG 01/161	tholeiitic rhyolite	rhyodacite	rhyodacite	rhyodacite	rhyolite
WR - Phase 2	CG 01/162	high-Mg tholeiite basalt	andesite	andesite	andesite	andesite
WR - Phase 2	CG 01/163	tholeiitic dacite	rhyodacite	rhyodacite	rhyodacite	rhyolite
WR - Phase 2	CG 01/82	tholeiitic rhyolite	rhyolite	-	-	-
WR - Phase 2	CG 01/83	tholeiitic rhyolite	rhyolite	-	-	-
WR - Phase 2	CG 01/84	tholeiitic rhyolite	rhyolite	rhyolite	rhyodacite	trachyte
WR - Phase 2	CG 01/85	calcalkaline basalt	andesite	-	-	-
WR - Phase 2	CG 01/86	tholeiitic andesite	andesite	-	-	-
WR - Phase 2	CG 01/87	high-Mg tholeiite basalt	andesite - trachyandesite	-	-	-
WR - Phase 2	CG 01/88	high-Mg tholeiite basalt	andesite	andesite	andesite	andesite
WR - Phase 2	CG 01/89	high-Mg tholeiite basalt	subalkaline basalt	-	-	-
WR - Phase 2	CG 01/90	high-Mg tholeiite basalt	andesite	andesite	andesite	andesite
WR - Phase 2	CG 01/91	tholeiitic andesite	andesite	-	-	-

Appendix 6. Comparison of results of classification diagrams for individual volcanic samples (WR White River Section; WM White Mfolozi Inlier)

Phase / Fmn	Sample No.	Jensen Cation	SiO_2 vs Zr/TiO_2	SiO_2 vs Nb/Y	Zr/TiO_2 vs Nb/Y	Zr/TiO_2 vs Ce
WR - Wagondrift Fmn	CG 01/12	high-Fe tholeiite basalt	subalkaline basalt	subalkaline basalt	subalkaline basalt	basalt
WR - Wagondrift Fmn	CG 01/13	high-Fe tholeiite basalt	subalkaline basalt	subalkaline basalt	subalkaline basalt	basalt
WR - Wagondrift Fmn	CG 01/15	high-Fe tholeiite basalt	subalkaline basalt	subalkaline basalt	subalkaline basalt	basalt
WR - Wagondrift Fmn	CG 01/16	high-Fe tholeiite basalt	subalkaline basalt	subalkaline basalt	subalkaline basalt	basalt
WR - Wagondrift Fmn	CG 01/17	high-Fe tholeiite basalt	subalkaline basalt	subalkaline basalt	subalkaline basalt	basalt
WR - Wagondrift Fmn	CG 01/18	high-Fe tholeiite basalt	subalkaline basalt	subalkaline basalt	subalkaline basalt	basalt
WR - Wagondrift Fmn	CG 01/19	high-Fe tholeiite basalt	subalkaline basalt	subalkaline basalt	andesite	basalt
WR - Wagondrift Fmn	CG 01/20	high-Fe tholeiite basalt	subalkaline basalt	subalkaline basalt	andesite	basalt
WR - Wagondrift Fmn	CG 01/21	high-Fe tholeiite basalt	subalkaline basalt	subalkaline basalt	basaltic andesite	basalt
WR - Wagondrift Fmn	CG 01/170	calcalkaline basalt	subalkaline basalt	subalkaline basalt	basaltic andesite	basalt
WR - Mantonga Fmn	CG 01/122	tholeiitic dacite	rhyodacite / dacite	rhyodacite / dacite	rhyodacite / dacite	trachyandesite
WR - Phase 1	2000/PG/20	calcalkaline andesite	andesite	andesite	andesite	basalt
WR - Phase 1	2000/PG/21	calcalkaline andesite	andesite	andesite	andesite	andesite
WR - Phase 1	2000/PG/22	high-Fe tholeiite basalt	andesite	andesite	andesite	andesite
WR - Phase 1	2000/PG/23	high-Fe tholeiite basalt	andesite	andesite	andesite	andesite
WR - Phase 1	2000/PG/24	tholeiitic andesite	andesite	andesite	andesite	andesite-basalt-trachyandesite boundary
WR - Phase 1	2000/PG/25	high-Fe tholeiite basalt	andesite	andesite	andesite	andesite
WR - Phase 1	2000/PG/26	high-Fe tholeiite basalt	andesite	andesite	andesite	andesite
WR - Phase 1	CG 01/1	calcalkaline basalt	andesite	andesite	andesite	andesite
WR - Phase 1	CG 01/2	calcalkaline basalt	andesite	andesite	andesite	andesite
WR - Phase 1	CG 01/3	calcalkaline basalt	andesite	andesite	andesite	andesite
WR - Phase 1	CG 01/4	high-Fe tholeiite basalt	andesite	andesite	andesite	andesite
WR - Phase 1	CG 01/5	tholeiitic andesite	rhyodacite / dacite	rhyodacite / dacite	andesite	andesite
WR - Phase 1	CG 01/6	calcalkaline basalt	andesite	andesite	andesite	andesite
WR - Phase 1	CG 01/7	tholeiitic andesite	andesite	andesite	andesite	basalt
WR - Phase 1	CG 01/47	high-Fe tholeiite basalt	andesite	andesite	andesite	andesite
WR - Phase 1	CG 01/48	high-Fe tholeiite basalt	andesite	andesite	andesite	andesite
WR - Phase 1	CG 01/49	calcalkaline basalt	andesite	andesite	andesite	andesite
WR - Phase 1	CG 01/50	high-Fe tholeiite basalt	andesite	andesite	andesite	andesite
WR - Phase 1	CG 01/51	high-Fe tholeiite basalt	andesite	andesite	andesite	andesite
WR - Phase 1	CG 01/123	high-Fe tholeiite basalt	subalkaline basalt	-	-	-
WR - Phase 1	CG 01/125	high-Fe tholeiite basalt	subalkaline basalt	subalkaline basalt	andesite	andesite
WR - Phase 1	CG 01/126	tholeiitic andesite	subalkaline basalt	-	-	-
WR - Phase 1	CG 01/127	high-Fe tholeiite basalt	andesite	-	-	-
WR - Phase 1	CG 01/128	high-Fe tholeiite basalt	andesite	andesite	andesite	basalt
WR - Phase 1	CG 01/130	high-Fe tholeiite basalt	andesite	-	-	-
WR - Phase 1	CG 01/131	tholeiitic andesite	andesite	andesite	andesite	andesite
WR - Phase 1	CG 01/132	high-Fe tholeiite basalt	andesite	-	-	-
WR - Phase 1	CG 01/133	tholeiitic andesite	andesite	-	-	-
WR - Phase 1	CG 01/134	high-Fe tholeiite basalt	andesite	-	-	-
WR - Phase 1	CG 01/135	tholeiitic andesite	andesite	-	-	-
WR - Phase 1	CG 01/167	high-Fe tholeiite basalt	subalkaline basalt	andesite	andesite	basalt
WR - Phase 2	CG 01/22	high-Mg tholeiite basalt	andesite	andesite	andesite	andesite
WR - Phase 2	CG 01/23	high-Mg tholeiite basalt	andesite	andesite	andesite	andesite